Jonathan Jones et al. *Editors*

Advanced GNSS Tropospheric Products for Monitoring Severe Weather Events and Climate

COST Action ES1206 Final Action Dissemination Report

cost
EUROPEAN COOPERATION IN SCIENCE & TECHNOLOGY

Springer

Advanced GNSS Tropospheric Products for Monitoring Severe Weather Events and Climate

Jonathan Jones • Guergana Guerova
Jan Douša • Galina Dick • Siebren de Haan
Eric Pottiaux • Olivier Bock • Rosa Pacione
Roeland van Malderen
Editors

Advanced GNSS Tropospheric Products for Monitoring Severe Weather Events and Climate

COST Action ES1206 Final Action Dissemination Report

cost
EUROPEAN COOPERATION IN SCIENCE & TECHNOLOGY

Springer

Funded by the Horizon 2020 Framework Programme of the European Union

Editors
Jonathan Jones
Met Office
Exeter, UK

Jan Douša
Geodetic Observatory Pecný, RIGTC
Ondřejov, Czech Republic

Siebren de Haan
Royal Netherlands Meteorological Institute
De Bilt, The Netherlands

Olivier Bock
IGN Institut national de l'information géographique et forestière
Paris, France

Roeland van Malderen
Royal Meteorological Institute (RMI)
Brussels, Belgium

Guergana Guerova
Physics Faculty, Department of Meteorology and Geophysics
Sofia University "St. Kliment Ohridski"
Sofia, Bulgaria

Galina Dick
GFZ German Research Centre for Geosciences
Helmholtz Centre Potsdam
Potsdam, Germany

Eric Pottiaux
Royal Observatory of Belgium
Brussels, Belgium

Rosa Pacione
e-GEOS/Centro di Geodesia Spaziale-Agenzia Spaziale Italiana
Matera, MT, Italy

This publication is based upon work from COST Action ES1206: Advanced Global Navigation Satellite Systems tropospheric products for monitoring severe weather events and climate, supported by COST (European Cooperation in Science and Technology). www.cost.eu

COST (European Cooperation in Science and Technology) is a funding agency for research and innovation networks. Our Actions help connect research initiatives across Europe and enable scientists to grow their ideas by sharing them with their peers. This boosts their research, career and innovation.

ISBN 978-3-030-13900-1 ISBN 978-3-030-13901-8 (eBook)
https://doi.org/10.1007/978-3-030-13901-8

Cover illustration: GNSS severe weather schematic, Sofia, Bulgaria, March 2018, Courtesy of Dr Tzvetan Simeonov, Sofia University.

This Springer imprint is published by the registered company Springer Nature Switzerland AG.
The registered company address is: Gewerbestrasse 11, 6330 Cham, Switzerland

Preface

This book presents the state of the art of atmospheric remote sensing using GNSS signal delays in Europe, conducted within COST Action ES1206 'Advanced Global Navigation Satellite Systems Tropospheric Products for Monitoring Severe Weather Events and Climate' (GNSS4SWEC, 2013–2017). It is well-suited for graduate students in the fields of geodesy and meteorology but also for a broader audience concerned with environmental remote sensing. The Action was initially suggested in mid-2011 during informal discussions at the third International Colloquium on Scientific and Fundamental Aspects of the Galileo Program, Copenhagen, and formally began at the kick-off meeting in Brussels, May 2013. As stated in the GNSS4SWEC Memorandum of Understanding (MoU), the main objective of the Action is to 'enhance existing and develop new, ground-based multi-Global Navigation Satellite Systems (GNSS) tropospheric products, assess their usefulness in severe weather forecasting and climate monitoring, and improve GNSS accuracy through enhanced atmospheric modelling'.

A previous COST Action (716) established and to some degree matured GNSS-meteorololgy in Western Europe, but its establishment across the whole of Europe was only achieved by GNSS4SWEC. Over 160 participants from 32 COST countries, 1 near-neighbour country and 4 international partner countries contributed to the work of the three Action working groups. GNSS4SWEC helped introduce GNSS meteorology to 11 European countries and in the establishment of 7 new GNSS Analysis Centres in previously data-sparse regions, e.g. south-east Europe and the Baltic region. Production and exploitation of next-generation GNSS tropospheric products with high spatio-temporal resolution for use in operational numerical weather prediction (e.g. within E-GVAP) are a major step forward (Chap. 3). The GNSS potential in nowcasting severe weather has been demonstrated using case studies, and its implementation in pre-operational tools is evolving at European National Meteorological Services (Chap. 4). The new field of GNSS climatology

was established as a result of GNSS4SWEC (Chap. 5). Chapters 6 and 7 present the national status reports and the outcomes of COST-funded short-term scientific missions (STSMs).

Enjoy reading!

Met Office, Exeter, United Kingdom — Jonathan Jones

Sofia University "St. Kliment Ohridski", Sofia, Bulgaria — Guergana Guerova

Geodetic Observatory Pecný, RIGTC, Ondřejov, Czech Republic — Jan Douša

GFZ German Research Centre for Geosciences, Potsdam, Germany — Galina Dick

Royal Netherlands Meteorological Institute, De Bilt, The Netherlands — Siebren de Haan

Royal Observatory of Belgium, Brussels, Belgium — Eric Pottiaux

IGN Institut national de l'information géographique et forestière, Paris, France — Olivier Bock

e-GEOS/Centro di Geodesia Spaziale-Agenzia Spaziale Italiana, Matera, Italy — Rosa Pacione

Royal Meteorological Institute (RMI), Brussels, Belgium — Roeland van Malderen

May 2019

Acknowledgement

Firstly, we would like to thank the COST Association in Brussels for the faith and vision to fund this COST Action and for their invaluable work encouraging and facilitating science and technology across Europe. In particular, we would like to thank Dr. Deniz Karaca and Ms. Tania Gonzalez-Ovin for the essential scientific and administrative support they have provided over the course of the Action.

We would like to thank all the GNSS network operators and data providers, as well as the IGS and EUREF – without which there would be no data for such scientific study. In addition, we would like to recognise and thank a number of European and national research projects whose support has been fundamental.

We would like to thank the support from all the participants' institutions (Appendix B), and special thanks must go to those people and institutions who have been involved in hosting meetings and workshops (Appendix A).

Finally, we would like to thank all of the participants of GNSS4SWEC; without your enthusiastic participation, none of this would have been possible. Particular thanks to a number of people who made significant contributions to coordination:

- Michal Kačmařík for coordinating and reporting on the WG1 benchmark campaign and slant delays intercomparisons and the help with the Final Report
- Hugues Brenot for coordinating and reporting on the WG1 sub-group for asymmetry modelling
- Florian Zus for coordinating and reporting on the WG1 sub-group for NWP tropospheric parameter modelling
- Pavel Václavovic for organising the WG1 real-time demonstration campaign and for organising the WG1 PPP sub-group
- Norman Teferle for coordinating the WG1 sub-group for ultra-fast products
- Zhiguo Deng for reporting on WG1 sub-group for multi-GNSS development
- Karolina Szafranek for reporting on WG1 sub-group new ACs and networks
- Wolfgang Söhne for support with completing the WG1 Final Report
- Jan Kaplon, Gregor Möller, Radmila Brožková and Pavla Skřivánková for support with the WG1 benchmark dataset

- Witold Rohm for organising the WG2 tomography sub-group
- Gemma Halloran for organising the WG2 numerical nowcasting and NWP assimilation sub-group
- Furqan Ahmed for coordinating and reporting on the WG3 ZTD datasets sub-group
- Anna Klos for coordinating and reporting on the WG3 homogenisation sub-group

May 2019 The Editors

Abstract

The path delay between a GNSS satellite and a ground-based GNSS receiver depends, after elimination of ionospheric effects using a combination of two GNSS frequencies, on the integral effect of the densities of dry air and water vapour along the signal path. The total delay in the signal from each satellite is known as the slant delay as the path is most likely to be non-azimuthal. The slant paths are then transferred into the vertical (or zenith) by an elevation-dependent mapping function, and this new parameter is known as the zenith total delay or ZTD. ZTD gives a measure for the integrated atmospheric condition and is now widely accepted as a standard product from a network of dual-frequency GNSS receivers. With further calculation, taking into account surface pressure and temperature, we can then convert a portion of the ZTD into an estimate of the integrated water vapour (IWV) content of the atmosphere.

As IWV may potentially change rapidly on very short timescales, it is the speed as well as accuracy at which IWV can be calculated which is of critical importance to short-term meteorological forecasting or 'nowcasting'. Often, rapid changes in IWV are associated with high humidity conditions linked to extreme weather events such as thunderstorms. Extreme weather events such as these are typically difficult to predict and track under traditional operational meteorological observing systems, and as they have the potential to cause great damage and risk to life, it is in the interests to both the public and national meteorological services to significantly improve nowcasting wherever possible. As such, the requirement for dense near real-time GNSS networks for meteorological applications becomes apparent. Furthermore, water vapour is one of the most important constituents of the atmosphere as moisture and latent heat are primarily transmitted through the water vapour phase. As such, water vapour is one of the most important greenhouse gases typically accounting for 60–70 % of atmospheric warming, and thus, accurate, long-term monitoring of atmospheric water vapour is of great importance to climatological research.

COST Action ES1206: Advanced Global Navigation Satellite Systems Tropospheric Products for Monitoring Severe Weather Events and Climate

(GNSS4SWEC) addresses new and improved capabilities from concurrent developments in both the GNSS and meteorological communities. For the first time, the synergy of three operational GNSS systems (GPS, GLONASS and Galileo) is used to develop new, more advanced tropospheric products, exploiting the full potential of multi-GNSS water vapour estimates on a wide range of temporal and spatial scales, from real-time monitoring and forecasting of severe weather to climate research.

The Action also promotes the use of meteorological data as an input to GNSS positioning, navigation and timing services and aims to stimulate knowledge transfer and data sharing throughout Europe.

Contents

1 Scientific Background 1
1.1 Atmospheric Water Vapour 1
1.2 Global Navigation Satellite Systems (GNSS) 6
1.2.1 GPS Basics 6
1.2.2 Delay in the Neutral Atmosphere 9
1.2.3 Zenith Delay Estimates 11
1.2.4 Derivation of IWV from ZTD 12
References 14

2 General Background 17
2.1 Introduction 18
2.2 The State-of-the-Art at the Start of the Action (E-GVAP) 19
2.3 Reasons for the Action 23
2.4 Objectives 24
2.5 Impacts and Benefits 25
2.5.1 Societal Benefits 25
2.5.2 Scientific Benefits 25
2.5.3 Technological Benefits 26
2.5.4 Economic Benefits 26
2.5.5 Target Groups and End-Users 26
2.6 Scientific Programme 27
2.7 Scientific Work Plans 28
2.7.1 Working Group 1: Advanced GNSS Processing Techniques 28
2.7.2 Working Group 2: Use of GNSS Tropospheric Products for High-Resolution, Rapid-Update NWP and Severe Weather Forecasting 29
2.7.3 Working Group 3: Use of GNSS Tropospheric Products for Climate Monitoring 30

3 Advanced GNSS Processing Techniques (Working Group 1) 33
3.1 Introduction 36
3.2 Campaigns for Development of Advanced Tropospheric Products 37
3.2.1 Benchmark Campaign – Common Data Set for New Product Development and Validation 37
3.2.2 GNSS Real-Time PPP Demonstration Campaign 45
3.3 Tropospheric Asymmetry Monitoring and Advantage of Multi-GNSS 48
3.3.1 Concept of Tropospheric Gradients 49
3.3.2 Global Validity and Behaviour of Tropospheric Gradients Estimated by GPS 53
3.3.3 Monitoring of Severe Weather from Wet Gradients, Residuals and Slants 55
3.3.4 Indicator of Tropospheric Activity Based on the Disruption of GNSS Signals 61
3.3.5 Validation of Slant Tropospheric Delays 71
3.3.6 Information Content in Post-fit Residuals, PPP vs DD Approach 84
3.3.7 Tropospheric Parameters from Multi-GNSS Analysis . . . 86
3.3.8 Multi-GNSS Solutions and Products 91
3.4 PPP and Ultra-Fast GNSS Tropospheric Products 92
3.4.1 Real-Time Data and Product Dissemination 94
3.4.2 BKG Real-Time Analysis Development and Contribution 96
3.4.3 Assessment of IGS RTS Orbits and Clock Corrections and GOP Real-Time Tropospheric Products 101
3.4.4 Real-Time Product Development and Evaluation at ROB 106
3.4.5 GFZ Real-Time Product Development and Assessment in RT Analysis 113
3.4.6 Contribution to RT Demonstration Campaign from ULX 114
3.4.7 New Adaptable Strategy for RT and NRT Troposphere Monitoring 119
3.4.8 Optimum Stochastic Modeling for GNSS Tropospheric Delay Estimation in Real-Time 124
3.5 Exploiting NWM-Based Products for Precise Positioning 126
3.5.1 Tropospheric Parameters from Numerical Weather Models 127
3.5.2 The Impact of Global and Regional Climatology on the Performance of Tropospheric Blind Models 133
3.5.3 Refined Discrete and Empirical Troposphere Mapping Functions VMF3 and GPT3 135

3.5.4 The Impact of NWM Forecast Length on ZTDs 136
3.5.5 Dual-Layer Tropospheric Correction Model Combining Data from GNSS and NWM 138
3.5.6 Tropospheric Refractivity and Zenith Path Delays from Least-Squares Collocation of Meteorological and GNSS Data 142
3.5.7 Improving Precise Point Positioning with Numerical Weather Models 144
3.5.8 Using External Tropospheric Corrections to Improve GNSS Positioning of Hot-Air Balloon 145
3.5.9 Real-Time PPP Augmented with High-Resolution NWM Model Data 149
3.5.10 Validation and Implementation of Direct Tropospheric Delay Estimation for Precise Real-Time Positioning 150
3.6 GNSS Data Reprocessing for Climate 158
3.6.1 EUREF Repro2 Contribution of Swisstopo 158
3.6.2 EUREF Repro2 Assessment of GOP Processing Variants 163
3.6.3 CORDEX.be Reprocessing 167
3.6.4 GRUAN Reprocessing 169
3.6.5 GFZ TIGA Reprocessing 170
3.6.6 ULX TIGA Reprocessing 172
3.7 New Analysis Centres, Networks and Solutions 174
3.7.1 Trop-NET System for Collaborative Ground-Based GNSS Meteorology 174
3.7.2 Sofia University GNSS Analysis Centre (SUGAC): First Processing Campaign 178
3.7.3 TU Wien Near Real-Time GNSS Analysis Centre in Austria (TUW AC): First Processing Results 182
3.7.4 New Operational Solutions from ROB in Support to Global NWP Models and Rapid-Update Numerical Nowcasting 183
3.7.5 New Methods to User GNSS Vapor Estimates for Meteorology (NUVEM) 185
3.7.6 Near Real-Time GNSS Processing at ASI/CGS, Italy . . . 187
3.7.7 New Analysis Centre (AUTh) and National Observatory of Athens (NOA) 189
3.7.8 New Analysis Centre in Iceland, Icelandic Meteorological Office (IMO) 193
3.7.9 New Analysis Centre in Hungary (BUTE) 194
References 194

4 Use of GNSS Tropospheric Products for High-Resolution, Rapid-Update NWP and Severe Weather Forecasting (Working Group 2) 203
4.1 Introduction 205
4.2 Non-numerical Nowcasting 206
4.2.1 Investigation of Fog in Bulgaria Using GNSS Tropospheric Products 206
4.2.2 WRF Model Evaluation with GNSS IWV for Intense Precipitation Cases in Bulgaria 210
4.2.3 Case Study of Foehn in Sofia with GNSS Tropospheric Products 217
4.2.4 A GNSS-Based Nowcasting Toolbox for Severe Weather in Belgium 221
4.3 Numerical Nowcasting and NWP Data Assimilation 235
4.3.1 HARMONIE-AROME Group 235
4.3.2 Assimilation of E-GVAP ZTD Data into the WRF Model 236
4.3.3 Improvement of Forecast Skill of the GLAMEPS Model 238
4.3.4 Slant Total Delay Assimilation in COSMO-DE: First Results 242
4.3.5 Data Assimilation Experiments with GNSS ZTD in AROME 3DVAR 247
4.4 Tomography 249
4.4.1 Nowcasting Using Tomography 250
4.4.2 Requirements for Assimilation of Tomography Results 250
4.4.3 Assimilation of Relative Humidity 251
4.4.4 Assimilation of Temperature and Specific Humidity 252
4.4.5 Assimilation of Wet Refractivity 255
4.4.6 Conclusions 257
4.5 Benchmark and Case Study Databases at the U.K. Met Office . . . 259
4.6 ZTD to IWV Conversion 260
References 262

5 Use of GNSS Tropospheric Products for Climate Monitoring (Working Group 3) 267
5.1 Introduction 270
5.1.1 Motivation 270
5.2 Available Reprocessed ZTD and IWV Datasets 273
5.2.1 Inventory of Available Reprocessed ZTD Datasets 273
5.2.2 IGS Repro1 as First Reference GNSS IWV Dataset 275
5.2.3 EPN Repro2 GNSS Reprocessing Campaign 279
5.2.4 VLBI Reprocessing Campaign 281
5.2.5 DORIS Reprocessing Campaign 282

5.3 Sensitivity Studies on GNSS Processing Options 284
5.3.1 An Overview of the GNSS Data Processing Strategies 284
5.3.2 Software Agreement 285
5.3.3 PPP vs. DD Processing Modes 287
5.3.4 Baseline Strategy in DD Processing 290
5.3.5 Mapping Functions 291
5.3.6 Trends in the IWV Estimated from Ground-Based GPS Data: Sensitivity to the Elevation Cutoff Angle 296
5.3.7 Improving Stochastic Tropospheric Model for Better Estimates During Extreme Weather Events 297
5.3.8 Multi-GNSS Data Processing 301
5.3.9 Impact of IGS Type Mean and EPN Individual Antenna Calibration Models 302
5.3.10 Impact of Non-Tidal Atmospheric Loading Models 303
5.3.11 Using Estimated Horizontal Gradients as a Tool for Assessment of GNSS Data Quality 304
5.3.12 Conclusions and Recommendations on Processing Options 312
5.4 Standardisation of ZTD Screening and IWV Conversion 314
5.4.1 ZTD Screening 314
5.4.2 ZTD to IWV Conversion 318
5.4.3 The Uncertainty of the Atmospheric Integrated Water Vapour Estimated from GNSS Observations 324
5.5 ZTD/IWV Homogenisation 326
5.5.1 Introduction 327
5.5.2 Methodology 328
5.5.3 Assessment of the Homogeneity of ERA-Interim 330
5.5.4 Synthetic Gataset Generation 331
5.5.5 Involved Homogenization Algorithms 332
5.5.6 Assessment of the Performance of the Tools on the Synthetic Datasets 335
5.5.7 Conclusions and Outlook 337
5.6 IWV Intercomparisons 339
5.6.1 A Literature Overview 339
5.6.2 A Comparison of Precipitable Water Vapour Products Over the Iberian Peninsula 347
5.6.3 Comparing Precipitable Water from Remote Sensing and Space Geodetic Techniques with Numerical Weather Models 351
5.6.4 Inter-Comparison Analysis of Tropospheric Parameters Derived from GPS and RAOB Data Observed in Sodankylä, Finland 355

5.7 IWV Trends & Variability from GNSS Data and Atmospheric Models . . . 358
5.7.1 Analysis of IWV Trends and Variability from GNSS and Re-Analyses . . . 358
5.7.2 Analysis of IWV Trends and Variability from GNSS and Satellite Data . . . 364
5.7.3 Evaluation of IWV Diurnal Variation in Regional Climate Models using GPS . . . 369
5.7.4 Validation of the Regional Climate Model ALARO-SURFEX by EPN Repro2 . . . 373
5.7.5 Evaluation of IWV Trends and Variability in a Global Climate Model . . . 374
5.7.6 Anomalies of Hydrological Cycle Components During the 2007 Heat Wave in Bulgaria . . . 381
5.8 Database, Formats and Dissemination . . . 384
5.8.1 GOP-TropDB – Comparison Tropospheric Database . . . 384
5.8.2 Tropo SINEX Format . . . 389
References . . . 390

6 National Status Reports . . . 403
6.1 COST Countries . . . 407
6.1.1 Austria . . . 407
6.1.2 Belgium . . . 408
6.1.3 Bulgaria . . . 410
6.1.4 Cyprus . . . 412
6.1.5 Czech Republic . . . 414
6.1.6 Denmark . . . 417
6.1.7 Estonia . . . 418
6.1.8 Finland . . . 419
6.1.9 France . . . 421
6.1.10 Germany . . . 422
6.1.11 Greece . . . 427
6.1.12 Hungary . . . 427
6.1.13 Iceland . . . 429
6.1.14 Israel . . . 431
6.1.15 Italy . . . 432
6.1.16 Lithuania . . . 435
6.1.17 Luxembourgh . . . 436
6.1.18 Poland . . . 439
6.1.19 Portugal . . . 442
6.1.20 Slovakia . . . 443
6.1.21 Spain . . . 446
6.1.22 Sweden . . . 449
6.1.23 Switzerland . . . 453
6.1.24 Turkey . . . 457

6.1.25 United Kingdom 458
6.2 COST International Partner Countries 463
6.2.1 Hong Kong 463
6.2.2 Australia 469
6.2.3 Canada 473
References 474

7 STSM Reports 483
References 507

Appendices 509
References 563

Glossary

3D-Var	Three-dimensional variational data assimilation system
4D-Var	Four-dimensional variational data assimilation system
AC	Analysis centre
ARP	Antenna reference point
ASI	Agenzia Spaziale Italiana (Italian Space Agency)
BKG	Bundesamt für Kartographie und Geodäsie, Germany
BNC	BKG Ntrip Client
BSW	Bernese Software
BUFR	Binary universal format for the representation of data (WMO)
CFSR	Climate Forecast System Reanalysis
CODE	Centre for Orbit Determination in Europe
CORDEX	Coordinated Downscaling Experiment
CORS	Continuously Operating (GNSS) Reference Stations
COST	Cooperation in the Field of Scientific and Technical Research
COST716	COST Action 716: Exploitation of Ground-Based GPS for Operational Numerical Weather Prediction and Climate Applications
DD	Double-difference method of GNSS processing
DMI	Danish Meteorological Institute
DORIS	Doppler Orbitography and Radiopositioning Integrated by Satellite
DWD	Deutscher Wetterdienst (the German National Meteorological Agency)
EC	European Community
ECMWF	European Centre for Medium Range Weather Forecasting
E-GVAP	The EIG EUMETNET GNSS Water Vapour Programme
EPN	EUREF Permanent Network
EPOS	GFZ GNSS processing software package
ERA-Clim	European Reanalysis of Global Climate Observations
ERA-Interim	ECMWF global atmospheric reanalysis
ERP	Earth rotation parameter

ESA	The European Space Agency
ETRS	European Terrestrial Reference System
EUPOS	The European Position Determination System
EUREF	IAG sub-commission for regional reference frames European Reference Frame
EUMETNET	European Meteorological Network
	FES2004
	Finite Element Solution 2004 (OTL model)
FTP	File Transfer Protocol (under TCP/IP)
Galileo	The European GNSS
GAMIT	GPS analysis software package from MIT and SIO
GCOS	WMO Global Climate Observing System
GEOSS	Global Earth Observation System of Systems
GFZ	GFZ German Research Centre for Geosciences
GIPSY-OASIS	GPS Inferred Positioning System Orbit Analysis Simulation Software
GLONASS	Globalnaya navigatsionnaya sputnikovaya sistema (the Russian GNSS system)
GMES	*Global Monitoring for Environment and Security*
GMF	Global mapping function
GNSS	Global navigation satellite system
GOME-2	*Global Ozone Monitoring Experiment-2*
GOP	Geodetic Observatory Pecny, Czech Republic
GPS	The NAVSTAR Global Positioning System (US GNSS)
GPT	Global pressure and temperature model
GRD	Tropospheric gradient
GTS	Global Telecommunication System
HIRLAM	High Resolution Limited Area Model
IAG	International Association of Geodesy
IASI	Infrared atmospheric sounding interferometer
IERS	International Earth Rotation and Reference Systems Service
IF DD	Ionosphere-free double difference
IGS	International GNSS Service
IGU	IGS ultra rapid products
IPCC AR5	Fifth Assessment Report of the Intergovernmental Panel on Climate Change
ITRF	International Terrestrial Reference Frame
IWV	Integrated water vapour
KNMI	Koninklijk Nederlands Meteorologisch Instituut
MC	Management Committee (of the Action)
MERRA	Modern-Era Retrospective analysis for Research and Applications
MIT	Massachusetts Institute of Technology
MOPS	Moisture observation pre-processing system
MoU	Memorandum of understanding

MSL	Mean sea level
NCEP	National Center for Environmental Prediction
NGAA	The Nordic GNSS Analysis Centre
NMHS	National Meteorological and Hydrological Services
NRT	Near real time
NTRIP	Networked transport of RTCM via Internet Protocol
NWM	Numerical weather model
NWP	Numerical weather prediction
OTL	Ocean tide loading
PCO	Phase centre offset
PCV	Antenna phase centre variation
PPP	Precise point positioning method of GNSS processing
PWV	Precipitable water vapour
RAOBS	Radiosonde observations
RINEX	Receiver independent exchange format
RMS	Root mean square
RO	Radio occultation
RTK	Real-time kinematic
RTS	Real-time service (of the IGS)
SCIAMACHY	Scanning Imaging Absorption Spectrometer for Atmospheric Chartography
SIO	Scripps Institution of Oceanography
SIWV	Slant integrated water vapour
SSM/I	Special Sensor Microwave Imager
SSMIS	Special Sensor Microwave Imager Sounder
SSR	State-space representation
STD	Slant total delay
StDev	Standard deviation
TIGA	The IGS Tide Gauge Benchmark Monitoring
TOUGH	Targeting Optimal Use of GPS Humidity Measurements in Meteorology
UCAR	University Consortium for Atmospheric Research
ULX	University of Luxembourg
UM	Unified Model
UTC	Universal time co-ordinated
VLBI	Very long baseline interferometry
VMF	Vienna Mapping Function
WG	Working group
WMO	World Meteorological Organization
WVR	Water vapour radiometer
ZHD	Zenith hydrostatic delay
ZTD	Zenith total delay
ZWD	Zenith Wet Delay

Chapter 1
Scientific Background

J. Jones

Abstract This chapter covers the fundamental science behind GNSS-meteorology. Firstly, atmospheric water vapour and it's role in meteorological and climate systems is covered. The Chapter then provides an overview of GNSS; how they fundamentally operate, how the atmosphere affects GNSS signals (and in particular, GNSS signal delays due to the neutral atmosphere), the conversion of atmospheric delays to integrated water vapour and the application of both signal delays and water vapour to modern meteorological observing systems.

1.1 Atmospheric Water Vapour

Water vapour is one of the most significant constituents of the atmosphere since it is the means by which moisture and energy (as latent heat) are transported through the troposphere and lower stratosphere. Aside from the role of water vapour in balancing the atmospheric heat budget, water vapour is obviously the source of precipitation. In any vertical column of air, the amount of water vapour provides operational meteorologists with a value of the maximum potential precipitation which could be retrieved from that column of air in optimal conditions. Also, as atmospheric water vapour is highly variable both temporally and spatially, it is a potential source of inaccuracy to the geodetic community, hence, accurate observations of atmospheric water vapour result in more accurate GNSS derived coordinates.

Although the actual amount of atmospheric water vapour is relatively low (~1%), the effect it has on the meteorology is very strong. It has the ability to cause temperature anomalies both large and small and, as mentioned, is also the main mechanism for atmospheric latent heat exchange. Furthermore, when looking at

Parts in this chapter are reprinted with kind permission from Jones (2010)

J. Jones (✉)
Met Office, Exeter, UK
e-mail: jonathan.jones@metoffice.gov.uk

J. Jones et al. (eds.), *Advanced GNSS Tropospheric Products for Monitoring Severe Weather Events and Climate*, https://doi.org/10.1007/978-3-030-13901-8_1

water vapour's role in the climate system, numerous scientific studies have determined that around 70% of atmospheric warming is attributable to atmospheric water vapour acting as a greenhouse gas (Houghton et al. 2001; Philipona et al. 2005).

In terms of definitions, water vapour is defined as the amount of water in gas phase (in grams per cubic metre) of air. Water vapour mixing ratio in a volume of air is the ratio of mass of water vapour and the mass of dry air. Specific humidity is the amount of water in gas phase (measured in grams in a total air volume with a mass of 1 kg). A commonly used parameter is relative humidity. Relative humidity is the ratio of the actual water vapour pressure in the air to that of the saturation (or equilibrium) water vapour pressure. Above the water vapour saturation pressure, at 100% relative humidity, any additional water vapour will condensate. The saturation pressure increases strongly with temperature, hence warm air can contain much more water vapour than cold air. Formation of clouds and precipitation is normally associated with lifting of air to levels with lower temperatures, where the air becomes over-saturated resulting in condensation.

Another way to express the water vapour content of an air parcel, is to combine all the water vapour in the vertically integrated total in any one column of air. The most commonly used terms in this case are Integrated Water Vapour (IWV) and Precipitable Water Vapour (PWV). Both terms represent the absolute total amount of water in the vertical column of air which could, hypothetically precipitate out with units of kg/m^2. The term of Integrated Water Vapour, or IWV, with units of kg/m^2 will generally be used in this report as is the standard convention in Europe. Also the unit, unlike the unit of mm which is commonly used for PWV, avoids any confusion with the units used in atmospheric delay, which are units of length. The actual amount is exactly the same, as 1 kg of water spread out over 1 m^2 would be exactly 1 mm in height.

It is important to remember that IWV is a cumulative total amount of water vapour, in principle all the way from the ground based GNSS antenna to the GNSS satellite at an altitude of around 20,000 km depending on GNSS constellation. However, water vapour is by no means distributed evenly in the vertical. The vast majority of the water vapour is limited to the warmest, bottom most portion of the lowest part of the atmosphere known as the troposphere, see Figs. 1.1 and 1.2.

In reality, the vast majority of all atmospheric water vapour is located in the bottom-most few km with a certain degree of variability depending on season, latitude and atmospheric conditions. A typical humidity profile for Camborne for July 2009 is shown in Fig. 1.2.

Due to its high variability, both temporally and spatially, water vapour is one of the most difficult quantities to predict with numerical weather prediction (NWP) models. Typically, NWP model fields are initialised using existing model data coupled with observational data. Historically, observations of water vapour were relatively scarce in meteorology with the majority of data obtained from geographically and temporally sparse radiosonde ascents. Given that approximately half of the energy in the atmosphere is transported by water vapour, other parameters such as

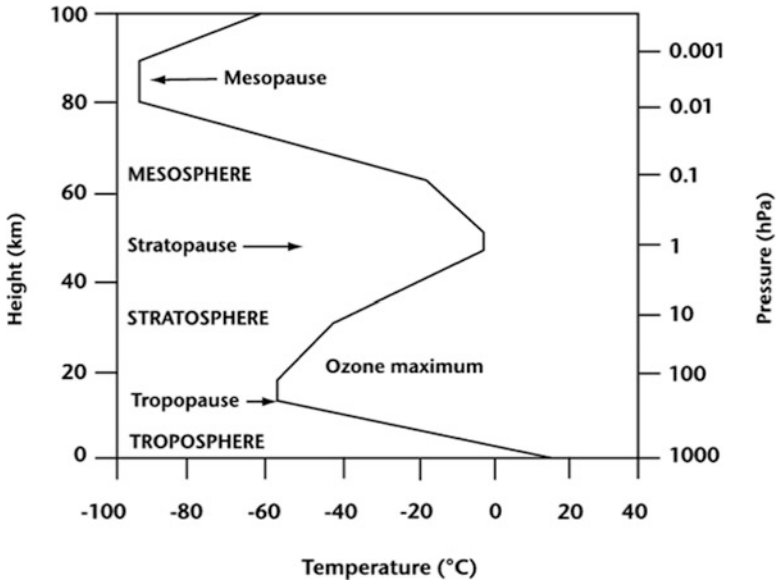

Fig. 1.1 Typical atmospheric temperature profile

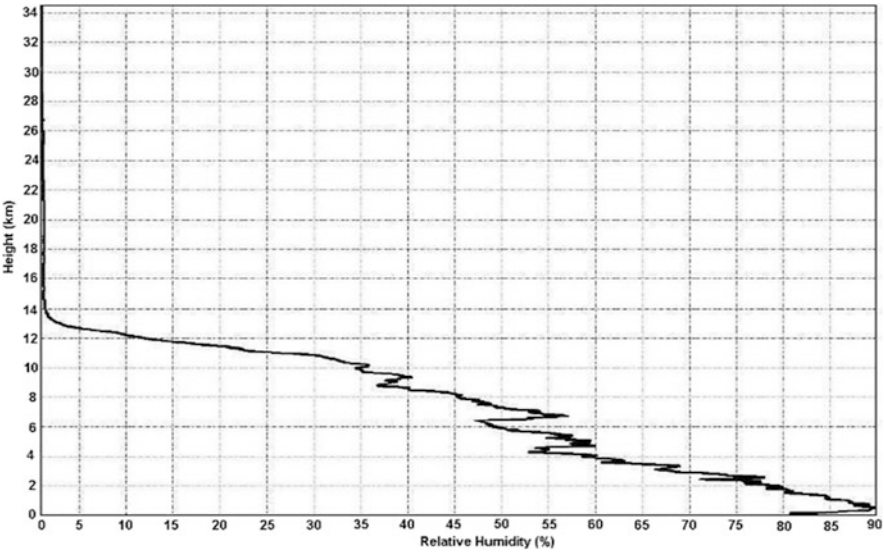

Fig. 1.2 Average monthly humidity profile, Camborne, UK. Composite of all RS92 operational radiosonde ascents from July 2009. (Courtesy of UK Met Office)

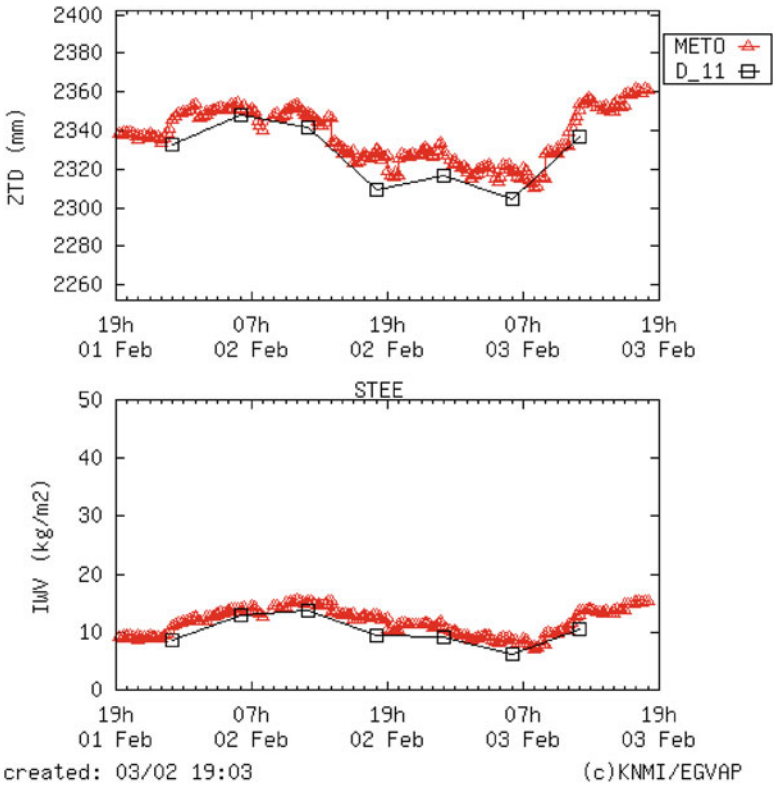

Fig. 1.3 Time series of ZTD and IWV (for Stevenage, UK, February 2010) illustrating the divergence of a NWP model which does not assimilate GNSS observations from reality

cloud cover and surface temperature are also better forecast with superior water vapour information. Due to the importance of water vapour in operational meteorology, improved knowledge and understanding of water vapour fields is one of the prime focuses for future observing systems and is key to improving future forecasting capability.

Figure 1.3 represents a time series of GPS ZTD and IWV estimates from the UK Met Office GNSS system (METO) compared against the HIRLAM 11 km unified NWP model (Unden et al. 2002) prior to the HIRLAM model assimilating GNSS ZTD observations.

In the future, added computing power will permit NWP models with ever increasing horizontal, vertical and temporal resolution. As such, with the advent of higher resolution NWP models will come the requirement for ever higher resolution observational data to initialise the models' starting conditions.

Besides the importance of accurate water vapour observations to operational meteorology, water vapour is one of the most important controlling factors in mean atmospheric temperature by the absorption of radiation. Life on Earth is very much dependent on what is commonly referred to as the greenhouse effect. In general terms, this effect is generally the absorption of solar radiation in the atmosphere, which maintains the Earth's atmosphere at a habitable temperature in which life can exist. Earth has an average temperature of around 14 °C whereas if it were not for the presence of gases such as water vapour and carbon dioxide in the atmosphere, the Earth would have a mean atmospheric temperature of around -18 °C and life would not be possible as we know it.

Water Vapour is one of the most crucial greenhouse gases and plays a vital role in the global climate system. This role is not only restricted to absorbing and radiating energy from the sun, but has direct effects on the formation of clouds and aerosols and also of the chemistry of the lower atmosphere. Despite its importance to atmospheric processes over a wide range of spatial and temporal scales, water vapour is one of the least understood and poorly described components of the Earth's atmosphere in current climate prediction models. Atmospheric water vapour allows short wavelength radiation to pass through the atmosphere, but absorbs long wavelength radiation emitted back by the Earth's surface. This trapped radiation causes the temperatures to increase.

A systematic increase in air temperature due to increasing levels of greenhouse gases, such as CO_2 and methane, enables the air to contain more water vapour. In addition, evaporation will increase where water is available (from oceans, lakes, plants, soil etc). The increase in water vapour levels leads itself to additional absorption of radiation in the lower atmosphere, but also leads to changes in the amount of cloud formation, precipitation, reflection of sunlight from cloud tops etc. Thus, water vapour is generally thought of as a feedback rather than a cause of global warming. Even so, water vapour's role in the climate system is still not very well understood. In many climate models, details in the representation of clouds can substantially affect the model estimates of cloud feedback and climate sensitivity (e.g., Senior and Mitchell 1993; Stainforth et al. 2005; Yokohata et al. 2005). Moreover, the spread of climate sensitivity estimates among current models arises primarily from inter-model differences in cloud feedbacks (Colman 2003; Soden and Held 2006; Webb et al. 2006) and as such, water vapour and it's attributable cloud feedbacks remain a large source of uncertainty in climate sensitivity estimates.

With the advent of high precision ground based geodetic GNSS networks and high quality GNSS processing schemes, we now have a novel approach for the long term monitoring of atmospheric water vapour. GNSS networks are increasing in their global coverage and if the data can be used for climate applications, they offer a huge resource in terms of monitoring atmospheric water vapour long-term. Furthermore, due to the instruments' stability, high level of reliability and low level of maintenance, GNSS sensors are especially suited to remote regions of the world which are typically data sparse. The applicability of GNSS as a tool for climate applications is discussed further in Chap. 5.

1.2 Global Navigation Satellite Systems (GNSS)

TRANSIT, was the first operational satellite navigation system. The system was developed to provide accurate location information to ballistic missile submarines. The system was rolled out for military use in January 1964 and subsequently to civilian users in July 1967. The system, using a constellation of five polar orbiting satellites in low Earth orbit (1075 km) was comprised of two carrier frequencies (150 and 400 MHz) which could be used to provide an hourly positioning estimate with an accuracy of between 200 and 400 m.

However, it wasn't until 1993 when the Global Positioning System (GPS) achieved operational capability that continuous three dimensional positioning and timing information became widely available allowing positioning accuracy down to the sub-decimetre level. The basic principle of GPS is that coded signals are transmitted by at least four satellites for the three dimensional position, plus the time element, to be determined. More information on the technique is given in the subsection below focusing on GPS basics. Whilst other GNSS systems are of course available and operational, the focus here is on GPS only - all other GNSS systems use the same basic principles (Fig. 1.4).

1.2.1 GPS Basics

All GNSS consist of three primary segments: space, ground and user. The space segment consists of satellites orbiting at an altitude of (in the case of GPS) approximately 20,200 km in orbital planes of 55 degrees to the equator. There must be at least 24 satellites operational to ensure at least 4 satellites are visible at any point on the Earth's surface, at any one time. The satellites transmit coded signals and other information (orbital parameters, satellite clock errors etc.) to the user. The ground segment consists of a master control station (in Colorado, USA for the GPS), as well

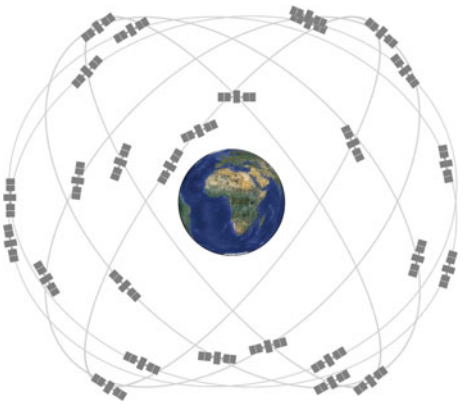

Fig. 1.4 Representation of a GNSS satellite constellation

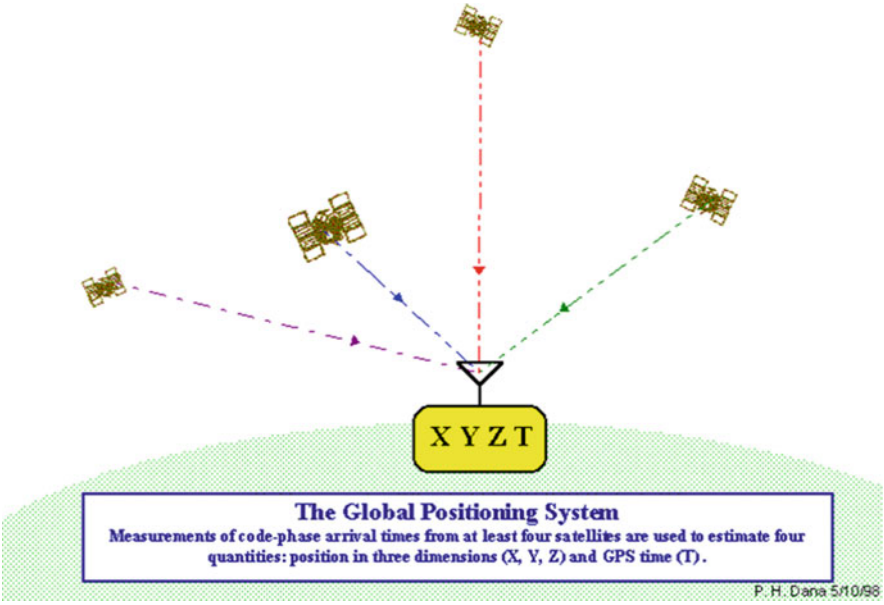

Fig. 1.5 Illustration of GPS positioning

as a number of global monitoring stations, which are responsible for estimating essential satellite information such as orbits and clock errors.

On each GPS satellite, an onboard satellite oscillator generates the fundamental frequency (f_0) of 10.23 MHz from which all other GPS signals are derived. Until relatively recently only two GPS sinusoidal carrier frequencies f_1 and f_2 (at 1575.42 MHz and 1227.60 MHz respectively) were generated which are right-hand polarized with respect to each other and are modulated with coded information. There are three codes imposed on the signal, the C/A (Coarse Acquisition or Clear-Access) code, the P (Precise or Protected) code and the navigation message. These codes have two states, a + 1 or −1 state. As such if the phase-modulated L1 and L2 codes can be decoded by a ground based GPS receiver (the user segment) they may give the user positioning and velocity information, as summarised in Fig. 1.5. In recent times, additional GPS frequencies are transmitted such as L5 and L2C, however, the fundementals of how the system is operated and it's application to meteorology is still largely based around the original two GPS frequencies.

The C/A code has a code sequence of 1023 bits in length and is transmitted with a frequency of 1.023 MHz. As such, it repeats itself once every millisecond and assuming the signal is travelling at the speed of light the distance between subsequent chips can be estimated to be ~300 m. The generation of the P-Code is very similar with the length of the code sequence being approximately 2.3547×1014 bits which corresponds to a time span of approximately 266 days. The P-Code repeats itself once every week and through a process known as anti-spoofing (AS), the P-code is encrypted to a Y-code.

After signals are received by a GPS receiver, the signals are initially split into their satellite specific pseudorandom noise or PRN number based on the C/A codes. A carrier reference code is generated by the GPS receiver, modulated with a copy of the satellite specific PRN code and time shifted to compare against the received code. If the receiver and satellite clock errors are ignored, this difference gives the travel time (τ) and when multiplied by the speed of light (c) gives the approximate range or pseudo-range to the satellite.

Phase positioning measurements are based on reconstructing the carrier phase of the signal and comparing against a signal copy generated by the GPS receiver. By observing the difference in the phase of the signals transmitted by the GPS satellite and those stored in the GPS receiver, the phase difference may be obtained which can be resolved to provide the user with a distance measurement. This expression may be written as:

$$\Delta\phi = \phi_{obs} - \phi_{rec} \tag{1.1}$$

Positioning using phase differencing has a much higher accuracy, although it does introduce an integer ambiguity (j_{amb}) which must be solved for. Furthermore additional delays in the signal propagation such as ionospheric delay (ΔL_{ion}), tropospheric delay (ΔL_{trp}) and clock differences between the satellite and receiver ($\tau_{sat} - \tau_{rec}$) must all be accounted for if precise, geodetic positioning is to be achieved. From Blewitt (1997) the pseudorange, multiplied by the frequency, λ, may be expressed as:

$$\lambda\Delta\phi = D + c(\tau_{sat} - \tau_{rec}) - \lambda j_{amb} + \Delta L_{trp} + \Delta L_{ion} + \mathrm{E} \tag{1.2}$$

Where D is the geometric range from receiver to satellite, c is the speed of light and E is the unknown errors such as receiver multipath. As there are more unknown parameters in Eq. 1.2 than known parameters, equations for a number of satellites are required if all parameters are to be solved for. Furthermore, satellite orbit and clock information must be known a-priori which can be obtained from the International GNSS Service (IGS), which is a voluntary federation of more than 200 worldwide organisations generating and providing free-of-charge GNSS products and services. With particular reference to this report, the IGS are essential in providing satellite clock corrections as well as both predicted and past satellite orbit information.

Even though the clock files provided by the IGS are of high quality there still remain clock errors in both satellite and receiver as well as un-calibrated phase errors which must be accounted for. These errors are common to all receivers and satellites and they can be eliminated by observing a number of satellites and receivers and forming what are known as baselines. Single difference baselines are formed by observing the same satellite by two receivers, in this way the satellite clocks and phase errors can be eliminated. By observing two satellites by two receivers the satellite clock, receiver clock and phase errors are all eliminated. However,

tropospheric errors can only be ignored if the baselines are relatively small and the stations are at roughly the same altitude, as the effect from the atmosphere will affect all signals in the same way.

The alternative to forming baselines between receivers to remove the clock errors, is to resolve the clock errors a-priori and thus introduce very accurate clock files into the processing in the first place. If this can be achieved, a network of GPS receivers can be processed in a station specific way, which is commonly referred to as Precise Point Positioning or PPP. The main benefits of PPP are that it is, at least for the coordinate and tropospheric estimation part, faster because the sites can be processed individually and the processing load can be shared over a number of CPUs/servers. Also, as the sites are processed individually, there is no risk of correlated errors as could be the case with the network solution. In reality however, any benefits in processing speed are often offset against the time it takes to generate the higher accuracy clocks and as such, the overall processing time for a national scale (approximately 200-receiver) network is often comparable to that taken by a double difference (DD) solution. It is when processing larger GNSS networks (300+ stations) where PPP typically has a speed advantage over DD. Furthermore, while a PPP system might not have any correlated errors between different parts of the network due to baselines, if any errors are introduced in the satellite clock determination part, those errors will be applied to the whole network being processed. For more information on the PPP method, see Kouba and Heroux (2001).

1.2.2 Delay in the Neutral Atmosphere

Once enough data has been collected from a number of satellites over a long enough time period, estimates can be generated of atmospheric delay as well as satellite clock errors and phase ambiguities. Due to the dispersive nature of the ionosphere it affects both GPS signals in the same way, by a mathematical combination of the L1 and L2 signals, a so-called ionosphere-free linear combination (L3) can be obtained and thus first order ionospheric delays can be eliminated. Second order effects are still present but their order of magnitude is so small they can be largely ignored for the purposes of this report.

$$L_3 = \frac{f_1^2}{f_1^2 - f_2^2} L_1 - \frac{f_2^2}{f_1^2 - f_2^2} L_2 \tag{1.3}$$

The atmosphere local to the GPS receiver is typically assumed to be horizontally homogenous and based on this assumption, slant path delays can be mapped into the vertical and the number of unknowns can be reduced further. While there is not enough power in the least squares adjustment to solve for slant paths directly, slant path delays are research topics at a number of atmospheric and geodetic institutes, but use of a-priori atmospheric model information is often necessary (Fig. 1.6). More

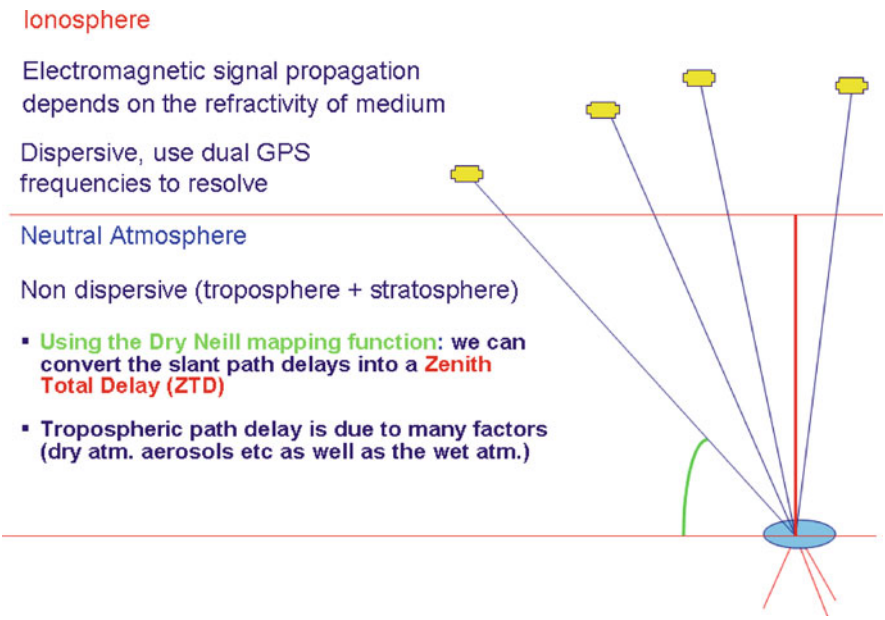

Fig. 1.6 Schematic of satellite signal path through atmosphere

information on slant delays and tomographic retrieval can be found in Chap. 3 of this report.

Tropospheric delay can be expressed as:

$$\Delta^T = \int_s n ds - \int_g dg \tag{1.4}$$

where n is the refractive index, s is the actual signal path and g is the hypothetical geometric path. It is possible to rewrite this as:

$$\Delta^T = \int_s (n-1) ds + \left(\int_s ds - \int_g dg \right) \tag{1.5}$$

This expression shows us that tropospheric delay is a combination of the excess geometric path length as well as the slowing of the signal propagation speed.

Excess geometric path length caused by changes in refractive index, n, is only of relevance at very high zenith angles where the signal is effectively being bent by the atmosphere and a bending angle is introduced. At the vast majority of satellite zenith angles, bending and thus excess path length is very small when compared to the delay of the signal due to propagation. From McClatchey et al. (1971) geometric delay at a zenith angle of 80° would only be in the region of ~4 cm whereas at lower zenith angles (i.e. higher elevation angles) the delay due to slowing of the signal contributes to around 99.7% of the atmospheric delay. In current practice, most GPS

receivers are set with an elevation cut off angles of either 5° or 10° which largely eliminates the geometric delay, as well as minimizing the multipath effect of signals being reflected off the Earth's surface or nearby objects.

As such we can we-write Eq. 1.5 to show that the tropospheric delay is due to the integrated refractivity along the signal propagation path:

$$\Delta^T = \int_s (n-1)ds = 10^{-6} \int_s Nds \tag{1.6}$$

where refractivity N is defined as $N = 10^6 (n-1)$ (according to Smith and Weintraub 1953; Thompson et al. 1986). In the microwave range however refractivity is related to atmospheric parameters through:

$$N = k_1 \frac{p_d}{T} Z_d^{-1} + k_2 \frac{e}{T} Z_w^{-1} + k3 \frac{e}{T^2} Z_w^{-1} \tag{1.7}$$

Where p_d is the pressure of dry air, e is the water vapour pressure, T is the temperature, Z_d and Z_w are the compressibility factors of dry air and water vapour respectively and k_1, k_2 and k_3 are thermodynamic coefficients with values of 77.6 $KhPa^{-1}$, 70.4 $KhPa^{-1}$ and 373,900 K^2 hPa^{-1} respectively, taken from Thayer (1974).

1.2.3 Zenith Delay Estimates

One of the standard outputs from a number of geodetic GNSS processing software is the Zenith Total Delay or ZTD, based on phase measurements from a network of ground based receivers. In GNSS-meteorology it is useful to reduce the term of ZTD into its constituent parts; Zenith Hydrostatic Delay (ZHD) and Zenith Wet Delay (ZWD). ZHD is responsible for the vast majority of the ZTD delay (typically around 90%) but is easily modeled if atmospheric pressure is known. It is the ZWD, which is of particular interest to meteorology, as it is this component which is related to humidity and can change rapidly both spatially and temporally. If we assume that the dry and wet components of Eq. 1.7 behave as ideal gases, Z_d and Z_w are equal to 1 (Bevis et al. 1992) and can therefore be eliminated. Such that when we separate the pressure into its dry and wet partial pressures we can express these terms as:

$$\rho_d = \frac{p_d}{R_d T} \tag{1.8}$$

and

$$\rho_w = \frac{e}{R_w T} \tag{1.9}$$

where R_d and R_w are the gas constants of dry air and water vapour respectively. The density of the 'real' air is simply $\rho_d + \rho_w$. Therefore the refractivity can be expressed as:

$$N = k_1 \frac{p_d}{T} + k_2 \frac{e}{T} + k3 \frac{e}{T^2} \tag{1.10}$$

which can be further reduced to:

$$N = k_1 \rho R_d + (k_2 R_w - k_1 R_d)\rho_w + \frac{k_3 \rho_w R_w}{T} \tag{1.11}$$

Since the path is assumed to be zenithal, ZTD is equal to Δ^T and therefore we can integrate Eq. 1.6, so that ZTD between the receiver altitude z_r and infinity is:

$$ZTD = 10^{-6} \int_{z_r}^{\infty} N dz \tag{1.12}$$

And therefore:

$$ZTD = 10^{-6} \int_{z_r}^{\infty} k_1 \rho R_d dz + 10^{-6} \int_{z_r}^{\infty} (k_2 R_w - k_1 R_d)\rho_w dz + 10^{-6} \int_{z_r}^{\infty} \frac{k_3 \rho_w R_w}{T} dz \tag{1.13}$$

1.2.4 Derivation of IWV from ZTD

The first term on the right hand side of Eq. 1.13 deals with the integration of the combined wet and dry air, The second and third terms integrate the water vapour density and ratio of water vapour density and temperature respectively. Furthermore by application of the hydrostatic equation:

$$dp = -g\rho dz \tag{1.14}$$

where g is the local gravitational acceleration, allows us to transform the first term of Eq. 1.13 to:

$$ZHD = 10^{-6}\frac{k_1 R_d}{g^*}p_r \tag{1.15}$$

where $g^*$is the local gravitational acceleration and the centre of mass of the vertical air column and the integration is performed between 0 and pressure at the receiver p_r. Equation 1.15 shows the dependency between receiver pressure and ZHD. However, as is illustrated in Eq. 1.13, other atmospheric parameters need to be known (temperature, humidity etc.) to determine the wet component of the delay. As this information is not necessarily available certain assumptions about the state of the atmosphere must be made.

By making additional assumptions about the vertical temperature and humidity structure, we can transform ZWD into a more meteorological term, integrated water vapour (IWV):

$$\mathrm{IWV} = \int_{z_r}^{\infty} \rho_w dz \tag{1.16}$$

So,

$$\begin{aligned}\mathrm{ZWD} &= 10^{-6}\int_{z_r}^{\infty}(k_2 R_w - k_1 R_d)\rho_w dz + 10^{-6}\int_{z_r}^{\infty}\frac{k_3 \rho_w R_w}{T}dz \\ &= 10^{-6}\left((k_2 R_w - k_1 R_d)\int_{z_r}^{\infty}\rho_w dz + 10^{-6}k_3 R_w \int_{z_r}^{\infty}\frac{\rho_w}{T}dz\right.\end{aligned} \tag{1.17}$$

To derive a relationship between ZWD and IWV we must first derive a mean temperature the vertical column of air above the GPS receiver

$$T_m = \frac{\int_{z_r}^{\infty}\rho_w dz}{\int_{z_r}^{\infty}(\rho_w/T)dz} \tag{1.18}$$

And as this relation is identical to

$$\int_{z_r}^{\infty}\frac{\rho_w}{T}dz = \frac{\int_{Z_r}^{\infty}\rho_w dz}{T_m} \tag{1.19}$$

The ZWD Eq. 1.17 can now be rewritten as

$$ZWD = 10^{-6}\left(k_2 R_w - k_1 R_d + k_3\frac{R_w}{T_m}\right)\int_{z_r}^{\infty}\rho_w dz \tag{1.20}$$

$$ZWD = 10^{-6}\left(k_2 R_w - k_1 R_d + k_3\frac{R_w}{T_m}\right)IWV \tag{1.21}$$

The conversion of ZTD into IWV thus depends largely on the mean temperature of the air column (T_m), which in turn depends on the vertical temperature and humidity profiles. The estimation of vertical temperature and humidity introduces error into the ZWD to IWV conversion and for this reason ZTD is more commonly assimilated into NWP assimilation schemes as opposed to IWV.

References

Bevis, M., Businger, S., Herring, T. A., Rocken, C., Anthes, R. A., & Ware, R. H. (1992). GPS meteorology: Sensing of atmospheric water vapor using the global positioning system. *Journal of Geophysical Research, 97*, 15787–15801.

Blewitt, G. (1997). Basics of the GPS technique: observation equations. In B. Jonsson (Ed.), *Geodetic applications of GPS* (pp. 9–54). Helsinki: National Land Survey of Sweden.

Colman, R. (2003). A comparison of climate feedbacks in general circulation models. *Climate Dynamics, 20*, 865–873.

Houghton, J. T., Ding, Y., Griggs, D. J., Noguer, M., van der Linden, P. J., Dai, X., Maskell, K., & Johnson, C. A. (Eds.). (2001). *Climate change 2001: The scientific basis*. Contribution of Working Group I to the third assessment report of the Intergovernmental Panel on Climate Change. Cambridge, UK: Cambridge University Press.

Jones, J. (2010). *An assessment of the quality of GPS water vapour estimates and their use in operational meteorology and climate monitoring*. PhD thesis, University of Nottingham. http://eprints.nottingham.ac.uk/11287/1/JJ_Thesis_Final.pdf

Kouba, J., & Heroux, P. (2001). Precise point positioning using IGS orbit and clock products. *GPS Solutions, 5*(2), 12–28.

McClatchey, R. A., Fenn, R. W., Selby, J. E. A., Volz, F. E., & Garing, J. S. (1971). *Optical properties of the atmosphere* (p. 85). Report AFRCL-71-0279. Air Force Cambridge Research Laboratories.

Philipona, R., Dürr, B., Ohmura, A., & Ruckstuhl, C. (2005). Anthropogenic greenhouse forcing and strong water vapour feedback increase temperature in Europe. *Geophysical Research Letters, 32*, L19809. https://doi.org/10.1029/2005GL023624.

Senior, C., & Mitchell, J. (1993). Carbon dioxide and climate. The impact of cloud parameterization. *Journal of Climate, 6*, 393–418.

Smith, E. K., & Weintraub, S. (1953). The constants in the equation for atmospheric refractive index at radio frequencies. *Proceedings of the IRE, 41*, 1035–1037.

Soden, B. J., & Held, I. M. (2006). An assessment of climate feedbacks in coupled ocean-atmosphere models. *Journal of Climate, 19*, 3354–3360.

Stainforth, D. A., Aina, T., Christensen, C., Collins, M., Faull, N., Frame, D. J., Kettleborough, J. A., Knight, S., Martin, A., Murphy, J. M., Piani, C., Sexton, D., Smith, L. A., Spicer, R. A., Thorpe, A. J., & Allen, M. R. (2005). Uncertainty in predictions of the climate response to rising levels of greenhouse gases. *Nature, 433*(403), 406.

Thayer, G. D. (1974). An improved equation for the radio refractive index of air. *Radio Science, 9*, 803–807.

Thompson, A. R., Moran, J. M., & Swenson, G. W. (1986). *Interferometry and synthesis in radio astronomy* (720pp.). New York: Wiley.

Unden, P., Rontu, L., Jarvinen, H., Lynch, P., Calvo, J., Cats, G., Cuhart, J., & Eerola, K. (2002). *HIRLAM-5 scientific documentation*. Technical report, HIRLAM-project, Norrkopping.

Webb, M. J., Senior, C., Sexton, D., Ingram, W., Williams, K., Ringer, M., Mcavaney, B., Colman, R., Soden, B., Gudgel, R., Knutston, T., Emori, S., Ogura, T., Tsushima, Y., Andronova, N., Li, B., Bony, S., & Taylor, K. (2006). On the contribution of local feedback mechanisms to the range of climate sensitivity in two GCM ensembles. *Climate Dynamics, 27*, 17–38.

Yokohata, T., Emori, S., Nozawa, T., Tsushima, Y., Ogura, T., & Kimoto, M. (2005). A simple scheme for climate feedback analysis. *Geophysical Research Letters, 32*, L19703. https://doi.org/10.1029/2005GL023673.

Chapter 2
General Background

J. Jones, G. Guerova, J. Douša, G. Dick, S. de Haan, E. Pottiaux, O. Bock, R. Pacione, and H. Vedel

J. Jones (✉)
Met Office, Exeter, UK
e-mail: jonathan.jones@metoffice.gov.uk

G. Guerova
Physics Faculty, Department of Meteorology and Geophysics, Sofia University "St. Kliment Ohridski", Sofia, Bulgaria
e-mail: guerova@phys.uni-sofia.bg

J. Douša
Geodetic Observatory Pecný, RIGTC, Ondřejov, Czech Republic
e-mail: jan.dousa@pecny.cz

G. Dick
GFZ German Research Centre for Geosciences, Helmholtz Centre Potsdam, Potsdam, Germany
e-mail: dick@gfz-potsdam.de

S. de Haan
Royal Netherlands Meteorological Institute, De Bilt, The Netherlands
e-mail: siebren.de.haan@knmi.nl

E. Pottiaux
Royal Observatory of Belgium, Brussels, Belgium
e-mail: eric.pottiaux@oma.be

O. Bock
IGN Institut national de l'information géographique et forestière, Paris, France
e-mail: olivier.bock@ign.fr

R. Pacione
e-GEOS/Centro di Geodesia Spaziale-Agenzia Spaziale Italiana, Matera, MT, Italy
e-mail: rosa.pacione@e-geos.it

H. Vedel
Danish Meteorological Institute, Copenhagen, Denmark
e-mail: hev@dmi.dk

J. Jones et al. (eds.), *Advanced GNSS Tropospheric Products for Monitoring Severe Weather Events and Climate*, https://doi.org/10.1007/978-3-030-13901-8_2

Abstract This Chapter gives a general overview of the motivations behind the COST Action, a state-of-the-art at the start of the Action, plus an overview of the EIG EUMETNET GNSS Water Vapour Programme, E-GVAP. The Chapter also gives a breakdown of the structure of the COST Action including the objectives, percieved benefits and a detailed breakdown of the scientific plans of each working group, as per the Memorandum of Understanding agreed with COST.

2.1 Introduction

To improve the forecasting of severe weather and monitoring climate change, it is vital to obtain atmospheric water vapour observations with high temporal and spatial resolutions. GNSS signal propagation is sensitive to atmospheric water vapour, and as many ground-based GNSS receivers are already installed, collection of those data is a cost-effective way to increase spatial resolution of water vapour observations. Furthermore, improved modelling of the atmospheric influence can contribute to the speed and precision of GNSS positioning, navigation, and timing services, making the collaboration between the geodetic and atmospheric communities mutually beneficial. This COST Action focuses on new and improved capabilities from concurrent developments in both the geodetic and atmospheric communities, to develop new GNSS tropospheric products and exploit the full potential of multi-GNSS (GPS, GLONASS, and Galileo readiness) observations on a wide range of temporal and spatial scales in weather forecasting and climate research.

The use of GNSS tropospheric products in climate science has been advertised for several years, but they are still not widely used, despite the excellent time stability of the observing system. This is in clear contrast to the advances of GNSS meteorology. The existence of more than 25 years of observations from permanent GNSS stations worldwide shows high potential for monitoring trends and variability in atmospheric water vapour. This COST Action looked to exploit homogeneous reprocessed GNSS tropospheric products, to detect climatic signals and to evaluate independent climate data records of IWV, which is recognised as an essential climate variable by the Global Climate Observing System (GCOS).

Successful development of new GNSS tropospheric products requires interaction and coordination between the meteorological and geodetic communities, as both data providers and data users. High-level expertise in these areas is available in relatively few countries and institutions, and needs to be spread across all of Europe. For such effort, COST constitutes a relevant mechanism for supporting a well-structured international effort, enabling scientists from European universities, National Meteorological and Hydrological Services (NMHSs) and geodetic institutions to cooperate.

Short-Term Scientific Missions (STSM), Expert Meetings, Training Schools and Workshops are ideally suited to enhance networking and cooperation between European experts, and are used to generate a higher level of scientific and technological interaction than otherwise possible.

2.2 The State-of-the-Art at the Start of the Action (E-GVAP)

Application of GNSS for Numerical Weather Prediction (NWP) was the focus of a number of previous EU projects (WAVEFRONT, MAGIC, TOUGH and COST Action 716). Following their successes, the application of GNSS for NWP is now a well-established technique in Europe. Since 2005, E-GVAP (EIG EUMETNET GNSS Water Vapour Programme, http://egvap.dmi.dk) has been responsible for the collection and quality control of operational GNSS tropospheric products for NWP in Europe.

The main purpose of E-GVAP is to provide its EIG EUMETNET members with GNSS-derived ZTD estimates and IWV in near real-time (NRT) for operational meteorology. A secondary purpose is to help advance the processing of GNSS data for estimation of atmospheric properties of importance to meteorology, and to advance the usage of such data in NWP and nowcasting schemes. Additionally, E-GVAP continues to attempt to expand into areas where coverage is currently poor, increase the homogeneity of data, validation and active quality control, and encourage the move to sub-hourly data processing and distribution. E-GVAP continues to help members access global data sets and also monitors research of next generation GNSS products.

Figure 2.1 shows the overall E-GVAP data flow, with the Analysis Centres (ACs) on the left, the data exchange and monitoring facilities to the right. Figure 2.2 shows a list of ACs. Notice that some of the ACs deliver several different ZTD products,

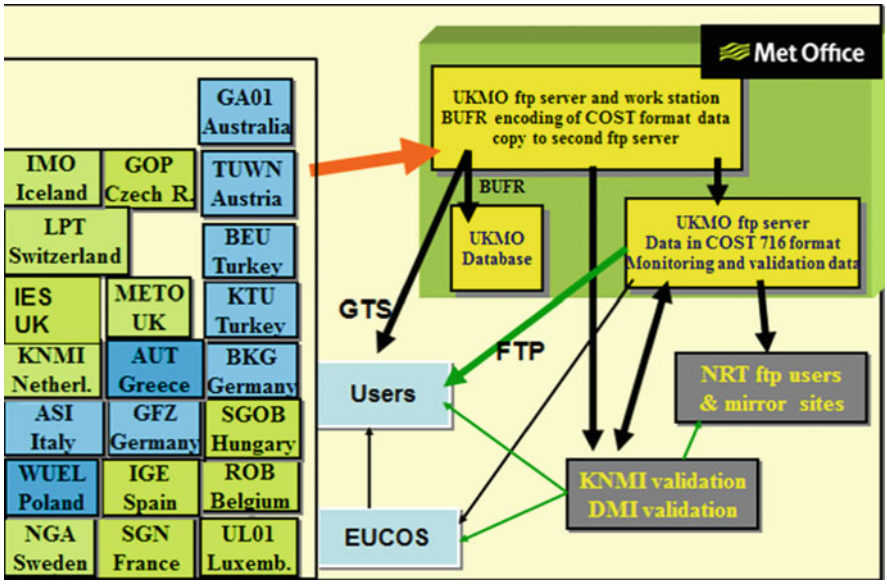

Fig. 2.1 The E-GVAP general setup

AC	Institution
AUT	Aristotle Univ. of Thessaloniki Analysis Center, Greee.
ASI	e-geos/Telespazio, Italy
BEU	Zonguldak University of Technology, Turkey
BKG	Federal Agency for Cartography and geodesy. Germany
GA01	Geoscience Australia New
GFZ	Helmholz Centre Potsdam, GFZ German Res. Cen. f Geosciences
GOPE	Geodectic Observatory Pecny, Czech Republic
IES	Inst. of Eng., Surv. And Space Geodesy, Univ of Nottingham, UK
IGE	Instituto Geografica National, Spain
IMO	Icelandic Met Office
KNMI	Royal Meteorological Institute of the Netherlands
KTU	Karadeniz Technival Univ. Analsis Center, Turkey
LPT	SwissTopo, Switzerland
METO	UK Met Office
NGA1	Lantmateriet (Swedish Mapping. Cadestre and Land Reg. Authority), Gavle, Sweden
ROB	Royal Observatory of Belgium
SGN	Institut Geographigue National, France
SGOB	Satellite Geod. Obs, IGCRS + Technical Univ. Budapest, Hungary
TUWN	Technical University Vienna, Austria
UL01	University of Luxembourg, Fac. Of Science and Communication
WUEL	Wroclaw University + Inst. Of Geodesy and Geoinformatics, Poland

Fig. 2.2 E-GVAP ACs

Table 2.1 Timeliness criteria for the ZTD timeliness monitoring

Level	Hourly ZTD estimation	Percentage	Sub-hourly ZTD estimation	Percentage
Threshold	120 min	–	30 min	90%
Target	90 min	90%	15 min	75%
Goal	60 min	75%	5 min	–

such as hourly, sub-hourly and/or global. The different products are identified by different solution naming, e.g. the AC METO (UK Met Office) provides three ZTD products; METR (UK region, sub-hourly), METG (global, hourly) and METO (European, hourly).

E-GVAP is based on a volunteer collaboration between GNSS geodetic institutions, the ACs and EUREF, and E-GVAP/EUMETNET. On the national level, E-GVAP members attempt to liaise with national geodetic institution to access raw GNSS data and ZTD estimates. In countries where there is no E-GVAP member, E-GVAP attempts to liaise with geodetic institutions directly on behalf of the national meteorological service. In Fig. 2.1 the blue ACs are ACs in non-member countries.

Timeliness

An essential requirement is to improve timeliness, to fulfill requirements from local, rapid refresh NWP and nowcasting. The timeliness criteria are shown in Table 2.1.

Quality
The criteria for ZTD precision is that ZTD OmB (GNSS ZTD estimate (Observation) minus NWP ZTD estimate (Background) standard deviation is <15 mm. The real ZTD uncertainty is significantly lower, as the main part of the OmB offsets are due to the NWP model itself (known from previous validation studies of GNSS vs radiosonde, vs. post-processed GNSS ZTDs, and also vs. IWV derived from microwave radiometers and VLBI.

Data Flow
Currently, more than 20 E-GVAP ACs produce GNSS tropospheric products for over 2500 ground-based GNSS stations, worldwide.The ACs uploads ZTDs to an ftp-server at the UK Met Office in COST716 format. Various checks on the content and format are carried out, the data is then BUFR encoded and distributed via the GTS. Additionally E-GVAP is developing an Active Quality Control (AQC) system which will be based on inter-comparison of ZTDs from GNSS sites for which ZTDs from at least three different ACs are available, valid at (approximately, fraction of hour) the same time. The full results of the AQC will be available via ftp. An automated warning will be submitted to users in case the AQC detects an AC & solution wide problem.

Organisation
Currently E-GVAP has two expert teams; the expert team on GNSS data processing and standards and the expert team on GNSS data usage. The teams meet annually in a combined meeting to which members of E-GVAP are also invited to enable efficient sharing of knowledge and guidance between data producers, data users and members. The expert team on GNSS data processing is extremely important to E-GVAP as it addresses common issues and helps AC coordination. Besides addressing E-GVAP specific issues, the meetings help coordinate activities on future research in GNSS-meteorology as many members of both expert teams are involved in such research besides their E-GVAP-specific work.

E-GVAP Expert Team on GNSS Data Processing and Standards
The main purpose of this team is to:

- Exchange knowledge on GNSS data processing, leading to best practices and improved homogeneity of the E-GVAP GNSS atmospheric delay products.
- Exchange knowledge on “next generation” GNSS data processing.
- Provide advice to E-GVAP on technical and scientific matters.
- Liaise with geodetic community

E-GVAP Expert Team on Data Usage
The main purpose of this team is to:

- Exchange knowledge on usage of E-GVAP data in meteorology, thereby providing feedback to the E-GVAP data producers, and provide material assisting members in using E-GVAP data.

- Exchange knowledge on usage of “next generation” GNSS in meteorology.
- Provide advice to E-GVAP on technical and scientific matters
- Liaise with the geodetic community.

Benefits to Users

Figure 2.3 is a recent example of NWP impact from different observing systems on a per-observation basis, with GNSS delays having the second largest impact. It both demonstrates that GNSS delays are useful, and that the NWP system is far from saturated with this type of humidity data. Hence, additional GNSS ZTDs will benefit the NWP system.

The current state-of-the-art is generally data assimilation in NWP models of hourly-updated Zenith Tropospheric Delays (ZTDs). However, there are big benefits to be obtained from innovation of the current GNSS products: most E-GVAP ACs analyse GPS-only, provide ZTD-only (no information on local in-homogeneities) and process GNSS data in a network solution (due to lack of high-quality, near real-time estimate of GNSS satellite clock errors, preventing use of the potentially faster Precise Point Positioning (PPP) technique). While the production, exploitation and evaluation of operational GNSS tropospheric products for NWP is well established in Northern and Western Europe, it is still an emerging R&D field in Eastern and

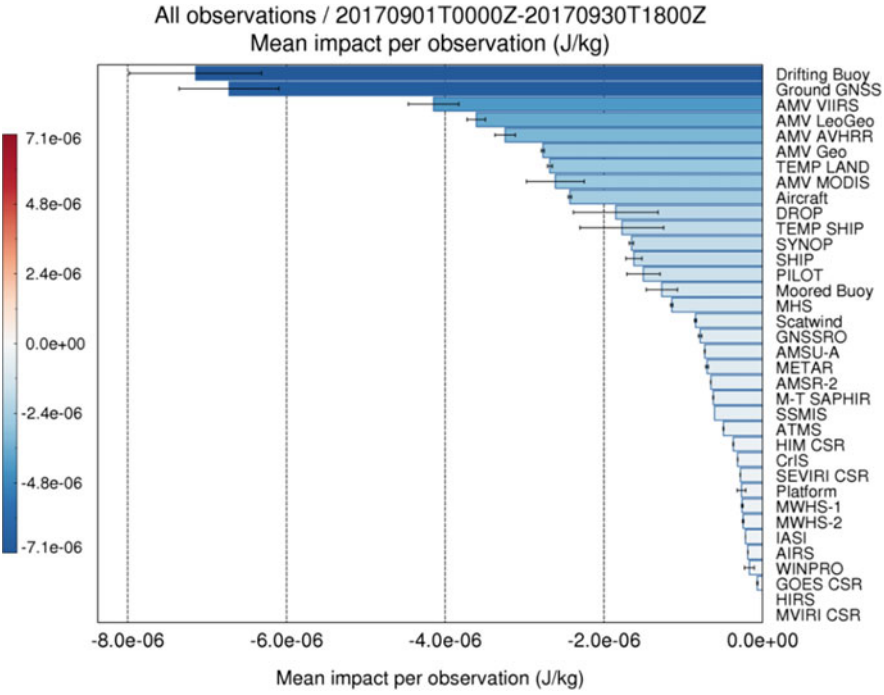

Fig. 2.3 Impact per observation of various types of observations in Met Office global NWP (Courtesy of Data Assimilation, UK Met Office)

South-Eastern Europe. More than 15 years of GNSS meteorology in Europe has already achieved outstanding cooperation not demonstrated elsewhere, overcoming difficulties such as cross-border data access.

It is now feasible to develop next-generation GNSS tropospheric products and applications that can enhance the quality of weather forecasts and monitoring of climate change, contributing to important societal and political needs. Of special interest in Europe are heavy precipitation events, flash floods, and heat waves. Such regional meteorological extremes are expected to increase in the future, as a result of global warming (IPCC AR5). Relevant areas of research are:

1. Severe weather forecasting: new GNSS products are required to provide more information on the spatial heterogeneity and rapid temporal variability of humidity in the troposphere.
2. Nowcasting: providing rapid updates in the analysis of the atmospheric state requires a transition from near real-time GNSS network processing (as implemented in E-GVAP) to real-time PPP processing.
3. Multi-GNSS analysis combining data from GPS, GLONASS, and Galileo in the future is expected to provide improved tropospheric products. Processing algorithms need to be modified and impact of use of additional observations needs to be assessed.
4. Climate monitoring through the evaluation of trends and variability in IWV for which the quality of reprocessed GNSS data and homogenised IWV estimates need to be assessed. The goal is to establish a new climate data record, taking benefit of more than 15 years of reprocessed ZTD estimates from hundreds of global and regional GNSS stations (e.g. http://acc.igs.org/reprocess.html and http://acc.igs.org/reprocess2.html).

2.3 Reasons for the Action

Coordinate the development and testing of new multi-GNSS products for operational NWP and forecasting of severe weather: Short-term, high-resolution NWP 'nowcasting' models require more detailed humidity observations, especially to resolve small-scale phenomena like deep convection. More advanced products such as horizontal ZTD gradients, slant delays (signal delay in the direction of each satellite) and 3-D refractivity or humidity fields (using tomography) can now be produced. Furthermore, multi-GNSS processing will improve the accuracy of tropospheric products due to improved coverage of azimuth and elevation angles.

Coordinate the development and testing of real-time GNSS processing algorithms for high-resolution, rapid-update analysis and nowcasting applications: New algorithms will be developed and tested in collaboration with ends users (forecasters).The benefits of rapid-update cycle NWP (e.g. with hourly data assimilation) will be assessed by coordinated case studies of severe weather events.

Enhance production, exchange and use of reprocessed GNSS products for climate monitoring: To meet the long-term stability requirement for climate data

record observations, the quality of GNSS data acquisition and processing are crucial. The Action will provide a framework for agreeing equipment standards, data formats, optimal data reprocessing using state-of-the-art GNSS algorithms and homogenisation methods to remove data discontinuities. The uncertainties in existing reprocessed GNSS IWV records, as well as those of data released during the course of the Action, will be assessed.

Improve GNSS processing and positioning: NWP data has recently been introduced as an input to GNSS processing for deriving improved mapping functions. In real-time GNSS processing there is currently an interest in using atmospheric NWP data to initialise PPP processing algorithms which can provide shorter convergence time and improve positioning. Establishing an atmospheric NWP data repository will drive the exploitation of NWP model data in real-time GNSS processing.

Strengthen the collaboration between GNSS experts and end-users: Workshops, Training Schools and STSMs will be efficient tools in bringing together scientists from various disciplines as well as linking with public and private data owners helping to promote free data exchange. Tighter cooperation between researchers and representatives from International and European organisations (GCOS, IAG, EGU, WMO, ECMWF etc.) will help guarantee that efforts will be conducted along high-priorities of both the scientific community as well as of political and economic stakeholders.

Increase observing network size, homogenise data quality and support knowledge transfer: This Action will encourage and facilitate the transfer of knowledge with possible establishment of GNSS ACs in Eastern and South-Eastern Europe, in cooperation with the European Position Determination System (EUPOS). Additionally, North African meteorological services are starting to use NWP models capable of assimilating GNSS tropospheric products and several national mapping agencies in this region already maintain operational GNSS networks.

2.4 Objectives

The aim of the Action is to enhance existing and develop new, ground-based multi-GNSS tropospheric products, to assess their usefulness in forecasting of severe weather and climate monitoring, and to improve GNSS real-time positioning accuracy through enhanced atmospheric modelling. A main focus is to strengthen and intensify this inter-disciplinary collaboration on a European level and to encourage cross-border cooperation.

Specific Objectives

- Develop new GNSS tropospheric products and assess their benefits in operational NWP and nowcasting, with a special focus on forecasting of severe weather.
- Coordinate the analysis of case studies to target known problems with modelling and forecasting of severe weather.

- Strengthen and extend the dialogue between GNSS tropospheric product providers and end-users from the meteorological and climate communities, stimulate transfer of knowledge and data exchange.
- Stimulate the exploitation of NWP data as an input to GNSS processing schemes, and assess the benefits for real-time GNSS positioning, navigation, and timing services.
- Generate recommendations on optimal GNSS reprocessing algorithms for climate applications and standardise the method of conversion between propagation delay and atmospheric water vapour with respect to climate standards.
- Coordinate the collection, archiving and exchange of raw GNSS data from various regional networks in Europe.
- Establish a database of reprocessed GNSS tropospheric products at global and regional scales and assess their quality by inter-comparison with in-situ and remote sensing techniques.
- Collaborate with the climate and meteorological communities, to assess and improve reanalyses and climate models (e.g. by assimilation of reprocessed GNSS tropospheric products) and investigate climate signals (trends and variability).

2.5 Impacts and Benefits

2.5.1 Societal Benefits

Better information about atmospheric humidity, particularly in climate-sensitive regions, is essential to improve the diagnosis of global warming, and for the validation of climate predictions on which socio-economic response strategies are based. The Action will foster a better understanding of atmospheric humidity and reduce uncertainties in climate predictions, enabling improved national, EU, and global policies mitigating negative effects of climate change. Furthermore, the Action will lead to improved forecasting of severe weather, which will have a positive impact on hazard management, lowering the risk of loss-of-life and the risk to national infrastructure. Direct and indirect societal benefits can be expected in the fields of disaster management, health, energy, water, agriculture and biodiversity.

2.5.2 Scientific Benefits

The Action will:

- Develop new multi-GNSS processing techniques, exploiting all GNSS constellations, leading to tropospheric products with improved timeliness, accuracy and reliability.

- Assess the quality of existing reprocessed GNSS tropospheric products, and define the requirements for the establishment of a GNSS climate data record.
- Coordinate the exploitation of ground-based GNSS and atmospheric data for the mutual benefit of both communities.
- Improve satellite-based positioning by using advanced signal propagation modelling and by use of NWP data to initialise PPP processing algorithms for real-time positioning.
- Link the activities of the existing tropospheric working groups (IGS, EUREF) and work in support of the operational goals of E-GVAP.
- NWP reanalysis, climate modelling, and calibration and validation of satellite water vapour related products will benefit from improvements in GNSS data processing.
- Work in support of GCOS, and spread expertise across Europe about GNSS atmospheric science through a well-organised panel of European experts and in liaison with the International Association of Geodesy.

2.5.3 Technological Benefits

The Action will provide recommendation on GNSS equipment standards, needs for collocated observations, optimal data processing, and methods for producing a GNSS climate dataset. Better modelling of tropospheric path delays in the processing algorithms will result in improved GNSS services for positioning, navigation, and timing.

2.5.4 Economic Benefits

A better understanding of atmospheric water vapour will improve mitigation of natural hazards, reducing the risk of economic disruption on national and international scales. Coordination throughout Europe is more cost-effective than solitary R&D in the atmospheric, climate, and geodetic communities. Long-term testing and validation will provide impetus to manufacturers to develop suitable, reliable, and cost-effective instruments.

2.5.5 Target Groups and End-Users

Target groups/end users of this Action are NMSs, climate research centres, and operational and research geodetic services, including those involved in E-GVAP, international boards for geodesy and geophysics (IUGG and IAG), and institutions working on climate change and weather watch (e.g., IPCC-AR5, GCOS, GEOSS

and GMES). They will be provided with data, scientific results and recommendations for operational use of GNSS observations and products.

2.6 Scientific Programme

The key questions to be addressed in this Action are:

- Which new GNSS processing techniques can deliver enhanced, more detailed GNSS tropospheric products suitable for high-resolution and rapid-update cycle NWP models?
- How far can new GNSS tropospheric products improve weather forecasting, and in particular forecasting of severe weather events?
- What is the added-value of combining observations from multiple GNSS systems (GPS, GLONASS, and Galileo readiness) on tropospheric products?
- What are the benefits of reprocessed GNSS tropospheric products (currently GPS-only) to the current state-of-the-art climate research?
- How can atmospheric NWP data improve real-time GNSS navigation, positioning and timing services?

The research activities will be contributing to five main areas:

1. Developing and testing of advanced GNSS processing techniques, making new products for use in operational nowcasting and forecasting of severe weather. Software developments are required to improve timeliness, enlarge data volume (more GNSS stations, new signals, higher resolution of tropospheric parameters) and to provide extended products. This task needs cooperation among experts in GNSS data processing, software developments, and end-users (forecasters).
2. Updating processing techniques and software and tackling specific problems to permit optimal usage of multi-GNSS data (e.g. combination of orbits, clocks, Earth rotation parameters). This task needs cooperation between geodesists and international bodies on references, conventions, and precise products (IAG, IERS, IGS, EUREF).
3. Optimising of present and future operational NWP systems to use of new ground-based GNSS tropospheric products for monitoring and forecasting severe weather. This task will assess the impact of assimilating new products (gradients, slant delays and new observables) on the quality of weather forecast. This task needs strong collaboration between the NWP and geodetic communities.
4. Evaluating and improving the quality of reprocessed ground-based GNSS tropospheric products for climate research (estimating water vapour trends and variability). This task will need cooperation between geodesists and climatologists, to agree on diagnostics for assessing the data records, and on recommendations on equipment, data reprocessing, and data formats. This task may also achieve a GNSS climate data record and assess and improve NWP reanalyses and climate models simulations.

5. Assessing atmospheric NWP data as an input to better GNSS navigation and precise real-time positioning products. This task will need a close cooperation of NWP operators and GNSS software and service developers.

2.7 Scientific Work Plans

The Action is organised into three Working Groups (WGs).

2.7.1 Working Group 1: Advanced GNSS Processing Techniques

This WG will coordinate the development of new/advanced GNSS processing techniques and products. The activities are:

- Develop, validate, and exchange GNSS processing algorithms and software, to enhance the existing temporal and spatial resolution of the operational GNSS tropospheric products suitable for high-resolution, rapid-update NWP and forecasting of severe weather and validate these new products.
- Assess methods for estimating gradients and slant delays for different GNSS processing methods (PPP and network solution).
- Study the potential of the IGS real-time precise orbits and clocks service to enable the faster and more efficient PPP GNSS data processing.
- Develop, validate and exchange GNSS processing algorithms to extend current GPS-only tropospheric products into the multi-GNSS products:
- Develop GPS and GLONASS products, and prepare for Galileo inclusion.
- Assess the consistency between stand-alone GPS and GLONASS products.
- Determine the potential of atmospheric NWP data as an input in real-time GNSS positioning, navigation, and timing services. Various approaches will be assessed.
- Enhance the production of multi-GNSS products, and check consistency and benefits of them.
- Develop new GNSS tropospheric products (gradients, slant delays, 3D water vapour and refractivity fields provided by tomographic reconstruction). Assess their potential for use in forecasting of severe weather and in high-resolution rapid-cycle NWP (hourly data assimilation).

Expected outcomes of WG1:

- Assessment reports and guidelines on new ultra-fast/real-time processing techniques, data format and products satisfying the needs for high-resolution, rapid-update NWP and forecasting severe weather.

- Assessment reports on the impact of multi-GNSS solutions on various GNSS tropospheric products.
- Define specific benchmark datasets designed for evaluation of the new tropospheric products.
- Prototype and report on use of atmospheric NWP data in support of real-time GNSS navigation and precise positioning.
- Establishment of GNSS Analysis Centres in Eastern Europe.

2.7.2 Working Group 2: Use of GNSS Tropospheric Products for High-Resolution, Rapid-Update NWP and Severe Weather Forecasting

This WG will coordinate the application of existing and development of new GNSS tropospheric products for high-resolution rapid-update NWP and forecasting of severe weather. The activities are:

- Create a standardised exchange format, and provide the gradients and slant delays from current networks through a central hub facility.
- Define and generate specific benchmark datasets in the form of GNSS observations, alternative water vapour and refractivity observations, and NWP products, for assessment and validation.
- Evaluate and validate the information content of the enhanced, new products provided by WG1, such as of gradients and slant delays (determine error sources, correlations etc.).
- Develop, validate, and exchange methods for initialization of NWP models using GNSS gradients and slant delays.
- Exchange methods of nowcasting applications of GNSS gradients and slant delays:
- Organize detailed analyses of special case studies.
- Establish a database with case studies of severe weather events.
- Organize user Workshops (audience forecasters/NWP modellers).
- Coordinate multi-model initialization experiments to obtain insight in the quality of different methods and models used in nowcasting and NWP.
- Assess the benefit of multi-GNSS tropospheric products in NWP and for severe weather forecasting.

Expected outcomes of WG2:

- Assessment reports and guidelines on standardised methods and data formats (in collaboration with WG1) for the initialization of NWP models using new/enhanced operational GNSS tropospheric products and for use in nowcasting.
- Promotion and dissemination of these standardised methods (STSMs, Training Schools, Workshops).

- Produce requirements for enhanced and new operational GNSS tropospheric products.
- Benchmark datasets for test, assessments and validations (for each method/product).
- Database with severe weather case studies.
- Recommendations and methods for operational GNSS nowcasting tools.
- Identify new ground-based GNSS data providers for operational NWP and severe weather monitoring in the data sparse regions such as Eastern and South-Eastern Europe.

2.7.3 Working Group 3: Use of GNSS Tropospheric Products for Climate Monitoring

This WG will coordinate the evaluation of existing and forthcoming GNSS tropospheric products and assess their potential for climate research. The activities are:

- Collect and intercompare various reprocessed GNSS tropospheric products (e.g. produced by IGS, EUREF ACs, and those released by several independent groups).
- Develop, validate and exchange methods to convert between ZTD and IWV. Models and methods will be re-assessed and clear standards will be defined.
- Detect and mitigate discontinuities in IWV time series due to changes in equipment. Test various algorithms used by the geodetic and the climate communities.
- Establish a GNSS climate data record based on existing and reprocessed and homogenised tropospheric products (ZTD and IWV).
- Intercompare and quantify reprocessed ground-based GNSS tropospheric products against IWV and ZTD from independent geodetic techniques (VLBI and DORIS) and atmospheric in-situ and remote sensing techniques (radiosondes, microwave radiometers, sun photometers, satellite water vapour products such as those from GOME(2), SCHIAMACHY, IASI, SSM/I, SSMIS and RO instruments and climate products from the EUMETSAT Climate and ROM SAFs).
- Evaluate the accuracy of NWP reanalysis products (e.g. ERA-Interim, MERRA, CFSR) and climate models simulations (e.g. IPCC-AR5, CORDEX), and provide feedback for improving modelling products through assimilation of high-quality reprocessed GNSS products in future global or regional reanalyses (e.g., ERA-CLIM, EURO-4M).
- Assess relevant diagnostics and indexes for quantifying climate trends and variability (e.g., inter-annual, intra-seasonal, and synoptic variability, seasonal and diurnal cycle) at global and regional scales.
- Bring together GNSS data owners, both private and public, on a European scale, with the goal of including additional Mediterranean partners, to attempt to agree on a strategy for collection of past, present and future data.

Expected outcomes of WG3:

- Assessment report of potential and existing GNSS datasets, metadata, and products for use in climate research.
- Guidelines on the data formats, processing, and homogenisation methods for enhanced use of reprocessed GNSS tropospheric products in climate research.
- A database of raw GNSS data and a consortium of GNSS data providers for climate research, at European and Mediterranean scale, and with connections to worldwide organisations (IGS, EUPOS, national positioning services, GNSS campaigns etc.).
- A new climate data record of GNSS ZTD and IWV, suitable for analysing climate trends and variability, and calibrating/validating independent datasets at global and regional scales.

Chapter 3
Advanced GNSS Processing Techniques (Working Group 1)

J. Douša, G. Dick, Y. Altiner, F. Alshawaf, J. Bosy, H. Brenot, E. Brockmann, R. Brožková, Z. Deng, W. Ding, K. Eben, M. Eliaš, R. Fernandes, A. Ganas, A. Geiger, G. Guerova, T. Hadaś, C. Hill, P. Hordyniec, F. Hurter, J. Jones, M. Kačmařík, K. Kaźmierski, J. Kaplon, P. Krč, D. Landskron, X. Li, C. Lu, J. P. Martins, G. Möller, L. Morel, G. Ófeigsson, R. Pacione, C. Pikridas, E. Pottiaux, J. Resler, W. Rohm, A. Sá, J. Sammer, T. Simeonov, W. Söhne, A. Stoycheva, A. Stürze, Sz. Rozsa, F. N. Teferle, S. Thorsteinsson, P. Václavovic, H. Valentim, B. Van Schaeybroeck, P. Viterbo, K. Wilgan, L. Yang, L. Zhao, N. Zinas, and F. Zus

In the following sections material is republished with kind permission: 3.2.1, 3.3.2–3.3.7, 3.4.3, 3.4.6, 3.4.7. 3.4.8, 3.5.3–3.5.6, 3.5.8, 3.5.9, 3.6.2 and 3.6.6.

J. Douša (✉)
Geodetic Observatory Pecný, RIGTC, Ondřejov, Czech Republic
e-mail: jan.dousa@pecny.cz

G. Dick
GFZ German Research Centre for Geosciences, Helmholtz Centre Potsdam, Potsdam, Germany
e-mail: dick@gfz-potsdam.de

Y. Altiner · W. Söhne · A. Stürze
BKG, Federal Agency for Cartography and Geodesy, Frankfurt, Germany
e-mail: yueksel.altiner@bkg.bund.de; wolfgang.soehne@bkg.bund.de; andrea.stuerze@bkg.bund.de

F. Alshawaf · Z. Deng · X. Li · C. Lu · F. Zus
GFZ German Research Centre for Geosciences, Potsdam, Germany
e-mail: fadwa.alshawaf@gfz-potsdam.de; deng@gfz-potsdam.de; lixin@gfz-potsdam.de; cuixian@gfz-potsdam.de; zusflo@gfz-potsdam.de

J. Bosy · T. Hadaś · P. Hordyniec · K. Kaźmierski · J. Kaplon · K. Wilgan
Wrocław University of Environmental and Life Sciences, Wrocław, Poland
e-mail: jaroslaw.bosy@up.wroc.pl; tomasz.hadas@upwr.edu.pl; pawel.hordyniec@upwr.edu.pl; kamil.kazmierski@up.wroc.pl; jan.kaplon@upwr.edu.pl; karina.wilgan@upwr.edu.pl

H. Brenot
Royal Belgian Institute for Space Aeronomy, Uccle, Belgium
e-mail: hugues.brenot@oma.be

E. Brockmann
Swiss Federal Office of Topography swisstopo, Wabern, Switzerland
e-mail: Elmar.Brockmann@swisstopo.ch

J. Jones et al. (eds.), *Advanced GNSS Tropospheric Products for Monitoring Severe Weather Events and Climate*, https://doi.org/10.1007/978-3-030-13901-8_3

R. Brožková
Czech Hydrometeorological Institute, Prague, Czech Republic
e-mail: radmila.brozkova@chmi.cz

W. Ding · F. N. Teferle
University of Luxembourg, Luxembourg, Luxembourg
e-mail: dingwenwu@asch.whigg.ac.cn; norman.teferle@uni.lu

K. Eben · P. Krč · J. Resler
Czech Institute of Computer Science, Academy of Sciences, Praha, Czech Republic
e-mail: eben@cs.cas.cz; krc@cs.cas.cz; resler@cs.cas.cz

M. Eliaš · P. Václavovic · L. Zhao
Geodetic Observatory Pecný, Research Institute of Geodesy, Topography and Cartography, Zdiby, Czech Republic
e-mail: michal.elias@pecny.cz; pavel.vaclavovic@pecny.cz; lewen.zhao@pecny.cz

R. Fernandes · H. Valentim
University of Beira Interior, Covilhã, Portugal
e-mail: rmanuel@di.ubi.pt; hugo.valentim@segal.ubi.pt

A. Ganas
National Observatory of Athens, Athens, Greece
e-mail: aganas@gein.noa.gr

A. Geiger · F. Hurter
ETH Zurich, Zürich, Switzerland
e-mail: alain.geiger@geod.baug.ethz.ch; fabian.hurter@geod.baug.ethz.ch

G. Guerova
Physics Faculty, Department of Meteorology and Geophysics, Sofia University "St. Kliment Ohridski", Sofia, Bulgaria
e-mail: guerova@phys.uni-sofia.bg

C. Hill · L. Yang
University of Nottingham, Nottingham, UK
e-mail: Chris.Hill@nottingham.ac.uk; lei.yang@nottingham.ac.uk

J. Jones
Met Office, Exeter, UK
e-mail: jonathan.jones@metoffice.gov.uk

M. Kačmařík
Institute of Geoinformatics, VŠB Technical University of Ostrava, Ostrava, Czech Republic
e-mail: michal.kacmarik@vsb.cz

D. Landskron · G. Möller · J. Sammer
Department of Geodesy and Geoinformation, TU Wien, Wien, Austria
e-mail: daniel.landskron@geo.tuwien.ac.at; gregor.moeller@geo.tuwien.ac.at; julia.sammer@student.tugraz.at

J. P. Martins · P. Viterbo
Instituto Português do Mar e da Atmosfera, Lisbon, Portugal
e-mail: joao.p.martins@ipma.pt; pedro.viterbo@ipma.pt

L. Morel
École Supérieure des Géomètres et Topographes, Le Mans, France
e-mail: laurent.morel@esgt.cnam.fr

G. Ófeigsson · S. Thorsteinsson
The Icelandic Meteorological Institute, Reykjavík, Iceland
e-mail: bgo@vedur.is; siggi@vedur.is

R. Pacione
e-GEOS/Centro di Geodesia Spaziale-Agenzia Spaziale Italiana, Matera, MT, Italy
e-mail: rosa.pacione@e-geos.it

C. Pikridas
Aristotle University of Thessaloniki, Thessaloniki, Greece
e-mail: cpik@topo.auth.gr

E. Pottiaux
Royal Observatory of Belgium, Brussels, Belgium
e-mail: eric.pottiaux@oma.be

W. Rohm
Institute of Geodesy and Geoinformatics, Wrocław University of Environmental and Life Sciences, Wroclaw, Poland
e-mail: witold.rohm@upwr.edu.pl

A. Sá
Polytechnic Institute of Guarda, Guarda, Portugal
e-mail: andre_sa@ipg.pt

T. Simeonov
Sofia University "St. Kliment Ohridski", Sofia, Bulgaria
e-mail: tzvetan.simeonov@gfz-potsdam.de

A. Stoycheva
National Institute of Meteorology and Hydrology, Sofia, Bulgaria
e-mail: anastassia.stoycheva@meteo.bg

Sz. Rozsa
Budapest University of Technology and Economics, Budapest, Hungary
e-mail: szrozsa@agt.bme.hu

B. Van Schaeybroeck
Royal Meteorological Institute of Belgium, Uccle, Belgium
e-mail: bertvs@meteo.be

N. Zinas
Tekmon Geomatics, Ioánnina, Greece
e-mail: nzinas@tekmon.gr

Abstract Over the last decade, near real-time analysis of GPS data has become a well-established atmospheric observing tool, primarily coordinated by the EIG EUMETNET GPS Water Vapour Programme (E-GVAP) in Europe. In the near future, four operational GNSS will be available for commercial and scientific applications with atmospheric science benefiting from new signals from up to 60 satellites observed at any one place and time, however, many challenges remain regarding their optimal combined utilization. Besides raw data streaming, recent availability of precise real-time orbit and clock corrections enable wide utilization of autonomous Precise Point Positioning (PPP), which is particularly efficient for high-rate, real-time and multi-GNSS analyses.

New GNSS constellation signals, products and processing methods suggest the development of advanced GNSS tropospheric products, in support of weather

numerical prediction and nowcasting will be substantially improved. Such examples are: ultra-fast and high-resolution tropospheric products available in real-time or on a sub-hourly basis, parameters monitoring tropospheric anisotropy above the station (such as horizontal gradients and tropospheric slant path delays), and indicators of severe weather such as extreme convection. Development of advanced GNSS tropospheric products within COST Action ES1206 benefited from two dedicated campaigns prepared for a collaborative effort: (1) the benchmark campaign and (2) the real-time demonstration campaign. The former served for estimating and assessing horizontal tropospheric gradients and tropospheric slant delays, estimated from GNSS, Water Vapour Radiometers and Numerical Weather Model (NWM) ray-tracing. The second campaign developed new software and strategies for real-time, multi-GNSS, high-rate tropospheric solutions including the assessment of pre-operational solutions.

The impact of selected processing strategies and precise models were assessed during a long-term GNSS reprocessing campaign aimed at providing homogeneous tropospheric products for climate research. Using information from modern NWM forecasting systems, a variety of tropospheric correction models for real-time kinematic GNSS positioning were developed and assessed. Finally, a transfer of knowledge such as support for establishing new GNSS Analysis Centres and inclusion of new networks into E-GVAP were completed.

3.1 Introduction

J. Douša
Geodetic Observatory Pecný, RIGTC, Ondřejov, Czech Republic
e-mail: jan.dousa@pecny.cz

G. Dick
GFZ German Research Centre for Geosciences, Helmholtz Centre Potsdam, Potsdam, Germany
e-mail: dick@gfz-potsdam.de

The GNSS4SWEC Working Group 1 (WG1) focused on development and utilization of advanced GNSS processing techniques for the purpose of both estimation and exploitation of tropospheric parameters within geodetic, meteorological and climate applications. The main goals of the WG1 are summarized within four defined domains:

1. Coordinating the development of advanced GNSS tropospheric products in support of weather forecasting, namely such as real-time parameter estimation, troposphere asymmetry monitoring and modelling, developing severe weather indicators, assessing the impact of hydrometeors, advantage of multi-GNSS data processing.
2. Exploiting NWM data in GNSS precise positioning and real-time kinematic applications, namely supported by mapping functions or mapping factors, a priori separation of hydrostatic contributions, tropospheric horizontal gradients, tropospheric parameter scaling and conversions factors.
3. Reprocessing of GNSS data and assessing precise models for the purpose of a long-term consistent tropospheric product provision in support of a climatology research.

4. Supporting the transfer of knowledge, tools and data exchange for extending existing products and establishment of new ACs or inclusions of new networks.

WG1 coordination was split into ten different sub-tasks, with many overlaps. For this reason, the structure of this chapter does not correspond to the WG1 sub-tasks, but reflects mainly goals specified above. An important role in new development was achieved by a collection of common data sets and the design of specific campaigns, which are described in Sect. 3.2. Development of advanced tropospheric products specified in the first goal are introduced in Sects. 3.3 and 3.4. Utilization of NWM-based products in precise GNSS analyses, i.e. corresponding to the second goal, is covered by Sect. 3.5. Various GNSS reprocessing and processing model assessments are then summarized in Sect. 3.6. Finally, the transfer of knowledge, the establishments of new ACs and integration of new networks is completed in Sect. 3.7. The definition of the SINEX_TRO V2 format, which was elaborated in a close collaboration with WG3, is included in appendix D.

3.2 Campaigns for Development of Advanced Tropospheric Products

The main goal of this section is to introduce two campaigns suitable for developing and evaluating advanced tropospheric products. The first is the so-called GNSS4SWEC WG1 Benchmark campaign which is considered as a cornerstone that helped to accomplish various WG1 objectives within the COST Action. The second is the Real-time demonstration campaign, which helped to develop, optimize and evaluate new real-time GNSS software and products.

3.2.1 Benchmark Campaign – Common Data Set for New Product Development and Validation[1]

M. Kačmařík
Institute of Geoinformatics, VŠB Technical University of Ostrava, Ostrava, Czech Republic
e-mail: michal.kacmarik@vsb.cz

J. Douša
Geodetic Observatory Pecný, RIGTC, Ondřejov, Czech Republic
e-mail: jan.dousa@pecny.cz

G. Dick
GFZ German Research Centre for Geosciences, Helmholtz Centre Potsdam, Potsdam, Germany
e-mail: dick@gfz-potsdam.de

[1]Parts from this section were previously published in Douša et al. 2016

F. Zus
GFZ German Research Centre for Geosciences, Potsdam, Germany
e-mail: zusflo@gfz-potsdam.de

R. Brožková
Czech Hydrometeorological Institute, Prague, Czech Republic
e-mail: radmila.brozkova@chmi.cz

H. Brenot
Royal Belgian Institute for Space Aeronomy, Uccle, Belgium
e-mail: hugues.brenot@oma.be

A. Stoycheva
National Institute of Meteorology and Hydrology, Sofia, Bulgaria
e-mail: anastassia.stoycheva@meteo.bg

G. Möller
Department of Geodesy and Geoinformation, TU Wien, Wien, Austria
e-mail: gregor.moeller@geo.tuwien.ac.at

J. Kaplon
Wrocław University of Environmental and Life Sciences, Wrocław, Poland
e-mail: jan.kaplon@upwr.edu.pl

Only basic information is presented here about the Benchmark campaign. For further information please see Douša et al. (2016).

3.2.1.1 Motivation

An idea to create a well-prepared and extensive common data set which would enable an effective collaboration within the WG1 itself, but also with other working groups, arosed during the first WG1 meeting in Valencia, October, 2013. The natural motivation for the campaign was to support the WG1 main goals, namely the development of advanced GNSS tropospheric products in support of weather forecasting and vice versa exploitation of numerical weather data in precise GNSS positioning. The Benchmark campaign planning started with inventory of requirements based on a wide discussion within the Action members. The following requests for the Benchmark data set were summarized as follows:

- Period covering a month at least to enable NWM and GNSS processing initializations and to cover different weather conditions – quiet and variable, optimally including a severe weather event.
- Availability of a dense network of GNSS reference stations in Europe with a limited scale, but including flat and mountainous areas.
- Availability of meteorological data from independent sources.

3.2.1.2 Description of Selected Spatial and Temporal Domain

Finally, an area in central Europe was selected covering Germany, the Czech Republic, Poland and Austria. Due to its size, the whole area was firstly divided into a 'core' domain where below mentioned severe weather events took place and an 'extended' domain which surrounded the 'core' one. In the second step both domains were geographically divided into several clusters to allow a reasonable GNSS data handling, see Fig. 3.1.

From the time perspective 2 months in June 2013 (May and June) were chosen. The weather conditions in the selected area during May 2013 were mostly quiet. On the contrary an extreme precipitation event lasting from May 31 to June 2 led to devastating flooding on Danube, Elbe and Vltava rivers. Since the event was only partly forecasted by NWM it was a suitable candidate for a GNSS meteorology benchmark campaign as it could provide additional observations for meteorological community. Significant precipitation periods hitting areas of smaller extent occurred also from June 9 to June 11 and from June 23 to June 26.

3.2.1.3 Description of Collected Data Set

The Benchmark data set contains following data: GNSS observations and auxiliary products, E-GVAP operational GNSS products, synoptic meteorological observations, NWM fields, radiosonde observations, WVR observations, meteorological radar images. Collected data from individual sources are briefly described in paragraphs below. The data set is stored on an ftp server at Geodetic Observatory Pecný

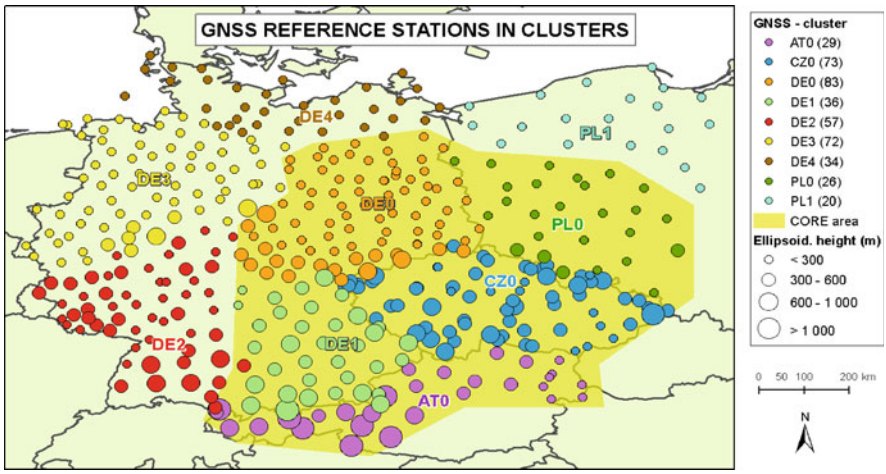

Fig. 3.1 Benchmark core (yellow area) and extended domains depicted together with nine clusters for GNSS stations (coloured points). The size of the points indicates height of GNSS reference stations above the WGS-84 ellipsoid

(GOP) and available to members of the COST ES1206 Action for research purposes. To obtain more information and access to the data set please send an email to michal.kacmarik@vsb.cz or jan.dousa@pecny.cz.

GNSS Observations observations from 430 GNSS reference stations in RINEX format with 30s sampling interval were collected in total from which 247 sites belonged to the 'core' domain. An average distance between two stations was about 50–70 km. From the total number of GNSS sites, 4 observed GPS, GLONASS and GALILEO satellites, 356 observed GPS and GLONASS satellites, and remaining 70 stations were equipped with GPS recievers only. Station metadata files were completed and checked carefully. A qualitative and quantitative control and a standard positioning were performed using G-Nut/Anubis software (Václavovic and Douša 2016). Besides multiple correction of metadata, 15 sites had to be rejected from the data set because of the data quality issues.

E-GVAP Operational GNSS Products operational near real-time tropospheric solutions provided by 14 analysis centres for all GNSS reference stations in Europe were collected for the campaign. These products contributed routinely to the E-GVAP (http://egvap.dmi.dk) and are stored in the COST-716 format with a temporal resolution of ZTD estimates from 5 to 60 min.

Synoptic Meteorological Data meteorological measurements of at least atmospheric air pressure, air temperature and relative humidity from 610 synoptic stations were collected. Original data were provided in various formats which were, additionally, converted into a single unified plain text format with a sampling interval ranging from 10 to 60 min.

NWM Data and Products NWM 3D data fields from the Czech Hydrometeorological Institute's (CHMI) local area model ALADIN-CZ were extracted in GRIB format. The horizontal resolution of the model is 4.7×4.7 km, outputs are provided at 87 model levels with a 6-h interval of analysis run (00:00, 06:00, 12:00 and 18:00 UTC) and 1-h interval for forecast range. The model didn't assimilate any GNSS tropospheric products for delivered fields and provided necessary parameters for derivation of hydrostatic and non-hydrostatic GNSS signal path delays as well as for calculating the effect on signal due to so called hydrometeors (e.g. ice and liquid water).

Radiosonde Data radio soundings from two different sources were collected providing profiles with full and reduced resolutions. Measurements with high resolution were available from two sites in the Czech Republic – Prague-Libuš and Prostějov, both provided by the CHMI. Altogether 278 files were obtained for the period of Benchmark campaign. Radiosonde data with reduced vertical resolution from 19 European stations were provided by E-GVAP based on the EUMETNET – EUREF MoU (Pottiaux et al. 2009).

Water Vapour Radiometer Data observations from two Water Vapour Radiometers (WVR) situated in Germany were collected. The first one was operated by German Research Centre for Geosciences (GFZ) in Potsdam (POTS) 30 km south-westward

from Berlin and provided measurements of IWV and liquid water in two modes: slant (GPS satellite tracking) and zenith. The second was operated by Deutscher Wetterdienst (DWD) at the Lindenberg meteorological observatory (LDBG) located approximately 100 km eastward from Berlin and provided the same parameters as the first mentioned WVR but only in the zenith direction.

Meteorological Radar Data raster images of combined observations from two C-band Doppler meteorological radars located in the Czech Republic and operated by the CHMI were collected. They represent a maximum reflectivity fields with side projections in horizontal resolution of 1 × 1 km and 30-min time interval. The area effectively covered by those two radars includes the territory of the Czech Republic and areas of approximately 100 km outside the Czech state boundary.

Data Acknowledgement the members of COST Action ES 1206 thank all the institutions that provided data for the campaign. GNSS data from the Austrian network EPOSA were provided by Österreichische Bundesbahnen Infrastruktur AG; GNSS data from SAPOS network in Germany by Zentrale Stelle SAPOS in Hannover; GNSS data from several networks in the Czech Republic – (1) CZEPOS by the Czech Land Survey Office, (2) Trimble VRS Now® by GEOTRONICS Praha, s.r.o. and (3) GEONAS and VESOG stations thanks to the project CzechGeo (LM2010008) operated by the Institute of Rock Structure and Mechanics of the Academy of Sciences of the Czech Republic and the Research Institute of Geodesy, Topography and Cartography, respectively; GNSS data from Polish ASG-EUPOS network by the Head Office of Geodesy and Cartography in Poland; Synoptic data by Zentralanstalt für Meteorologie und Geodynamik, ZAMG (Austria), Deutscher Wetterdienst, DWD (Germany), Czech Hydrometeorological Institute, CHMI (the Czech Republic) and Polish Institute of Meteorology and Water Management (Poland). Finally, special thanks come to people assisting in collecting all the data and metadata, namely: Dr. Jan Řezníček (GNSS/CZEPOS), Dr. Uwe Feldmann-Westendorff and Dr. Markus Ramatschi (GNSS/SAPOS), Dr. Petr Novák (RADAR/CHMI), Dr. Martin Motl (RAOBS/CHMI), Dr. Anna Valeriánová (SYNOP/CHMI), Dr. Pavla Skřivánková (CHMI), Dr. Roland Potthast (SYNOP/DWD), Dr. Jürgen Güldner (WVR-Lindenberg/DWD) and Dr. Stefan Heise (WVR-Potsdam/GFZ).

3.2.1.4 Reference Products and Their Initial Validation

After the data preparation, quality checking and cleaning, GNSS and NWM reference (tropospheric) products were generated and consequently initially validated. Results of these steps provided a first insight into variations of parameters and atmospheric conditions during the Benchmark campaign and were helpful for more detailed planning of following Benchmark-related activities. Following paragraphs provide basic information about mentioned reference products and their validation.

GNSS Reference Tropospheric Products two institutions delivered their GNSS tropospheric products for all GNSS reference stations within the Benchmark data set. The first reference one was generated at GOP using the BSW52 (Dach et al. 2015) with the network processing approach using double-differenced GNSS observations. The strategy for daily solutions was consistent with the GOP contribution to the EUREF Repro2 campaign (Douša et al. 2017). The second reference tropospheric product was delivered by GFZ using the GFZ EPOS software (Gendt et al. 2004; Ge et al. 2006) based on undifferenced GNSS observations and PPP approach. GOP solution used CODE precise orbit and clock products while GFZ solution was based on GFZ own precise products. The models were in case of both GOP and GFZ solutions compliant with the IERS Conventions (Petit and Luzum 2010).

NWM Derived Tropospheric Products analogously to the situation with GNSS reference products also NWM derived reference tropospheric products were independently generated by GOP and GFZ. GOP used their G-Nut/Shu software (Douša and Eliaš 2014) and provided three products. Two were based on global numerical weather models – the European Centre for Medium-Range Weather Forecasts (ECMWF) ERA-Interim (Dee et al. 2011) and the Global Forecast System (GFS) of the National Centres for Environmental Prediction (NCEP) available at http://www.ftp.ncep.noaa.gov/data/nccf/com/gfs/prod/, and one was based on regional model ALADIN-CZ which was provided within the Benchmark dataset. The following tropospheric and meteorological parameters were calculated for all stations: zenith hydrostatic and wet delays, air pressure, partial water vapour pressure, mean temperature, temperature lapse rate, water vapour pressure and zenith wet delay exponential decay rates. GFZ used their direct numerical simulation (DNS) tool (Zus et al. 2014) in order to derive the following parameters from two global NWMs (ERA-Interim and GFS): zenith hydrostatic and zenith wet delays, horizontal (1st, 2nd order) tropospheric gradients and coefficients of hydrostatic and wet mapping functions.

Validation of Reference Tropospheric Products Values of ZTD, ZWD and horizontal tropospheric gradients derived from described GNSS and NWM reference products were compared to study the quality and mutual agreement. Table 3.1 summarizes comparison results of GNSS ZTDs with those derived from NWMs. Mean statistics over all 430 sites demonstrated that both GNSS reference products based on a completely different software and strategy performed very similarly when compared to NWM products. Also, both software used for derivation of GNSS related tropospheric parameters from NWM fields agreed very well. In case of individual NWM the high-resolution ALADIN-CZ model outperformed both global reanalysis models in the Benchmark domain and period mainly in terms of standard deviation. For the NCEP's GFS products a negative mean bias of about 5 mm was observed compared to all other solutions. This bias stems from the bias in ZWD values and its possible explanation is the low vertical resolution of GFS model which resulted in larger interpolation errors. A comparable bias for GFS model was reported by Urquhart et al. (2011).

Table 3.1 Comparison of zenith total delays from NWM and GNSS (mean values, 430 sites)

NWM source (software)	Grid resolution	Analysis [hour]	Forecast [hour]	GNSS source (software)	Pairs #	Excl #	Bias [mm]	Sdev [mm]	RMS [mm]
ERA (Shu)	1 deg	6	0	GOP (BSW52)	224	2	+0.0	9.6	10.0
ERA (Shu)	1 deg	6	0	GFZ (EPOS-8)	224	3	+0.3	9.7	10.0
ERA (DNS)	1 deg	6	0	GOP (BSW52)	224	3	−0.4	9.4	9.8
ERA (DNS)	1 deg	6	0	GFZ (EPOS-8)	224	3	−0.1	9.6	9.8
GFS (DNS)	1 deg	6	3	GOP (BSW52)	224	7	−4.9	11.0	12.0
GFS (DNS)	1 deg	6	3	GFZ (EPOS-8)	223	7	−4.5	10.9	11.8
ALADIN (Shu)	4.7 km	6	0,1,2,3,4,5	GOP (BSW52)	1343	20	+0.8	7.6	7.8
ALADIN (Shu)	4.7 km	6	0,1,2,3,4,5	GFZ (EPOS-8)	1343	22	+0.6	7.3	7.5

Results of individual GNSS and NWM reference products were studied also using maps showing differences between ZTDs from GNSS GOP product and individual NWM products. Generally, a good homogeneity was observed from the statistical results. Exceptions existed mainly in relation to the orography which triggered larger differences between models particularly in mountain areas with complex terrain where regional model ALADIN-CZ performed better than both global models.

3.2.1.5 List of Benchmark Campaign Participants and Users

- G. Möller (TU Wien). In the first instance, we will use RINEX data to compute STDs using different processing strategies. In addition, the GNSS GOP products are used as input for GNSS tomography and assimilation studies.
- E. Pottiaux (ROB). The idea is to use the Benchmark campaign to assess the different tropospheric products (RT, sub-hourly, hourly and post-processing – ZTD, gradients and possibly slant delays from the BSW52) and refine my processing strategies. By taking part myself in the Benchmark processing, I also would like to stimulate the interaction with WG2 developments.
- J. Douša et al. (GOP). Generation of the reference GNSS tropospheric products. Development of the software and the strategy for optimal provision of real-time products and asymmetry monitoring, slant delay retrievals. Assessment of NWM-derived tropospheric products and developing the combination of GNSS and NWM data.
- G. Dick et al. (GFZ). Generation of the reference GNSS tropospheric products.
- M. Kačmařík (TU Ostrava). Inter-comparison of tropospheric slant delays form GNSS, NWM and WVR at dual-station.
- W. Rohm et al. (WUELS). We would like to join the Benchmark campaign by providing Slant Delays for selected stations (same as Michal's) based on the GNSS observations and ray-tracing.
- H. Brenot (BIRA). I would like to look at hydrometeors delays from ALADIN outputs and to show their impact for the severe flood event of June.
- K. Eben (ICS ASCR). Assimilation of NRT ZTDs into the WRF mesoscale model.
- T. Hadaś et al. (WUELS). The goal is to use the stored real-time products for simulated real-time troposphere monitoring (ZTD estimates using original software), to optimize the methodology and algorithms, to compare results with other real-time AC.
- L. Morel (Le CNAM). To process some stations of the benchmark campaign and to deliver CNAM results (GAMIT processing).
- S. Nahmani (IGN). I want to verify some of my results on these specific stations.
- P. Gołaszewski (UWM). My research is focused on real time and post-processed ZTD/ZWD estimation. Using this data will allow me to present the results on the COST workshop in Potsdam, in September this year. I am interested in using

pseudo real-time demonstration (for ZTD estimation) and observation data for post-processing.

- S. de Haan (KNMI). My plan is to eventually assimilate the slant observations in Harmonie. But first, I am going to compare the observation with my model equivalent.
- Arpaci (UBIMET). We will carry out case studies to examine the impact of the assimilation on the forecast quality. Especially the catastrophic flooding from June 2013, which affected big parts of central Europe seems to be an ideal evaluation case study scenario. We will compute WRF model runs with ZTD assimilation and compare them with runs without data assimilation. UBIMET will carry out eye to eye verifications, Upper Air verifications (using sounding and aircraft data) and surface verifications using VERA analysis data.
- D. Kwasniak (UWM). I want to use them for my research about GPS positioning using a new positioning method called MAFA method. Results of this research I want to present on 17th Czech-Polish Workshop.
- Y. Altiner et al. (BKG). Want to obtain the access for a processing the Benchmark GNSS data in real-time simulated mode.

3.2.2 GNSS Real-Time PPP Demonstration Campaign

P. Václavovic
Geodetic Observatory Pecný, Research Institute of Geodesy, Topography and Cartography, Zdiby, Czech Republic
e-mail: pavel.vaclavovic@pecny.cz

J. Douša
Geodetic Observatory Pecný, RIGTC, Ondřejov, Czech Republic
e-mail: jan.dousa@pecny.cz

F. N. Teferle
University of Luxembourg, Luxembourg, Luxembourg
e-mail: norman.teferle@uni.lu

Providing new real-time or ultra-fast tropospheric products, such as ZTD, GRD, STD, IWV maps or other derived products estimated using data from GNSS permanent networks, is interesting for numerical and non-numerical weather nowcasting and severe weather event monitoring (Guerova et al. 2016a, b). The Precise Point Positioning (PPP) processing strategy plays a key role in the production of real-time tropospheric parameters because of its high processing efficiency, and the sensitivity to the absolute value of the tropospheric delay. It enables to exploit optimally data from all available GNSS multi-constellations, and facilitates the production of all interesting GNSS parameters such as ZTDs, GRDs or STDs.

Most importantly, the PPP is supported with the global orbit and clock products provided by the RTS (Caissy et al. 2012) of IGS (Dow et al. 2009).

During the period 2015–2017, the COST Action ES1206 WG1 played an initiative role in the coordination of the development and the evaluation of GNSS real-time tropospheric products thanks to the design of the GNSS4SWEC Real-time Demonstration Campaign which is briefly introduced in this subsection.

3.2.2.1 Campaign Design and Contribution Specifications

A list of common stations was selected from the E-GVAP supersites, EPN and IGS sites, which were limited by a maximum of 50 in total, regionally and globally distributed:

- E-GVAP super-sites (5): BRST, GOPE, ONSA, YEBE, ZIM2
- EPN sites (10): CASC, HERT, HOFN, MALL, MATE, NICO, PDEL, POTS, REYK, WTZR
- IGS sites (17): ADIS, ALBH, ALGO, ALIC, AUCK, DUBO, LHAZ, NKLG, NRMD, OHI3, POVE, THTI, ULAB, UNSA, WIND, YAR3, YELL

Station metadata are introduced using the RINEX skeleton files which are available from EPN CB (http://www.epncb.oma.be/stations/log/skl) and IGS CB (http://igscb.jpl.nasa.gov/igscb/station/general/skel). The strategy for tropospheric estimation is generally free when optimized with respect to the individual software capabilities and following the state-of-the-art models, in particular IERS conventions, antenna phase offsets and variations, a priori tropospheric model, and mapping functions, and others.

Use of GNSS systems GPS and GPS + GLONASS is recommended if supported by the software and real-time data streams, other systems are optional, however, the constellation has to be properly defined in the header of the COST-716 file using the PCD flag. The GPS and GPS + GLONASS solutions are provided in different files and different names and individual solution (including variants) has to be specified by the fourth character in the processing centre name. The character 'G' will be used for GPS-only results, and the character 'R' will be used for GPS + GLONASS. In order to support GPS + GLONASS, the IGS03 real-time product is mandatory for the utilization to guarantee a consistency of mandatory products and enable to compare the results. Thus even GPS-only solution should use the IGS03 stream, for others solutions the precise ephemeris source is optional.

Parameters must be estimated with a 5-min resolution (parameter sampling rate). If the higher sampling rate is used in the processing delivered product files should be reduced to 5 min.

Parameters to be estimated: ZTD (mandatory) with the product sampling rate of 5 min (processing sampling rate can be higher), horizontal tropospheric gradients (optionally) and coordinates (mandatory) estimated as static parameters. The contributors submit files with troposphere parameters every hour to the ftp-server at the Geodetic Observatory Pecny after the registering of the product. The product file is

converted to the latest COST-716 format with the file name following the COST-716 conventions, i.e. using *"demo"* product status. Analysis centre providing more product lines should be uploaded as separate COST-716 files when using a specific analysis centre acronym (i.e. consisting of a unique analysis centre and a product line).

3.2.2.2 Contribution and Monitoring

From April 2015 till the end of the COST Action, eight agencies succeeded to start the real-time processing and provide partial contribution at least to the GNSS4SWEC Real-Time Demonstration Campaign. Real-time/ultra-fast solutions were provided using six different software and using various flavours of processing options (Table 3.2). Truly real-time solutions using the operational processing engine was provided by seven contributors.

For the purpose of a feedback to such product providers, a dedicated web service for an easy monitoring and comparison of individual contributions Fig. 3.2. The access has been made available also to a wide community (in particular interested from the GNSS4SWEC WG2) at http://www.pecny.cz/COST/RT-TROPO to enable visualising site-specific time series of recently estimated ZTD and gradient parameters from real-time solutions. For the comparison purpose, also near real-time regional and global solutions from the GOP analysis centre operationally contributing to the EIG EUMETNET GNSS Water Vapour Programme, E-GVAP (http://egvap.dmi.d) were included in the real-time demonstration monitoring.

Table 3.2 Contributions to GNSS4SWEC Real-Time Demonstration campaign

AC	Running agency	Software	Start	Update	Solutions
GOP	Geodetic Observatory Pecný, RIGTC	G-Nut/ Tefnut	9.4. 2015	Real-time	GPS, GLO, gradients
TUW	Technical University Vienna	TUW software	15.4. 2015	Real-time	GPS
ROB	Royal Observatory of Belgium	G-Nut/ Tefnut	23.4. 2015	Real-time	GPS, GLO, gradients
ASI	Agenzia Spaziale Italiana/Centro di Geodesia Spaziale, Matera	Gipsy-Oasis	5.5. 2015	Hourly	GPS, gradients
ULX	University of Luxembourg	BNC	15.6. 2015	Real-time	GPS
TUO	Technical University of Ostrava	RTKLib	5.11.2015	Real-time	GPS
BKG	Bundesamt für Kartographie und Geodäsie	BNC	1.3.2016	Real-time	GPS, GLO
GFZ	GFZ German Research Centre for Geosciencies	EPOS-RT	16.2.1017	Real-time	GPS, GLO

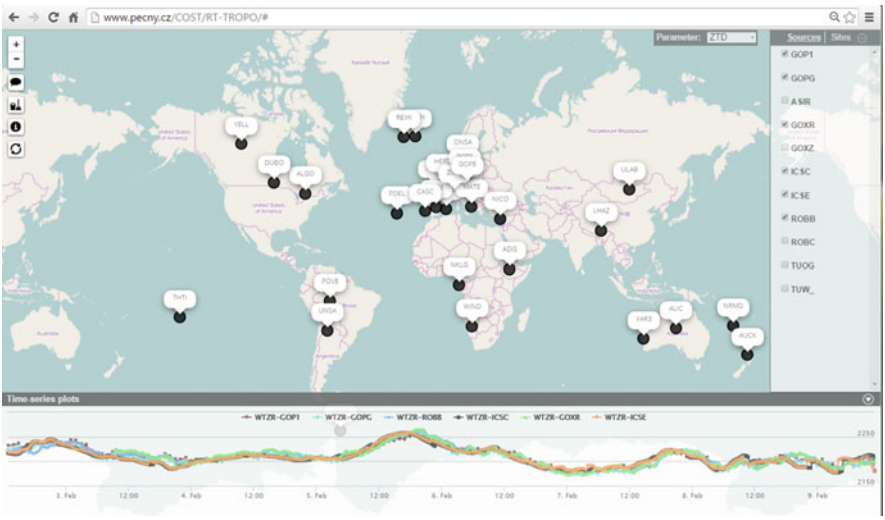

Fig. 3.2 Web service for the monitoring of the GNSS4SWEC Real-Time Demonstration campaign

3.2.2.3 Link to 4.3.7 IAG Working Group

The activity within the GNSS4SWEC project plays also a key role in the IAG Working Group 4.3.7 'Real-Time troposphere monitoring' which has been established with the following objectives for the period of 2015–2019:

- Stimulate the development of software that enable routine production of real-time/ultra-fast tropospheric products.
- Develop optimal strategies suitable for numerical or non-numerical weather nowcasting applications, and severe weather event monitoring.
- Demonstrate a reliable high-temporal resolution real-time/ultra-fast production, assess applied method, software and precise real-time orbit and clock products.
- Evaluate real-time/ultra-fast tropospheric parameters and their potential for applications in meteorology.
- Setting up a link to the users, review product format and requirements.

3.3 Tropospheric Asymmetry Monitoring and Advantage of Multi-GNSS

This section focuses on the detection of meteorological heterogeneities surrounding ground-based GNSS stations, in particular the disturbance of GNSS signal through the neutral atmosphere as retrieved by geodetic software with gradient and residual contributions to Slant Total Delay (STD). The STD of the neutral atmosphere, measured by GNSS technique, is the result of the adjustment of two components –

isotropic and anisotropic. The ZTD of the neutral atmosphere represents the isotropic contribution above a GNSS site. To adjust the anisotropic contribution, the concept of horizontal gradients has been introduced in GNSS software.

Additionally, this section included selected results of the multi-GNSS processing, which is expected to foster and improve tropospheric parameters, in particularly a possibility to monitor anisotrophy by estimating tropospheric horizontal gradients or retrieving STDs from carrier-phase post-fit residuals for more satellites in view.

3.3.1 Concept of Tropospheric Gradients

H. Brenot
Royal Belgian Institute for Space Aeronomy, Uccle, Belgium
e-mail: hugues.brenot@oma.be

The accuracy of slant delay measurements of neutral atmosphere (L_{atm}) and the number of visible satellites are critical for identifying the exact location of small-scale asymmetric tropospheric structures (Fig. 3.3).

$$\mathrm{STD} = L_{atm}(\epsilon, \alpha) = 10^{-6} \int_S N\left(\vec{\mathrm{P}}\right) ds \tag{3.1}$$

L_{atm} is commonly called slant tropospheric delay (for the elevation ϵ and the azimuth α). Its formulation shows a dependency on the atmospheric refractivity (N) and the position of source of signal ($\vec{\mathrm{P}}$). The adjustment of the slant path delay of GNSS signal (L_{atm}) through a blob of water vapour, can be well retrieved taking into account the 1st order anisotropic character of the neutral atmosphere (model presented Fig. 3.3; see Gradinarsky 2002).

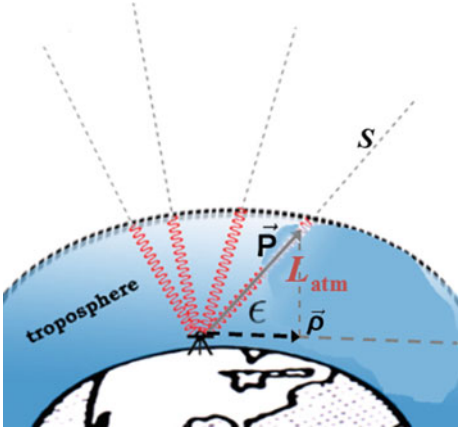

Fig. 3.3 Illustration of tropospheric heterogeneity affecting path travel (S) of GNSS signal. $\vec{P}$ is the vector position along the satellite direction (S) at the elevation (ϵ), and ρ is its projection on the horizontal plan

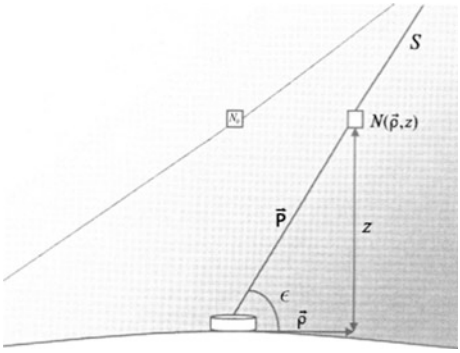

Fig. 3.4 Example of the distribution of the atmospheric refractivity (N) above a GNSS site for which a model of a flat tilted atmosphere is considered to retrieve delay gradient. The tilted line on the top, corresponds to the isoline for a constant refractivity N_0

The atmospheric anisotropy reflects the fact that the speed of microwave signals emitted from satellites and recorded by ground-based receivers differs according to the azimuthal direction through the neutral atmosphere (and the asymmetrical distribution of components surroundings a GNSS station). An inclined plane model of troposphere (Fig. 3.4) schematised by linear thickness and density variations is considered to define horizontal gradients during the adjustments of tropospheric parameters (Davis et al. 1993; Gradinarsky 2002). The correction provided by gradients possesses its own mapping function, mf_{az} (Chen and Herring 1997). The expression of azimuthal anisotropic contribution (L_{az}) to the reconstruction of slant delays depends on the satellite direction (elevation and azimuth).

According to Davis et al. (1993), the first order Taylor expansion (when ρ tends to $\vec{0}$) of the atmospheric refractivity (N) can be formulated

$$N(\vec{\rho}, z) = N_o(z) + \left.\frac{\partial N(\vec{\rho}, z)}{\partial \vec{\rho}}\right|_{\vec{\rho}\to\vec{0}} = N_o + \vec{\xi}\ (z).\ \vec{\rho} \tag{3.2}$$

This expresses the 1st order anisotropy around a site. The assumption of a straight line propagation is considered, with no time dependency of N (Gradinarsky 2002). N_0 is the isotropic contribution to N with cylindrical symmetry, and $\vec{\xi}$ is the horizontal refractivity gradient. Both depend on the altitude z (function of the elevation ϵ). Using expression Eq. 3.2 injected in Eq. 3.1, the formulation of L_{atm} is obtained:

$$\begin{aligned} L_{atm}(\epsilon, \alpha) &= 10^{-6}\int_S N_o(z)\, ds + 10^{-6}\int_S \vec{\xi}\ (z).\ \vec{\rho}\ \ ds \\ &= L_{sym}\ (\epsilon) + L_{az}\ (\epsilon, \alpha) \end{aligned} \tag{3.3}$$

L_{sym} is the symmetric contribution to ZTD mapped in direction of satellite, and L_{az} is the asymmetric contribution to the total delay (with azimuthal dependency). Vector position $(\vec{\rho})$ in the horizontal plan can be expressed using the orthonormal base $(\overrightarrow{u_{NS}}\ ,\ \overrightarrow{u_{EW}})$ of the North-South (NS) and East-West (EW) directions:

$$\vec{\rho} \quad = z.\cot(\epsilon).\left(\cos(\alpha)\ \overrightarrow{u_{NS}} + \sin(\alpha)\ \overrightarrow{u_{EW}}\right) \tag{3.4}$$

A way to link the differential of length along the path of GNSS signal (ds) and the differential of length along the vertical (dz) is to use mapping function (Niell 1996; Böhm et al. 2006a, b) which can depend on the elevation ($m_0(\epsilon)$)

$$ds \quad = m_0(\epsilon)\ .\ dz \tag{3.5}$$

The refractivity gradient can be expressed in the base $\left(\overrightarrow{u_{NS}}\ ,\ \overrightarrow{u_{EW}}\right)$:

$$\vec{\xi}\ (z) = \xi_{NS}(z)\ \overrightarrow{u_{NS}} + \xi_{EW}(z)\ \overrightarrow{u_{EW}} \tag{3.6}$$

Considering Eqs. 3.3, 3.5 and 3.6, L_{az} can be formulated

$$L_{az}(\epsilon,\alpha) = 10^{-6}.\ m_0(\epsilon).\cot(\epsilon).(G_{NS}.\cos(\alpha) + G_{EW}.\sin(\alpha)) \tag{3.7}$$

(G_{NS}, G_{EW}) are the components of the horizontal delay gradients $\left(\vec{\mathrm{G}}\right)$ in the base $\left(\overrightarrow{u_{NS}}\ ,\ \overrightarrow{u_{EW}}\right)$ expressed as

$$\vec{\mathrm{G}} = G_{NS}\ \overrightarrow{u_{NS}} + G_{EW}\ \overrightarrow{u_{EW}} = \begin{pmatrix} G_{NS} \\ G_{EW} \end{pmatrix} \tag{3.8}$$

The analytic formulation of (G_{NS}, G_{EW}) is following

$$\begin{pmatrix} G_{NS} \\ G_{EW} \end{pmatrix} = \begin{pmatrix} \int_0^\infty z.\xi_{NS}(z)\ dz \\ \int_0^\infty z.\xi_{EW}(z)\ dz \end{pmatrix} \tag{3.9}$$

The unit of delay gradient is the same as for the delay – the unit of length [m]. The delay gradient $\left(\vec{\mathrm{G}}\right)$ can be defined as a correction of phase residual projections depending on the elevation and azimuth angles of visible satellites. An interpretation of the horizontal gradient is for example that, a gradient component of 1 mm at the zenith will show a higher correction for elevation of 45° and 25° (correction of about 2 mm and 4 mm, respectively).

Following the implementation of tropospheric delay (ZTD), the horizontal delay gradient is the second tropospheric parameter implemented in the least-squares adjustment proceeded by geodetic software in the analysis of GNSS data (Davis et al. 1993; MacMillan 1995; Alber et al. 1997; Chen and Herring 1997; Bar-Sever and Kroger 1998). Initially, horizontal gradients were introduced into the calculations in order to improve positioning solutions, showing a 15% improvement for the horizontal repeatability (Bar-Sever and Kroger 1998) and a 25% improvement

between wet delays from GNSS and WVR. Afterwards, the potential of delay gradient for GNSS meteorology has been investigated. Walpersdorf et al. (2001) have showed how the use of GNSS gradient can describe the approach of a front towards Marseille in the south-east of France in 1998. Iwabuchi et al. (2003) also showed that the temporal and spatial variations of GNSS gradients matched well with the moisture field determined by ZTD and with the meteorological condition in summer 1996 over the Japan Islands (in particular during the passage of a weather front).

The interest of using GNSS gradient for monitoring severe weather is still investigated, especially to improve our understanding of meteorological situation. For example, during the flash-flood event of September 2002 (southeastern France), three phases have been identified by Delrieu et al. (2005) and confirmed by GNSS data (Brenot et al. 2006). The maximum daily precipitation reached 691 mm. Figure 3.5 shows the path of a MCS over CHRN station during the Phase III (from 01:00 to 18:00 UTC on 9 September 2002). It can be seen that horizontal gradient can clearly be used to monitor tropospheric structure (MCS or blob of water vapour). Just after this rainfall event (in Autumn 2002), a dense network of 20 GPS stations has been installed by the Mediterranean Hydrometeorological Observatory Cévennes-Vivarais (OHM-CV) to proceed monitoring of convective systems and Cévenol effect, eastwards of Mont Aigoual (AIGO station located at 30 km of this dense network; see Fig. 3.5). Using different configurations in calculations (settings, geometry, constrains), the precision of NS and EW delay gradients components (zenith direction) has been evaluated to 0.35–0.7 mm and 0.2–0.5 mm respectively (Brenot et al. 2014a, b). The lack of GPS satellites at low elevation in the North for a

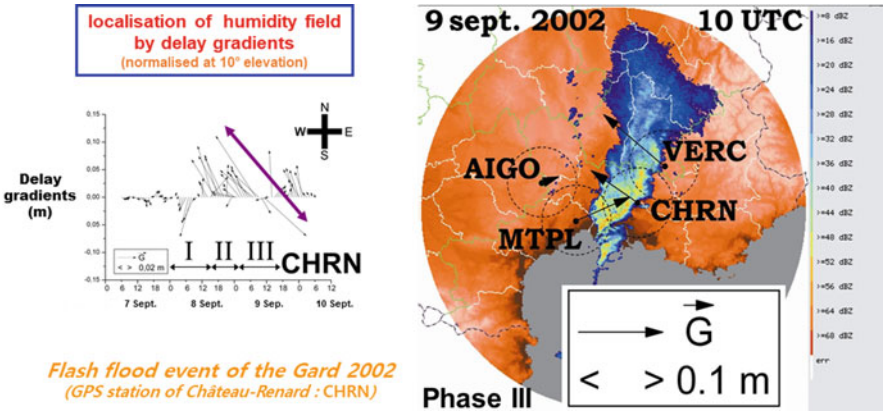

Fig. 3.5 (left) Time-series of delay gradients over Château-Renard (CHRN) GPS station during the flash-flood event of September 2002 (over Bouche-du-Rhône, between Montpellier and Marseille, France). Purple double-arrow shows the path of a quasi-stationary Mesoscale Convective System (MCS) over CHRN station. (right) GNSS delay gradients are superposed over radar reflectivity localising the MCS close to MTPL, CHRN and VERC stations. Dash circles show representativity areas of gradients (for a cutoff angle of 10°).

network located at a latitude of 45°N, explains why the precision of the NS component is less good than the EW one.

3.3.2 *Global Validity and Behaviour of Tropospheric Gradients Estimated by GPS*[2]

L. Morel
École Supérieure des Géomètres et Topographes, Le Mans, France
e-mail: laurent.morel@esgt.cnam.fr

Estimation of tropospheric gradients in GNSS data processing is a well-known technique to improve positioning. Today, they are routinely estimated by several global and regional GNSS analysis centres but they are still not yet used for operational meteorology. We have studied the physical meaning of tropospheric gradients estimated from GPS observations recorded by several permanent stations located all around the world. In a first study with several stations on Corsica island, we estimated ZTD and tropospheric gradients using two software: GAMIT/GLOBK (GAMIT version 10.5) and GIPSY-OASIS II version 6.3 in order to analyse the differences in the tropospheric results (ZWD and gradients) coming from the processing strategy (double-differences for GAMIT/Globk versus zero-difference for GIPSY-OASIS). That study allowed to confirm a strong correlation between the two software for ZWD estimation (98%) and a good correlation for gradient estimation (70%). No direct correlation with elevation or geographical location has been noticed but the gradients were oriented inward land (Fig. 3.6), in opposite direction from tropospheric humidity field processed by ERA – Interim and with a direction relatively stable along the year (Morel et al. 2014).

In a following study with 14 stations all around the world, selected due to their proximity of the relief, we also observed that gradient directions were stable over the time and pointed toward the relief for most of the stations selected. Correlation coefficients were processed between gradients (yearly mean values (Ge, Gn) as vector component) and direction of the steep slopes (obtained by analysing Digital Elevation Model at 20 km, 40 km and 60 km around the station), see Table 3.3. These results gave us a first step for a physical meaning to gradients when stations are close to high mountains. We can notice 10 stations with a correlation coefficient > 0.4 (60 km) and 2 stations without any correlation (BOGT and CHWK) but surrounded by mountains. Now, we are going to continue the study with more stations and years and quantify multipath effect.

[2]Parts from this section were previously published in Morel et al. 2014

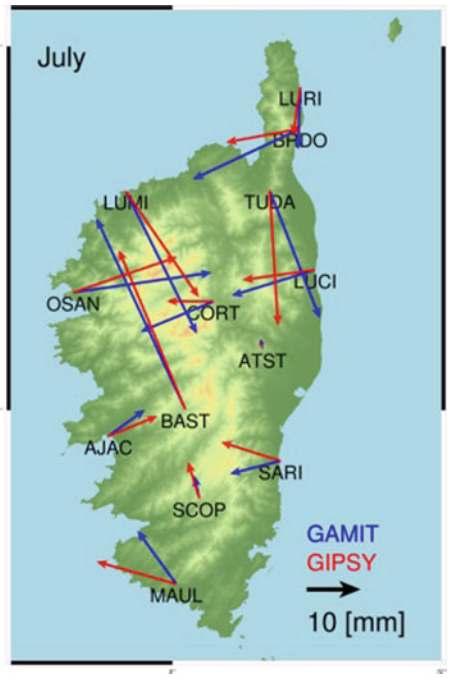

Fig. 3.6 Monthly mean gradient magnitude and direction (blue arrows estimated by GAMIT and red arrows estimated by GIPSY-OASIS) for all stations in Corsica Island over the year 2011. Gradient vectors are drawn considering monthly mean values (Ge, Gn) as vector components

Table 3.3 Correlation coefficient between gradient and relief around 14 stations (red: negative correlation, orange: weak correlation and green: strong correlation)

	20 km	40 km	60km
ARAN	-0,618	-0,266	0,248
BOGT	-0,682	-0,731	-0,766
CHAM	0,154	0,446	0,429
CHUM	0,057	0,706	0,790
CHWK	-0,003	-0,575	-0,656
CIT1	0,711	0,719	0,723
COMO	0,855	0,850	0,881
CRAL	0,800	0,862	0,908
IENG	-0,244	0,809	0,801
KIT3	-0,195	0,223	0,582
NIST	0,211	0,084	0,134
RIOP	-0,170	0,103	0,227
THTI	0,399	0,354	
UNSA	0,814	0,757	0,537

3.3.3 *Monitoring of Severe Weather from Wet Gradients, Residuals and Slants*[3]

H. Brenot
Royal Belgian Institute for Space Aeronomy, Uccle, Belgium
e-mail: hugues.brenot@oma.be

To retrieve Slant Wet delays (SWD) in direction of GNSS satellites (for elevation ϵ and azimuth α), two contributions are commonly considered (see Eq. 3.10): the isotropic contributions (L_{sym}^{wet}) with spherical symmetry and derived from Zenith Wet Delays (ZWD), and the anisotropic contributions (L_{asym}^{wet}) with azimuthal asymmetry and derived from horizontal wet gradients and residuals.

$$\mathrm{SWD} = L_{sym}^{wet}(\epsilon) + L_{asym}^{wet}(\epsilon, \alpha) \tag{3.10}$$

with

$$L_{sym}^{wet}(\epsilon) = \mathrm{ZWD}_{\mathrm{adjusted}} \cdot \mathrm{mf}_{\mathrm{sym}}^{\mathrm{wet}}(\epsilon) \tag{3.11}$$

The GNSS technique retrieves Zenith Tropospheric Delay (ZTD) of the neutral atmosphere using an a priori ZHD ($\mathrm{ZHD}_{\mathrm{apriori}}$) and adjusting a ZWD ($\mathrm{ZWD}_{\mathrm{adjusted}} = \mathrm{ZTD} - \mathrm{ZHD}_{\mathrm{apriori}}$). $\mathrm{ZHD}_{\mathrm{apriori}}$ is generally obtained using the formula of Saastamoinen (1972); see also Davis et al. (1985) and Elgered et al. (1991). L_{sym}^{wet} depends on the elevation (ϵ) of each satellite and using a wet mapping function, e.g. GMF (Boehm et al. 2006a, b).

Concerning the wet anisotropic contribution (L_{asym}^{wet}), the 1st and the 2nd order contributions can be considered by using respectively the wet gradients (L_{az}^{wet}) and the one-way post-fit residuals (L_{res}), as formulated in Eq. 3.12. Generally, the contribution of residuals is not considered because it can be highly affected by multipath and artefacts in calculations. This study tries to show you the interest of using residuals, as retrieved by GAMIT software (Herring et al. 2010). The 1st order contribution to L_{az}^{wet} is estimated with gradient wet components ($G_{\mathrm{NS}}^{\mathrm{wet}}$, $G_{\mathrm{EW}}^{\mathrm{wet}}$) that is connected to the azimuth (α), and with the use of gradient mapping function $\left(\mathrm{mf}_{\mathrm{az}}^{\mathrm{wet}} = 1/(\sin\epsilon\tan\epsilon + \mathrm{C})\right)$ which depends on satellite's elevation and on a constant C (Chen and Herring 1997).

$$L_{asym}^{wet}(\epsilon, \alpha) = L_{az}^{wet}(\epsilon, \alpha) + L_{res}(\epsilon, \alpha) \tag{3.12}$$

with

[3]Parts from this section were previously published in Brenot et al. (2013)

$$L_{az}^{wet}(\epsilon,\alpha) = \mathrm{mf}_{\mathrm{az}}^{\mathrm{wet}}(\epsilon,\mathrm{C}).\left(G_{\mathrm{NS}}^{\mathrm{wet}}.\cos(\alpha) + G_{\mathrm{EW}}^{\mathrm{wet}}.\sin(\alpha)\right)$$

The gradient components (G_{NS}, G_{EW}) retrieved by GNSS technique are total. This means there is no distinction between wet and hydrostatic gradients (Chen and Herring 1997; Flores et al. 2000). In geodetic software it is commonly considered that C = 0.0032 (Herring 1992), but for the estimation of the asymmetric wet delay (L_{az}^{wet}), C = 0.0031 can be used (Chen and Herring 1997). The wet gradient $\overrightarrow{\mathrm{G}^{\mathrm{wet}}}$ is expressed by the difference of the hydrostatic to the total component.

$$\overrightarrow{\mathrm{G}^{\mathrm{wet}}} = \begin{pmatrix} G_{\mathrm{NS}}^{\mathrm{wet}} \\ G_{\mathrm{EW}}^{\mathrm{wet}} \end{pmatrix} = \begin{pmatrix} G_{NS} \\ G_{EW} \end{pmatrix} - \begin{pmatrix} G_{\mathrm{NS}}^{\mathrm{hydrostatic}} \\ G_{\mathrm{EW}}^{\mathrm{hydrostatic}} \end{pmatrix} \tag{3.13}$$

To obtain the hydrostatic gradient components, a characterisation of the surface pressure field around each GNSS station is required. In that case, the hydrostatic gradient can be established by fitting a plane through the pressure measurements (Champollion et al. 2004; Brenot et al. 2014a, b). From the pressure field near a GNSS site, the spatial variations of the hydrostatic delay per unit of distance (km) in the north-south ($Z_{\mathrm{NS}}^{\mathrm{hydrostatic}}$) and east-west ($Z_{\mathrm{EW}}^{\mathrm{hydrostatic}}$) directions can be calculated. Generally, for a case study, surface pressure measurements around all GNSS stations are not available. Outputs from numerical weather model can be considered. Assuming an exponential law in the hydrostatic refractivity and considering the scale height of the gradients in the hydrostatic delays set to $H = 13$ km (as suggested by Chen and Herring 1997), the spatial variations of the hydrostatic delay can be converted in hydrostatic gradients (Elósegui et al. 1999; Ruffini et al. 1999; Flores et al. 2000) to obtain wet gradient components (Eq. 3.14).

$$\begin{pmatrix} G_{\mathrm{NS}}^{\mathrm{wet}} \\ G_{\mathrm{EW}}^{\mathrm{wet}} \end{pmatrix} = \begin{pmatrix} G_{NS} \\ G_{EW} \end{pmatrix} - H.\begin{pmatrix} Z_{\mathrm{NS}}^{\mathrm{hydrostatic}} \\ Z_{\mathrm{EW}}^{\mathrm{hydrostatic}} \end{pmatrix} \tag{3.14}$$

The 2nd order asymmetric contribution from residuals (L_{res}), can be considered if a station is weakly affected by multipath or these avoided by Multipath Stacking Methods (MPS), as introduced by Elósegui et al. (1995) and Shoji et al. (2004). By using MPS, low elevation measurements can be improved by identifying and avoiding non-tropospheric signature in data. Estimates of slant delays can also be improved by using Phase Centre Variation model (PCV) for the antenna (Shoji et al. 2004). This aspect is not treated in this study, as well as the questioning of artefacts in calculations. This study investigates the contribution of residuals (L_{res}) to wet delays without any correction of multipath and PCV model.

Brenot et al. (2013) have studied in detail the rainfall event of 28–29 June 2005. This paper shows the critical role of GNSS horizontal gradients of the water vapour content to detect small scale structures of the troposphere (i.e. convective cells), and presents a strategy to identify typical water vapour configurations (dry/wet dipole in

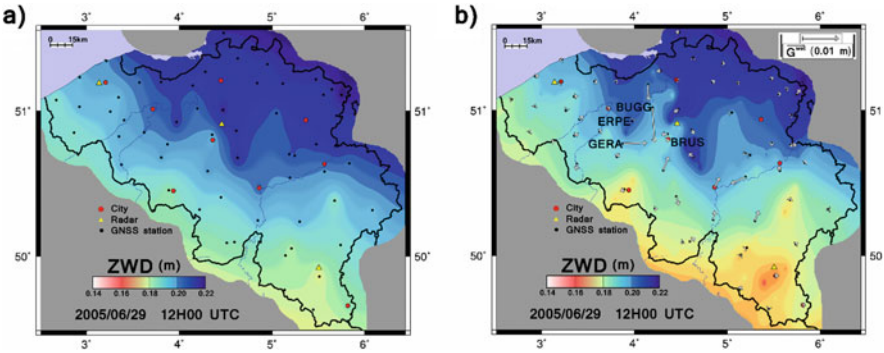

Fig. 3.7 (**a**) Imaging of the 2D field of ZWD with a classic interpolation (stations are plotted using black circles); (**b**) improvement of this field by GNSS gradients. Wet gradients $\overrightarrow{G^{wet}}$ are plotted using grey arrows at each GNSS site. BUGG, ERPE, GERA and BRUS stations are plotted. Locations of 9 major Belgium cities (red circles) and meteorological radars (yellow triangles) are also plotted on these 2D maps

time and space) and obtain preliminary signs of the initiation of deep convection. The complementary objective of this work is to investigate, step by step, the use of wet gradient to improve 2D field of ZWD and visualise water vapour blobs, and the use of SWD delays to monitor small scale tropospheric structure of convective cells.

Total GNSS gradients has been used by Brenot et al. (2013, 2014a, b) to improve the spatial resolution of the 2D field of ZTD (using Hermite interpolation or pseudo-observation defined by gradients). The strategy of Brenot et al. (2013) with additional pseudo-observations has been transferred to the improvement of the 2D field of ZWD with wet gradients $\overrightarrow{G^{wet}}$ (comparison between classic interpolation and improved ZWD field is shown in Fig. 3.7). The grey arrows in Fig. 3.7b, represent $\overrightarrow{G^{wet}}$ (expressed in the zenith direction) with amplitudes of about 0.01 m and more for stations GERA and BUGG at 12:00 UTC on 29 June 2005. A relevant way to visualise, in time, isotropic and anisotropic contributions to wet delays, is proposed in Fig. 3.8. Such a graph acts by superimposing horizontal wet gradient to ZWD. Four stations have been selected (ERPE, BUGG, GERA and BRUS), as being several time close or overflown by convective cells. Let's focus our attention on the time window (10:00 to 14:00 UTC) when these four stations measure high anisotropic contributions (wet gradient higher than 0.01 m).

The morning of the 29th June 2005, the wet delay is gradually decreasing for the four stations (as shown in Fig. 3.8), then a sudden increase is observed (starting at 11:00 UTC for ERPE and GERA, and 12:00 UTC for BRUS and BUGG). Figure 3.9 shows the spatial distribution of wet delay all over Belgium at 12:15, 12:30, 13:00 and 13:15 UTC. Low ZWD is observed by BUGG station at 12:15 in Fig. 3.9a. At this moment, the initiation of convection is taking place between BUGG and BRUS (dry/wet dipole). At 12:30 UTC (in Fig. 3.9b), a strong contrast of moistening is still

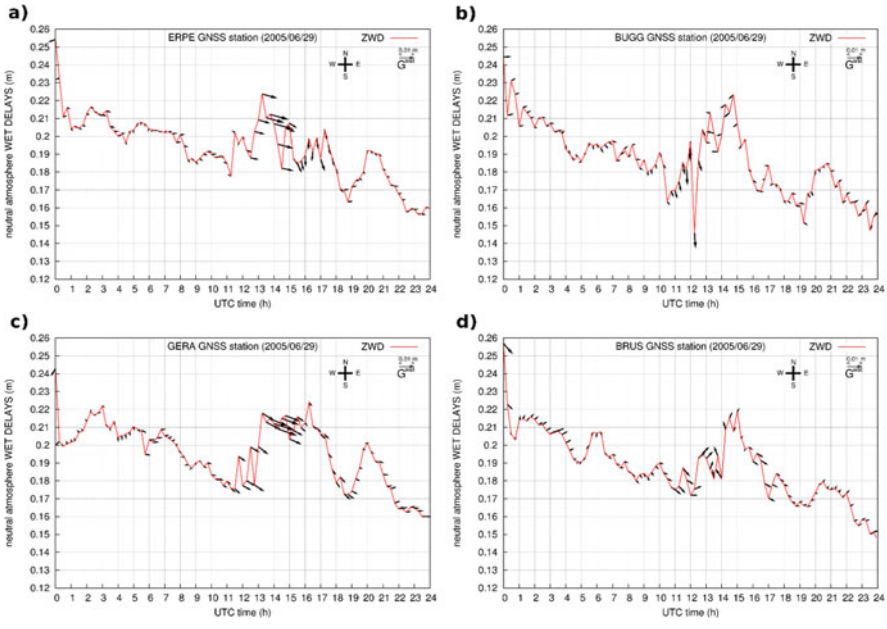

Fig. 3.8 Visualisation of isotropic (ZWD) and anisotropic (wet gradient, $\vec{G}^{wet}$) contributions to delays on 29 June 2005 for 4 stations (**a**) ERPE, (**b**) BUGG, (**c**) GERA, and (**d**) BRUS

observed between BRUS and BUGG with significant rainfall. Wet gradients of BUGG and BRUS stations point to area with high precipitation.

At 13:00 UTC, the flux of water vapour from north to south is separated by a drier area on the north and east side of BRUS, where the initiation of deep convection is taking place (on the east side of BRUS). The strength of the rapid flux of moistening is shown by a strong increase of the field of ZWD close to BUGG and ERPE and in the north-west of Belgium (see Fig. 3.9c). Wet gradient amplitudes higher than 0.015 m have been observed for several stations during this rainfall event (and especially during this time window), notably at NAMR station (south-east of BRUS in Fig. 3.9d); see Brenot et al. (2013). Looking at the improved 2D field in Fig. 3.9, dry/wet contrast of ZWD field is a good indicator of preliminary signs of deep convection and heavy precipitation.

An investigation of the interest of SWD for monitoring small-scale structures (sub-kilometric size) for these four stations is presented in Fig. 3.10 (time window from 10:00 to 14:00 UTC). Using skyplots, the three contributions to SWD (isotropic contribution by ZWD and L_{sym}^{wet}, and anisotropic contributions by wet gradients and residuals, respectively L_{az}^{wet} and L_{res}) are shown for GNSS signals from two satellites recorded by four stations.

Small wet gradients and residuals are observed between 10:00 and 12:00 UTC for these four stations (except a wet structure at 11:00 on the west side of ERPE and

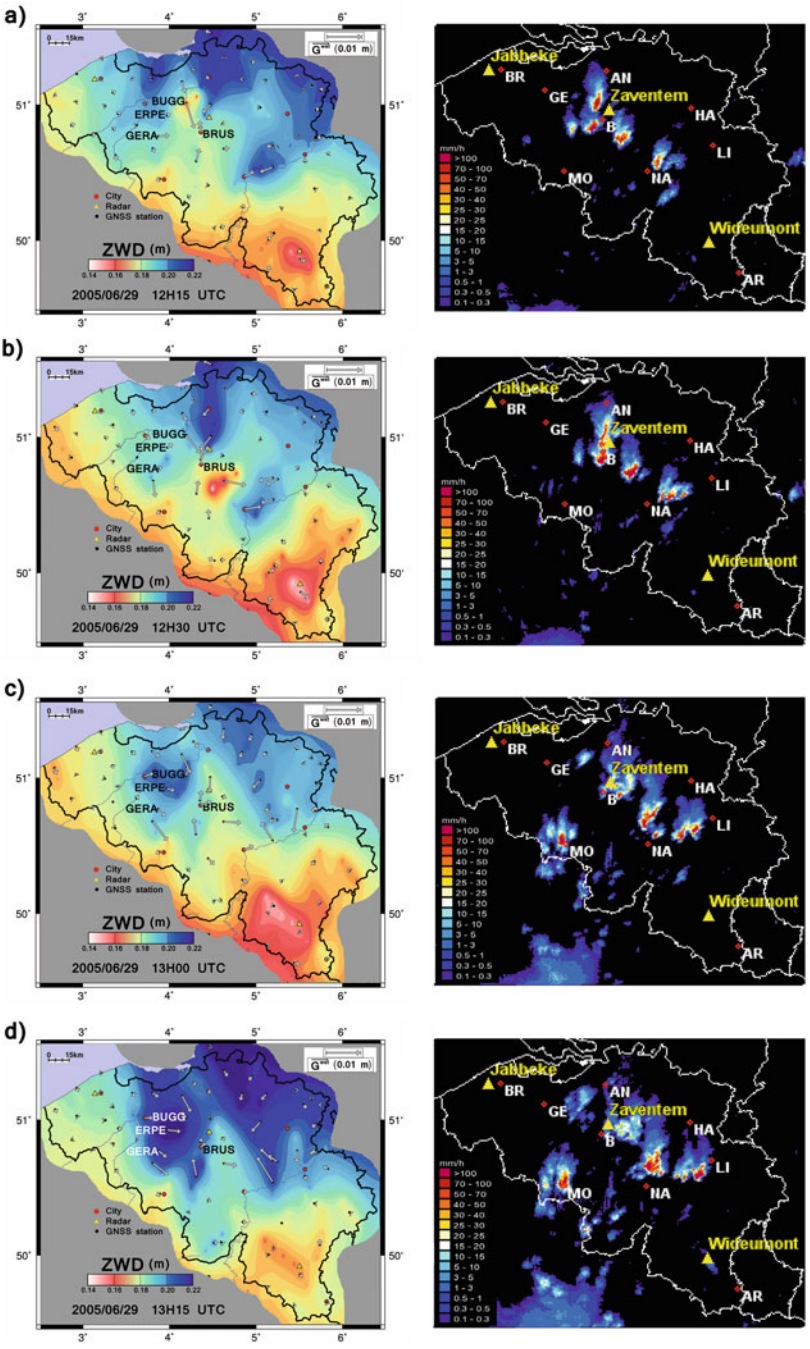

Fig. 3.9 (left) 2D fields of ZWD improved by, $\overrightarrow{G^{wet}}$ at (**a**) 12:15, (**b**) 12:30, (**c**) 13:00 and (**d**) 13:15 UTC on 29 June 2005; (right) Radar precipitation at (**a**) 12:15, (**b**) 12:30, (**c**) 13:00 and (**d**) 13:15 UTC on 29 June 2005.

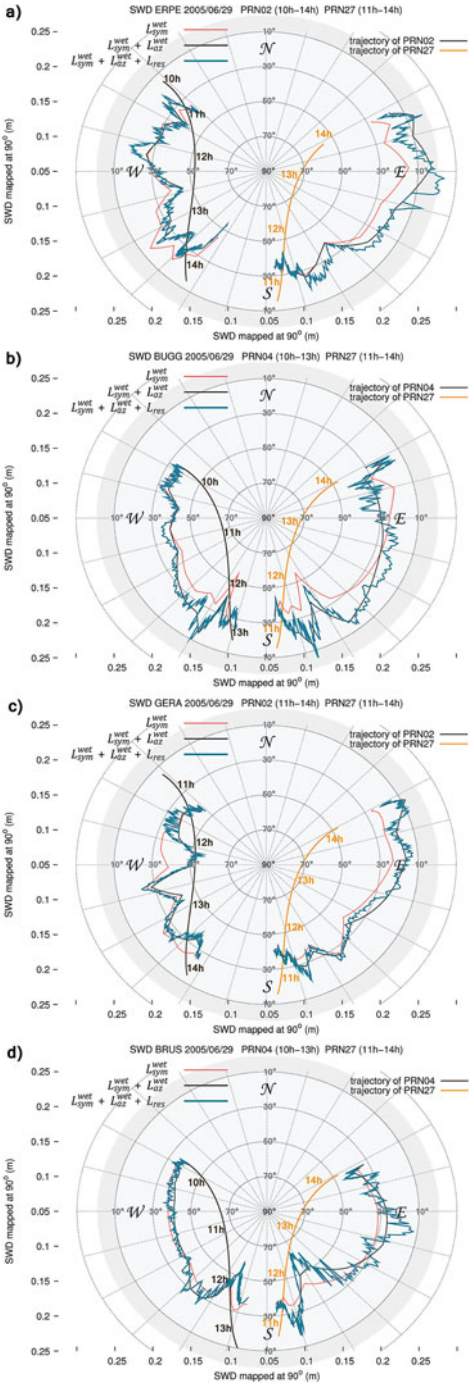

Fig. 3.10 Skyplots for 4 GNSS stations of couples SWD/satellites trajectories on 29 June 2005, (**a**) ERPE, (**b**) BUGG, (**c**) GERA, and (**d**) BRUS

BUGG, 15 min later, specifically where the initiation of a convective system took place). Between 12:00 and 14:00, several tropospheric structures are identified by the four stations, showing a base of anisotropic contribution provided by the wet gradient and a precise time-space detection by the residuals.

Even similarity and correlation with radar precipitation is not obvious, neither straightforward. It can be noticed that at 12:15, a blob of water vapour is detected on the west side of ERPE. For BUGG station, the negative residuals of PRN27 satellite at 12:15, decrease the anisotropy seen by the wet gradients (showing that the highest density of humidity of the wet structure is not located at 60° of elevation). No significant structure is seen by L_{res} for GERA station. However, a tropospheric structure is detected by residuals of PRN27 BRUS station (in the south – south-east direction for elevations between 40° and 50°).

At 12:30, the wet gradients of BRUS indicate the north, and L_{res} of PRN27 is negative for elevation between 50° and 70°, showing a drier structure (convective system has moved eastward). A wet structure is seen by L_{res} of PRN27 for ERPE station (located north-west of BRUS).

Between 13:00 and 13:30, PRN27 residuals of ERPE and BRUS stations indicate wet structure in the east direction for an elevation of 70°. BUGG residuals show a wet structure in the south-east.

There is a clear identification of sub-kilometric meteorological structure by one-way post fit residuals. Even no correction of multipath and PCV model has been applied (Elósegui et al. 1995; Shoji et al. 2004), a way to justify that the structures detected by residuals have properly a tropospheric origin is to compare L_{res} on 29 June with the one measured the day before, for which the trajectories of satellites are very similar. On 28 June, the tropospheric activity was moderate. Figure 3.11 shows clearly low residuals on 28 June, justifying that the structures detected on 29 June are due to tropospheric activity (no multipath or artefact effect). If a GNSS station is a good candidate (confirmation of the tropospheric origin of residuals), the 2nd order asymmetric contribution from residuals (L_{res}), can be considered in meteorological applications (assimilation in numerical weather forecasts or imaging for nowcasting). This study shows a good potential for residuals and SWD for detecting small scale tropospheric structures affecting signal propagation between GNSS satellites and stations.

3.3.4 *Indicator of Tropospheric Activity Based on the Disruption of GNSS Signals*[4]

H. Brenot
Royal Belgian Institute for Space Aeronomy, Uccle, Belgium
e-mail: hugues.brenot@oma.be

[4]Parts from this section were previously published in Brenot and Warnant (2008)

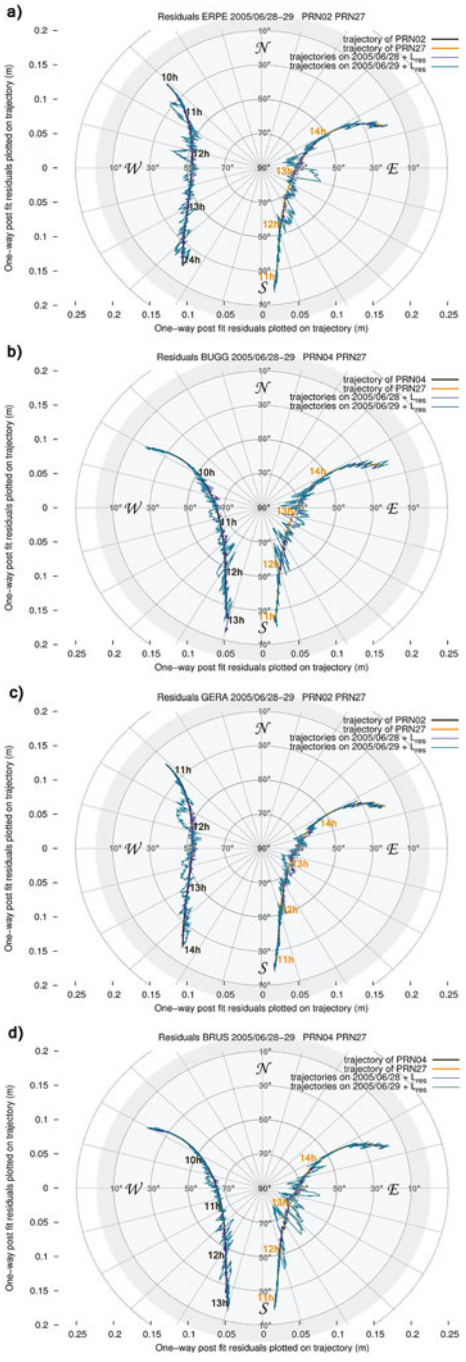

Fig. 3.11 Skyplots for 4 GNSS stations of one-way post fit residuals (L_{res}) and satellites trajectories on 28–29 June 2005, (**a**) ERPE, (**b**) BUGG, (**c**) GERA, and (**d**) BRUS

The aim of this subsection is to find a new indicator of small-scale tropospheric activity. Different candidates of tropospheric effects indicators can be considered according to GNSS carrier phase measurements (King et al. 1985; Dong and Bock 1989; Blewitt 1989; Leick 1989; Teunissen et al. 1998). However, ZTD and gradients are not the best candidate being the results of a time and space average. STDs show a good potential to detect small-scale meteorological structure (see Sect. 3.3.5). Nevertheless, double differences (L_1, L_2) of the ionosphere-free combination of GNSS phase observations can be used as an additional detection of the presence of small-scale structures in the troposphere. Small-scale structures induce disturbances on phase measurements. This study considers stations for which the positions and the geometric distances D_{AB}^{ij} are precisely known between couples of satellites and ground-based receivers. The tropospheric perturbation T_{AB}^{ij} and the ambiguity $N_{AB,IF}^{ij}$ remains the only unknown parameters in the double difference of phase of the ionosphere-free (IF) combination $\phi_{AB,IF}^{ij}$ (for a simplified mathematical model of phase measurements (Seeber 2003; Leick 2004; Brenot and Warnant 2008). A new observable of phase $\Phi_{AB,IF}^{ij}$ can be estimated:

$$\Phi_{AB,IF}^{ij} = \phi_{AB,IF}^{ij} - \frac{f_1}{c} D_{AB}^{ij} = \frac{f_1}{c} T_{AB}^{ij} + N_{AB,IF}^{ij} \tag{3.15}$$

c is the speed of electromagnetic waves, (f_1, f_2) carrier frequencies of (L_1 or L_2). The ambiguity term ($N_{AB,IF}^{ij}$) has the following expression:

$$N_{AB,IF}^{ij} = \left(N_{A,IF}^{i} - N_{B,IF}^{i}\right) - \left(N_{A,IF}^{j} - N_{B,IF}^{j}\right) \tag{3.16}$$

Ambiguities ($N_{A,IF}^{i}$, $N_{B,IF}^{i}$, $N_{A,IF}^{j}$ and $N_{B,IF}^{j}$) are defined using ionosphere-free combination. The phase ambiguity term ($N_{AB,IF}^{ij}$) is a real number with a constant value.

Figure 3.12 shows an example of tropospheric perturbation T_{AB}^{ij} and ambiguity $N_{AB,IF}^{ij}$ presented by the phase observable $\Phi_{AB,IF}^{ij}$ (called IF Double Difference and expressed in cycles) on 29 June 2005 for BRUS-GILL baseline (4 km) and the couple of satellites (27-08). Without the presence of the troposphere, a constant real value of the IF DD should be observed according to the ambiguity $N_{AB,IF}^{ij}$ (which can be a real number). The error induced by the troposphere on the IF Double Difference observable $\Phi_{AB,IF}^{ij}$ time-series is clearly shown in Fig. 3.12 between 12:00 and 13:00 UTC. According to radar imaging important precipitations (higher than 100 mm/h) took place over and north-east of OLLN station at 12:30 UTC the 29th June 2005 (location of strong tropospheric activity).

A high content of water vapour and the existence of hydrometeors induces a strong perturbation of atmospheric refractivity (Brenot et al. 2006). Perturbation of refractivity can clearly explain sudden variability of tropospheric error T_A^i measured by station A for a signal emitted by a satellite i. The following expression presents

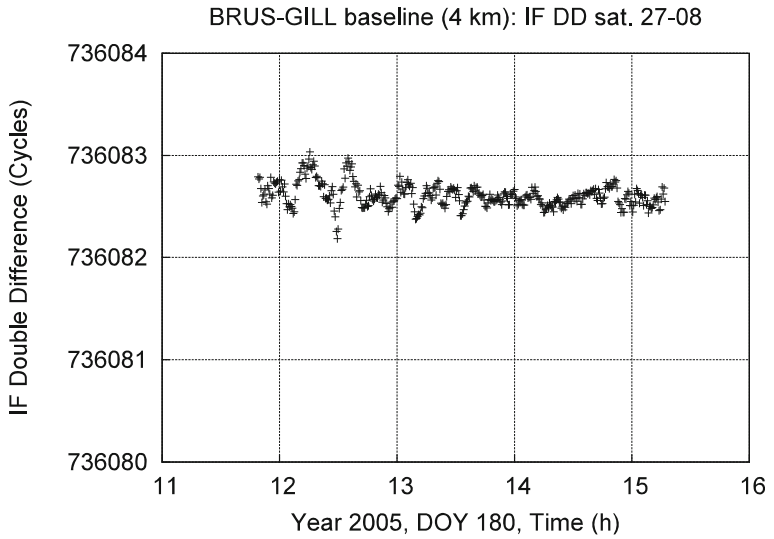

Fig. 3.12 IF Double Difference of BRUS-GILL baseline the 29th June 2005 (Day Of Year 180)

the relation of tropospheric error T_A^i (*i. e.* generally called STD) with neutral atmosphere refractivity (N):

$$T_A^i = 10^{-6} \int N \; ds \tag{3.17}$$

ds is a differential distance according to path travel of signal between satellite i and station A. The tropospheric error T_{AB}^{ij} induces the perturbation of the phase observable $\Phi_{AB,IF}^{ij}$, as defined by Eq. 3.15, representing the double difference of phase of the ionosphere-free combination with a correction of the geometric distances. This tropospheric error has the following expression:

$$T_{AB}^{ij} = \left(T_A^i - T_B^i\right) - \left(T_A^j - T_B^j\right) \tag{3.18}$$

Sudden perturbations of tropospheric errors (T_A^i,T_B^i,T_A^j and T_B^j) by a small-scale structures induce direct perturbations of T_{AB}^{ij} and $\Phi_{AB,IF}^{ij}$. Considering two epochs of measurements (epoch t_0 and epoch t_0 + Δt, for example Δt = 5 min), Fig. 3.13 illustrates the direct impact of the occurrence of a small-scale tropospheric structure on phase measurements (observables $\Phi_{AB,IF}^{ij}$ and T_{AB}^{ij}).

The resolution of the ambiguities is required. For a selected Day Of Year (DOY), reference satellites are chosen to form double differences (DD) and maximise the time periods. The atmospheric scans by these couples of satellites are sufficient to represent the tropospheric activity. Considering NAMR-OLLN baseline DOY 180 of 2005 (couple of satellites 10–21) and BRUS-BERT baseline DOY 365 of

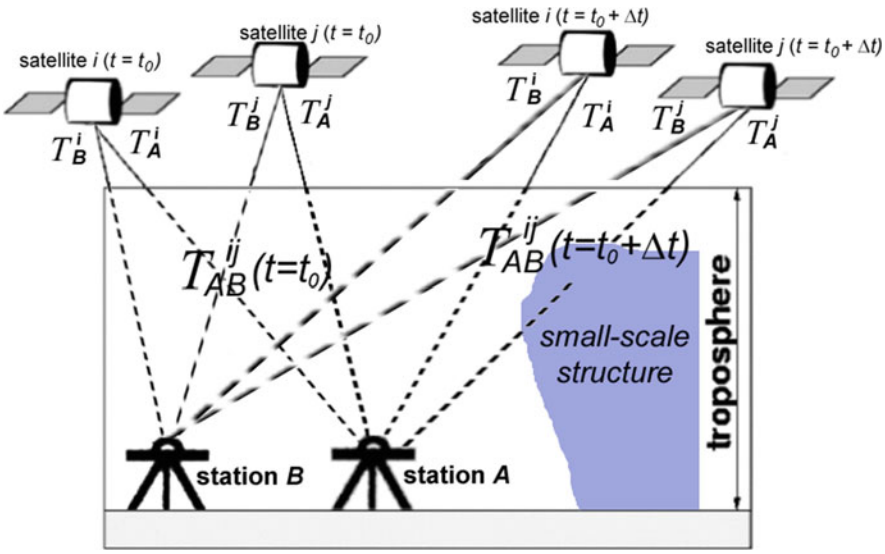

Fig. 3.13 Perturbation of TABij induced by a small-scale tropospheric structure for two epochs of measurements (epoch t = t0 and epoch t = t0 + Δt)

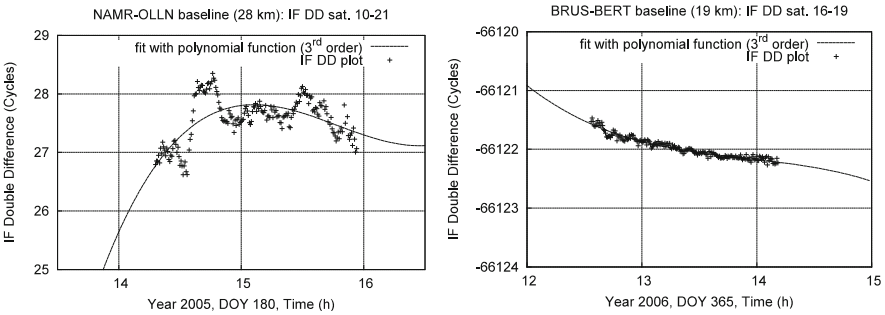

Fig. 3.14 IF Double Difference of NAMR-OLLN baseline the 29th of June 2005 event (DOY 180) on the left, BRUS-BERT baseline on the right (no meteorological event on 31 December 2005, DOY 365). The fits of DD time-series with polynomial functions of the 3rd order are shown

2006 (couple of satellites 16–19), Fig. 3.14 shows IF Double Differences time-series (observable of phase $\Phi_{AB,IF}^{ij}$ of Eq, 3.15) for these two baselines (called IF DD plotted with crosses).

The impact on DD depends on the elevation of considered satellites. This is a specificity of the tropospheric activity. In order to display only the influence of small-scale structures on DD time-series, fits of IF DD time-series have been assessed using polynomial functions of the 3rd order (dashed line Fig. 3.14) and

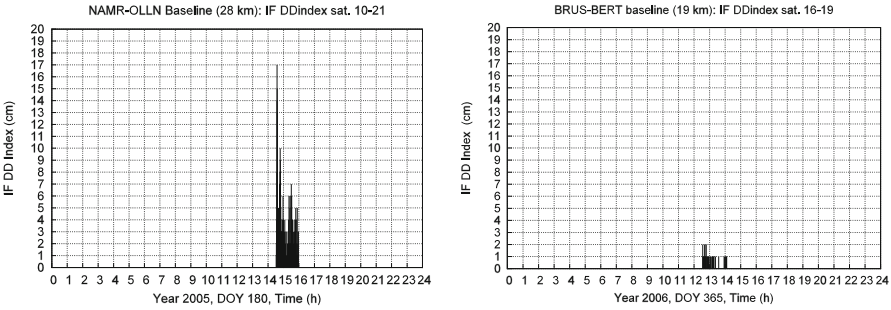

Fig. 3.15 1 h radar precipitation accumulation starting at (**a**) 16:00 UTC, (**b**) 17:00 UTC, (**c**) 18:00 UTC, and (**d**) 19:00 UTC on 2006/10/01

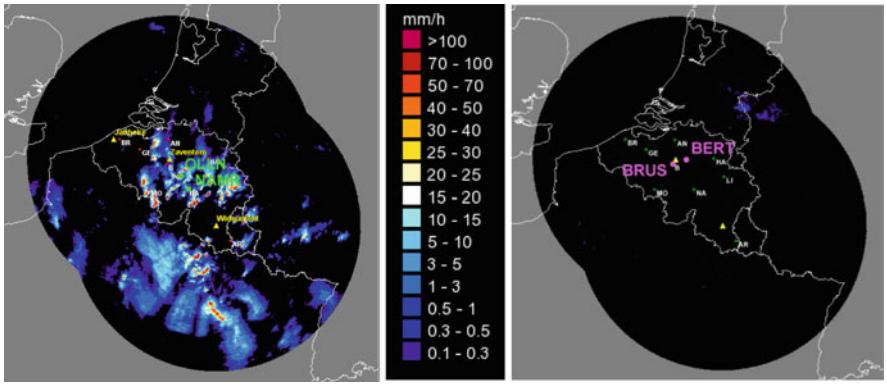

Fig. 3.16 Radar precipitation on 29 June 2005 at 14:30 UTC (left), and on 31 December 2006 at 13:15 UTC (right)

the biases between IF DD and the respective fits**,** called IF DD Residuals, can be obtained.

The estimation of the bias to the fit removes elevation effects. Then small-scale structures are clearly identified for NAMR-OLLN baseline on the 29th of June 2005 (in Fig. 3.14 between 14:00 and 15:00 UTC). Figure 3.15 shows a time-series of IF DD Index. To obtain this Index of the tropospheric activity, absolute values of IF DD Residuals (in cycles) is converted into centimetres (multiplying by the wave length: 19.029 cm).

According to radar imaging of rain rate (in Fig. 3.16 on the left), the tropospheric small-scale activity around *Namur* (NAMR and OLLN stations) during DOY 180 of 2005 can be easily observed between 14:00 and 15:00 UTC. Note that a strong tropospheric activity was also observed between 12:00 and 13:00 UTC this day (see Figs. 3.14 and 3.15; see also Brenot et al. 2013). No tropospheric activity took place around *Brussels* (station BRUS) DOY 365 of 2006 at 13:15 UTC (see radar imaging in Fig. 3.16 on the right).

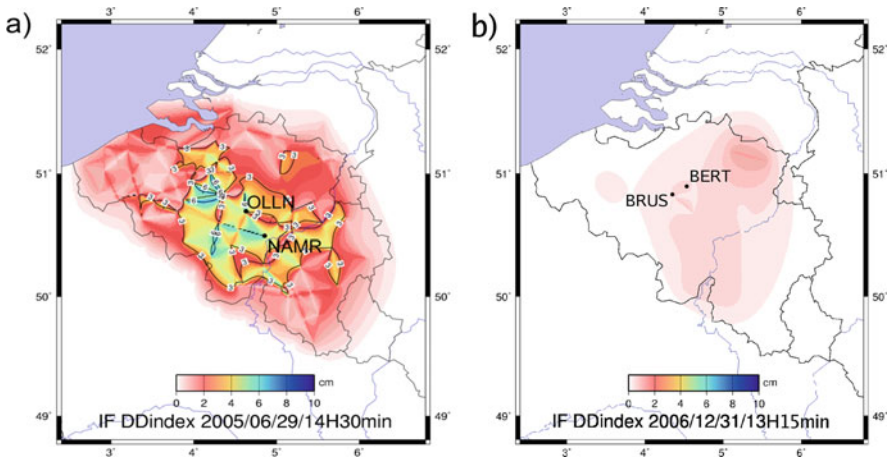

Fig. 3.17 Imaging of maximal IF DD Index detected (**a**) 29 June 2005 at 14:30 UTC; (**b**) 31 December 2006 at 13:15 UTC

Considering all the couples of satellites for a selected baseline and all the available phase measurements, the daily tropospheric activity (superposition of all the IF DD Index of the selected satellites-stations couples) can be shown (see Brenot and Warnant 2008).

Considering every baseline of the Belgian network, IF DD Index imaging are shown Fig. 3.17. In this imaging, geometric segments (each one corresponding to a baseline) are affected by the maximum IF DD Index estimated at a given moment (at 14:30 UTC on 2005/06/29 and 13:15 UTC on 2006/12/31, for the two examples presented) according to all the couples of satellites considered in our system.

Note that the rainfall cell present over OLLN station does not appear with ZTD imaging due to the time and space average. Horizontal delay gradient points a direction where the local anisotropy is maximal. However gradient represents a time and space average which punctually (at 12:30 UTC) do not show exactly the location of small-scale structure (in the north-east direction of OLLN station), as seen by IF DD Index.

The IF DD Index imaging (Fig. 3.17a) is clearly sensitive to sudden perturbation of tropospheric activity. That means sensitive to the occurrence of tropospheric small-scale structures which locally affect transmission of signals from GNSS satellites at a given epoch and not for a time and space average measurements. IF DD Index shows strong perturbations of GNSS signal propagation induced by the troposphere around OLLN station between 14:30 and 15:00 UTC (Brenot and Warnant 2008). The presence of water vapour and hydrometeors above OLLN and on the north-east side of this station, affects Double-Difference observations for OLLN-NAMR baseline the 29th June of 2005 (DOY 180). The deep convection process and the thermally driven turbulent mixing that moves air parcels from the lower to the upper atmosphere, shows a vertical extension up to 14 km close to

BRUS, MECH and BUGG stations, with occurrence of heavy rain and, for some area, hail stones at 12:20 UTC (Brenot et al. 2013).

Using a dense network of GNSS stations (e.g. the Belgian dense network with baselines from 5 to 30 km), a relevant monitoring of tropospheric structure can be established with IF DD Index. As an example of severe weather, the month of September and the start of autumn 2006 was exceptionally hot and dry. During the last days of September, sea breeze was finally bringing humidity in the warm low layer. At higher altitude, a strong dynamic was taking place with strong jets maintaining powerful forcing able to generate the sturdiest thunderstorms. The differences of wind direction from low to high levels, so called wind shear, in association with strong flux of water vapour and moistening of low level, led to a critical situation on 1st October 2006. The tropospheric activity took place during all this day, initiating locally deep convection and generating specific conditions for the establishment of supercells that can stay active during few hours.

One of these supercells has created a convenient meteorological situation for the formation of a tornado (see photography in Fig. 3.18). This supercell (associated with heavy rainfall from a cumulonimbus cloud, as seen on radar imaging on the south of Brussels in Fig. 3.19), has generated this tornado close to BRUS and LEEU stations. Taking the northeast direction after its creation and avoiding densely built area, the tornado nevertheless reached farms located along its trajectory. Several buildings have been seriously damaged. Figure 3.18b presents the probability of hail (maximum values) during the 1st October 2006 event (DOY 274). The passage of the supercell on the south side of *Brussels* can be observed. Several other supercells are also shown (wind direction oriented from south-west to north-east). Operational hail detection products are derived from the height of the freezing level and from 45 dBZ echotop values provided by single-polarization C-band weather radar (Delobbe and Holleman 2006). The supercell close to *Brussels* (BRUS station) and *Sint-Pieters-Leeuw* (LEEU station) can clearly be observed by daily IF DD Index (Fig. 3.19) applied for a baseline of 8 km.

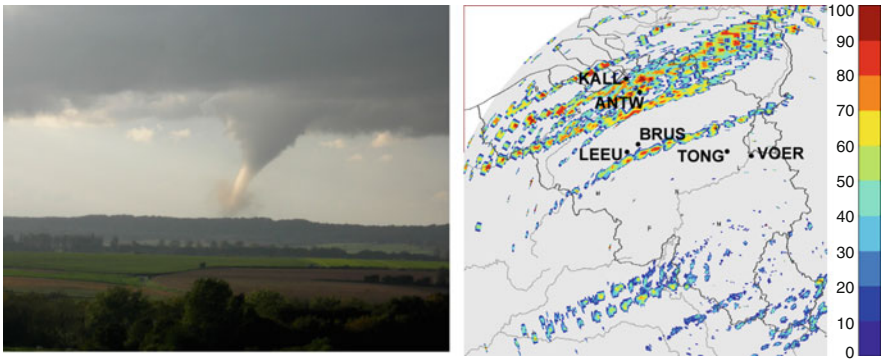

Fig. 3.18 Photography of the tornado of Petit-Roeulx-lez-Braine (source: C. De Keyser) at 16:00 UTC on 2006/10/01 (left); daily probability of hail (in %) for this day, with positions and names of 6 GNSS stations; courtesy of Laurent Delobbe (right)

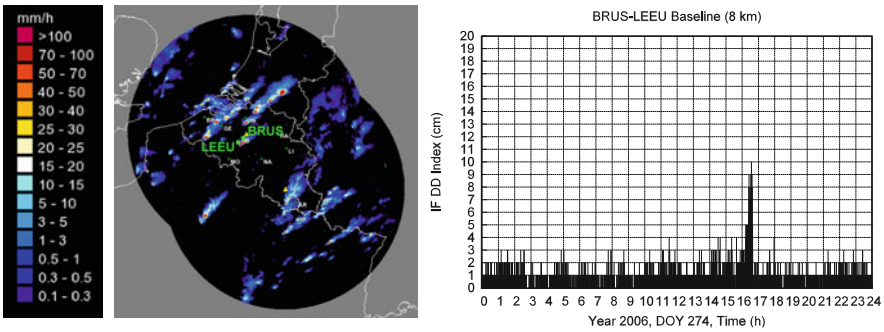

Fig. 3.19 Radar imaging on the 1st of October 2006 at 16:25 UTC (left); daily IF DD Index for BRUS-LEEU baseline (right)

Note that the tropospheric daily IF DD Index detects strong activity DOY 274 for baseline ANTW-KALL. On the other hand, a quiet tropospheric activity is observed for the baseline VOER-TONG.

The interest of looking at radar imaging of hail probability is that the possible production of hail requires an important vertical extension and a consequent amount of water vapour, linked with the existence of hydrometeors. The IF DD Index at 16:25 UTC in Fig. 3.19 shows high level of activity with Index more than 10 cm.

In Fig. 3.20, 1 h radar precipitation accumulation shows that supercells have traveled from south-west to north-east. Baselines BUGG-NIKL, BREC-HERE, DIES-MOL0, LEEU-NIVL, BRUS-NIVL, BERT-OLLN and BREE-MAAS are plotted on these radar imaging. For these baselines, IF DD Index tropospheric activities are presented in Fig. 3.21.

According to radar precipitation accumulation imaging (Fig. 3.20), the description of Fig. 3.21 (left) is the following: at about 16:00 UTC, tropospheric activity for baseline BUGG-NIKL (up to 7 cm) was occurring close to BUGG station (cell C of Fig. 3.20a). This same cell C was located then close to HERE station at about 17:00 UTC and induced an IF DD Index up to 7 cm for BREC-HERE baseline. Around 18:00 UTC, the cell B was approaching over BUGG station (in Fig. 3.20b) and inducing IF DD Index up to 10 cm for BUGG-NIKL baseline. The passage of the cell B can clearly be observed with IF DD Index presented in Fig. 3.21 between 18:00 and 19:30 UTC. Around 19:00 UTC, the cell B (in Fig. 3.20c) was above HERE station (IF DD Index up to 11 cm for BREC-HERE baseline), and at 19:20 UTC (in Fig. 3.20d) above MOL0 station (IF DD Index up to 8 cm for DIES-MOL0 baseline).

According to radar precipitation accumulation imaging (in Fig. 3.20), the description of Fig. 3.21 (right) is the following: at 16:20 UTC, tropospheric activity has taken place around LEEU and NIVL stations (IF DD Index up to 8 cm for baseline LEEU-NIVL). Between 16:30 and 17:00 UTC the supercell A has moved from south-west to east of *Brussels* (successively IF DD Index of 6 cm for BRUS-NIVL and BERT-OLLN baselines). Around 18:40 UTC, the cell A was close to MAAS station and induced IF DD Index up to 7 cm for BREE-MAAS baseline. The passage of the supercell A is clearly shown from 16:00 to 19:00 UTC on IF DD Index.

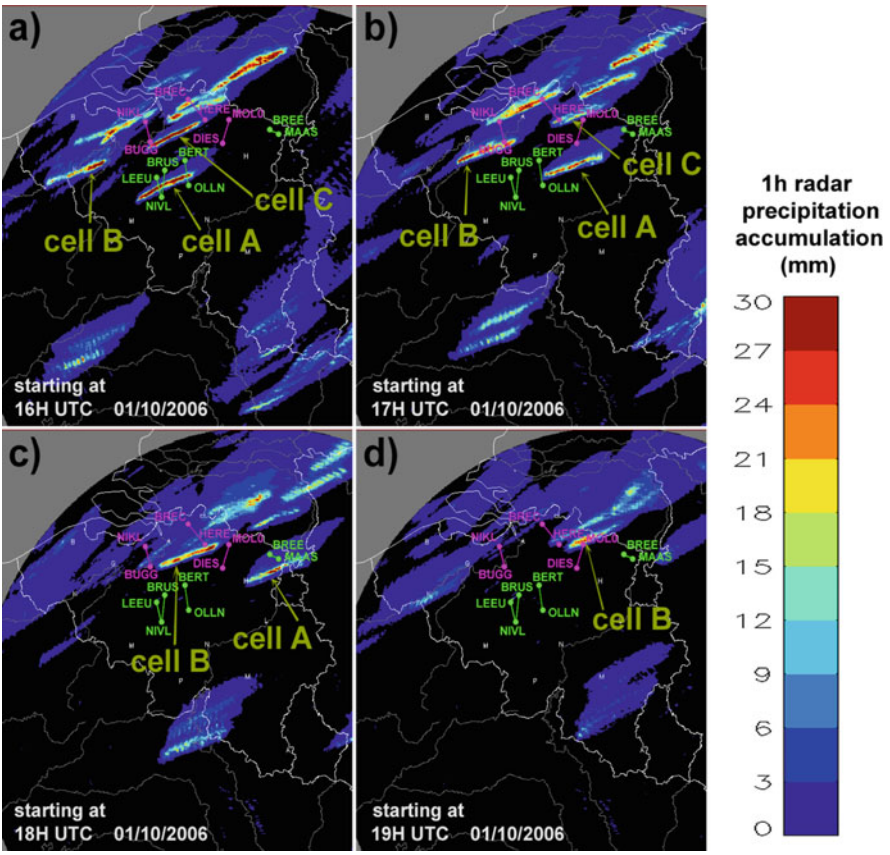

Fig. 3.20 1 h radar precipitation accumulation starting at (**a**) 16:00 UTC, (**b**) 17:00 UTC, (**c**) 18:00 UTC, and (**d**) 19:00 UTC on 2006/10/01

The contribution of hydrometeors in association with water vapour bubble to strong IF DD Index of tropospheric activity is indisputable. The blobs of water vapour surround rainfall cells with a high vertical extension (up to 10 km for cells B and C and up to 11 for cell A, as estimated by the maximum radar reflectivity from the weather radar of Wideumont).

The implementation of this index started in the frame of the GALOCAD/ESA project (2006–2008). The aim was to find relevant tropospheric and ionospheric indicators to warn the impact on NRT positioning solutions, i.e. effect in RTK-architecture for a dense network of stations (Brenot and Warnant 2008; Warnant et al. 2008, Wautelet et al. 2008; Brenot et al. 2014a, b).

To summarise, this study presents GNSS indicators of meteorological activity that allow the detection of small-scale structures in the neutral atmosphere. The scope is to present a new NRT index of meteorological activity based on double-difference of the ionosphere-free combination (so called IF DD index). Contrary to

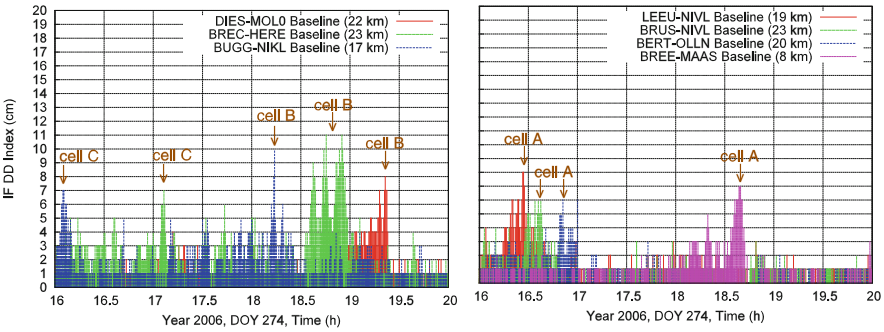

Fig. 3.21 Daily IF DD index (2006/10/01) for BUGG-NIKL, BREC-HERE and DIES-MOL0 baselines (left), and for LEEU-NIVL, BRUS-NIVL, BERT-OLLN and BREE-MAAS baselines (right)

ZTD imaging and horizontal delay gradients measurements from geodetic software (result of a mean time and space solution), the IF DD Index imaging is clearly sensitive to sudden disturbances of tropospheric activity. That means sensitive to the occurrence of tropospheric small-scale structures which locally affect couples of satellites emitted signals considered in NRT applications (i.e. GNSS meteorology or positioning) at a given epoch. The use of the IF DD Index can be planed operationally in NRT meteorological or geodetic system using dense networks, being useful for forecasters and nowcasting.

The next step of this work can be to improve the time and space imaging of the IF DD Index using multi-GNSS satellites, in collaboration with forecasters. The contribution of hydrometeors to IF DD Index need to be investigated studying correlation with radar reflectivity. The use of the geometry-free combination (GF) can also be used to define an indicator of ionospheric activity (GF DD Index). This work based on DD difference can also be transferred to of L_1, L_2 and IF combination to obtain IF Index of the tropospheric activity between a satellite and a ground-based station. As a first investigation the flash-flood event in the Gard region, on 8–9 September 2002, has been tested (Brenot et al. 2006), showing in Fig. 3.22 strong tropospheric activity when convective cells were located close to CHRN station.

3.3.5 Validation of Slant Tropospheric Delays[5]

M. Kačmařík
Institute of Geoinformatics, VŠB Technical University of Ostrava, Ostrava, Czech Republic
e-mail: michal.kacmarik@vsb.cz

[5]Parts from this section were previously published in Kačmařík et al. (2017)

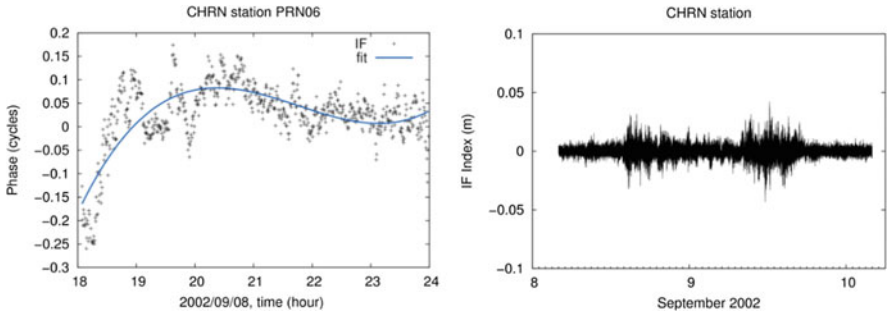

Fig. 3.22 Time-series of IF combination (GPS satellite PRN06) and its fit for CHRN station on 8–9 September 2002 (left); IF Index for all the signals emitted from satellites and recorded by CHRN on 8–9 September 2002 (right)

J. Douša
Geodetic Observatory Pecný, RIGTC, Ondřejov, Czech Republic
e-mail: jan.dousa@pecny.cz

P. Václavovic
Geodetic Observatory Pecný, Research Institute of Geodesy, Topography and Cartography, Zdiby, Czech Republic
e-mail: pavel.vaclavovic@pecny.cz

G. Dick
GFZ German Research Centre for Geosciences, Helmholtz Centre Potsdam, Potsdam, Germany
e-mail: dick@gfz-potsdam.de

F. Zus
GFZ German Research Centre for Geosciences, Potsdam, Germany
e-mail: zusflo@gfz-potsdam.de

H. Brenot
Royal Belgian Institute for Space Aeronomy, Uccle, Belgium
e-mail: hugues.brenot@oma.be

G. Möller
Department of Geodesy and Geoinformation, TU Wien, Wien, Austria
e-mail: gregor.moeller@geo.tuwien.ac.at

E. Pottiaux
Royal Observatory of Belgium, Brussels, Belgium
e-mail: eric.pottiaux@oma.be

P. Hordyniec
Wrocław University of Environmental and Life Sciences, Wrocław, Poland
e-mail: pawel.hordyniec@upwr.edu.pl

J. Kaplon
Wrocław University of Environmental and Life Sciences, Wrocław, Poland
e-mail: jan.kaplon@upwr.edu.pl

L. Morel
École Supérieure des Géomètres et Topographes, Le Mans, France
e-mail: laurent.morel@esgt.cnam.fr

Tropospheric STD represents the total delay that undergoes the GNSS radio-signal due to the neutral atmosphere along the path from a satellite to a ground receiver antenna. It is evident that STDs can provide much more information about the distribution of water vapor in the troposphere than classical ZTDs. With a continuous development of NWM forecasting and nowcasting tools a demand for high-quality humidity observations with high spatial and high temporal resolutions is growing at side of a meteorological community. On the other hand, despite a set of studies which dealt with this topic there is still not a uniform consensus on how to reconstruct STDs from GNSS processing results. Therefore, we decided to realize an extensive inter-technique validation of STDs using data from Benchmark data set and try to answer at least some of the opened questions. A summary of obtained results is given here, however, we refer the reader to the publication of Kačmařík et al. (2017) for a much more detailed presentation.

3.3.5.1 Description of STD Validation Study

From the complete Benchmark data set, we selected a subset of 10 GNSS reference stations situated at six different locations (Table 3.4). It also includes collocated (dual) GNSS stations playing an important role in the validation since they track GNSS satellites with the same azimuth and elevation angles, so that they should deliver the same or very similar tropospheric parameters used for STD reconstructions.

Seven institutions delivered their STD solutions for this validation study, namely Ecole Supérieure des Géomètres et Topographes (ESGT CNAM), Geodetic Observatory Pecný (GOP, RIGTC), Helmholtz Centre Potsdam – German Research Centre for Geosciences (GFZ), Royal Observatory of Belgium (ROB), VŠB-Technical University of Ostrava (TUO), Vienna University of Technology (TUW), and Wroclaw University of Environmental and Life Sciences (WUELS). Principal information about individual solutions are given in Table 3.5.

In total, we validated eleven solutions computed with five different GNSS processing software. Considering all available GNSS solutions, only GOP used a stochastic modelling approach to estimate all parameters. Additionally, GOP provided two solutions: (1) GOP_F using Kalman filter (forward filter only), i.e. capable of providing ZTD, tropospheric gradients and STDs in real time, and (2) GOP_S applying the backward smoothing algorithm (Václavovic and Douša 2015) on top of the Kalman filter. The latter improves the quality of all estimated parameters during

Table 3.4 Characteristics of 10 GNSS reference stations

Name	Latitude [°]	Longitude [°]	Height [m]	Network	Dual station	Receiver	Antenna
GOPE	49.914	14.786	593	IGS, EPN		TPS NET-G3	TPSCR.G3 TPSH
KIBG	47.449	12.309	877			TPS GB-1000	TPSCR3_GGD CONE
LDB0	52.210	14.118	160		LDB2	JAVAD TRE_G2T	JAV_GRANT-G3T NONE
LDB2	52.209	14.121	160		LDB0	JPS LEGACY	LEIAR25.R4 LEIT
POTM	52.379	13.066	145		POTS	JAVAD TRE_G3TH	JAV_GRANT-G3T NONE
POTS	52.379	13.066	144	IGS, EPN	POTM	JAVAD TRE_G3TH DELTA	JAV_RINGANT_G3T NONE
SAAL	47.426	12.832	796			TPS GB-1000	TPSCR3_GGD CONE
WTZR	49.144	12.879	666	IGS, EPN	WTZS, WTZZ	LEICA GRX1200 + GNSS	LEIAR25.R3 LEIT
WTZS	49.145	12.895	663	IGS	WTZR, WTZZ	SEPT POLARX2	LEIAR25.R3 LEIT
WTZZ	49.144	12.879	666	IGS	WTZR, WTZS	JAVAD TRE_G3TH DELTA	LEIAR25.R3 LEIT

Table 3.5 Information about GNSS-based STD solutions used in the validation

Solution Name	Institution	Strategy	Software	GNSS	Elev. cut-off	Mapping function	ZTD/gradients interval	Post-fit residuals
CNAM	ESGT CNAM	DD	GAMIT	GPS	3 °	VMF1	1 h/1 h	NO
GFZ	GFZ Potsdam	PPP	EPOS 8	GPS	7 °	GMF	15 min/1 h	YES
GOP_F	GO Pecný	PPP	G-Nut/Tefnut	GPS	7 °	GMF	2.5 min/2.5 min	YES
GOP_S	GO Pecný	PPP	G-Nut/Tefnut	GPS	7 °	GMF	2.5 min/2.5 min	YES
ROB_G	ROB	DD	BSW52	GPS + GLO	3 °	GMF	15 min/1 h	YES
ROB_V	ROB	DD	BSW52	GPS + GLO	3 °	VMF1	15 min/1 h	YES
TUO_R	TU Ostrava	DD	BSW52	GPS + GLO	3 °	VMF1	1 h/3 h	NO
TUO_G	TU Ostrava	DD	BSW52	GPS	3 °	VMF1	1 h/3 h	NO
TUW_3	TU Vienna	PPP	NAPEOS	GPS + GLO	3 °	GMF	30 min/1 h	YES
TUW_7	TU Vienna	PPP	NAPEOS	GPS + GLO	7 °	GMF	30 min/1 h	YES
WUE	WUELS	PPP	BSW52	GPS	3 °	VMF1	2.5 min/1 h	YES

the batch processing interval and eliminates effects such as the PPP convergence or re-convergence. Some institutions delivered also two STD solutions which differ in a single processing setting. The aim was to evaluate their impact on STDs: a) TUO_G and TUO_R exploit GPS-only and GPS + GLONASS observations respectively, b) TUW_3 and TUW_7 apply an elevation cut-off angle of 3 and 7 degrees respectively, and c) ROB_G and ROB_V use the GMF and VMF1 mapping functions respectively. Additionally, ROB solutions are the only ones based on the processing of double-difference (DD) observations and providing ZD carrier-phase post-fit residuals converted from the original DD residuals using the technique described in Alber et al. (2000).

For an independent validation of STDs from GNSS processing we used STDs derived from NWM via ray-tracing and from observations of Water Vapor Radiometer (WVR). In case of NWM derived STDs, four institutions delivered their solutions based on three different NWMs: ALADIN-CZ (4.7 km resolution, limited-area hydrostatic model, operational analysis in 6-h interval with forecasts for 0, 1, 2, 3, 5, 6 h, http://www.umr-cnrm.fr/aladin/), ERA-Interim (1° horizontal resolution, 6-h reanalysis), and NCEP-GFS (1° horizontal resolution, 6-h operational analysis, https://www.ncdc.noaa.gov/data-access/model-data/model-datasets/global-forcast-system-gfs). None of these NWM assimilates data from ground GNSS stations. For more information about the models, see Douša et al. (2016) and specifically Trojáková (2016) for the ALADIN-CZ model and Dee et al. (2011) for the ERA-Interim reanalysis. First, STD solutions using the ERA-Interim and NCEP-GFS models were delivered by GFZ Potsdam using acronym ERA/GFZ and GFS/GFZ, respectively. Two STD solutions were then delivered for the ALADIN-CZ model: (a) ALA/BIRA generated at Royal Belgian Institute for Space Aeronomy (BIRA), and (b) ALA/WUELS delivered by Wroclaw University of Environmental and Life Sciences. For a description of these solutions we refer to Kačmařík et al. (2017).

In case of WVR we used the instrument operated at GFZ Potsdam. The instrument is situated on the same roof as the GNSS reference stations POTM and POTS. The WVR is switching between ‘zenith mode’ when it is measuring IWV and ‘slant mode’ when it is tracking GPS satellites using an in-built GPS receiver. In the latter case, Slant Integrated Water Vapour (SIWV) values are delivered for the direction of satellites. Our study focuses on the comparison of STDs, not SIWV. It was thus necessary to convert the WVR SIWV into STDs. The used conversion of WVR SIWVs to STDs aimed at minimum distorting the accuracy of original WVR observations and is described in Kačmařík et al. (2017).

3.3.5.2 Introduction to STD Estimation from GNSS Observations

The tropospheric STD is being reconstructed from tropospheric parameters valid in zenith direction which are being estimated during GNSS observation processing. It can be expressed by Eq. 3.19, where ZHD and ZWD represent Zenith Hydrostatic

and Wet delay, respectively, G horizontal tropospheric gradient and *ele* is the elevation angle and *azi* is the azimuth angle of observation.

$$STD(ele, azi) = ZHD \cdot mf_h(ele) + ZWD \cdot mf_w(ele) + G(ele, azi) + RES - MPT \tag{3.19}$$

The elevation angle dependency of STD is described by the mapping functions, separately for the hydrostatic (mf_h) and the wet (mf_w) components. Additionally, post-fit residuals (RES) may contain un-modelled tropospheric effects not covered by the estimated tropospheric parameters. Obviously, residuals contain also other un-modelled effects such as multipath (MPT), however, potentially including also errors from antenna phase centre variations or systematics in satellite clocks. For eliminating such systematic effects, cleaning of post-fit residuals was applied by generating elevation/azimuth-dependent correction maps as described by Shoji et al. (2004). We thus computed mean values of post-fit residuals in 1 × 1 degree bins using the whole benchmark period for each solution and station. Computed means were then subtracted from the original post-fit residuals to generate solutions using cleaned residuals. Therefore, whenever zero-differenced (ZD) post-fit residuals were available for any solution delivered to the validation, three variants of the solution were used: (1) solution without residuals (nonRES), (2) solution with raw residuals (rawRES), and (3) solution with cleaned residuals (clnRES).

Example maps obtained with gradient estimation, polar 1 × 1 degree bins for multipath determination and 2 sigma outlier rejection threshold are presented on Fig. 3.23 for LDB0. Kapłon et al. (2017) later realized a set of tests to evaluate the impact of strategy of STDs calculation on STD differences obtained from GNSS and

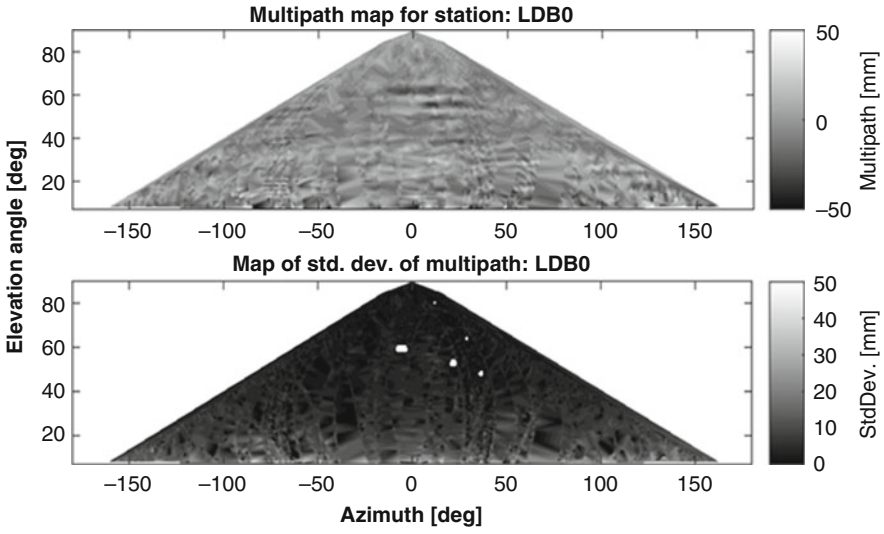

Fig. 3.23 Example equal area maps of multipath effect for LDB0 station

raytracing through the GFS NWM model including testing the impact of method of multipath effect calculation: polar degree bins (1 × 1, 2 × 2 and 5 × 5 degree) or equal area bins (Huisman et al. 2009) of 1, 2 or 5 degree height, level of outliers reduction (2 or 3 sigma) on STDs. Summarizing results of these tests, all 24 variants of multipath maps provided very similar results with a slight edge for variants using the smallest 1 × 1 degree bins.

3.3.5.3 Methodology of STD Comparisons

Since NWM outputs are restricted to the time resolution of their predictions (typically 1, 3 or 6 h) and since WVR is able to track only one satellite at one moment, all three sources provide different numbers of STDs per day. Therefore, three different comparisons were realized: (1) results for GNSS versus GNSS comparisons, (2) results for GNSS versus NWM comparisons, and (3) results for GNSS versus WVR comparisons. All the presented results were obtained over the whole benchmark period of 56 days. No outlier detection and removal procedure was applied during the statistics computation within the study. Two variants of the comparisons are presented: 'ZENITH' and 'SLANT'. 'ZENITH' stands for original STDs mapped back to zenith direction using 1/sin(ele) formula. Such mapping aimed at normalizing STD differences for their evaluation in a single unit. The 'SLANT' type of comparison denotes an evaluation of STDs at their actual elevation angles. To be more specific, STDs were grouped into individual elevation bins of 5 degrees, i.e. for example all STDs with an elevation angle between 10 and 15 degrees were evaluated as a single unit. The cut-off angle of 7 degrees was used in all GNSS versus GNSS and GNSS versus NWM comparisons. In GNSS versus WVR comparisons 15 degrees cut-off was applied to exclude problematic WVR observations from low elevation angles.

3.3.5.4 GNSS Versus GNSS: Evaluation of All GNSS Solutions Versus the Reference GNSS Solution

Individual GNSS solutions were first compared to the GFZ solution in the zenith direction (ZENITH). Figure 3.24 shows all the solutions using STDs calculated from the estimated ZTD and horizontal gradient parameters, i.e. without adding post-fit residuals. Adding raw or clean residuals, applied consistently to both compared and reference solutions, provided very similar graphs (not displayed). Colours in the Figure indicate the processing software used in individual solutions. Medians of all solutions (dotted lines in each bin) are displayed for each station in order to highlight differences among the stations. These were observed mainly as biases ranging from −3.6 mm to 0.6 mm. The better agreement between GOP and GFZ solutions could be attributed to a similar strategy of both solutions compared to others. It is particularly visible for LDB0 and POTM stations where median values over all solutions differ by −2.3 mm and − 3.6 mm, respectively. The reason for the

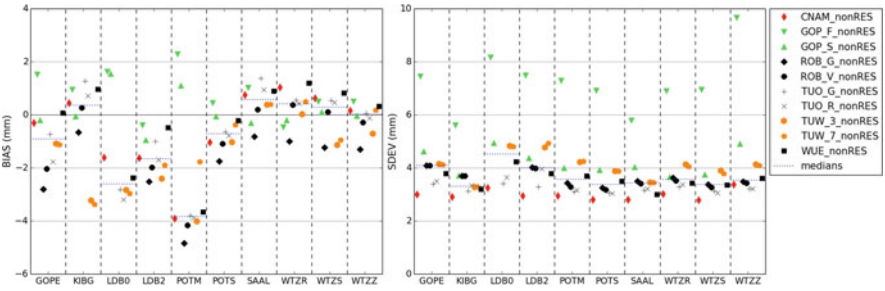

Fig. 3.24 Comparison of individual GNSS STD solutions against GFZ solution, all without using residuals (nonRES) and projected in the zenith direction: bias (left) and standard deviation (right). The median value of all solutions at each station is represented by the dotted blue line in each bin

divergent behaviour at the two stations has not been identified although site metadata were cross-checked carefully. A significant difference can also be noticed for TUW_3 and TUW_7 at the station KIBG where these solutions used individual antenna calibration files while all others solution used type mean calibration (Schmid et al. 2016). Plots with standard deviations show agreements within 3–5 mm among all the stations and all solutions. The only exception is the GOP_F solution representing a simulated real-time analysis applying only a Kalman filter (not backward smoothing) and providing results by a factor of 2 worse compared to the others in terms of precision.

3.3.5.5 GNSS Versus GNSS: Evaluation in the Slant Direction

Figure 3.25 provides an evaluation of the STDs at their original elevation angles for the station POTS. Four individual panels show bias (top left), normalized bias (NBIAS, top right), standard deviation (bottom left), and normalized standard deviation (NSDEV, bottom right). Normalized bias and normalized standard deviation were computed to see the dependence of relative errors in STDs at different elevations. For its computation, absolute differences of STDs from two solutions were divided by the STD values from the reference solution.

We found that the agreement among individual solutions compared to the GFZ STDs is rather stable above the elevation angle of 30 degrees. Corresponding biases of individual elevation bins are within ± 4 mm and standard deviations are slowly increasing up to 10 mm at 30 degrees. With elevation angles decreasing below 30 degrees the biases slightly increase for some solutions. Normalized standard deviation remains almost constant over all elevation angles indicating a very consistent relative performance of STDs among all the solutions. A similar behaviour is present at all stations although the absolute values can be higher for some stations or solutions, namely GOP_F for LDB0 and WTZZ with standard deviations reaching up to 72 mm.

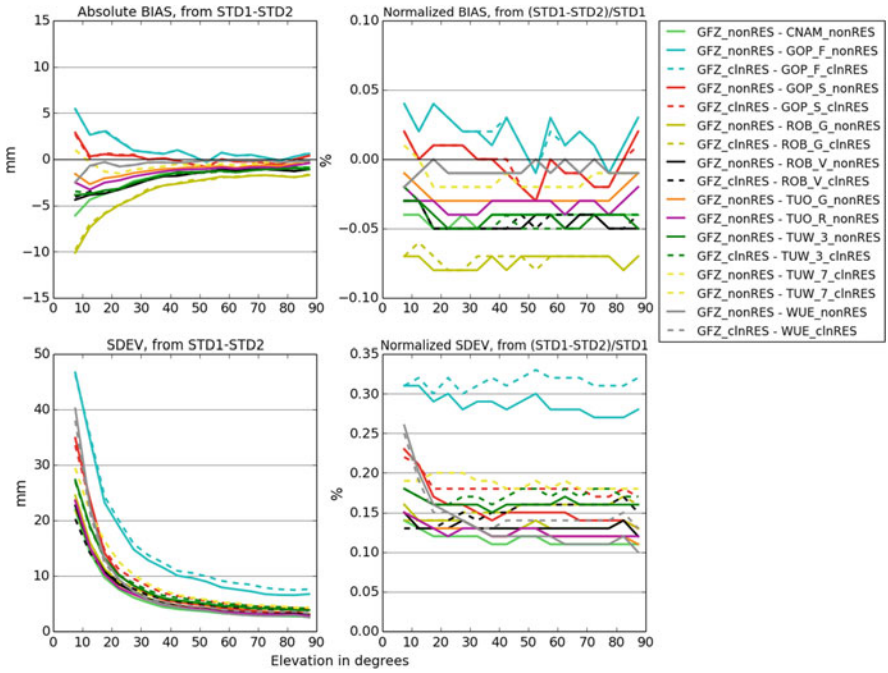

Fig. 3.25 Comparison of individual GNSS STD solutions against GFZ STD solution at station POTS, in slant directions

3.3.5.6 GNSS Versus NWM: Summary of Results

A summary of the GNSS versus NWM validation is presented in Table 3.6. For each reference station a median of bias and a median of standard deviation in the zenith direction between all GNSS solutions and a particular NWM-based solution are given. If we consider ALA/BIRA and ERA/GFZ only, without the two mountainous stations KIBG and SAAL, absolute biases between NWM and GNSS solutions stay mostly below 3 mm, which represents a very good agreement between these independent sources used for retrieving slant delays. Standard deviations generally range from 8 mm to 12 mm in the zenith projection, with an exception of ALA/WUELS showing lower precision by a factor of 2.5.

3.3.5.7 GNSS Versus WVR: Summary of Results

A bias of about 5.5 mm in the zenith direction was found between WVR and GNSS solutions at station POTS while the bias at station POTM was around 10 mm. The difference between stations POTM and POTS are probably related to issues with GNSS data processing at POTM. The bias between POTS and WVR roughly corresponds to 1 kg/m^2 of IWV, what can be addressed as the achievable accuracy

Table 3.6 Medians of bias and standard deviation values of differences between all GNSS solutions and a particular NWM-based solution at each reference station, expressed in the zenith direction

Station	Bias (mm)				Standard deviation (mm)			
	ALA/ BIRA	ERA/ GFZ	GFS/ GFZ	ALA/ WUELS	ALA/ BIRA	ERA/ GFZ	GFS/ GFZ	ALA/ WUELS
GOPE	0.3	3.3	8.6	11.5	8.3	10.3	7.1	22.4
KIBG	−19.3	4.9	9.6	22.5	11.6	17.8	11.0	26.7
LDB0	−2.0	0.7	5.5	10.6	9.9	10.3	8.5	26.2
LDB2	−1.6	0.9	6.1	15.1	9.1	10.1	8.6	25.4
POTM	3.4	6.3	12.5	18.9	8.0	10.6	9.4	26.2
POTS	−1.7	1.4	7.6	12.5	7.7	10.3	9.2	25.8
SAAL	−19.4	7.8	11.7	24.3	12.7	17.9	11.8	22.9
WTZR	−4.8	−1.5	4.9	10.2	11.0	11.8	8.5	23.1
WTZS	−3.5	−0.9	4.2	10.8	11.4	12.3	8.7	23.7
WTZZ	−2.1	0.9	6.0	11.6	11.3	12.0	8.9	23.7

of any technique, however, WVR accuracy is more dependent on a proper instrument calibration. Values of standard deviation around 12 mm in the zenith direction, were higher than those observed in GNSS versus GNSS comparisons and slightly higher than from GNSS versus NWM comparisons.

3.3.5.8 Results at Collocated Stations

For the GNSS versus NWM and GNSS versus WVR comparisons at individual stations slightly higher values of standard deviations were always found for GNSS solutions applying raw or cleaned residuals in contrast to versions of solutions without any residuals (Kačmařík et al. 2017). However, since two erroneous techniques were always confronted to each other without knowing the true reference, these results do not tell anything about potential of post-fit residuals.

For these reasons, we assessed all GNSS solutions at the collocated (dual) stations because for them we are able to provide troposphere-free differences of STDs to evaluate noise of GNSS STD retrievals. Dual stations were available in the benchmark campaign at three different locations in Germany. The first two sites collocate twin GNSS reference stations (LDB0 + LDB2 and POTM+POTS), the third location collocate three individual reference stations (WTZR+WTZS+WTZZ).

During normal weather conditions, the tropospheric variation is reasonably smooth, meaning it can be well represented by GNSS STDs reconstructed only from ZTDs and horizontal gradients. However, during high temporal or spatial variabilities in the troposphere, post-fit residuals certainly contain tropospheric signals which are not modelled. If they surpass the observation noise and other residual errors from GNSS models, cleaned residuals should be considered in the GNSS STD model as described in Eq. 3.19. In order to initially address optimal STD modelling under different weather conditions within the benchmark, we tried to

identify days with a high variability in the troposphere. Daily standard deviations of cleaned post-fit residuals were computed individually for each day of the benchmark, for every station and GNSS solution for 1-degree elevation angle bins. We studied their daily variations considering the GNSS model applied. If cleaned post-fit residuals consist of the noise of observations only, the variation in time should be negligible. However, the days showing significantly higher values, correlated at collocated stations, indicated highly variable tropospheric conditions.

Three such days were identified at LDB0, LDB2, POTM and POTS stations (May 31, June 20, June 23) and 2 days at WTZR and WTZS stations (June 19, June 20). They all very well correspond to the days initiating heavy precipitations in the domain, Douša et al. (2016). Typical differences between raw and clean residuals are displayed in Fig. 3.26 for all elevations during the normal day (June 19, DOY 170) and the following day with high variability in the troposphere (DOY 171, June 20) for POTM and POTS stations using GFZ solution. Obviously, the variability of clean residuals (black dots) and their 2-sigma envelops are higher by a factor of two for the day of year 171 compared to 170. The variability is clearly visible over all elevations, but the increase is slightly higher at low elevations. The plot demonstrates the different quality of GNSS observations, particularly related to a multipath effect displayed by 2-sigma envelop (green curves). The multipath level is much lower for station POTS which is using a choke ring antenna compared to station POTM which is not using a choke ring. The similar situation was found for stations LDB0 and LDB2. Variability of 2-sigma envelopes of clean residuals (red curves) indicates a higher sensitivity of clean residuals to the weather conditions compared to station selection and observation quality, thus suggesting a significant

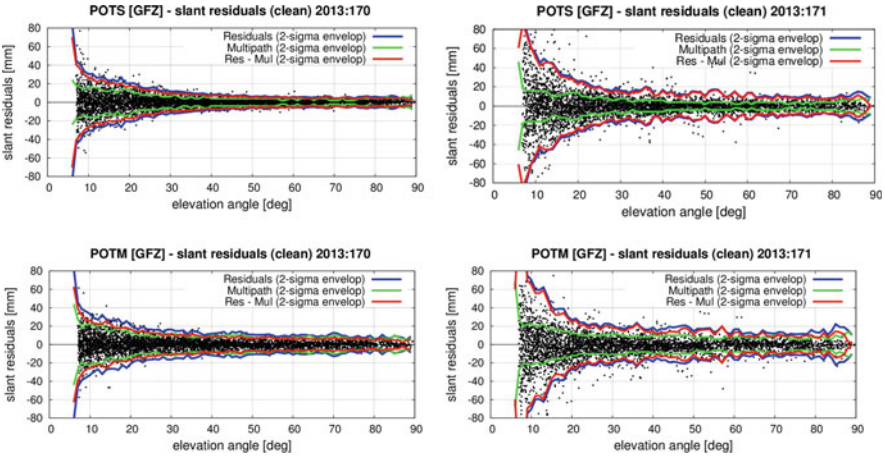

Fig. 3.26 Comparison of individual GNSS STD solutions against GFZ STD solution at station POTS, in slant directions. Elevation-dependent variability of clean residuals (black dots) and their 2-sigma envelops (red curves) are showed for June 19 (DOY 171) and June 20 (DOY 170) and stations POTS and POTM. Additionally, plots display 2-sigma envelopes for raw residuals (blue curves) and multipath (green curves)

contribution from the troposphere to the cleaned residuals. In the same context, raw residuals show much higher sensitivity to the observation quality compared to different weather conditions, which is particularly true in case of LDB0 and LDB2 stations.

In a next step elevation-dependent differences of STDs from all three versions (without residuals, with raw residuals, with clean residuals) were analysed for days with high and low variability of residuals. We noticed following:

(a) STD differences are more or less similar for both days, i.e. no significantly different between days with normal and high variations in the troposphere. It suggests that increased residuals contain strong contributions from the tropospheric effect that could not have been assimilated into ZTDs and tropospheric horizontal gradients
(b) STD differences using raw residuals were always the largest ones and they varied with the elevation angle,
(c) relative performance of differences from STDs with clean residuals and without residuals for different days remained similar. Uncertainties of the simplified STDs at low elevations surpassed additional uncertainties due to applying clean residuals. According to the magnitude of clean residuals at low elevations (Fig. 3.26), the small uncertainties from calculated differences indicated the presence of tropospheric signals in the residuals at low elevations, roughly below 30 degrees. It seemed to be almost independent from the weather conditions and is supposed to represent mainly unmodelled horizontal asymmetry in the troposphere.

Figure 3.27 displays results for comparisons of individual collocated stations in slant directions calculated from all days of the benchmark. The same statistics and plots (not displayed) were prepared also for days identified with 'severe' weather conditions, but only minor differences were observed. Strong variations are observed mainly in normalized biases over all elevation angles for the solutions using raw post-fit residuals (rawRES) regardless weather conditions. These are clearly related to local effects such as multipath or modelling instrumented related effects (phase centre offsets and variations) and disappear after using the cleaned residuals (clnRES). The standard deviations and normalized standard deviations at all stations are clearly the lowest for variants without using post-fit residuals (nonRES), slightly higher using cleaned residuals, and significantly higher when using raw residuals, i.e. corresponding to above performed inter-technique validations.

3.3.5.9 Future Work

Three institutions (GFZ, GOP, ROB) delivered GNSS STD solutions not only for the ten GNSS reference stations but for the whole GNSS network within the Benchmark data set. Our future study will therefore focus on (a) larger comparison within the network of stations, (b) an evaluation of azimuthal dependency of post-fit

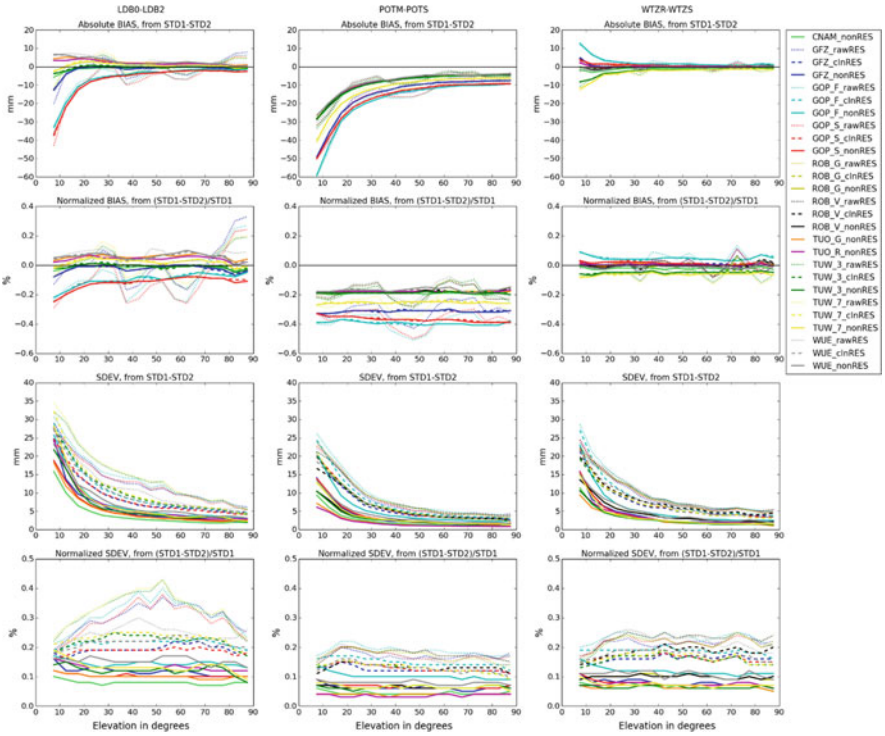

Fig. 3.27 Comparison of GNSS STDs at dual stations computed over whole benchmark period from individual GNSS solutions in the slant direction for dual stations from left to right: LDB0-LDB2, POTM-POTS, WTZR-WTZS. Statistical parameters from top to bottom: bias, normalized bias, standard deviation, normalized standard deviation

residuals under severe weather conditions and (c) an evaluation of GNSS STDs estimated from real-time and post-processed solutions using a stochastic approach.

3.3.6 Information Content in Post-fit Residuals, PPP vs DD Approach[6]

G. Möller
Department of Geodesy and Geoinformation, TU Wien, Wien, Austria
e-mail: gregor.moeller@geo.tuwien.ac.at

Based on real GNSS measurements, the tropospheric signal in post-fit residuals is difficult to assess since it is superimposed by a series of other unmodelled effects like

[6]Parts from this section were previously published in Möller (2017)

observation noise, multipath, satellite clock or orbit errors. Nevertheless, observation stacking methods as applied in (Kačmařík et al. 2017; Möller 2017) allow for the reduction of common parts like multipath or clock errors, but only when longer time periods or larger GNSS networks are processed. Hence, within the COST action an initiative was carried out which addresses the general tropospheric signal in GNSS post-fit residuals, with focus on differenced data processing.

Theoretically, the precise point positioning (PPP) and the double difference approach (DD) are equivalent with respect to redundancy and with respect to the estimates, in case a correct stochastic model is introduced. Practically, the DD approach has some advantages in data processing since the satellite and receiver clock errors and therewith the hardware biases cancel out, which allows the fixing of integer ambiguities. Further, also the pre-processing is less critical since the receiver clock error has to be known only with μs-accuracy.

Unfortunately the greatest strength of double-difference processing, the elimination of common effects, is also a shortcoming at the same time in small networks (< 500 km). In such networks, tropospheric parameters cannot be estimated in an absolute sense but rather with respect to a reference station. Therefore, reference values (station coordinates and ZTD) have to be introduced, at least for one station, and constrained to their given values. Then the tropospheric parameters can be estimated like in PPP processing, except for the reference station. In order to analyse satellite or station specific effects in double-difference residuals (DDR), the residuals have to be converted into zero-difference residuals (ZDR), also known as pseudo-ZDR since certain conditions have to be applied for the reconstruction. (Alber et al. 2000) suggested a two-step approach in which the DDR vector is converted into a pseudo-ZDR vector, assuming zero-mean conditions.

In order to analyse the applicability of this approach and in general of the tropospheric signal in DDR, two sets of dual-frequency GPS observations were simulated for 12 stations in Austria. Both sets differ only with respect to the applied troposphere model. While no troposphere model was applied to the first set of observations, ZTDs and East-West gradients were simulated for the second set.

The observations of all 12 stations were processed in PPP and double-difference approach. If both, ZTD and gradients are estimated, the simulated STD could be recovered with sub-mm accuracy and the post-fit residuals became negligible. If only the ZTD is estimated, it is expected that an anisotropic delay remains in the post-fit residuals. It turned out that in case of PPP methods the anisotropic delay, except for a small offset which was absorbed by the ambiguity parameter, could be recovered from the PPP post-fit residuals but unfortunately not from the DDR. If only a single baseline is processed, the DDR and also the reconstructed pseudo-ZDR are almost zero since the anisotropic effects were differenced out in data processing. In best case, the resulting STD bias and standard deviation was −1 mm +/−37 mm. This was obtained by fixing the ZTD and by taking all possible baselines between the 12 stations into account for the reconstruction of pseudo-ZDR using the method proposed by (Alber et al. 2000). However, a comparable result (0 mm +/−38 mm) is obtained if no residuals are added to the isotropic STD.

In practice, the ZTD is not known and therewith cannot be fixed to its given value. Thus an additional solution was created whereby ZTD but no gradient parameters were estimated. This results in an increase of bias and standard deviation (84 mm +/− 105 mm). This example underscores the importance to estimate gradient parameters in addition to ZTDs. An unmodelled east-west gradient of 2 mm introduced a ZTD error of 35 mm +/− 13 mm. For more details the reader is referred to (Möller 2017).

It becomes obvious that the applied reconstruction method proposed by (Alber et al. 2000) is less suited for the reconstruction of pseudo-ZDR in small networks. The reconstructed values are mostly too small. In addition, jumps appear in the time series every time a satellite rises or sets. The magnitude of the jumps can be reduced by downweighting of low elevation satellites; however, the reconstruction process cannot be significantly improved therewith. In consequence, for analysis of satellite or station specific effects in post-fit residuals we recommend undifferenced GNSS data processing strategies, especially in small GNSS networks.

3.3.7 Tropospheric Parameters from Multi-GNSS Analysis[7]

P. Václavovic
Geodetic Observatory Pecný, Research Institute of Geodesy, Topography and Cartography, Zdiby, Czech Republic
e-mail: pavel.vaclavovic@pecny.cz

J. Douša
Geodetic Observatory Pecný, RIGTC, Ondřejov, Czech Republic
e-mail: jan.dousa@pecny.cz

Nowadays, multi-GNSS offers new satellites and signals which are expected to strengthen all estimated parameters, in particular the ZTD and horizontal linear tropospheric gradients, or to densify slant tropospheric delays for monitoring the troposphere asymmetry at individual GNSS sites. Currently, data from the US NAVSTAR Global Positioning System (GPS) and the Russian GLONASS constellation are commonly used to produce different products within scientific services. Essential models for these two systems has been already established, and their mutual combination provides better precision then the processing from any standalone system. Besides others, limitations for the use of GNSS data from other global systems, the European Galileo and the Chinese BeiDou, persist mainly in (1) incompleteness of the constellations, (2) lack of precise models and calibrations for new signals, receiver and satellite instrumentations, and (3) lack of precise orbit and clock products supporting the ultra-fast processing mode. The situation will

[7]Parts from this section were previously published in Douša et al. (2018a).

change soon as both global systems will become operational in next years and the IGS Multi-GNSS Experiment (MGEX, http://mgex.igs.org, Montenbruck et al. 2017) is continuously filling the gaps in data, metadata, models, formats, standards and products for an optimal exploitation of all global satellite constellations and their regional augmentations.

3.3.7.1 Evaluation of Results from Collocated GNSS Stations

The impact of using multi-constellation data on the tropospheric parameter estimation can be optimally assessed using closely collocated GNSS stations, e.g. within few meters. Although different instrumentation-specific effects, such as phase centre modelling and the quality of a receiver tracking, can affect analyses at both stations, the station should principally observe the same tropospheric delays. For the purpose of our evaluation, we selected two IGS station pairs, ZIM2-ZIMJ (Zimmerwald, Switzerland) and MAT1-MATE (Matera, Italy), all collecting data from GPS, GLONASS and Galileo systems within 10 m and 2.5 m in horizontal and vertical distances, respectively. We used the GFZ MGEX (GBM) product (Deng et al. 2017) and CODE MGEX (COM) product (Prange et al. 2017) as multi-GNSS reference solutions for the comparison. We assessed not only the impact of using more constellations but also the impact of different strategies for the parameter estimation. The first approach is the Kalman filter usable mainly for real-time, and the second strategy is the backward smoothing designed for improving the precision of parameters in post-processing (Václavovic and Douša 2015).

Solutions improved by introducing multi-constellations and the backward smoothing are demonstrated in the time series of ZTD and horizontal gradient differences obtained from the two collocated stations, ZIM2 and ZIMJ, Fig. 3.28. Results of the single−/multi-constellations are visualized by different colours: (1) standalone GPS in red, (2) GPS + GLO in green, and (3) GPS + GLO + GAL in blue. A positive effect is visible for all parameters, and is similar using both the Kalman filter and the backward smoothing, i.e. for both real-time and post-processing strategy. Scatters of multi-constellation solutions are smaller compared to the standalone GPS solution. More significant effect is visible for the smoothed gradient parameters. Theoretically, zero differences are expected for the collocated stations with the same antenna height. However, a vertical difference between ZIM2 and ZIMJ is about 2 m which can cause about 0.5 mm difference in ZTDs when considering the pressure decreases approximately by 11.3 Pa/m near the geoid and the 100 Pa difference in the atmospheric pressure causes a 2.27 mm difference in ZHD (Saastamoinen 1972). As we observe a ZTD difference about 2–3 mm, it can be still attributed to remaining station-specific systematic errors, e.g. such as phase centre offset and variation models.

Numerical statistics (biases and standard deviations) characterize an impact of single- and multi-constellation solutions on the estimated ZTDs and horizontal linear gradients when using the Kalman filter, Table 3.7. It should be noted, that GLONASS (R) and Galileo (E) observations were down-weighted by a factor of

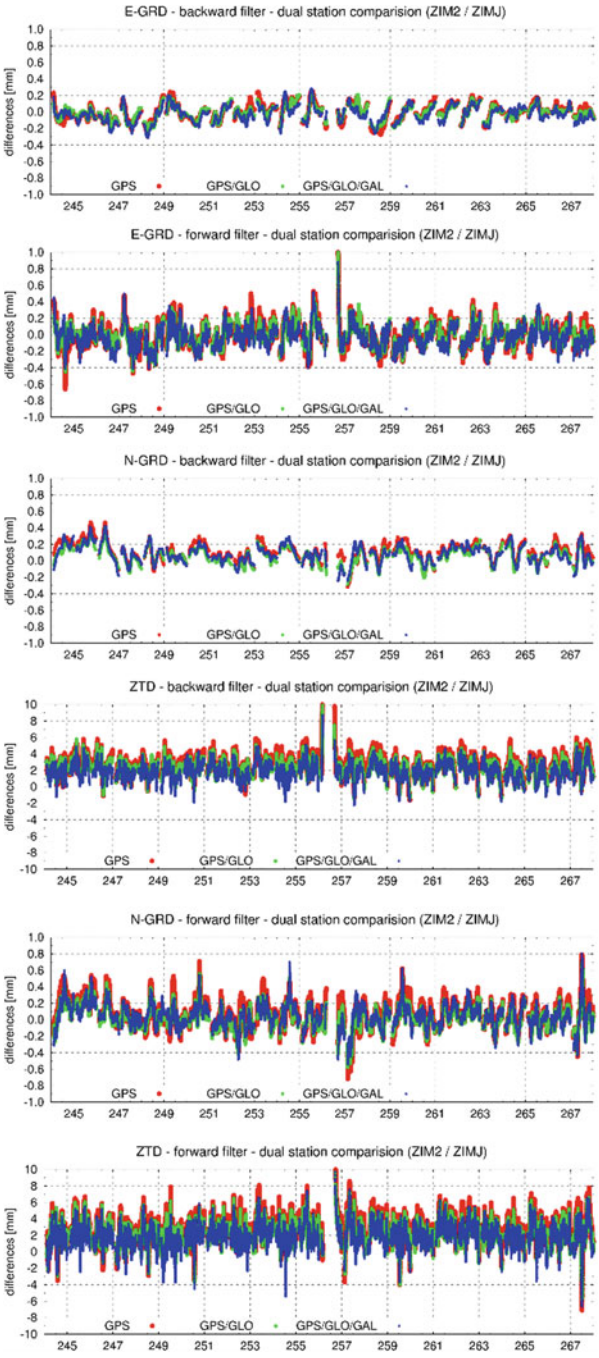

Fig. 3.28 Time series of ZTD (top), north gradient (middle) and east gradient (bottom) differences at Zimmerwald dual-station when using the Kalman filter (left) and the backward smoothing (right)

Table 3.7 Statistics (BIAS ± SDEV) for Kalman filter using GPS (G), GLONASS (R) and Galileo (E)

Station pair	GNSS	BIAS ± SDEV ZTD [mm]	BIAS ± SDEV N-GRD [mm]	BIAS ± SDEV E-GRD [mm]
ZIM2-ZIMJ	G	+2.8 ± 1.4	+0.08 ± 0.17	−0.02 ± 0.14
ZIM2-ZIMJ	GR	+2.4 ± 1.3	+0.02 ± 0.14	−0.02 ± 0.12
ZIM2-ZIMJ	GRE	+2.0 ± 1.3	+0.03 ± 0.14	−0.04 ± 0.13
MAT1-MATE	G	−0.5 ± 2.4	−0.03 ± 0.18	+0.18 ± 0.25
MAT1-MATE	GR	+0.1 ± 2.3	+0.01 ± 0.15	+0.14 ± 0.22
MAT1-MATE	GRE	+0.1 ± 2.2	+0.00 ± 0.15	+0.13 ± 0.21

2 with respect to GPS (G) to reflect lower accuracy of precise products and models. A positive effect of multi-constellation is visible at all parameters, and particularly in terms of the standard deviation, while the impact of GLONASS is more significant compared to Galileo. It is expected due to a lower number of operational Galileo satellites as well as longer support of GLONASS with precise models and products in the scientific community. As already discussed, ZIM2-ZIMJ differences indicate a bias of about 2–3 mm in ZTD which has been decreased partly in multi-GNSS solutions. The improvements in all parameters reached 15–30% in terms of RMSE at both dual-stations. Table 3.8 then shows the impact of the backward smoothing on all solutions using single- or multi-constellation data. All the above mentioned characteristics are similar to the Kalman filter, and the backward smoothing then improved mainly standard deviations (by about 25%).

3.3.7.2 Carrier-Phase Post-fit Residuals and Slant Delays

Figure 3.29 shows the carrier-phase post-fit residuals when using the Kalman filter PPP (left) and the backward smoothing PPP (right) for multi-GNSS solutions supported with the COM (top) and GBM (bottom) MGEX products. The carrier-phase residuals are useful indicators of an overall performance of the solution including the quality of input products and models. Showing plots for the ZIM2 station only, below discussed characteristics are common to other stations too. First, we observe a common elevation-dependent pattern of characteristics of post-fit residuals when using elevation-dependent observation weighting. Second, the backward smoothing does not change the distribution of the carrier-phase post-fit residuals significantly. The main effect of the backward smoothing is thus understood mainly as improved accuracy of the estimated parameters. The tropospheric slant delays reconstructed from the model parameters and post-fit residuals will thus

Table 3.8 Statistics (BIAS ± SDEV) for backward smoothing using GPS (G), GLONASS (R), Galileo (E)

Station pair	GNSS	BIAS ± SDEV ZTD [mm]	BIAS ± SDEV N-GRD [mm]	BIAS ± SDEV E-GRD [mm]
ZIM2-ZIMJ	G	+2.7 ± 1.1	+0.11 ± 0.12	−0.02 ± 0.10
ZIM2-ZIMJ	GR	+2.3 ± 1.0	+0.06 ± 0.11	−0.02 ± 0.09
ZIM2-ZIMJ	GRE	+1.9 ± 1.0	+0.07 ± 0.12	−0.04 ± 0.09
MAT1-MATE	G	−1.3 ± 1.6	−0.04 ± 0.15	+0.22 ± 0.19
MAT1-MATE	GR	+0.6 ± 1.4	+0.00 ± 0.12	+0.16 ± 0.17
MAT1-MATE	GRE	+0.5 ± 1.4	−0.01 ± 0.11	+0.16 ± 0.16

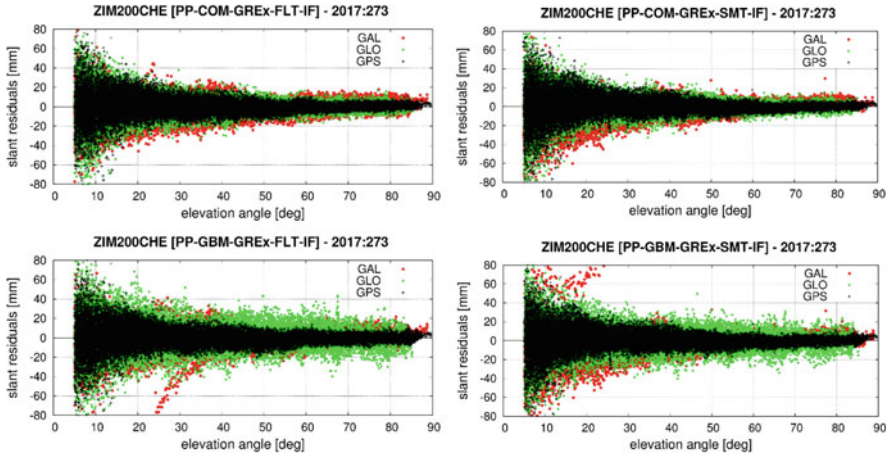

Fig. 3.29 Carrier-phase post-fit residuals from the Kalman filter (left) and the backward smoothing (right)

benefit primarily from the improvement of the parameters. Third, the GPS residuals (black) are the smallest and compact compared to other systems indicating actual quality of precise models and products. Galileo shows the largest residuals, however, we had to substitute various precise models, in particular station antenna phase centre offsets and variations by using the values from GPS models. Due to the same reason, we may notice systematic changes in the elevation-dependent redistribution of Galileo residuals (red) after applying the backward smoothing. Fourth, we can notice about twice larger post-fit residuals GLONASS (green) when using the GBM product compared to the COM product. As the characteristics are common to all the stations, it indicates a lower quality of GLONASS orbits and clocks from the

GBM product or some inconsistent models used for the product generation and in the PPP software.

3.3.8 *Multi-GNSS Solutions and Products*

Z. Deng
GFZ German Research Centre for Geosciences, Potsdam, Germany
e-mail: deng@gfz-potsdam.de

GPS PWV is considered to have observation noise of about 1~2 mm, but GPS PWV sometimes shows larger noise and jumps for some stations and/or at certain times, suggesting that a lower number of GPS satellites and poor line-of-sight condition limits the quality of ZTD estimates in such stations and at such times. Many GPS networks are now being upgraded to multi-GNSS observation networks, and this upgrade is expected to be beneficial for GNSS tropospheric monitoring. The IGS network is being upgraded to be capable to observe multi-GNSS (GPS, GLONASS, Galileo, BeiDou and QZSS) signals. GFZ has started to provide multi-GNSS orbit and clock for all the constellations (GBM) since middle 2014 (Fig. 3.30).

To validate ZTD results from a global GPS-only and multi-GNSS analysis we processed multi-GNSS station data from the global ground tracking MGEX-network (Fig. 3.31) spanning a 3-month time period from December 2014 to February 2015. Color indicates maximum number of satellites available in addition to GPS per observation epoch.

Multi-GNSS and GPS-only global network solutions were generated to study the impact of including additional GNSS on estimated ZTD. ZTD difference time series

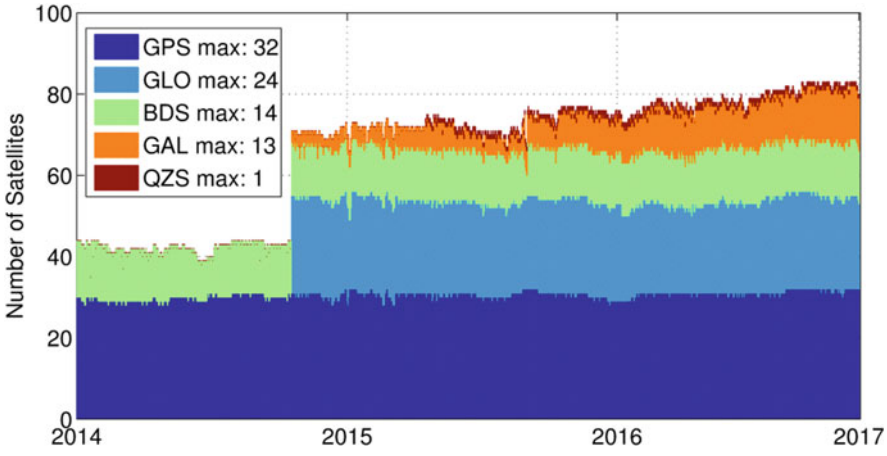

Fig. 3.30 Number of satellites per GNSS constellation included in the global multi-GNSS observation data processing

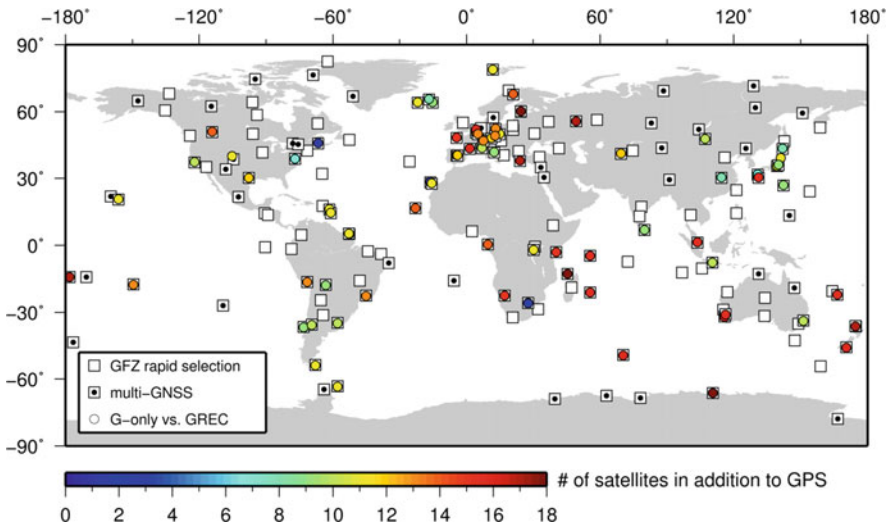

Fig. 3.31 Site selection for multi-GNSS processing derived from pre-defined sites associated to GFZ Rapid routine solution

were computed for sites which provided multi-GNSS observation data. Dots depict sites suitable for comparing GPS-only versus multi-GNSS (GREC) results. Figure 3.32 shows the mean bias of the resulting ZTD differences which varies in the range of ±1.5 mm. No specific latitude or longitude dependency could be identified. Moreover, there is no obvious correlation between the magnitude of the bias and the number of additional satellites used to estimate the ZTDs (compare to Fig. 3.31). Figure 3.33 shows associated standard deviations derived from the ZTD difference time series with values below 3.5 mm (Deng et al. 2015).

ZTDs estimated with multi-GNSS processing are more stable than those based on GPS only. Sudden jumps observed in GPS-only ZTD are significantly reduced with the multi-GNSS processing. Because the number of satellites in multi-GNSS solution is more than twice that of only GPS observation, the noise due to rising and setting satellites is mitigated thus reducing the size of sudden jumps in ZTD.

3.4 PPP and Ultra-Fast GNSS Tropospheric Products

A majority of E-GVAP ACs till now uses a double-difference observation processing in the network solution. This strategy eliminates clock errors at GNSS receiver and satellite while public products were not available in near real-time (NRT). The situation has changed in 2012, when the IGS introduced the Real-Time Service (RTS, http://rts.igs.org) providing GPS and GLONASS orbit and clock corrections by combining contributions from several IGS real-time analysis centres

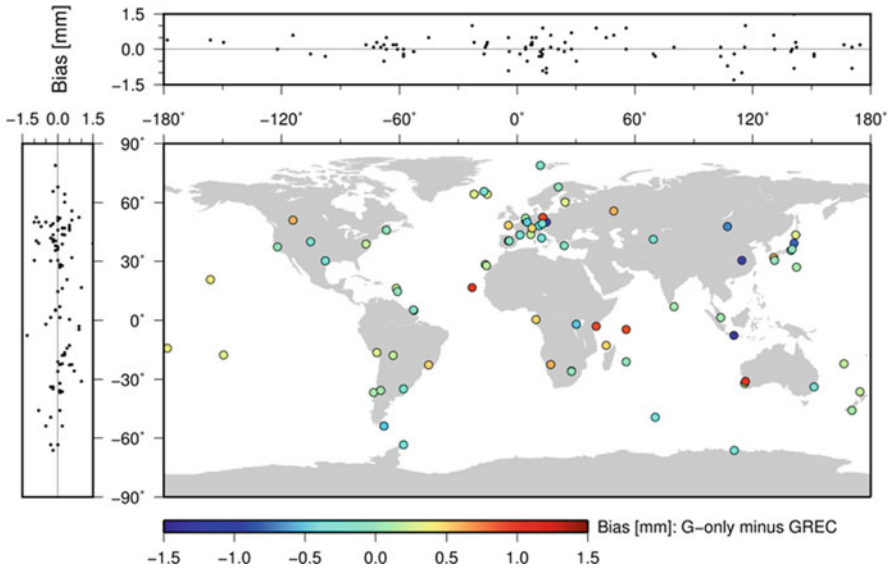

Fig. 3.32 Mean bias for zenith total delay estimates between GPS-only and multi-GNSS (GRCE) solution. Differences are shown only for those sites actually providing multi-GNSS observation. Left and top subfigures show mean bias distribution w.r.t. latitude and longitude, respectively

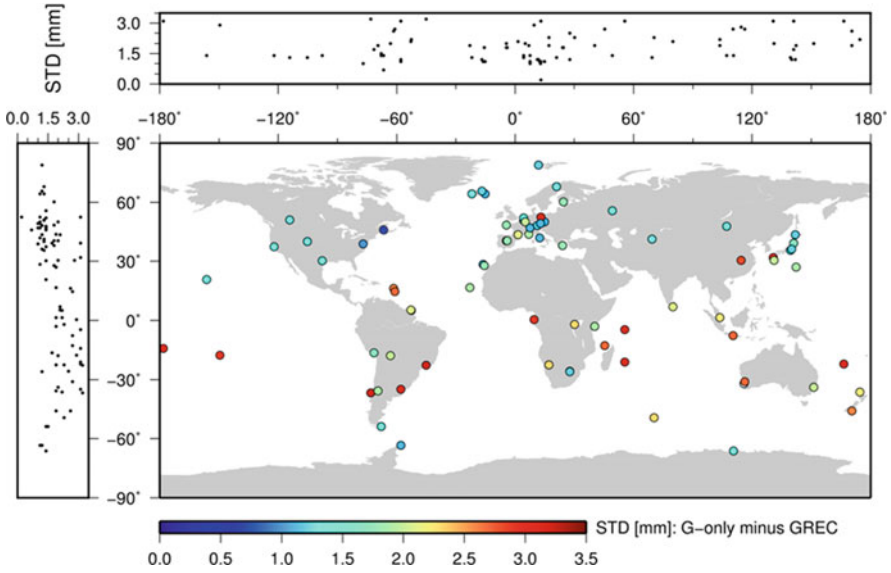

Fig. 3.33 Shows associated standard deviations (StDev) derived from the ZTD difference time series with values below 3.5 mm. In contradiction to the biases, the STDs reveal a small latitude dependency with larger magnitudes for sites below the equator

(Caissy et al. 2012). The IGS RTS aims at supporting real-time (RT) analyses with the Precise Point Positioning (PPP) method (Zumberge et al. 1997). The PPP is based on original observations or their linear combination without differencing between receivers or satellites. Though German Research Centre for Geosciences (GFZ) has provided a NRT PPP ZTD product (Dick et al. 2001; Gendt et al. 2004) since 2001, it was possible only thanks to their two-step processing approach consisting of (1) a global NRT solution for determining consistent satellite clock and orbit products and (2) a distributed PPP processing for ZTD estimated for each station individually. With the availability of global real-time data flow, software and standards specified for precise product dissemination, the PPP is becoming more popular for the troposphere monitoring.

Compared to the traditional approach in E-GVAP dominated by the double-difference network processing, the PPP offers several advantages: (a) an easy production in real-time or NRT fashion, (b) flexible use of central or distributed processing scheme including a receiver built-in solution, (c) an estimation of tropospheric parameters in the absolute sense with a high spatio-temporal resolution, and (d) an optimal support of all satellite constellations and new signals including multiple frequencies; all profiting from a highly efficient and autonomous processing approach. The price for mentioned advantages is however paid by several disadvantages. Compared to the strategy using double differences, all observation models need to be carefully applied to reach the best accuracy. In addition, integer ambiguity resolution is possible only if precise observation phase biases are available, thus often non-integer-fixed ambiguities are usually estimated.

3.4.1 Real-Time Data and Product Dissemination

Y. Altiner
BKG, Federal Agency for Cartography and Geodesy, Frankfurt, Germany
e-mail: yueksel.altiner@bkg.bund.de

W. Söhne
BKG, Federal Agency for Cartography and Geodesy, Frankfurt, Germany
e-mail: wolfgang.soehne@bkg.bund.de

A. Stürze
BKG, Federal Agency for Cartography and Geodesy, Frankfurt, Germany
e-mail: andrea.stuerze@bkg.bund.de

PPP is a method for high accuracy positioning using observations from a single GNSS receiver, suited for both, real-time and post-processing implementations. Traditionally, PPP is an idea of a post-processing technique for efficient evaluation of GNSS data from large scale networks. But it also enables a real-time positioning for stable (static) and movable (kinematic) objects with an accuracy of centimeter and sub-decimeter level, respectively. The fundamental advantage of PPP is that the

number of simultaneously observed stations within a global network can be significantly increased without decrease in accuracy of station coordinates.

This benefit and the short duration of data processing has given the PPP method popularity to be used it efficiently also in the field of climate research, in particular to support weather forecasting techniques for medium or large scale areas. Using PPP, estimation of coordinates for positioning and determination of ZTD is possible every second (real-time PPP). However, for PPP in real-time some parameters, such as precise satellite coordinates (orbit), earth orientation parameters, and satellite clock corrections are needed from an external source, e.g., available online from the IGS RTS.

The IGS RTS is generating and providing the variables of the SSR related to the orbits and clocks of GNSS satellites, an indispensable essential for real-time PPP (http://www.igs.org/rts). The RTS products created by several analysis centres contain GNSS satellite orbit and clock corrections to the broadcast ephemeris. Orbit corrections are provided as along-track, cross-track and radial offsets to the Broadcast Ephemeris in the ECF reference frame (Earth-centred and Earth-fixed). RTS corrected orbits are expressed within the ITRF implemented during the real-time GNSS observations. Clock corrections are expressed as offsets to the Broadcast Ephemeris satellite. Hereby, attention should be paid that the reference point of the satellite clocks is selected in accordance with the reference point of the satellite orbits.

The IGS RTS is providing three combination solutions, IGS01, IGS02 and IGS03. While IGS01 is generated on the basis of epoch-wise combination, the Kalman filter technique is exploited for producing IGS02 and IGS03. Two different agencies are responsible for these RT products: European Space Agency (ESA) provides IGS01 and BKG provides IGS02 and IGS03. All mentioned streams include orbits/clock corrections to GPS satellites, and only IGS03 supports also GLONASS constellation. While IGS01 and IGS02 are combined from up to eight individual solutions, IGS03 has only four individual contributors.

The RTS correction streams are formatted with respect to the RTCM (Radio Technical Commission for Maritime Services) standard for SSR and are transmitted using the NTRIP protocol (Networked Transport of RTCM via Internet Protocol). NTRIP was developed in co-operation between the Informatikzentrum Dortmund in Germany and BKG (http://igs.bkg.bund.de/ntrip) and initiated as an industrial standard since 2004 (Weber et al. 2005). Afterwards, NTRIP was standardized by the Special Committee 104 “DGNSS” of RTCM. The communication between the major components of the NTRIP, i.e. the server, the caster and the client are handled through HTTP ports. It is to mention that the major software components of the NTRIP are developed under “GNU General Public License”. NTRIP allows disseminating hundreds of data and product streams simultaneously for a few thousand users when applying the modified Internet Radio Broadcasting Software. It is also to note that a GNSS stream typically needs not more than 5 kbit/s bandwidth. The currently used version 2 of NTRIP, downward compatible to version 1, was completed in 2009. BKG supports the distribution of the new technology by providing the so-called Professional NTRIP Caster. This tool has been developed in

cooperation of BKG with Alberding Company in Germany for administration, configuration, and implementation the piece of software running using the LINUX operating system and is widely used within the IGS and EUREF (http://www.epncb.oma.be/). Meanwhile, almost every new GNSS receiver is coming with the NTRIP option.

3.4.2 BKG Real-Time Analysis Development and Contribution

Y. Altiner
BKG, Federal Agency for Cartography and Geodesy, Frankfurt, Germany
e-mail: yueksel.altiner@bkg.bund.de

W. Söhne
BKG, Federal Agency for Cartography and Geodesy, Frankfurt, Germany
e-mail: wolfgang.soehne@bkg.bund.de

A. Stürze
BKG, Federal Agency for Cartography and Geodesy, Frankfurt, Germany
e-mail: andrea.stuerze@bkg.bund.de

Since April 2016, BKG is contributing to the COST real-time demonstration campaign for troposphere estimation providing solutions processed with BNC, BKG's own software tool. The development of BNC started in 2005 by BKG in collaboration with different partners, e.g. with Technical University Prague, Czech Republic, and Alberding Company, Germany. BNC is a software for simultaneously retrieving, decoding, converting and processing or analyzing real-time GNSS data streams applying the NTRIP standard. BNC has been developed within the framework of EUREF and the IGS. Although BNC is primarily intended for real-time GNSS applications, it may also be run offline by transmission of data from an external file to simulate real-time observation conditions or for post-processing implementations. BNC provides also different modes of data evaluation like "graphics or interactive" mode to illustrate the processing state and results and "no windows" mode as well.

A major module of the BNC is the option "Real-Time PPP" for positioning in real-time according to the SSR model which was first provided in 2010. To meet requirements of the PPP in real-time using the state variables of the SSR model, within this version additional messages are provided to the user, among others, satellite orbit and clock corrections for GPS as well as GPS and GLONASS combination, and ionospheric corrections as well as biases for code and phase data. The PPP module of BKG allows users a real-time positioning worldwide at sub-decimeter-level using code and phase data in ionosphere-free solutions using P3 or L3 linear combinations in static or kinematic mode within an observation time of 10 min. In 2011, the "Real-Time PPP" module was expanded by incorporating the

PPP implementation for post-processing to work offline including data from external files. In 2014, BNC comes into being able to process data of multiple stations in a single BNC job (one job for all stations). Within this version (BNC 2.12), the troposphere parameters estimated by the data processing is provided by SINEX-TRO format (v0.01) to allow the usage of the TRO-file as a priori or a posteriori model for GNSS applications (Weber et al. 2016).

Within the RT demonstration campaign, ZTD values were evaluated in 5-min intervals for 22 mount-points at the beginning. As of October 2017, all 32 mount-points are implemented. As agreed, orbit and clock corrections from the IGS03 product are used. Streaming of broadcast ephemeris is taking place through the real-time access to the broadcast ephemeris stream of BKG "RTCM3EPH" for GPS and GLONASS. It should be noted that the IGS03 correction stream is a combined stream of four individual solutions providing GPS and GLONASS and is done by BKG with BNC.

The evaluation of ZTD implemented by BNC is using the Kalman filtering method. One important parameter to set in the configuration file is the white noise (signal) for 1 h which can be according to the weather conditions. The standard value for the variation of the white noise is 36 $mm/h^{1/2}$. Other effects or parameters influencing the accuracy of positioning so far considered by BNC are listed in Table 3.9. Processing of data within the demonstration campaign takes place using an elevation cut-off angle of 7° for observation usage and considering the float ambiguity resolution.

To study the impact assessment of GNSS processing on tropospheric products, two different products are created by BKG. A GPS-only and a combined GPS plus GLONASS product is computed and submitted separately as GPS and GPS + GLO products on hourly basis to the central analysis centre of the project (http://www.pecny.cz/COST/RT-TROPO/). Each hourly solution contains 12 ZTD-values and each ZTD-value represents a time span of 5 min within the relevant hourly solution.

In total, 10,234 files were submitted on hourly basis from March 14, 2016 to July 31, 2017 including solutions using the real-time GPS measurements and state

Table 3.9 Important effects so far considered by BNC within data processing

Effect	Considered
Earth's tide	Yes
Earth's rotation (Movement of pol)	Yes
Phase-wind up	Yes
Ionosphere	First order terms eliminated using L3
Troposphere	Determined
Multipath (phase shift of the signal)	No
Atmospheric and hydrological loading	No
Ocean tides	No
Offset and phase centre variations of satellite and ground antennas (PCV)	Yes

variables from the IGS03 product stream. For GPS + GLO, the quantity of the submitted hourly files reached to a total number of 8988 between March 18, 2016 and July 31, 2017. Data transmission continues also beyond the date 31.7.2017 (Fig. 3.34).

The internal precision in terms of agreement of both BKG solutions – GPS-only versus GPS + GLONASS – is shown in Figs. 3.35, 3.36 and 3.37. The example covering a 15-day period in July 2017 shows a good overall agreement for the ZTD

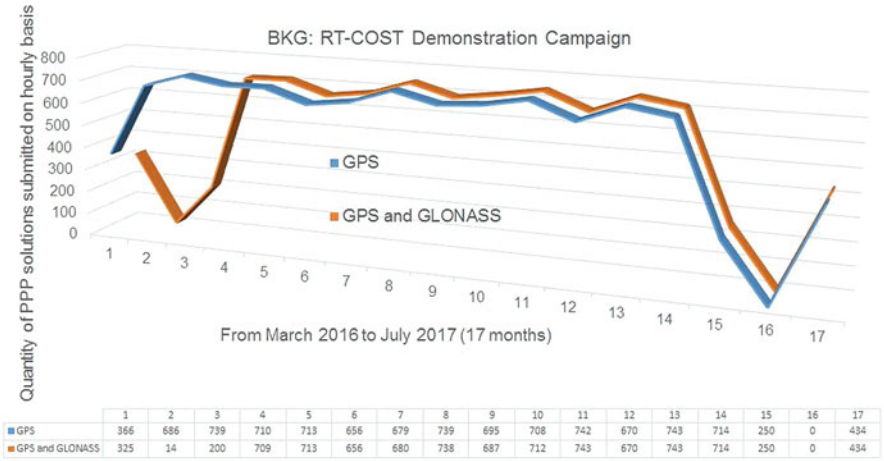

	1	2	3	4	5	6	7	8	9	10	11	12	13	14	15	16	17
GPS	366	686	739	710	713	656	679	739	695	708	742	670	743	714	250	0	434
GPS and GLONASS	325	14	200	709	713	656	680	738	687	712	743	670	743	714	250	0	434

Fig. 3.34 The quantity of ZTD processed by PPP using orbit and clock corrections from IGS03 product for GPS and GPS + GLO observations. The solutions were created in 5-min intervals and combined to a single file on hourly basis to be submitted to the central analysis centre of the project (http://www.pecny.cz/COST/RT-TROPO/). Each submitted hourly solution contains 12 ZTD-values and each ZTD-value represents a time span of 5 min within the relevant hourly solution

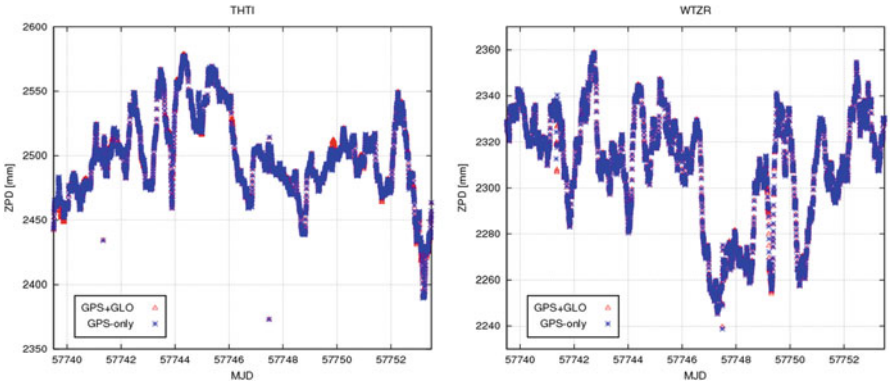

Fig. 3.35 Time series of ZTD estimates from BKG's real-time solutions (GPS-only and GPS + GLONASS) as taken from the uploaded COST format files for stations THTI (left) and WTZR (right)

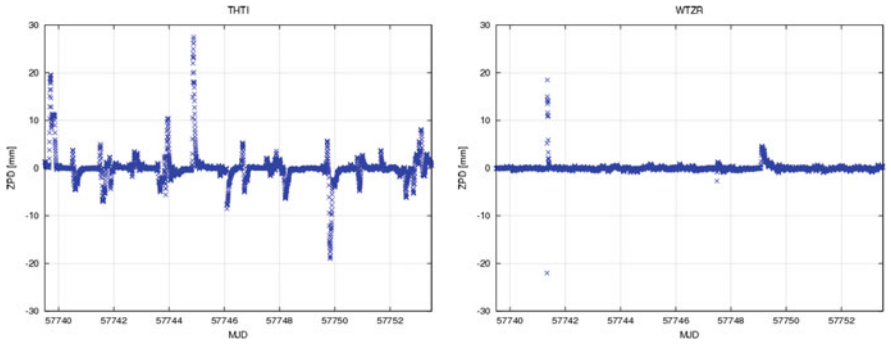

Fig. 3.36 Time series of differences of ZTD estimates between BKG's real-time solutions "GPS-only" minus "GPS + GLONASS" for stations THTI (left) and WTZR (right). The plots are showing increased differences during periods of re-initialization of at least one of both solutions

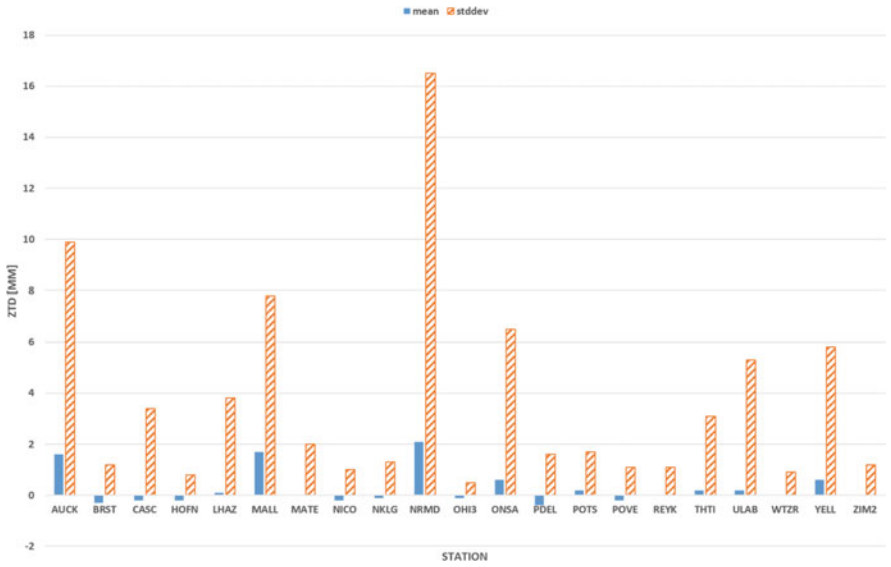

Fig. 3.37 Mean of differences between time series of ZTD estimates from BKG's real-time solutions GPS-only minus GPS + GLONASS for 15 days in July 2017. Only three of 21 stations show a bias of almost 2 mm ZTD. The large standard deviation for station NRMD cannot be explained by frequent re-initialization; the time series show larger portions of disagreement

time series for Tahiti (Fig. 3.35 left) and Wettzell. A closer look into the differences, however, shows some portion of disagreement. This can be explained by re-initialization of at least one of both solutions. Figure 3.37 shows the statistics for 21 stations (station ADIS was only occasionally available in the GPS + GLO solution). For the majority of the stations the mean bias is well below 2 mm ZTD.

Regarding the submitted ZTDs of BKG within the demonstration campaign, a statistical study for station WTZR was conducted in relation to the EUREF weekly

combined solutions (Table 3.10). To do this, the EUREF weekly combined ZTD solutions were considered as target values and BKG real-time GPS and GPS + GLO solutions as measured values, respectively. The measured values from BKG were subtracted from the EUREF target values. In total, 8451 ZTD values from each solution were included to this statistical study. The correlation between the differences of GPS and GNSS solutions in relation to the EUREF combined solutions amounts to 85%. This suggests good coincidence between both solutions (GPS and GPS + GLO). The average differences for GPS and GPS + GLO are on the order of 11.4 mm and 8.6 mm, respectively. Contrary to the average, the standard deviation of GPS is smaller than the standard deviation of GPS + GLO (11.4 mm and 12.9 mm, respectively).

To illustrate the relation of the GPS and GPS + GLO solutions to the EUREF combined solution the total 8451 ZTD values were reduced to 253 through choosing a random value for each day at 15:30 as illustrated in Fig. 3.38. It is important here to

Table 3.10 Statistical aspects between ZTDs determined by BKG for station WTZR using GPS and GPS + GLO real-time corrections and the combined EUREF weekly solution. In total, 8451 ZTD values from each solution were included in the study. Averages and standard deviations, shown in bold, determined relative to the EUREF combined ZTD solution (EUREF minus BKG-GPS and EUREF minus BKG-GNSS)

Solution for station WTZR	Average in mm	Std. dev. in mm	Average of std. dev. in mm
BKG-GPS	11,8	11,4	0,7
BKG-GPS + GLO	8,1	12,9	0,7
EUREF			0,5

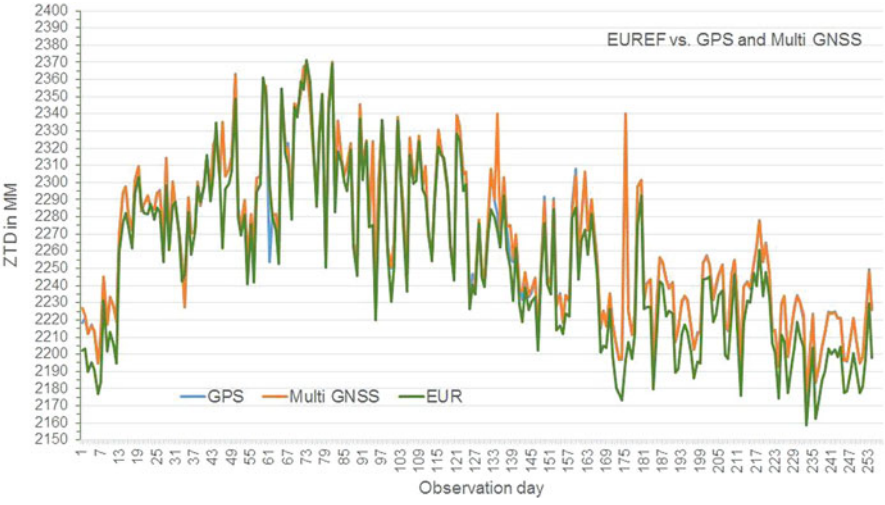

Fig. 3.38 Relation of the GPS and GPS + GLO solutions to the EUREF combined solution for station WTZR. 8451 ZTD values from each solution were reduced to 253 through choosing of a random value for each day at 15:30. The results suggest good coincidence between the GPS and GPS + GLO solutions using the real-time orbit and clock corrections

notice that the EUREF weekly combinations include the results of several ACs which are derived using the final orbits of the IGS. Each AC does not use the same software for data processing, and network geometries of ACs are also different. Some studies conducted by BKG between the results of the real-time, near real-time und post-processing applications also suggest the good quality of real-time PPP with respect to the determination of ZTD (Altiner et al. 2009, 2010 and 2011).

3.4.3 Assessment of IGS RTS Orbits and Clock Corrections and GOP Real-Time Tropospheric Products[8]

L. Zhao
Geodetic Observatory Pecný, Research Institute of Geodesy, Topography and Cartography, Zdiby, Czech Republic
e-mail: lewen.zhao@pecny.cz

P. Václavovic
Geodetic Observatory Pecný, Research Institute of Geodesy, Topography and Cartography, Zdiby, Czech Republic
e-mail: pavel.vaclavovic@pecny.cz

J. Douša
Geodetic Observatory Pecný, RIGTC, Ondřejov, Czech Republic
e-mail: jan.dousa@pecny.cz

The accuracy of the RT ZTD calculated with the PPP method strongly depends on the quality of RT GNSS orbit and clock corrections (Douša and Václavovic 2014; Hadaś and Bosy 2015). We evaluated publicly available global RT products and we summarized our ZTD contributions to the RT Demonstration Campaign initiated in 2015 by this COST Action. We also studied the impact of IGS RTS (Caissy et al. 2012) on the simulated RT ZTD estimates within the GNSS4SWEC Benchmark Campaign (Douša et al. 2016).

3.4.3.1 Assessment of Real-Time Orbit and Clock Corrections

We investigated the performance of four real-time products (Douša et al. 2018a) having been collected and archived at Geodetic Observatory Pecny (GOP) using the BNC Software (Weber et al. 2016) since 2013: IGS01, IGS02 and IGS03 the official IGS RTS combined products, and CNS91 (also known as CLK91) as an individual solution provided by CNES RT AC (Laurichesse 2011). Two different strategies and

[8]Parts from this section were previously published in Douša et al. (2018a).

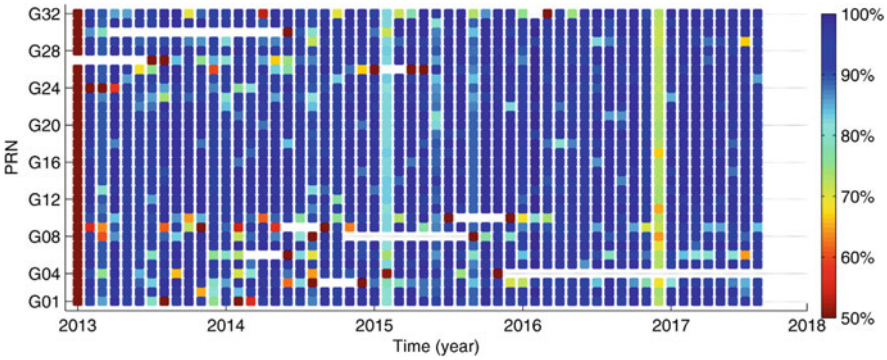

Fig. 3.39 Monthly statistics of availability of satellite corrections from IGS01 RT stream

software are used for combining the IGS RTS (Hadaś and Bosy 2015). All mentioned streams include orbits/clock corrections to GPS satellites, and only IGS03 supports also GLONASS constellation. Navigation data from MGEX (Montenbruck et al. 2017) needs to be used together with the RT corrections to recover the precise satellite orbit and clocks. First, the availability and completeness of RT corrections were checked and, second, satellite orbit and clocks were compared to IGS final orbit and clocks, both during the period of 2013–2017.

Figure 3.39 depicts monthly completeness of RT corrections for all GPS satellites from the IGS01 combined products. The others IGS products and the CNES product are generally showing similar performance. From the comparison, we can classify problems into three groups: (1) temporal unavailability period of some satellites, e.g. G03, G04, (2) source-specific unavailability, e.g. G01 for CNS91, and (3) satellite-specific incompleteness. The first group is usually caused by the loss of observations due to the upgrade of satellite, such as replacing the old Block IIA satellites with the new Block IIF satellites or a maintenance identified by satellite unhealthy status. The second and third groups of gaps are caused by data unavailability from a global network and the processing strategy including outlier detection in the product generation. The availability of the corrections is significantly lower for some months (June 2015, December 2016) compared to others which was caused by the internet connection failures at GOP when receiving the streams. The source-specific loss of data at IGS02 and CNS91 streams are visible in June 2015 and, these are mainly due to the inconsistent navigation message Issue of Date (IOD) available from the MGEX broadcast and those referred by RT corrections. It can be thus recommended to use consistent RT navigation data and precise correction streams optimally guaranteed by the same provider. In general, the availability of RT corrections is well over 90% for most satellites which agrees with findings in (Hadaś and Bosy 2015). It indicates that the RT corrections were provided continuously for use in troposphere monitoring, however, problems can be expected in a kinematic positioning which is more sensitive to the product incompleteness.

Table 3.11 RT clocks and orbits components compared to the IGS final products

	RMSE [mm]					SDEV [mm]
	Radial	Along	Cross	3D	Clock	Clock
IGS01	1.84	2.83	2.38	4.34	5.72	2.95
IGS02	2.35	3.71	3.04	5.63	10.08	3.52
IGS03	2.41	3.82	3.10	5.70	10.28	3.03
CNS91	2.68	3.07	2.47	5.01	11.16	2.29

Apart from the availability of the corrections, the precision is critical for the user performance. The orbits are compared in 5-min intervals for three components: radial, along-track and cross-track while the clock comparison is based on the second order difference method. The IGS08 and the IGS14 model is used to correct satellite PCOs prior and after January 29, 2017, respectively, corresponding to the adoption of the IGS14 reference frame (Rebischung et al. 2016). The clock datum is estimated by calculating average over all satellites clocks at each epoch. The datum inconsistencies are then eliminated through single-differences between individual satellite clocks and the clock datum. The single-differences from the real-time clocks are compared to those from the IGS final product. The root-mean-square error (RMSE) of RT orbits and clocks are calculated for each day while outliers are removed using a fixed threshold. Although there is a strong correlation between clocks and radial orbit component, we haven't corrected this dependency. Table 3.11 gives summary statistics for all products over all days.

The orbit difference in radial component shows the smallest RMSE for all products, whereas the along-track and cross-track components reached slightly larger values. The IGS01 orbit shows the best agreement with respect to the IGS final orbits. Largest differences are observed for the orbits from IGS03, which might be attributed to a different outlier detection method applied when including GLONASS satellites. Time evolution of the orbit comparison for each product and specific component is shown in Fig. 3.40. Coordinate differences greater than 30 cm are plotted at the top horizontal lines of each graph. Orbits from the IGS01 stream are less affected by the outliers compared to IGS02 and IGS03 products as indicated by outliers mainly during March 2015. The switch from the IGS08 to the IGS14 PCO model (January 28, 2017) can be observed in statistics of the radial component. It seems that the CNS91 product used the new IGS14 model as of March 9, 2017, while official IGS solutions are difficult to recognize due to most likely asynchronous switches by different contributing providers. Otherwise, the orbit accuracy for all products shows an overall good consistency over the period.

Table 3.11 also summarizes RMSE and standard deviation (SDEV) of the real-time clock corrections. The former represents the accuracy relevant for the processing of code pseudoranges while the latter characterizes the precision important for the carrier-phase processing. It can be also interpreted from the PPP point of view combining both observation types as follows – the former have a positive impact on the PPP convergence time while the latter enable more precise positioning within already converged solution (Ye et al. 2018). Obviously, this is the case of

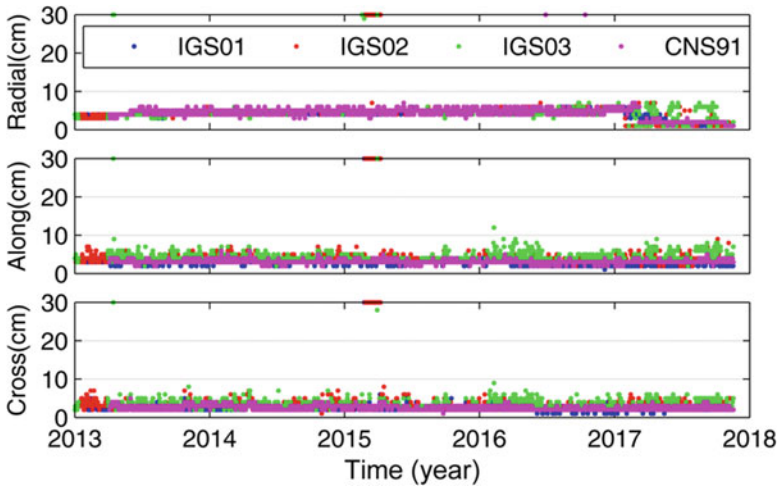

Fig. 3.40 Daily RMS of real-time orbits with respect to IGS final orbit

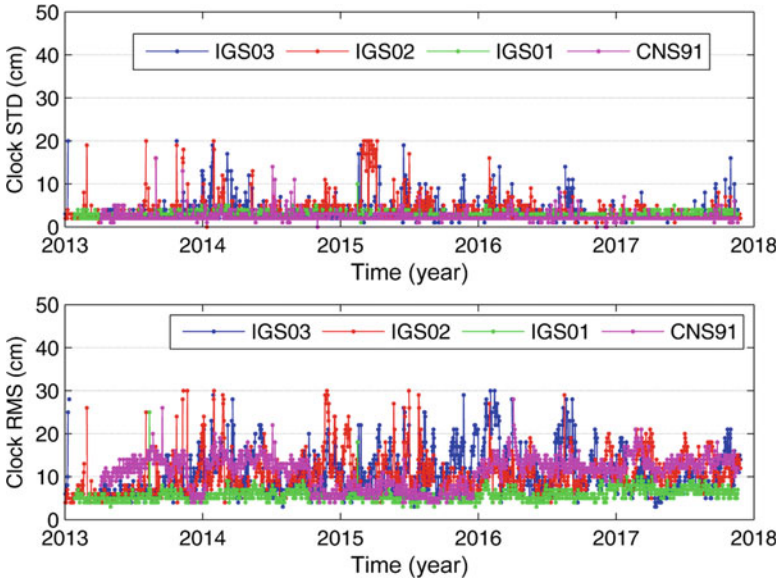

Fig. 3.41 Daily statistics SDEV (top) and RMSE (bottom) of real-time clocks

IGS01 and CNS91 products when the first is more accurate, but the second more precise for the PPP application. The IGS02 and IGS03 products performs slightly worse in terms of both RMSE and SDEV.

Figure 3.41 finally shows time series of the clock SDEV and RMSE statistics. The former (top plot) indicates a comparable high quality over the period for IGS01

and CNS91, while more outliers are observed for IGS02 and IGS03 including the problematic period in 2015 identified in the orbit availability evaluation. The clock RMSE from IGS01 is the lowest and the most stable compared to the others during the period while, the RMSE of CNS91 clocks was more accurate during 2015 when compared to the other years.

3.4.3.2 Impact of IGS RTS Products on ZTD Estimates

The impact of the IGS RTS products on PPP ZTD estimates was assessed by exploiting the GNSS4SWEC Benchmark campaign with 400 GNSS stations in central Europe during the period of May–June, 2013. The ZTD was calculated using the G-Nut/Tefnut software in the post-processing mode when supported with two precise products: (1) IGS final orbits and clocks, and (2) IGS RTS orbit and clock corrections. Two reference solutions were provided for the benchmark using different software and processing strategies (Douša et al. 2016). GOP used the BSW and the double-difference processing (DD) and GFZ used the EPOS software and the PPP method. Statistics from the comparison of both testing solutions with respect to both reference products are given in Table 3.12. Generally, the results indicate a good agreement, however, the impact of the IGS RTS products (IGS01) on ZTDs is clearly visible in two aspects: a) a common systematic error of 2.4–2.8 mm, and b) a lower precision of 13–17%. Interestingly, a better agreement in terms of SDEV is reached between 10% and 20% when using two PPP solutions (G-Nut/Tefnut vs EPOS software) compared to the processing strategies (DD vs PPP). The results also showed that input products and the processing strategy might result in a similar impact on the ZTD estimates which can reach up to 20% in terms of accuracy. Finally, it should be noted that the PPP ZTD estimation used a stochastic model and an epoch-wise filtering method in the G-Nut/Tefnut software (Václavovic et al. 2013), while a deterministic model with the least-squares batch adjustment used in the EPOS software.

Table 3.12 Summary statistics from the comparison of PPP ZTD results using two inputs (IGS01 RT vs. IGS final) w.r.t. EUREF reprocessing

G-Nut/Tefnut PPP Input precise products	ZTD reference product	Bias [mm]	STD [mm]	RMS [mm]
IGS final (SP3 files)	GOP final (BSW52/DD)	+0.9	5.1	5.2
IGS01 RT corrections	GOP final (BSW52/DD)	+2.4	5.8	6.4
IGS final (SP3 files)	GFZ final (EPOS/PPP)	+0.4	4.1	4.2
IGS01 RT corrections	GFZ final (EPOS/PPP)	+2.8	4.9	5.7

3.4.3.3 Long-Term Quality of Operational RT ZTD Production

The RT ZTD from the demonstration campaign is evaluated for 18 European stations during the initial year of the GNSS4SWEC Real-time Demonstration campaign. Two GOP solutions using the IGS03 product are compared with respect to the EUREF 2nd reprocessing combined tropospheric product (Pacione et al. 2017): (1) GOPR – standalone GPS solution, and (2) GOPQ – GPS + GLONASS solution. In Table 3.13, we can observe a systematic error in ZTD of about 2 mm in the long-term evaluation, similar as observed in the simulated real-time processing in the benchmark campaign, see the previous subsections. Although GLONASS observations are down-weighted by a factor of 2 in our solution in order to reflect the lower quality of GLONASS precise products, a small positive impact on the ZTD is observed in terms of mean bias (10%) and mean SDEV (7%), both calculated over 18 stations.

Figure 3.42 shows the comparison of the GOPR solution with respect to the EUREF combined product during the first year of the RT demonstration campaign. Monthly mean ZTD biases, standard deviations and their 1-sigma scatter calculated over all 18 stations indicate a long-term stability of the operational real-time production with a small seasonal effect in SDEV due to a less accurate troposphere modelling during the summer period (Douša and Václavovic 2016).

3.4.4 Real-Time Product Development and Evaluation at ROB

E. Pottiaux
Royal Observatory of Belgium, Brussels, Belgium
e-mail: eric.pottiaux@oma.be

In the framework of COST Action ES1206 (GNSS4SWEC), the Royal Observatory of Belgium (ROB) collaborated with the Geodetic Observatory Pecny (GOP) to use their Real-Time Precise-Point-Positioning (RT-PPP) software G-Nut/Tefnut for the real-time monitoring of the troposphere, to help support nowcasting of severe weather in Belgium. On June 21, 2014, ROB started to use G-Nut/Tefnut to produce real-time tropospheric products (ZTD and horizontal gradients) using 4 different processing strategies (Table 3.14), with a particular focus on Belgium.

Table 3.13 Summary statistics over 18 stations from routine RT product using GPS and GPS + GLO data

Solution description	BIAS [mm] mean ± sdev	SDEV [mm] mean ± sdev	RMSE [mm] mean ± sdev
GOPQ – GPS + GLO	1.8 ± 2.9	6.7 ± 1.2	7.5 ± 2.5
GOPR – GPS	2.0 ± 2.8	7.2 ± 1.0	7.9 ± 1.5

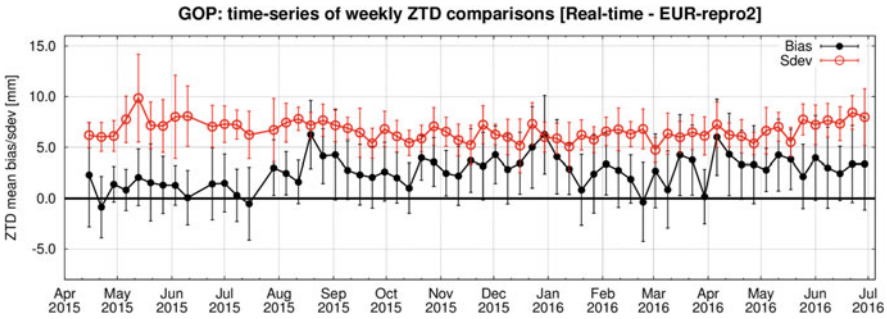

Fig. 3.42 Monthly summary biases and standard deviations of real-time ZTDs over 18 stations

Table 3.14 Setup of the different ROB's RT-PPP Processing

Common parameters to all solutions		
Parameter	**Setup**	
Coordinates	Static estimation	
Tropospheric parameters	ZTD + horizontal gradients	
Tropospheric model	Saastamoinen + GMF + Chen and Herring	
Cut-off angle	3°	
Time resolution	10 s	
Latency	100 s	
Ocean tide loading Coef.	FES2004	
Antenna model	IGS08 Antex file	
Solution naming & differences		
Solution name	**GNSS observations**	**CLK + ORB product**
ROBA	GPS-only	IGS02 (GPS only)
ROBB	GPS	IGS03 (GPS + GLONASS)
ROBC	GPS + GLONASS	IGS03 (GPS + GLONASS)
ROBD	GPS + GLONASS	CNS91 (GPS + GLONASS)

Based on these developments, ROB also participated in the RT-PPP demonstration campaign, with the main goals to extensively develop, test, and validate real-time processing methods and tropospheric products that can help supporting nowcasting and forecasting of severe weather and foster the link to WG2 activities. ROB processes thus real-time GNSS observations from the 32 GNSS sites requested to participate in the demonstration campaign, along with those from 153 additional GNSS sites located worldwide (Fig. 3.43, left), including the complete Belgian dense network (Fig. 3.43, right). In total, 185 GNSS Stations are included in ROB's RT-PPP processing with G-Nut/Tefnut (Fig. 3.44). These 185 stations are equipped with 73 different combinations of GNSS receivers and antennas (26 receiver types, 40 antenna type, Fig. 3.45), allowing thereby to study and assess the performances of this RT-PPP processing w.r.t. the equipment, and in fine to fine-tune accordingly the processing strategy. All RT-PPP products are formatted in both

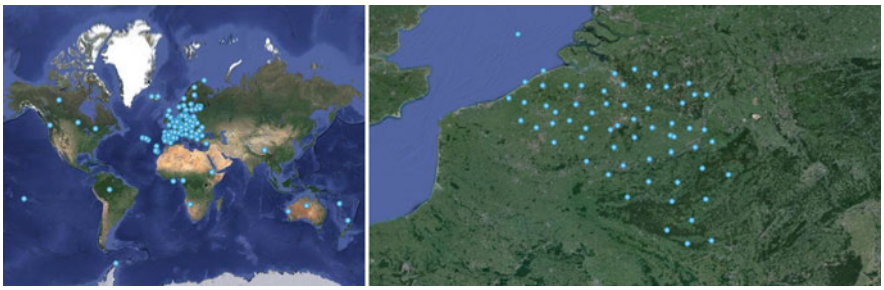

Fig. 3.43 (Left) Location of the GNSS stations included in the RT-PPP operated by ROB using the G-Nut/Tefnut software from GOP. (Right): The location of the GNSS stations of the Belgian Dense network included in this processing

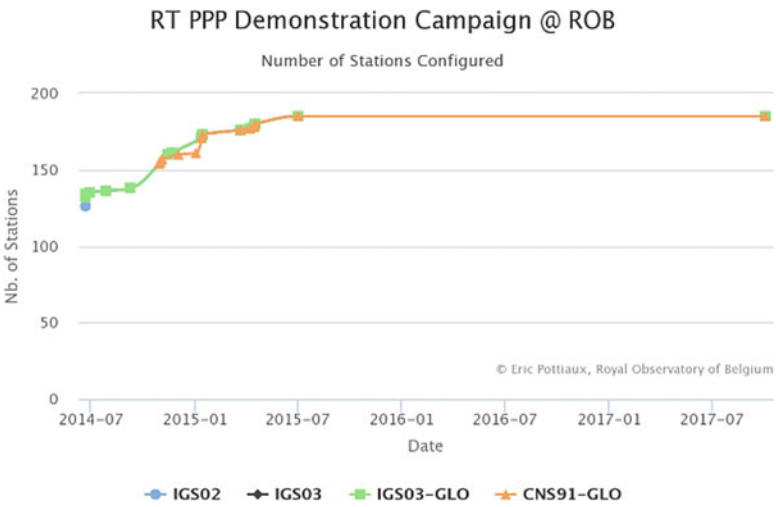

Fig. 3.44 Number of GNSS stations included in the RT-PPP Processing operated by ROB

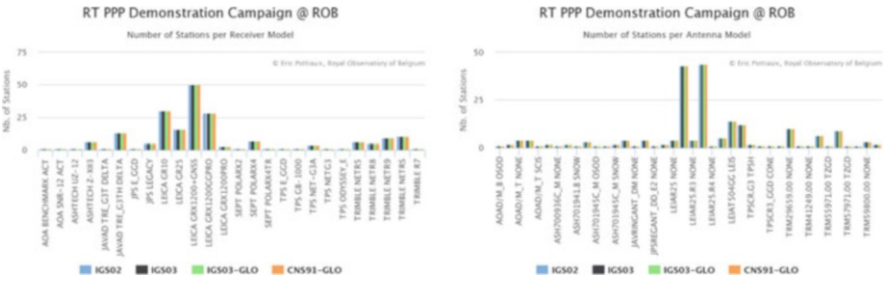

Fig. 3.45 Number of stations equipped with a specific type of GNSS receiver (left) or antenna (right) and included in ROB's operational RT-PPP processing campaign

in the COST-716 v2.2a and in the SINEX_TRO v2.00 format to ease exchange and validation. Upload of these products (only the stations contributing to the WG1 RT demonstration campaign) is done every hour to a central hub at GOP, and can be visualized at http://www.pecny.cz/COST/RT-TROPO.

3.4.4.1 Monitoring and Validation

Developing and maintaining such new RT-PPP processing systems and products requires regular assessment, adaptation, and fine-tuning cycles. Therefore, ROB developed its own monitoring/validation system consisting of MySQL databases, statistical assessment programs, and a web-based user-interface to monitor continuously his RT-PPP processing system (graphs, reports...). The system is capable of monitoring/carrying out:

- The campaign setup and its evolution
- Inconsistency checks (configuration, equipment, models...)
- The performances of the products at all GNSS stations included in the RT-PPP processing (the monitoring system developed by GOP can only monitor 17% of them), at various time scale and epochs (biases, precision, geographical dependency...)
- Alarm systems in case of problem (dataflow, processing...)

To validate the performances of the products at all stations and all time scales (e.g. a very rapid monitoring require the use of e.g. NRT products), the monitoring system uses various reference products listed in Table 3.15, from post-processed to NRT, some computed in PPP, some in Double-Difference (DD) approach etc. In all cases, the validation starts with a screening of the RT-PPP results to reject convergence period. This screening is using the RMS of the coordinates, ZTD and horizontal gradients, as well as the GDOP values, and the number of satellite measurements used to compute the tropospheric products at each single epoch. The advantages of this approach is that it can be implemented as a "real-time

Table 3.15 List of reference products chosen to validate the RT-PPP products operationally computed by ROB

Solution	Software	Orb. & Clk.	Multi-GNSS	Time Res.	Latency	NB. Sta.	TRO Est.
IGS	BSW50	IGS final	GPS only	5 min	3–4 weeks	30	ZTD + GRD
ROB PPP	BSW52	CODE final	GPS + GLO	5 min	3 weeks	All	ZTD + GRD
ROB DD	BSW52	CODE final	GPS + GLO	1 h	3 weeks	All	ZTD + GRD
ROB NRT E-GVAP	BSW52	IGS ultra-rapid	GPS only	15 min	1 h	All	ZTD only

filtering" at the production level to screen out potential performance degradations before using the product in actual meteorological applications. In most cases, this filtering works well and had a low percentage of rejected values (<1%).

Having various reference products is justified by their respective advantages and drawbacks, namely IGS for a standard reference product (but having only 30 common stations), consistency for PPP approaches (but probably less precise/accurate than the double-difference approach), accuracy/precision for final products (but large latency of the monitoring), and short-latency monitoring in the case of NRT solutions.

The first long-term validation has been carried out with this system over the period July 1st 2014–March 31st 2015 (9 months). Globally and at the long-term level, the 4 solutions listed in Table 3.14 agrees very well with the IGS Final products (22 stations considered altogether). The linear regressions (computed over ~600,000 samples) between RT-PPP and the IGS products have a correlation coefficient above 0.99, a slope of ~0.99, and almost a zero intercept (0.02–0.03 mm). The bias is however station dependent, consistent at the mm level for all products, and ranges from −5 to 16 mm (Fig. 3.46). The standard deviation is also station dependent and ranges typically from 5 to 10 mm (Fig. 3.47), with a maximal value

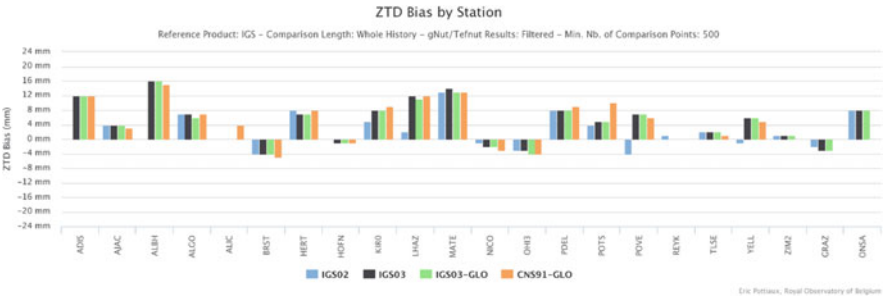

Fig. 3.46 Bias observed between the ZTDs from each ROB's RT-PPP product and the IGS final troposphere product over the period July 1st 2014–March 31st 2015

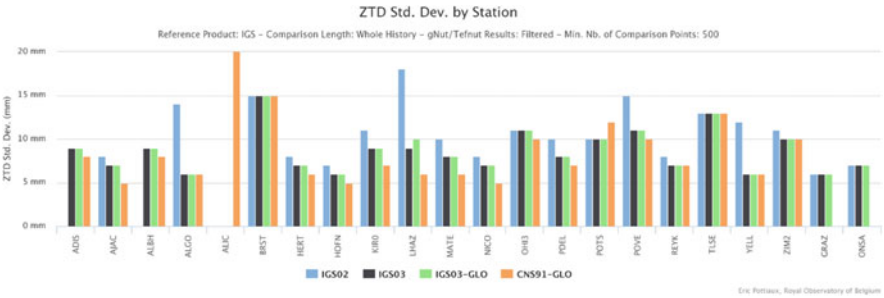

Fig. 3.47 Standard deviation observed between the ZTDs from each ROB's RT-PPP product and the IGS final troposphere product over the period July 1st 2014–March 31st 2015

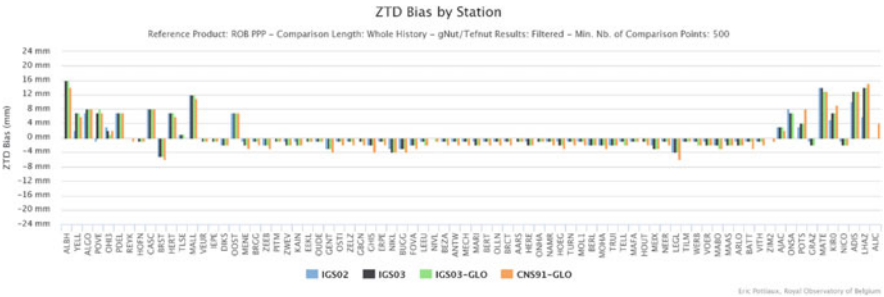

Fig. 3.48 Bias observed between the ZTDs from each ROB's RT-PPP product and the ROB final PPP troposphere product over the period July 1st 2014–March 31st 2015. Stations are ordered by increasing longitude

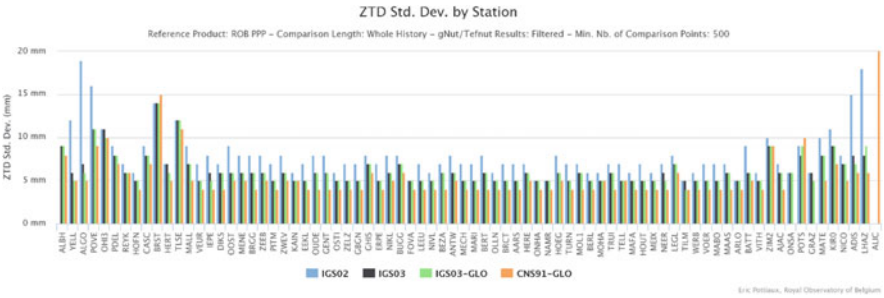

Fig. 3.49 Standard deviation observed between the ZTDs from each ROB's RT-PPP product and the ROB final PPP troposphere product over the period July 1st 2014–March 31st 2015. Stations are ordered by increasing longitude

observed of 26 mm (ALIC). No clear geographical dependency (longitude, latitude, and altitude) of the bias or the standard deviation could be observed in this comparison.

The comparison between the 4 RT-PPP solutions and the ROB's PPP post-processing reference solution showed very similar results (Figs. 3.48 and 3.49), with typical biases ranging from −5 to 16 mm, typical standard deviations ranging from 4 to 7 mm (i.e. slightly better than when compared to the IGS final product), and correlation coefficient above 0.99. One can also remark that the RT-PPP solutions performs very well and homogenously in Belgium: all stations in the middle of the graphs (i.e. from VEUR to VITH) have lower biases ranging from −1 to 4 mm. We can also note the slightly better global performance obtained with the CNS91 orbit and clock product. This lower standard deviation can be due to a faster convergence time for the solution using CNS91 in GPS + GLONASS mode, but this still needs to be confirmed. Finally, processing jointly GPS + GLONASS observations (ROBC, IGS03-GLO) provides consistent solutions as processing GPS-only observations (ROBB, IGS03), in general at the 1–2 mm level.

In conclusion, ROB started in June 2014 to compute operationally RT-PPP products as a demonstration campaign using the G-Nut/Tefnut software from GOP. This campaign has run now for more than 3 years. Results obtained so far are very promising but leave space for further studies and improvements. This RT-PPP production and their related developments will continue in the framework of the IAG WG 4.3.7 'Real-time GNSS tropospheric products', with the aim on a more longer term to be operationally provided to E-GVAP. As the next natural step in the developments, ROB participates in a case study that aims to simulate the RT-PPP processing in off-line mode. The goals of this case study are explained in the next paragraph.

3.4.4.2 Assessment of RT Products in Simulated RT Analysis of Benchmark Data

As we said, the RT-PPP demonstration campaign provided promising results but also leaved space for specific studies and improvements. Such kind of studies, like studying the optimal processing settings according to e.g. weather type (severe versus normal condition), studying the influence of the station equipment, or optimizing the convergence period etc. requires to be able to replay the processing several times on the same dataset by changing solely one processing parameter at a time. In other words: simulating the real-time processing in an offline mode for fine-tunings and assessments. One perfect candidate for this is the WG1 Benchmark campaign, and at the end of the COST Action, we started the real-time benchmark campaign with the following main objectives:

- Processing (a core group of) stations of the Benchmark campaign in simulated real-time PPP mode with various real-time orbits and clocks products to produce a final assessment of the capability of each real-time orbit and clock product.
- Develop optimal strategies for the estimation of ZTDs and tropospheric gradients at high (time) resolution (e.g. 5 min), and assess them to reference solutions and/or ZTD/GRD from NWM.
- Investigate the capability of dynamically constrain ZTDs and GRDs according to the weather conditions (calm, moderate, turbulent, severe, etc.). This is very important for natural hazard warnings.
- Produce a dataset of simulated real-time tropospheric products (ZTD, horizontal gradients, SPD) using the final fine-tuning of all previous steps that can be re-used to assess the capability/performances of these products in real studies/applications (e.g. a nowcasting case of severe weather).
- Production of IWV in almost real-time for non-numerical nowcasting applications.
- Standardize methods and format, and provide guidelines towards operational production of real-time tropospheric products (link to E-GVAP).

In that context, ROB processed the complete WG1 benchmark dataset in simulated real-time offline mode with various processing options and various orbit and

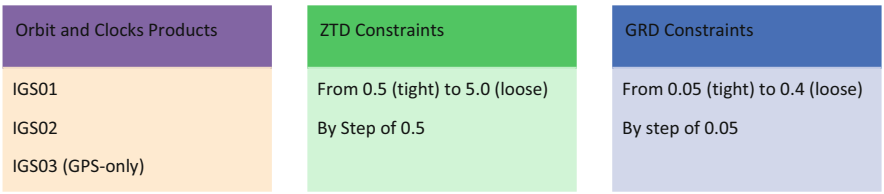

Fig. 3.50 The different processing configuration tested by ROB in the context of the real-time PPP benchmark campaign (simulated real-time PPP offline processing). It includes 4 orbit and clock products configurations (no offline version of the CNS91 product could be found), 10 ZTD constraints setup, and 8 horizontal gradients constraints setup

clock products, focusing on providing the final assessment of the orbit and clock products, on testing different ZTD & GRD (dynamical/optimal) constrains, on studying the dependency of the performance w.r.t. to the equipment (see text of the RT demonstration campaign), and on convergence periods. Similarly as for the regular assessment of the real-time demonstration campaign, we also reprocessed the benchmark campaign with the BSW52 to produce final reference tropospheric products both in PPP and in double-difference approach. In total, 320 flavors of the RT-PPP products are available for inter-comparison (Fig. 3.50) and assessments. These results have been produced towards the end of the COST Action but will be analyzed in the context of the IAG WG 4.3.7.

3.4.5 GFZ Real-Time Product Development and Assessment in RT Analysis

C. Lu
GFZ German Research Centre for Geosciences, Potsdam, Germany
e-mail: cuixian@gfz-potsdam.de

X. Li
GFZ German Research Centre for Geosciences, Potsdam, Germany
e-mail: lixin@gfz-potsdam.de

The multi-constellation Global Navigation Satellite Systems (GNSS) offers promising potential for the retrieval of real-time (RT) atmospheric parameters to support time-critical meteorological applications, such as nowcasting or regional short-term forecasts. In this study, we processed GNSS data from the globally distributed Multi-GNSS Experiment (MGEX) network of about 30 ground stations by using the precise point positioning (PPP) technique for retrieving RT multi-GNSS tropospheric delays. RT satellite orbit and clock product streams from the International GNSS Service (IGS) were used. Meanwhile, we assessed the quality of clock and orbit products provided by different IGS RTS ACs, called CLK01, CLK81, CLK92, GFZC2, and GFZD2, respectively. Using the RT orbit and clock products, the

performances of the RT ZTD retrieved from single-system as well as from multi-GNSS combined observations are evaluated by comparing with the U.S. Naval Observatory (USNO) final troposphere products. With the addition of multi-GNSS observations, RT ZTD estimates with higher accuracy and enhanced reliability can be obtained compared to the single-system solution. Comparing with the GPS-only solution, the improvements in the initialization time of ZTD estimates are about 5.8% and 8.1% with the dual-system and the four-system combinations, respectively. The RT ZTD estimates retrieved with the GFZC2 products outperform those derived from the other IGS RTS products, Fig. 3.51. In the GFZC2 solution, the accuracy of about 5.05 mm for the RT estimated ZTD can be achieved with fixing station coordinates. The results also confirm that the accuracy improvement (about 22.2%) can be achieved for the real-time estimated ZTDs by using multi-GNSS observables compared to the GPS-only solution. In the multi-GNSS solution, the accuracy of real-time retrieved ZTDs can be improved by a factor of up to 2.7 in the fixing coordinate mode comparing with that in the kinematic mode, Fig. 3.52.

3.4.6 Contribution to RT Demonstration Campaign from ULX[9]

W. Ding
University of Luxembourg, Luxembourg, Luxembourg
e-mail: dingwenwu@asch.whigg.ac.cn

F. N. Teferle
University of Luxembourg, Luxembourg, Luxembourg
e-mail: norman.teferle@uni.lu

After initial RT solutions based on BNC were abandoned, ULX modified the PPP-Wizard developed by CNES to provide a real-time solution to the RT-Demonstration Campaign. These solutions included GPS, GLO and GAL observations and employed the real-time products from CNES CLK93, including satellite orbit, clock and code/phase biases. The latter allowed PPP ambiguity resolution for GPS using a zero-difference ambiguity resolution approach (see Table 3.16). The modifications of PPP-Wizard included:

- Apply Antenna Reference Point (ARP) correction from igs08.atx
- Apply receiver PCO + PCV correction from igs08.atx
- Solid earth tide + ocean tide loading correction (FES2004)
- ZTD (GPT and Saastamoinen) + ZWD (modeled as random walk process)
- Troposphere Mapping Function (GMF)
- Elevation dependent weighting strategy (Q = 1/cos(zen)**2)
- Of particular interest was the impact of multi-GNSS on initialization times.

[9]Parts from this section were previously published in Ding et al. (2017).

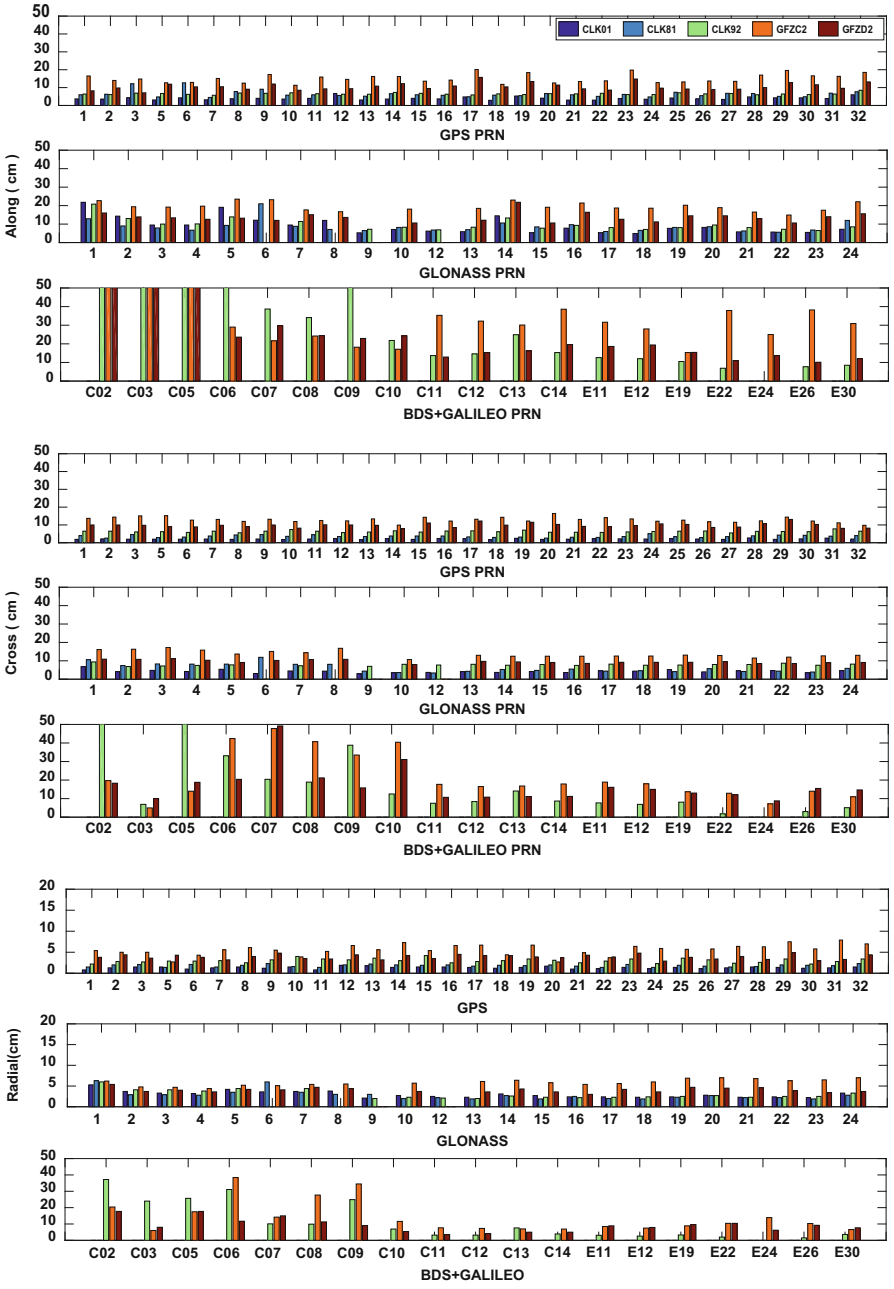

Fig. 3.51 RMS values of the differences between IGS RTS orbits (CLK01, CLK81, CLK92, GFZC2, and GFZD2) and GFZ final orbits for the four systems (i.e., GPS, GLONASS, Galileo, and BDS) in the along (top), cross (middle) and radial (bottom) components, respectively

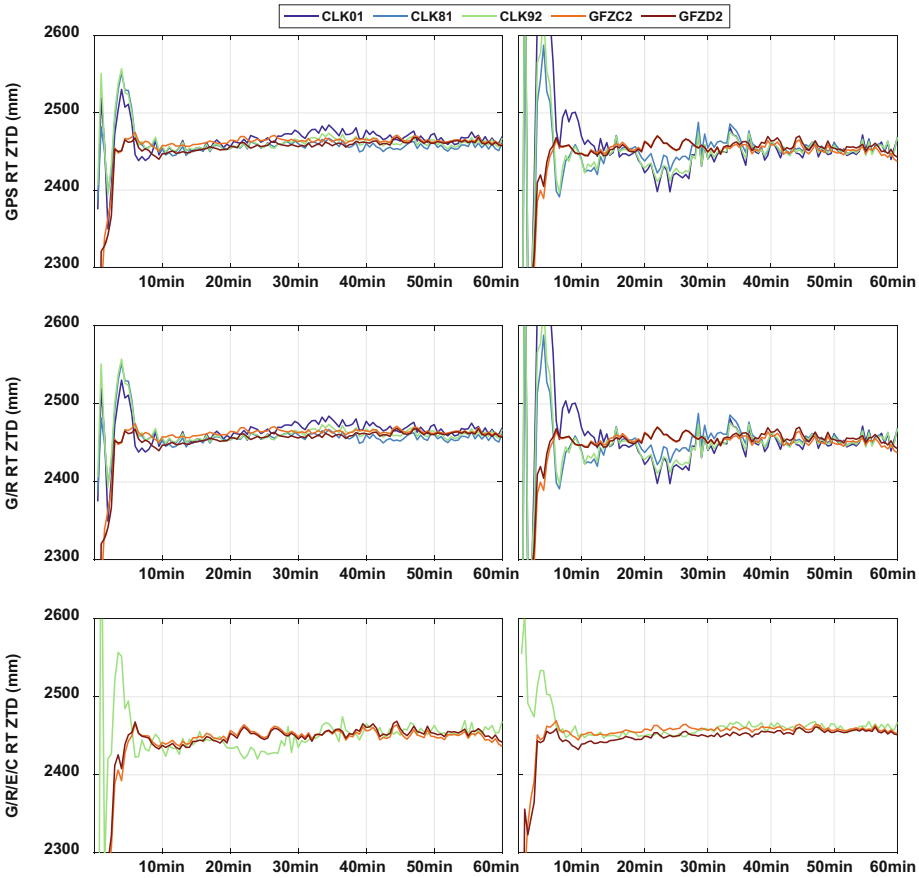

Fig. 3.52 RT ZTD estimates at station ONS1 derived from the GPS-only ("GPS", top), the combined GPS/GLONASS ("G/R", middle), and the combined GPS/GLONASS/Galileo/BDS ("G/R/E/C", bottom) solutions in fixing coordinate (left panels) and kinematic processing (right panels) modes by employing different IGS RTS over the first 2 h of DOY 090, 2017

Table 3.16 List of data processing modes investigated at ULX

Modes	Details
RFLT	Float PPP solution based on GLONASS-only observations
GFLT	Float PPP solution based on GPS-only observations
GFIX	Fixed PPP solution based on GPS-only observations
MFLT	Float PPP solution based on GPS/GLONASS observations
MFIX	Fixed PPP solution based on GPS/GLONASS/Galileo observations

Reproduced from Ding et al. (2017)

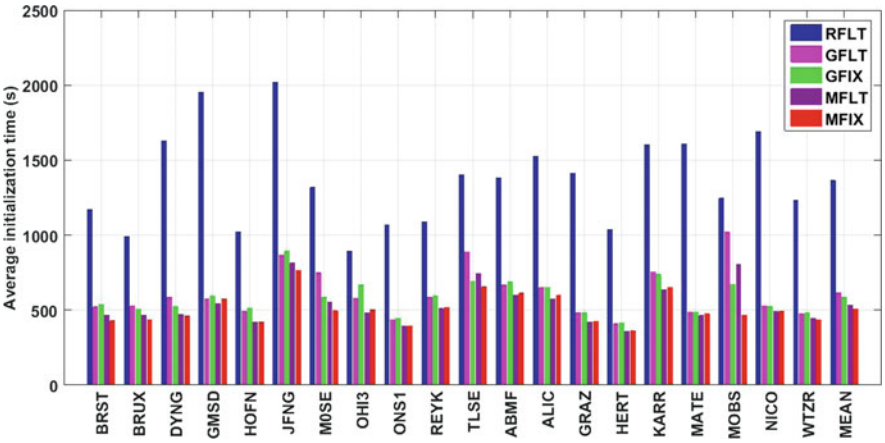

Fig. 3.53 Average initialization time in all data processing modes. (Reproduced from Ding et al. 2017)

From Fig. 3.53 it can be found that the initialization time required by the RFLT solution is still the longest. It exceeds 30 min for two stations. Compared with that, the initialization time for the GFLT solution is shorter for all stations. The average value is 613 s (approx. 10.2 min). By applying ambiguity resolution, the initialization time becomes shorter for most of the stations, and is 583.6 s (approx. 9.7 min) on average. The initialization process can also be accelerated by utilizing GNSS observations, for which it can be achieved on average in 533 s (approx. 8.9 min). Again, this suggests that the effect of the observation geometry is larger than that of ambiguity resolution in accelerating the initialization process, especially considering that an initialization time is required to achieve the first ambiguity resolution. When applying all three GNSS and ambiguity resolution in the MFIX solution, the initialization process is finished on average in 508.3 s (approx. 8.5 min), and there are only small differences between different stations, which leads to the highest consistency in the solutions and reveals the benefit of GNSS observation and ambiguity resolution for severe weather event monitoring (for more details see Ding et al. 2017).

Furthermore, the solutions from the five different RT data processing modes can be compared to the benchmark troposphere products from CODE and USNO, both being GPS + GLONASS solutions (Table 3.17).

The statistics with respect to the two types of benchmark products are similar, which further validates the reliability and consistency of the reference products. The RMS of the RFLT solution for nearly all stations is smaller than 15 mm, and the average value is about 11.16 and 13.98 mm with respect to the final troposphere products from CODE and USNO. Compared with that, the RMS of the GFLT solution is better. The RMS of all stations is better than 12 mm except MOBS, and is about 9 mm on average. The worse performance of the RFLT solution may

Table 3.17 Mean accuracy of processing modes with respect to final troposphere products from CODE and USNO (reproduced from Ding et al. 2017)

	CODE			USNO		
	Mean(mm)	STD(mm)	RMS(mm)	Mean(mm)	STD(mm)	RMS(mm)
RFLT	0.82	11.26	11.61	0.61	13.67	13.98
GFLT	−0.83	6.32	7.05	−0.59	8.27	8.95
GFIX	−2.09	5.65	6.37	−2.03	7.45	8.17
MFLT	−0.47	6.41	6.87	−0.41	8.27	8.69
MFIX	−1.48	5.96	6.42	−1.52	7.69	8.14

come from two points: (1) the number of GLONASS satellites is less than for GPS; (2) the accuracy of satellite products for GLONASS is worse than for GPS (Dach and Jean 2015). However, considering the accuracy requirements (10–15 mm) in updating NWP models, the RT troposphere estimates based on GPS or GLONASS only observations can both fulfill the requirements (De Haan 2006).

Applying ambiguity resolution, the GFIX solution is further improved up to 0.8 mm on average compared to the GFLT solution. However, the mean bias becomes slightly bigger. Combining the observations of two systems, the MFLT solution is only 0.18 mm and 0.26 mm improved on average with respect to CODE and USNO products, which reveals that the accuracy is not greatly improved by incorporating GLONASS observations. In addition, the accuracy even becomes a little worse for some stations, which may be correlated with the weighting strategy between two systems and needs further research in the future. At last, the mean RMS of the MFIX solution is 6.42 mm and 8.14 mm with respect to CODE and UNSO products, respectively. It is the best solution among all the data processing modes, which again reveals the effect in utilizing GNSS observations and ambiguity resolution.

A further comparison was performed with respect to radiosonde observations (Fig. 3.54). To summarize the accuracy of the 13 stations, we sort the results according to the distance between the GNSS station and the nearby radiosonde launch site. Since the mean bias of RT ZTD are monitored and will be corrected in the assimilation procedure, we will only calculate the standard deviation (StDev) of all stations (Bennitt and Jupp 2012). Based on the results, the accuracy of the RFLT solution is the worst, of which the StDev is especially larger and exceeds 15 mm in several stations. Among the other solutions, the StDevs are all smaller than 15 mm except for ABMF and JFNG. On average, the StDevs of the two single system solutions are 14.6 mm and 9.1 mm each, which again reveals that they can fulfill the requirements in monitoring severe weather events.

However, compared with the GFLT solutions, we notice that the accuracies of the GFIX and MFLT solutions become a little lower for many stations. Since there is only one radiosonde observation in each day, this might be a consequence of the instability of GPS phase bias information and the satellite orbit/clock products for GLONASS. Additional details can be found in Ding et al. 2017.

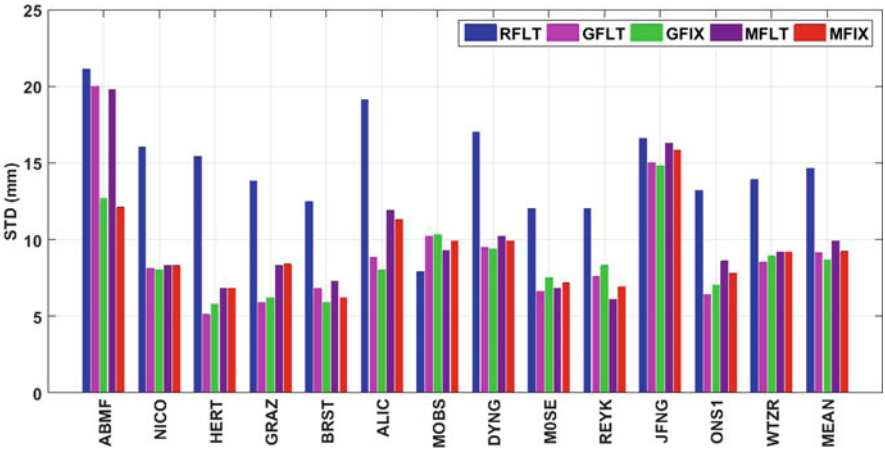

Fig. 3.54 Standard deviation of RT ZTD errors with respect to the radiosonde observations in all data processing modes (reproduced from Ding et al. 2017)

3.4.7 New Adaptable Strategy for RT and NRT Troposphere Monitoring[10]

P. Václavovic
Geodetic Observatory Pecný, Research Institute of Geodesy, Topography and Cartography, Zdiby, Czech Republic
e-mail: pavel.vaclavovic@pecny.cz

J. Douša
Geodetic Observatory Pecný, RIGTC, Ondřejov, Czech Republic
e-mail: jan.dousa@pecny.cz

In order to optimize the accuracy and the timeliness of tropospheric parameters with possibly prioritizing the product latency in real-time (RT) or its accuracy in near real-time (NRT), we have developed a new adaptable strategy in the G-Nut/Tefnut software (Douša et al. 2018a) exploiting the Precise Point Positioning, PPP (Zumberge et al. 1997). We aimed to support various users from a single processing PPP engine combining RT and NRT analysis modes. All the parameters, ZTD, GRD and STD, are estimated consistently for both product lines when supported by real-time orbit and clock products. The strategy based on data from an individual station only is also ready to exploit optimally all available multi-GNSS observations when supported by precise products.

[10]Parts from this section were previously published in Douša et al. (2018a).

3.4.7.1 Epoch-Wise Filtering vs. Batch Processing

Nowadays, a common procedure of the NRT analysis within the EIG EUMETNET GNSS Water Vapour Programme (E-GVAP, http://egvap.dmi.dk) is based on the least-squares adjustment (LSQ) analysis and a piece-wise linear function of the modelling of tropospheric parameters within the processing interval. By using the BSW52 (Dach et al. 2015), Geodetic Observatory Pecný (GOP) applies the same strategy in all long-term contributions to E-GVAP (Douša 2001a, b, Douša and Bennitt 2013). The estimated tropospheric parameters for such case are displayed in Fig. 3.55 by black dots and the piece-wise deterministic model by dash lines connecting the parameters within each hourly product update; not necessarily connected at update boundaries. According to the E-GVAP conventions, the last product value is shifted by 1 min (HR:59) in order to avoid a duplicate value with the next hour product update.

So far, the tropospheric horizontal linear gradients and slant delays were not provided by GOP because of two reasons: (1) not being yet assimilated into numerical weather models (NWM), and (2) significantly increase the number of parameters in the network solution and, consequently, the computation time. From this point of view, the epoch-wise processing (e.g. Kalman filter) is an optimal strategy as it, contrary to the LSQ, estimates recurrently all unknown parameters in every epoch. One of the consequences is that only previous observations contribute to a current estimate and thus the solution needs a certain time to converge. However, an accuracy of parameters estimated during the initial convergence, or any later re-convergence, can be improved only by using the backward smoothing algorithm (Václavovic and Douša 2015) additionally using both past and following observations for improving the precision at every epoch. As a consequence, the backward smoothing was designed for the post-processing solutions and it can substitute the LSQ in a number of applications. In the first step of the filter, parameters are predicted via adding particular amount of noise to diagonal elements of the variance-covariance matrix belonging to dynamic parameters. When new observations are available the state vector with its variance-covariance matrix are

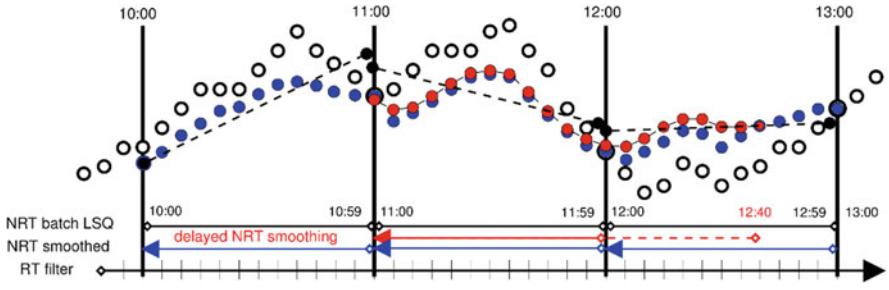

Fig. 3.55 Various strategies of the troposphere modelling: (1) piece-wise model (black dots connected with dash lines) and (2) stochastic modelling by real-time Kalman filter (white points), hourly backward smoothing (blue points), and 45-min postponed hourly backward smoothing (red points)

updated. Results from the prediction as well as from the update needs to be stored for future smoothing. Since the standard Kalman filter and also smoother can suffer from numerical instabilities due to the round-off error we have implemented alternative forms of the algorithms exploiting Cholesky and Singular Value Decompositions of the variance-covariance matrix instead of the original one.

3.4.7.2 RT and NRT Combined Processing Supported by Observations from Files or Streams

In E-GVAP, the NRT products are updated on hourly basis and the delivery requirement to the E-GVAP server at UK Met Office is 45 min after the last observation used in the analysis. The NRT LSQ batch processing, initiated every hour when obtaining a majority of data files, is thus a relevant solution for this purpose when using hourly data files. Although the backward smoothing approach is the most beneficial for the post-processing solutions, it can be effectively used in NRT applications too. We have thus used it for the new adaptable strategy combining a continuously running forward filter with a regularly triggered backward smoothing filter. The former is aimed for the estimating epoch-wise tropospheric parameters in real-time indicated by white points in Fig. 3.55. The backward smoothing is started periodically at a pre-defined time stamp as indicated at HR:00 in the Figure. It uses the initial state vector from the same epoch provided by the real-time filter for recalculating the past parameters from the Kalman filter. Obviously, such recalculation is able to refine significantly older parameters, but cannot improve parameters at the initial epochs of the backward smoothing. The length of the smoothing period can be set flexibly to reflect an actual user preference for a higher accuracy or a shorter latency of the product. In such way, the standard E-GVAP NRT tropospheric product can also be provided on hourly basis as shown by blue points in the Figure.

Initially, the new adaptable strategy was designed to use the precise orbit and clock corrections disseminated through RT streams, it can however exploit observations coming from both real-time (streams) and near real-time (hourly or sub-hourly files). While the former is necessarily used in a simultaneous RT and NRT product generation, the latter is applicable for NRT only. In any case, both data flows can be mixed and analysed for each station independently. Additional advantage of the NRT analysis utilizing the backward smoothing and RT observations may profit from the 45-min requirement in E-GVAP for the product delivery in NRT. By starting the backward smoothing shortly before the delivery request, indicated in Fig. 3.55 by the red arrow starting at 12:40, new observations can further improve the accuracy of NRT product, in particular last parameters of the NRT product and still reduce systematic errors typical for data interval boundaries.

3.4.7.3 Estimating High-Resolution ZTDs and Horizontal Gradients

Estimating high-resolution parameters with the batch LSQ can be more difficult due to increasing size of normal equations, in particular for the network processing, and consequently extending the processing time due to the inversion of the large matrix of the solution. On the contrary, the described combination of the Kalman filter and smother seems to be more convenient for monitoring dynamical processes when high-resolution parameters are required. Since only observations from past epochs are used in the Kalman filter processing, achieved parameters cannot react on their fast change, and batch processing can reach better precision in this case. However, when backward smoothing is applied, following observations improve the state vector estimation when preserving high resolution from the previous forward filter.

Such situation is presented in Fig. 3.56 showing the ZTDs from different solutions during the fast change in the troposphere, indicated with a sudden decrease of ZTD by 6–7 cm during 2.5 h at POTS station on May 10, 2013. Obviously, the post-processing 15-min ZTDs from the GFZ solution using the EPOS software (Gendt et al. 2004) implementing the LSQ processing (gray points) and the daily smoothed 30-s stochastic ZTDs from our software (black dots) are in a very good agreement. Note that ZTDs from our solution is resampled to 5 min in the Figure. Due to the use of past observations only, the real-time Kalman filter (red points) shows a delay in the change of estimated parameter. The random walk for ZTD was set to 5 mm/h$^{1/2}$. The Figure reveals a characteristic behaviour for the real-time processing when using past observations in stochastic parameter estimation. We can observe significant improvements mainly in reducing the systematic behaviour for the 1-h backward smoothing (green points). The main improvement can be reached within 15–30 min, as indicated for the ZTD from the backward smoothing at 12:00, 13:00 and 14:00. Interestingly, the ZTD from the 2-h smoothing already shows a very good agreement with the post-processing LSQ solution. It shows a potential improvement discussed in the previous subsections and postponing the NRT smoothing by at least 30 min if RT observations are available.

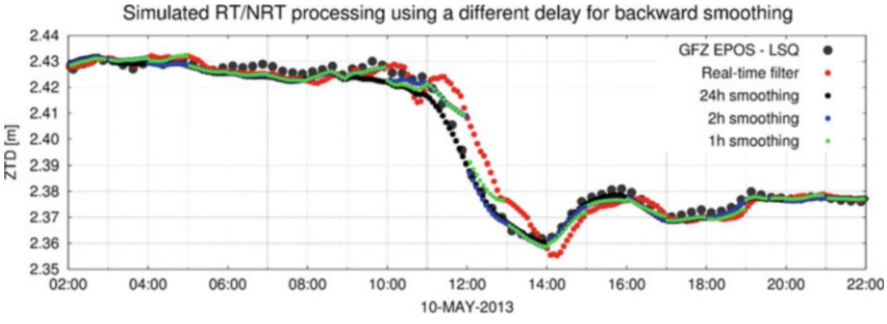

Fig. 3.56 Real-time (red), near real-time (green, blue) and reference (black) ZTD estimates during a fast change in the troposphere

3.4.7.4 Assessment of New Method Compared to the Existing E-GVAP Processing

The new strategy has been initially developed and assessed using the GNSS4SWEC Benchmark campaign (Douša et al. 2016) and firstly compared to the GOP NRT tropospheric solution contributing operationally to E-GVAP. Thought the new strategy can provide RT and NRT products in high temporal resolution, we compared only the ZTD as a product of HH:00 and HH:59 time stamps in every hour representing the standard NRT E-GVAP product, see Fig. 3.55.

Table 3.18 summarizes results of three strategies and six ZTD solutions using 13 EUREF stations selected from the benchmark campaign and exploiting the EUREF combined ZTD product as a reference for all comparisons (Pacione et al. 2017). The table shows summary statistics indicating similar improvements in terms of the standard deviation over all ZTDs estimated at HH:00 in NRT independently on applied products (IGS RTS vs. IGS final products), processing strategies and software (G-Nut/Tefnut PPP vs. BSW52 DD). Compared to the Kalman filter ZTD estimated at the last epoch (HH:59), the backward smoothing running on hourly basis showed the improvement of 20% and 24% for the IGS RTS and the IGS final product, respectively. The E-GVAP/GOP product demonstrates a similar improvement (24%) comparing ZTD from HH:00 against HH:59, which corresponds to our previous results (Douša and Souček 2005). The new adaptable PPP solution using the IGS final orbits reached the same accuracy as the E-GVAP/GOP product using the IGS ultra-rapid orbits and NRT DD network solution from the BSW. On the other hand, the use of IGS RTS products instead of IGS final products in PPP indicates a degradation of 18% in ZTD SDEV and a 2.5 mm bias. It should be finally noted, that the E-GVAP/GOP solution and the reference EUREF solution are based on a similar processing strategy and the software, while the new strategy is significantly different.

Table 3.18 Summary statistics of three processing strategies and six ZTD solutions compared to EUREF combined tropospheric product

Solution	Software	Strategy description	Latency	Mean BIAS	Mean SDEV
RT PPP (HR:59)	G-Nut/ Tefnut	Kalman filter, simulated real-time solution	<5 min	2.4 mm	5.7 mm
NRT PPP (HR:00)	G-Nut/ Tefnut	Hourly backward smoothing in real-time	~ 60 min	2.5 mm	4.6 mm
PP PPP (HR:59)	G-Nut/ Tefnut	Kalman filter in offline processing, IGS final	< 5 min	0.1 mm	4.7 mm
PP PPP (HR:00)	G-Nut/ Tefnut	Hourly backward smoothing with IGS final	~ 60 min	−0.2 mm	3.6 mm
NRT DD (HR:59)	BSW52	Last ZTD of hourly PW linear LSQ	~ 90 min	0.4 mm	4.9 mm
NRT DD (HR:00)	BSW52	First ZTD of hourly PW linear LSQ	~ 30 min	0.2 mm	3.7 mm

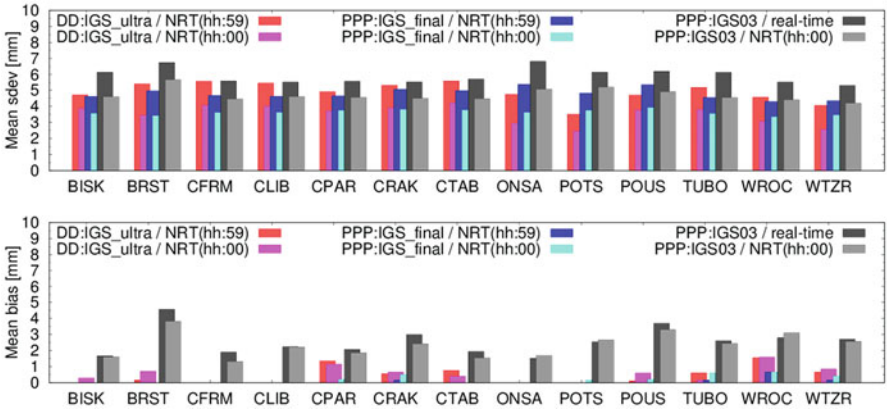

Fig. 3.57 ZTD standard deviations and biases for 13 EUREF stations and six processing strategies compared to the reference EUREF product

Figure 3.57 shows standard deviations and biases individually for all stations comparing the first ZTDs (HH:00) and the last ZTDs (HH:59). The statistics of ZTDs from the E-GVAP/GOP solution (PPP:DD-ultra) are plotted in red and pink for HH:00 and HH:59, respectively. The results from the new strategy using the PPP with IGS final orbit and clock products (PPP:IGS-final) are shown in dark and light blue and, using IGS RTS (PPP:IGS03) in black and grey. Standard deviations for all the stations show a similar improvement in the ZTD SDEV over all the strategies, software and precise products. However, there is no significant impact of the strategy on systematic errors, and we can observe only a common positive bias attributed to the use of the IGS RTS products.

3.4.8 Optimum Stochastic Modeling for GNSS Tropospheric Delay Estimation in Real-Time[11]

T. Hadaś
Wrocław University of Environmental and Life Sciences, Wrocław, Poland
e-mail: tomasz.hadas@upwr.edu.pl

K. Kaźmierski
Wrocław University of Environmental and Life Sciences, Wrocław, Poland
e-mail: kamil.kazmierski@up.wroc.pl

P. Hordyniec
Wrocław University of Environmental and Life Sciences, Wrocław, Poland
e-mail: pawel.hordyniec@upwr.edu.pl

[11]Parts from this section were previously published in Hadaś et al. (2017).

J. Bosy
Wrocław University of Environmental and Life Sciences, Wrocław, Poland
e-mail: jaroslaw.bosy@up.wroc.pl

F. N. Teferle
University of Luxembourg, Luxembourg, Luxembourg
e-mail: norman.teferle@uni.lu

It is commonly accepted by the GNSS community to constrain epoch-wise ZWD estimates, usually by estimating ZWD as a random walk parameter. Wrocław University of Environmental and Life Sciences (WUELS) have shown that the optimum ZWD constraints in real-time GNSS processing, modelled as a random-walk process, should be time and location specific. A typical approach is to perform an initial empirical testing in order to obtain the effective constraining. As an alternative, WUELS proposed to take benefit from numerical weather prediction models to define optimum random walk process noise (RWPN). Two different strategies were proposed and validated.

In the first approach an archived ZTD time series can be used to calculate a grid of yearly means of the difference of ZWD between two consecutive epochs divided by the root square of the time lapsed, which can be considered as a random walk process noise. Using archived VMF-G grids, we obtained RWPN global grids for hydrostatic and wet parameter (Fig. 3.58). We noticed that grids are nearly identical year by year, with differences below 1 mm/√h for hydrostatic and wet grids. This means that a single RWPN grid can be implemented in a software as a look up table to define the optimum wet RWPN value for any station located worldwide. It was shown that RWPN values from grids are similar to those obtain with empirical testing (see Fig. 3.58).

Alternatively, a short-term weather forecast can be used to perform ray-tracing in order to obtain forecast of ZTD and then to calculate RWPN dynamically in real-time. This approach was validated using forecast from GFS4 model. In this case

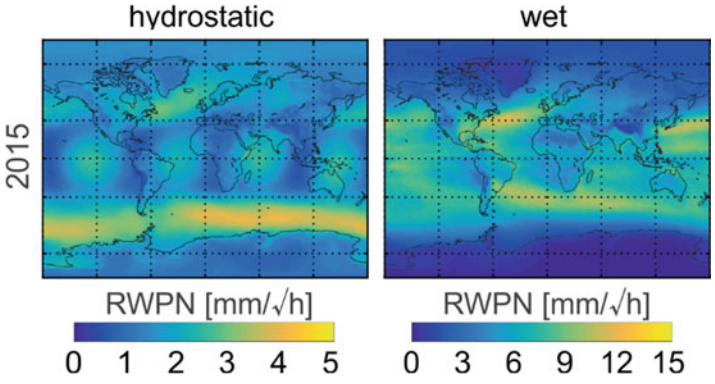

Fig. 3.58 Hydrostatic (left) and wet (right) yearly mean RWPN grid for 2015

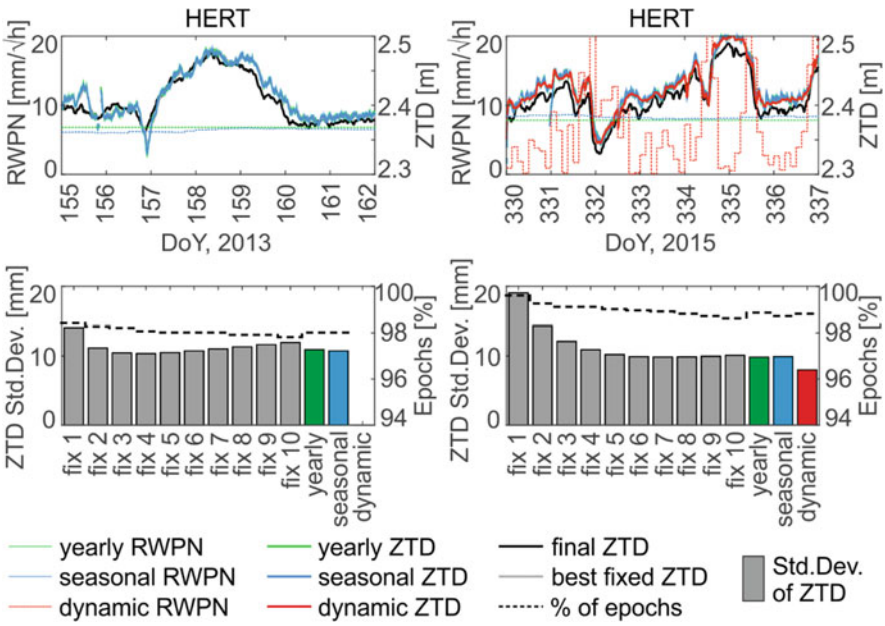

Fig. 3.59 Comparison of wet RWPN, ZTD time series, standard deviations of real-time ZTD residuals

superior results were obtained, by means on the accuracy and precision of estimated tropospheric delay (see Fig. 3.59). The advantage of this approach is that the wet RWPN is regularly adjusted to the current tropospheric conditions. Its value remains low, when ZTD is stable over time, and rises when a rapid change of ZTD is expected. More details can be found in Hadaś et al. (2017).

3.5 Exploiting NWM-Based Products for Precise Positioning

Numerical Weather Model (NWM) data and/or derived climatologies are increasingly used in precise geodetic applications. A prominent example is the Vienna Mapping Function, VMF (Boehm et al. 2006a), and the Global Mapping Function, GMF, (Boehm et al. 2006b). In recent years, the tropospheric models became more sophisticated including NWM tropospheric (1st/2nd order) gradient estimates, NWM tropospheric mapping factors, advantages of utilization of high-resolution NWM models and NWM predictions, and others. The use of NWM-derived parameters plays more significant role in both a long-term reprocessing and real-time kinematic positioning. The following section provides an overview of achievements in this respect within the COST Action.

3.5.1 Tropospheric Parameters from Numerical Weather Models

F. Zus
GFZ German Research Centre for Geosciences, Potsdam, Germany
e-mail: zusflo@gfz-potsdam.de

The tropospheric delay T is approximated as

$$T(e,a) = mf_h(ah,bh,ch,e)\cdot Z_H + mf_w(aw,bw,cw,e)\cdot Z_W + mf_G(C,e)[N\cos(a) + E\sin(a)] \quad (3.20)$$

where e and a denote the elevation and azimuth angle of the station satellite link, mf_h and mf_w denote the hydrostatic and non-hydrostatic Mapping Function (MF), $\mathrm{mf_g}$ denotes the gradient MF, Z_h and Z_w are the zenith hydrostatic and non-hydrostatic delay, and N and E denote the (first-order) gradient components. The elevation angle dependency of the hydrostatic (non-hydrostatic) MF is based on the continued fraction form proposed by Marini (1972) and normalized by Herring (1992) to yield the unity at zenith

$$m(a,b,c,e) = (1 + a/(1 + b/(1 + c)))/(\sin(e) + a/(\sin(e) + b/(\sin(e) + c))) \quad (3.21)$$

The elevation angle dependency of the gradient MF is based on the form proposed by Chen and Herring (1997):

$$mg(C,e) = 1/(\sin(e)\tan(e) + C) \quad (3.22)$$

where $C = 0.003$. Therefore, provided that the tropospheric parameters *ah, bh, ch, aw, bw, cw, zh, zw*, N and E are known, the tropospheric delay can be assembled for any station satellite link. The tropospheric parameters are determined from ray-traced tropospheric delays. The required pressure, temperature and humidity fields are taken from a Numerical Weather Model (NWM). At GFZ Potsdam the algorithm proposed by Zus et al. (2014) is used to compute mapping factors and slant factors, i.e. the ratios of slant and zenith delays. Note that mapping factors are computed under the assumption of a spherically layered troposphere. From the mapping factors and slant factors the tropospheric parameters are estimated by least-squares fitting. This is done separately for the mapping function coefficients and the gradient components.

3.5.1.1 Mapping Function Coefficients

For each station, 10 hydrostatic (non-hydrostatic) mapping factors are computed for elevation angles of 3, 5, 7, 10, 15, 20, 30, 50, 70, 90 degree, and the hydrostatic (non-hydrostatic) MF coefficients are determined by least-squares fitting (Zus et al. 2015a).

3.5.1.2 Gradient Components

At first, 120 slant factors and corresponding mapping factors are computed at elevation angles 3, 5, 7, 10, 15, 20, 30, 50, 70, 90 degree and the azimuth angles 0, 30, 60, 90, 120, 150, 180, 210, 240, 270, 300, 330 degree. Second, zenith delays are applied to obtain azimuth-dependent and azimuth-independent slant total delays. Third, the differences between azimuth-dependent and azimuth-independent slant total delays are computed. Finally, the gradient components are determined by least-squares fitting (Zus et al. 2015b).

3.5.1.3 Tropospheric Model Errors

The pressure, temperature and humidity fields are taken from Global Forecast System (GFS) of the National Centers for Environmental Prediction (NCEP). The NCEP's GFS analyses are available every 6 h (00:00, 06:00, 12:00, 18:00 UTC) with a horizontal resolution of 0.5 degree on 31 pressure levels. Tropospheric parameters are derived for a grid with a resolution of 0.5 degree. For any gridpoint on Earh's surface we examine how well the modeled tropospheric delays, i.e., the tropospheric delays assembled from the tropospheric parameters, match the true (ray-traced) tropospheric delays. This is done by calculating the elevation angle dependent postfit-residual.

$$R(e) = \sqrt{\frac{\sum \left(T\left(e, a_j\right) - S\left(e, a_j\right)\right)^2}{n}} \tag{3.23}$$

where T denotes the assembled tropospheric delay and S denotes the ray-traced tropospheric delay. The elevation angles are chosen to be 3, 5, 7, 10, 15, 20, 30, 50, 70, 90 degree and the azimuth angles are chosen to be 0, 30, 60, 90, 120, 150, 180, 210, 240, 270, 300, 330 degree. As an example we consider a single epoch (first of May 2017, 12:00 UTC).

At first, we examine azimuth independent tropospheric delays. Figure 3.60 shows the residuals for an elevation angle of 7°. The residuals are well below 1 mm for any point on Earth's surface. For comparison Figure 3.61 shows the residual for an elevation angle of 7° if we replace the NWM based MF by the GMF (Boehm et al. 2006a, b). Clearly, as the GMF is based on a climatology it cannot capture the short-

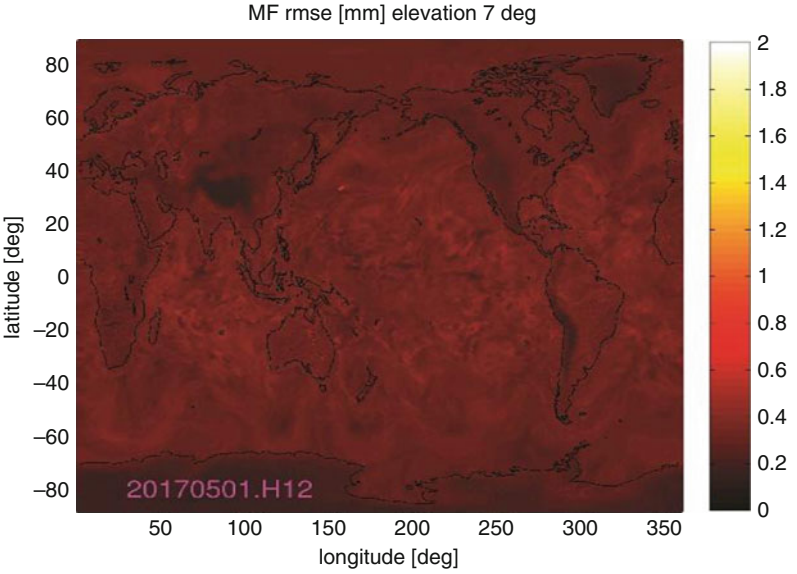

Fig. 3.60 We examine azimuth independent tropospheric delays (1st of May 2017, 12:00 UTC). The scatter plot shows the tropospheric residuals for an elevation angle of 7°

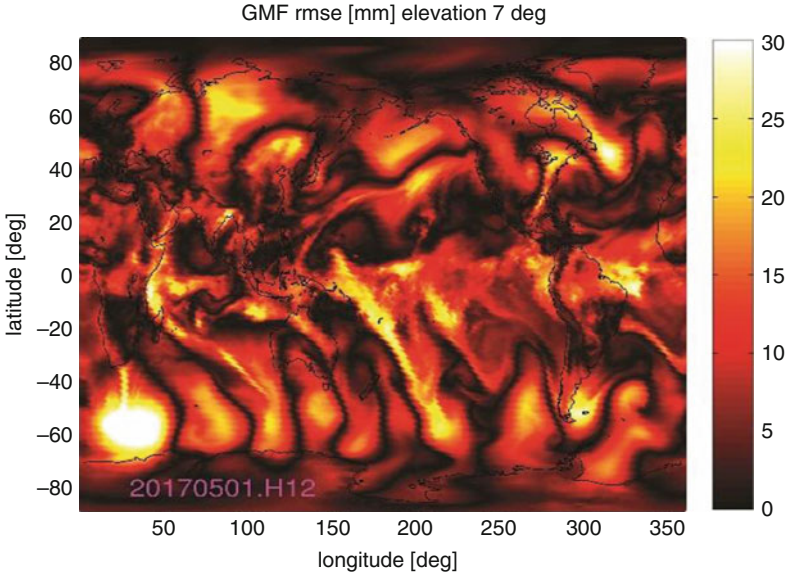

Fig. 3.61 We examine azimuth independent tropospheric delays (1st of May 2017, 12:00 UTC). The NWM based MF is replaced by the GMF. The scatter plot shows the tropospheric residuals for an elevation angle of 7°

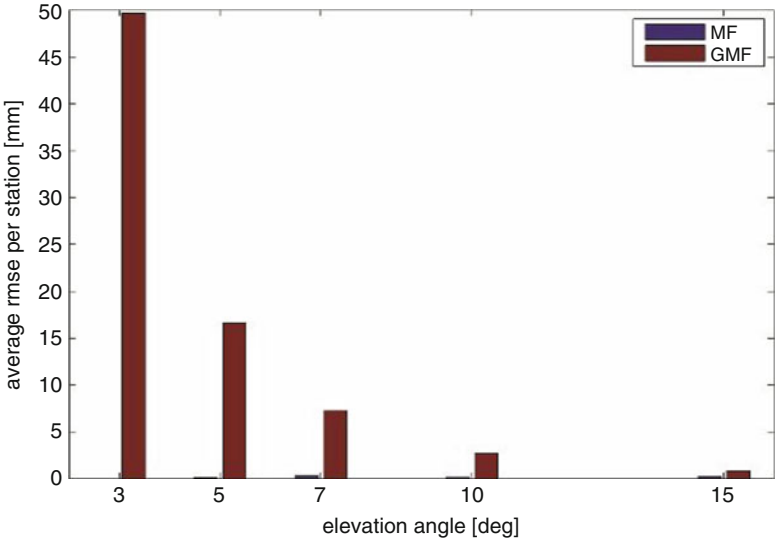

Fig. 3.62 We examine azimuth independent tropospheric delays (1st of May 2017, 12:00 UTC). The bar plot shows the average residual per grid point as a function of the elevation angle. Different colors show different options; NWM based MF and GMF

term variability of the troposphere and hence the residuals are larger. Figure 3.62 shows the average residual per grid point as a function of the elevation angle. The residuals for the NWM based MF are well below 1 mm for any elevation angle emphasizing the fact that the three term continued fraction form of the mapping function works with an exquisite level of precision. Hence, if the troposphere is indeed spherically layered, the tropospheric model (its functional form) can be regarded error free.

Next, we examine azimuth dependent tropospheric delays. Figure 3.63 shows the residuals for an elevation angle of 7° when no gradients are applied and Fig. 3.64 shows the residuals for an elevation angle of 7° when gradients are applied. As to expect the residuals are significantly reduced when gradients are applied. The residuals can be reduced by adding higher-order gradients to the tropospheric delay model. In essence, the tropospheric delay is approximated as

$$\begin{aligned} T(e,a) = {} & mf_h(ah,bh,ch,e)\cdot Z_H + mf_w(aw,bw,cw,e)\cdot Z_W \\ & + mf_G(C,e)[G_N\cos(a) + G_E\sin(a)] \\ & + mf_G(C,e)[\mathrm{Fcos}(a)\cos(\mathrm{a}) + \mathrm{Gcos}(a)\sin(\mathrm{a}) + \mathrm{Hsin}(a)\sin(\mathrm{a})] \end{aligned} \tag{3.24}$$

where *F, G* and *H* denote higher-order gradient components.

Figure 3.65 shows the residuals for an elevation angle of 7° when first- and higher-order gradients are applied. Finally, Fig. 3.66 shows the average residual per grid point as a function of the elevation angle. The application of higher-order

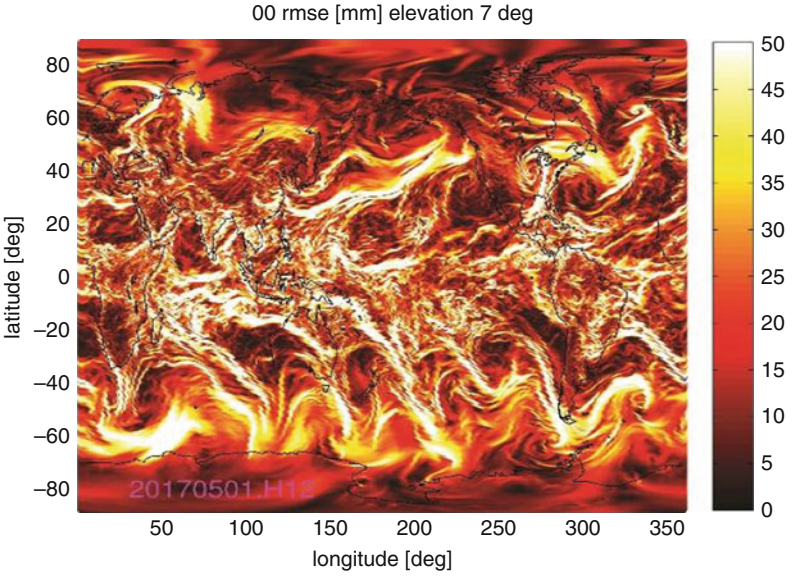

Fig. 3.63 We examine azimuth dependent tropospheric delays (1st of May 2017, 12:00 UTC). The scatter plot shows the tropospheric residuals for an elevation angle of 7 ° when no gradients are applied

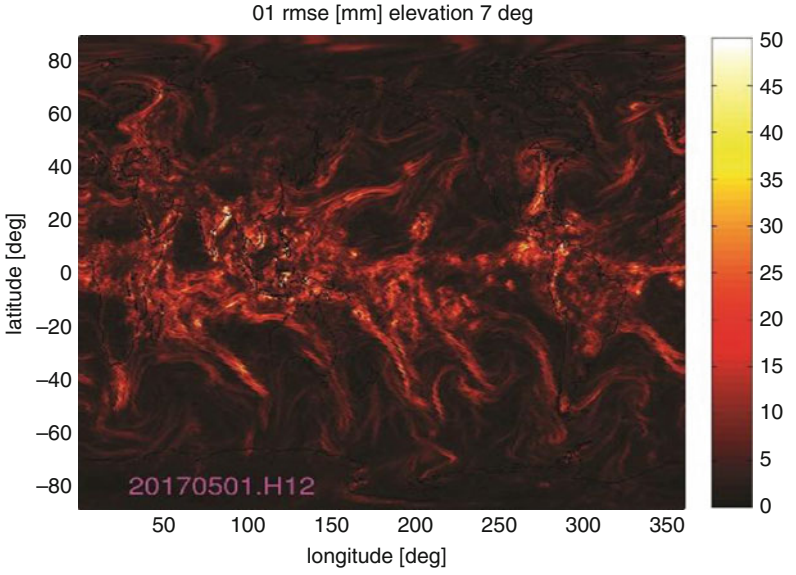

Fig. 3.64 We examine azimuth dependent tropospheric delays (1st of May 2017, 12:00 UTC). The scatter plot shows the tropospheric residuals for an elevation angle of 7 ° when first-order gradients are applied

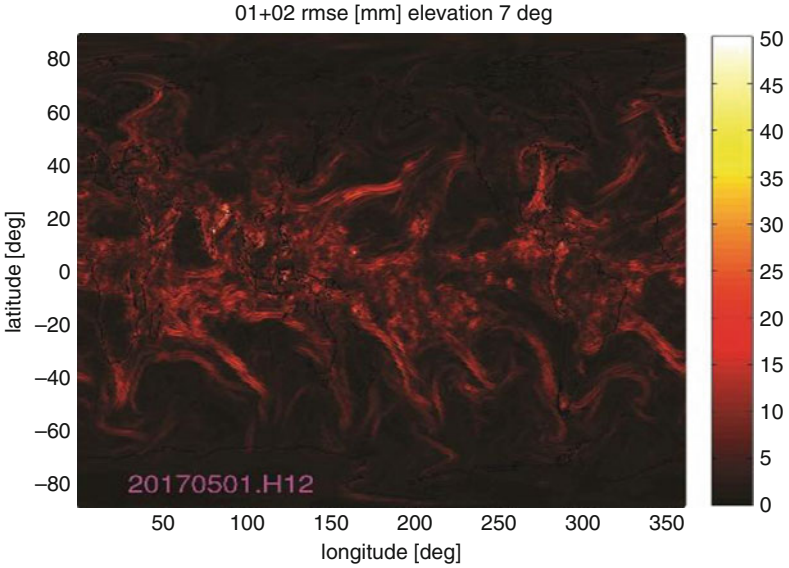

Fig. 3.65 We examine azimuth dependent tropospheric delays (1st of May 2017, 12:00 UTC). The scatter plot shows the tropospheric residuals for an elevation angle of 7 ° when first- and higher-order gradients are applied.

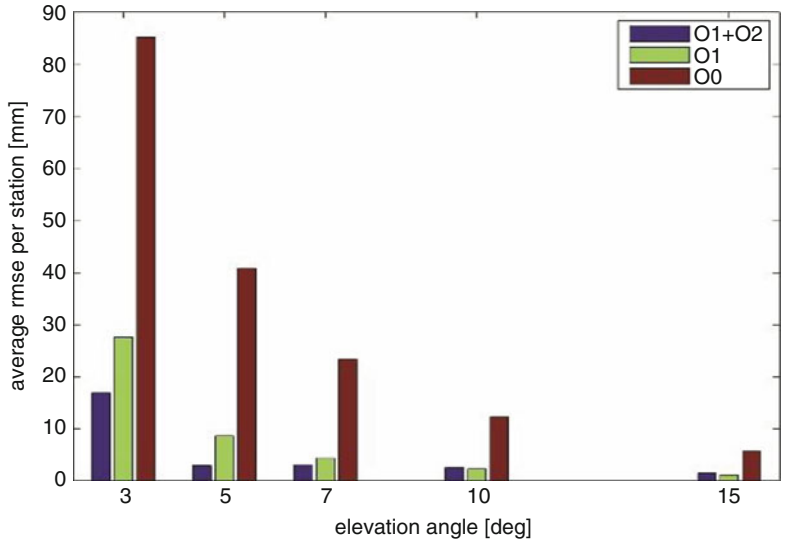

Fig. 3.66 We examine azimuth independent tropospheric delays (1st of May 2017, 12:00 UTC). The bar plot shows the average residual per grid point as a function of the elevation angle. Different colors show different options; no gradients applied, first-order gradients applied and first- and higher-order gradients applied.

gradients reduces the residual in particular for elevation angles below 10°. We recall that the underlying NWM has a horizontal resolution of 0.5 degree. Small scale tropospheric features cannot be represented by the low horizontal resolution. Larger residuals are expected when the horizontal resolution of the underlying NWM increases.

3.5.2 *The Impact of Global and Regional Climatology on the Performance of Tropospheric Blind Models*

G. Möller
Department of Geodesy and Geoinformation, TU Wien, Wien, Austria
e-mail: gregor.moeller@geo.tuwien.ac.at

J. Sammer
Department of Geodesy and Geoinformation, TU Wien, Wien, Austria
e-mail: julia.sammer@student.tugraz.at

For tropospheric delay modelling usually the concept of mapping functions is used:

$$\Delta L(\varepsilon) = \Delta L_h^z \cdot mf_h(\varepsilon) + \Delta L_w^z \cdot mf_w(\varepsilon) \tag{3.25}$$

It describes the total slant delay ΔL at elevation angle ε as as the sum of a hydrostatic and a wet component. Each component can be expressed as the product of a zenith delay and the corresponding mapping function.

Empirical troposphere models like GPT2w (Böhm et al. 2015) can provide this information for any user position and epoch. In particular, GPT2w is based on global $1^\circ \times 1^\circ$ gridded values of tropospheric state parameters like surface pressure for modelling the zenith hydrostatic delay or water vapour pressure, weighted mean temperature and water vapour decrease factor for modelling of the zenith wet delay. In addition, mapping coefficients are provided separately for the hydrostatic and the wet mapping function, to further reduce the mapping error, especially below 15 degrees elevation angle (Möller et al. 2014).

Comparison with time series of the IGS reveal that GPT2w allows for modelling of the zenith tropospheric delay with a bias of less than 1 mm and a RMS of about 3.6 cm, see (Böhm et al. 2015). However, to further improve the model performance on regional level, the global $1^\circ \times 1^\circ$ grid was replaced by a regional $0.2^\circ \times 0.3^\circ$ grid.

Analogous to the global grid, on the regional climatological grid tropospheric parameters are provided as mean, annual and semi-annual coefficients. The regional coefficients were derived from 3 years of ALARO model data, as provided by the Central Institute for Meteorology and Geodynamics (ZAMG), Austria on 18 pressure levels with a temporal resolution of 3 h.

Figure 3.67 shows time series of pressure (p), temperature (T), temperature lapse rate (dT), mean temperature (Tm), water vapour pressure (e) and water vapour

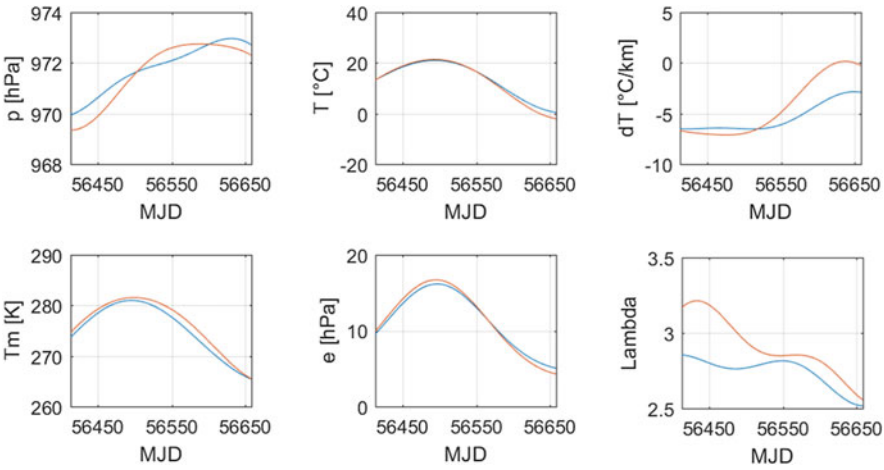

Fig. 3.67 Meteorological parameters as obtained from GPT2w (blue) and GPT2w ALARO (red) at GNSS station HART, Austria. Analysed period: May–Dec 2013

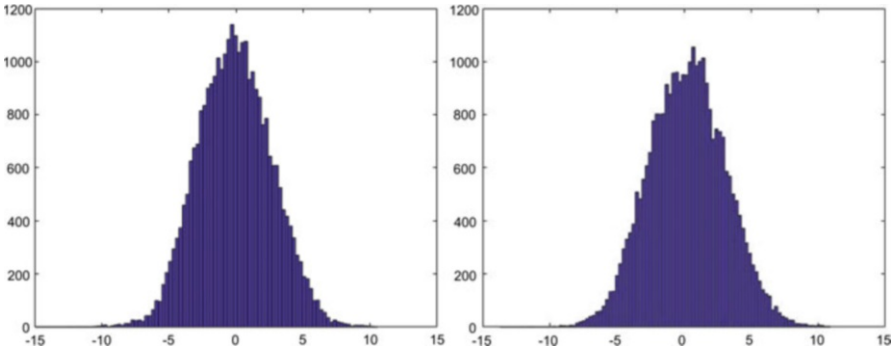

Fig. 3.68 Histogram of ZTD residuals (GNSS minus model) as obtained at 45 GNSS in Austria. (Left) GNSS minus GPT2w, (right) GNSS minus GPT2w ALARO. Analysed period: May–Dec 2013

decrease factor (Lambda), as obtained from both grids, exemplary for GNSS station HART, Austria. The regional model (GPT2w ALARO) shows in general a more distinct seasonal signal than the global GPT2w. Especially in temperature lapse rate and water vapour decrease factor, significant differences can be observed.

In order to evaluate the impact on the delay modelling based on both grids, ZTD time series were derived for about 45 GNSS sites in Austria and neighbouring countries. Figure 3.68 shows the ZTD residuals for GPT2w and GPT2w ALARO with respect to ZTDs derived from dual-frequency GNSS observations at GNSS site.

The regional grid helps to further reduce the ZTD bias at GNSS sites, which are located north and south of the main Alpine ridge. Nevertheless, averaged over all

GNSS station and over the period May to December 2013, the mean bias (GPT2w: −2 mm and GPT2w ALARO: 3 mm) and standard deviation (GPT2w: 29 mm and GPT2w ALARO: 30 mm) of GPT2w ALARO is very comparable to the global GPT2w. In consequence, it is concluded that a higher spatial resolution does not lead consequently to a better performance of the tropospheric blind model, even not in the Alpine area. In order to further increase the performance of tropospheric blind models in future other strategies have to be discovered.

3.5.3 *Refined Discrete and Empirical Troposphere Mapping Functions VMF3 and GPT3*[12]

D. Landskron
Department of Geodesy and Geoinformation, TU Wien, Wien, Austria
e-mail: daniel.landskron@geo.tuwien.ac.at

J. Boehm
Department of Geodesy and Geoinformation, TU Wien, Wien, Austria
e-mail: Johannes.Boehm@geo.tuwien.ac.at

The Vienna Mapping Functions 3 (VMF3) is a refinement of VMF1 with the aim of even higher precision. It eliminates shortcomings in the empirical coefficients b and c and is not only tuned for the specific elevation angle of 3°, but for the whole elevation range through least-squares adjustments. The new mapping function coefficients were determined on the basis of ray-traced delays of the ray-tracer RADIATE (Hofmeister and Böhm 2017). Comparing modeled slant delays of VMF3 and VMF1 with the underlying ray-traced delays proves the high quality of VMF3, in particular at low elevation angles. In consequence, when requiring highest precision, VMF3 is to be preferable to VMF1. For more details, the reader is referred to Landskron and Böhm (2017).

Figure 3.69 shows the empirical (blind) troposphere model Global Pressure and Temperature 3, GPT3 (Landskron and Böhm 2017) as a refinement of the model Global Pressure and Temperature 2 wet, GPT2w (Böhm et al. 2015), with re-calculated mapping function coefficients and empirical horizontal gradients, available in a horizontal resolution of 5° × 5° and 1° × 1°. The meteorological quantities remain unchanged. The empirical mapping factors from GPT3 are averaged from the VMF3 applying information from 2D ray-tracing through numerical weather models of the ECMWF.

GPT3 is full consistent with VMF3 and can be used for GNSS as well as VLBI analysis. It is unique in such a way as it provides the entire information which is required in order to model a priori the troposphere delay dependent on elevation angle and azimuth.

[12]Parts from this section were previously published in Landskron and Böhm (2017).

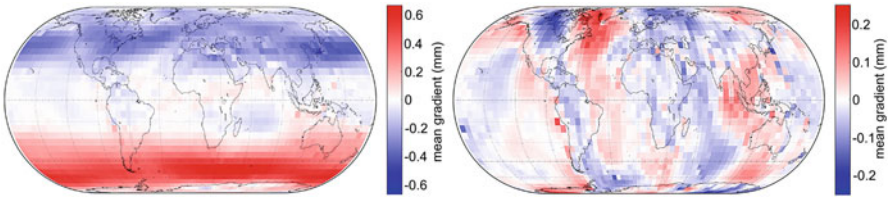

Fig. 3.69 Hydrostatic north gradient (left) and hydrostatic east gradient (right) from GPT3. While the north gradient shows systematic features for the northern and southern hemisphere owing to the atmospheric bulge, the east gradient is rather affected by the land-ocean distribution

3.5.4 The Impact of NWM Forecast Length on ZTDs[13]

J. Douša
Geodetic Observatory Pecný, RIGTC, Ondřejov, Czech Republic
e-mail: jan.dousa@pecny.cz

P. Václavovic
Geodetic Observatory Pecný, Research Institute of Geodesy, Topography and Cartography, Zdiby, Czech Republic
e-mail: pavel.vaclavovic@pecny.cz

M. Eliaš
Geodetic Observatory Pecný, Research Institute of Geodesy, Topography and Cartography, Zdiby, Czech Republic
e-mail: michal.elias@pecny.cz

P. Krč
Czech Institute of Computer Science, Academy of Sciences, Praha, Czech Republic
e-mail: krc@cs.cas.cz

K. Eben
Czech Institute of Computer Science, Academy of Sciences, Praha, Czech Republic
e-mail: eben@cs.cas.cz

J. Resler
Czech Institute of Computer Science, Academy of Sciences, Praha, Czech Republic
e-mail: resler@cs.cas.cz

To study the impact of the GNSS tropospheric corrections on the NWP prediction length, we calculated ZTDs for stations in the Benchmark campaign using the G-Nut/Shu software and the Weather Research and Forecasting (WRF) models operated routinely by the Institute of Computer Science, Academy of Sciences,

[13]Parts from this section were previously published in Douša et al. (2015a, b).

Czech Republic (ICS ASCR). The two same WRF-ICS analyses have routinely contributed to the Real-time Demonstration campaign since July 2015 and can be characterized as follows: (a) two regional domains 9 × 9 km (EU9) and 3 × 3 km (CZ3), (b) uniform horizontal grid represented using the Lambert Conformal Conic projection (LCC), (c) grid unstaggered dimensions (west-east = 418 grid points; south-north = 302 grid points), (d) 38 vertical levels with the top level at 50 hPa, (e) four forecasts per day: 00:00, 06:00, 12:00 and 18:00 UTC, (f) a 1-h temporal resolution in each forecast, and (g) a 13-h length of the forecast.

The data used for the WRF-ICS analysis computation are collected within a 6-h window surrounding the synoptic time *T*. The analysis then emerges on the web site of NCEP about 3 h 25 min after the synoptic time. The global model runs the forecasts for increasing time horizons up to 14 days. The resulted forecasts are successively uploaded until about *T + 5 h*. The mesoscale WRF model starts its simulation run at the synoptic time *T*, using previous analysis (*T-6 h*) and the time window from *T-6 h* to *T*. The so called grid nudging is performed at this level. In this way the mesoscale model reaches a state in time *T*, being a downscaled analysis. Grid nudging ensures that the mesoscale model doesn't diverge too far from the global analysis in time *T*. The mesoscale simulation starts at approximately *T + 3 h* 35 min real time and during the grid nudging phase and the subsequent spinup phase, i.e. while simulating hours (*T, T + 6*), the mesoscale model simulation catches up the real time, until about *T + 4 h* 30 min real time. About *T + 7 h* real time when depending of computing resources, the forecast horizon *T + 78 h* is produced.

Based on the WRF-ICS different forecasting intervals counted from the time *T*: *0-6 h* (spinup), *6-12 h* (forecast) and *12–18 h* (forecast), we calculated ZTDs for all Benchmark stations during May/June 2013 and compared then with reference GNSS ZTD parameters. Figure 3.70 shows the comparisons of the NWP-based ZTDs with

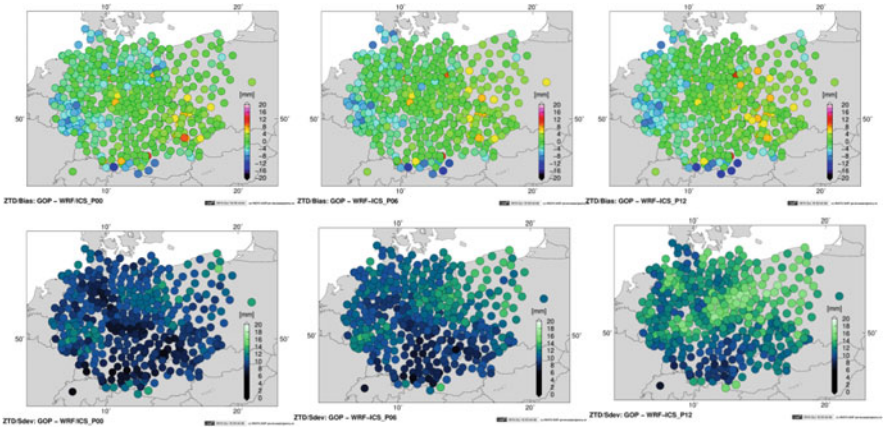

Fig. 3.70 ZTD biases (top) and standard deviations (bottom) calculated for 420 stations of the GNSS4SWEC Benchmark campaign over 2 weeks in May–June 2013 NWP models compared to GOP GNSS reference solution. From left to right three prediction intervals are shown: 0–6 h (left), 6–12 h (middle) and 12–18 (right)

Table 3.19 Summary statistics for the prediction length

NWP domain	Forecast window	Bias [mm]	Sdev [mm]	RMS [mm]
D01/EUR	0–6 h	−1.50	9.93	10.42
D01/EUR	6–12 h	−0.89	10.95	11.55
D01/EUR	12–18 h	−0.51	12.91	13.48
D02/CZ	0–6 h	+2.05	9.14	9.84
D02/CZ	6–12 h	+2.46	10.33	11.90
D02/CZ	12–18 h	+3.20	12.83	13.50

respect to GNSS reference solution in geographical plots. Biases (top) and standard deviations (bottom) are shown for the three prediction windows (left to right). Table 3.19 then provides a summary statistics for ZTDs calculated from two WRF domains. We focused on assessing zenith tropospheric delays potentially usable as external corrections for GNSS real-time applications such as positioning and navigation. Statistics for 14 days and 420 stations of the GNSS4SWEC Benchmark campaign [6] summarize ZTDs calculated from the spinup (0–6 h) and forecast intervals (6–12 h and 12–18 h). The summary shows that the quality of ZTD within the prediction windows up to 18-h resulted in RMS of 9.5–13.5 mm. It demonstrated a slow degradation of ZTDs from NWM approximately at a rate of 1–2%/h, which can be characterized by 1–2 mm/h. A degradation of mean biases was not observed. ZTDs usable in real-time GNSS applications correspond to the prediction of 6–12 h in the standard WRF operation.

3.5.5 Dual-Layer Tropospheric Correction Model Combining Data from GNSS and NWM[14]

J. Douša
Geodetic Observatory Pecný, RIGTC, Ondřejov, Czech Republic
e-mail: jan.dousa@pecny.cz

M. Eliaš
Geodetic Observatory Pecný, Research Institute of Geodesy, Topography and Cartography, Zdiby, Czech Republic
e-mail: michal.elias@pecny.cz

P. Václavovic
Geodetic Observatory Pecný, Research Institute of Geodesy, Topography and Cartography, Zdiby, Czech Republic
e-mail: pavel.vaclavovic@pecny.cz

[14]Parts from this section were previously published in Douša et al. 2018b.

K. Eben
Czech Institute of Computer Science, Academy of Sciences, Praha, Czech Republic
e-mail: eben@cs.cas.cz

Various tropospheric models for GNSS real-time positioning have been developed at GOP recently taking advantages of recent enhancements in the troposphere modelling (1) analytical ZWD calculation based on the concept of Askne and Nordius (1987) when combining exponential decay parameters from the water vapor pressure vertical profile and ZWD profile (Douša and Eliaš 2014), (2) more precise vertical approximation for the ZWD parameter using new parameter for modelling of ZWD exponential decay expressed either for a dependency on pressure or altitude (Douša and Eliaš 2014), (3) more simple and accurate tropospheric model based on user parameters related to the hydrostatic and non-hydrostatic zenith delays (Douša et al. 2015a, b), and (4) a flexible parameterization of new and legacy ZWD modelling approaches in various user modes, (Douša et al. 2015a, b).

Based on the abovementioned enhancements in the modelling of tropospheric corrections, GOP has developed a new concept of a dual-layer tropospheric correction model for GNSS precise real-time positioning applications which optimally benefit from the synergy between NWM and GNSS data. The idea behind is to combine and predict optimally hydrostatic and wet components of the total zenith path delay in support of real-time GNSS positioning applications. In a simple form it resembles the approach of an assimilation of GNSS ZTD into the numerical weather forecast, however, targeting the GNSS user parameters, i.e. tropospheric path delays of an electromagnetic signal up to 15GHz frequencies.

The new concept aimed at enhancing the original GOP augmentation model introduced in Douša et al. (2015a, b) by combining NWM data with ZTDs estimated from GNSS permanent stations in regional networks. The first layer is represented with the background NWM-driven model available anytime for the region of interest when derived purely from a NWM forecast provided from several hours up to 1–2 days. The first-layer parameters are predicted from NWM data fields and provides the background ZHD, ZWD together with auxiliary parameters for the parameter vertical scaling. The second layer improves mainly the ZWD, or more precisely, optimized corrections complementary to the NWM-derived hydrostatic corrections of the tropospheric effect on the at radio-frequency electromagnetic signal.

The description of the combination method is given in the paper by Douša et al. (2017) and includes four test cases for optimal method of ZWD combination from GNSS and NWM. Two NWM models were used: (1) global ERA-Interim reanalysis (Dee et al. 2011) provided by ECMWF (we used 6-h updates with $1^\circ \times 1^\circ$ horizontal resolution), and (2) high-resolution regional NWM prediction (European model with 9×9 km horizontal uniform resolution, hourly updated) provided from an operational short-time prediction from the mesoscale WRF model operated by the Institute of Computer Science (ICS), Academy of Sciences of the Czech Republic. The input GNSS ZTDs stems from the analysis of GNSS data of the GNSS4SWEC WG1 Benchmark dataset (Douša et al. 2016) provided by GOP as the GNSS reference solution.

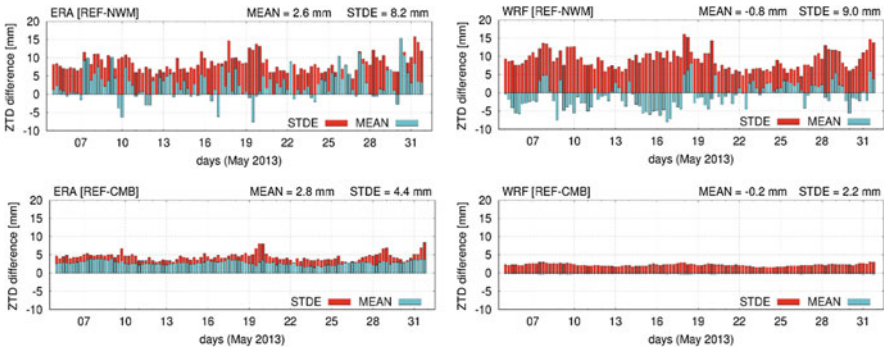

Fig. 3.71 Mean statistics of a single-layer model (top) and dual-layer (bottom) ZTDs with respect to GNSS ZTDs using a closed-loop test case and ERA Interim (left) and WRF-ICS (right) models during May, 2013

The concept was implemented in the G-Nut/Shu software for the testing and assessing different variants of ZWD weighting method. The closed-loop results demonstrated that the new combination concept provides highly accurate and stable results despite of several involved approximations, see Fig. 3.71. The GNSS data were able to improve significantly the non-hydrostatic part of the NWM-based tropospheric model, however it is able to correct also possible errors in the hydrostatic component coming from the underlying NWM data. The most significant improvement of using the second model layer was reached in term of ZTD standard deviations, in total over 43%, when assessed using products from independent GNSS stations. An improvement has also been observed in term of systematic errors, but these were almost negligible in the total statistics. The most important result of the combination of GNSS and NWM data was found in term of stability in the session-to-session performance of the dual-layer model ZTD statistics. The scatters in session-to-session mean standard deviations were reduced from 8.7 to 4.4 mm and from 9.6 to 3.0 mm for the WRF-ICS model when using GNSS ZTD and ZTD together with horizontal gradients, respectively, see Table 3.20.

The GNSS contribution to the dual-layer augmentation model consists particularly in a local phenomena where the model resolution plays a key role for an optimal assimilation of GNSS ZTDs into the model. We demonstrated a fast decrease of the statistics when simulating a higher horizontal resolution for the ERA-Interim model and obtaining comparable or better results to those resulting from the high-resolution WRF-ICS model. Comparing several ZWD weighing methods in the combination, optimal results were achieved by replacing the original NWM ZWDs with GNSS ZWDs if these were interpolated robustly to the model grid points.

Using tropospheric horizontal gradients estimated for each GNSS station, we developed a method to calculate so-called pseudo-ZTDs to densify GNSS ZTD field for its optimal contribution to the combination with NWM ZWDs stemming from the WRF-ICS high-resolution model, example is given in Fig. 3.72. The combination of GNSS ZTDs and pseudo-ZTDs with NWM showed up to 70% improvement

Table 3.20 ZTD mean statistics of GNSS and ERA-Interim data weighting within the ZWD combination and improvements with respect to the background NWM model (last line)

	Data reduction:	None	R3 (33%)	R2 (50%)
Variant	Data weighting [mm]	bias/sdev [mm]	bias/sdev [mm]	bias/sdev [mm]
First layer (ERA)	$\sigma_{GNSS} = 10.0$; $\sigma_{NWM} = \infty$	+2.6 / 9.3	+2.6 / 9.3	+2.7 / 9.4
First layer (WRF)	$\sigma_{GNSS} = 10.0$; $\sigma_{NWM} = \infty$	−0.8 / 9.6	−0.7 / 9.5	−0.8 / 9.6
Second layer (ERA)	$\sigma_{GNSS} = \infty$; $\sigma_{NWM} = 10.0$	+2.8 / 5.3	+2.7 / 5.2	+3.0 / 5.5
Second layer (WRF)	$\sigma_{GNSS} = \infty$; $\sigma_{NWM} = 10.0$	−0.2 / 2.4	−0.2 / 2.9	−0.0 / 3.0

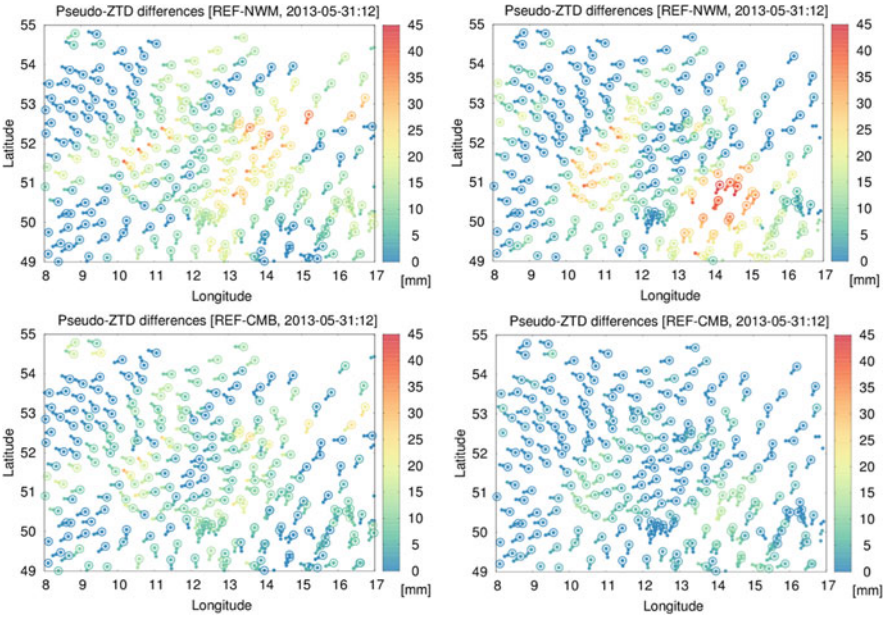

Fig. 3.72 Differences of ZTDs (points with circles) and pseudo-ZTDs at distances of 15 km and 25 km (small points) with respect to the reference GNSS ZTDs are showed for the model first layer (top panels) and for the model second layer (bottom panels) and ERA-Interim (left panels) and WRF-ICS (right panels), on May 31, 12:00 UTC, 2013

for standard deviations compared to the NWM model, and about 35% improvement compared to the initial GNSS ZTDs and NWM data combined model. As expected in this test case, we haven't observed any improvement in case of the ERA-Interim model.

As the developed method of NWM and GNSS data combination demonstrated a high accuracy and stability over time, it is very promising for implementation of a

service for tropospheric corrections for real-time precise positioning. Currently, we are implementing the operational prototype combining the existing GOP services for tropospheric parameters estimated (near) real-time (Douša and Václavovic 2014, 2016) provided in support of the numerical weather forecasting, and the existing demonstration prototype for the GOP model background layer utilizing the WRF-ICS operational weather forecast for Europe. More details can be found in Douša et al. 2018a, b.

3.5.6 *Tropospheric Refractivity and Zenith Path Delays from Least-Squares Collocation of Meteorological and GNSS Data*[15]

K. Wilgan
Wrocław University of Environmental and Life Sciences, Wrocław, Poland
e-mail: karina.wilgan@upwr.edu.pl

W. Rohm
Institute of Geodesy and Geoinformatics, Wrocław University of Environmental and Life Sciences, Wrocław, Poland
e-mail: witold.rohm@upwr.edu.pl

J. Bosy
Wrocław University of Environmental and Life Sciences, Wrocław, Poland
e-mail: jaroslaw.bosy@up.wroc.pl

F. Hurter
ETH Zurich, Zürich, Switzerland
e-mail: fabian.hurter@geod.baug.ethz.ch

A. Geiger
ETH Zurich, Zürich, Switzerland
e-mail: alain.geiger@geod.baug.ethz.ch

This subsection summarizes results of the troposphere model tested in two countries with different orography: Switzerland (mountainous) and Poland (mostly flat). The troposphere model is based on the least-squares collocation technique, where each observation is divided into a deterministic part, a correlated stochastic part (signal) and an uncorrelated stochastic part (noise). The selected parameters from different data sources are estimated simultaneously in the least-squares sense taking into account the two kinds of errors. The advantage of this method is a relatively easy implementation of additional data sources. Using the computed model coefficients it is possible to reconstruct the value of considered parameter at any time and place.

[15]Parts from this section were previously published in Wilgan et al. (2017a)

Calculations were made using the software COMEDIE (Collocation of Meteorological Data for Estimation and Interpretation of tropospheric path delays), developed at ETH Zürich.

For Switzerland, the profiles of total refractivity were calculated from three data sets: (1) the total refractivity calculated from ground-based meteorological measurements, (2) the total refractivity calculated from meteorological measurements and ZTD from GNSS stations and (3) the total refractivity calculated from meteorological measurements, ZTD GNSS and horizontal gradients of ZTD from GNSS stations. The data set (2) exhibits the best agreement with the reference RS data. The data set (1) based on the ground-based meteorological data also gives a good information about the tropospheric state, but only up to the height of the highest station. Above that height, it is necessary to use an additional data source, such as the ZTD GNSS, to provide an information about tropospheric parameters in the vertical profiles. Unfortunately, adding the horizontal gradients of ZTD in data set (3) did not improve the troposphere model.

In the countries located mainly on lowlands such as Poland, the height distribution of ground-based meteorological stations is too flat to reconstruct the refractivity profiles with the collocation technique. Thus, the troposphere model is built based on NWP data of 10 km $\times$ 10 km spatial resolution, 34 height levels and time resolution of 1 h. The total refractivity profiles and ZTD values were calculated from 4 data sets: (1) NWP WRF model, (2) WRF model integrated with ZTD GNSS, (3) ZTD GNSS only, and (4) WRF model, ZTD GNSS and ground-based meteorological measurements. The obtained total refractivity profiles were compared with the reference radiosonde (RS) data and obtained ZTD with the reference GNSS data from post-processing. For total refractivity, the best agreement with reference RS data was achieved from the WRF model integrated with GNSS data (data set 2). Including the ground-based meteorological data (data set 4) did not improve the model. Data set (1) exhibited similar agreement with RS measurements as data set (2), only in the upper layers of the model there was a displacement of 2 ppm. The data set (3) showed much worse accuracy with the discrepancies at lower altitudes even at the level of -30 ppm. Such large differences are a result of an attempt to reconstruct a whole profile of refractivity from a single ZTD value. In the next step, the model of ZTD from COMEDIE was compared with the reference near-real time GNSS data. The comparisons were made for 9 days in May 2014 that included a severe weather event. The data sets of the highest agreement with the reference GNSS data are (2) and (3) with the average biases of 3.7 mm and 3.8 mm and standard deviation of 16.7 mm and 17.2 mm, respectively. The collocation based only on the WRF model (data set 1) overestimates the ZTD values. The reason for such behavior is that the humidity values provided by the WRF model after the rainfall are too high, which directly affects the ZTD values. To sum up, the integration of NWP and GNSS data is essential to provide accurate models for both total refractivity and ZTDs. More details can be found in Wilgan et al. 2017a, b.

3.5.7 *Improving Precise Point Positioning with Numerical Weather Models*

C. Lu
GFZ German Research Centre for Geosciences, Potsdam, Germany
e-mail: cuixian@gfz-potsdam.de

Precise positioning with the current Chinese BeiDou Navigation Satellite System is proven to be of comparable accuracy to the Global Positioning System (GPS), which is at centimeter level for the horizontal components and sub-decimeter level for the vertical component. But the BeiDou precise point positioning (PPP) shows its limitation in requiring a relatively long convergence time. In this study, we develop a numerical weather model (NWM) augmented PPP processing algorithm to improve BeiDou precise positioning. Tropospheric delay parameters, i.e., zenith delays, mapping functions, and horizontal delay gradients, derived from short-range forecasts from the Global Forecast System (GFS) of the National Centers for Environmental Prediction (NCEP) are applied into BeiDou real-time PPP. Observational data from stations that are capable of tracking the BeiDou constellation from the IGS Multi-GNSS Experiments (MGEX) network are processed, with the introduced NWM augmented PPP and the standard PPP processing. The accuracy of tropospheric delays derived from NCEP is assessed against with the IGS final tropospheric delay products, Fig. 3.73. The positioning results show that an improvement of convergence time up to 60.0% and 66.7% for the east and vertical components, respectively, can be achieved with the NWM augmented PPP solution compared to the standard PPP solutions, while only slight improvement of the solution convergence can be found for the north component Fig. 3.74. A positioning accuracy of 5.7 cm and 5.9 cm for the east component is achieved with the standard PPP that estimates gradients and the one that estimates no gradients, respectively, in comparison to 3.5 cm of the NWM augmented PPP, showing an improvement of 38.6% and 40.1%. Compared to the accuracy of 3.7 cm and 4.1 cm for the north component derived from the two standard PPP solutions, the one of the NWM augmented PPP solution is improved to 2.0 cm, by about 45.9% and 51.2%. The

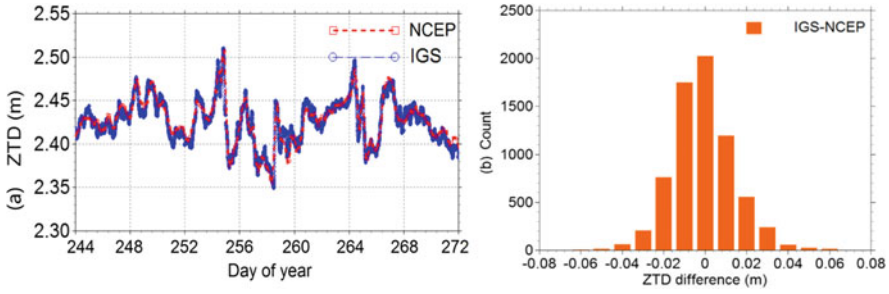

Fig. 3.73 (**a**) The time series of NCEP and IGS ZTD at station BRST for September, 2015 – day of year 244–272. The NCEP ZTD are shown in red, and IGS ZTD in blue. (**b**) Distribution of ZTD differences between NCEP and IGS

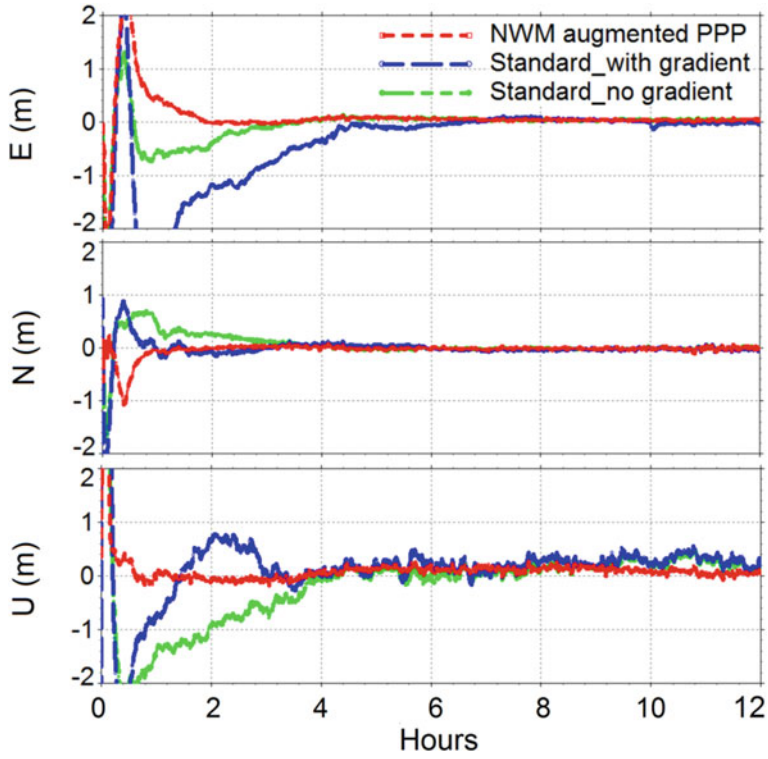

Fig. 3.74 The BeiDou RT-PPP solutions at station GMSD (Japan, 30.56 °N, 131.02° E) on September 1, 2015 (DOY 244 of 2015). The NWM augmented PPP solution is shown in red, the standard PPP solution that estimates gradients in blue, and the standard PPP solution that estimates no gradients in green

positioning accuracy for the up component improves from 11.4 cm and 13.2 cm with the two standard PPP solutions to 8.0 cm with the NWM augmented PPP solution, an improvement of 29.8% and 39.4%, respectively.

3.5.8 Using External Tropospheric Corrections to Improve GNSS Positioning of Hot-Air Balloon[16]

P. Václavovic
Geodetic Observatory Pecný, Research Institute of Geodesy, Topography and Cartography, Zdiby, Czech Republic
e-mail: pavel.vaclavovic@pecny.cz

[16]Parts from this section were previously published in Vaclavovic et al. (2017).

J. Douša
Geodetic Observatory Pecný, RIGTC, Ondřejov, Czech Republic
e-mail: jan.dousa@pecny.cz

M. Eliaš
Geodetic Observatory Pecný, Research Institute of Geodesy, Topography and Cartography, Zdiby, Czech Republic
e-mail: michal.elias@pecny.cz

Tropospheric delay of a GNSS signal has to be considered in any precise positioning solution. When a receiver remain in a static position, which is the case of all permanent stations, coordinates are significantly constrained, and the correlation between station height and ZTD is not critical. Moreover, tropospheric parameters can be also constrained during stable weather condition. However, when a receiver is in movement, particularly in vertical direction, the height-ZTD mutual correlation can significantly decrease an accuracy of position results. It is particularly true for Precise Point Positioning because any biases are neither eliminated nor reduced. It should be noted, that known precise troposphere can improve also static receiver positioning, namely in terms of reducing convergence time due to diminishing state vector dimension and better observation model after cold start. Consequently, introducing ZTD from an external source can play important role in making the solution more robust and accurate. Sources for the tropospheric parameters can be models produced on the bases of meteorological data, tropospheric products from GNSS analyses, or their optimal combination.

Geodetic Observatory Pecny has demonstrated how the correlation between height and ZTD critically influences position estimates of kinematic receiver. For this purpose, an experiment with a hot air balloon carrying a GNSS receiver together with several meteorological sensors has been arranged (Fig. 3.75). The receiver with other necessary equipment were mounted on the balloon basket and flied more than 2000 meters above the earth surface (Václavovic et al. 2017). Figure 3.76 demonstrates a vertical profile of the flight divided into five flight phases: (1) Initial, (2) Ascent, (3) Descent, (4) Landing, and (5) Finish. In order to obtain stable solution without initial convergence typical for the PPP method, the receiver remained in its static position during the initial and finish flight phases. Collected multi-GNSS (GPS, GLONASS, Galileo, BeiDou) high rate observations with meteorological measurements (atmospheric pressure, relative humidity, air temperature) were processed by the G-Nut/Geb software using the PPP method, which requires modeling all errors with the highest accuracy. This is accomplished using corrections from external precise models or products, such as satellite orbits and clocks, satellite attitude models, atmospheric delays, receiver and satellite antenna phase centre offsets and variations, relativistic and phase windup effects. Experimental campaign observations were processed utilizing real-time orbits and clocks of GPS and GLONASS satellites provided by the Centre National d'Etudes Spatiales, CNES (Laurichesse et al. 2013). The products are disseminated in a real-time stream, and

Fig. 3.75 Mounting GNSS antenna and meteorological sensors on the balloon basket (left) and the balloon during ascending (right)

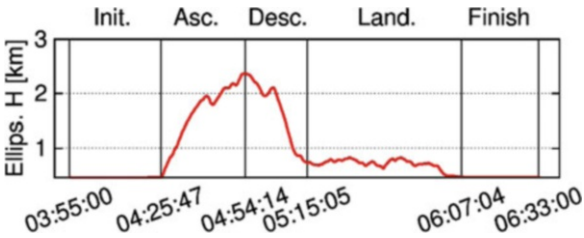

Fig. 3.76 Experimental vertical profile and definition of flight phases

they had been stored in daily files using the BKG NTRIP Client (BNC) (Weber et al. 2016).

We applied two principal strategies for ZTD modeling: (1) estimating along with all other unknowns in the adjustment, (2) introducing from an external tropospheric model. The tropospheric model used in this study was the Weather Research and Forecasting (WRF) model provided by the Institute of Computer Science, Academy of Science of the Czech Republic. A methodology for deriving ZTD from such WRF model has been developed at GOP and published in Douša and Eliaš 2014.

Estimating ZTD simultaneously with the rover height resulted in a strong dependency of kinematic solution on the ZTD random walk noise setting. The effect was attributed to a strong mutual correlation described by the correlation coefficient reaching up to −0.9 for a very loose ZTD constraining spectral density 500 mm/$h^{1/2}$ of the stochastic process random walk (red line in Fig. 3.77). Depending on ZTD random walk setting, the rover height discrepancies reached up to 30–50 cm. The study suggests that ZTD should be tightly constrained in a vertically kinematic solution to stabilize the results; however the constraining influences the accuracy of estimated height in case of strong rover dynamics. The solution using not only GPS satellites but also GLONASS became more stable due to a better satellite

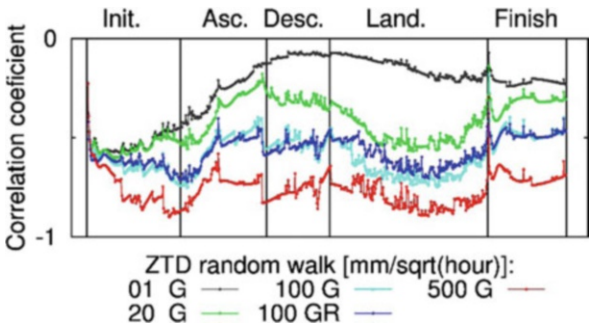

Fig. 3.77 Dependence of the correlation coefficient between ZTD and height on random walk settings

geometry and a better decorrelation of estimated parameters. To achieve the best accuracy, a careful offline analysis of an optimal random walk setting for estimated ZTD should be done and, optionally, dynamically adapted. Findings of such analyses are not available in real-time, however, when a precise external tropospheric model is applied, the offline analyses is not necessary.

The precise tropospheric model improved mainly solutions under the conditions of poor satellite geometry which was simulated by reducing available GPS constellation. Therefore, a significantly smaller dependence of positioning precision on the ZTD constraining was observed when using multi-constellation observation compared to single-constellation. Kinematic processing is usually difficult in real-time because receiver movement cannot be sufficiently predicted; therefore, large noise has to be introduced in the Kalman filter prediction. However, when post-processing is applicable the backward smoothing can be applied (Václavovic and Douša 2015). It the experiment, such improvement was described by the factor of two. The combination of multi-GNSS observations and the backward smoothing algorithm reached the best agreement between different solution variants using different troposphere constraining.

As an optimal setting for ZTD constraining is not able to recommend, precise kinematic positioning may benefit from external tropospheric corrections. Current accuracy of NWM forecasts already provides corrections at the centimeter level, which is similar or even better when compared to values estimated from GNSS data, in particular when a standalone GNSS is used. The NWM-driven PPP solution of our vertical experiment resulted in 9–12 cm and 5–6 cm uncertainties in the rover altitude using the Kalman filter and the backward smoothing, respectively. Compared to the standard PPP, it indicates better performance by a factor of 1–2 depending on the availability of GNSS constellations, the troposphere constraining and the processing strategy used. To conclude, if observation conditions are difficult, such as with high GDOP values, external corrections from the augmented tropospheric model can significantly improve the robustness and the accuracy of the rover height in precise positioning of prevailing vertical dynamics. More details can be found in Václavovic et al. 2017.

3.5.9 Real-Time PPP Augmented with High-Resolution NWM Model Data[17]

K. Wilgan
Wrocław University of Environmental and Life Sciences, Wrocław, Poland
e-mail: karina.wilgan@upwr.edu.pl

T. Hadaś
Wrocław University of Environmental and Life Sciences, Wrocław, Poland
e-mail: tomasz.hadas@upwr.edu.pl

P. Hordyniec
Wrocław University of Environmental and Life Sciences, Wrocław, Poland
e-mail: pawel.hordyniec@upwr.edu.pl

J. Bosy
Wrocław University of Environmental and Life Sciences, Wrocław, Poland
e-mail: jaroslaw.bosy@up.wroc.pl

We proposed a high-resolution model of troposphere corrections for Poland based on numerical weather prediction (NWP) model and GNSS data from post-processing. The chosen NWP model is Weather Research and Forecasting (WRF). In current configuration, the model outputs are given in a form of a dense horizontal grid (4 km × 4 km) with 47 height levels. Another factor that can impact the positioning accuracy and convergence time is the choice of mapping functions used to reduce the zenith delay to the slant delay. The most commonly used VMF are based on the ECMWF model with spatial resolution of about 40 km and temporal resolution of 6 h. In this article, the mapping functions based on a WRF model with higher spatial and temporal resolutions were proposed.

The tropospheric corrections model was applied into real-time PPP software GNSS-WARP (Wroclaw Algorithms for Real-time Positioning) developed at Institute of Geodesy and Geoinformatics, Wroclaw University of Environmental and Life Sciences. The study was conducted for 14 Polish EPN stations during three periods, with different troposphere conditions.

The performance tests were conducted in six GNSS data processing variants, including two commonly used variants using a priori ZTD and mapping functions from UNB3m and VMF1-FC models, one with a priori ZTD and mapping functions calculated directly from WRF model and three variants using the aforementioned mapping functions but with ZTD model based on GNSS and WRF data used as a priori troposphere and to constrain tropospheric estimates. The application of a high-resolution WRF/GNSS-based ZTD model and mapping functions results in the best agreement with the official EPN coordinates. Three types of coordinates: static, kinematic and reinitialized kinematic were estimated. In both, static and kinematic

[17]Parts from this section were previously published in Wilgan et al. (2017b).

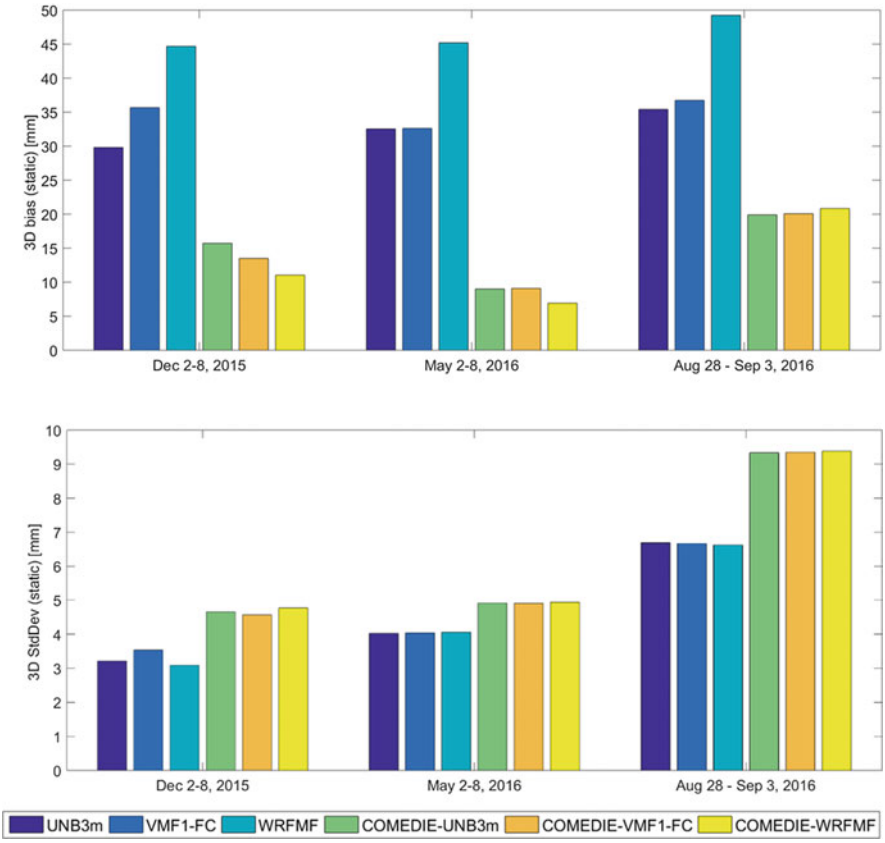

Fig. 3.78 Mean 3D biases and 3D StDev of static coordinate residuals (estimated – EPN official) averaged from 14 Polish EPN stations

mode the application of high-resolution WRF/GNSS-based model resulted in an average reduction of 3D bias by 20 and 10 mm respectively, but an increase of 3D standard deviations by 1.5 and 4 mm respectively (Figs. 3.78 and 3.79). This approach also shortens the convergence time, e.g. for a 10 cm convergence level, by 13% for the horizontal components and by 20% for the vertical component (Fig. 3.80). More details can be found in Wilgan et al. 2017a, b.

3.5.10 Validation and Implementation of Direct Tropospheric Delay Estimation for Precise Real-Time Positioning

L. Yang
University of Nottingham, Nottingham, UK
e-mail: lei.yang@nottingham.ac.uk

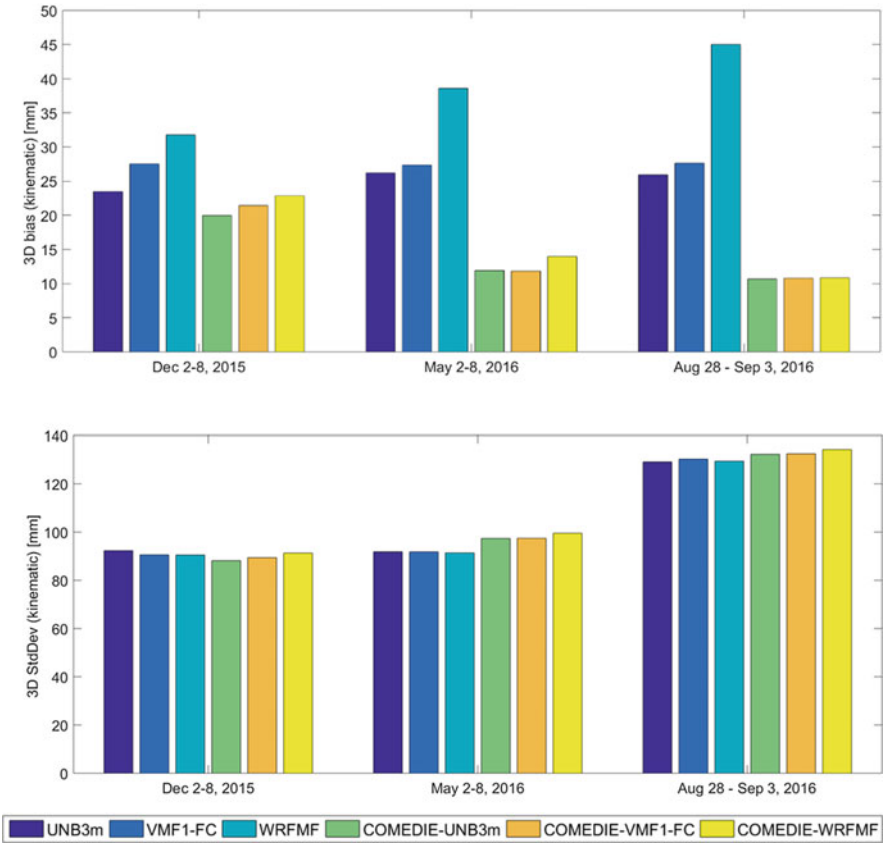

Fig. 3.79 Mean 3D biases and 3D StDev of kinematic coordinate residuals (estimated – EPN official) averaged from 14 Polish EPN stations

C. Hill
University of Nottingham, Nottingham, UK
e-mail: Chris.Hill@nottingham.ac.uk

J. Jones
Met Office, Exeter, UK
e-mail: jonathan.jones@metoffice.gov.uk

Unmitigated tropospheric delay remains one of the major error sources in PPP. Due to the lack of real information, conventional empirical models (for both ZTD and mapping functions) have limitations in terms of positioning accuracy and convergence time, especially during active tropospheric conditions. Aiming to overcome these limitations and improve PPP performance, we investigated the feasibility of integrating the real atmospheric condition from NWM into PPP, as an external

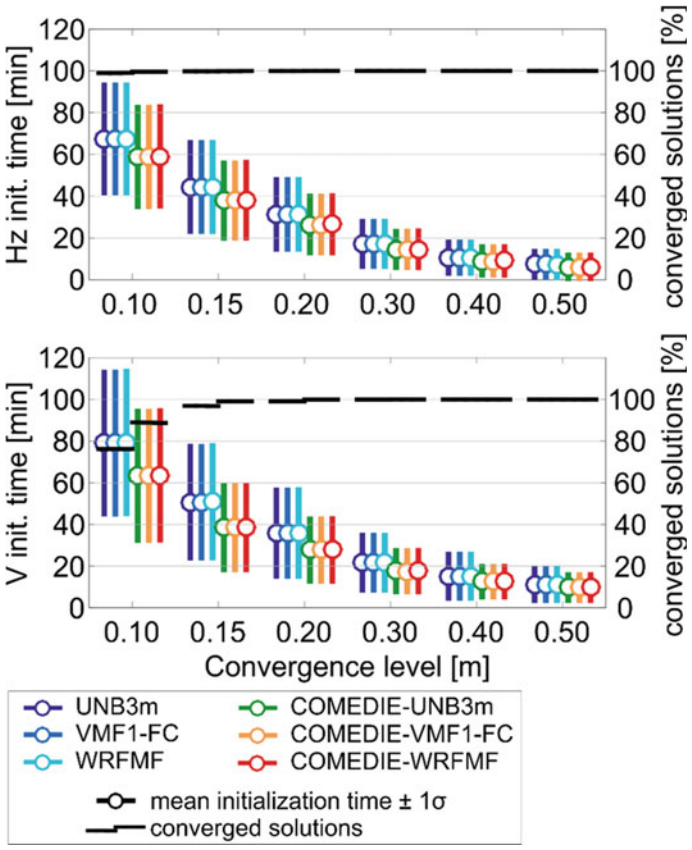

Fig. 3.80 Convergence time for different levels of convergence for horizontal (up) and vertical (bottom) components and a percentage of converged solutions

correction service. The main challenge is to capture and abstract the most effective information from NWP data, and transmit to the user in a bandwidth-economic way.

The fundamental concept proposed is a multiple-tiered data transmission structure. The tiers will provide quality information in different levels of details. The content of the tiers is shown in Fig. 3.81. In the whole service area, the atmospheric conditions are monitored in grid cells. The higher tiers are only produced and transmitted where/when they could bring additional accuracy compared to the lower tiers. An indication type of flag map is produced in real-time to inform users of the number of active tiers available at the users' grid cell. This tiered transmission scheme could effectively reduce the transmission bandwidth consumed, while keeping a certain guarantee of accuracy.

In this project, the state of the art Unified Model (UM) produced by the UK Met Office (UKMO) is selected for the underpinning NWP. To investigate the

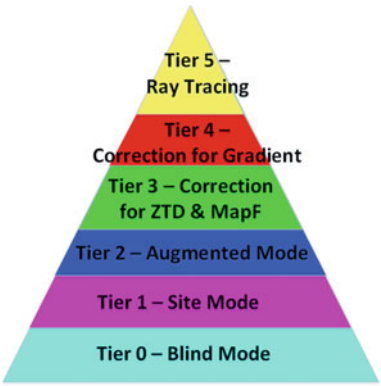

Fig. 3.81 Tiered troposphere delay correction structure

performance of the proposed correction service, statistical analysis is carried out using data over 12 months in 2014 with a 6-h interval at 108 CORS stations in the UK.

3.5.10.1 Impact of the Multiple Tiers

In Fig. 3.82, the RMS errors of different ZTD estimation methods are compared, (using DD solution as the reference). Three different empirical ZTD estimations (Tier 0, which does require any external information), i.e. the MOPS model, the GPT2 model and the ESA Blind (ESA-B) mode model, show very similar performance. While clear improvements can be observed for the higher tier solutions. Comparing to the ESA-B solution, there is a 27.3% improvement for the ESA site mode (Tier 1, which provides surface meteorological parameters), 45.2% for the ESA augmented mode (Tier 2, which provides vertical lapse rates of meteorological parameters) and 73.9% for the zenith ray tracing solution (which provides the ultimate on-site ZTD correction). Clearly the more real information provided, the better the ZTD estimation accuracy achieved.

Figure 3.83 provides the slant tropospheric delay (STD) error comparison between the solutions of Tier 0 (ESA blind mode), Tier 1 (ESA site mode), Tier 2 (ESA augmented mode), Tier 3 (ZTD and mapping function correction) and Tier 4 (gradient correction). The Tier 3 solutions are further split into the ZTD only correction and the ZTD plus mapping function correction. Ray tracing is used as the reference. The mean error and standard deviation of each solution are plotted in individual figures in the left, and the RMS errors of all solutions are plotted together against elevation in the right.

It can be seen that, from the blind mode to the site mode and then the augmented mode, both mean error and standard deviation are improved in general, which results in the improved RMS errors in turn. The improvement from blind mode to site mode

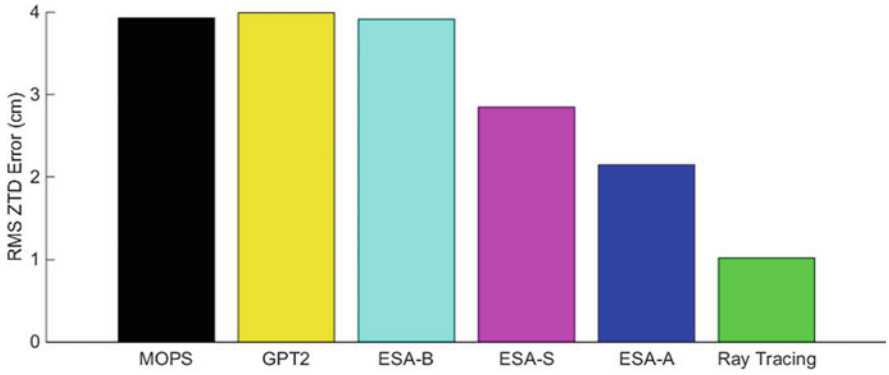

Fig. 3.82 RMS of ZTD error from different estimation methods

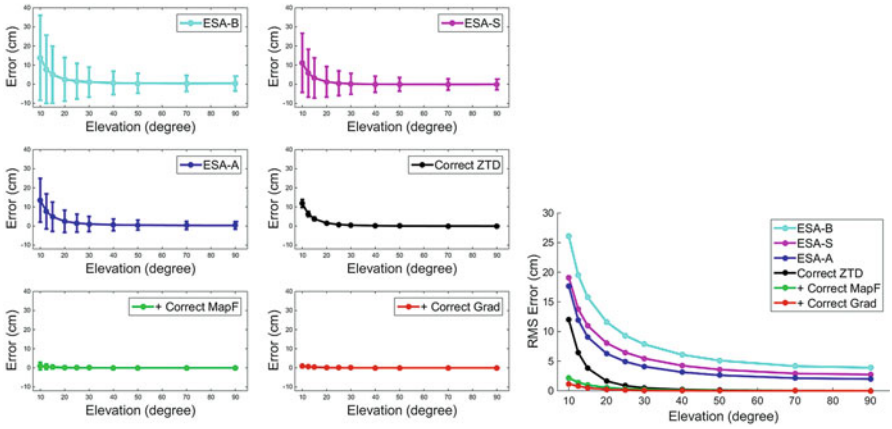

Fig. 3.83 TSD RMS error against elevation, for different tiers

is larger than the improvement from site mode to augmented mode indicating that, although the real vertical rates of change are beneficial, the real surface parameters play a more important role in the STD estimation. The ZTD correction could effectively reduce the mean error offset at higher elevations, as well as the uncertainty in the lower elevation area. This is because if the ZTD is not estimated properly, the error could be magnified by the mapping function. Even with the ZTD correction, the RMS error at 10° elevation is still higher than 10 cm. Both mapping function and gradient correction could reduce the error in the lower elevation, while the former has a stronger impact. Therefore, it is recommended that the mapping function shall be corrected earlier than the gradient. It can also be seen that at the 10° elevation, the improvement from the mapping function correction

will be larger than the improvement from the ZTD correction, and could reduce the RMS error to centimetre level.

3.5.10.2 Flag Map

One of the key features in our proposed tiered troposphere delay correction scheme is the flag map. This map is updated in real time, and provides users with local information, that to which correction tier the user should use to guarantee a certain STD estimation accuracy. The size of this flag map is quite small, thus is suitable for broadcast in a transmission medium with limited bandwidth, such as a communication satellite. Figure 3.84 shows an example of the tiered structure flag map, which is consist of 60 by 90 grid squares (~17 km × 17 km) for the UK region.

Figure 3.85 shows the total occurrence probability of each tier, from the statistic of 12 months in the UK CORS stations. Each subfigure presents different elevation settings, ranging from 10° to 70°. In each subfigure, the x axis is various thresholds that could be pre-set as the accuracy targets, and the y axis gives the chance (in percentage) of each correction tier being required.

At high elevations, a simple empirical estimation approach would be able to meet a lenient accuracy target. With an increasingly strict threshold, real information is required to replace empirical values to suppress the modelling error. When the elevation gets lower, the STD modelling assumptions based on the empirical mapping function and balanced local atmosphere profile will gradually become less valid, and the error they bring cannot be ignored.

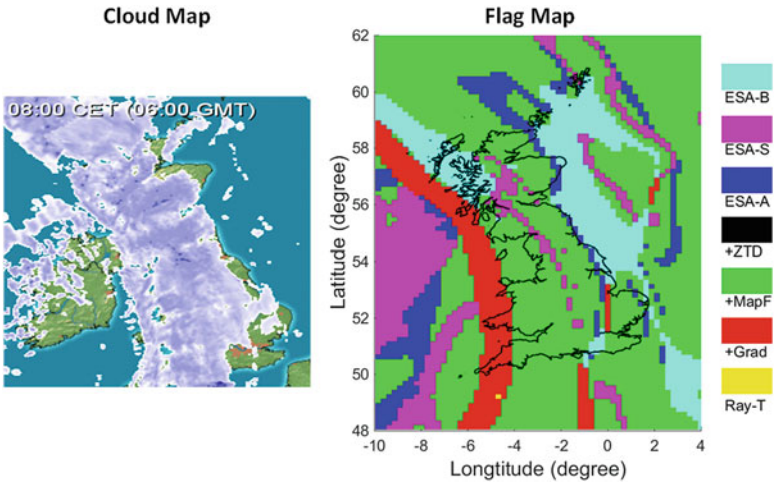

Fig. 3.84 Example of the flag map for the tiered structure (06th Oct 2014 0600 GMT)

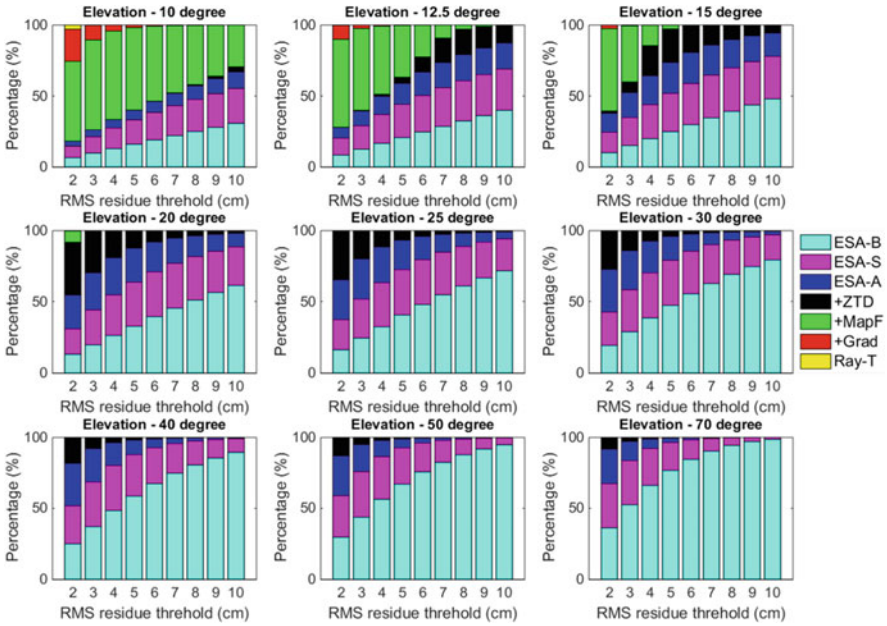

Fig. 3.85 The chance of each tier to be applied, against different threshold

3.5.10.3 PPP Improvement

Figure 3.86 uses four storm event cases (at each row) to indicate the PPP performance improvement from the proposed correction scheme, in which the red lines indicate the traditional PPP solution using empirical tropospheric modelling and the green lines indicate PPP with external tropospheric correction. In the left column, the convergence times for 10 cm (dash line) and 5 cm (solid line) are shown. And in the right column, the positioning standard deviation in 3D (solid line) and height component (dash line), at the end epoch after the 1-h PPP solution, are shown. The positive impact of the proposed external correction can be observed from both aspects.

3.5.10.4 Bandwidth

Bandwidth is a key issue in for the proposed troposphere correction scheme, since if the bandwidth required is too high to be transmitted, the whole scheme is not practical. A customized transmission has been designed in this project, which only transmits the necessary information to where it is required and hence effectively reduce the total required bandwidth and also help in multiplexing the transmission channel.

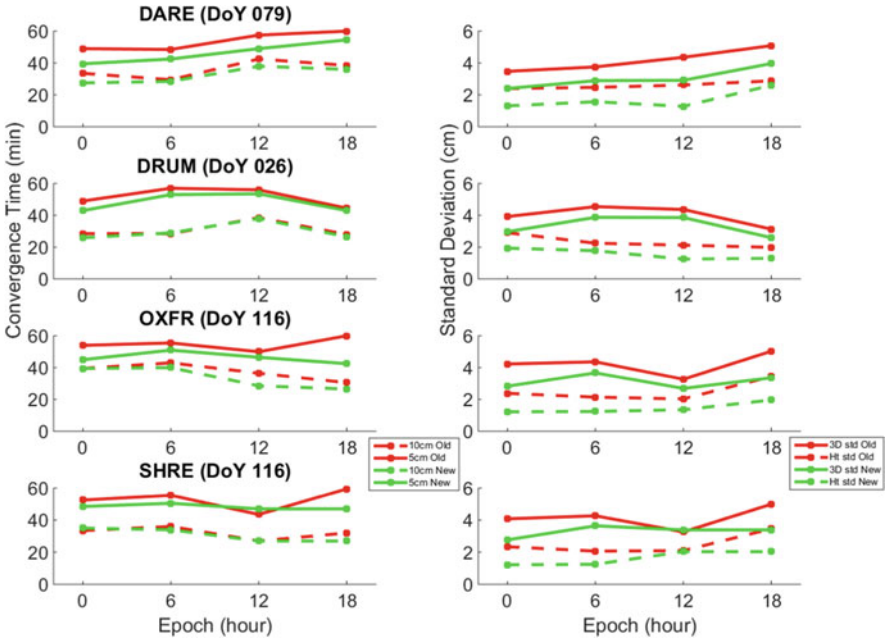

Fig. 3.86 Comparison of PPP convergence time and standard deviation after 1 h

Table 3.21 Summary of transmission design details for each tier, for UK coverage

Tier	1	2	3	4	5
Bandwidth (kbps)	4.74	2.60	0~5.21	0~2.60	397~531

In Table 3.21 the required transmission bandwidth is estimated. It can be seen that, for the UK coverage, the total required bandwidth for tier 1–4 will be 7.34~15.15 kbps, and 397~529 kbps for Tier 5. Meanwhile, the size of each flag map message will be 110 Bytes, which could be easily broadcasted. Tier 1–4 and the flag map message could be easily fit into communication satellite bandwidth nowadays. Tier 5 information is better to be transmitted via 4/5G network and through a two-way communication once required.

3.5.10.5 Summary

- Real time ray tracing could provide an accurate STD estimation, and thus improve PPP results.
- Although the required troposphere condition data for the real time 3D full ray tracing is huge, a tiered correction structure and flag maps mechanism has been

designed to reduce data transmission volume effectively. The data are only transmitted for the time and place when they are required.
- Statistical results show that only very occasionally is the full ray tracing correction required, and for most of the time, the mapping function correction could allow the user to satisfy STD estimation accuracy.
- The total bandwidth required for the UK coverage is 7.34~15.15 kbps for Tier 1–4, and 397~529 kbps for Tier 5. The flag map message size is 110B each. Apart from Tier 5, other information could be easily transmitted via communication satellite.
- The current drawback of the whole proposed solution is the NWP data resolution, especially in time (currently 6-h interval).

3.6 GNSS Data Reprocessing for Climate

One of the important tasks of the WG1 of the COST Action was the homogeneous reprocessing of GNSS data for climate applications in support of WG3. Main focus of WG1 was to study the impact of precise models and processing strategy for providing a long-term tropospheric parameters with an optimal accuracy, a high reliability and a consistent quality. This section gives an overview of the reprocessing activities during the COST Action period, while WG3-related activities are described in Chap. 5, including reprocessing product validation, combination, quality control and homogenization.

This section introduces contributions to the GNSS second reprocessing performed within the IAG sub-commission for the European Reference Frames (EUREF) and within the IGS TIGA campaign. Although these were primarily designed for contribution to geodetic applications, within the COST Action a significant effort was additionally dedicated to an optimal estimation of tropospheric parameters on regional and global scales. A special activity supporting directly the climate community has been then started by establishing the GRUAN Central Processing Centre at GFZ for a long-term ground-based GNSS precipitable water estimation.

3.6.1 EUREF Repro2 Contribution of Swisstopo

E. Brockmann
Swiss Federal Office of Topography swisstopo, Wabern, Switzerland
e-mail: Elmar.Brockmann@swisstopo.ch

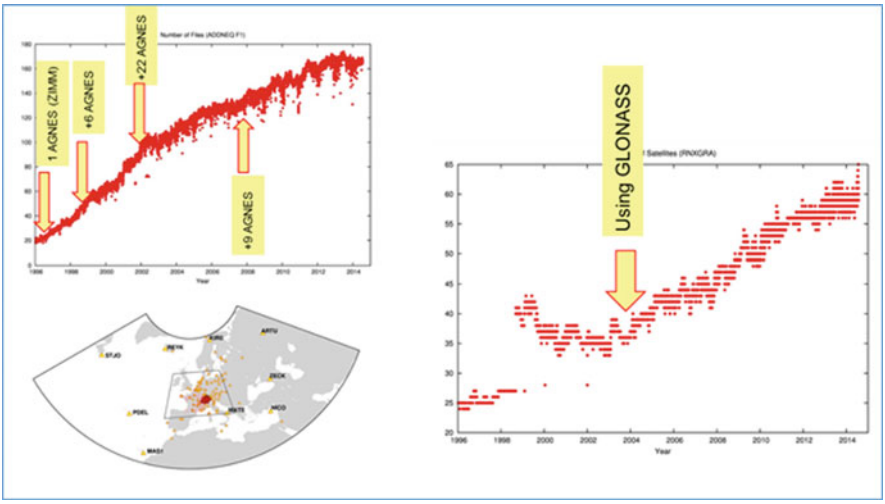

Fig. 3.87 Key parameters of swisstopo repro2

The Swisstopo finished a reprocessing in 2014 covering a homogeneous processing of a time span starting beginning 1996 till almost the end of 2014. Some key parameters are given in Fig. 3.87. The number of stations increased from 20 to 170. The stations are mostly located in central Europe. Some boundary stations were included to enable a better decorrelation between troposphere parameters with station height. The number of satellites increased from 25 in 1996 to 65 in 2014. Since 2004, the number of satellites increased due to the improved GLONASS constellation.

The reprocessing was performed with the BSW52 using most up-to-date models in a homogeneous way. Orbit and earth rotation parameters were used from the CODE repro2 products. The important processing options are given in Table 3.22.

Figure 3.88 shows that daily solutions are even more stable in view of the Helmert transformation parameters than the previous weekly solutions.

Overlapping 3-day solutions are calculated to optimize the ZTD estimates at midnight (see Fig. 3.89).

Moreover, variations on the processing options were carried out in order to find the best possible modelling options and in order to do some sensitivity studies:

- GMF/GPT mapping, atmosphere loading (ATL) + IGS08 group antenna PCV (submitted as LP0 to EUREF: Oct. 23. 2014)
- VMF mapping, IGS08 antenna model but with individual antenna PCV where available, atmospheric tidal loading ATL, non-tidal atmospheric pressure loading ALP (submitted to EUREF as LP1: March 20, 2015).
- Same as above, but GPS-only (idea borne on Thessaloniki workshop 2014, results generated in June 2015 and presented at Wroclaw COST meeting end of September 2015)

Table 3.22 Basic processing options used for swisstopo repro2

Software	BSW52 (+)
Satellite systems	GPS + GLO (ab 2004)
Elevation cutoff angle	3°
Observation weighting	COSZ elevation-dependent weighting
Antenna	I08 absolute antenna model (group values)
Troposphere	GMF and DRY GMF mapping for the a priori values and while estimating hourly ZPD parameters using WET GMF
Troposphere gradients	Chen Herring for tropospheric gradient estimation
Tides	Atmospheric tidal loading applied
Conventions	IERS2010
Ocean tides	FES2004
Gravity field	EGM08
Ionosphere	CODE 2-h resolution; including higher order terms
Reference frame	IGb08
Network	Max. 180 stations
Time span	DOY 007, 1996 till DOY 207, 2014
Orbits/EOP	CODE reprocessing series 2011 (till DOY 106, 2011) and CODE reprocessing series 2013 (till DOY 362, 2013), CODE operational series in 2014

- The impact of additional GLONASS observations on the long-term (comparison of the before mentioned last two repro2 series) was especially analyzed in this project. The impact of the additional GLONASS observations is negligible when analyzing ZTD trends. Further conclusions can be drawn from the comparisons between different ZTD time series:
- Formal errors of ZTD estimates are smaller with more GLONASS observations (max. 10%) included
- Influence of GMF versus VMF: no significant rate, standard deviation 0.5–2.5 mm ZTD (109 sites with long time series)
- Difference to CODE global Repro: no significant rate, standard deviation 2.0–5.0 mm ZTD (39 sites with long time series);
- Influence additional GLONASS observations: no significant rate, standard deviation: 0.4–1.5 mm (111 sites) (MODA exception). This is In fact a little higher (also GPS-only time counted), but strongly dependant on the used a priori ZTD constraints, there is only a statistical effect but no significant bias.

Comparisons with e.g. radio sondes have much bigger differences (see Fig. 3.90). In case of PAYE we see a standard deviation of 8–9 mm ZTD. The estimated rate of 5 mm/10 years. is also dependent on changes at the radio sonde station. In 2009, a

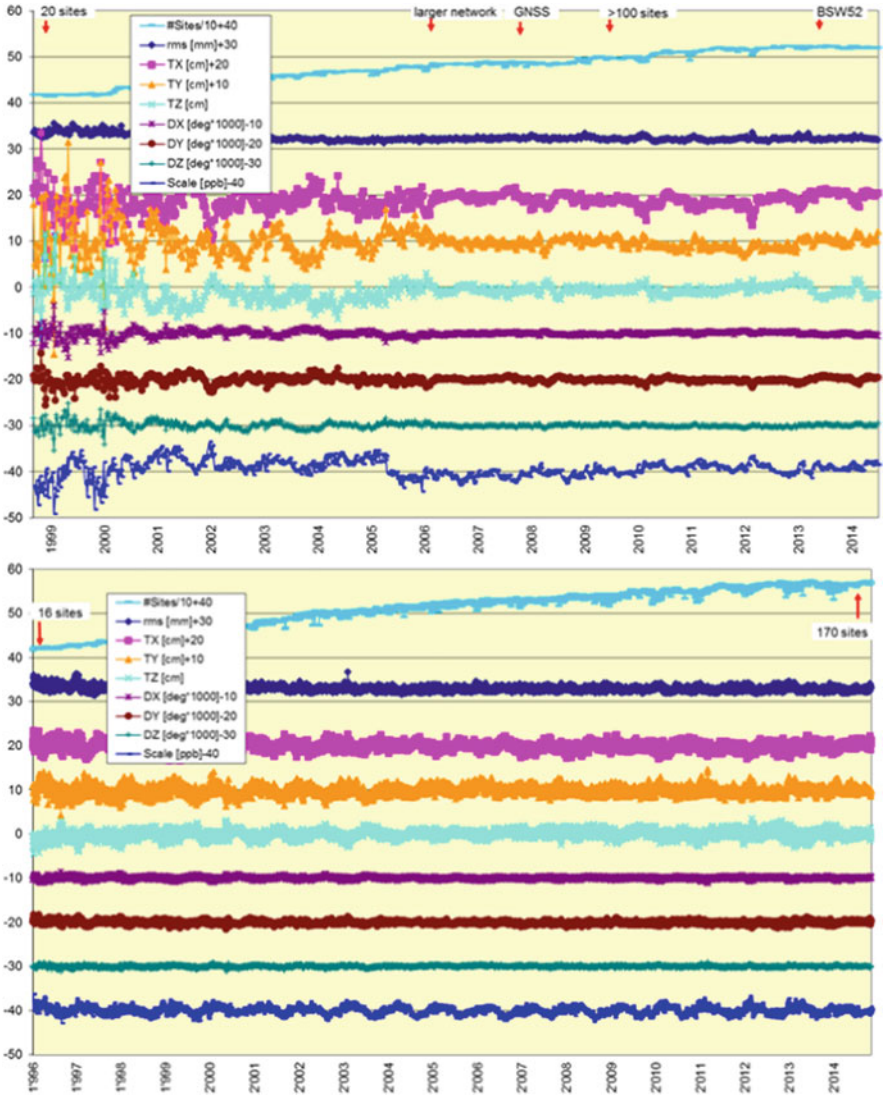

Fig. 3.88 Stability of the solutions expressed in Helmert Parameters between each individual solution with respect to the combined solution (operational older weekly solution top, swisstopo repro2 daily solution bottom)

new humidity sensor was used. Trend estimates on the raw ZTD time series are quite sensitive – especially the various antenna changes at the GNSS stations generate quite significant jumps in station heights as well as in the ZTDs.

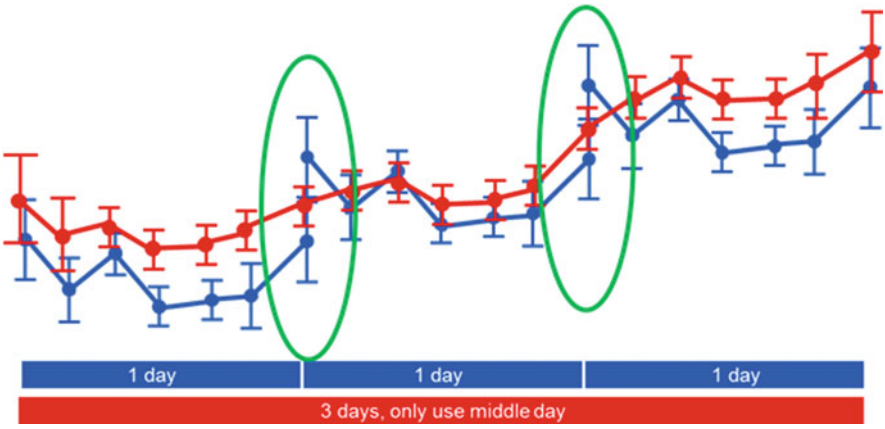

Fig. 3.89 3-day solutions to optimize the ZTD estimates at midnight

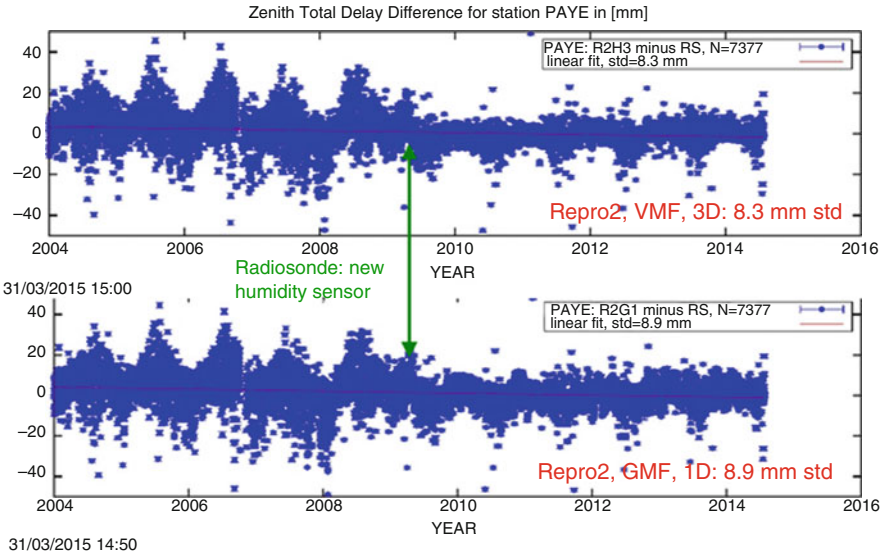

Fig. 3.90 Swisstopo Repro2 (VMF 3 days upper diagram, GMF 1 day lower diagram) compared with radio sonde derived ZTD estimates for station PAYE

3.6.2 EUREF Repro2 Assessment of GOP Processing Variants[18]

J. Douša
Geodetic Observatory Pecný, RIGTC, Ondřejov, Czech Republic
e-mail: jan.dousa@pecny.cz

P. Václavovic
Geodetic Observatory Pecný, Research Institute of Geodesy, Topography and Cartography, Zdiby, Czech Republic
e-mail: pavel.vaclavovic@pecny.cz

The results of the 2nd reprocessing of all data available from 1996 to 2014 from all stations (>300) of the European GNSS permanent network are introduced as performed at the Geodetic Observatory Pecný (GOP) (Douša et al. 2017). The reanalysis was completed during the 2nd EUREF reprocessing to support mainly the realization of a new European terrestrial reference system. The BSW52 (Dach et al. 2015) was used together with CODE precise products (Dach et al. 2014).

Within the COST ES1206 project, a new set of GNSS tropospheric parameter time series was provided for applications in climate research. To achieve this goal, we improved our strategy for combining tropospheric parameters over three consecutive days that guarantees a continuity of all estimated tropospheric parameters, zenith tropospheric delays (ZTD) and tropospheric horizontal linear gradients, at all mid-nights and during transitions of GPS weeks. Basic characteristics of the 2nd reprocessing are provided in Table 3.23.

Within the reprocessing, we performed additionally seven solution variants in order to study an optimal troposphere modelling, Table 3.24. We assessed variants in terms of the coordinate repeatability by using internal evalautions of coordinate repatability. Then, we compared ZTDs and tropospheric horizontal gradients with independent values obtained from ERA-Interim numerical weather reanalysis (Dee et al. 2011).

Generally, the results of the GOP Repro2 yielded improvements of approximately 50% and 25% for the horizontal and vertical component repeatability, respectively, when compared to the results of the GOP Repro1 solution. Vertical repeatability was reduced from 4.14 mm to 3.73 mm when using the VMF1 mapping function (Boehm et al. 2006a, b), a priori ZHD, and non-tidal atmospheric loading corrections from actual weather data. Increasing the elevation cut-off angle from 3° to 7°/10° increased RMS errors of residuals from the coordinates' repeatability. These findings were confirmed also by the independent assessment of tropospheric parameters using NWM reanalysis data. The differences of particular solutions were statistically analysed to demonstrate the impact of the different modelling on ZTDs, see

[18]Parts from this section were previously published in Douša et al. (2017).

Table 3.23 Characteristics of GOP reprocessing models

Analysis options	Description
Products	CODE precise orbit and earth rotation parameters from the IGS 2nd reprocessing.
Observations	Dual-frequency code and phase GPS observations from L1 and L2 carriers. Elevation cut-off angle 3°, elevation-dependent weighting $1/\cos^2$ (zenith), double-difference observations and with 3-min sampling rate.
Reference frame	IGb08 realization, core stations set as fiducial after a consistency checking. Coordinates estimated using a minimum constraint.
Antenna model	GOP: IGS08_1832 model (receiver and satellite phase Centre offsets and variations).
Troposphere	A priori zenith hydrostatic delay/mapping function: GPT/GMFh (GO0) and VMF1/VMF1 h (GO1-GO6). Estimated ZWD corrections every hour using VMF1w mapping function; 5 m and 1 m for absolute and relative constraints, respectively. Estimated horizontal NS and EW tropospheric gradients every 6 h (GO0-GO5) or 24 h (GO6) without a priori tropospheric gradients and constraints.
Ionosphere	Eliminated using ionosphere-free linear combination (GO0-GO6). Applying higher-order effects estimated using CODE global ionosphere product (GO5).
Loading effects	Atmospheric tidal loading and hydrology loading not applied. Ocean tidal loading FES2004 used. Non-tidal atmospheric loading introduced in advanced variants from the model from TU-Vienna (GO4-GO6).

Table 3.24 GOP solution variants for the assessment of selected models and settings

Solution ID	Specific settings and differences	Remarks and rationales
GO0	GMF and 3° cut-off	Legacy solution for Repro1
GO1	VMF1 and 3° cut-off	New candidate for Repro2
GO2	=GO1; 7° cut-off	Impact of elevation cut-off angle
GO3	=GO1; 10° cut-off	Impact of elevation cut-off angle
GO4	=GO1; atmospheric loading	Non-tidal atmospheric loading applied
GO5	=GO4; higher-order ionosphere	Higher-order ionosphere effect not applied
GO6	=GO4; 24-h gradients	Stacking tropospheric gradients to 24-h sampling

Table 3.25. Although the VMF1 mapping function outperformed GMF in term of standard deviation for the elevation cut-off angle of 3° (GO0 vs GO1), the impact is smaller than for the others effects, i.e. due to elevation cut-off angle (GO2 vs GO1, GO3 vs GO1) and non-tidal atmospheric modelling (GO4 vs GO1). The results get worse for both ZTD and tropospheric gradients when raising the elevation cut-off angle from 3° to 7° (GO2) or 10° (GO3). No significant impact of modelling of high-order ionospheric effects (GO5) was observed; the effect is systematic for regional network and was eliminated by applying fiducial stations. Figure 3.91 shows a significant improvement for gradients (negligible impact on ZTD) when combining

Table 3.25 Median, minimum and maximum values of total ZTD biases and standard deviation over all stations

Compared solution variants	ZTD bias median [mm]	ZTD bias min [mm]	ZTD bias max [mm]	ZTD sdev median [mm]	ZTD sdev min [mm]	ZTD sdev max [mm]
GO1 vs GO0	−0.36	−1.52	+0.70	2.01	0.69	3.82
GO2 vs GO1	+0.03	−0.81	+1.66	0.66	0.15	1.29
GO3 vs GO1	+0.03	−2.22	+2.66	1.10	0.31	2.04
GO4 vs GO1	+0.05	−3.29	+5.55	1.37	0.68	4.72
GO5 vs GO4	−0.02	−0.31	+0.07	0.07	0.04	0.30
GO6 vs GO4	−0.02	−0.23	+0.16	1.24	0.76	2.46

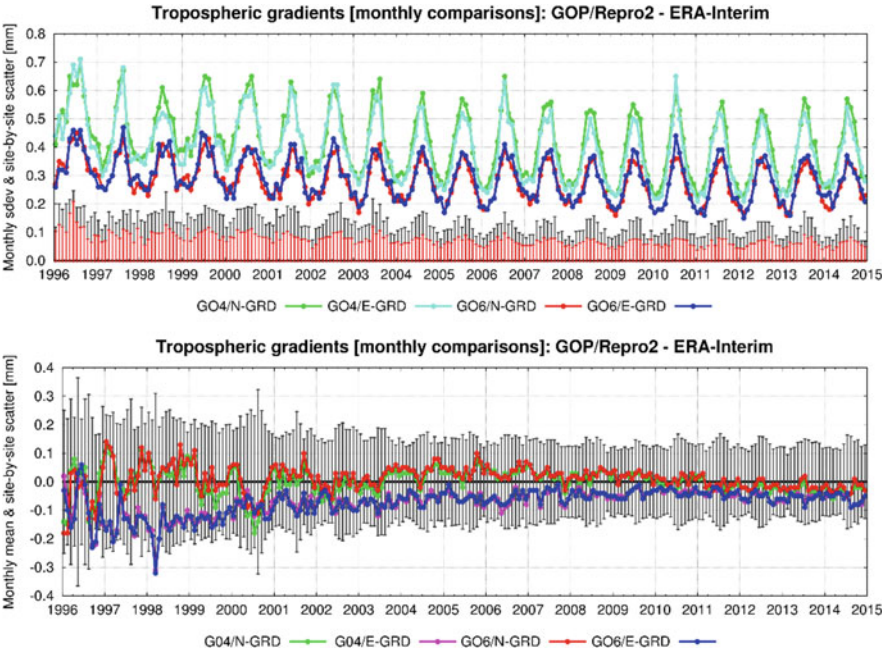

Fig. 3.91 Monthly means of bias and standard deviation of tropospheric horizontal north (N-GRD) and east (E-GRD) gradients compared to those obtained by ERA-Interim. Error bars indicate standard errors of mean values over all compared stations plotted from the zero y-axis to emphasise seasonal variations and trends. Error bars are displayed for north gradients only, however, being representative for the east gradients too

gradient parameters from the original 6-h into 24-h time resolution without applying constrains. The 6-h gradients were able to absorb some remaining errors in GNSS model.

We also studied a temporal and spatial variation of ZTD differences from seven solution variants, for details see Douša et al. 2017. Figure 3.92 shows latitudinal

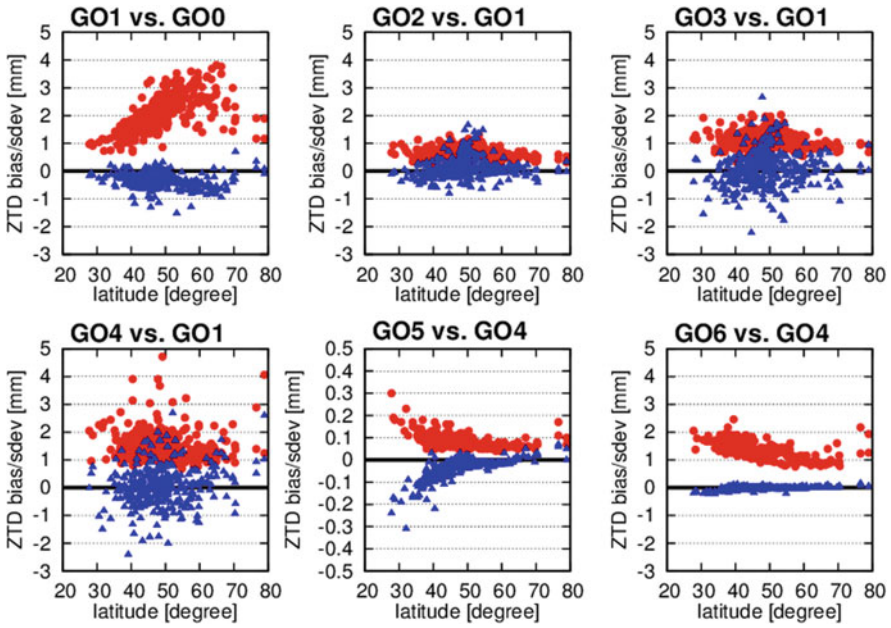

Fig. 3.92 Dependence of ZTD biases (blue) and standard deviations (red) from inter-comparisons of GOP 2nd reprocessing solution variants on station latitude. Note different y-range for the GO5 vs. GO4 comparison

dependence of the ZTD differences, while dependences on height, time and geographical location are not showed here.

Based on the reanalysis variants, we recommend using low-elevation observations together with the VMF1 mapping function, precise a priori ZHD values and consistent model of non-tidal atmospheric loading. The daily piecewise linear function model showed better stability for estimated gradients while did not indicate a worse repeatability of coordinates estimates. For saving the time, we could recommend such (unconstrained) approach for an optimal modelling of the first-order tropospheric asymmetry. The main difficulties faced during the 2nd reprocessing was the quality of the GNSS historical data containing a large variety of problems. To provide high-accuracy GNSS tropospheric products, the elimination of problematic data was more critical compared to estimating coordinates on a daily only. The 3rd EUREF reprocessing should thus exploit more complex data quality control in order to optimize the reprocessing and the quality of tropospheric products.

3.6.3 CORDEX.be Reprocessing

E. Pottiaux
Royal Observatory of Belgium, Brussels, Belgium
e-mail: eric.pottiaux@oma.be

B. Van Schaeybroeck
Royal Meteorological Institute of Belgium, Uccle, Belgium
e-mail: bertvs@meteo.be

The CORDEX.be stands for "COordinated Regional Climate Downscaling EXperiment and beyond" (http://cordex.meteo.be/). This national project brings together the Belgian climate and impact modelling research groups into one research network as the first step towards the realization of climate services. The philosophy of CORDEX.be is inspired by the World Climate Research Programme (WCRP) project CORDEX ("COordinated Regional Climate Downscaling Experiment", http://www.cordex.org/) project, but – as the ".be" in the acronym indicates – the project aims to go beyond for Belgium.

CORDEX.be has 4 main targets (see http://cordex.meteo.be/meteo/view/en/29026726-Targets.html): (1) to contribute to the international CORDEX project, (2) to go beyond by running 4 High-Resolution Limited Area Models (ALARO-0, MAR, and two flavours of COSMO-CLM, all with a resolution of ± 4 km, but with different forcing strategies), (3) to go beyond by running 4 Local-Impact Models (Wave and storm surge, urban, crop Isoprene or vegetation emission models), and (4) to infer the climate uncertainties to the Belgian level. In addition, a specific task is dedicated to the validation of the high-resolution climate simulations using GNSS-derived products. The main objective of this task is to go beyond the standard verification procedure of climate simulations. The traditional manner is to compare the results from climate runs with long-term ground-based surface meteorological observations. Instead, here we will implement a verification based on products estimated from continuously operating GNSS (Global Navigation Satellite Systems, such as the American GPS) stations.

Therefore, a careful reprocessing of the historical observations at about 320 world-wide GNSS stations (Fig. 3.93, left) has been carried out with a focus on the period 2000–2010 (i.e. the period requested by the CORDEX.be partners for the assessment of the climate models), allowing both the validation of the standard CORDEX runs and the high-resolution runs. Unfortunately, from these 320, only 20 GNSS stations (Fig. 3.93, right) which were operating almost continuously and providing high-quality observations throughout the requested validation period (2000–2010) are located in the restricted high-resolution climate model domain, but many other European GNSS sites can still be use to validate the standard 12.5 and 50 km resolution European CORDEX runs.

First results of this GNSS-based validation of the hourly ZTDs derived from the high-resolution model output is given in Fig. 3.94 (only for two climate models, MAR and COSMO-CLM, but with different forcing scenarios for MAR: NCEP,

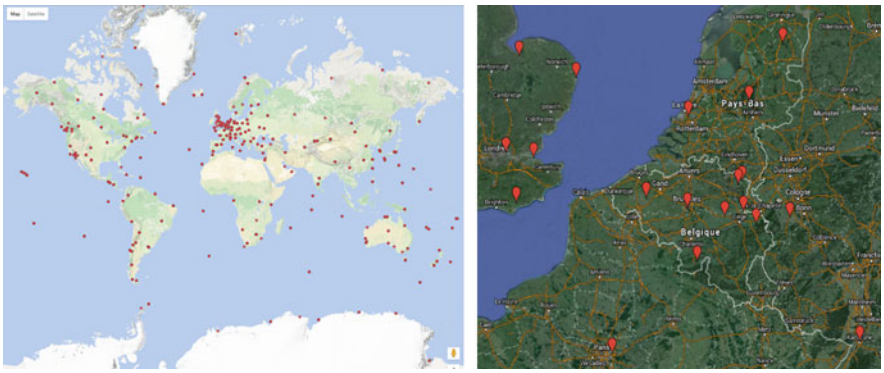

Fig. 3.93 Left: All GNSS stations included in the reprocessing. Right: GNSS stations located in the high-resolution climate domains of CORDEX.be

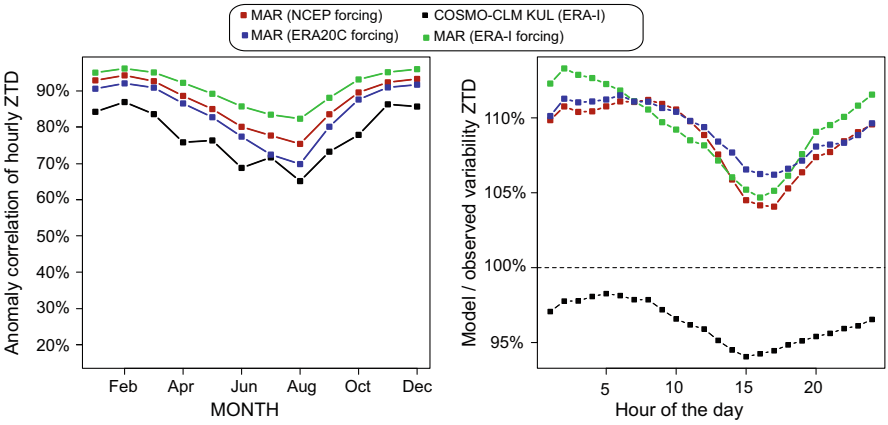

Fig. 3.94 Anomaly correlation (left) and variability ratio (right) of hourly ZTD values between different model simulations and the GNSS-derived observations for the different months of the year. The models considered are the H-Res simulations of COSMO-CLM (driven by ERA-Interim), and MAR (driven by NCEP-NCAR-v1, ERA-Interim and ERA20C). Averages are taken over seven Belgian GNSS stations

ERA20C and ERA-Interim). It is seen that all model-based ZTDs correlate pretty well with the GNSS-based ZTDs. The annual cycle (Fig. 3.94, left) from all models shows a better agreement during the winter months while more pronounced departure is visible during the summer months. Very similar yearly patterns in the anomaly correlation is visible for the two climate models and the various forcing scenarios represented. For the daily cycle (Fig. 3.94, right), also very similar daily patterns in the "model over observed variability of the ZTD" is visible in all cases, with a peak drop in the mid-late afternoon. The current working hypothesis is that the higher the water vapour variability, the higher the departure between model and observation is visible. In terms of forcing the climate model runs: as expected for the

MAR results, results with ERA-Interim forcing are better than forcing with NCEP-NCAR-v1 reanalysis which in turn are better ERA20C forcing. The better scores for MAR with respect to COSMO-CLM may be caused by contrasting coupling strategies. More specifically, whereas MAR is directly forced at the boundaries by reanalysis, COSMO-CLM uses an additional nesting to obtain the highest spatial resolution of 2.8 km. This validation work is still ongoing and more detailed assessments will be undertaken in the future.

3.6.4 GRUAN Reprocessing

G. Dick
GFZ German Research Centre for Geosciences, Helmholtz Centre Potsdam, Potsdam, Germany
e-mail: dick@gfz-potsdam.de

F. Alshawaf
GFZ German Research Centre for Geosciences, Potsdam, Germany
e-mail: fadwa.alshawaf@gfz-potsdam.de

The Global Climate Observing System (GCOS) Reference Upper Air Network (GRUAN) of the World Meteorological Organization (WMO) is an international reference observing network, designed to meet requirements of climate research. Upper air observations within GRUAN will provide long-term high-quality climate records. A GNSS receiver is part of the GRUAN station equipment with highest priority for deriving PWV. Due to its long-term experience in GNSS data processing, GFZ was selected by WMO as a Central GRUAN GNSS Data Processing Centre. GFZ operates also a number of GNSS stations on GRUAN sites, see Fig. 3.95.

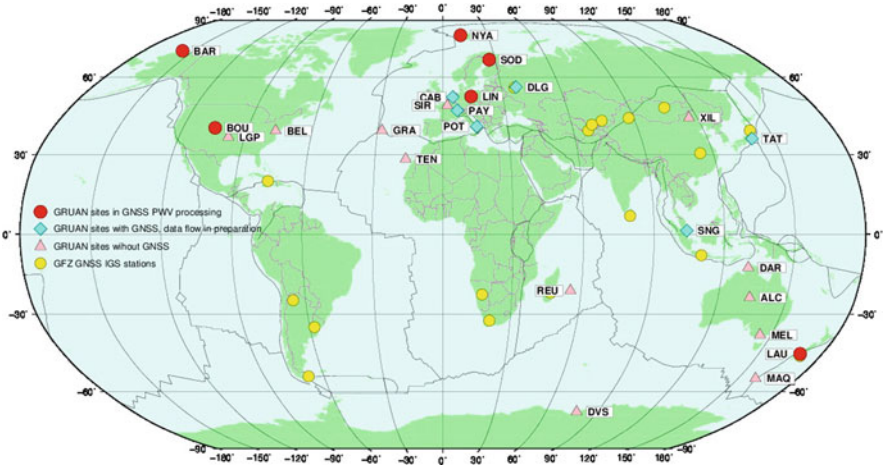

Fig. 3.95 GRUAN network with GNSS stations on GRUAN sites operated by GFZ (in red)

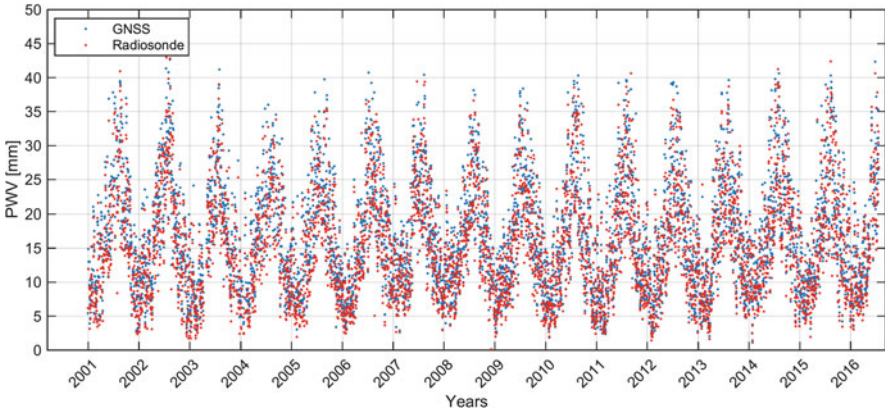

Fig. 3.96 GNSS-derived PWV results from reprocessed data for 2001–2016 compared with radiosonde measurements at GRUAN site Lindenberg (Germany)

The GRUAN GNSS Processing Centre at GFZ with EPOS software covers a fully automated processing chain starting with collecting of raw GNSS observations and resulting with climate relevant validated PWV products, which are available online. PWV uncertainty estimation (Ning et al. 2016), comparisons with radiosonde (RS) measurements (Figs. 3.96 and 3.97) as well as PWV trend estimation (Fig. 3.98) are essential parts of the GNSS data analysis at GFZ for climatological applications.

3.6.5 GFZ TIGA Reprocessing

Z. Deng
GFZ German Research Centre for Geosciences, Potsdam, Germany
e-mail: deng@gfz-potsdam.de

Being a modern geodetic measuring method, GNSS (Global Navigation Satellite Systems) has reached an important role in geosciences. Within the scope of the Tide Gauge Benchmark Monitoring Working Group (TIGA-WG) of the IGS, GFZ analyses and reprocesses GNSS data of stations near tide gauges (Deng et al. 2014). This allows us to monitor tide gauges for vertical land deformations, e.g. due to postglacial uplift. TIGA also contributes to the calibration of satellite altimeters and the unification of height systems (Hunegnaw et al. 2017). In conjunction with circa 400 global IGS stations, GFZ processes data of almost 500 GNSS stations near tide gauges between 1994 and today (Fig. 3.99). In the first TIGA combination there are contributions from 3 international ACs. The GFZ TIGA solution shows the best accuracy among the three submitted solutions (Hunegnaw et al. 2017).

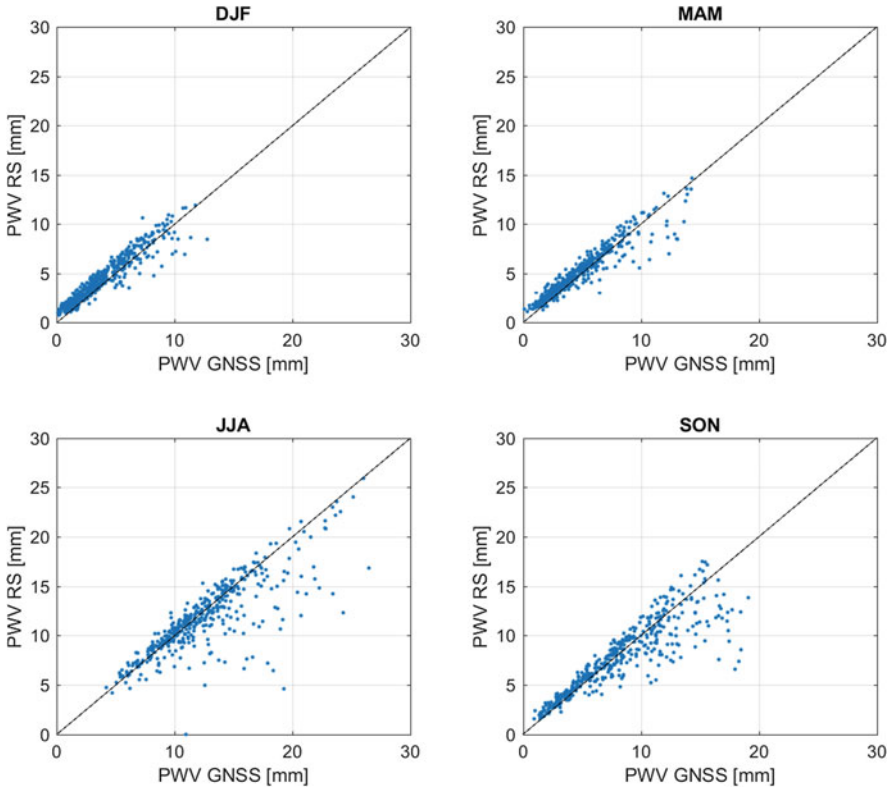

Fig. 3.97 GNSS-derived PWV results from reprocessed data for 2011–2016 compared seasonally with radiosonde measurements at GRUAN site Ny-Alesund (Norway). Seasonal differences between GNSS PWV and RS can be explained by different behaviour of RS during warmer and colder months

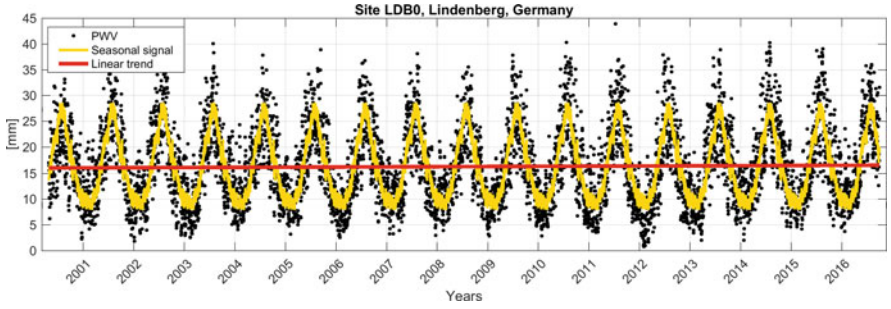

Fig. 3.98 Example of PWV trend estimation from reprocessed GNSS data for 2000–2016 at GRUAN site Lindenberg. Trend value is 0.31 mm/decade, sigma of the trend is 0.075 mm/decade

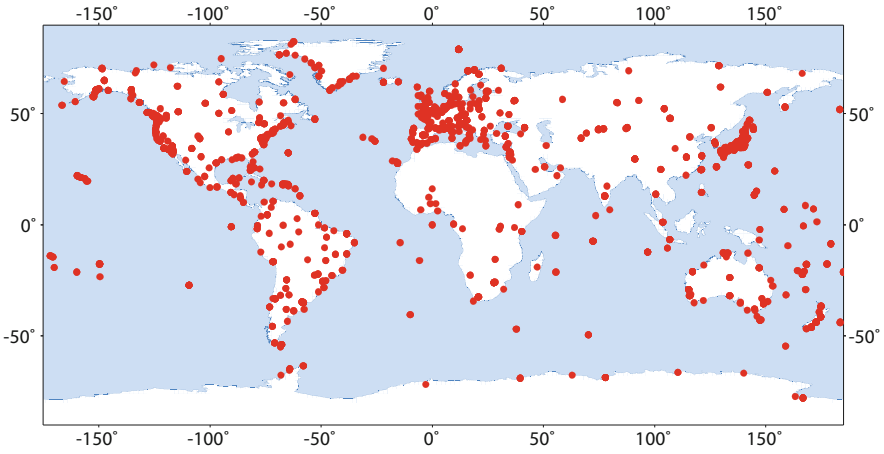

Fig. 3.99 GNSS stations processed at GFZ in the framework of TIGA

Since the GFZ TIGA processing complied with the accords of the 2nd IGS reprocessing campaign, our reprocessed solutions contributed to the determination of the ITRF2014 (Rebischung et al. 2016). In that context the GFZ solution contained the most stations among all of the nine solutions. Because it is the only solution that contains all IGS stations, the IGS Analysis Centre Working Group decided at the 2017 IGS Workshop in Paris, to routinely deliver the GFZ TIGA solution to the IGS in order to ensure, that all IGS stations are contained in the combined weekly IGS solutions.

GFZ TIGA products are available via FTP servers of GFZ and CDDIS. The GFZ FTP server provides daily and weekly files for coordinates, orbits and Earth rotation parameters (ftp://ftp.gfz-potsdam.de/pub/transfer/kg_igs/igstiga/solutions/). In addition to coordinate and orbit products, troposphere parameters are provided, which can be used for climate studies (ftp://ftp.gfz-potsdam.de/GNSS/products/tiga_repro2_tro/).

3.6.6 ULX TIGA Reprocessing[19]

F. N. Teferle
University of Luxembourg, Luxembourg, Luxembourg
e-mail: norman.teferle@uni.lu

ULX, as one of the IGS Tide Gauge Benchmark Monitoring (TIGA) Working Group AC has carried out a second reprocessing campaign in line with IGS. Using the latest

[19]Parts from this section were previously published in Hunegnaw et al. (2015).

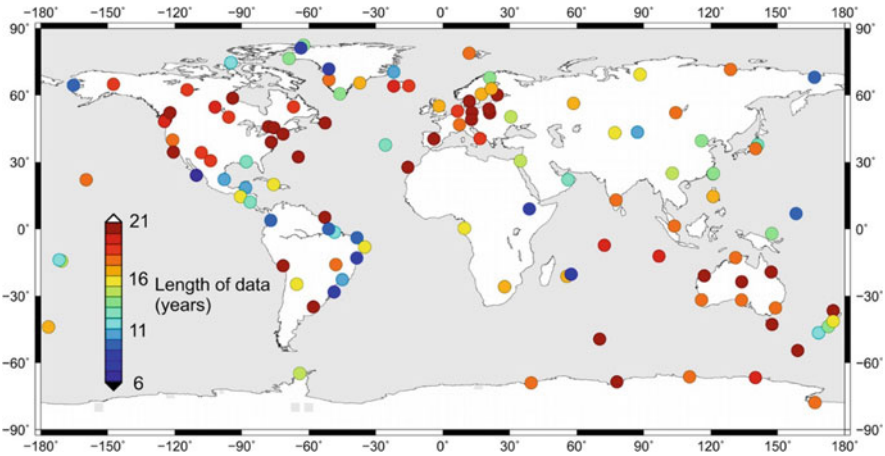

Fig. 3.100 120 selected global stations from the reprocessed TIGA solution. The selection is based on the time length of the ZTD time series and their quality. We have only selected those sites having a minimum length of 6 years

available bias models and methodology the different IGS ACs re-analyzed the full history of GPS data collected by the global tracking network from 1995 to 2015. The consortium of the British Isles continuous GNSS Facility (BIGF) and the University of Luxembourg TIGA Analysis Centre (BLT) completed a new global solution using <750 GPS stations. Figure 3.100 shows a map of 120 stations. As it can be seen, the stations are globally distributed and the timeseries varies from 6 to 21 years in length.

The re-processing follows a double difference network strategy using the BSW52 (Dach et al. 2015), incorporates recent bias model developments, the latest IERS 2010 conventions (Petit and Luzum 2010) and IGS recommendations. Further details are detailed in (Hunegnaw et al. 2015). The selected station network included all IGb08 core stations (Rebischung et al. 2012) and more or less the complete archive of TIGA, which encompasses a large number of GPS stations at or near the global network of tide gauges. The GPS data was re-processed using the CODE final precise orbits and Earth orientation parameters. We employed the IGS08 satellites and receiver antenna phase centre models and adopted an elevation cut-off angle of 3° (Dach et al. 2016). In our solution we make use of the VMF1 (Boehm et al. 2006a, b) that allows to describe the atmosphere with the finest detail, leading to the highest precision in the derived tropospheric parameters.

In BSW52, the ZHD is parameterized as a piece-wise function variation of the delay using a piece-wise linear interpolation between temporal nodes. Observations of atmospheric pressure at the GPS station offer high precision for the ZHD estimates and minimize station height errors (Tregoning and Herring 2006). However, many of the TIGA and IGS stations do not possess integrated meteorological sensors. Thus, ZHD in units of meters was a priori obtained reliably from surface pressure data from the gridded output of the ECMWF NWP model and is provided

by VMF1 using the modified Saastamoinen model, which assumes that the atmosphere is in hydrostatic equilibrium (Davis et al. 1985). We estimate the ZTD parameters in an interval of 1 h with a loose constraint of 5 m. In addition, horizontal gradients in the North-South and East-West directions are estimated in a 24-h interval with the same 5 m loose relative constraint. In this manner more than two decades of ZTD time series along with station positions are available from our re-processing. Figure 3.100 shows a selection of 120 global stations for which we have carried out the further analysis described in this study. However, as the station positions are affected by on average two discontinuities per station per decade, the ZTD time series need to be homogenized before being useful for further application. The results for these 120 stations in terms of a statistical analysis of the periodic signals and stochastic porperties of the related ZWD time series can be found in Klos et al. (2018).

3.7 New Analysis Centres, Networks and Solutions

In this section, the new ACs are mainly presented, however, including also new networks and strategies as well as the shared system for facilitating a collaboration between existing and new ACs. Some of the new ACs are located in Eastern and South-Eastern Europe (Bulgaria, Greece, Turkey, Romania), i.e. large areas where no operational products existed so far, others have been established in countries like Austria, Iceland and Portugal. All of them has developed or gained the expertise thanks to the COST Action. Creating of new GNSS ACs thus fulfilled one of the very important goals of the Action: to increase the observing network and to facilitate the transfer of knowledge for establishment of new GNSS ACs. Now, almost all of the new ACs contribute to E-GVAP – the EUMETNET EIG GNSS Water Vapour Programme (http://egvap.dmi.dk).

3.7.1 Trop-NET System for Collaborative Ground-Based GNSS Meteorology

J. Douša
Geodetic Observatory Pecný, RIGTC, Ondřejov, Czech Republic
e-mail: jan.dousa@pecny.cz

The Trop-NET system has been developed at the Geodetic Observatory Pecny (GOP), Czech Republic, in support of the GNSS4SWEC transfer of knowledge. The goal was to facilitate establishment of new analysis centres for near real-time troposphere monitoring in support of numerical weather prediction within the EUMETNET EIG GNSS Water Vapour Programme – E-GVAP (http://egvap.dmi.

dk). Three short-term scientific missions has been carried out within the transfer of knowledge, see the STSM summary in Appendices.

The ground-based GNSS near real-time processing using a batch approach requires following aspects: (1) hourly data provision, (2) predicted orbit products and precise models, (3) efficient and robust procedure for fully automated operation, and (4) a continuous monitoring and product evaluations. Since 1997, GOP has been developing a flexible system for automated GNSS processing using the BSW and BPE. The system also included data/product flow and supports scientific applications for estimating various parameters in a flexible update rate for different purposes/services:

- near real-time GPS regional troposphere monitoring (EGVAP)
- near real-time GPS + GLONASS regional troposphere monitoring (EGVAP)
- near real-time GPS global troposphere monitoring (EGVAP)
- ultra-rapid GPS and GLONASS orbit determination (IGS)
- rapid (daily), final (weekly) GPS solution for reference frame (EUREF)
- homogeneous re-processing of full EPN (EUREF)
- daily/hourly data flow at the local data centre (EUREF)

All these applications are based on a common module library continuously extended for a higher flexibility and robustness with a near real-time GNSS analysis for the troposphere monitoring as the earliest application (Douša 2001a, b). Due to initial limits in hardware and software, frequent instabilities of data flow, low quality of 24-h predicted orbit products, the system designed had to be highly efficient, fully self-supporting and maximally robust. During the decade, enhancements were done particularly by extending the library for ultra-rapid orbit determination (Douša 2004a, b, 2010), GLONASS processing (Douša 2012), global NRT troposphere solution (Douša and Bennitt 2013) and long-term coordinate and troposphere re-analysis (Douša et al. 2017).

The above mentioned experience leaded to the idea of sharing the library for a collaborative use within the GNSS4SWEC project. For this purpose, the Trop-NET package has been completed for easier dissemination, configuration and maintenance in different environments. Main goals within the COST ES1206 were: (a) facilitate the establishment of new analysis centres, (b) improve the product coverage and its homogeneity over Europe, (c) give a possibility to share future developments, and (d) enable coordinated solution updates. Currently, the Trop-NET pack is maintained by GOP using the Subversion repository. The system consists of several modules supporting individual settings for different user scenarios (Fig. 3.101). The distributed processing is supported by three core modules: (1) for data and product download and mirroring, (2) for GNSS data processing, and (3) for product uploading. Additionally, the system includes central components currently maintained by GOP such as software distribution and update system, NRT product monitoring system, long-term product evaluation system and information systems. Additional modules are considered for future development, for example conversion of ZTD into IWV, animation plots or local monitoring.

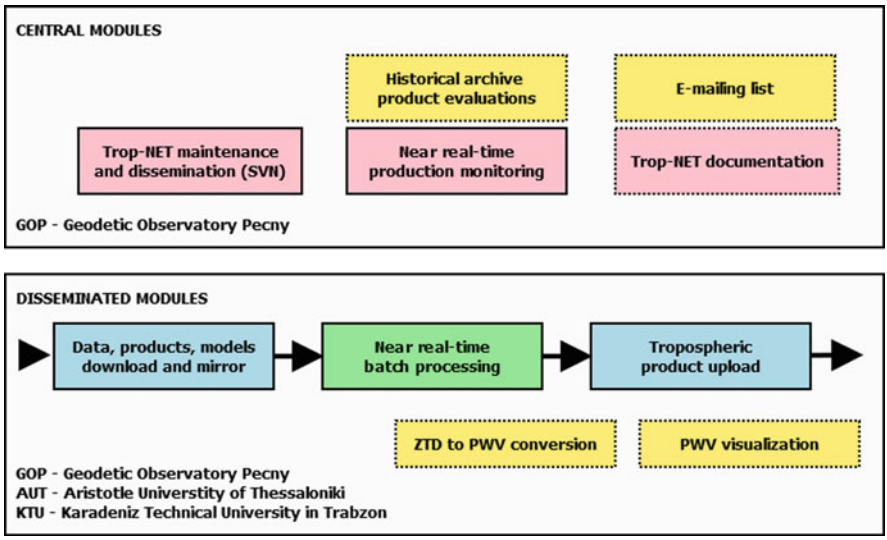

Fig. 3.101 Trop-Net modules – central (up) and disseminated (bottom)

3.7.1.1 Strategy for NRT Troposphere Monitoring

Several aspects are considered generally as important for developing the near real-time GNSS troposphere estimates: (a) high efficiency and low latency of GNSS processing, (b) precise station coordinates fully consistent with troposphere estimates, and (c) robust system operated with a minimum manual interventions. For this purpose, the Trop-NET system implemented three processing levels with intermediate solutions combined into a final solution, however, still efficient in near real-time fashion (Douša 2004a, b), Fig. 3.102:

1. Processing of small network clusters using a short-term data batch (yellow and green).
2. Stacking of clusters in spatial domain into a single session network solution (grey).
3. Stacking of network solutions in long-term solutions using previous solutions (blue).

Originally, the Trop-NET system applied the 1-h session because of a limited computer power in early 2000. In order to support global solution and for a reliable integer ambiguity resolution at long baselines, the processing batch has been extended to the 4-h session (Douša and Bennitt 2013). Hence, the level of processing the original GNSS data remains redundant for 3 h as visible in Fig. 3.103. The session network and sub-network solutions are temporarily saved in the form of normal equations as intermediate products archived for next 30 days at least.

Various numbers of intermediate solutions are combined when estimating different parameters – tropospheric path delays, receiver coordinates or resolving integer

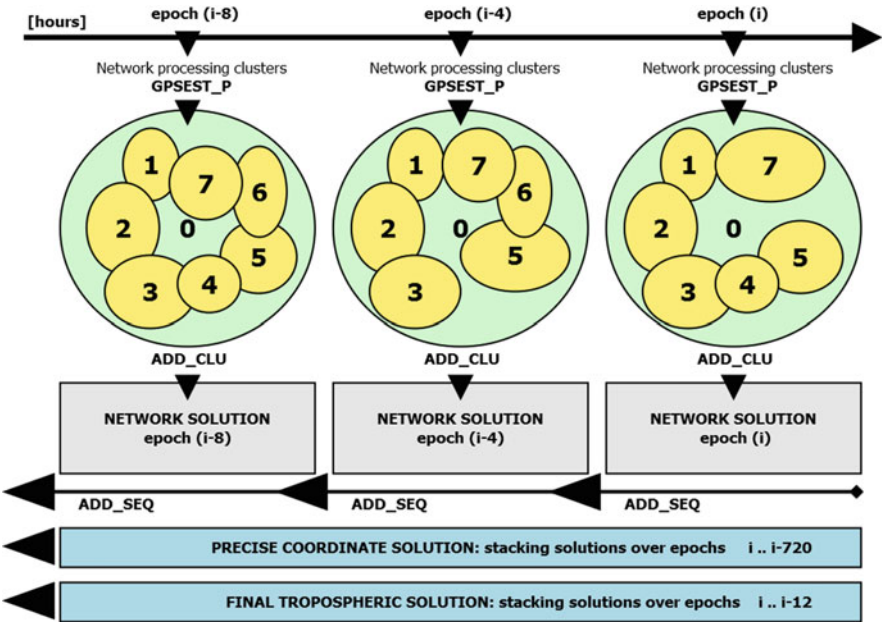

Fig. 3.102 Trop-NET processing in network clusters, spatial and temporal stacking solutions

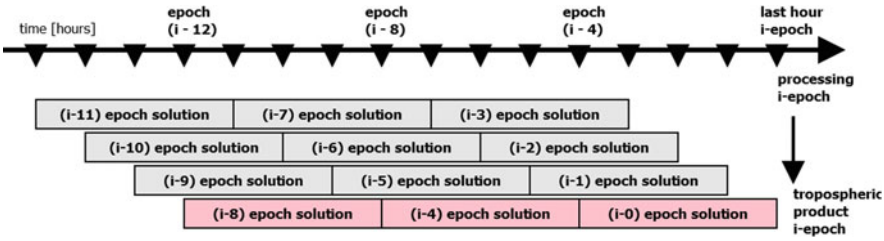

Fig. 3.103 Trop-NET processing redundancy

phase ambiguities. Initially, all parameters are always estimated step-by-step using the 4-h session when original GNSS observations are processed and precise satellite positions introduced as known. First coordinates and tropospheric parameters are then estimated from previous solutions of 1–2 days only before these are introduced for resolving integer phase ambiguities. In later steps, the coordinates are estimated from the time span of 28 days along with introducing integer phase ambiguities and still estimating unresolved ambiguities as float values. Such coordinates are estimated within each individual hourly NRT solution and tied to the actual reference datum. Such approach keeps the system free from any external process and provides additional advantages: (a) all models being implicitly consistent for coordinate and troposphere estimates, (b) coordinates are automatically updated within the system

without need of an external information about their changes in time (implicitly supports solutions in tectonically active areas such as Greece, Turkey and Iceland), (c) any new station is configured once only with an implicit initialization of station coordinates which is usually done from two past days. The tropospheric parameters are finally estimated using the 12-h session when combining normal equations in temporal domain. The ambiguities are estimated along with tropospheric parameters in the final step because it guarantees more stable tropospheric product compared to the ambiguities-fixed solution when using a short data session only.

Different parallelization strategies are used in various processing steps. The 'pre-definition' regional clusters are used whenever necessarily applying a full correlation model for the sub-network solution and such solutions are usually used also for storing solution normal equations. On the other hand, adaptable strategy for parallel processing uses optimal groups of sites or baselines, often suitable for autonomous site or independent baseline processing. The examples are RINEX conversions, pseudorange smoothing, receiver clock synchronization, ambiguity resolution etc. The processing of regional clusters based on pre-defined configurations may still be automatically adapted, e.g. merging too small clusters. The adaptation of clusters uses several scenarios for generating optimal groups: (a) sorting station- or baseline-specific observation files, (b) using actually available stations, or (c) following clusters from any previous step of the processing.

The processing system finally provides automatic warning and error messages either via e-mail or via SMS indicating a temporary solution problem. A warning message often informs about a temporary exclusion of station due to the incompatibility of the file header and the station metadata which always requires a station manual reconfiguration. An error indicating a solution crash often represents a temporary lack of data/products which is possibly within upcoming hours, or if caused by a system-specific reason might need a manual intervention. The status of processing solutions and monitoring indicators are archived along with the products.

3.7.2 Sofia University GNSS Analysis Centre (SUGAC): First Processing Campaign

3.7.2.1 Motivation

T. Simeonov
Sofia University "St. Kliment Ohridski", Sofia, Bulgaria

G. Guerova
Physics Faculty, Department of Meteorology and Geophysics, Sofia University "St. Kliment Ohridski", Sofia, Bulgaria
e-mail: guerova@phys.uni-sofia.bg

In Europe GNSS meteorology is a well-established field in both research and operation, however, large regional differences were acknowledged in GNSS4SWEC MoU, namely "while the production, exploitation and evaluation of operational

GNSS tropospheric products for NWP is well established in the Northern and Western Europe, it is still an emerging R&D field in Eastern and South-Eastern Europe". In 2014, with the signature of national agreement between Sofia University and Bulgarian BuliPOS GNSS network, the Sofia University GNSS Analysis Centre (SUGAC, http://suada.phys.uni-sofia.bg/) was established to fill the gap of production of GNSS tropospheric products for Bulgaria and South-East Europe (Simeonov et al. 2015). The GNSS4SWEC supported STSM for knowledge transfer and processing of 1 year of tropospheric products from Bulgaria.

3.7.2.2 Main results

The first SUGAC processing campaign took place during the STSM of Tzvetan Simeonov to University of Luxembourg (for details see Chap. 7). 7 stations from the BULiPOS network (red pointers in Fig. 3.104) were processed using the NAvigation Package for Earth Observation Satellites (NAPEOS) software version 3.3.1. NAPEOS is developed and maintained by the European Space Operations Centre of the European Space Agency (ESA). First SUGAC processing campaign was performed using the Global Mapping Function and 10° elevation angle cutoff. The RINEX files were processed using the PPP strategy and IGS satellite orbits and clocks. ZTD was computed every 300 s (5 min) for one year – 2013. The ZTD data was used to: (1) estimate IWV and (2) evaluate the numerical weather prediction

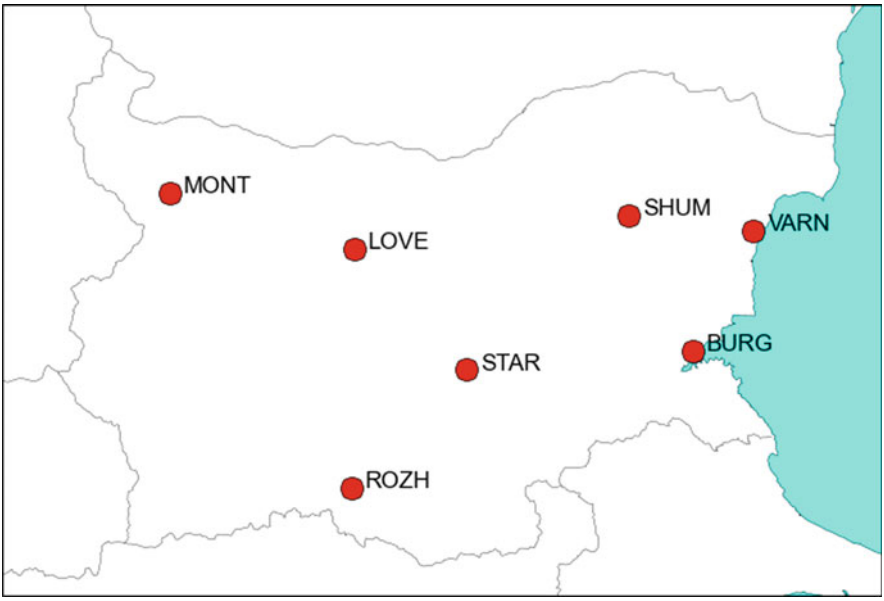

Fig. 3.104 Map of Bulgaria with marked (red dots) ground based stations of the BuliPOS GNSS network used in first SUGAC processing campaign

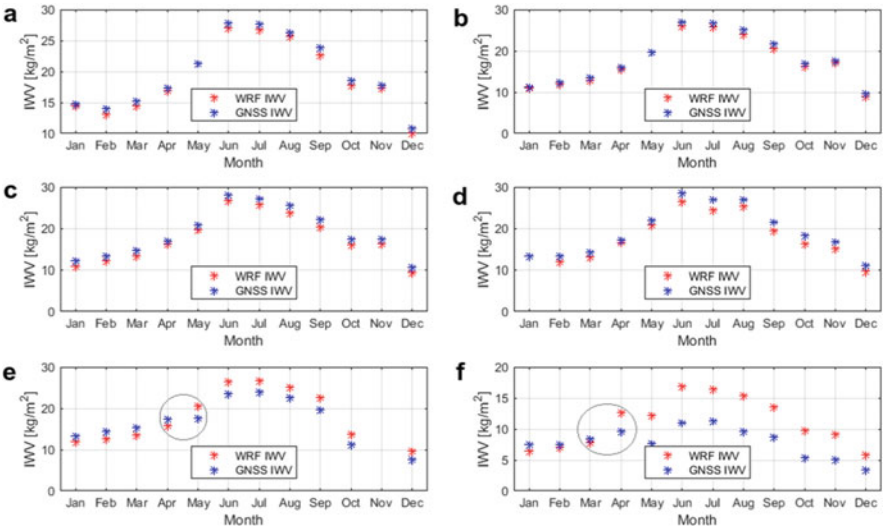

Fig. 3.105 Monthly mean IWV from GNSS (blue markers) and WRF (red markers) for: (**a**) Burgas, (**b**) Shumen, (**c**) Stara Zagora, (**d**) Montana, (**e**) Varna and (**f**) Rozhen in 2013

(NWP) model for Bulgaria (Simeonov et al. 2016). In order to derive IWV with sub-hourly temporal resolution the surface pressure and temperature from the Weather Research and Forecast (WRF) NWP model were used. WRF model simulations were initialized at 00:00 UTC and computed on horizontal mesh of 9 km with 44 vertical levels over Bulgaria. Separately the IWV from WRF is computed by integrating the vertical profile of the water vapour density. The comparisons of monthly mean GNSS and WRF IWV at stations Burgas, Shumen, Stara Zagora, Montana, Varna and Rozhen are presented in Fig. 3.105. At all stations, with exception of Rozhen, the monthly mean IWV minimum is 10 [kg/m^2] in December 2013 and the maximum is up to 25 [kg/m^2] in June 2013. For station Burgas (Fig. 3.105a) good agreement between the monthly mean IWV from GNSS and WRF is seen with correlation coefficient between 0.96 and 0.84 and Root Mean Square Error (RMSE) between 1.8 and 2.8 [kg/m^2] (Fig. 3.106). The maximum and minimum correlation is seen in winter and autumn, and spring and summer, respectively. Between stations Shumen (Fig. 3.105b) and Stara Zagora (Fig. 3.105c) similarities in the IWV can be observed. The two stations also share low RMSE of 2.3 and 2.5 [kg/m^2] respectively. For Shumen the lowest correlation is observed in April and it remains low during the spring months. For Stara Zagora the correlation coefficient stays low in summer with minimum from April till August. Montana (Fig. 3.105d) is in Northwest Bulgaria where the influence of the Balkan mountains is significant and the interaction with synoptic flows plays a major role for the IWV distribution. The lowest GNSS and WRF IWV values are seen for December 12 [kg/m^2] and the highest for June with 27 [kg/m^2]. For Varna (Fig. 3.105e) of interest is the difference between GNSS and WRF, which is seen in January–April

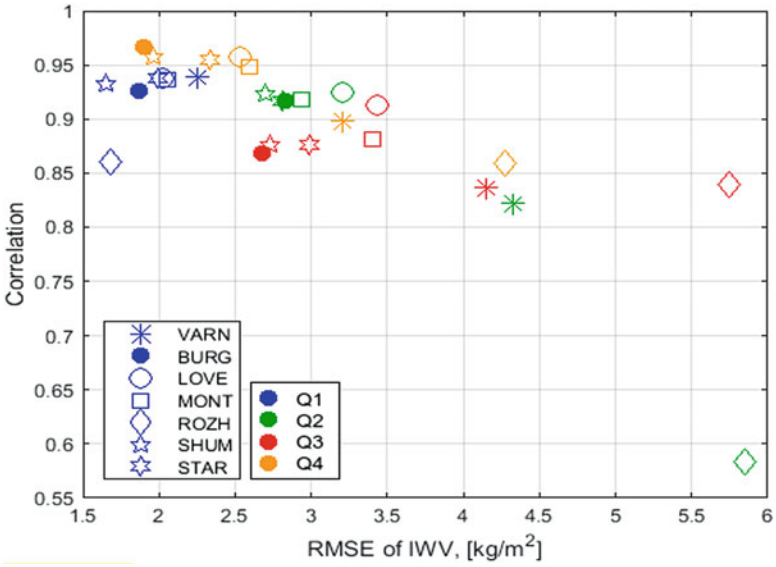

Fig. 3.106 IWV RMSE and correlation between model and GNSS datasets for the Bulipos Network for 2013. Colors indicate: blue – first quarter of the year (JFM), green – second quarter (AMJ), red – third quarter (JAS), orange – fourth quarter (OND)

and May–December period (marked with gray circle). From January to April the IWV in the WRF is lower than the GNSS and from May to December it is the opposite. Similar GNSS IWV jump between April and May is seen at Rozhen (gray circle on Fig. 3.105f). The reason for IWV jump at station Varna is identified to be change of antenna type in the RINEX file. However, for station Rozhen the reason for the IWV change needs further investigation. A summary of the correlation and RMSE for each season is presented in Fig. 3.106. For the cold part of the year (January to March and October to December) the correlation between the model and observation is highest and the RMSE is below 2.6 [kg/m^2]. The warm part of the year quarter 2 and 3 (April–September) is with RMSE over 2.6 [kg/m^2] and correlation below 0.9. This is expected and is related to the increased atmospheric dynamics and summer time instability and convection, which are a well-known weakness of the NWP models. A detailed investigation of WRF model performance in summer is given in Chap. 4 of this report (Slavchev and Guerova).

3.7.2.3 Future Work

The first SUGAC processing campaign was a first step in building expertise in Bulgaria with processing GNSS for remote-sensing the troposphere. The work will continue by developing a pilot transnational severe weather service exploiting GNSS

tropospheric products to enhance the safety, the quality of life and environmental protection in the Balkan-Mediterranean region (Bulgaria, Cyprus and Greece).

3.7.3 TU Wien Near Real-Time GNSS Analysis Centre in Austria (TUW AC): First Processing Results

G. Möller
Department of Geodesy and Geoinformation, TU Wien, Wien, Austria
e-mail: gregor.moeller@geo.tuwien.ac.at

Since March 2017 TU Wien provides near real-time ZTDs for selected GNSS reference sites in Austria and neighbouring countries, see Fig. 3.107.

The processing is based on dual-frequency GPS and GLONASS observations, which are provided on a routine basis from the national reference network provider EPOSA (www.eposa.at) in hourly batches. The processing is carried out at TU Wien using the BSW52 double-difference processing strategy. The routines for processing were established within the national research project GNSS-MET Austria in the years 2009–2010 (see Karabatic et al. 2011) and were further refined during the framework of the COST action. For reliable ambiguity resolution, the observations available within the last 8 h are processed altogether. Therefore, it can be guaranteed that at least 65% (long term average) of the ambiguities can be fixed to their integer values. The accuracy of the tropospheric estimates is evaluated regularly at selected IGS sites against the final IGS tropospheric estimates.

Figure 3.108 shows the results of the comparison, exemplary for station GRAZ over the first 31 days in 2018. Therefore, from each near real-time solution only the estimates of the last hour were considered. Except of a few outliers, the differences in

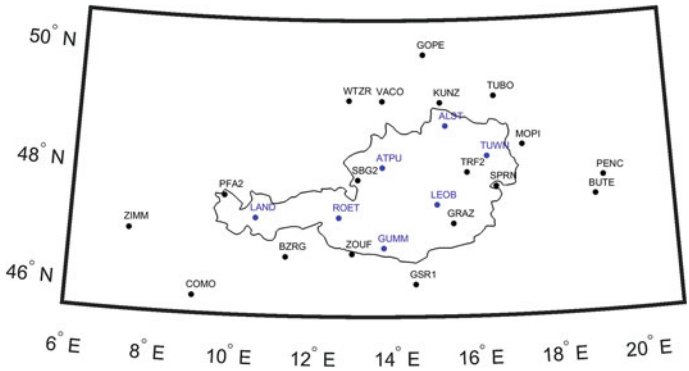

Fig. 3.107 GNSS station distribution. (Blue) GNSS stations of the Austrian reference network EPOSA, (black) IGS and EUREF stations

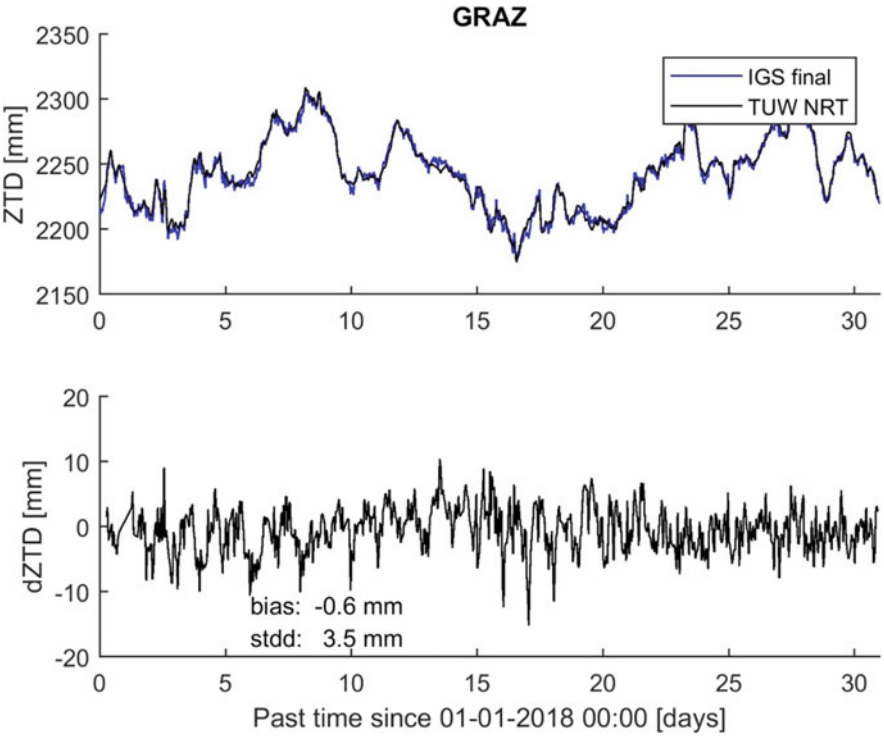

Fig. 3.108 Comparison of TUW near real-time ZTDs with IGS final ZTDs at GNSS site Graz, Austria. Analysed period: First 31 days in 2018

ZTD vary between +/−1 cm with a mean bias of −1 mm and a standard deviation of of about +/−4 mm. A similar result is obtained for other IGS sites.

3.7.4 New Operational Solutions from ROB in Support to Global NWP Models and Rapid-Update Numerical Nowcasting

E. Pottiaux
Royal Observatory of Belgium, Brussels, Belgium
e-mail: eric.pottiaux@oma.be

Fostered by the successful developments done by ROB in the context of this COST Action ES1206, the existing near real-time regional troposphere monitoring operated continuously by ROB in the framework of E-GVAP was upgraded to the latest BSW52, using now GPS + GLONASS observations, and processing them in a double-difference batch approach with the latest modelling techniques. In that

process, a special attention was given to develop a highly flexible and robust processing chain using the BSW52 and the BPE (similar philosophy as the system developed by GOP and described in Sect. 3.6.1), allowing thereby using the same core processing system for various specific applications. This core systems also aims to minimize the manual intervention.

As a consequence, we could extend our support to the meteorological community by developing two new troposphere monitoring systems:

1. A 15-min updated regional troposphere monitoring to support nowcasting applications, and
2. A near real-time global troposphere monitoring to support global NWP models.

Similarly to the legacy ROB solution to E-GVAP, these two new contributions uses the BSW52, GPS + GLONASS observations, the latest modelling techniques, and are now fully operationally provided to all E-GVAP partners. These new monitoring systems are shortly describes below.

3.7.4.1 New Sub-Hourly GPS + GLONASS Troposphere Monitoring

The sub-hourly operational solution operated by ROB includes about 235 GNSS stations providing real-time observations throughout several NTRIP broadcaster servers (Fig. 3.109). Its main objective is to enable rapid-update cycle NWP data assimilation and non-numerical nowcasting applications in the BENELUX + UK regions. This solution has an update cycle of 15 min, and is uploaded to E-GVAP (named ROBQ) with a latency of max 10–15 min after the last observation included in the processing. As expected due to the strong requirement of latency, the precision of the solution is slightly less good than for a standard regional near real-time solution, but it remains within the requirements imposed for such applications (Offiler et al. 2010). Further developments and improvements are still expected to improve this support.

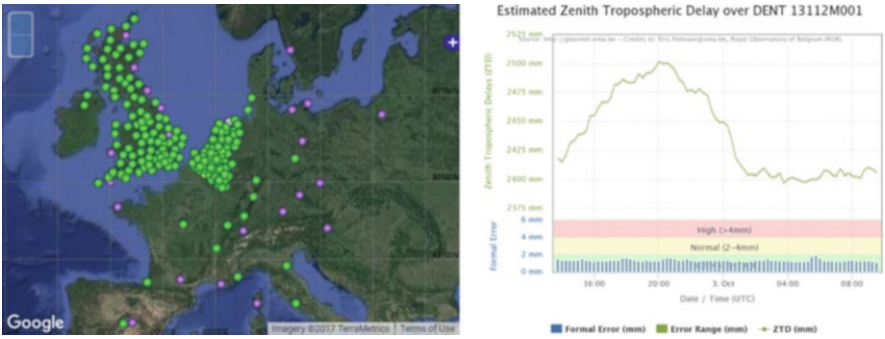

Fig. 3.109 Left: Location of the GNSS stations currently included in ROB's 15-min updated operational contribution to E-GVAP. Right: ZTD time series (and its formal error below) for the Belgian EPN station located in Denterghem from this solution (ROBQ, Status: 3 October 2017)

3.7.4.2 New Near Real-Time GPS + GLONASS Global Troposphere Monitoring

The global operational solutions operated by ROB includes about 315 GNSS stations (named ROBG, Fig. 3.110). Its main objective is to support data assimilation in global NWP models such as those from the U.K Met Office and Météo France. It also potentially supports meteorological agencies outside Europe but collaborating with E-GVAP (e.g. Environment Canada) to access our products. The precision of the solution is similar to the one of the standard regional near real-time solution. With ROB's global solution, E-GVAP has now (solely) 3 global solutions (ROB, GOP and U.K. Met Office). This allows redundancy and a combination process (ASIC solution by ASI/e-Geos) at common GNSS sites, but ROBG also improves the global coverage by processing sites that are not (yet) processed by the two other ACs. Further works on this solution include performance tuning, and adding more sites in specific area such as in Antarctica to further improve the spatial coverage for global NWP models.

3.7.5 New Methods to User GNSS Vapor Estimates for Meteorology (NUVEM)

R. Fernandes
University of Beira Interior, Covilhã, Portugal
e-mail: rmanuel@di.ubi.pt

H. Valentim
University of Beira Interior, Covilhã, Portugal
e-mail: hugo.valentim@segal.ubi.pt

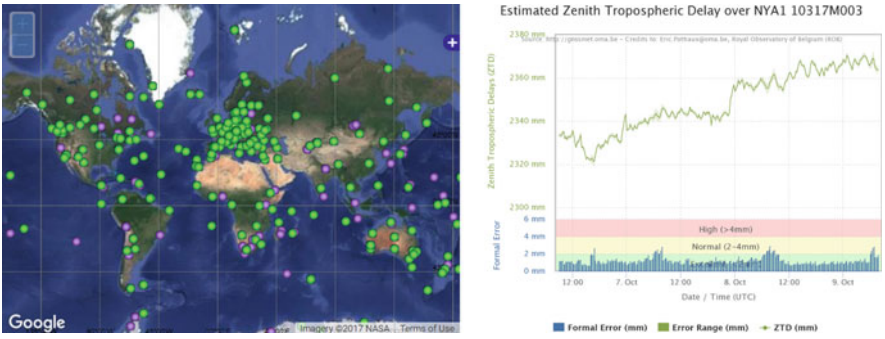

Fig. 3.110 Left: Location of the GNSS stations currently included in ROB's hourly-updated global operational contribution to E-GVAP (ROBG, Status: 3 October 2017). Right: ZTD time series (and its formal error below) for the EPN station NYA1 located in Ny-Alesund, Norway

P. Viterbo
Instituto Português do Mar e da Atmosfera, Lisbon, Portugal
e-mail: pedro.viterbo@ipma.pt

J. P. Martins
Instituto Português do Mar e da Atmosfera, Lisbon, Portugal
e-mail: joao.p.martins@ipma.pt

A. Sá
Polytechnic Institute of Guarda, Guarda, Portugal
e-mail: andre_sa@ipg.pt

J. Jones
Met Office, Exeter, UK
e-mail: jonathan.jones@metoffice.gov.uk

The goal was to include GNSS PWV estimates in weather forecast of Portugal, especially in the decision process of warning dissemination of severe weather situations. For that purpose, Instituto Português do Mar e da Atmosfera (IPMA) and Space and Earth Analysis Laboratory (SEGAL) set up a scheme that provides PWV based on GNSS estimates. Scripts were developed to automatically retrieve the raw GNSS from ftp servers to the server at SEGAL each hour. NUVEM is using 146 stations from 6 GNSS networks over Portugal and Spain, see Fig. 3.111.

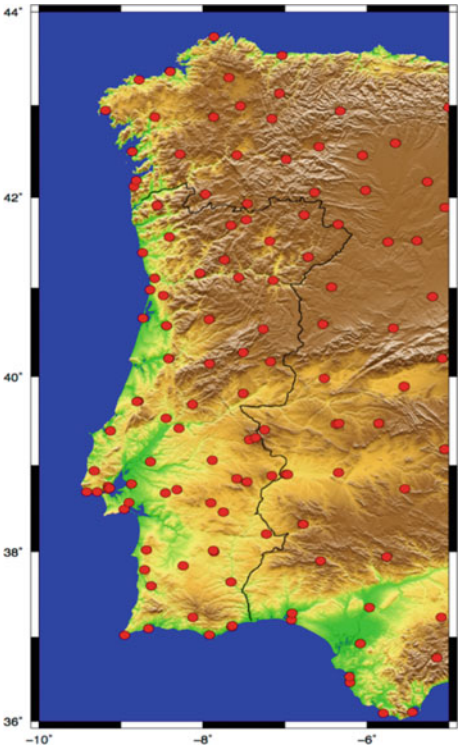

Fig. 3.111 Stations used to estimate the PWV solutions in the framework of NUVEM project

3.7.5.1 GNSS Data Providers

Portugal: RENEP (1); SERVIR (2)

1. http://www.dgterritorio.pt/cartografia_e_geodesia/geodesia/redes_geodesicas/renep/
2. http://www.igeoe.pt/servir/servir.asp

Spain: IGN (3); Castilla (4); Extremadura (5); Andalucia (6)

1. http://www.fomento.es
2. http://gnss.itacyl.es
3. http://194.224.247.162:8080/WebExtremadura/
4. http://www.juntadeandalucia.es/obraspublicasytransportes/redandaluzadeposicionamiento/rap/

The product (GNSS-PWV maps) is available every 5 min with a 2 h delay and can be checked through a dedicated website (http://nuvem.di.ubi.pt/) that was created for the NUVEM project, where all relevant information, including operational results were/are being published.

The ZTDs are estimated at SEGAL, which collects data provided by GNSS networks and information about the GNSS satellite orbits provided by the NASA Jet Propulsion Laboratory as inputs to the GIPSY-OASIS software that is responsible for calculating the ZTD. The conversion of ZTD to PWV is also performed at SEGAL and requires additional information about the pressure and temperature in the vicinity of the GNSS stations. In the developed scheme, these variables are extracted and interpolated for each of the stations by IPMA from the forecasts provided by the ECMWF and are sent to the SEGAL as soon as forecasts are available, with up to about 12 h in advance of their use by the GIPSY. The PWV estimates are then sent to the IPMA, where they are archived and made available to the Operational Centre of Time Forecasting in the form of maps every 15 min, although the available information allows maps every 5 min. In the moment, the products currently available for free by JPL only allow 2 h delay estimates, limiting their use in the context of nowcasting.

Although the project is over, SEGAL and IPMA still maintain the operation and there are plans to improve the products (better outlier detection, quality flagging of the retrievals, reducing delay, increasing availability, etc. as well as comparison to other data sources).

3.7.6 Near Real-Time GNSS Processing at ASI/CGS, Italy

R. Pacione
e-GEOS/Centro di Geodesia Spaziale-Agenzia Spaziale Italiana, Matera, MT, Italy
e-mail: rosa.pacione@e-geos.it

ASI/CGS has been processing Near-Real Time data for E-GVAP since its beginning. During the years of the COST Action ES1206, the existing Near Real-Time network continuously analysed by ASI/CGS in the framework of E-GVAP was upgraded by adding as many GNSS stations as possible in order to homogenize the coverage of troposphere products over Italy.

GNSS data belonging to the following regional GNSS networks: Veneto, Liguria, Piemonte, Friuli Venezia Giulia, Trentino, Umbria, Puglia, Calabria, Lazio, Abruzzo, Campania and the NetGeo commercial GNSS network for the Sardinia Island were added to the core network based on EPN and ASI stations. As of today, about 250 stations in the Central Mediterranean part of Europe are recognized by the NRT processing system.

In the E-GVAP framework, ASI/CGS is participating as Analysis Centre and acts as Combination Centre delivering four tropospheric solutions:

1. Near Real Time ZTD (Operational, labelled ASI_): every hour, 15′ ZTD estimates with a 1h45′ latency for an European network of more than 250 sites (Fig. 3.112, left);
2. Near Real Time Combined ZTD (Operational, labelled ASIC): every hour, the 15′ ZTD estimates from the contributing E-GVAP Analysis Centres are combined and made available to the project, using a combination scheme outlined in Pacione et al. 2011. On hourly basis about 550 stations on a global scale are combined (Fig. 3.112, right);
3. Near Real Time ZTD (Test, labelled ASIR): the aim of this solution is to evaluate IGS RT products in hourly PPP for NWP application;
4. Sub-hourly ZTD (Test, labelled ASIS): the aim of this solution is to test RT GNSS observation and products in sub-hourly PPP for now-casting application.

For ASI_, ASIR and ASIS solutions, GIPSY-OASIS II software (Webb and Zumberge 1997) is used for data reduction. In particular, for ASI_ the standard

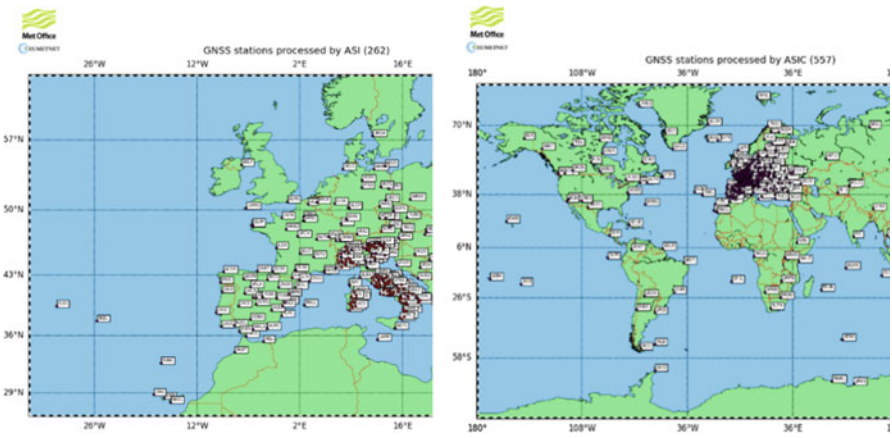

Fig. 3.112 Left: ASI E-GVAP operational network, Right: ASI E-GVAP Combined Network

technique of network adjustment is used fixing the IGS Ultra Rapid orbits. A 4-h sliding window approach for data handling is applied with a sampling rate of 5 min and an elevation cut-off angle for the data of 100. The ZWD is estimated every 5 min with a stochastic model (random walk) and a constraint of 20 mm/h$^{1/2}$. The station coordinates are kept fixed to values provided by combining 1 month of daily post-processed solutions and are updated every 30 days taking into account the tectonic movements of the area as reported in Pacione and Vespe 2008.

3.7.7 New Analysis Centre (AUTh) and National Observatory of Athens (NOA)

C. Pikridas
Aristotle University of Thessaloniki, Thessaloniki, Greece
e-mail: cpik@topo.auth.gr

N. Zinas
Tekmon Geomatics, Ioánnina, Greece
e-mail: nzinas@tekmon.gr

A. Ganas
National Observatory of Athens, Athens, Greece
e-mail: aganas@gein.noa.gr

3.7.7.1 New Analysis Centre (AUTh)

In the frame of a Short Term Scientific Mission on October 2014, a new analysis centre (AC) for near real-time GNSS tropospheric monitoring in Greece was established at the Department of Surveying Engineering of the Aristotle University of Thessaloniki (AUTh). Since then the AUTh Analysis Centre contributes to the EGVAP hourly ZTDs from many permanent GNSS stations in Greece (Fig. 3.113) using the Trop-NET Engine.

The AC provides a unique contribution of tropospheric products to the meteorological community for the E-GVAP project that cover the whole of Greece. During the STSM the GOP's (Geodetic Observatory Pecný) TropNET engine was installed. AUTh AC operates the BSW52 and handles GNSS data from its own and collaborated networks. Additionally, 36 GNSS stations (Fig. 3.114) from IGS and EUREF are included in the network processing scheme for datum definition and consistent absolute tropospheric estimation.

The near real-time (NRT) processing engine includes the following three modules:

1. flexible data, metadata, precise product and model downloading or mirroring,

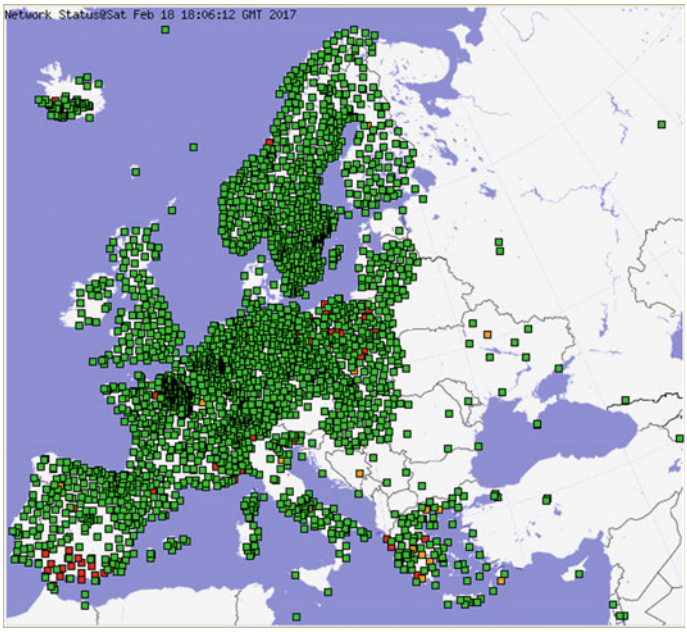

Fig. 3.113 GNSS stations in Greece contributing to E-GVAP

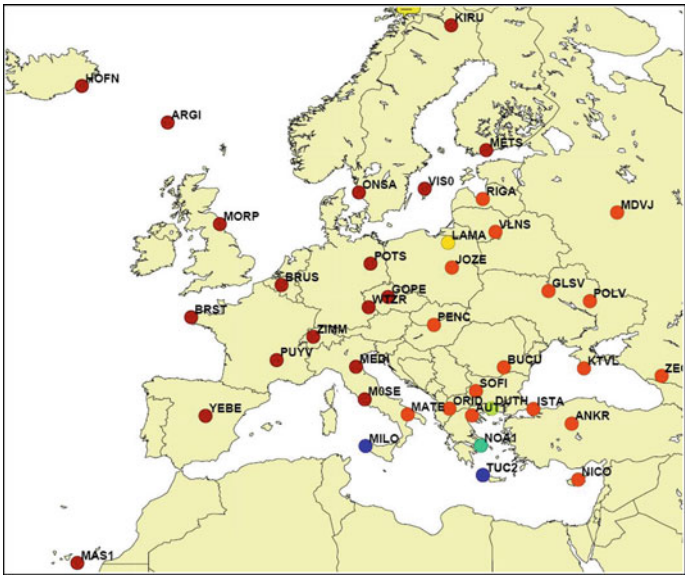

Fig. 3.114 IGS and EUREF GNSS stations

2. module for GNSS processing based on BSW52 and the BPE, and
3. tropospheric product filtering module for converting in the COST-716 format version 2.2. Currently the tropospheric products are uploaded to the GOP data centre, Met-Office and AUTh ftp archive.

In order to have a continuous quality monitoring of the estimated results (like coordinates) and product evaluation the AUTh AC research team (GNSS_QC) developed various scripts for automatic plots of ZTD and coordinates values for each GNSS station (Fig. 3.115).

Finally, in collaboration with two other COST participating countries, Bulgaria and Cyprus, the AUTh Research team received funding under the frame of the European Territorial Cooperation Programme "Interreg V-B Balkan-Mediterranean 2014–2020" for the project BeRTISS (Balkan-Meditteranean Real Time Severe weather Service).

The main objective of BeRTISS is to develop and establish a pilot transnational severe weather service by exploiting Global Navigation Satellite Systems (GNSS) tropospheric products to enhance the quality and safety of life in the Balkan-Mediterranean region. This monitoring service will provide continuous and uninterruptible information for nowcasting, forecasting and early warning for

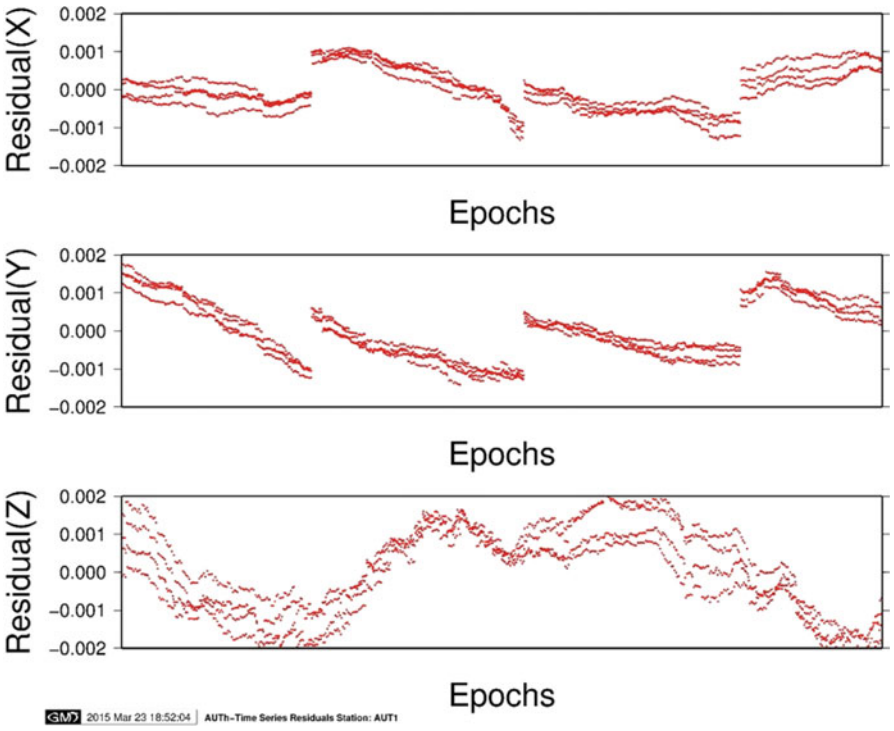

Fig. 3.115 Coordinate residuals for GNSS reference station AUT1

PWV using the GNSS derived tropospheric products and WRF (Weather Research and Forecasting) model that will be tangible and visible to the public through a dedicated web-platform. In detail, the aims of the project are: (1) Integration of networks of GNSS stations located in the three countries in a unified system, (2) Collection, processing and analysis of GNSS observations and tropospheric products, (3) Calculation of the meteorological parameter IWV/PWV for more accurate short-term prediction of severe weather events and (4) Creation of a dedicated website to provide in near real-time the National Meteorological Services and the public with PWV data and warnings of severe weather events.

BeRTISS comprises the continuation of the EU-COST Action "GNSS4SWEC" in particular with respect to the expansion of GNSS tropospheric products in one of the Europe's most remote region and vulnerable to climate change.

3.7.7.2 National Observatory of Athens (NOA)

National Observatory of Athens (NOA) operates NOANET the nationwide geodetic network of 22 CORS stations (www.gein.noa.gr/gps.html). NOANET daily 30-s data are distributed via the GSAC web service http://194.177.194.238:8080/noanetgsac/ as part of the ongoing project EPOS-IP https://epos-ip.org/. In total the NOA GSAC distributes data from 62 CORS stations in SE Europe. In addition, NOA (1) conducted several GPS field campaigns (re-measuring the position of benchmarks) of the CRL/Lefkada/Messinia network in scheduled missions (2) continued installation and maintenance of CORS stations, in the CRL area, in Rhodes (station KATC owned by UNAVCO) and in Messinia (new station ANIK) and (3) conducted installation and maintenance of six (6) continuous GNSS stations in the Ionian Sea area after the 17 November 2015 Earthquake in Lefkada (DRAN, EXAN, ASSO, FISK, KIPO, VLSM).

NOA continues to apply space geodesy techniques (SAR interferometry and GNSS) as an important tool for mapping regional surface deformations due to tectonic motions and large earthquakes (e.g. Ganas et al. 2015; 2016; 2017; ongoing research by Athanassios Ganas, Panagiotis Elias, Panagiotis Argyrakis and Alexandra Moshou). In addition, NOA is engaged in research activities within the CRL project (http://crlab.eu/) with emphasis on the effect of the troposphere (ongoing research by Nikos Roukounakis and Panagiotis Elias). The troposphere introduces a path delay in the radio signal, which, in the case of GPS, can be partially removed with the use of specialized mapping functions. Moreover, tropospheric stratification and short wavelength spatial turbulences produce an additive noise to the ground deformation calculated by the (multitemporal) INSAR methodology. The objective is to further correct the vertical component in GPS measurements with the use of a high resolution meteorological model (WRF), producing a 3D tomography of the troposphere. Thus, the knowledge of the tropospheric parameters along the propagation medium can be used to estimate and minimize the effect of this noise, so that the remaining signal represents the deformation mostly due to tectonic or other geophysical processes (Roukounakis et al. 2015). The data-contributing stations

belong to the Corinth Rift Laboratory and NOANET networks, which monitor the seismicity of the region on a permanent basis. Results are compared with tropospheric delays derived from WRF re-analysis.

3.7.8 New Analysis Centre in Iceland, Icelandic Meteorological Office (IMO)

S. Thorsteinsson
The Icelandic Meteorological Institute, Reykjavík, Iceland
e-mail: siggi@vedur.is

B. G. Ófeigsson
The Icelandic Meteorological Institute, Reykjavík, Iceland
e-mail: bgo@vedur.is

Icelandic Meteorological Office (IMO) operates most monitoring networks of natural hazards in Iceland, see Fig. 3.116. Its operations range from Meteorological monitoring, Hydrological monitoring to volcano and seismic hazard monitoring. As

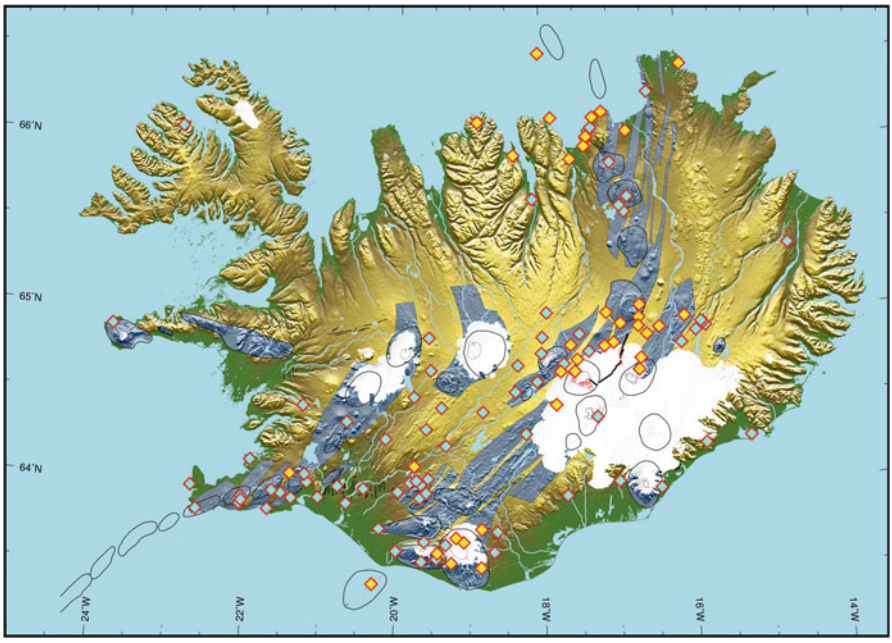

Fig. 3.116 Continuous GNSS network in Iceland (ISGPS). The diamonds mark the location of a GNSS station

a part of this monitoring effort IMO operates a continuous GNSS network mostly used for volcano monitoring.

With the support of Geodetic Obseratory Pecný (GOP), IMO established an analysis centre for near real-time regional troposphere monitoring, using GOP's Trop-NET system in March 2016. Since then the majority of Icelandic continuous GNSS stations already operated by IMO are routinely processed. The analyses is now a part of IMO's continuous operational systems where it has become one of the analysis centres providing GNSS ZTD data to E-GVAP.

IMO has started and plans to continue to do assimilation impact studies with the GNSS ZTD data as well as from 4 GNSS sites in Greenland gotten from E-GVAP in HARMONIE on the 2.5 km IGB grid domain. New decision regarding the common operational system between IMO and the Danish Meteorological Institute (DMI) is to extend the domain to cover the whole Greenland and Iceland and its surrounding islands, termed IGB domain. The HARMONIE tools and the Icelandic processing GNSS ZTD centre that we have developed in COST ES1206 to monitor convective clouds and severe weather conditions will become useful for IMO.

3.7.9 New Analysis Centre in Hungary (BUTE)

Sz. Rozsa
Budapest University of Technology and Economics, Budapest, Hungary
e-mail: szrozsa@agt.bme.hu

The new Analysis Centre (SGO1) was set up in 2014. It processes the Hungarian active GNSS network (37 stations with the mean distance of 60 kms) including some permanent stations from the neighbouring countries (19) as well as some EUREF station as fiducial stations. The near realtime processing is done using BSW52 and the estimated ZTD values are automatically transmitted to the E-GVAP programme.

References

Alber, C., Ware, R. H., Rocken, C., & Solheim, F. S. (1997). GPS surveying with 1 mm precision using corrections for atmospheric slant path delays. *Geophysical Research Letters, 24*, 1859–1862.

Alber, C., Ware, R., Rocken, C., & Braun, J. (2000). Obtaining single path phase delays from GPS double differences. *Geophysical Research Letters, 27*, 2661–2664. https://doi.org/10.1029/2000gl011525.

Altiner, Y., Söhne, W., & Weber, G. (2009). *Echtzeitnahe Schätzung troposphärischer Laufzeit-Verzögerung und Koordinatenüberwachung*, AVN 2/2009, pp. 42–47.

Altiner, Y., Mervart, L., Söhne, W., & Weber, G. (2010). *Real-time PPP results from global orbit and clock corrections.* https://igsac-cnes.cls.fr/documents/egu10/EGU2010-11969_Altiner.pdf

Altiner, Y., Söhne, W., & Weber, G. (2011). *Von NRT zu RT*. http://www.uni-stuttgart.de/gi/research/Geodaetische_Woche/2011/Session4/S4-18-Altiner.pdf

Askne, J., & Nordius, H. (1987). Estimation of tropospheric delay for microwaves from surface weather data. *Radio Science, 22*(3), 379–386.

Bar-Sever, Y. E., & Kroger, P. M. (1998). Estimating horizontal gradients of tropospheric path delay with a single GPS receiver. *Journal of Geophysical Research, 103*, 5019–5035.

Bennitt, G., & Jupp, A. (2012). Operational assimilation of GPS zenith total delay observations into the UK met Office numerical weather prediction models. *Monthly Weather Review, 140*(8), 2706–2719. https://doi.org/10.1175/MWR-D-11-00156.1.

Blewitt, G. (1989). Carrier phase ambiguity resolution for the global positioning system applied to geodetic baselines up to 2000 km. *Journal of Geophysical Research, 94*, 10,187–10,203. https://doi.org/10.1029/JB094iB08p10187.

Boehm, J., Niell, A., Tregoning, P., & Schuh, H. (2006a). Global mapping function (GMF): A new empirical mapping function based on numerical weather model data. *Geophysical Research Letters, 33*, L07304. https://doi.org/10.1029/2005GL025546.

Boehm, J., Werl, B., & Schuh, H. (2006b). Troposphere mapping functions for GPS and very long baseline interferometry from European Centre for Medium-Range Weather Forecasts operational analysis data. *Journal of Geophysical Research, 111*, B02406. https://doi.org/10.1029/2005JB003629.

Böhm, J., Möller, G., Schindelegger, M., Pain, G., & Weber, R. (2015). Development of an improved empirical model for slant delays in the troposphere (GPT2w). *GPS Solutions, Springer, 19*(3), 433–441.

Brenot, H., & Warnant, R. (2008). *Characterization of the tropospheric small-scale activity*, Technical Report ESA, WP250, GALOCAD project. https://orbi.uliege.be/jspui/bitstream/2268/84849/1/GALOCAD-WP250-Report-OUT250-1_v2.pdf

Brenot, H., Ducrocq, V., Walpersdorf, A., Champollion, C., & Caumont, O. (2006). GPS zenith delay sensitivity evaluated from high-resolution numerical weather prediction simulations of the 8–9 September 2002 flash flood over southeastern France. *Journal of Geophysical Research, 111*, D15105. https://doi.org/10.1029/2004JD005726.

Brenot, H., Neméghaire, J., Delobbe, L., Clerbaux, N., De Meutter, P., Deckmyn, A., Delcloo, A., Frappez, L., & Van Roozendael, M. (2013). Preliminary signs of the initiation of deep convection by GNSS. *Atmospheric Chemistry and Physics*, *13*, 5425–5449. https://doi.org/10.5194/acp-13-5425-2013 (licensed under CC BY 3.0, https://creativecommons.org/licenses/by/3.0/).

Brenot, H., Wautelet, G., Warnant, R., Nemeghaire, J., & Van Roozendael, M. (2014a) *GNSS meteorology and impact on NRT position*. Proceedings of the European Navigation Conference (ENC), Rotterdam, The Netherlands.

Brenot, H., Walpersdorf, A., Reverdy, M., van Baelen, J., Ducrocq, V., Champollion, C., Masson, F., Doerflinger, E., Collard, P., & Giroux, P. (2014b). A GPS network for tropospheric tomography in the framework of the Mediterranean hydrometeorological observatory Cévennes-Vivarais (southeastern France). *Atmospheric Measurement Techniques, 7*, 553–578. https://doi.org/10.5194/amt-7-553-2014.

Caissy, M., Agrotis, L., Weber, G., Hernandez-Pajares, M., & Hugentobler, U. (2012). INNOVATION-coming soon-the international GNSS real-time service. *GPS World, 23*, 52–58.

Champollion, C., Masson, F., Van Baelen, J., Walpersdorf, A., Chéry, J., & Doerflinger, E. (2004). GPS monitoring of the tropospheric water vapour distribution and variation during the September 9, 2002, torrential precipitation episode in the Cévennes (southern France). *Journal of Geophysical Research, 109*, D24.

Chen, G., & Herring, T. A. (1997). Effects of Atmospheric Azimuthal Asymetry on the Analysis of Space Geodetic Data. *Geophysical Research Letters, 102*(20), 489–420. 502.

Dach, R., & Jean, Y. (2015). *International GNSS service, technical report 2014*. Pasadena: IGS Central Bureau.

Dach, R., Schaer, S., Lutz, S., Baumann, C., Bock, H., Orliac, E., Prange, L., Thaller, D., Mervart, L., Jäggi, A., Beutler, G., Brockmann, E., Ineichen, D., Wiget, A., Weber, G., Habrich, H., Söhne, W., & Ihde, J. (2014). Steigenberger, P., and Hugentobler, U: CODE IGS Analysis

Center Technical Report 2013, Dach, R., & Jean, Y. (Eds.), IGS 2013 Technical Report, pp. 21–34.
Dach, R., Lutz, S., Walser, P., & Fridez, P. (2015). *Bernese GNSS Software Version 5.2*, University of Bern, Bern Open Publishing. https://doi.org/10.7892/boris.72297.
Dach, R., Stefan, S., Arnold, D., Orliac, E., Prange, L., Suśnik, A., Villiger, A., & Jäggi, A. (2016) *CODE final product series for the IGS*, Published by Astronomical Institute, University of Bern. https://doi.org/10.7892/boris.75876.
Davis, J. L., Herring, T. A., Shapiro, I. I., Rogers, A. E. E., & Elgered, G. (1985). Geodesy by interferometry: Effects of atmospheric modeling errors on estimates of baseline length. *Radio Science, 20*, 1593–1607.
Davis, J. L., Elgered, G., Niell, A. E., & Kuehn, C. E. (1993). Groundbased measurements of gradients in the "wet" radio refractivity of air. *Radio Science, 28*, 1003–1018.
De Haan, S. (2006). National/regional operational procedures of GPS water vapour networks and agreed international procedures, Rep WMO/TD-No, 1340:20, KNMI, Netherlands.
Dee, D. P., et al. (2011). The ERA-Interim reanalysis: Configuration and performance of the data assimilation system. *Quarterly Journal of the Royal Meteorological Society, 137*(656), 553–597.
Delobbe, L., & Holleman, I. (2006). Uncertainties in radar echo top heights used for hail detection. *Meteorological Applications, 13*, 361–374.
Delrieu, G., Nicol, J., Yates, E., Kirstetter, P.-E., Creutin, J.-D., Anquetin, S., Obled, C., Saulnier, G.-M., Ducrocq, V., Gaume, E., Payrastre, O., Andrieu, H., Ayral, P.-A., Bouvier, C., Neppel, L., Livet, M., Lang, M., Parent du-Châtelet, J., Walpersdorf, A., & Wobrock, W. (2005). The Catastrophic Flash-Flood Event of 8–9 September 2002 in the Gard Region, France: a First Case Study for the Cévennes-Vivarais Mediterranean Hydrometeorological Observatory, *Journal of Hydrometeorology, 6*, 34–51. https://doi.org/10.1175/JHM400.1.
Deng, Z., Schöne, T., & Gendt, G. (2014). *Status of the TIGA Tide Gauge Data Reprocessing at GFZ*. International Association of Geodesy Symposia, October 2014.
Deng, Z., Uhlemann, M., Fritsche, M., Dick, G., & Wickert, J. (2015). *Troposphere parameters derived from multi-GNSS data processing at GFZ*. Wien, EGU 2015.
Deng, Z., Nischan, T., & Bradke, M. (2017). Multi-GNSS Rapid Orbit-, Clock- & EOP-Product Series. GFZ Data Services. https://doi.org/10.5880/GFZ.1.1.2017.002.
Dick, G., Gendt, G., & Reigber, C. (2001). First experience with near real-time water vapor estimation in a German GPS network. *Journal of Atmospheric and Solar – Terrestrial Physics, 63*, 1295–1304. https://doi.org/10.1016/S1364-6826(00)00248-0.
Ding, W., Teferle, F. N., Kazmierski, K., Laurichesse, D., & Yuan, Y. (2017). An evaluation of real-time troposphere estimation based on GNSS Precise Point Positioning. *Journal of Geophysical Research Atmosphere, 122*(5), 2779–2790. https://doi.org/10.1002/2016JD025727.
Dong, D.-N., & Bock, Y. (1989). Global positioning system network analysis with phase ambiguity resolution applied to crustal deformation studies in California. *Journal of Geophysical Research, 94*, 3949–3966. https://doi.org/10.1029/JB094iB04p03949.
Douša, J. (2001a). Towards an operational near-real time precipitable water vapor estimation. *Physics andChemistry of the Earth, Part. A, 26*, 189–194. https://doi.org/10.1016/S1464-1895(01)00045-X.
Douša, J. (2001b). The impact of ultra-rapid orbits on precipitable water vapor estimation using ground GPS network. *Physics and Chemistry of the Earth, 26*(6–8), 393–398.
Douša, J. (2004a). Evaluation of tropospheric parameters estimated in various routine analysis. *Physics and Chemistry of the Earth, 29*(2–3), 167–175.
Douša, J. (2004b). Precise orbits for ground-based GPS meteorology: Processing strategy and quality assessment of the orbits determined at geodetic observatory pecný. *Journal of the Meteorological Society of Japan, 82*, 371–380.
Douša, J. (2010). Precise near real-time GNSS analyses at geodetic observatory pecný – Precise orbit determination and water vapour monitoring. *Acta Geodynamics et Geomaterialia, 7*(157), 1–11.

Douša, J. (2012). Developments of the GLONASS ultra-rapid orbit determination at geodetic observatory pecný. In S. Kenyon, M. C. Pacino, & U. Marti (Eds.), *Geodesy of planet earth* (IAG Symposia Series) (Vol. 136, pp. 1029–1036). Dordrecht: Springer.

Douša, J., & Bennitt, G. V. (2013). Estimation and evaluation of hourly updated global GPS zenith Total delays over ten months. *GPS Solutions, 17*, 453–464. https://doi.org/10.1007/s10291-012-0291-7.

Douša, J., & Eliaš, M. (2014). An improved model for calculating tropospheric wet delay. *Geophysical Research Letters, 41*, 4389–4397.

Douša, J., & Souček, P. (2005). The results of near real-time COST-716 GPS campaign from geodetic observatory Pecný, In J. Sledzinski (Eds.), *Proceedings of the EGU G9 symposium* (pp. 139–150). Reports on Geodesy, Warsaw University of Technology, Institute of Geodesy and Geodetic Astronomy, Warsaw, Poland.

Douša, J., & Václavovic, P. (2014). Real-time zenith tropospheric delays in support of numerical weather prediction applications. *Advances in Space Research, 53*(9), 1347–1358. https://doi.org/10.1016/j.asr.2014.02.021.

Douša, J., & Václavovic, P. (2016). *Evaluation of ground-based GNSS tropospheric products at Geodetic Observatory Pecný*. Proceedings of the IAG Symposia Series, Springer, Rizos Ch. & Willis P. (Eds.). 143:759–766. 10.1007/1345_2015_157.

Douša, J., Elias, M., Veerman H., van Leeuwen, S. S., Zelle, H., de Haan, S., Martellucci, A., & Perez, R. O. (2015a). *High accuracy tropospheric delay determination based on improved modelling and high resolution numerical weather model*. Proceedings of the ION GNSS 2015, Institute of Navigation, Tampa, Florida, USA, September 14–18, pp. 3734–3744.

Douša, J., Václavovic, P., Krč, P., Eliaš, M., Eben, E., & Resler, J. (2015b). NWM forecast monitoring with near real-time GNSS products, In *Proceedings of the 5th scientific Galileo Colloquium*, Braunschweig, Germany, October 27–29. http://old.esaconferencebureau.com/docs/default-source/15a08_session1/044-dousa.pdf?sfvrsn=2

Douša, J., Dick, G., Kačmařík, M., Brožková, R., Zus, F., Brenot, H., Stoycheva, A., Möller, G., & Kaplon, J. (2016). Benchmark campaign and case study episode in Central Europe for development and assessment of advanced GNSS tropospheric models and products. *Atmospheric Measurement Techniques, 9*, 2989–3008. https://doi.org/10.5194/amt-9-2989-2016. (licensed under CC BY 3.0, https://creativecommons.org/licenses/by/3.0/).

Douša, J., Václavovic, P., & Eliaš, M. (2017). Tropospheric products of the second European GNSS reprocessing (1996–2014). *Atmospheric Measurement Techniques, 10*, 1–19. https://doi.org/10.5194/amt-10-1-2017. (licensed under CC BY 3.0, https://creativecommons.org/licenses/by/3.0/).

Douša, J., Václavovic, P., Zhao, L., & Kačmařík, M. (2018a). New adaptable all-in-one strategy for estimating advanced tropospheric parameters and using real-time orbits and clocks. *Remote Sensing, 10*, 232. https://doi.org/10.3390/rs10020232. (licensed under CC BY 4.0, https://creativecommons.org/licenses/by/4.0/).

Douša, J., Eliaš, M., Václavovic, P., Eben, K., & Krc, P. (2018b). A two-stage tropospheric correction combining data from GNSS and numerical weather model. *GPS Solutions, 22*, 77. https://doi.org/10.1007/s10291-018-0742-x.

Dow, J. M., Neilan, R. E., & Rizos, C. (2009). The international GNSS service in a changing landscape of global navigation satellite systems. *Journal of Geodesy, 83*, 191–198. https://doi.org/10.1007/s00190-008-0300-3.

Elgered, G., Davis, J. L., Herring, T. A., & Shapiro, I. I. (1991). Geodesy by radio interferometry: Water vapour radiometry for estimation of the wet delay. *Journal of Geophysical Research, 96*, 6541–6555.

Elósegui, P., Davis, J. L., Jaldehag, R. T. K., Niell, A. E., & Shapiro, I. I. (1995). Geodesy using the global positioning system: The effects of signal scattering on estimates of site position. *Journal of Geophysical Research, 100*, 99219934.

Elósegui, P., Davis, J. L., Gradinarsky, L. P., Elgered, G., Johansson, J. M., Tahmoush, D. A., & Ruis, A. (1999). Sensing atmospheric structure using small-scale space geodetic networks. *Geophysical Research Letters, 26*, 2445–2448.

Flores, A., Ruffini, G., & Rius, A. (2000). 4D tropospheric tomography using GPS slant wet delays. *Annales de Geophysique, 18*, 223–234. https://doi.org/10.1007/s00585-000-0223-7.

Ge, M., Gendt, G., Dick, G., Zhang, F. P., & Rothacher, M. (2006). A new data processing strategy for huge GNSS global networks. *Journal of Geodesy, 80*(4), 199–203.

Gendt, G., Dick, G., Reigber, C., Tomassini, M., Liu, Y., & Ramatschi, M. (2004). Near real time GPS water vapor monitoring for numerical weather prediction in Germany. *Journal of the Meteorological Society of Japan, 82*, 361–370.

Gradinarsky, L. P. (2002). *Sensing atmospheric water vapor using radio waves*, Ph.D. thesis, School of Electrical Engineering, Chalmers University of Technology, Göteborg, Sweden.

Guerova, G., Jones, J., Douša, J., Dick, G., de Haan, S., Pottiaux, E., Bock, O., Pacione, R., Elgered, G., Vedel, H., & Bender, M. (2016a). Review of the state of the art and future prospects of the ground-based GNSS meteorology in Europe. *Atmospheric Measurement Techniques, 9*, 5385–5406. https://doi.org/10.5194/amt-9-5385-2016.

Guerova, G., Simeonov, Tzv.,& Vassileva, K. (2016b). Comparison of GNSS tropospheric products obtained by two processing strategies. In *Proceedings of international SYMPOSIUM on modern technologies, education and professional practice in geodesy and related fields.* Sofia, Bulgaria, 3–4/11/2016, 8 p. ISSN 2367-6051. Available at: http://suada.phys.uni-sofia.bg/wordpress/wp-content/uploads/2017/07/Guerova_etal_Sofia-Symposium_2016.pdf

Hadaś, T., & Bosy, J. (2015). IGS RTS precise orbits and clocks verification and quality degradation over time. *GPS Solutions, 19*, 93–105. https://doi.org/10.1007/s10291-014-0369-5.

Hadaś, T., Teferle, F. N., Kaźmierski, K., Hordyniec, P., & Bosy, J. (2017). Optimum stochastic modeling for GNSS tropospheric delay estimation in real-time. *GPS Solutions, 21*(3), 1069–1081. Berlin – Heidelberg.

Herring, T. A. (1992). Modeling atmospheric delays in te analysis of space geodetic data. In *Proceedings of the symposium on refraction of transatmospheric signals in geodesy*. Netherlands Geodetic Commission, Publications on Geodesy, Delft, the Netherlands.

Herring, T. A., King, R. W., & McClusky, S. C. (2010). *Documentation for the GAMIT GPS analysis software*, version 10.4, Technical report. Cambridge: Massachusetts Institute of Technology.

Hofmeister, A., & Böhm, J. (2017). Application of ray-traced tropospheric slant delays to geodetic VLBI analysis. *The Journal of Geodesy, 91*(8), 945–964.

Huisman L., van der Marel H., & Teunissen P. (2009). CORS local-site finger-printing using undifferenced least squares GNSS phase residuals. In *International global navigation satellite systems society IGNSS symposium 2009*, Holiday Inn, Surfers Paradise, Qld, Australia, December 1–3

Hunegnaw, A., Teferle, F. N., Bingley, R., & Hansen, D. (2015). Status of TIGA activities at the British Isles continuous GNSS facility and the University of Luxembourg, C. Rizos & P. Willis (Eds.), *International Association of Geodesy Symposia, 143*:617–623. https://doi.org/10.1007/1345-2015-77. Cham: Springer.

Hunegnaw, A., Teferle, F. N., Abraha, K. E., Santamaría-Gómez, A., Gravelle, M., Wöppelman, G., Schöne, T., Deng, Z., Bingley, R., Hansen, D., Sanchez, L., & Moore, M. (2017). *On the Scientific Applications of IGS Products: An Assessment of the Reprocessed TIGA Solutions and Combined Products*. IGS Workshop 2017, Paris.

Iwabuchi, T., Miyazaki, S., Heki, K., Naito, I., & Hatanaka, Y. (2003). An impact of estimating tropospheric delay gradients on tropospheric delay estimations in the summer using the Japanese nationwide GPS array. *Journal of Geophysical Research, 108*, 4315. https://doi.org/10.1029/2002JD002214.

Kačmařík, M., Douša, J., Dick, G., Zus, F., Brenot, H., Möller, G., Pottiaux, E., Kapłon, J., Hordyniec, P., Václavovic, P., & Morel, L. (2017). Inter-technique validation of tropospheric slant total delays. *Atmospheric Measurement Techniques, 10*, 2183–2208. https://doi.org/10.5194/amt-10-2183-2017. (licensed under CC BY 3.0, https://creativecommons.org/licenses/by/3.0/).

Kapłon, J., Hordyniec, P., & Rohm, W. (2017). *Analysis of systematic effects in slant total delay estimation with PPP*. Presentation G06-1-06 at IAG-IASPEI 2017 Joint Scientific Assembly of the International Association of Geodesy (IAG) and International Association of Seismology and Physics of the Earth's Interior (IASPEI), Kobe, Japan, August 1.

Karabatic, A., Weber, R., & Haiden, T. (2011). Near real-time estimation of tropospheric water vapour content from ground based GNSS data and its potential contribution to weather now-casting in Austria. *Advances in Space Research, 47*(10), 1691–1703. https://doi.org/10.1016/j.asr.2010.10.028.

King, R. W., Masters, E. G., Rizos, C., Stolz, A., & Collins, J. (1985). *Surveying with GPS*, Monograph 9, School of Surveying, University of New South Wales, Kensington, Australia.

Klos, A., Hunegnaw, A., Teferle, F. N., Abraha, K. E., Ahmed, F., & Bogusz, J. (2018). Statistical significance of trends in Zenith Wet Delay from re-processed GPS solutions. *GPS Solutions, 22*, 51. https://doi.org/10.1007/s10291-018-0717-y.

Landskron, D., & Böhm, J. (2017). VMF3/GPT3: Refined discrete and empirical troposphere mapping functions. *The Journal of Geodesy*. https://doi.org/10.1007/s00190-017-1066-2. (licensed under CC BY 4.0, https://creativecommons.org/licenses/by/4.0/).

Laurichesse, D. (2011). The CNES real-time PPP with undifferenced integer ambiguity resolution demonstrator. In *Proceedings of the ION GNSS 2011*, Portland, Oregon.

Laurichesse, D., Cerri, L., Berthias, J. P., & Mercier, F. (2013). Real time precise GPS constellation and clocks estimation by means of a Kalman filter. In *Proceedings ION GNSS 2013* (pp. 1155–1163), Institute of Navigation, Nashville, Tennessee, USA, September 16–20.

Leick, A. (1989). *GPS satellite surveying*. New York: Wiley-Interscience.

Leick, A. (2004). *GPS satellite surveying* (3rd ed., 435p). New York: Wiley.

MacMillan, D. S. (1995). Atmospheric gradients from very long baseline interferometry observations. *Geophysical Research Letters, 22*(9), 97–102. https://doi.org/10.1029/95GL00887.

Marini, J. W. (1972). Correction of satellite tracking data for an arbitrary tropospheric profile. *Radio Science, 7*(2), 223–231.

Möller, G. (2017) *Reconstruction of 3D wet refractivity fields in the lower atmosphere along bended GNSS signal paths*, Dissertation, TU Wien, Department of Geodesy and Geoinformation. http://repositum.tuwien.ac.at/obvutwhs/content/titleinfo/2268559

Möller, G., Weber, R., & Böhm, J. (2014). Improved troposphere blind models based on numerical weather data. *NAVIGATION: Journal of the Institute of Navigation, 61*(3), 203–211.

Montenbruck, O., Steigenberger, P., Prange, L., Deng, Z., Zhao, Q., Perosanz, F., Romero, I., Noll, C., Stürze, A., Weber, G., Schmid, R., MacLeod, K., & Schaer, S. (2017). The Multi-GNSS Experiment (MGEX) of the International GNSS Service (IGS) – Achievements, prospects and challenges. *Advances in Space Research, 59*, 1671–1697. https://doi.org/10.1016/j.asr.2017.01.011.

Morel, L., Pottiaux, E., Durand, F., Fund, F., Boniface, K., de Oliveira, P. S., & Van Baelen, J. (2014). Validity and behaviour of tropospheric gradients estimated by GPS in Corsica. *Advances in Space Research*. https://doi.org/10.1016/j.asr.2014.10.004.

Niell, A. E. (1996). Global mapping functions for the atmosphere delay at radio wavelengths. *Journal of Geophysical Research, 101*, 3227–3246. https://doi.org/10.1029/95JB03048.

Ning, T., Wang, J., Elgered, G., Dick, G., Wickert, J., Bradke, M., & Sommer, M. (2016). The uncertainty of the atmospheric integrated water vapour estimated from GNSS observations. *Atmospheric Measurement Techniques, 9*, 79–92. https://doi.org/10.5194/amt-9-79-2016.

Offiler, D. et al. (2010). *EIG EUMETNET GNSS Water Vapour Programme (E-GVAP-II)*, Product Requirements Document, Version 1.0 – 21 December 2010.

Pacione, R., & Vespe, F. (2008). Comparative studies for the assessment of the quality of near-real time GPS-derived atmospheric parameters. *Journal of Atmospheric and Oceanic Technology, 25*, 701–714.

Pacione, R., Pace, B., de Haan, S., Vedel, H., Lanotte, R., & Vespe, F. (2011). Combination methods of tropospheric time series. *Advances in Space Research, 47*, 323–335. https://doi.org/10.1016/j.asr.2010.07.021.

Pacione, R., Araszkiewicz, A., Brockmann, E., & Douša, J. (2017). EPN-Repro2: A reference GNSS tropospheric data set over Europe. *Atmospheric Measurement Techniques, 10*, 1689–1705. https://doi.org/10.5194/amt-10-1689-2017.

Petit, G., Luzum, B. (red.), IERS Conventions. (2010). IERS Technical Note No. 36, Frankfurt am Main: Verlag des Bundesamts für Kartographie und Geodäsie, ISBN 3-89888-989-6

Pottiaux, E., Brockmann, E., Söhne, W., & Bruyninx, C. (2009). The EUREF – EUMETNET collaboration: First experience and potential benefits. *Bulletin of Geodesy and Geomatics, 3*, 269–288.

Prange, L., Orliac, E., Dach, R., Arnold, D., Beutler, G., Schaer, S., & Jäggi, A. (2017). CODE's five-system orbit and clock solution—The challenges of multi-GNSS data analysis. *Journal of Geodesy, 91*, 345–360. https://doi.org/10.1007/s00190-016-0968-8.

Rebischung, P., Griffiths, J., Ray, J., Schmid, R., Collilieux, X., & Garayt, B. (2012). IGS08: The IGS realization of ITRF2008. *GPS Solutions, 16*, 483494. https://doi.org/10.1007/s10291-011-0248-2.

Rebischung, P., Altamimi, Z., Ray, J., & Garayt, B. (2016). The IGS contribution to ITRF2014. *Journal of Geodesy, 90*, 611–630. https://doi.org/10.1007/s00190-016-0897-6.

Roukounakis, N., et al. (2015). Improvement of the vertical component of GPS and INSAR measurements in the western Corinth Gulf (Greece), by the use of high-resolution meteorological modeling of the lower troposphere: The PaTrop Experiment, 12th European Conference on Applications of Meteorology (ECAM), EMS2015-544;11 September 2015, Sofia, Bulgaria.

Ruffini, G., Kruse, L. P., Rius, A., Bürki, B., & Cucurull, L. (1999). Estimation of tropospheric zenith delay and gradients over the Madrid area using GPS and WVR data. *Geophysical Research Letters, 26*(4), 447–450. https://doi.org/10.1029/1998GL900238.

Saastamoinen, J. (1972). Atmospheric correction for the troposphere and stratosphere in radio ranging of satellites. *The Geophysical Monograph Series, 15*, 247–251.

Schmid, R., Dach, R., Collilieux, X., Jäggi, A., Schmitz, M., & Dilssner, F. (2016). Absolute IGS antenna phase center model igs08.atx: status and potential improvements. *Journal of Geodesy, 90*(4), 343–364.

Seeber, G. (2003). *Satellite geodesy* (2nd ed., 589p). New York: de Gruyter.

Shoji, Y., Nakamura, H., Iwabuchi, T., Aonashi, K., Seko, H., Mishima, K., Itagaki, A., Ichikawa, R., & Ohtani, R. (2004). Tsukuba GPS dense net campaign observation: Improvement in GPS analysis of slant path delay by stacking one-way post phase residuals. *Journal of the Meteorological Society of Japan, 82*(1B), 301–314. https://doi.org/10.2151/jmsj.2004.301.

Simeonov Tzv., Sidorov, D., Teferle, N, Guerova, G., Egova, E., Vassileva, K., Milev, I., & Milev, G. (2015). Sofia University GNSS Analysis Centre, FIG working week, 17–21/05/2015, Sofia, Bulgaria. https://www.Figurenet/resources/proceedings/fig_proceedings/fig2015/papers/ts08g/TS08G_simeonov_sidorov_et_al_7677.pdf

Simeonov, T., Sidorov, D., Teferle, F. N., Milev, G., & Guerova, G. (2016). Evaluation of IWV from the numerical weather prediction WRF model with PPP GNSS processing for Bulgaria. *Atmospheric Measurement Techniques Discussions*. https://doi.org/10.5194/amt-2016-152. https://www.atmos-meas-tech-discuss.net/amt-2016-152/amt-2016-152.pdf.

Teunissen, P., Kleusberg, A., Bock, Y., Beutler, G., Weber, R., Langley, R. B., van der Marel, H., Blewitt, G., Gload, C., & Colombo, O. L. (1998). *GPS for geodesy* (2nd ed.). Berlin: Springer.

Tregoning, P., & Herring, T. A. (2006). Impact of a priori zenith hydrostatic delay errors on GPS estimates of station heights and zenith total delays. *Geophysical Research Letters, 33*(L23303). https://doi.org/10.1029/2006GL027706.

Trojáková, A. (2016). The NWP activities at CHMI, Joint 26th ALADIN Workshop & HIRLAM All Staff Meeting 2016, Lisbon, Portugal, April 4–8.

Urquhart, L., Santos, M., Nievinski, F., & Boehm, J. (2011). Generation and Assessment of VMF1-Type Grids using North-American Numerical Weather Models, XXV IUGG General Assembly, Melbourne, Australia, June 28th – July 7th. Available at http://unb-vmf1.gge.unb.ca/Publications.html

Václavovic, P., & Douša, J. (2015). Backward smoothing for precise GNSS applications. *Advances in Space Research, 56*(8), 627–1634. https://doi.org/10.1016/j.asr.2015.07.020.

Václavovic, P., & Douša, J. (2016). G-Nut/Anubis – Open-source tool for multi-GNSS data monitoring. In *IAG Symposium*. Berlin/Heidelberg: Springer. ISBN-13: 978-3-319-30895-1, *143*, 775–782.

Václavovic, P., Douša, J., & Gyori, G. (2013). G-Nut software library – State of development and first results. *Acta Geodynamica et Geomaterialia, 10*(4), 431–436. https://doi.org/10.13168/AGG.2013.0042.

Václavovic, P., Douša, J., Elias, M., & Kostelecky, J. (2017). Using external tropospheric corrections to improve GNSS positioning of hot-air balloon. *GPS Solutions, 21*(4), 1479–1489. https://doi.org/10.1007/s10291-017-0628-3.

Walpersdorf, A., Calais, E., Haase, J., Eymard, L., Desbois, M., & Vedel, H. (2001). Atmospheric Gradients Estimated by GPS Compared to a High Resolution Numerical Weather Prediction (NWP) Model. *Physics and Chemistry of the Earth, 26*, 147–152.

Warnant, R., Wautelet, G., Spits, J., & Lejeune, S. (2008) *Characterization of the ionospheric small-scale activity.* Technical Report ESA, WP220, GALOCAD project.

Wautelet, G., Lejeune, S., Stankov, S., Brenot, H., & Warnant, R. (2008) *Effects of small-scale atmospheric activity on precise positioning.* Technical Report ESA, WP230, GALOCAD project.

Webb, F. H., & Zumberge, J. F. (1997). An Introduction to GIPSY/OASIS II. JPL D-11088.

Weber, G., Dettmering, D., Gebhard H., & Kalafus, R. (2005) Networked Transport of RTCM via Internet Protocol (Ntrip) – IP Streaming for Real-Time GNSS Applications. In *Proceedings ION-GNSS 18th international technical meeting of the satellite division* (pp. 2243–2247).

Weber, G., Mervart, L., Stürze, A., Rülke, A., & Stöcker, D. (2016). BKG Ntrip Client (BNC) Version 2.12, Mitteilungen des Bundesamtes für Kartographie und Geodäsie, Band 49, ISBN 978-3-86482-083-0.

Wilgan, K., Hurter, F., Geiger, A., Rohm, W., & Bosy, J. (2017a). Tropospheric refractivity and zenith path delays from least-squares collocation of meteorological and GNSS data. *The Journal of Geodesy, 91*(2), 117–134. (licensed under CC BY 4.0, https://creativecommons.org/licenses/by/4.0/).

Wilgan, K., Hadaś, T., Hordyniec, T., & Bosy, J. (2017b). Real-time PPP augmented with high-resolution NWM model data. *GPS Solutions, 23*(3), 1341–1353. (licensed under CC BY 4.0, https://creativecommons.org/licenses/by/4.0/).

Ye, S., Zhao, L., Song, J., Chen, D., & Jiang, W. (2018). Analysis of estimated satellite clock biases and their effects on precise point positioning. *GPS Solutions, 22*, 16. https://doi.org/10.1007/s10291-017-0680-z.

Zumberge, J. F., Heflin, M. B., Jefferson, D. C., Watkins, M. M., & Webb, F. H. (1997). Precise point positioning for the efficient and robust analysis of GPS data from large networks. *Journal of Geophysical Research, 102*, 5005–5017. https://doi.org/10.1029/96JB03860.

Zus, F., Dick, G., Heise, S., Douša, J., & Wickert, J. (2014). The rapid and precise computation of GPS slant total delays and mapping factors utilizing a numerical weather model. *Radio Science, 49*(3), 207–216.

Zus, F., Dick, G., Douša, J., & Wickert, J. (2015a). Systematic errors of mapping functions which are based on the VMF1 concept. *GPS Solutions, 19*, 277–286.

Zus, F., Dick, G., Heise, S., & Wickert, J. (2015b). A forward operator and its adjoint for GPS slant total delays. *Radio Science, 50*, 393–405.

Chapter 4
Use of GNSS Tropospheric Products for High-Resolution, Rapid-Update NWP and Severe Weather Forecasting (Working Group 2)

S. de Haan, E. Pottiaux, J. Sánchez-Arriola, M. Bender, J. Berckmans, H. Brenot, C. Bruyninx, L. De Cruz, G. Dick, N. Dymarska, K. Eben, G. Guerova, J. Jones, P. Krč, M. Lindskog, M. Mile, G. Möller, N. Penov, J. Resler, W. Rohm, M. Slavchev, K. Stoev, A. Stoycheva, E. Trzcina, and F. Zus

Section 4.2.1 contains material that is republished with kind permission.

S. de Haan
Royal Netherlands Meteorological Institute, De Bilt, The Netherlands
e-mail: siebren.de.haan@knmi.nl

E. Pottiaux (✉) · C. Bruyninx
Royal Observatory of Belgium, Brussels, Belgium
e-mail: eric.pottiaux@oma.be; carine.bruyninx@oma.be

J. Sánchez-Arriola
AEMET, Santander, Spain
e-mail: jsancheza@aemet.es

M. Bender
Deutscher Wetterdienst, Offenbach, Germany
e-mail: michael.bender@dwd.de

J. Berckmans · L. De Cruz
Royal Meteorological Institute of Belgium, Brussels, Belgium
e-mail: julieb@meteo.be; lesley.decruz@meteo.be

H. Brenot
Royal Belgian Institute for Space Aeronomy, Uccle, Belgium
e-mail: hugues.brenot@oma.be

G. Dick
GFZ German Research Centre for Geosciences, Helmholtz Centre Potsdam, Potsdam, Germany
e-mail: dick@gfz-potsdam.de

N. Dymarska · G. Möller
Department of Geodesy and Geoinformation, TU Wien, Wien, Austria
e-mail: natalia.dymarska@geo.tuwien.ac.at; gregor.moeller@geo.tuwien.ac.at

J. Jones et al. (eds.), *Advanced GNSS Tropospheric Products for Monitoring Severe Weather Events and Climate*, https://doi.org/10.1007/978-3-030-13901-8_4

K. Eben · P. Krč · J. Resler
Institute of Computer Science of the Czech Academy of Sciences, Prague, Czech Republic
e-mail: eben@cs.cas.cz; krc@cs.cas.cz; resler@cs.cas.cz

G. Guerova
Physics Faculty, Department of Meteorology and Geophysics, Sofia University "St. Kliment Ohridski", Sofia, Bulgaria
e-mail: guerova@phys.uni-sofia.bg

J. Jones
Met Office, Exeter, UK
e-mail: jonathan.jones@metoffice.gov.uk

M. Lindskog
Swedish Meteorological and Hydrological Institute, Norrkoping, Sweden
e-mail: magnus.lindskog@smhi.se

M. Mile
Hungarian Meteorological Service, Budapest, Hungary
e-mail: mile.m@met.hu

N. Penov · K. Stoev (✉)
GNSS Meteorology Group Sofia University "St. Kliment Ohridski", Sofia, Bulgaria
e-mail: npenov@uni-sofia.bg; krasi@phys.uni-sofia.bg

W. Rohm · E. Trzcina
Institute of Geodesy and Geoinformatics, Wrocław University of Environmental and Life Sciences, Wrocław, Poland
e-mail: witold.rohm@igig.up.wroc.pl; estera.trzcina@igig.up.wroc.pl

M. Slavchev · A. Stoycheva
National Institute of Meteorology and Hydrology, Sofia, Bulgaria
e-mail: martin.slavchev@meteo.bg; anastassia.stoycheva@meteo.bg

F. Zus
GFZ German Research Centre for Geosciences, Potsdam, Germany
e-mail: zusflo@gfz-potsdam.de

Abstract For more than a decade, GNSS-meteorology has been increasingly used operationally in Europe particularly for data assimilation in Numerical Weather Prediction (NWP) models, mainly thanks to the EIG EUMETNET GNSS Water Vapour Program (E-GVAP, 2005-today). As such, GNSS has become a well-established, mature observing technique for data assimilation applications. Over this period however, scientists and specialists in GNSS-meteorology noted the clear potential for enhancements and novelties in the domain. The work carried out by the COST Action ES1206 Working Group 2 members addressed these potential enhancements and novelties from the meteorological point of view, in collaboration with WG1. This included the establishment of discussion channels with forecasters in order to determine which GNSS products would be best suited for their day-to-day operational requirements. Particular areas of interest include engaging more operational forecasters (e.g. use of meteorological case studies), especially for non-numerical nowcasting of severe weather, and getting more meteorological agencies to assimilate GNSS products in regions of Europe where they were not yet/well exploited. It also included the development of the techniques and tools

necessary to benefit from the brand new products developed by the Action WG1 and WG2 members, namely real-time GNSS tropospheric products for rapid-cycle NWP and non-numerical nowcasting, data assimilation of horizontal tropospheric gradients and tropospheric slant delays as well as tomographic products. Finally, the work carried out by the WG2 members brought operational improvements through dialog, transfer of knowledge, and standardisation (e.g. the new standardized tropo-SINEX format or the development of assimilation operators). The major WG2 outcomes are discussed in this Chapter.

4.1 Introduction

S. de Haan
Royal Netherlands Meteorological Institute, De Bilt, The Netherlands
e-mail: siebren.de.haan@knmi.nl

E. Pottiaux
Royal Observatory of Belgium, Brussels, Belgium
e-mail: eric.pottiaux@oma.be

J. Jones
Met Office, Exeter, UK
e-mail: jonathan.jones@metoffice.gov.uk

GNSS4SWEC Working Group 2 (WG2) was established primarily to define and improve the use of GNSS tropospheric products for high-resolution, rapid-update numerical (i.e. NWP) and for non-numerical (e.g. forecaster visualisation) nowcasting, with a specific focus on severe weather events. Historically, the primary user of GNSS-meteorological outputs (i.e. ZTD and IWV) were the NWP community, using ZTD for assimilation into local and regional NWP models. Whilst the NWP community still represents a very important user of GNSS products, other users are becoming more evident such as the forecaster and climate communities, and it is an overall aim of this COST Action to better engage these communities. With regards to WG2, forecasters at a number of national meteorological and hydrological agencies were engaged to publicise the usefulness of GNSS-derived IWV fields (images and animations) in certain conditions, and also to better understand the role and requirements of the forecaster when considering future products.

As well as assessing the use of the more traditional GNSS-tropospheric products (i.e. ZTD and IWV), WG2 also looks to assess the impact of more advanced tropospheric products developed by WG1 such as slants and gradients in NWP schemes, and also assesses the benefits and status of GNSS-tomography.

A number of work packages were defined to more efficiently organise the activity in the different fields. The main areas of focus were:

WP 2.1 Non-numerical Nowcasting (Sect. 4.2)

- Review and exchange tools and methods for non-numerical GNSS nowcasting.
- Assess the benefit of new/enhance GNSS products (real-time, gradients, slants etc.) for non-numerical nowcasting.

- Organize detailed analyses of special case studies by non-numerical nowcasting (fog, foehn, precipitation etc.), and to establish a database of severe weather case studies that can be re-used.
- Draw recommendations for operational GNSS nowcasting.

WP 2.2 Numerical Nowcasting and NWP Assimilation (Sect. 4.3)

- Develop, validate and exchange methods for the initialization of NWP models using new/enhanced operational GNSS tropospheric products (e.g. gradients and slants), and for use in nowcasting.
- Evaluate and validate the information content of the enhanced, new products provided by WG1, such as gradients and slant delays (determine error sources, correlations etc.).
- Assess the benefit of multi-GNSS tropospheric products to NWP and severe weather forecasting.

WP 2.3 Tomography (Sect. 4.4)

- Review the status of tomography w.r.t. nowcasting and NWP data assimilation.
- Organise inter-comparison and validate tomography products.
- Organise a specific tomography case study.
- Identify tomography products capability in term of requirement for NWP and nowcasting.
- Develop operational tomography products and evaluate them.

WP 2.4 Benchmark and Case Study Databases (Sect. 4.5)

- Define and generate specific benchmark datasets in the form of GNSS observations, alternative water vapour and refractivity observations and NWP products, for test, assessment, and validation
- Establish a database with severe weather case studies (data, documentation etc.).
- Establish a database with meteorological data to enhance real-time GNSS positioning.

WP 2.5 ZTD2IWV Conversion (Sect. 4.6)

- Develop, validate and exchange methods to convert between ZTD and IWV.

4.2 Non-numerical Nowcasting

4.2.1 Investigation of Fog in Bulgaria Using GNSS Tropospheric Products[1]

A. Stoycheva
National Institute of Meteorology and Hydrology, Sofia, Bulgaria
e-mail: anastassia.stoycheva@meteo.bg

[1]Parts from this section were previously published in Stoycheva et al. (2017) and Stoycheva and Guerova (2015).

N. Penov
Sofia University "St. Kliment Ohridski", Sofia, Bulgaria
e-mail: npenov@uni-sofia.bg

G. Guerova
Physics Faculty, Department of Meteorology and Geophysics, Sofia University "St. Kliment Ohridski", Sofia, Bulgaria
e-mail: guerova@phys.uni-sofia.bg

Despite the continuous improvement of weather prediction fog diagnosis and forecasting remains a challenge with large economic losses for public services and in particular aviation where the cost of flight delays and re-scheduling is estimated to hundreds million euros per year. Today operational fog forecasting is mainly done with "in-house" developed tools. The aim of this work is to investigate the benefit of GNSS tropospheric products in operational fog forecasting in Bulgaria.

Three Fog Case Studies

Fog is low level phenomenon caused by suspended in the air water droplets resulting in visibility below 1000 m. Typical fog conditions for Bulgaria are anti-cyclonic weather with surface: (1) relative humidity over 90–95%, (2) light wind (below 2 m/s) and (3) temperature in the range ± 5 °C. Presented are three case studies of fog development and dissipation in three regions of Bulgaria namely: (1) Danubian plain (blue circles in Fig. 4.1), (2) Sofia valley (yellow circle in Fig. 4.1) and (3) Plovdiv plain (red circle in Fig. 4.1).

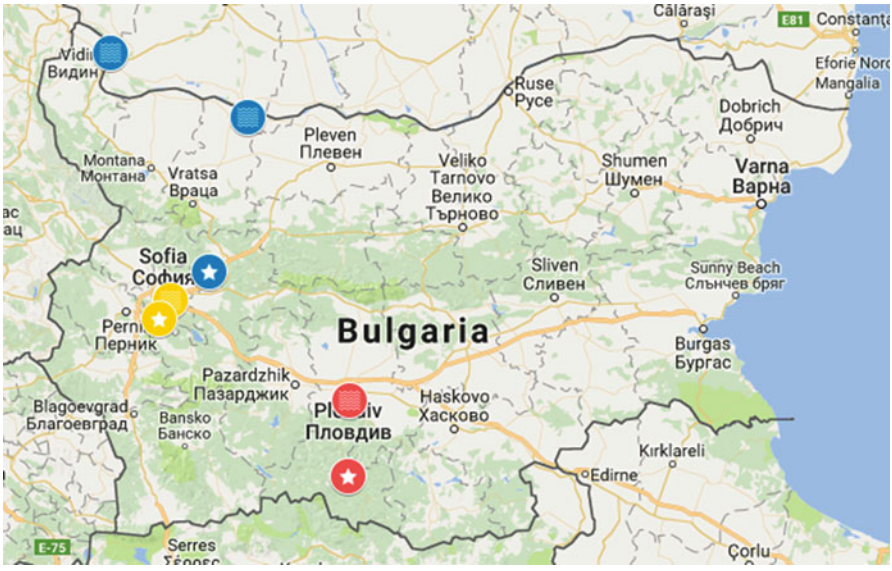

Fig. 4.1 Map of Bulgaria with marked locations of the case studies. Blue circles – Danubian plain fog (11–13 November 2012), yellow circles – Sofia valley fog (1–11 January 2014) and red circles – Plovdiv plain fog (13–16 December 2014)

Table 4.1 Names and altitude of the GNSS (column 2) and synop (column 3 and 4) stations used for case studies (column 1)

Case	GNSS stations	Synop low elevation station	Synop elevated station	Stability Index name
Case 1 11–13.11.2012	Vidin (31 m asl.)	Vidin (31 m asl.)	Murgash (1687 m asl.)	Vidin Stability Index (VSI)
	Oriahovo (29 m asl.)	Oriahovo (29 m asl.)		Oriahovo Stability Index (OSI)
Case 2 1–11.01.2014	Sofia (1164 m asl.)	Sofia (595 m asl.)	Cherni vrah (2292 m asl.)	Sofia Stability Index (SSI)
	Sredets (534 m asl.)			
Case 3 13–16.12.2014	Plovdiv (154 m asl.)	Plovdiv (154 m asl.)	Rozhen (1754 m asl.)	Plovdiv Stability Index (PSI)
	Rozhen (1754 m asl.)			

For each case IWV is derived from GNSS ZTD as described in Stoycheva et al. (2017). In addition, for case 2 the IWV difference is calculated by subtracting IWV from Sredec and Sofia. Equivalent potential temperature (EPT) is calculated following Holton (1972). Computed is also stability index (Stoycheva et al. 2017) using surface temperature observations at low level and elevated mountain synoptic station (marked with star in Fig. 4.1). In Table 4.1 are given the names and altitude of the GNSS (column 2) and synop (column 3 and 4) stations used for each case study.

Case Study 1: Danubian Plain

Presented in Stoycheva and Guerova (2015) are four fog case studies in the Danubian plain. Here is revisited the fog on 10–13 November 2012. In Fig. 4.2 are shown with grey bars the period with fog and with lines the EPT (dashed black), IWV (solid black) and stability indexes (solid red) for Vidin (VSI) and Oriahovo (OSI). The foggy periods in Vidin and Oriahovo differ and most notably the fog starts in Oriahovo 21 h earlier than in Vidin. Comparison of the diurnal cycle of EPT (Fig. 4.2a, b) on 11 November gives that a clear minimum is registered at 6:00 UTC in Oriahovo while at the same time in Vidin EPT remains constant for 6 h between 0:00 and 6:00 UTC. Interestingly, IWV has sharp increase in Vidin (9:00 UTC) while in Oriahovo it decreases (Fig. 4.2b and d). This can be explained with change of the air mass and in particular, IWV, being an integral characteristic of the troposphere, reflects the air mass transformation over time. The north-westerly air mass advection is confirmed in satellite images (not shown) and is registered 9 h later (18:00 UTC) in Oriahovo (Fig. 4.2d). The GNSS derived IWV give an indication of new air mass advection at altitude and the fog formation shows high sensitivity to upper level (1–2 km) advection. It is to be noted that VSI and OSI values are above 1 during the fog on 12–13 November and once the fog disperses drop. However, OSI is not sensitive for the visibility improvement on 12 November but the small IWV changes between 6:00 and 15:00 UTC give indication for transition between liquid

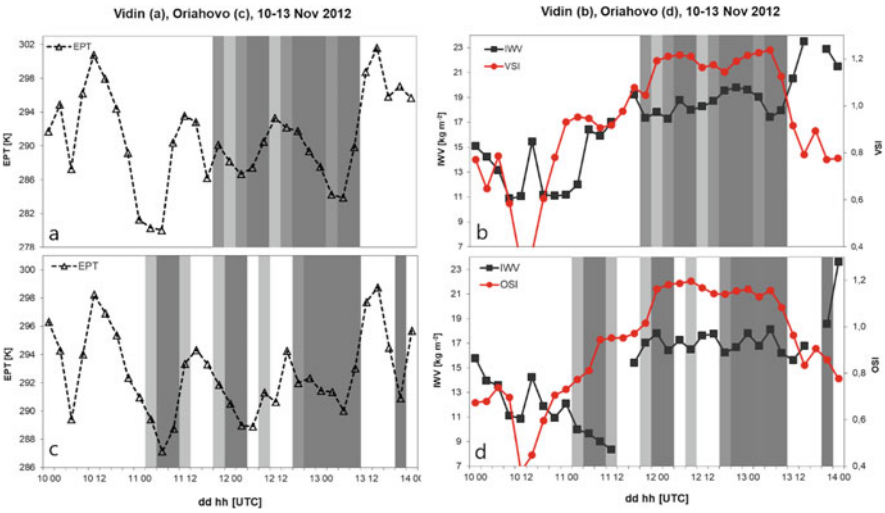

Fig. 4.2 Fog in Danubian plain 11–13 November 2012. The grey bars mark foggy periods. (**a**) and (**c**) EPT at Vidin and Oriahovo (dashed black line). (**b**) IWV in Vidin (solid black line) and VSI (solid red line). (**d**) IWV in Oriahovo (solid black line) and OSI (solid red line)

water and water vapour i.e. vapour increase with fog dispersion and drop with fog onset.

Case Study 2: Sofia Valley

Fog with duration under 24 h is mainly radiation fog with weak temperature inversion generally dispersed by noon. However, when a warm air is advected at the altitude in December and January the weak inversion transforms into powerful one with the fog layer strengthening day by day resulting in a prolonged fog lasting several days. The persistent fog (with duration over 24 h) is a result of interaction between surface, boundary layer and changes at the altitude, which makes prediction of visibility improvement or non-improvements around noon challenging. Here we review the presented in Stoycheva et al. (2017) case of persistent fog in Sofia valley in January 2014. Presented on Fig. 4.3 are the fog registrations in Sofia. The fog is separated in: (a) part I from 3 to 5 January (51 h), and (b) part II from 7 to 10 January (84 h). The part I and II are separated by 39 h with no fog (12:00 UTC on 5 January to 0:00 UTC on 7 January). As seen from Fig. 4.3a the EPT has a marked decrease for fog formation and increase with fog dispersion. In addition, it has a maximum during visibility improvement at 12:00 UTC on 3, 4, and 8 January. A transition of the air mass is recorded between fog part I and II, which is clearly visible in the sharp IWV increase from 10 to 18 kg/m^2 between 0:00 and 12:00 UTC on 5 January (black line on Fig. 4.3b). The Sofia Stability Index (SSI) has higher than 1 values for part II fog (red line in Fig. 4.3b). The SSI increase correlates well with the increase of horizontal visibilities in particular around midday on 8 and 9 January. With SSI drop below 0.8 at 15:00 UTC on 11 January the fog is dispersed. To study the IWV changes at the lower 600 m we compute a daily IWV difference (Sredec minus

Sofia). As seen in Fig. 4.3c the daily mean IWV difference (black dots) do not mark the days with fog but the within day variation of the IWV difference is smaller for the days with fog on 3, 4, 8, and 9 January (black whiskers in Fig. 4.3c). For comparison are given also the IWV differences from the Weather Research and Forecast (WRF) model. The model set-up is described in Stoycheva et al. (2017). The daily mean IWV from GNSS and WRF (red dots and whiskers in Fig. 4.3c) has correlation of 0.66 but the lower variance during fog is not reproduced in the model. As discussed in Stoycheva et al. (2017) the model does not simulate well the temperature inversion layers. The lack of adequate simulation of temperature profile and the inversion layer are the main reason for poor model skills in fog diagnoses and prognoses.

Case Study 3: Plovdiv Plain

In Plovdiv plain the fog is registered for 3-hour interval on 1 January and then for 33-hour period between 1 and 3 January 2013. Clearly seen from Fig. 4.4a is that EPT decreases with fog formation and increase with fog dispersion. The Plovdiv Stability Index (red line in Fig. 4.4b) has upward trend during fog formation (9 and 21:00 UTC on 1 January) and drops with fog dispersion (9:00 UTC on 3 January). The gap in the IWV data does not allow drawing major conclusions but the IWV decreases with fog formation with about 0.5 kg/m^2 between 18:00 and 21:00 UTC on 1 January and increases with fog dispersion by 1 kg/m^2 between 6:00 and 9:00 UTC on 3 January.

Conclusions

Investigation of fog formation and dispersion at different regions in Bulgaria shows that changes of the air mass are critical for timely fog prediction. The high temporal resolution of GNSS derived IWV plays a critical role in detecting local changes in the air mass and this makes it of particular interest for operational fog forecasting in particular for persistent fog. IWV decrease was found to result in fog formation while IWV increase to fog dispersion. We demonstrate the added value of IWV, equivalent potential temperature and stability index for studying fog. The results from this study are beneficial for development of a pilot transnational service exploiting GNSS tropospheric products to enhance the safety, the quality of life and environmental protection in the Balkan-Mediterranean region.

4.2.2 WRF Model Evaluation with GNSS IWV for Intense Precipitation Cases in Bulgaria

M. Slavchev
National Institute of Meteorology and Hydrology, Sofia, Bulgaria
e-mail: martin.slavchev@meteo.bg

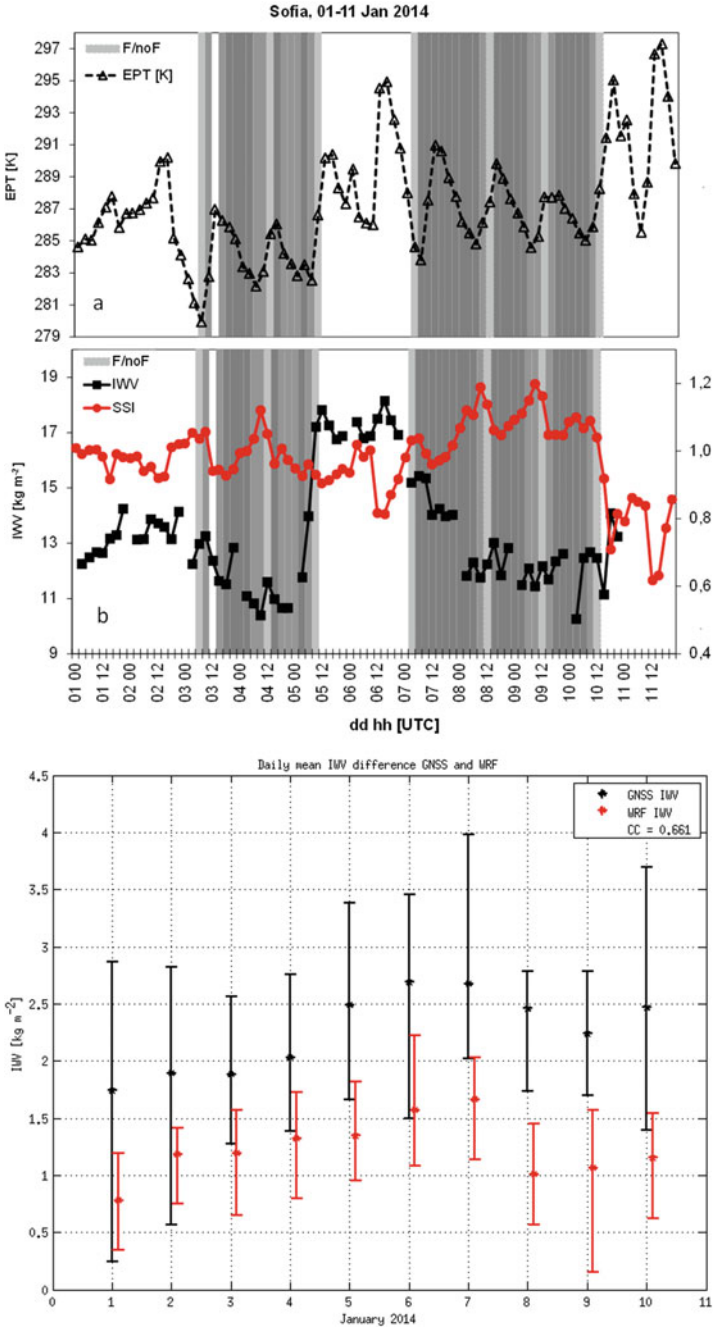

Fig. 4.3 Persistent fog over Sofia valley 1–11 January 2014. With grey bars are marked fog periods. (**a**) EPT in Sofia (dashed black line). (**b**) IWV (solid black line) and Sofia Stability Index (SSI, solid red line). (**c**) daily mean IWV difference from GNSS (black dots and whiskers) and WRF model (red dots and whiskers)

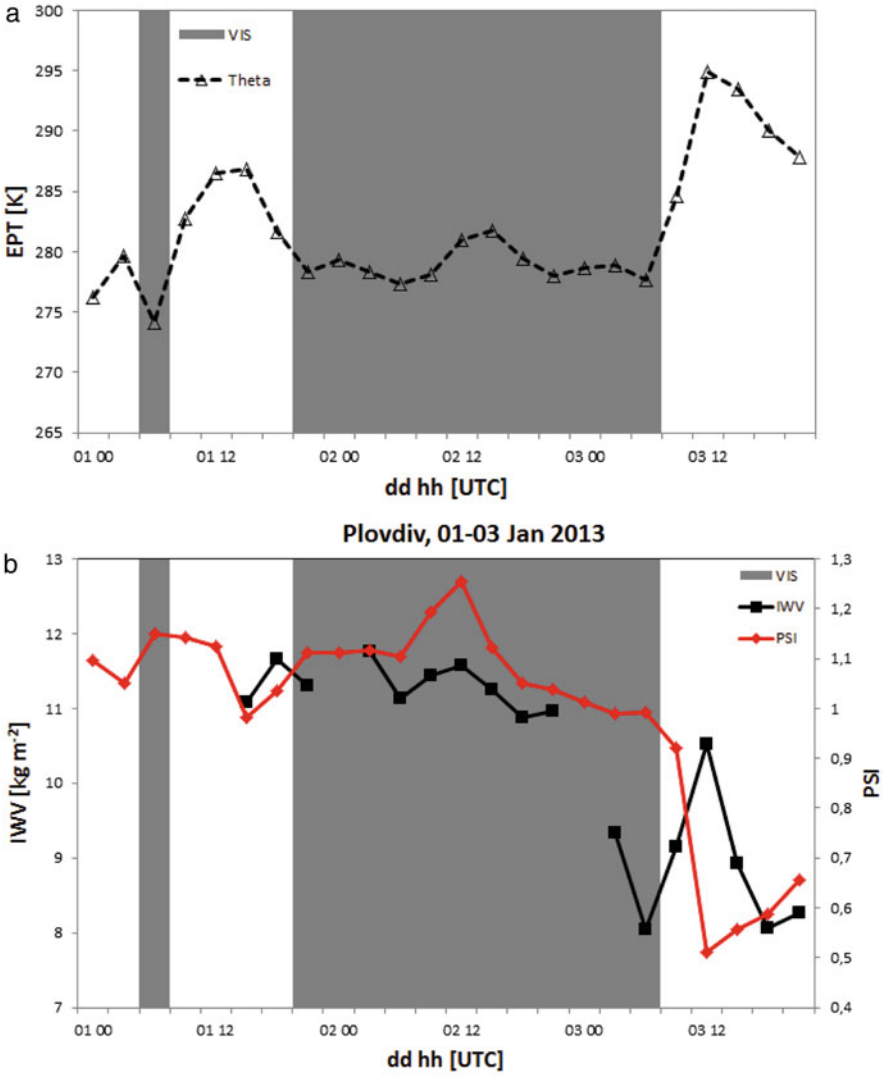

Fig. 4.4 Fog in Plovdiv plain 1–3 January 2013. Gray bars mark the fog periods. (**a**) EPT in Plovdiv (dashed black line). (**b**) IWV (solid black line) and Plovdiv Stability Index (PSI, solid red line)

G. Guerova
Physics Faculty, Department of Meteorology and Geophysics, Sofia University "St. Kliment Ohridski", Sofia, Bulgaria
e-mail: guerova@phys.uni-sofia.bg

Predicting formation and development of vigorous thunderstorms producing intense precipitation and hail is a complex process, which among other environmental conditions depend on accurate estimation of water vapour distribution in space and time. The goal of this work is to use GNSS derived IWV to evaluate the Weather Research and Forecasting (WRF) model skills for predicting the temporal and spatial variability during 20 intense precipitation events in Bulgaria during 2012.

In the last decade, nowcasting severe weather events is rapidly developing using both observations and Numerical Weather Prediction (NWP) models with high spatio-temporal variability and updates. However, prediction of correct time and location of precipitation is a known difficulty in particular in regions with complex topography like Bulgaria, which territory has 41% plateaus and hills (200–600 m asl.) and 20% low and medium-high mountains (600–1500 m asl.). In this work are selected and analysed 20 intense precipitation cases with frontal or convective origin. Conducted are 24-h forecast runs with WRF model v3.4.1 (http://www.wrf-model.org/index.php) and horizontal resolution 4 km and 44 vertical levels for Bulgaria (yellow rectangle in Fig. 4.5a. The used parameterization schemes are: (1) Double-moment 6 class scheme for microphysics, (2) Rapid Radiative Transfer Model/Dudhia scheme for long/short wave radiation, (3) Noah land surface model for land surface and (4) Yonsei University scheme for atmospheric boundary layer. Two experiments are performed by different cumulus parameterization set-up namely: (1) no parameterized convection (NCP) and (2) Kain-Fritsch (KF) cumulus parameterization. The IWV is derived for 30 GNSS stations from the Zenitgeo permanent network in Bulgaria (http://www.zenitgeo.com/about-us.html) and 80 from Greece (Fig. 4.5b). Schematic illustration of IWV computation from WRF and GNSS is given in Fig. 4.4. It is to be noted that the GNSS IWV is computed using surface pressure and temperature from the WRF model. Two

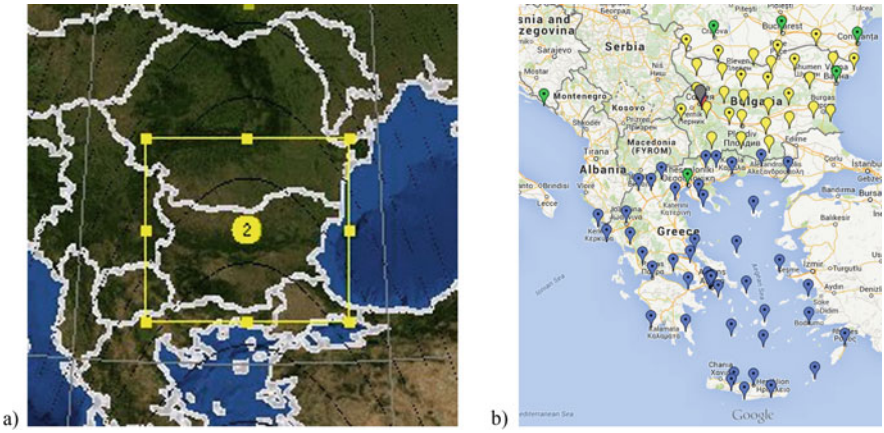

Fig. 4.5 (**a**) WRF model domain used in this work. (**b**) Map of South-east Europe with marled the GNSS stations in Bulgaria (yellow pointers) and Greece (blue pointers)

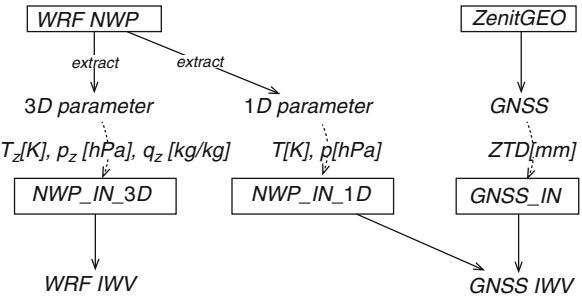

Fig. 4.6 IWV derivation from WRF and GNSS and WRF

dimensional (2D) IWV maps are produced via interpolation between the GNSS stations and application for altitude correction (Guerova 2013) (Fig. 4.6).

A detailed investigation of WRF model is conducted for the period from 8 to 28 May 2012 which covers 6 of the selected 20 cases. In Figs. 4.7a and b, IWV from GNSS (black dots) and two simulations namely WRF/KF (blue dots) and WRF/NCP (red dots) for Vidin (North-west Bulgaria) and Plovdiv (central Bulgaria) are shown. The WRF/KF simulation has consistently higher IWV, with mean of 31.0 and 31.4 kg/m^2, compared to the observed 28.8 and 28.0 kg/m^2. On the other side the WRF/NCP simulation tends to: (1) underestimate the IWV by about 3.3 and 2.6 kg/m^2, (2) has closer to the observed root mean square error (RMS) and (3) has higher correlation namely 0.83 and 0.78 for Vidin and Plovdiv respectively. For comparison correlation between GNSS and KF simulation is 0.74 and 0.56 for Vidin and Plovdiv correspondingly. Interestingly, there is IWV difference of 5.6 and 6.0 kg/m^2 between two model simulations, which shows that the WRF model has a high sensitivity to the convective processes during the selected period and also indicates potential for further improvement by assimilation of the GNSS IWV. It is to be noted that similar results are obtained for the remaining GNSS stations.

In Fig. 4.8a and b the IWV correlation coefficients for Plovdiv from GNSS and WRF/NCP for 10 cases with intense precipitation with mesoscale convective system origin (MSC) and 10 with frontal passage, respectively are shown. The visual inspection shows that the model has a better skill in simulating IWV for the frontal precipitation (Fig. 4.6b) with 7 out of 10 cases with correlation over 0.7. The correlation higher than 0.7 is registered for only 3 MCS cases.

On 27 June, intense MSC precipitation (74 mm) is registered between 9:00 and 15:00 UTC in northeast Bulgarian coast. From 2D GNSS IWV maps (Fig. 4.9) large variation in spatial distribution of IWV is seen with dry air mass covering only North Bulgaria at 00:00 UTC and then also South Bulgaria at 06:00 UTC. Within 6-hour period the IWV in South Bulgaria dropped by 10 kg/m^2 from 35 kg/m^2 at 00:00 UTC (Fig. 4.5a) to 25 kg/m^2 at 06 (Fig. 4.9c). The strong north-south gradient of IWV over the Balkan peninsula is seen also at 12:00 and 18:00 UTC (Fig. 4.9e and g). Large IWV gradient is confirmed by the SEVIRI-Meteosat maps in Fig. 4.9b, d, f and h (http://www.eumetrain.org/eport/tooltip/euro/sphr_tpw.html).

Evaluation of WRF model skills in IWV simulation of 20 intense precipitation cases in Bulgaria show: (1) high sensitivity to the selection of the convective scheme

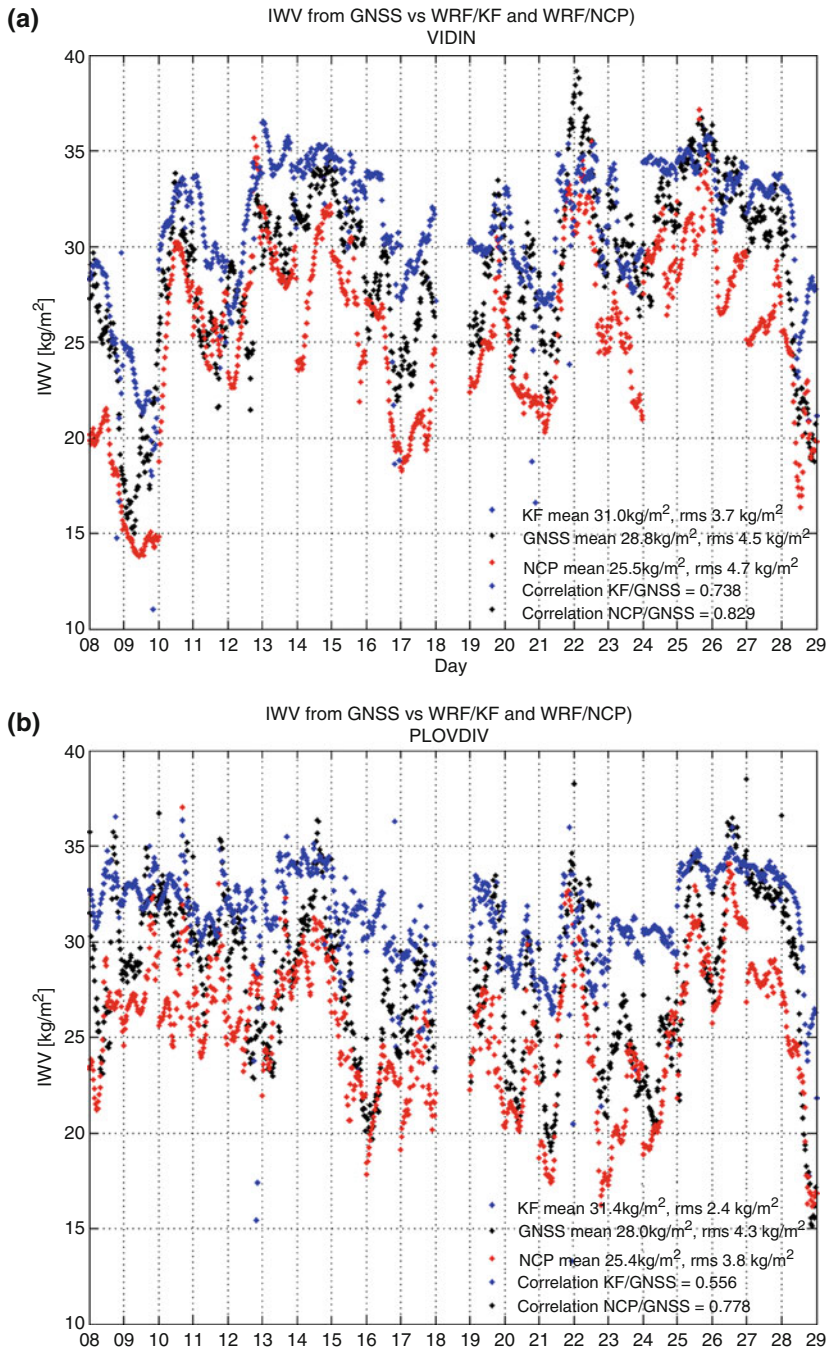

Fig. 4.7 IWV GNSS vs WRF/KF and WRF/NCP for: (**a**) Vidin and (**b**) Plovdiv 8–28 May 2012

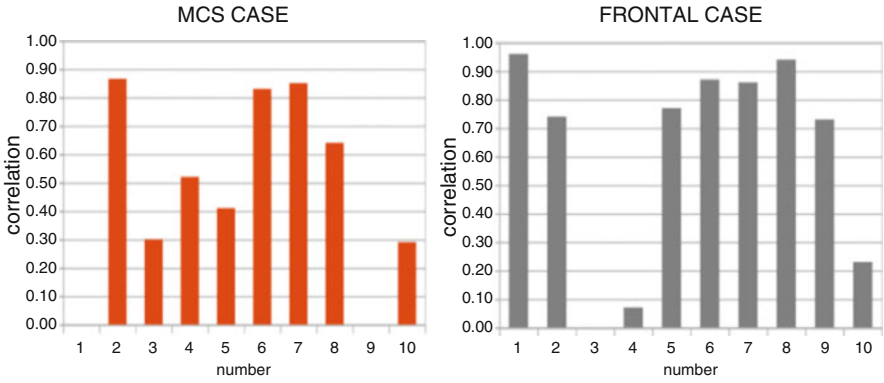

Fig. 4.8 Correlation coefficients between IWV from GNSS and WRF for (**a**) MSC and (**b**) frontal cases

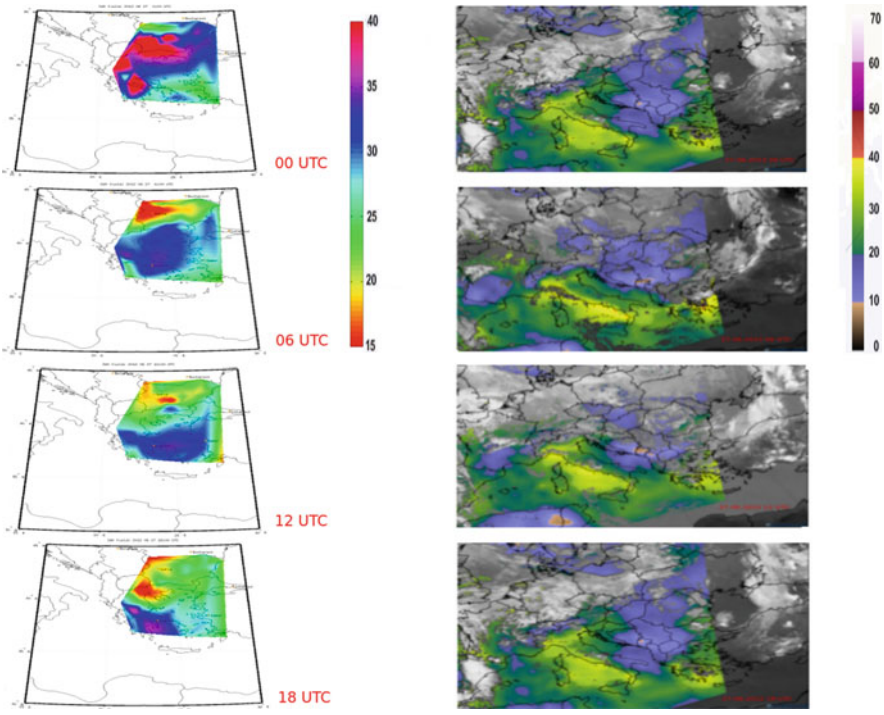

Fig. 4.9 2D maps of the GNSS IWV on 27 June at: (**a**) 00:00 UTC, (**c**) 06:00 UTC, (**e**) 12:00 UTC and (**g**) 18:00 UTC. 2D maps of the Meteosat-IWV on 27 June at: (**b**) 00:00 UTC, (**d**) 06:00 UTC, (**f**) 12:00 UTC and (**h**) 18:00 UTC. Note the difference in the colour map

of the model, (2) better model performance for frontal precipitation cases compared to the mesoscale convective systems and (3) potential for model improvement by assimilation of GNSS IWV. The work will continue by developing a pilot transnational severe weather service exploiting GNSS tropospheric products in collaboration with the colleagues from Cyprus and Greece.

4.2.3 *Case Study of Foehn in Sofia with GNSS Tropospheric Products*

K. Stoev
Sofia University "St. Kliment Ohridski", Sofia, Bulgaria
e-mail: krasi@phys.uni-sofia.bg

G. Guerova
Physics Faculty, Department of Meteorology and Geophysics, Sofia University "St. Kliment Ohridski", Sofia, Bulgaria
e-mail: guerova@phys.uni-sofia.bg

Foehn is an extreme weather event by wind speed and its accurate prediction is still a challenge in operational forecasting. The aim of this study is to use the GNSS derived water vapour to study the Foehn onset in Sofia valley.

Foehn is a warm and dry wind that blows on the downwind side of a mountain and due to its high wind speed and pulsating nature, it is also an extreme weather event impacting aviation, construction, agriculture and spread of fires. The Foehn in Sofia occurs usually during a south or southwest airflow. Passing over the Vitosha mountain the air descends to Sofia valley and adiabatically warms and dries. A cloud-wall forms on the upward side of the Vitosha mountain (blue shading in Fig. 4.10a) and an Altocumulus lenticularis cloud is observed from Sofia (grey shading in Fig. 4.10a). In this work we derive water vapour from IGS station in Sofia (SOFI, black pointer in Fig. 4.10a). Following Stoycheva et al. (2017) we compute Equivalent Potential Temperature (EPT) and Sofia Stability Index (SSI) using surface temperature observations from synoptic station in Sofia (600 m asl., blue pointer in Fig. 4.10a) and Cherni vrah (2290 m asl. Not shown). The Foehn in Sofia is related to the development and the trajectory of cyclonic vortices. In Fig. 4.10b are illustrated the cyclone tracks for four case studies.

Stoev and Guerova (2017) study Foehn in Sofia for the 40-year period (1975–2014) and report 280 days, summarized in 201 synoptic situations. The annual average number of the days with Foehn is 7. However, the number of days was found to be higher for the 1975–1990 period compared to 1990–2014. As seen from Fig. 4.11 this is also reflected in the number of days with wind speed classified according to the severe weather criteria of Meteoalarm. Namely, for the 1975–1990 period 26 Foehn days are with the wind speed below 14 m/s (green bars in Fig. 4.11), 69 days are with wind speed from 14 to 19 m/s (yellow bars in Fig. 4.11), 40 days are

Fig. 4.10 (**a**) Map of Sofia valley and Vitosha mountain with GNSS station SOFI (black pointer) and Sofia synoptic station (blue pointer). The shaded blue area is the location of the cloud wall. (**b**) Cyclone tracks: (1) 24–26 March 2004 (F1 blue line), (2) 26–28 December 2004 (F2 black line), (3) 21–25 March 2008 (F3 green line) and (4) 3–7 December 2008 (F4 red line)

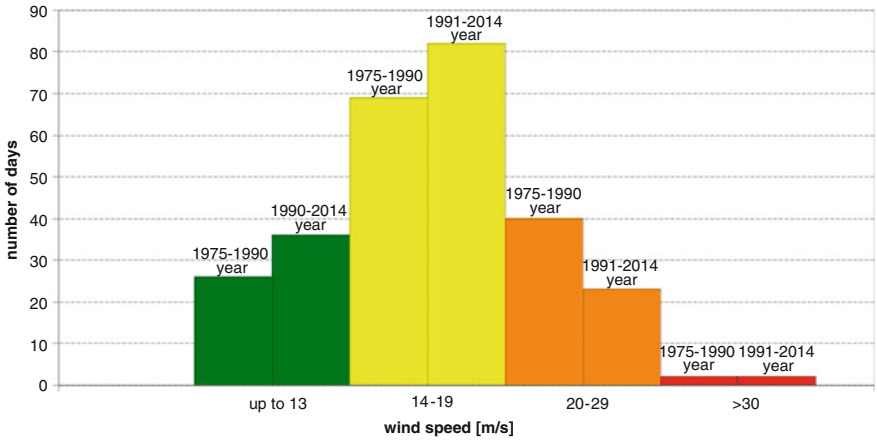

Fig. 4.11 Number of days with Foehn in Sofia for the 1975–1990 (left bars) and 1990–2014 (right bars). The colour code is following Meteoalarm severe weather criteria i.e. "green" for wind speed below 14 m/s, "yellow" for wind speed 14–19 m/s, "orange" for wind speed 20–29 m/s and "red" for wind speed higher than 30 m/s

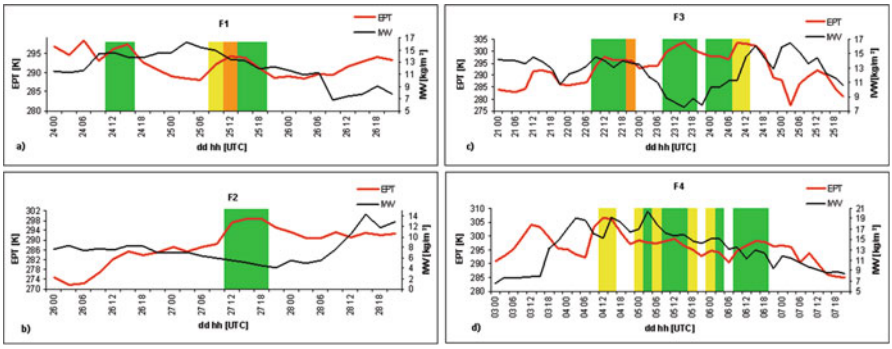

Fig. 4.12 EPT (red line) and IWV (black line), bars mark the foehn periods and bar colour corresponds to the Meteoalarm code for: (**a**) F1, (**b**) F2, (**c**) F3 and (**d**) F4

with wind speed 20–29 m/s (orange bars in Fig. 4.11). Compared to 1975–1990 for the 1990–2014 period the number of days with wind speed below 14 m/s and 14–19 m/s is higher but the lower number of days is recorded with wind speed 20–29 m/s.

Based on GNSS data availability four Foehn cases in 2004 and 2008 are investigated in this work namely: (1) *24–26 March 2004 (F1), (2) 26–28 December 2004 (F2), (3) 21–25 March 2008 (F3) and (4) 3–7 December 2008 (F4).* As seen in Fig. 4.12a two Foehn events are registered on 24 (12:00–18:00 UTC) and 25 March 2004 (9:00–21:00 UTC). Both of them start with EPT increase of 3.2 K/3 h and 4 K/

3 h correspondingly (Fig. 4.12a). The IWV decrease is registered during the foehn but no marked changes are observed before the Foehn start (Fig. 4.12a). The SSI has sharp decrease from 0.59 at 9:00 UTC to 0.29 at 12:00 UTC on 24 March (Fig. 4.12a). The Foehn is observed for a 9-hour period (12:00–21:00 UTC) on 27 December 2004. The EPT increased from 288.3 K at 9:00 UTC to 297.3 K at 12:00 UTC (Fig. 4.12b) and SSI decreased from 0.85 to 0.65 (Fig. 4.13b). IWV decreases linearly between 3:00 and 21:00 UTC on 27 December.

Foehn outbreaks with different duration are registered on 22, 23 and 24 March 2008. Marked increase of EPT from 287 to 294 K and from 293.9 to 299.8 K is seen between 6:00 and 9:00 UTC on both 22 and 23 March (Fig. 4.12c), correspondingly. It is to be noted while on 24 the EPT is constant. On 23 March, IWV starts to decrease from 13.5 kg/m^2 at 0:00 UTC to 8.8 kg/m^2 at 9:00 UTC (Fig. 4.12c). SSI drops from 0.61 to 0.36 between 6:00 and 9:00 UTC on 22 March (Fig. 4.13c). Foehn wind with different duration is registered on 4, 5 and 6 December 2008. As seen from Fig. 4.12d the EPT increased by: (a) 3.3 K/3 h (303–306.3 K), (b) 1.3 K/3 h (297.2–298.5 K), (c) 1.7 K/3 h (293–294.7 K) and (d) 4.5 K/3 h (290.2–294.5 K). The SSI decreased by: (a) 0.19 (0.79–0.6) 9:00 to 12:00 UTC on 4 December, (b) 0.4 (0.7–0.3) 21:00 to 0:00 UTC on 4–5 December, (c) 0.2 (0.5–0.3) 21:00 to 0:00 UTC on 5–6 December and (d) 0.2 (0.6–0.4) 6:00 to 9:00 UTC 6 December (Fig. 4.13d). On 5 December, IWV has steady decrease from 20.4 kg/m^2 at 3:00 UTC to 14.3 kg/m^2 at 21:00 UTC.

It can be concluded that the start of Foehn in Sofia is associated with sharp increase of equivalent potential temperature and drop of the Sofia Stability Index. However, the water vapour at SOFI station does not reflect the air mass change namely decrease with Foehn start. The likely reason is the SOFI station location, which is on the side of the Vitosha mountain. It is to be noted that the Foehn is very

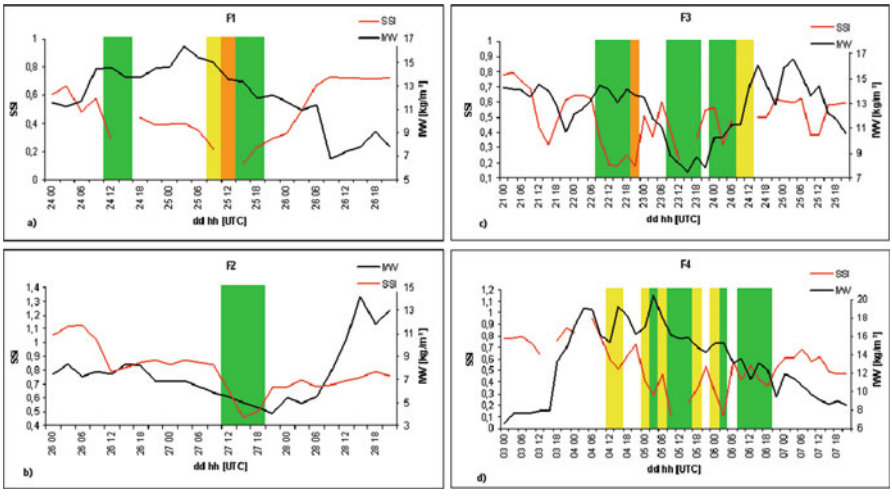

Fig. 4.13 SSI (red line) and IWV (black line) bars mark the foehn periods and bar colour corresponds to the Meteoalarm code for: (**a**) F1, (**b**) F2, (**c**) F3 and (**d**) F4

local phenomenon thus the station position plays a critical role. The work will continue by conducting case studies using GNSS station located in Sofia valley as a part of a pilot transnational severe weather service exploiting GNSS tropospheric products for the Balkan-Mediterranean region.

4.2.4 A GNSS-Based Nowcasting Toolbox for Severe Weather in Belgium

E. Pottiaux
Royal Observatory of Belgium, Brussels, Belgium
e-mail: eric.pottiaux@oma.be

C. Bruyninx
Royal Observatory of Belgium, Brussels, Belgium
e-mail: carine.bruyninx@oma.be

J. Berckmans
Royal Meteorological Institute of Belgium, Brussels, Belgium
e-mail: julieb@meteo.be

S. de Haan
Royal Netherlands Meteorological Institute, De Bilt, The Netherlands
e-mail: siebren.de.haan@knmi.nl

At the beginning of COST Action GNSS4SWEC, a workshop dedicated to review the state-of-the-art was organised in Munich, Germany. In that context, the Royal Observatory of Belgium (ROB) decided to review potential methods and products to develop a comprehensive prototype toolbox for non-numerical nowcasting that can be used to study severe weather cases, with a focus over Belgium and the BENELUX. This toolbox was then used on a real severe weather case study to evaluate its potential and performances, draw a non-exhaustive inventory of problems encountered and open questions related to non-numerical GNSS-nowcasting, fostering discussions within WG2 and new developments in the field.

The Case Study

To develop and assess our GNSS nowcasting toolbox, we chose to focus on a severe weather case that happened in a nowcasting domain (Lon: E 1°–E 7.5°, Lat: N 48.5°–N 53.5°) similar to the one used by the INCA-BE nowcasting tool and the operational NWP ALARO 4 km resolution model operated at Royal Meteorological Institute (RMI) of Belgium. This case happened at the end of the summer 2012 (16–26 September 2012), with a passage of a cold front with a warm front ahead on 23–25 September 2012. The synoptic situation is shown in Fig. 4.14. These fronts came from France and moved in the northeast direction, crossing Belgium and evacuating by the Netherlands. The system turned into the formation of an occluded front, which curved around the depression (i.e. back-bent occlusion) located south of

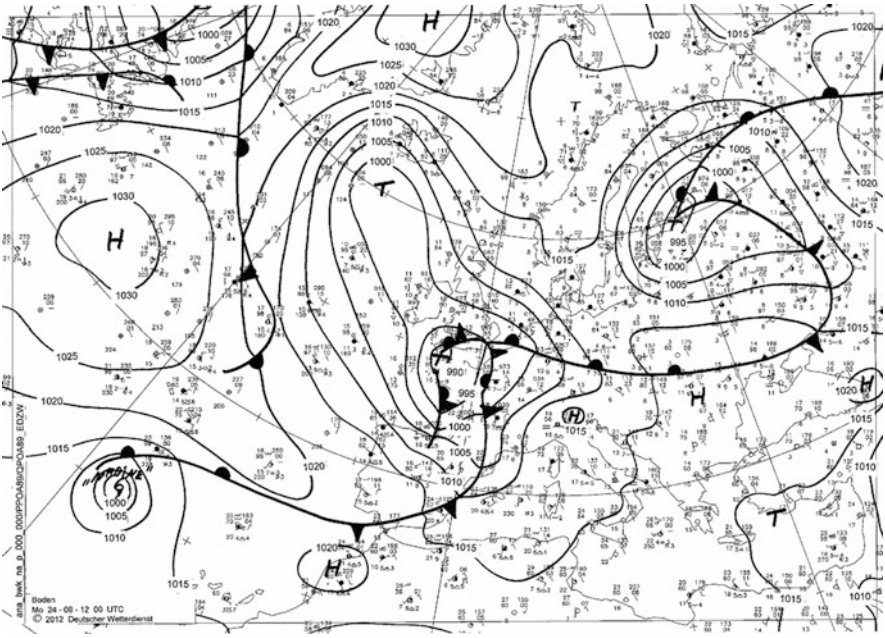

Fig. 4.14 Synoptic situation 24th Sept 2012 at 12:00 UTC. (Courtesy of DWD)

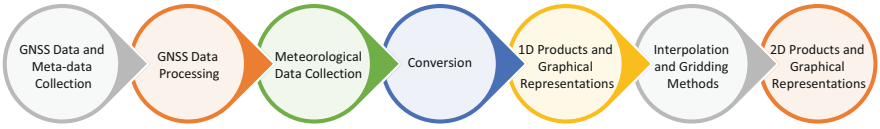

Fig. 4.15 Schematic structure of the toolbox in modules

U.K. During the night of the 23–24 September 2012, the weather system produced deep convective cells bringing heavy precipitation and severe wind in Belgium.

The Toolbox

The comprehensive toolbox developed includes several modules (Fig. 4.15) that relate to the data collection, data processing, and graphical representation.

GNSS Data Collection and Processing

To feed the toolbox with tropospheric products, the historical raw daily observations from 331 GNSS stations were collected from the EPN (EUREF Permanent Network, http://epncb.oma.be) and IGS (International GNSS Service, http://igscb.jpl.nasa.gov) networks, and completed with observations from the national densification networks in Belgium, France, Netherlands, and UK (Fig. 4.16). These historical daily observations have been analysed using the Bernese GNSS software (Dach et al. 2015) with the Precise Point Positioning (PPP) method (in post-processing) to

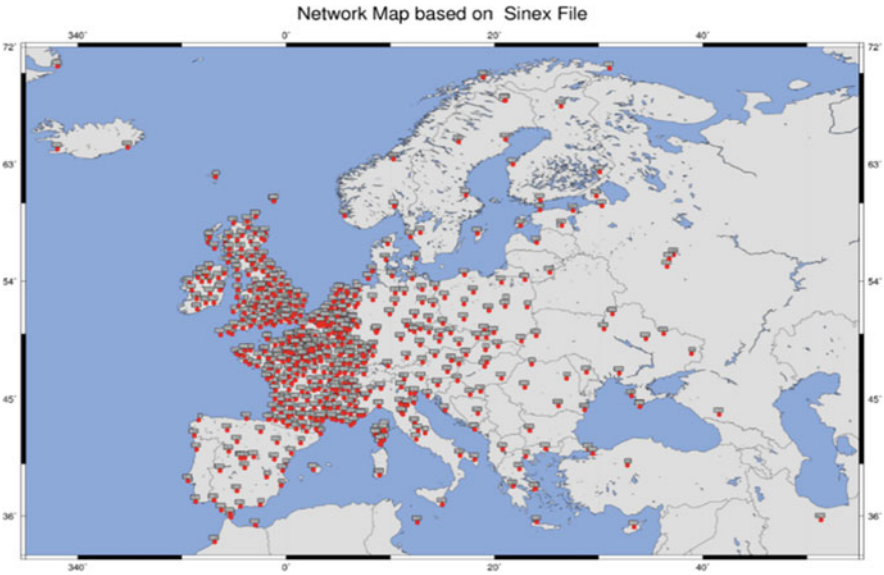

Fig. 4.16 Network of GNSS Stations processed during the case study

estimate tropospheric parameters with a time resolution of 5 min. The tropospheric parameters include Zenith tropospheric Total Delays (ZTDs) and tropospheric horizontal gradients (GRDs). Although not yet considered in the present study, ZTDs and GRDs can be used to reconstruct the slant tropospheric delays, and their potential for non-numerical nowcasting will be investigated in the future.

Meteorological Data Collection and IWV Conversion

The estimated ZTD were then converted into Integrated Water Vapour (IWV). For this, we chose a quite conservative and well-established approach found in the literature (Rocken et al. 1995; Wang et al. 2005, 2007; Heise et al. 2009; Vey et al. 2009; Ning et al. 2013; van Malderen et al. 2014) (Fig. 4.18). The conversion requires surface pressure and surface temperature data at the GNSS station location. Therefore, we collected meteorological data from 135 meteorological sensors (red dots in Fig. 4.17). These sensors belong to the RMI (Belgium), KNMI (The Netherlands), and the Integrated Surface Data (ISD, NOAA) observation networks. To obtain the surface pressure and temperature at the GNSS station, we used the nearest meteorological sensor (i.e. no time nor spatial interpolation was carried out), with a max distance of 50 km, a max altitude difference of 500 m, and a max time differences between meteorological and ZTDs observation epochs of 5 min to ensure the quality of the conversion. Even if more sophisticated approaches can be applied (e.g. a weighted mean interpolation in space and a temporal interpolation), the current simple approach gave satisfactory results for our study.

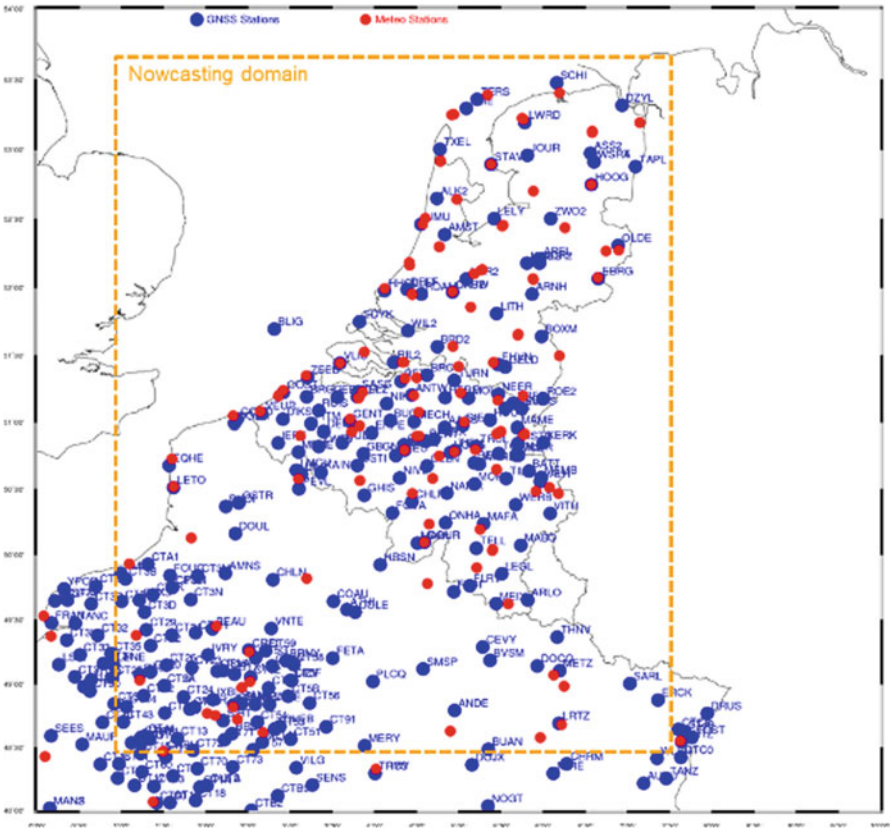

Fig. 4.17 Location of the GNSS stations (blue dots) and meteorological sensors (red dots) located in the nowcasting domain considered (orange dashed line)

Conversion Error and User Product Requirement

Using the method presented in Fig. 4.18, the nearest meteorological sensor, and the findings presented in (Bevis et al. 1994; Ning et al. 2013), we estimated that the total uncertainty of our IWVs is in the 0.75–1.03 mm range. This means that the requirement for non-numerical nowcasting (Table 4.2) are achieved.

Basic Graphical Representation

Most graphical modules of the toolbox relies on the Generic Mapping Tools (GMT, http://gmt.soest.hawaii.edu/home). They enable the representation of the products (e.g. the IWV) both in time and in space. It includes time series (Fig. 4.20) and maps (Fig. 4.19) representations. These graphical outputs can then directly be published on a web user-interface to enable studying and interpreting the weather conditions.

Interpolation Methods for Reconstructing Grids

In addition to the point representation in space shown in Fig. 4.19, we wanted the toolbox to be able to fully represent the IWV field over the complete nowcasting

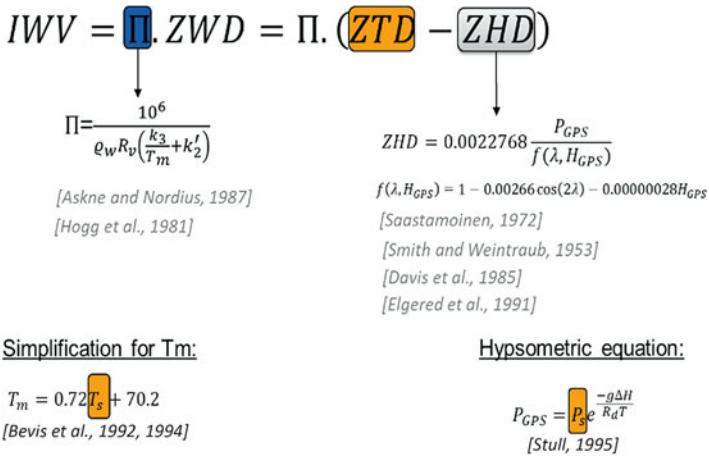

Fig. 4.18 Scheme of the method used to convert ZTDs to IWVs

Table 4.2 Requirement imposed on IWV observations for non-numerical nowcasting applications as stated in the E-GVAP Product Requirement Document [E-GVAP PDR]

	Threshold	Breakthrough	Goal
Accuracy	5 kg/m^2	2 kg/m^2	1 kg/m^2
Timeliness	30 min	10 min	5 min

domain. Therefore, four interpolation methods have been implemented, and their performances intercompared. These methods are the optimal triangulation (Watson 1982), the Nearest Neighbour, the Continuous Curvature Spline in Tension (Smith and Wessel 1990), and the Ordinary Krigging (Matheron 1962, 1963a, b) methods. An example of this comparison is given in Fig. 4.21. The optimal triangulation and nearest neighbour methods gave unsatisfactory results (with sometimes unrealistic IWV local field, incomplete domain fill, artefacts...) while the continuous curvature spline in tension and ordinary Krigging methods gave a more realistic IWV field representation over the full nowcasting domain. The two latest methods are also the two methods that match the more closely together. The Krigging method has the advantage to be capable to take into account the uncertainties in the input data, and to enable the estimation of the variance of the estimated grid, i.e. the uncertainty of our IWV field over the whole domain. For example, in the case presented in Fig. 4.21 the error variance of the estimated IWV field remained below 1.2 mm (Fig. 4.22, right), satisfying the nowcasting requirements (Table 4.2). We thus opted for the Ordinary Krigging method to reconstruct maps with a time resolution of 5 min and a spatial resolution of 0.05° lon. × 0.05° lat. The toolbox also allows applying a mask over some regions like the Channel and U.K. as shown in the figures below.

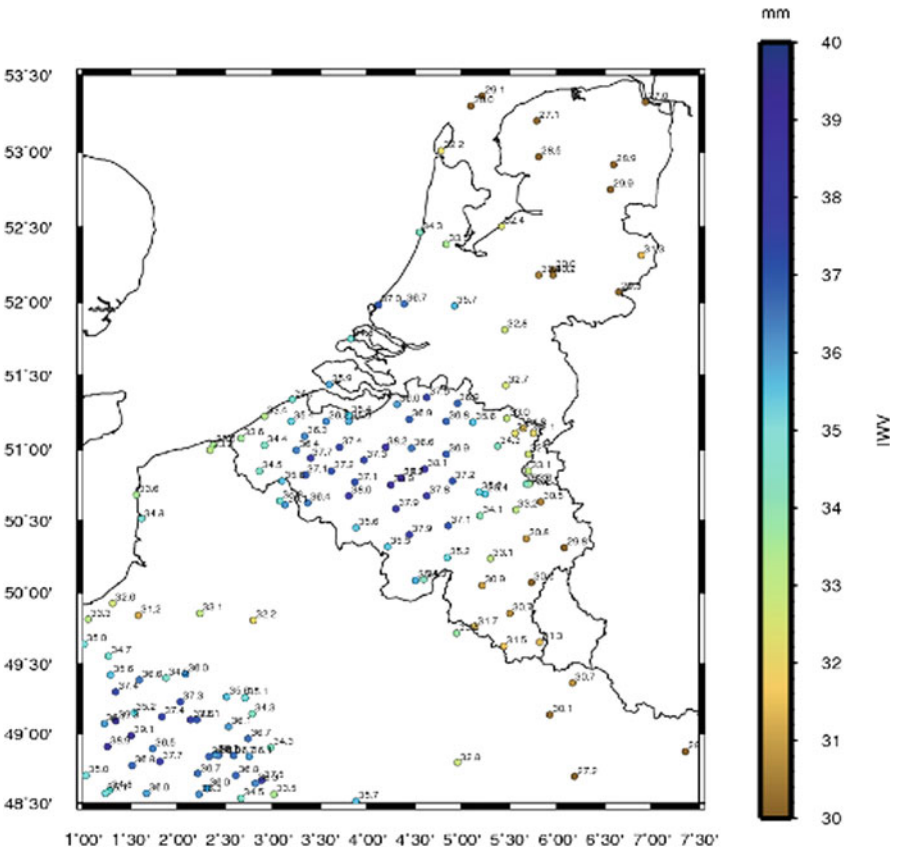

Fig. 4.19 Spatial representation of the IWV at each GNSS station at epoch 23 Sep. 2012 23:00 UTC

Exploiting the Horizontal Gradients to Access the Horizontal Inhomogeneity
During the GNSS data processing, N-S and E-W tropospheric horizontal gradients (GRDs) were estimated simultaneously to the ZTDs with a time resolution of 5 min. The GRD estimation follows the methodology proposed in (Chen and Herring 1997), and represents the first-order heterogeneities in the tropospheric delay (mainly due to water vapour but not only). These GRDs can be used to study the location of water vapour inhomogeneities in the atmosphere. The toolbox allows representing them in the form of time series (Fig. 4.23) or superimposed them over 2D grid maps (e.g. IWV maps, Fig. 4.24).

During our analysis we noticed at several occasions that horizontal gradients at nearby or collocated GNSS stations showed sometimes a very good agreement but sometimes emphasized very different directions (e.g. in Fig. 4.25). Therefore, we currently recommend a careful usage of horizontal gradients until further investigations on the validation and representativeness of the GRDs are carried out. Such investigations can e.g. be done based on long-term GRD observations at collocated

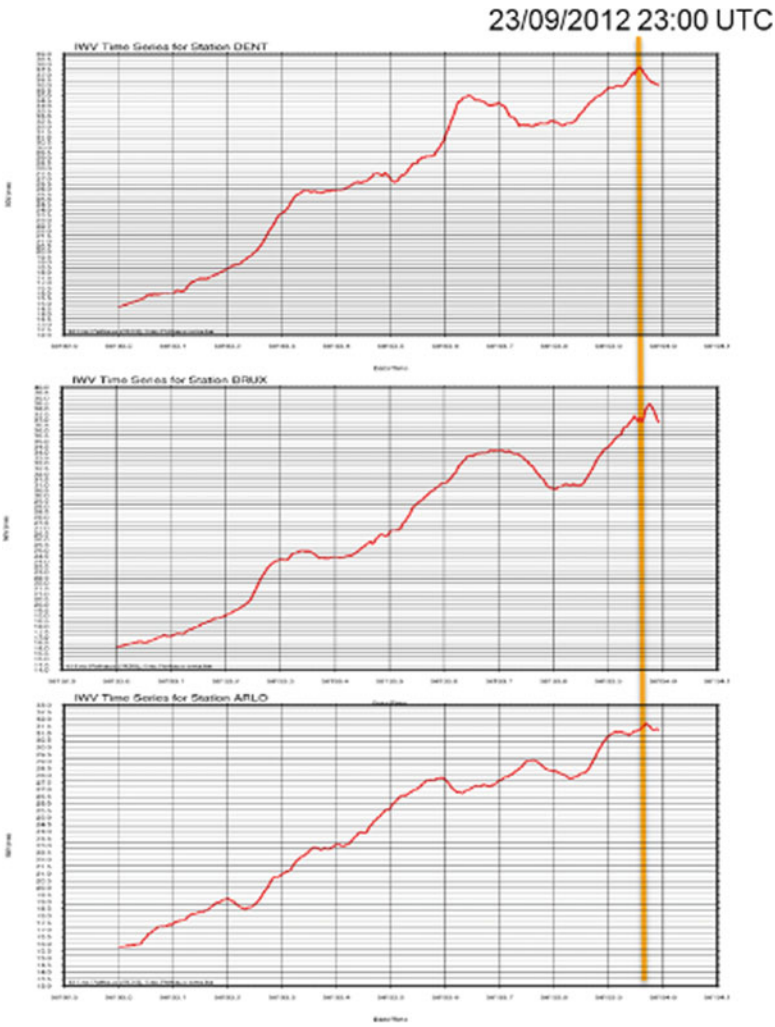

Fig. 4.20 Time series of the IWV at three Belgian stations (top: Dentergem, middle: Brussels, bottom: Arlon)

GNSS stations, and cross validated with external source of information whenever possible (e.g. output of NWP models that doesn't assimilate GNSS products). In addition, the impact of the antenna calibration model on the estimation of the horizontal gradients should be investigated (e.g. type mean versus individual calibration, and antenna misalignment).

Computing Reconstructed Grid Derivatives

Once the 2D grid map has been reconstructed based on the Ordinary Krigging interpolation method, the 2D map of partial derivatives in the N-S and E-W

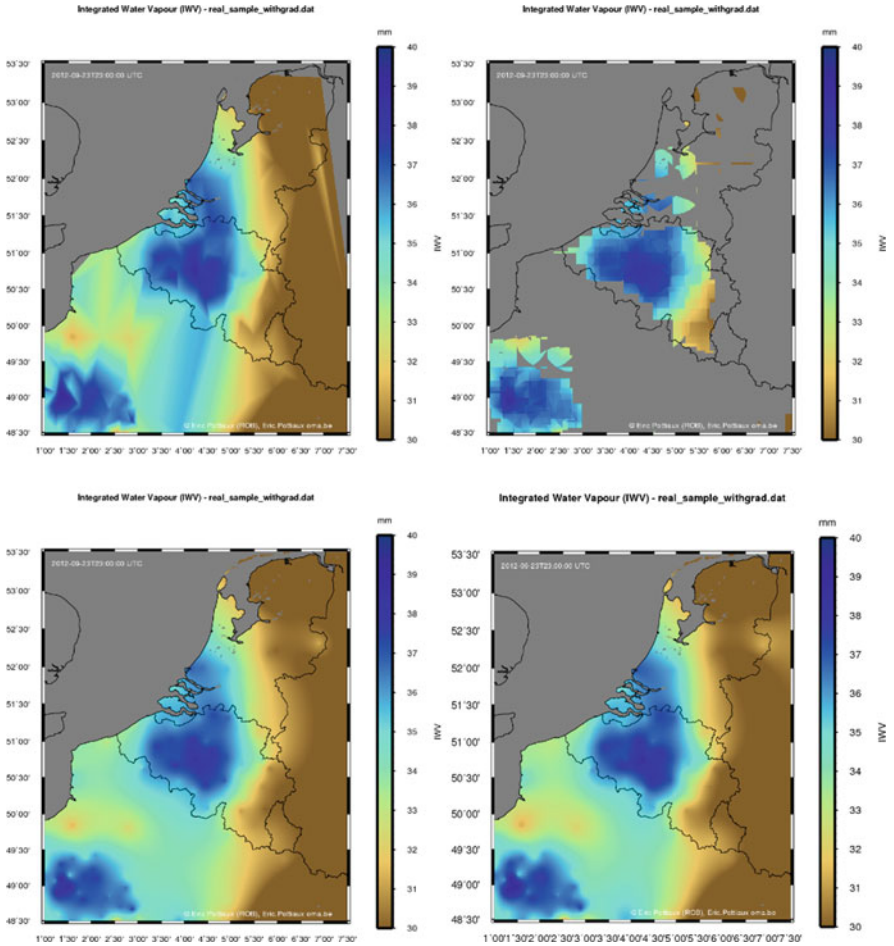

Fig. 4.21 IWV maps derived from the four interpolation methods implemented (Top left: optimal triangulation, top right: nearest neighbour, bottom left: continuous curvature spline in tension, and bottom right: ordinary krigging) on 23rd Sep. 2012 at 23:00 UTC. Grids are clipped to remove the field over the Channel and U.K

directions can be computed from the original grid, e.g. for the IWG grid. These partial derivative maps can then be used to study the heterogeneities in the IWV field and might also be used to intercompare with the horizontal gradient components computed during the GNSS processing. Figure 4.26 show an example of the 2D map of the partial derivative norm at each IWV grid cell projected in the N-S (left plot) and E-W (right plot) directions with superimposed the GRDs estimated from the GNSS processing (red vectors). Similar plots can be constructed for the phase (direction) of the partial derivatives of the IWV grid.

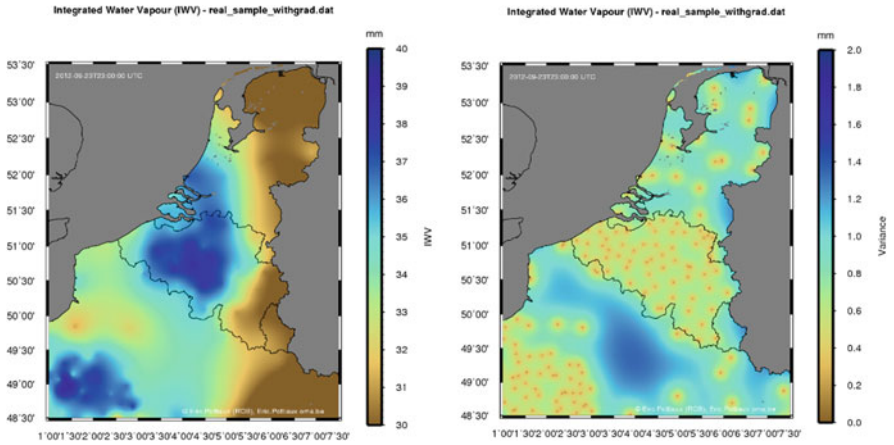

Fig. 4.22 Estimated IWV map based on the ordinary Krigging method (left) and its associated error variance (right)

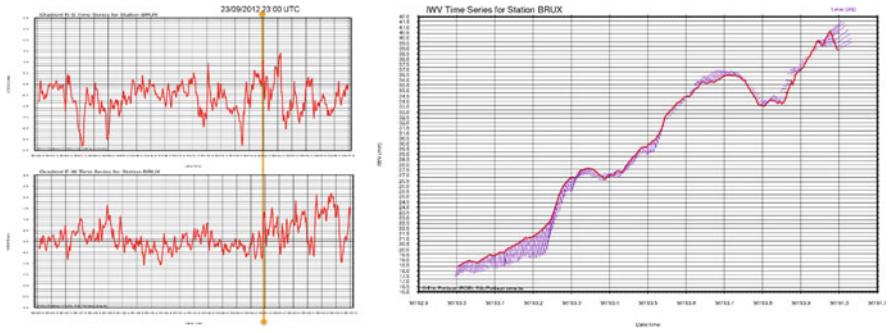

Fig. 4.23 (Left) Time series of the N-S (top) and E-W (bottom) GRDs estimated at the station BRUX in Brussels, Belgium. (Right) Time series of the ZTDs (in red) at the same station BRUX. Purple vectors superimpose the horizontal gradient attached at the ZTD point. The length of the vector represents the amplitude of the GRD and the direction of the vector gives the direction of the gradient in the horizontal plane (North is pointing to the top of the figure, East at the right...)

Extracting Tracks Through the Reconstructed Grid

Another important capability of the toolbox is to enable the extraction of specific profile along a track in the interpolated grid field, as specified by its origin and destination coordinates. An example is given in Fig. 4.27 with an IWV grid map. Extracting track profile enable e.g. to study the IWV distribution along a path crossing a specific region. Such specific region can e.g. be a deep convection cell causing severe rain as illustrated with the radar image in Fig. 4.27. Similarly as for IWV, track profiles can be extracted from other 2D grid field representation (e.g. partial derivative grids) reconstructed by the toolbox, and presented later (e.g. partial derivatives) (Fig. 4.28).

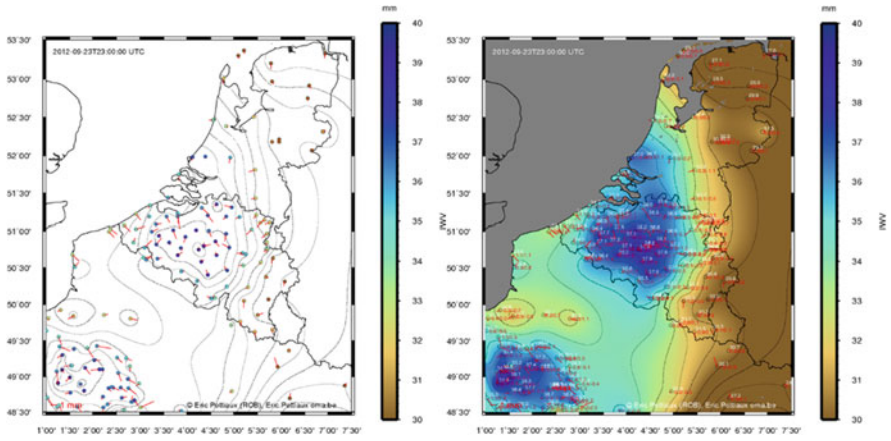

Fig. 4.24 Red vectors attached at the GNSS station location represent the tropospheric GRDs. The length of the vector matches the amplitude of the GRDs while the direction of the vector matches the orientation of the horizontal gradients

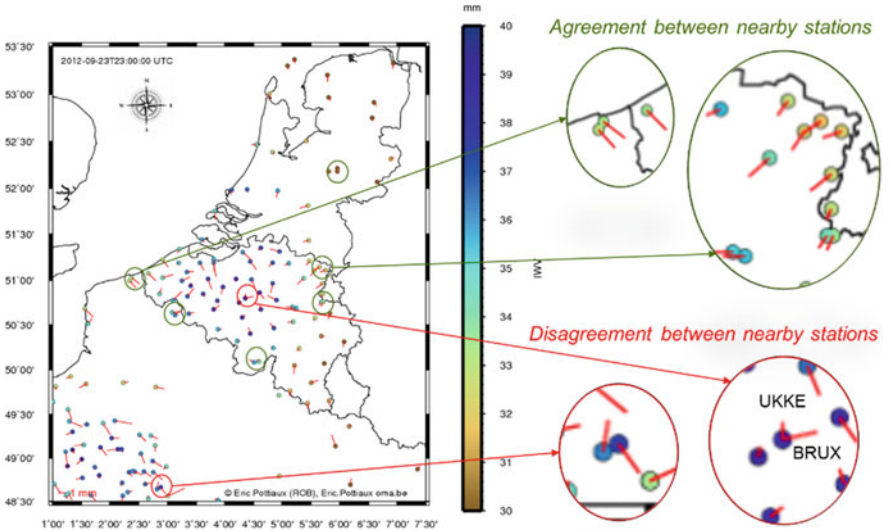

Fig. 4.25 Horizontal gradients superimposed on top of a point-wise ZTD map representation showing that GRDs sometimes agree very well but sometimes differs significantly in direction at nearby and collocated GNSS stations

Fluxes – Rate of Change – Post-fit Residuals Analysis

The developed toolbox also computes the fluxes or rate of changes of the IWV, and of the GRDs to detect sudden changes in water vapour distribution that might be associated with severe weather events like a deep convective system. An example is given in Fig. 4.30 showing the time series of the rate of change of the IWV (top), N-S

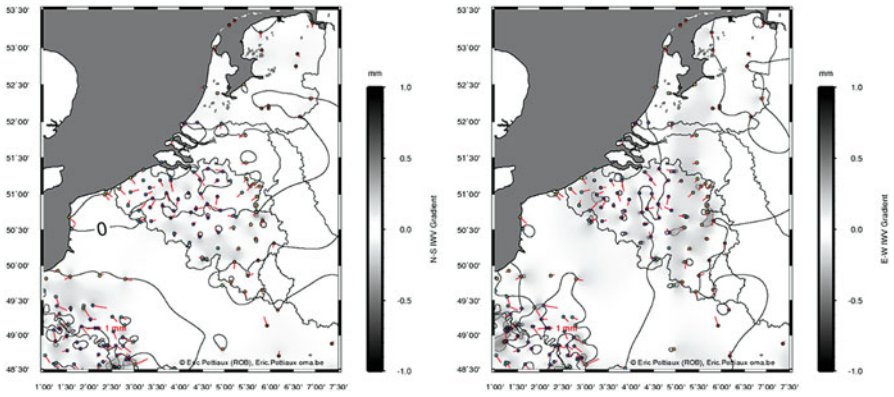

Fig. 4.26 Amplitude of the partial derivatives of the ZTD grid in the N-S (left) and E-W (right) direction. Superimposed (in red) the vector of the horizontal gradient estimated during the GNSS processing

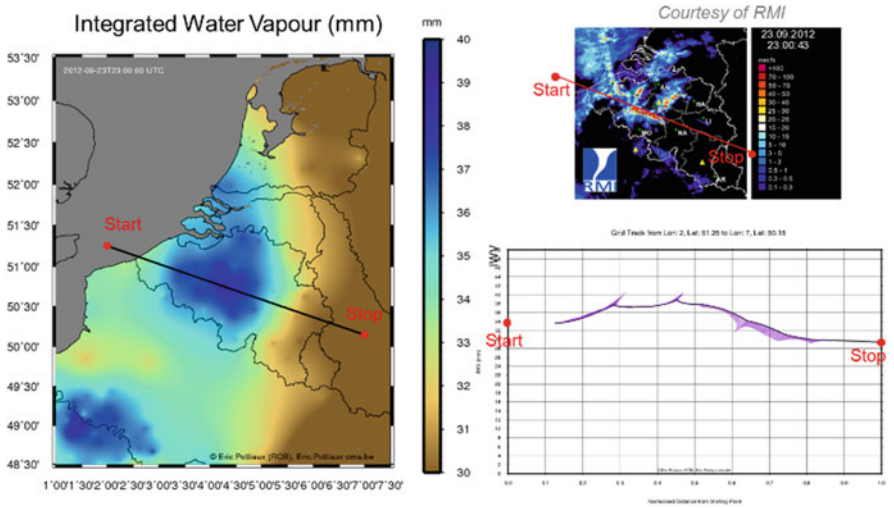

Fig. 4.27 (Left) IWV map reconstructed with Krigging interpolation on 23 Sep. 2012 23:00 UTC, and the track path superposed. (Top right) the corresponding radar image with the same track path aligned to a rain cell. (Bottom right) the IWV profile along the track

(middle), and E-W (bottom) gradients at Brussels, Belgium. A clear and sudden signature can be noticed at the moment when a deep convective system was passing over Brussels (orange vertical line). Once the fluxes/rate of change of these quantities are computed, the toolbox is also capable to reconstruct the 2D field of these rate of change (based on the interpolation methods presented above) to enable the study of their spatial and spatio-temporal (e.g. film) behaviours (Fig. 4.30). Finally, this information can also be combined with the analysis of the ionosphere-free carrier-

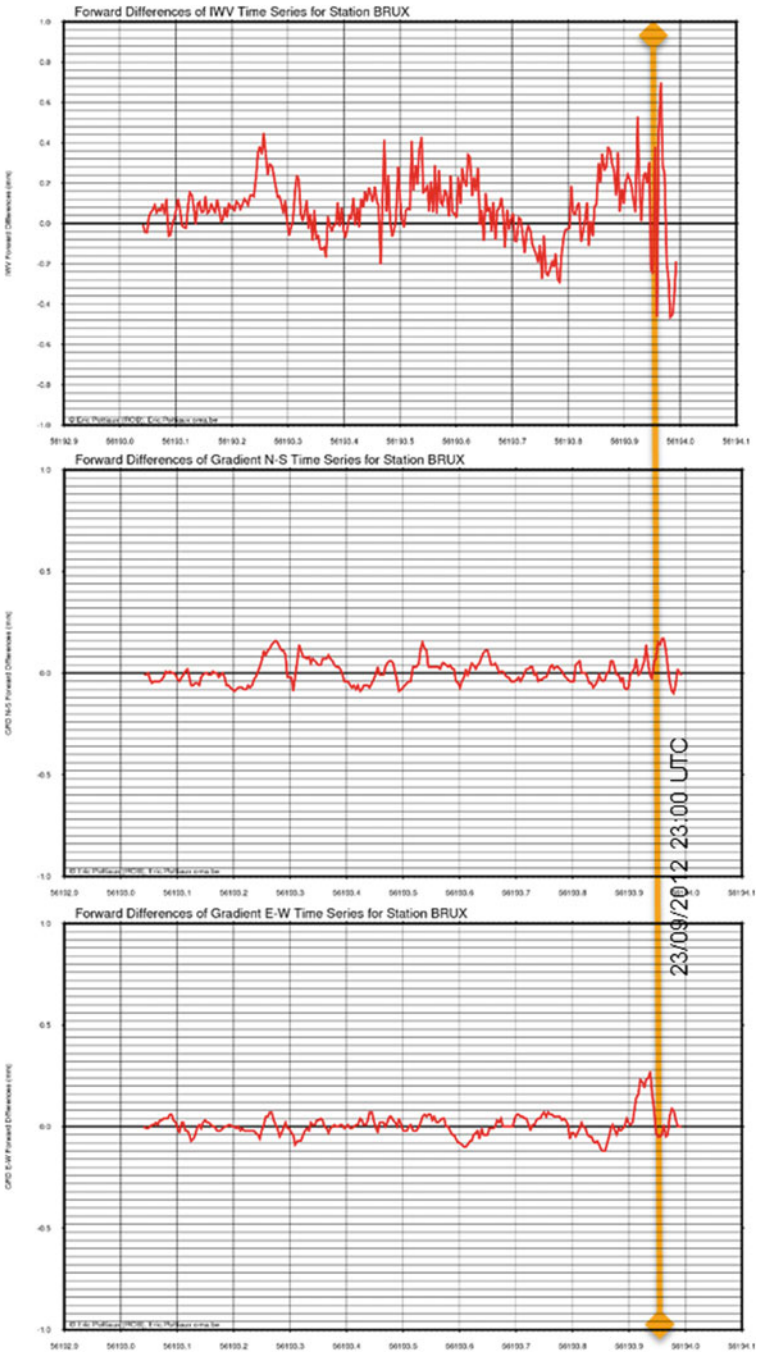

Fig. 4.28 Time series of the rate of change of the ZTD (top), N-S (middle) and E-W (bottom) GRD at Brussels, Belgium

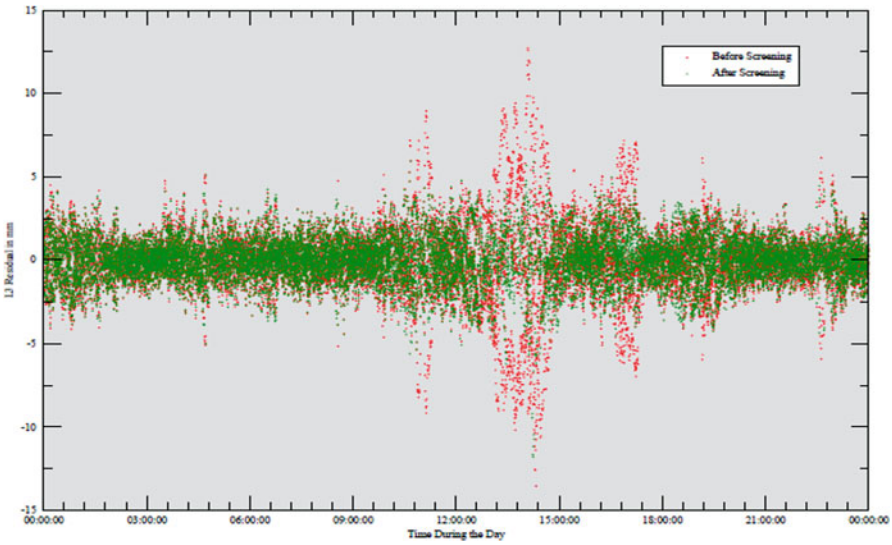

Fig. 4.29 Ionosphere-free carrier-phase double-difference post-fit residuals before (red dots) and after (green dots) data cleaning for the baseline Dentergem – Waremme, Belgium, during 29 June 2005. The passage of a deep convective system leading to a hailstorm

phase double-difference post-fit residuals before and after data cleaning as shown in Fig. 4.29 [Pottiaux 2010]. Altogether, these fluxes/rate of change, and post-fit residuals quantities are very important quantities in the process of setting up automatic detection of severe events and alarms systems based on critical values (Fig. 4.30).

Conclusions and Open Questions

With the development of a prototype GNSS-based nowcasting toolbox, the Royal Observatory of Belgium (ROB) aimed to demonstrate the feasibility, and to foster GNSS-based non-numerical nowcasting in Belgium and the BENELUX. The current toolbox includes numerous 1D and 2D representation of various tropospheric quantities (ZTD, IWV, GRD, fluxes/rate of change...) with sufficient precision to allow studying the spatio-temporal evolution of water vapour for nowcasting. 2D representation can be stacked over time to create movies representing the time evolution. The toolbox also enables the operation of automatic detection of severe events, and to trigger alarms (e.g. based on the rate of change and post-fit residuals), albeit the necessary critical values and pattern recognition should be further studied.

During the developments, a list of further investigations was established, and includes e.g. assessing the horizontal gradients and studying their representativeness in some cases, an automatic access to and an enhancing of the use of surface pressure and temperature data (e.g. interpolation method for the conversion or testing the use of the forecast fields from high-resolution NWP models), and accessing GNSS tropospheric products with a latency below 5 min to operate such toolbox in live conditions.

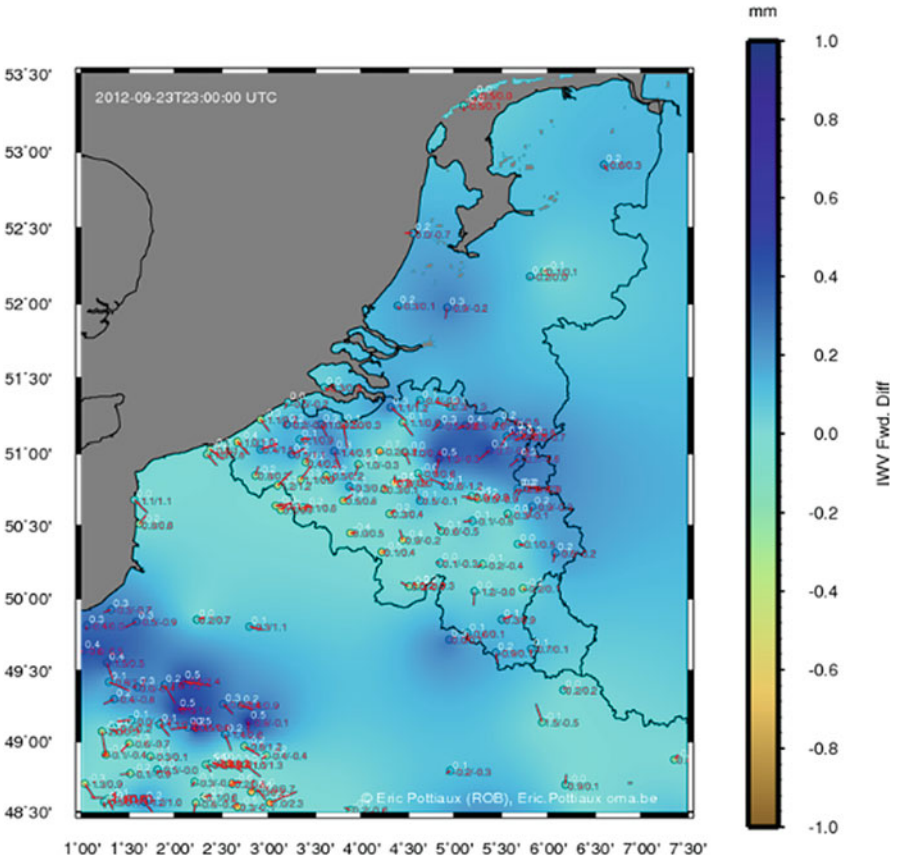

Fig. 4.30 2D field of the rate of change of the IWV in the nowcasting domain superimposed with the horizontal gradient information.

Operating live this toolbox requires indeed a real-time access and processing of the GNSS observations. Therefore, within the real-time demonstration campaign of the WG1, ROB collaborated with the GOP (Geodetic Observatory in Pecný) to use their GNut/Tefnut software, and to setup at ROB a prototype real-time processing of GNSS observations in this nowcasting domain, including the Belgian dense network. This activity was started during the context of a Short-Term Scientific Mission (STSM) of the Action, and enable to feed the toolbox with real-time ZTD, GRD and slant delays.

Until now, we operated the toolbox over a single case study to demonstrate its potential. Of course, the next natural step would be to operate it, and to test it over a wider variety of cases. For this, operating live the toolbox would be very beneficial. This would also enable to contribute updating and extending the requirements imposed for non-numerical nowcasting as found in the current version of the E-GVAP Product Requirement Document [E-GVAP PDR].

Finally, as shown with one example of radar images, this toolbox would highly benefit of a synergetic use with other meteorological observation sources such as radars, Meteosat, winds, lightning, SSMI... observations, as it was already demonstrated in the literature (Mazany et al. 2002; de Haan et al. 2004, 2009). However, one has to note that this synergetic use would probably better find its place directly within a nowcasting suite such as the INCA-BE rather than in a separate toolbox.

Acknowledgments
This research has been carried out with the support of the Solar-Terrestrial Centre of Excellence (STCE).

4.3 Numerical Nowcasting and NWP Data Assimilation

4.3.1 HARMONIE-AROME Group

M. Lindskog
Swedish Meteorological and Hydrological Institute, Norrkoping, Sweden
e-mail: magnus.lindskog@smhi.se

J. Sánchez-Arriola
AEMET, Santander, Spain
e-mail: jsancheza@aemet.es

The benefit of using GNSS ZTD in the state-of the art HARMONIE-AROME km scale data assimilation and forecasting system has been demonstrated (Sánchez-Arriola et al. 2016). A 3-dimensional variational data assimilation was applied and the importance of using an extensive observation handling was pointed out, and in particular the benefit of using an adaptive so called variational bias correction. For HARMONIE-AROME the sensitivity of the bias correction to adding additional refinements in the form of various additional predictors was small (Lindskog et al. 2017). On the other hand, results were found to be sensitive to the spatial density of the GNSS ZTD observations, due to the fact that a higher observation density does not necessarily imply better model skill, but no clear recommendation on optimal data density for a particular modelling system yet exist.

Since June 2016 Lantmäteriet (Swedish Mapping, Cadastre and Land Registration Authority) became NGAA, one of the analysis centres in E-GVAP and is in charge of the data processing for the GNSS stations in Sweden, Finland, Norway, Denmark and some IGS stations in order to provide near real-time (NRT) ZTDs. Currently NGAA has two NRT ZTD products (NGA1 and NGA2) produced. The NGA1 product is obtained from the BSW52 network solution while NGA2 is given by the GIPSY/OASIS II v.6.2 data processing using the Precise Point Positioning (PPP) strategy. We have validated the NGAA products by the ZTDs estimated by a post-processing using the IGS final satellite orbits and clock products. Two products give very similar results with a mean difference smaller than −0.5 mm and standard

deviations less than 5 mm with respect to the ZTDs from the post-processing. In addition, products of NGAA have also been compared and used within the state-of-the-art MetCoOp operational modelling system (Muller et al. 2017). The NGAA product has been shown to be beneficial to the forecast quality (Lindskog et al. 2017) and the NGAA product is now used operationally within the operational MetCoOp modelling system.

4.3.2 *Assimilation of E-GVAP ZTD Data into the WRF Model*

K. Eben · J. Resler · P. Krč
Institute of Computer Science of the Czech Academy of Sciences, Prague, Czech Republic
e-mail: eben@cs.cas.cz

We have performed several experiments, assimilating the ZTD from the E-GVAP database together with other data into the WRF model, using 3DVar assimilation package, WRFDA. In particular, we have investigated the synergy of the OPERA radar composite with E-GVAP data. We have tested different assimilation methods, among others the hybrid ensemble/3DVar method.

The OPERA radar composite provides a large source of European-wide data on radar reflectivity. E GVAP and OPERA bear different kind of information on water vapour in the atmosphere and both have a potential for data assimilation. Several simulations have been performed and analysis increments have been compared, using different background covariance models and analysis methods. Besides the standard 3DVar we used the ensemble/3DVAR hybrid method of Wang et al. (2008) with five control variables. This method combines the flow-dependent covariance derived from the ensemble with the climatologic (static) background covariance. The static part of the covariance was generated from historical data by the NMC method. The ensemble part was computed by means of downscaling the NCEP/GEFS ensemble using the WRF model. As expected, the hybrid method improves the estimate of the background covariance matrix. The NCEP/GEFS ensemble (20 members) seems to be suitable for use within the hybrid method. Figure 4.31 shows an example of a Pseudo single-observation test, where the pseudo observation is 1 cm above the model value of the ZTD.

For the benchmark test case (high precipitation episode in Bohemia in July 2013) we have performed several simulations of a forecast with the WRF model. We have compared water vapour increments when assimilating either E-GVAP ZTD or OPERA reflectivities. Water vapour increments from both radar and ZTD observations occur in higher model levels (model level 15 in Fig. 4.32 below) and are to some extent complementary. A typical pattern can be seen in Fig. 4.32.

Both ZTD and maximum reflectivity from OPERA have been assimilated, on the top of conventional observations. Starting from assimilated fields, a 24-hour

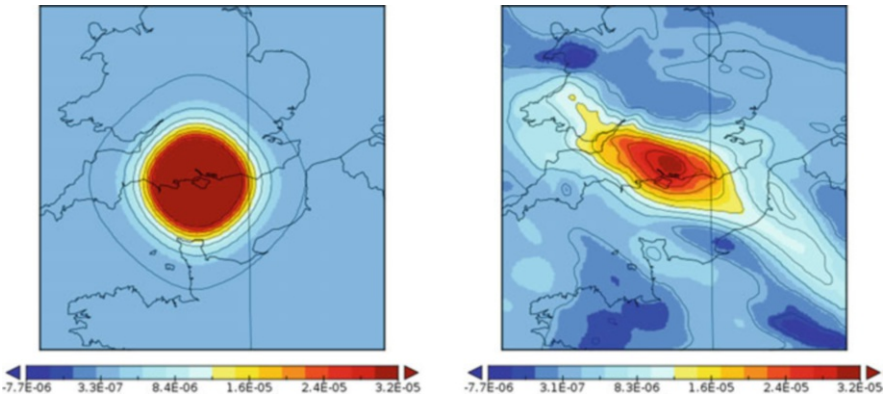

Fig. 4.31 Pseudo single-observation test. Left: analysis increment, static (isotropic) background covariance generated by the NMC method. Right: increment, hybrid covariance matrix with ensemble part derived from downscaled GEFS ensemble

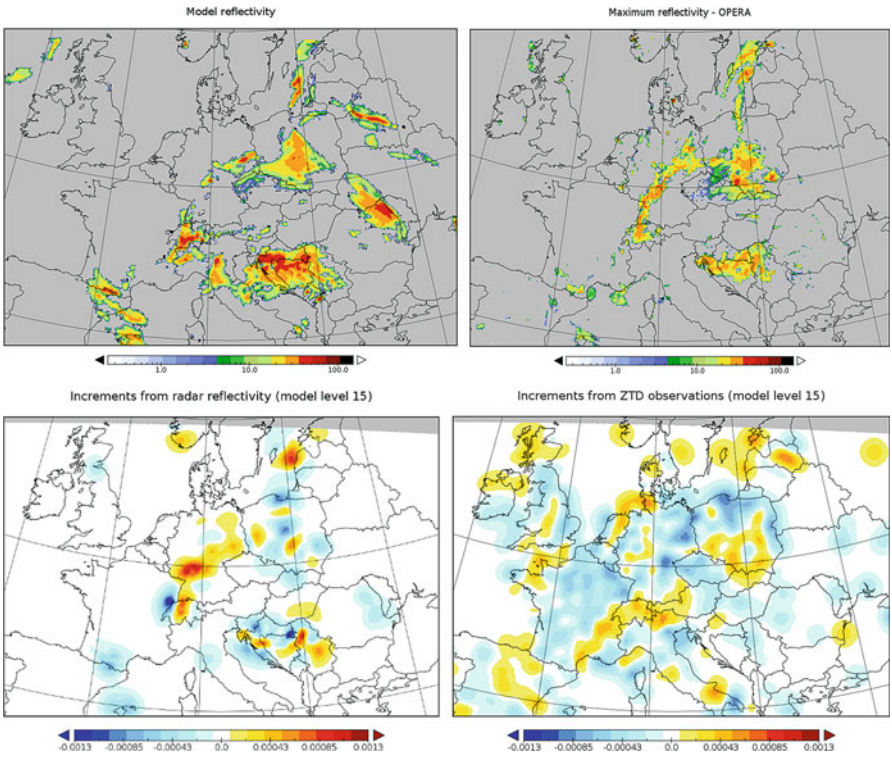

Fig. 4.32 A sample from an intensive rain episode (01 June 2013 03:00). Upper left: model maximum reflectivity, upper right: observed maximum reflectivity in OPERA composite. Lower left: Water vapour analysis increments from E-GVAP ZTD, lower right: analysis increments from OPERA reflectivity. There is no clear agreement between increments from ZTD and from reflectivity. The absence of ZTD increments in Serbia region is caused by the lack of measurements

accumulated precipitation has been forecast. The accordance of the forecast with observations is good. For 24-hour accumulated precipitation, however, only minor and non-systematic improvement over the operational forecast has been observed (Fig. 4.33).

The experiments confirm the widely accepted fact that GNSS observations represent a valuable source of data for assimilation. They provide an additional information on water vapour profile, which is complementary to radar reflectivities. The NCEP/GEFS ensemble seems to be promising in providing ensemble perturbations for the hybrid ensemble/3DVar method. The sensitivity of the forecast to background covariance is high and several settings of the methods need to be tuned before a stable forecast improvement may be expected.

Acknowledgements
The work was supported by grant 13-34856S of the Grant Agency of the Czech Republic (GA ČR) "Advanced random field methods in data assimilation for short-term weather prediction".

4.3.3 Improvement of Forecast Skill of the GLAMEPS Model

L. De Cruz
Royal Meteorological Institute of Belgium, Brussels, Belgium
e-mail: lesley.decruz@meteo.be

E. Pottiaux
Royal Observatory of Belgium, Brussels, Belgium
e-mail: eric.pottiaux@oma.be

During the course of this COST Action, a Belgian nationally funded project was run at the Royal Meteorological Institute (RMI) of Belgium with the aim to improve the forecast skill of the probabilistic Grand Limited-Area Model Ensemble Prediction System (GLAMEPS) system (Smet et al. 2012; De Cruz and Duerinckx 2015). Key to the skill of the probabilistic forecast delivered by GLAMEPS is the accuracy of the constituent models of this ensemble. The progress in both data assimilation (DA) methods and novel observations have been indispensable in the increase in forecast skill of Numerical Weather Prediction (NWP) models in the past decades. As such, it is crucial that the current trend towards higher spatial resolutions in both deterministic and probabilistic models, such as GLAMEPS, is accompanied by a corresponding improvement in the model initialization. To this end, precipitation radar and GNSS tropospheric delay estimates (3D-var approach) data assimilation was implemented for the Belgian Local Area Model (LAM) ALARO.

ZTD Assimilation System
Where possible, the precipitation radar data assimilation was built upon the methods developed at Météo France for the assimilation of radar data using the Bayesian

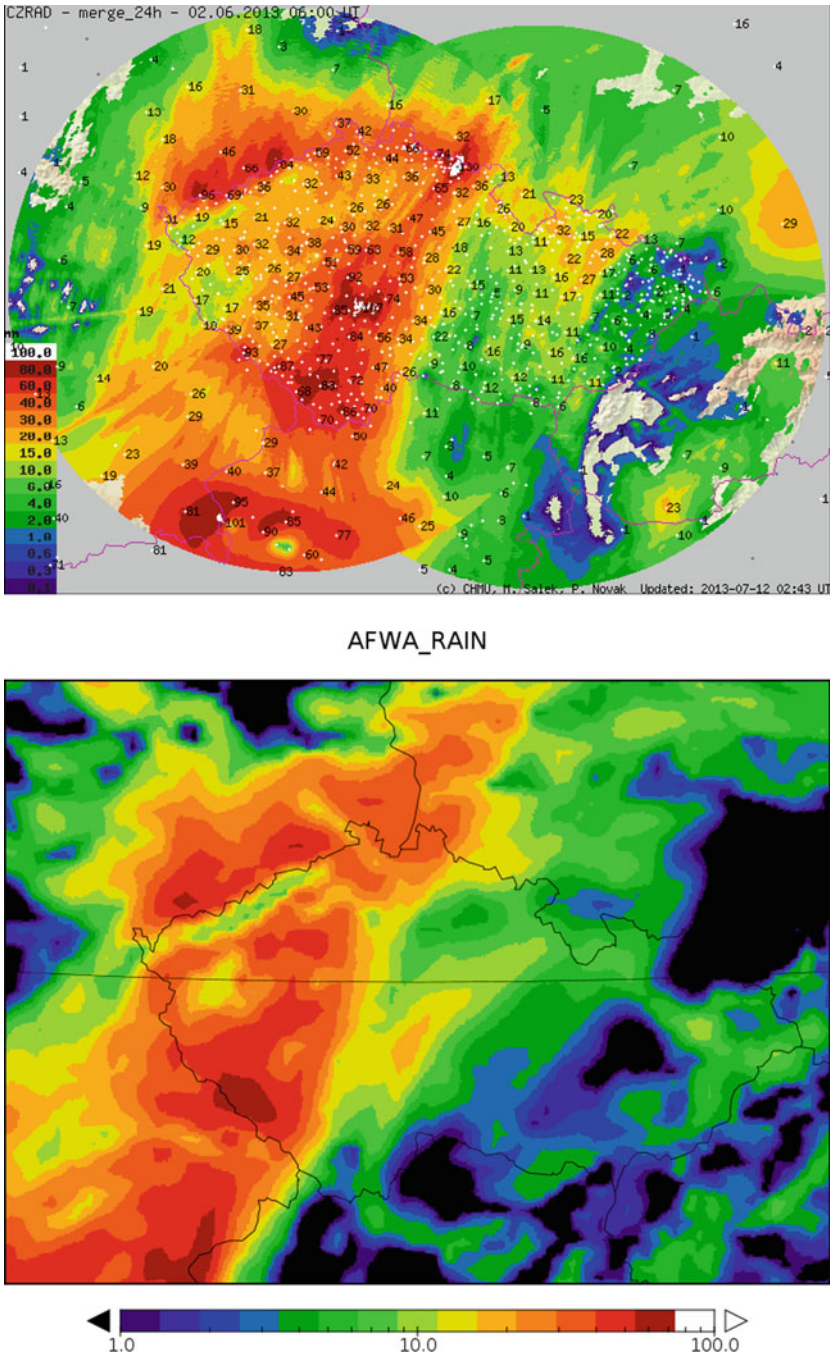

Fig. 4.33 Top: Estimated precipitation from radar and rain gauge sets (source: Czech Hydrometeorological institute). Bottom: WRF forecast of 24 h accumulated precipitation (1 June 2013 06:00–2 June 2013 06:00), starting from analysis with assimilated E GVAP ZTD and OPERA reflectivities. Time of analysis 01 June 2013 00:00

1D + 3DVar approach. This approach has been shown to significantly increase forecast skill in the first 12 h lead time (Caumont et al. 2010; Wattrelot et al. 2014). Then, the ZTD data assimilation system was developed based on the current 3D-Var system which was built for the assimilation of conventional data. The observation operator for the ZTD is calculated as the integral of the index of refractivity in the air column above the GNSS station location. This integral depends on the model pressure, temperature and partial pressure of water vapour. The GNSS ZTDs were processed and provided by the Royal Observatory of Belgium (ROB) (Pottiaux 2010; Bruyninx et al. 2012). It benefits from observations from the very dense network of GNSS tracking stations available in Belgium. In addition to radar and GNSS ZTDs, conventional ("SYNOP") observations such as weather station and sounding data were also assimilated.

Before assimilation of the ZTD data, a number of pre-processing steps were performed:

- Static bias correction, which is performed by calculating the differences between the simulated and observed ZTDs in a passive model run of 30 days (i.e., with assimilation of conventional data but not ZTDs). The static bias correction also takes into account the constant bias due to the fraction of the atmosphere above the highest model level.
- Based on the above error statistics, a white-list has been built for the GNSS stations.
- Spatial thinning was performed at the level of 10 km. Temporally, only the observations at assimilation time were retained: for example, in a 6 h update cycle, only the observations at 00, 06, 12, 18 h were retained.
- The hydrostatic correction, that accounts for the difference between the model altitude and the true altitude of the GNSS station, is accounted for in the observation operator.

The assimilation of ZTDs has a clear impact on moisture-related variables, as illustrated by the total precipitable water (TWP) in Fig. 4.34.

Results

The assimilation of ZTD data was shown to improve the representation of humidity in the low to middle troposphere (Yan et al. 2009), the prediction of precipitation patterns (Poli et al. 2007; Vedel et al. 2004), and cloud forecasts (Bennitt and Jupp 2012). In order to evaluate the impact of ZTDs assimilation in the RMI system setup, two case studies were selected: The Pentecost storm (June 7-8-9 2014) and the storm of September 23-24-25 2012 which hit much of Western Europe.

As a first preliminary result (De Cruz et al. 2015), the assimilation of ZTDs yields a neutral to positive impact. For the Pentecost storm, the assimilation of SYNOP data + non-bias corrected ZTDs slightly improved the Root Mean Square Error (RMSE) and bias of the 2 m relative humidity (RH2m) for short (< 9 h) forecast range compared to SYNOP data only, as shown in Fig. 4.35. For the second case study, there is a neutral impact on the scores.

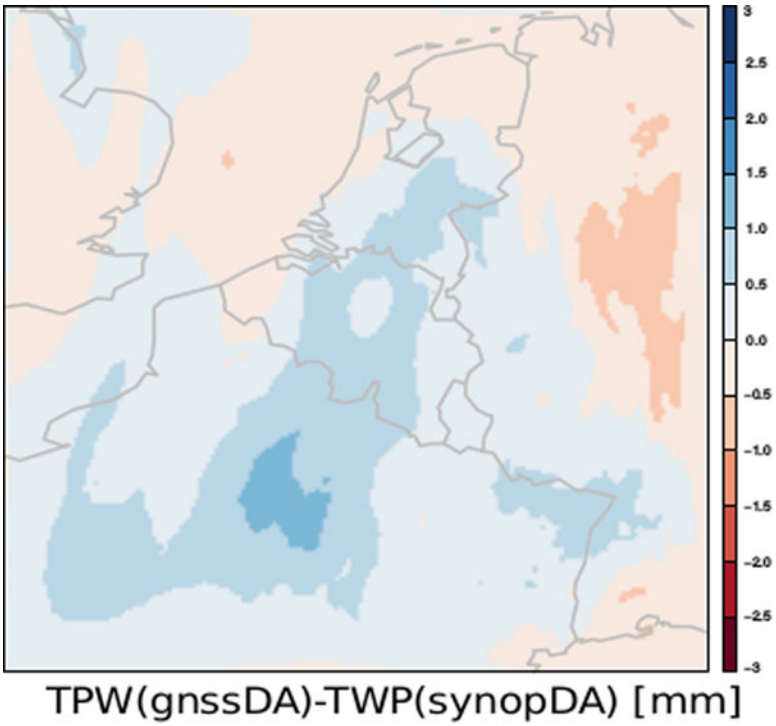

Fig. 4.34 Difference in Total Precipitable Water (TPW in mm) between a forecast with assimilated ZTDs versus a forecast in which only SYNOP data were assimilated.

While the preliminary results for the assimilation of non-bias corrected ZTDs are encouraging, it was found that applying a static bias correction largely cancels the positive effect of ZTD assimilation on the RH2m RMSE and bias. This may indicate that static bias correction currently represents the model biases rather than the biases present in the data (or representation difference), which effectively neutralizes the impact of the data assimilation. Possible causes are the overestimation of the ZTD observation errors with respect to the background (model) errors.

To solve the problems inherent to static bias correction, we intend to adopt variational bias correction, an algorithm to adaptively tune the background and observation error covariance matrix.

Acknowledgments

Engagement de chercheurs supplémentaires dans le cadre de la loi du 18 juillet 1997 et de l'A.R. du 19 août 1997. MO/34/021- Report: 2014–2015 « Développement du système international de prévision probabiliste à méso-échelle GLAMEPS ». The contribution of ROB to E-GVAP is supported by the Solar-Terrestrial Centre of Excellence (STCE).

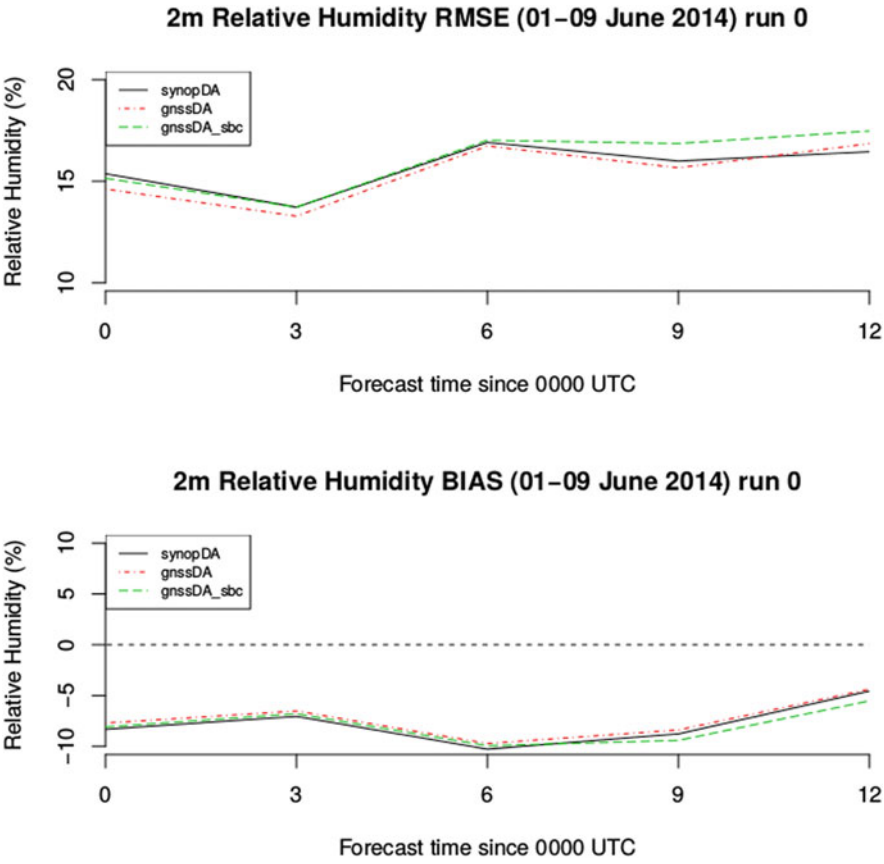

Fig. 4.35 RMSE (top) and bias (bottom) for the 2 m relative humidity during the case study of the Pentecost Storm of 2014

4.3.4 Slant Total Delay Assimilation in COSMO-DE: First Results

M. Bender
Deutscher Wetterdienst, Offenbach, Germany
e-mail: michael.bender@dwd.de

Slant total delays (STDs) provide directional information about the atmospheric state along the signal path between individual GNSS satellites and the receiver. Regarding the improved STD processing strategies described in Sect. 3.2, the assimilation of STDs into numerical weather models has the potential to supersede the assimilation of zenith total delays (ZTDs) which is currently operational at most European weather centres. In order to investigate the impact of STD assimilation into high-

resolution regional weather models the German Weather Service (DWD) developed a STD observation operator for COSMO/KENDA. This subsection gives a short description of the STD operator, the COSMO model and assimilation system and the current state of STD assimilation experiments at the DWD.

STD Observation Operator

The STD is defined by the difference between the optical path length of the GNSS signal in the atmosphere and the geometric distance G between satellite and receiver:

$$\mathrm{STD} = \int_S n(s)\, ds - G \tag{4.1}$$

The refractive index $n(s)$ along the signal path S depends on the temperature T, the pressure p and the relative humidity rh. The STD observation operator needs to evaluate this integral for a given atmospheric state, i.e. the 3D fields provided by a numerical weather model. The curved signal path S also depends on the atmospheric state and is not known in advance. The STD operator has to implement a ray tracer which estimates S, some interpolation from the discrete model fields on the signal path and the numerical integration of Eq. (4.1).

The ray tracer is the main component of the STD operator. It finds the signal path S by minimizing Eq. (4.1) and thereby evaluates the integral $\int n\, ds$. The raytracing algorithm used at the DWD is based on Fermat's principle, i.e. a variational approach for finding the minimum optical path length as described in (Zus et al. 2012, 2014). The minimization is done in a special Cartesian reference system linked to the satellite receiver axis. All required quantities, such as receiver positions, grid node coordinates, etc. are transformed to this reference frame assuming an ellipsoidal shape of the Earth. The curved signal path is approximated iteratively by computing the refractivities and their gradients along an estimated signal path which is refined in each iteration. The interpolation is done in three steps: (1) the refractivity is computed at adjacent grid nodes, (2) for each column the refractivities are vertically interpolated to the given height assuming an exponential profile, and (3) a bilinear horizontal interpolation provides the refractivity at the given point. A cubic four-point interpolation of unequally spaced data is used to approximate the integral in Eq. (4.1).

Validation of the STD Observation Operator

The new STD operator was tested using one month of operational COSMO-DE analyses and the latest STD product provided by the GFZ. For this test hourly analyses from March 2015 where read and the STD operator was running for all STD observations from that hour. The observation minus model statistics is shown in Fig. 4.36. In order to emulate the first guess check which removes "poor" observations from the assimilation all data with a relative difference greater than 1.5%, equivalent to about 3.5 cm in the zenith, were removed. In total 19,450,701 STDs were processed and 31,671 = 0.16% were removed.

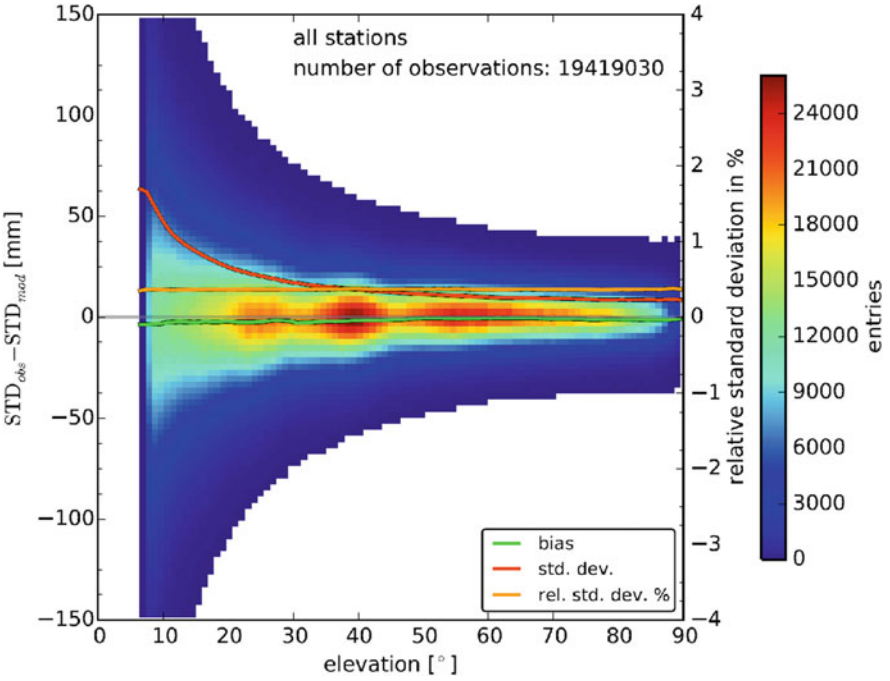

Fig. 4.36 Distribution of $STD_{obs} - STD_{mod}$ for all elevations ε. The variation of the bias (green line, mm) and the standard deviation (red line, mm) with the elevation is shown together with the relative standard deviation (orange line in %, right scale)

The 2D histogram in Fig. 4.36 shows a rather narrow distribution with a standard deviation of about 10 mm near the zenith ($\varepsilon \leq 90°$). At lower elevations $\varepsilon < 30°$ the standard deviation increases considerably up to about 65 mm. Such a behaviour could be expected as both the error of the processed STD data and the accumulated error of the weather model fields increase with decreasing elevation.

Altogether, the results were quite promising: The STDs from the new EPOS 8 version of the GFZ processing system show almost no bias with respect to the COSMO-DE model. The standard deviation is within the range of the expected STD observation error and the relative standard deviation is almost constant for all elevations down to 7°, which indicates, that neither the STD processing error nor the operator error increase disproportionally at low elevations.

COSMO: Model and Assimilation System

The DWD operates the limited-area numerical weather prediction model COSMO-DE (Baldauf et al. 2011) with a horizontal resolution of 2.8 km and 50 hybrid vertical layers up to 22 km. Hourly lateral boundary conditions are provided by the ICON global model with a global horizontal resolution of 13 km which is refined to 7.5 km over Europe. Observations are assimilated in an hourly cycle using an ensemble Kalman filter for convective-scale data assimilation (KENDA, Schraff

et al. 2016) which is based on a local ensemble transform Kalman filter (LETKF, Hunt et al. 2007). The operational COSMO-DE setup runs with an ensemble of 40 members and uses latent heat nudging of radar precipitation (Stephan et al. 2008).

The LETKF computes the analysis as a linear combination of the background ensemble where the weights of individual ensemble members depend on the differences between the observations and their model equivalents. The linear combinations are computed for each point of the analysis grid regarding all observations within the localisation radius. Currently, an analysis grid with 10 km horizontal resolution and 30 vertical layers is used. The LETKF approach is equivalent to propagating a flow dependent model error background covariance matrix.

First STD Assimilation Experiments

A number of STD assimilation experiments were executed in a quasi-operational environment, which emulates the full assimilation and forecast cycle of the operational COSMO-DE/KENDA system at the DWD. Conventional observations, such as synoptic data, radiosonde profiles, wind profiler data and aircraft observations were assimilated by the LETKF and the latent heat nudging was active during the COSMO-DE runs.

Some of these experiments showed promising results. One experiment for the period 17.5.–29.5.2014 showed a positive impact on the precipitation forecast validated with radar observations (Fig. 4.37). The equitable threat score (ETS) could be improved during the first 20 forecast hours which shows that the humidity information from the GNSS STDs makes a positive contribution to the model. However, the validation with other observations, especially radiosonde profiles, was slightly negative. In this experiment, the STDs were located at the GNSS station positions.

The processing of STDs with the LETKF leads to a fundamental problem with the assimilation of non-local observations with a local filter. The LETKF creates independent analyses for each point of the analysis grid, which requires observations with well-defined positions. Furthermore, the analysis depends on the differences $\delta y = y_o - H(x^b)$ at these points. In case of STDs it's not obvious what is the position of the STD and the observations represent the atmospheric state along the whole signal path without any information about local variations. Therefore, it is not optimal to assign δy to a certain point or set of points.

While there is no well-defined position of a STD it can be assumed that the position should be somewhere on the GNSS signal path. To select certain positions a reference height can be set within the STD operator. The operator estimates the position on the signal path with the given height and assigns the STD to that position. For a reference height of 0 m, all STDs will be located at the GNSS receiver positions, for increasing heights the horizontal STD positions will be shifted towards the GNSS satellite.

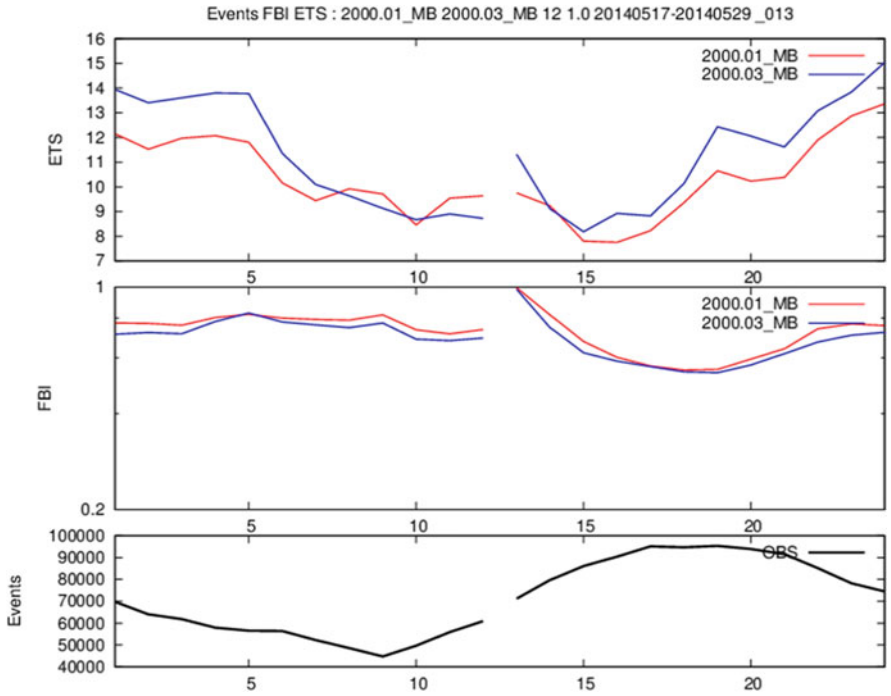

Fig. 4.37 Radar verification of precipitation, 17.5.–29.5.2014, 12:00 UTC forecasts, precipitation threshold 1 mm/h. The reference experiment (blue line) is compared with an STD assimilation experiment (red line). The equitable threat score (ETS), the frequency bias (FBI) and the total number of events (COSMO grid cells with rain) are shown

Another problem is the choice of the localisation radius. In the current implementation, the horizontal localisation radius defines a circle around the observation while the vertical localisation radius is a pressure range below and above the observations. There is no option to specify some direction, e.g. along the signal path.

To address this problem experiments with different STD positions and localisation radii were carried out and combined with different choices of the assumed STD error and of spatial and temporal thinning. The results are not yet consistent and work is in progress. However, it seems that a temporal thinning of the STD observations is necessary. STD observations with a sampling interval of 2.5 min, as provided by the GFZ, strongly outnumber all other observations and add up to more than 90% of all observations.

4.3.5 *Data Assimilation Experiments with GNSS ZTD in AROME 3DVAR*

M. Mile
Hungarian Meteorological Service, Budapest, Hungary
e-mail: mile.m@met.hu

At the Hungarian Meteorological Service (OMSZ) the use of GNSS ZTD is recognized as an important non-conventional observation source for local operational data assimilation (DA) systems. In the frame of GNSS4SWEC COST Action, DA studies were started in order to determine the impact of ZTD measurements on mesoscale AROME analyses and forecasts. During the first studies, observations from Hungarian E-GVAP network so called SGO1 have been evaluated and in latter studies, the observation set was extended with Czech GOP1 and Polish WUEL data as well. The domain of AROME and a typical distribution of GNSS ZTD observations for a particular case study are highlighted in the figures below (Figs. 4.38 and 4.39).

To assimilate GNSS ZTD a proper pre-selection of GNSS sites and an accurate bias correction have to be done. In the early studies, the pre-selection thresholds and static bias correction settings were employed after Poli et al. (2007) and Yan et al. (2008) in the Hungarian AROME 3D-Var assimilation system. The recent version of AROME DA consists only conventional observations (i.e. SYNOP, aircraft and radiosonde measurements) and the assimilation of ZTD on the top of conventional data showed positive impact on AROME winter skill and mostly neutral on summer forecasts. After these first encouraging results, the more advanced variational bias

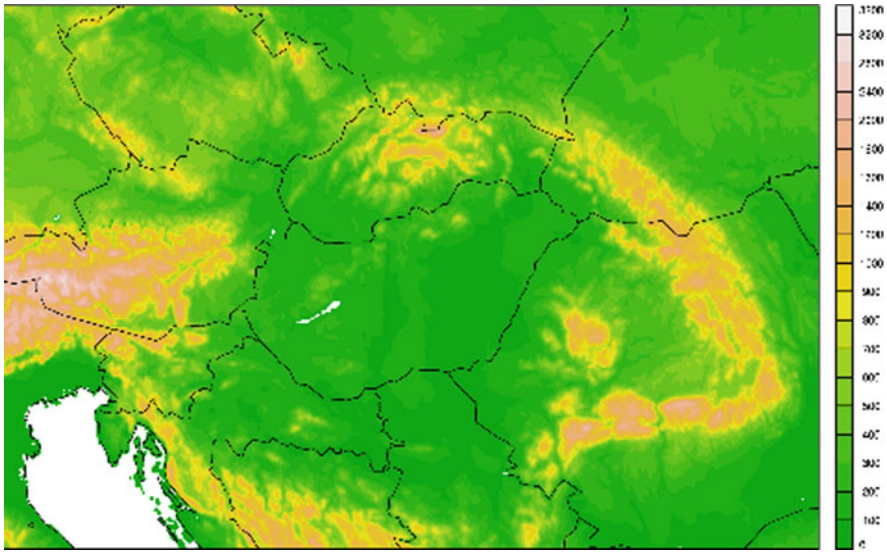

Fig. 4.38 The domain of mesoscale AROME NWP system at OMSZ

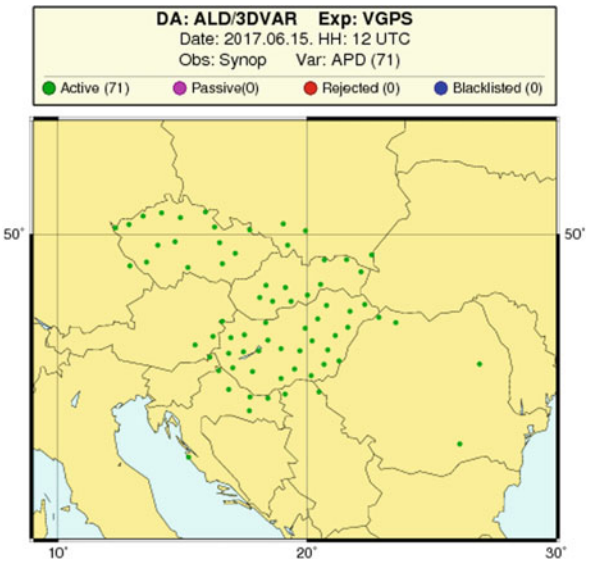

Fig. 4.39 Observation status monitoring of GNSS ZTD from SGO1, GOP1 and WUEL E-GVAP networks for 12:00 UTC AROME analyses at 15th of June, 2017

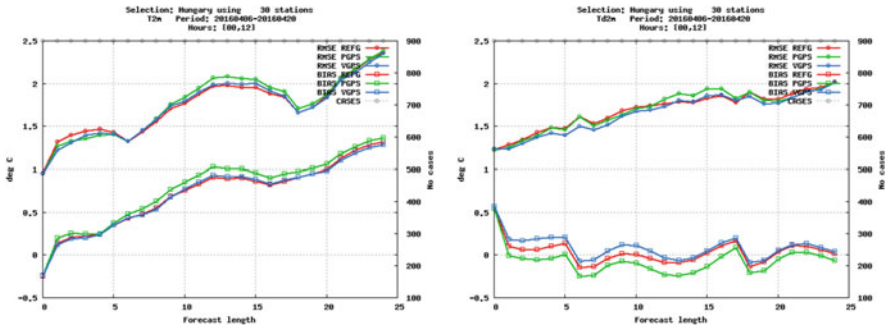

Fig. 4.40 Assimilation impact study: RMSE and BIAS scores of AROME forecasts corresponding to the operational AROME with conventional observations (REFG – red), AROME with conventional plus GNSS ZTD based on static bias correction (PGPS – green) and AROME with conventional plus GNSS ZTD based on variational bias correction (VGPS – blue) for 2 m temperature and dew point temperature

correction (VARBC) approach (Sánchez-Arriola et al. 2016) was applied and tested which provides adaptive bias correction better matched to the future needs of an operational implementation. The benefit of the variational bias correction and the assimilation of ZTD can be seen in Fig. 4.40 above.

The latest experiments included computation of optimal thinning distance (~20 km), evaluation of the optimal VARBC predictor selection, observation monitoring and diagnostic studies (Degree of Freedom for signal, etc.).

4.4 Tomography

W. Rohm
Institute of Geodesy and Geoinformatics, Wrocław University of Environmental and Life Sciences, Wrocław, Poland
e-mail: witold.rohm@igig.up.wroc.pl

E. Trzcina
Institute of Geodesy and Geoinformatics, Wrocław University of Environmental and Life Sciences, Wroclaw, Poland
e-mail: estera.trzcina@igig.up.wroc.pl

G. Möller
Department of Geodesy and Geoinformation, TU Wien, Wien, Austria
e-mail: gregor.moeller@geo.tuwien.ac.at

N. Dymarska
Department of Geodesy and Geoinformation, TU Wien, Wien, Austria
e-mail: natalia.dymarska@geo.tuwien.ac.at

H. Brenot
Royal Belgian Institute for Space Aeronomy, Uccle, Belgium
e-mail: hugues.brenot@oma.be

GNSS tomography is a novel technique that takes advantage of slant troposphere observations between GNSS receivers and satellites, traces these signals through the 3D grid of voxels and estimates through an inversion process the refractivity of the water vapour content within each voxel. The inversion is a highly variable and ill-posed process, hence the methodology to obtain reasonably well resolved troposphere field is a challenging task. The last 10–15 years of GNSS tomography development was focused on the numerical methods to stabilize the solution and get more out of the limited number of observations. As this has been achieved to the great extent, currently we are facing new challenges and possibilities for GNSS tomography in meteorology.

One of the key bottleneck limiting ingest of slant troposphere observations in numerical weather prediction models is a large number of numerical operations required to calculate model-based slants. Additionally, there is a great debate within meteorologists' society as to how assign uncertainty of the slant or zenith delay measurements. The measurement is taken at the station location but the quantity is measured along some trajectory. Using GNSS tomography methodology one can estimate refractivity or water vapour content in a 3D grid with full variance-covariance matrix, which can be used directly in the assimilation process.

On the other hand, same information, i.e. 3D water vapour distribution, but delivered in Near Real-Time or Real-Time using batch processing or stream processing could be another data source for forecasters as an additional tool for assessing

precipitable water content over area covered by the GNSS network. This might be of benefit e.g. in cases with moist unstable air being advected over the domain of interest.

4.4.1 Nowcasting Using Tomography

Severe weather is a growing threat to people and infrastructure all around the world, in Europe the most common event is extensive and prolonged precipitation that may cause a large scale flooding. This weather type is associated with widespread precipitation caused by the convergence on macro scale of air masses in cyclonic systems. Extreme widespread rainfall triggered by convergence on macro scale 5 are usually formed as a result of intensive cyclogenesis organized in the form of quasi-stationary thermal asymmetric appearing from the low barometric pressure of the southern sector of the Central Europe. Such low barometric pressure provides power in moist air from the sector from S through SE and E to NE, which ascends over the cold air coming from the sector NW and N. Frontal surface separating two air masses is predominantly anabatic cold front. As such events are very well studied in literature and predicted to the great extent with sufficient accuracy, we decided to apply GNSS tomography model TOMO2 to resolve the water vapour content before, during and after the event. The applied technique allows getting full picture of troposphere at all locations covered by GNSS network. In this study, we investigate: (1) the meteorological correctness of the tomography retrieval, (2) whether the new temporal and spatial resolution of the troposphere water vapour content will provide new information regarding these well studied events. Two events were investigated: one in May 2014 and one in August/September 2014, the tomography retrievals are compared with radiosonde profiles and numerical weather prediction (NWP) model. We show better agreement of tomography data with radiosonde data than NWP has with radiosonde, we also show the intersections through the cold front and associated atmosphere profile variability. The overall picture of water vapour supply to the rain bands locations is also well represented.

4.4.2 Requirements for Assimilation of Tomography Results

After discussion with Met Office experts following requirements in regards to the troposphere profiles retrieved from tomographic models (Table 4.3) were established.

The criteria set up by Met Office experts are quite tight especially as to what vertical resolution of tomography model retrievals they are interested in. The tomography profile quality is a function of interstation distance, terrain undulation, STDs quality and as such, it is rather infrastructure dependent. Currently the European reference network does not provide enough station density to achieve such high standard results of tomography retrieval over the whole domain, therefore we propose to use limited area models.

Table 4.3 The set of requirements that tomographic retrieval should fulfil in order to be assimilated in the NWP models

Parameter	Requirements minimum (target)
Number of horizontal layers	16 (20)
Bottom layer	<2.0 km (0.5 km)
Top layer	6 km
Inversions	Resolved
Height difference between receivers	~300 m (1000 m)
Distance between receivers	<20 km
Cut-off angle	5 deg. (1.4 deg)
Bending impact	Resolved 59 mm (2397 mm)

According to Seidel et al. (2010) the radiosonde balloon mean drift w.r.t. the pressure levels (approx. height) in the northern hemisphere mid latitude is as follows: 850 hPa (~1500 m) – 2 km, 700 hPa (~3200 m) – 5 km, 500 hPa (~5800 m) – 10 km 300 hPa (~9500 m)- 20 km, 100 hPa (~16,000 m) – 55 km. Therefore, it puts another constraint of 10 km voxel size in the bottom part of the troposphere. Ascend time for radiosonde is 5 min to 2 km and 1.5 h to the top of the troposphere, thus the maximum integration time for tomography should not exceed 1 h.

4.4.3 Assimilation of Relative Humidity

For assimilation purposes, a tomography dataset was provided with one-hour temporal resolution for the first two weeks in April 2016. The tomography model covers the area from 14.2° E to 23.8° E (grid point every 0.8°) and 49.25°N to 54.75° N (grid point every 0.5°), including nine height levels (290, 790, 1290, 1790, 2290, 2790, 3790, 5290 and 6790 m).

The assimilation itself was carried out using the Weather Research and Forecasting Data Assimilation System (WRFDA). WRFDA was configured using two nested domains with a spatial resolution of 12 km × 12 km (259 × 282 grids) and 4 km × 4 km (238 × 220 grids, Fig. 4.41), respectively. Vertically, all domains have 48 levels. Data from the Global Forecasting System (GFS) are used as initial and boundary conditions, available every 6 h. WRFDA allows using both 3D and 4D data assimilation. Here we have used a 3D data assimilation approach (3DVAR). 3DVAR is a variational method based on minimization of a cost function. For assimilation of tomography data, the WRFDA standard observation operator for upper air sounding was applied. Therefore, the wet refractivity fields as obtained from the tomography solution, were converted into time series of relative humidity (in %).

The forecast was started at 00:00 UTC for each day the period covered with TOMO data (01.04.2016–14.04.2016). The lead time was 48 h and meteorological information was written every 1 h to the output file for further post processing. Both

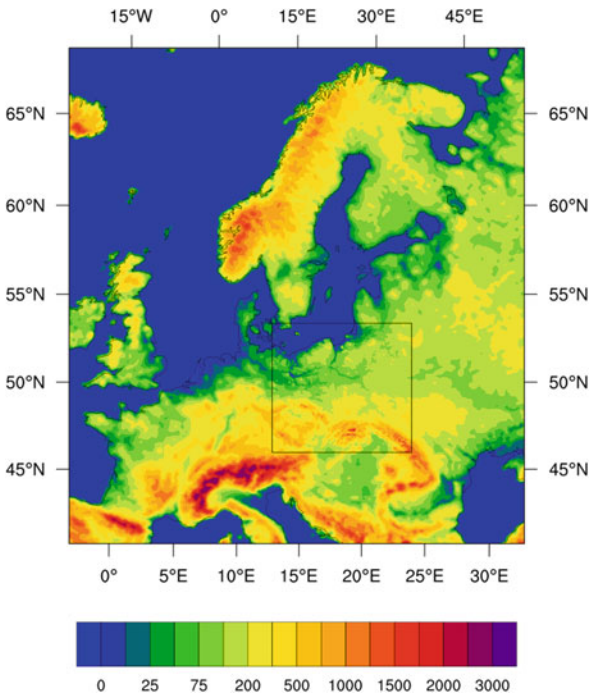

Fig. 4.41 WRF model domains and terrain elevation (msl)

runs (base run and with TOMO data assimilated for the nested domain) were compared to quantify the differences. The differences were calculated for air temperature at 2 m (T2), mixing ratio at 2 m (Q2), rainfall (RAIN; accumulated since the first hour of the model run) and wind speed at 10 m.

Figure 4.42 presents the forecast started at 01.04.2016 00:00 UTC, lead time 6 h, for air temperature at 2 m and accumulated rainfall. There are significant differences in spatial distribution of both meteorological variables. The largest differences between the base run and the model run with TOMO data assimilated are obtained close to the front line. For air temperatures, the differences exceed +/− 2 K. For the majority of the model domain area, air temperatures at 2 m are higher for the base run than for the TOMO assimilation run. For rainfall (accumulated for 6 h) the differences exceed 10 mm.

Verification of the temperature measurements indicate a mixed negative and positive impact (Fig. 4.43) which should be linked with very long assimilation window (13 h) of a fast changing parameter (RH).

4.4.4 Assimilation of Temperature and Specific Humidity

For tomography assimilation studies at the Central Institute for Meteorology and Geodynamics (ZAMG), Austria, May and June 2013 were selected as study period.

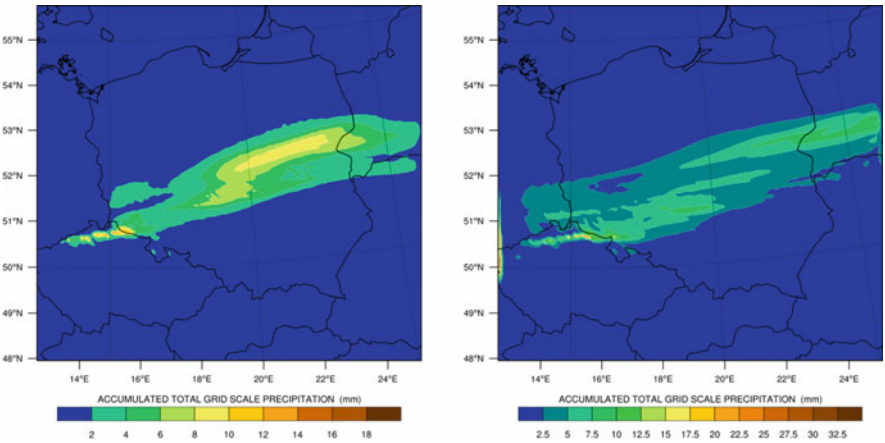

Fig. 4.42 Forecasted accumulated rainfall for the model run without data assimilation left and with data assimilation right. Forecast start time 01.04.2016 00:00 UTC, lead time 6 h

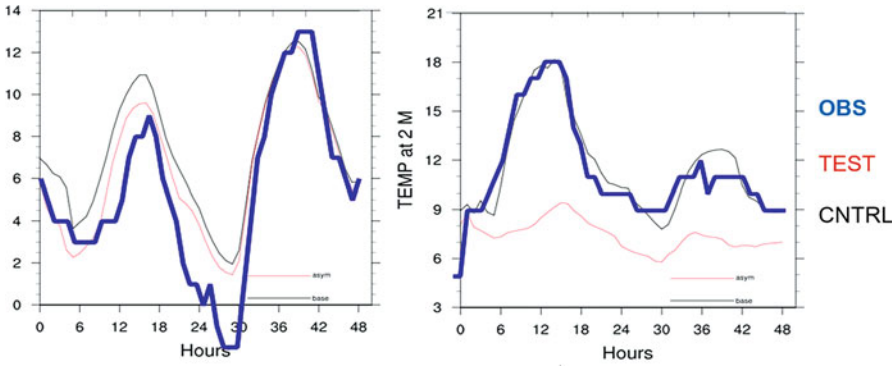

Fig. 4.43 Forecasted temperature for the model run without data assimilation (black line), with data assimilation (red line), against observations at the EPWR station (blue line). For 01.04.2016 + 48 h left and 07.04.2016 + 48 h right.

Within this period, a series of extratropical cyclones of type 'Vb' (Grams et al. 2014) with origin in the Mediterranean and South-East Europe brought very moist and warm air around the Alps, which finally caused a century flood event, affecting the Danube and Elbe catchment areas. Especially end of May and beginning of June INCA precipitation analysis (Möller et al. 2016) revealed heavy precipitation events, with up to 300 mm accumulated precipitation in 72 h over South-East Germany and Austria.

In order to study the atmospheric processes within this period more in detail, a tomography dataset was computed over the entire period of two months with three-hour temporal resolution. The resulting wet refractivity fields reflect the atmospheric

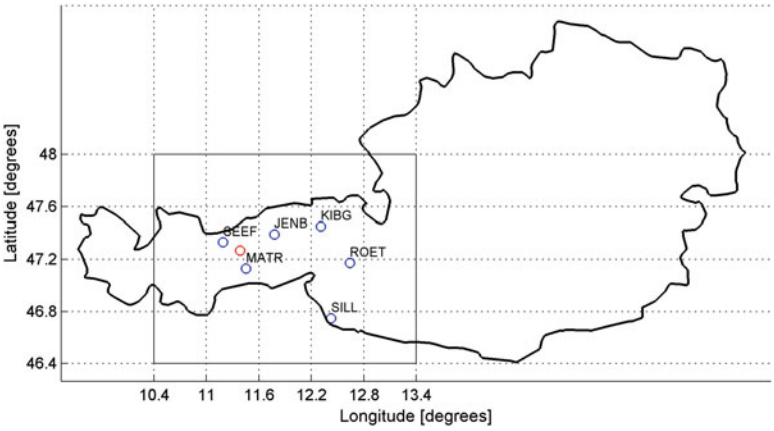

Fig. 4.44 Voxel model and GNSS station distribution in Western Austria. The red circle indicates the location of the radiosonde launch at Innsbruck airport

conditions within the area of Western Austria, parts of Germany and Italy, see Fig. 4.44. For more details about the tomography processing strategy, the reader is referred to (Möller 2017).

Comparisons with radiometer data at Innsbruck airport reveal that the tomography solution, i.e. the obtained wet refractivity fields are significantly less biased than operational numerical weather model data (ALARO), see Fig. 4.45. In consequence, during the assimilation tests a significant impact on the forecast field, especially on the vertical structure of the humidity field is expected.

The assimilation itself was carried out at ZAMG by setting up an extended observation system simulation experiment. Over a period of 14 days (23.05.–05.06.2013) the operational AROME model (2.5 km horizontal resolution, 48 h integration time) was driven with a basic set of conventional and non-conventional observations. On top of this basic setup, different assimilation tests were performed, including the assimilation of ZTDs and wet refractivities.

In contrast to previously described assimilation runs, the wet refractivity fields were transformed into profiles of specific humidity and temperature using a 1DVAR approach, which could be assimilated as conventional T, q-profiles into AROME using a 3DVAR approach. In total 112 AROME model runs had to be performed and evaluated. From this runs we have seen that assimilation of refractivity tends to have a drying effect on the AROME forecast, especially at lower atmospheric levels.

For further analysis, the amplitude score was computed for each model run. This score evaluates the quality of area mean precipitation forecasts with respect to gridded observation data (which is INCA in our case). An A score of '0' would indicate a perfect correspondence between forecast and observation date while values <0 can be interpreted as underestimation and values >0 as overestimation by the model.

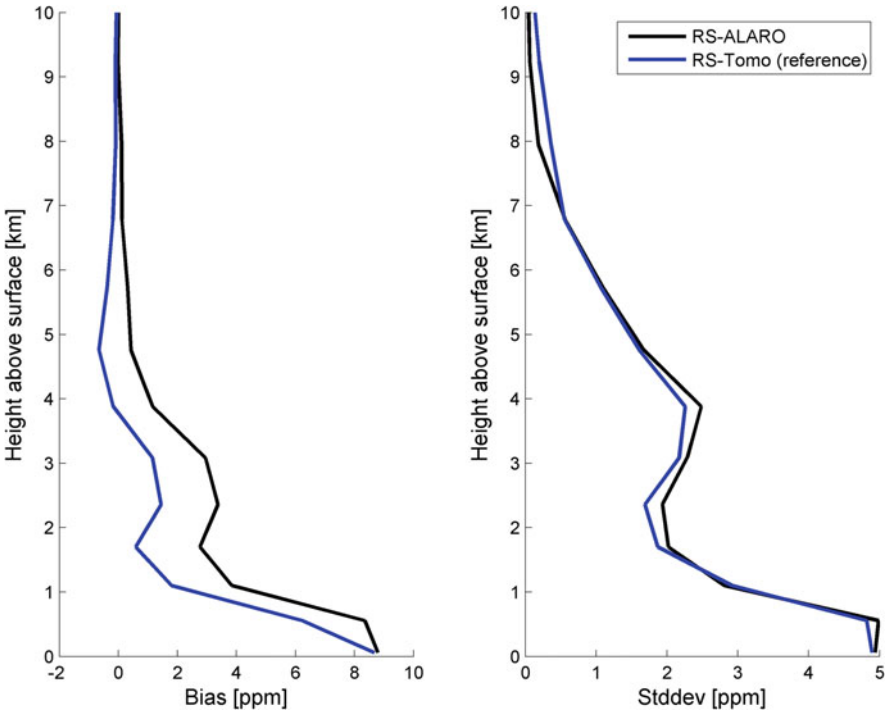

Fig. 4.45 Statistic of the comparison of ALARO and tomography derived wet refractivities with radiosonde profiles. Analysed period: May 2013

Figure 4.46 shows the amplitude score for various assimilation scenarios. It clearly shows that the experiment runs using refractivity observations in the assimilation (ZG02 and ZG04) produce significantly less precipitation than the reference run (ZG01) and the runs using ZTD observations during the first 9 or even 12 h of the forecast (ZG03 and ZG05). According to the amplitude score, the bias correction of ZTD data tends to decrease precipitation in early forecast hours, this gets visible when comparing ZG03 and ZG05.

From the results, we can assume that applying a (variational) bias correction might reduce the amplitude of the drying effect and decrease the overall impact of this observation type. Overall, the results of these assimilation tests clearly show the potential of 3D refractivity observations.

4.4.5 Assimilation of Wet Refractivity

For the described test case, a tomography dataset was derived from slant wet delays, observed at 72 GNSS sites in Eastern Germany and parts of Czech Republic in May and June, 2013. Therefore, the same tomography processing strategy was applied as

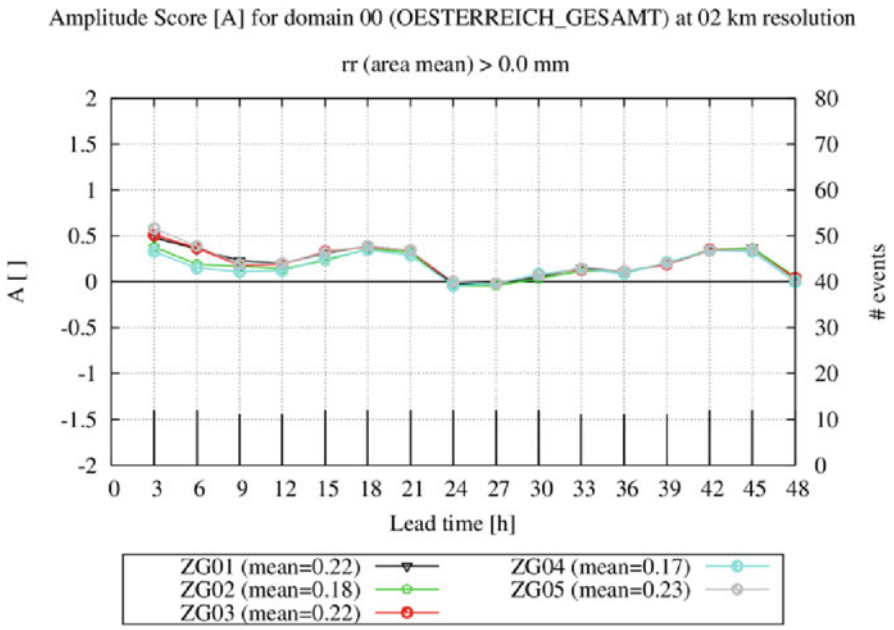

Fig. 4.46 Mean amplitude score (A) as a function of forecast lead time

described in the previous subsection using the ATom tomography package, which was developed at TU Wien. For the assimilation, the Weather Research and Forecasting Data Assimilation System (WRFDA) was configured for the area of Central Europe (Fig. 4.47) with 36 km horizontal spacing and 35 vertical levels. The model top was defined at 50 hPa air pressure.

In total a one-day long assimilation experiment was performed, with (GPS NW) and without (CTRL) GNSS tomography product assimilation. Thereby two solutions were tested: (1) assimilation of relative humidity profiles, (2) assimilation of refractivity observations. The WRF model background (initial and boundary conditions) was derived from NCEP FNL (final) operational global analysis data with $1^\circ \times 1^\circ$ horizontal resolution and 26 vertical layers. In case of assimilation, the model is started at 06:00, 12:00 and 18:00 UTC and is integrated for 6 h (so-called cycle-mode). After that, refractivity fields are applied to the 6-h forecast field through WRF 3DVAR assimilation with a 3-h time window.

For evaluation of the assimilation results, comparisons with radiosonde data were carried out. Figure 4.48 shows the obtained vertical profiles of relative humidity and wind speed, exemplary for RS stations 12,425 and 10,184.

The correlation coefficients (R) between RS and WRF forecasted relative humidity (RH), wind speed (WS) and temperature (T) are summarized in Table 4.4. While in terms of temperature, the correlation remains close to one, the correlation of the relative humidity profiles increased after assimilation of the refractivity fields, from 0.52 to 0.65 (10184), or 0.77 to 0.81 (10393). In contrast

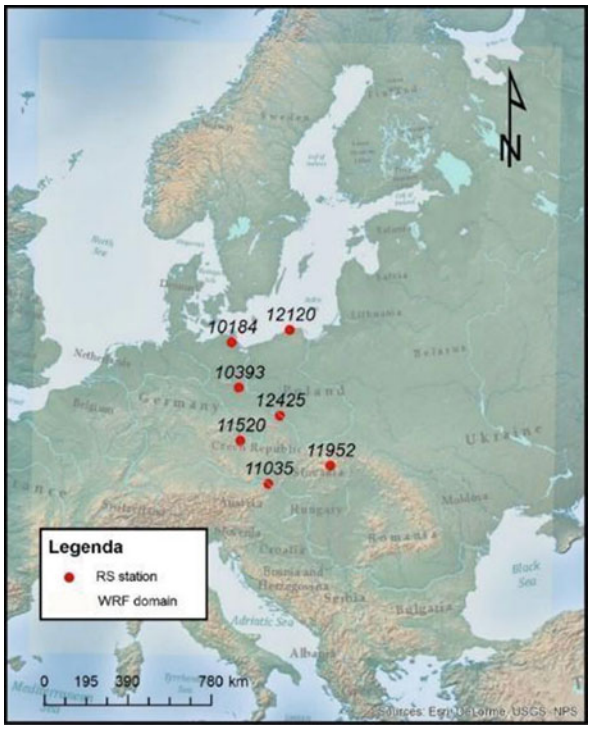

Fig. 4.47 CASE2 WRF model domain including the locations of the radiosonde stations used for model evaluation

the correlation of wind speed decreased after assimilation from 0.78 to 0.75 (10184). This is probably related to the dry part of refractivity, which was added for assimilation purposes.

4.4.6 Conclusions

In conclusion, the assimilation of the tomography outputs into WRF DA is possible using available modules, dedicated for other observations. Two solutions were tested: (1) assimilation as relative humidity profiles, (2) assimilation as refractivity observations.

In case 1, the results show that the impact of GNSS tomography data assimilation on meteorological forecast is significant. Large changes were observed for air temperature at 2 m, mixing ratio at 2 m, rainfall and wind speed. The impact of data assimilation varies spatially and changes with general synoptic situation. Data assimilation strongly affects first 24 h of the forecast, but for several cases it was also significant for the entire forecast (48 h).

In case 2, larger changes in the initial conditions of the model appear and a noticeable, positive impact on the relative humidity forecasts is obtained.

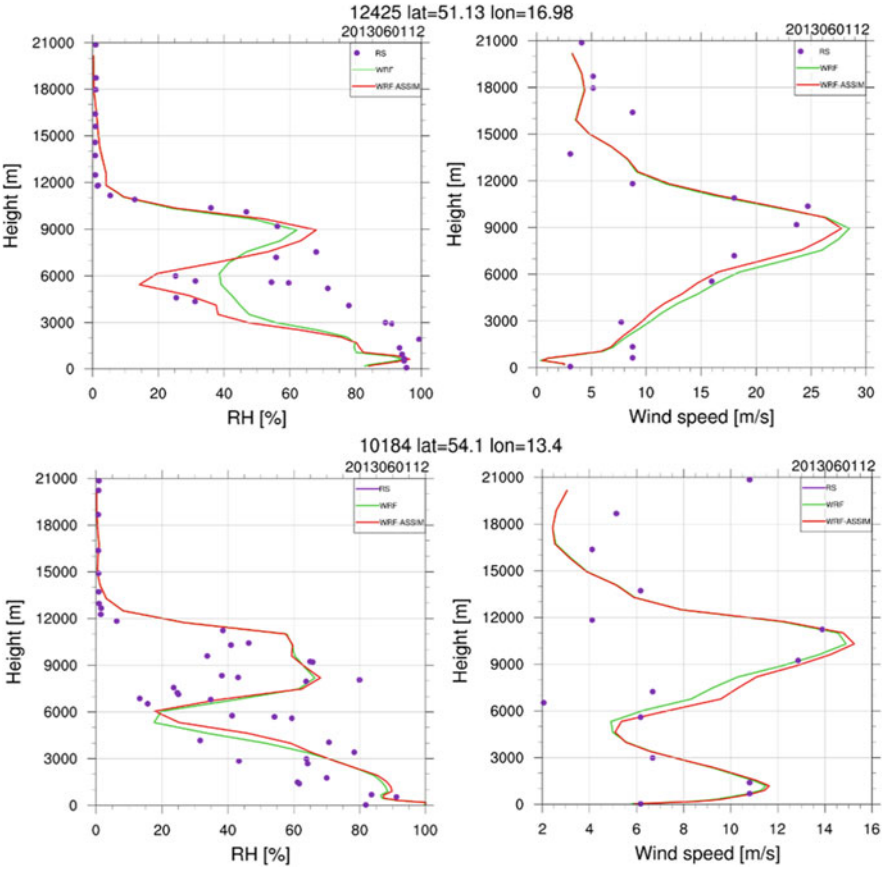

Fig. 4.48 The profiles of the relative humidity (left) and the wind speed for RS (purple) and WRF (red – after refractivity assimilation, green – control dataset) data. Plots for 12,425 (top) and 10,184 (bottom) RS stations

Table 4.4 Correlation between RS and WRF data for 5 RS stations. Date time is 2013-06-01 12:00 UTC

	R [%]					
	RH		WS		T	
Station	CTRL	after assim.	CTRL	after assim.	CTRL	after assim.
10,184	0.58	0.62	0.78	0.75	1.00	1.00
12,120	0.45	0.49	0.88	0.86	1.00	1.00
10,393	0.77	0.81	0.76	0.69	1.00	1.00
12,425	0.93	0.88	0.89	0.90	1.00	1.00
11,520	0.84	0.78	0.88	0.82	1.00	1.00
11,035	0.70	0.71	0.92	0.88	1.00	1.00
11,952	0.86	0.88	0.46	0.44	1.00	1.00
mean	0.73	0.74	0.79	0.76	1.00	1.00

4.5 Benchmark and Case Study Databases at the U.K. Met Office

J. Jones
Met Office, Exeter, UK
e-mail: jonathan.jones@metoffice.gov.uk

This sub-WG was established to define and generate specific benchmark datasets in the form of GNSS observations, alternative water vapour and refractivity observations, and NWP products, for test, assessment and validation for each method/product in conjunction with WG1. Only by validation of traditional and more advanced GNSS tropospheric products (developed in WG1) will the scientific community (specifically the forecasting community) have a better understanding of the benefit of GNSS-tropospheric products to meteorology.

Benchmark Campaign
During the first year of the Action, a benchmark area/time period was determined for the testing and validation of advanced GNSS tropospheric products and processing algorithms developed by WG1. After consideration of a number of areas and events, it was determined that the benchmark campaign should be focused on the areas of Germany/Poland (with some data from surrounding countries) which suffered extremely heavy precipitation in the period of May–June 2003, causing severe flooding of the Danube, Moldau and Ebla rivers.

A database was established at the Geodetic Observatory, Pecny, Czech Republic in conjunction with the International GNSS Service, which met the requirements of the benchmark database, (http://www.pecny.cz/gop/index.php/gop-tropdb). The database contains the following datasets:

- GNSS: ~500 stations, SYNOP: ~200 stations
- NWM: regional (Aladin-CZ), global (ERA-Interim, NCEP GFS)
- RAOBS: 2 high-resolution
- WVR: Potsdam, Lindenberg
- RADAR images: Brdy, Skalka

- Reference products
- GNSS: Bernese (GOP), EPOS (GFZ)
- NWP: G-Nut/Shu (GOP), DNS (GFZ)

More information on the benchmark campaign can be found in detail in subsection 4.1.1 of this report.

Severe Weather Case Study Database
A database was established on a publicly-facing ftp server at the UK Met Office (ftp.metoffice.gov.uk) for the collection and ditribution of severe weather case studies. The case studies uploaded to the database are those found in Sect. 4.2 of this Report plus additional severe weather case studies from events in Austria, Czech Republic, Italy, Lithuania, the Netherlands and the UK.

The database will be supported long-term for the benefit of scientific research and forecaster use. The database is user/password controlled, so please contact jonathan.jones@metoffice.gov.uk for access.

NWP Database for Input to GNSS Processing

This task was created to establish and feed a database with live meteorological data to be used as an input to real-time GNSS positioning. ZTD estimates rely on mapping functions to estimate the atmospheric condition. Advance knowledge of the atmosphere can not only lead to more realistic ZTD and IWV estimates, but also improve GNSS convergence time, thus aiding the positioning community.

The creation of a database at the UK Met Office for the provision of live (i.e. real-time) NWP unified model (UM) output to aid real-time positioning was unfortunately not possible due to UM licence restrictions. Whilst providing the GNSS community with live data was not possible, the provision of offline data for post-processing applications was possible. As is documented in subsection 3.4.10 of this report, a European Space Agency (ESA) funded project, 'RTTSD – Validation and Implementation of Direct Tropospheric Delay Estimation for Precise Real-Time positioning' was established between the University of Nottingham (UoN) and the Met Office, whereby the UoN used data from the Met Office UM model (accessible via the British Isles Atmospheric Data Centre (BADC)), as an input to real-time PPP processing to improve GNSS solution convergence time, with the longer-term view of providing industry with a GNSS quality flag warning system. Please see subsection 3.4.10 for more details.

Additional data for future studies should be requested on a case-by-case basis to the UK Met Office.

4.6 ZTD to IWV Conversion

UK Met Office Operational conversion of ZTD to IWV

J. Jones
Met Office, Exeter, UK
e-mail: jonathan.jones@metoffice.gov.uk

At the UK Met Office, IWV is derived from ZTD using surface meteorological observations retrieved from the Met Office database, the MetDB. On an hourly or sub-hourly basis (determined by the frequency of the GNSS processing system), the database is interrogated and meteorological parameters for all 8000+ global surface sites are extracted. The parameters are; site identifier, latitude, longitude, height, date, time, temperature, dew point temperature and MSL pressure.

Latitude and longitude are read into a MySQL database and values are compared against the latitude and longitude of the GNSS sites used for that particular processing campaign, and thus meteorological data from the nearest surface-

observing site to each GNSS site is chosen. If data from the nearest site is not available, then the next nearest site's data is used, and so on. The temperature and dew point temperature are used as-is, but the MSL pressure must be converted to the pressure at the GNSS antenna height using the formula of Saastamoinen (1972).

In an ideal world, high quality pressure and temperature sensors would be collocated alongside the GNSS antennae, however this is not practical in reality primarily in terms of the cost and infrastructure requirements. Using the nearest sites' pressure is generally deemed adequate as pressure fields do not vary greatly in the horizontal on the scales in this scenario (generally <40 km), however care must be taken as a 1 hPa pressure error typically leads to errors in IWV of around 0.4 km/m^2. For reference, 1 °C temperature error typically leads to an error of around 0.1 km/m^2 in IWV.

Additionally, the forecast field of a rapid-cycle NPW model could be used to obtain the parameters necessary for ZTD to IWV conversion, and this could be an interesting option to investigate further in the future.

GFZ

G. Dick
GFZ German Research Centre for Geosciences, Helmholtz Centre Potsdam, Potsdam, Germany
e-mail: dick@gfz-potsdam.de

F. Zus
GFZ German Research Centre for Geosciences, Potsdam, Germany
e-mail: zusflo@gfz-potsdam.de

For conversion of the adjusted ZTD into the integrated water vapour (IWV), the meteorological surface data at the stations is needed (the pressure for getting the zenith wet delay; the temperature profile, approximated by linear regression from surface data). For some stations, e.g. the 24 GFZ-DWD sites, local measurements are available. However, for most of the sites the needed pressure and temperature have to be interpolated using the synoptic sites of the DWD (about 200 sites with hourly sampling rate of data). For each site, the smallest surrounding station triangle is used for a linear interpolation, correcting for the height differences beforehand. Stations with a height over 1000 m are excluded because of limitations of interpolation accuracy caused by errors in height correction. The quality of the interpolation is normally 0.3 hPa (RMS). In mountainous regions, the error can reach higher values, but 0.5–1 hPa (corresponding to about 0.2–0.4 mm IWV) can be accepted for numerical weather prediction if these are only random fluctuations, however, there are only a few sites that do not meet this limit. The pressure data are checked beforehand by mutual interpolation to eliminate sites, which can be regarded as outliers in the pressure field over Germany. That means, each pressure value is compared to the interpolated value using surrounding sited, and it is excluded if the difference exceeded given accuracy limit.

Additionally, in the case that pressure and temperature observations are not available (e.g. the meteorological sensors are not co-located) the pressure and

temperature values can be obtained from Numerical Weather Model (NWM) data. Since the grid points of the NWM are not co-located with the GPS stations, pressure and temperature values are obtained by interpolation utilizing the nearest grid points.

Further Reading

The empirical conversion of ZTD to IWV is covered in subsect. 1.2.4. A review of conversion methods with a view of determining a climatological standard are covered in subsect. 5.4.2.

References

Askne, J., & Nordius, H. (1987, May–June). Estimation of tropospheric delay for microwaves from surface weather data. *Radio Science*, *22*(3), 379–386. https://doi.org/10.1029/RS022i003p00379.

Baldauf, M., Seifert, A., Förstner, J., Majewski, D., Raschendorfer, M., & Reinhardt, T. (2011). Operational convective-scale numerical weather prediction with the COSMO model: Description and sensitivities. *Monthly Weather Review, 139*(12), 3887–3905.

Bennitt, G. V., & Jupp, A. (2012). Operational assimilation of GPS Zenith total delay observations into the Met office numerical weather prediction models. *Monthly Weather Review, 140*, 2706–2719.

Bevis, M., Businger, S., & Herring, T. (1992). GPS meteorology: Remote sensing of atmospheric water vapour using the Global Positioning System. *Journal of Geophysical Research: Atmospheres, 97*(D14), 15787–15801. https://doi.org/10.1029/92JD01517.

Bevis, M., Businger, S., Chiswell, S., Herring, T., Anthes, R., Rocken, Ch., & Ware, R. (1994, March). GPS meteorology: Mapping zenith wet delays onto precipitable water. *Journal of Applied Meteorology and Climatology*, *33*(3), 379–386. https://doi.org/10.1175/1520-0450(1994)033%3C0379:GMMZWD%3E2.0.CO;2.

Bruyninx, C., Habrich, H., Söhne, W., Kenyeres, A., Stangl, G., & Völksen, C. (2012), Enhancement of the EUREF permanent network services and products. In *Geodesy for planet Earth*, vol. 136 of IAG symposia series (pp. 27–35). Springer.

Caumont, O., Ducrocq, V., Wattrelot, É., Jaubert, G., & Pradier-Vabre, S. (2010). 1D+3DVar assimilation of radar reflectivity data: A proof of concept. *Tellus A, 62*, 173–187.

Chen, G., & Herring, T. (1997, September). Effects of atmospheric azimuthal asymmetry on the analysis of space geodetic data. *Journal of Geophysical Research: Solid Earth*, *102*(B9), 20489–20502. https://doi.org/10.1029/97JB01739.

Dach, R., Lutz, S., Walser, P., & Fridez, P. (Eds) (2015). *Bernese GNSS Software Version 5.2. User manual*. Astronomical Institute, University of Bern, Bern Open Publishing. https://doi.org/10.7892/boris.72297. isbn:978-3-906813-05-9.

Davis, J., Herring, T., Shapiro, I., Rogers, A., & Elgered, G. (1985, November–December). Geodesy by radio interferometry: Effects of atmospheric modelling errors on estimates of baseline length. *Radio Science, 20*(6), 1593–1607. https://doi.org/10.1029/RS020i006p01593.

De Cruz, L., & Duerinckx, A.(2015, April 13–16). *Assimilation of GNSS and radar data in ALARO cy38t1 at RMIB*. Joint 25th ALADIN Workshop & HIRLAM All Staff Meeting, Helsingor, Denmark.

De Cruz, L., Duerinckx, A., & Pottiaux, E. (2015, May 11–13). *GNSS assimilation in NWP: Case studies for Belgium*. COST ES1206 – GNSS4SWEC: 2nd Workshop, Thessaloniki, Greece.

De Haan, S., Barlag, S., Klein Blatink, H., Debie, F., & van der Marel, H. (2004, April). Synergetic use of GPS water vapour and meteosat images for synoptic weather forecasting. *Journal of Applied Meteorology and Climatology*, *43*(3), 514–518. https://doi.org/10.1175/1520-0450(2004)043%3C0514:SUOGWV%3E2.0.CO;2.

De Haan, S., Holleman, I., & Holtslag, A. (2009). Real-time water vapour maps from a GPS surface network: Construction, validation, and applications. *Journal of Applied Meteorology and Climatology, 48*(7), 1302–1316. https://doi.org/10.1175/2008JAMC2024.1.

E-GVAP PDR. (2010, December 21). *Product requirements document v 1.0*. Prepared by the Met Office. http://egvap.dmi.dk/support/formats/egvap_prd_v10.pdf

Elgered, G., Davis, J., Herring, T., & Shapiro, I. (1991, April). Geodesy by radio interferometry: Water vapour radiometry for estimation of the wet delay. *Journal of Geophysical Research – Solid Earth 96*(B4), 6541–6555. https://doi.org/10.1029/90JB00834.

Grams, C. M., Binder, H., Pfahl, S., Piaget, N., & Wernli, H. (2014). Atmospheric processes triggering the central European floods in June 2013. *Natural Hazards and Earth System Sciences, 14*(7), 1691–1702.

Guerova, G. (2013). Ground-based GNSS Meteorology: Case studies for Bulgaria/Southeast Europe. In *Proceedings of the 4th International colloquium – Scientific and fundamental aspects of the Galileo programme*, Prague, Czech Republic, 4–6.12.2013. http://suada.phys.uni-sofia.bg/wordpress/wp-content/uploads/2015/02/2923524_guerova.pdf

Heise, S., Dick, G., Gendt, G., Schmidt, T., & Wickert, J. (2009). Integrated water vapour from IGS ground-based GPS observations: Initial results from a 5-min data set. *Annales de Geophysique, 27*, 2851–2859. https://doi.org/10.5194/angeo-27-2851-2009.

Hogg, D., Guiraud, F., & Decker, M. (1981). Measurement of excess transmission length on Earth–space paths. *Astronomy and Astrophysics, 95*, 304–307.

Holton, J. R. (1972). *An introduction to dynamic meteorology* (p. 319). New York: Academic.

Hunt, B. R., Kostelich, E. J., & Szunyogh, I. (2007). Efficient data assimilation for spatiotemporal chaos: A local ensemble transform Kalman filter. *Physica D: Nonlinear Phenomena, 230*(1–2), 112–126.

Lindskog, M., Ridal, M., Thorsteinsson, S., & Ning, T. (2017). *Data assimilation of GNSS Zenith Total Delays from a Nordic processing centre*. Submitted to Atmospheric Chemistry Physics.

Matheron, G. (1962). *Traité de géostatique appliquée.* Tome I, Mémoires du Bureau de Recherche Géologiques et Minières, N°14, Edt. Technip, Paris.

Matheron, G. (1963a). Principles of Geostatics. *Economic Geology, 58*(8), 1246–1266. https://doi.org/10.2113/gsecongeo.58.8.1246.

Matheron, G. (1963b). *Traité de géostatique appliquée*. Tome II: le Krigeage, Mémoires du Bureau de Recherche Géologiques et Minières, N°24, Edt. B. R. G. M., Paris.

Mazany, R., Businger, S., & Gutman, S. (2002, October). A lightning prediction index that utilizes GPS integrated precipitable water vapour. *Weather and Forecasting*, *17*, 1034–1047.

Möller, G. (2017). *Reconstruction of 3D wet refractivity fields in the lower atmosphere along bended GNSS signal paths*. Dissertation, TU Wien, Department of Geodesy and Geoinformation, 211p.

Möller, G., Wittmann, C., Yan, X., Umnig, E., Joldzic, N., & Weber, R. (2016). *3D ground based GNSS atmospheric tomography*. Final Report GNSS-ATom project 840098, 49p.

Muller, M., Homleid, M., Ivarsson, K.-I., Koltzow, M., Lindskog, M., Midtbo, K.-H., Andrae, U., Aspelien, T., Berggren, L., Bjorge, D., Dahlgren, P., Kristiansen, J., Randriamampianina, R., Ridal, M., & Vigne, O. (2017). AROME-MetCoOp: A nordic convective-scale operational weather prediction model. *Weather and Forecasting, 32*, 609–627. https://doi.org/10.1175/WAF-D-16-0099.1.

Ning, T., Elgered, G., Willén, U., & Johansson, J. (2013). Evaluation of the atmospheric water vapour content in a regional climate model using ground-based GPS measurements. *Journal of Geophysical Research: Atmospheres, 118*(2), 329–339. https://doi.org/10.1029/2012JD018053.

Poli, P., Moll, P., Rabier, F., Desroziers, G., Chapnik, B., Berre, L., Healy, S. B., Andersson, E., & El Guelai, F.-Z. (2007). Forecast impact studies of Zenith total delay data from European near real-time Gps stations in Météo France 4DVAR. *Journal of Geophysical Research: Atmospheres*, *112*(D6). Wiley Online Library.

Pottiaux, E. (2010). *Sounding the Earth's atmospheric water vapour using signals emitted by global navigation satellite systems*. PhD. thesis in Sciences, 200. Université Catholique de Louvain.

Rocken, C., Van Hove, T., Johnson, J., Solheim, F., Ware, R., Bevis, M., Chiswell, S., & Businger, S. (1995), GPS/STORM–GPS sensing of atmospheric water vapour for meteorology. *Journal of Atmospheric and Oceanic Technology*, *12*, 468–478. https://doi.org/10.1175/1520-0426(1995)012<0468:GSOAWV>2.0.CO;2.

Saastamoinen, J. (1972). Atmospheric corrections for the troposphere and stratosphere in radio ranging of satellites. In S. W. Henriksen et al. (Eds.), *The use of artificial satellites for geodesy* (Monograph series) (Vol. 15, pp. 247–251). Washington DC: AGU.

Sánchez Arriola, J., Lindskog, M., Thorsteinsson, S., & Bojarova, J. (2016). Variational bias correction of GNSS ZTD in the HARMONIE modelling system. *Journal of Applied Meteorology and Climatology, 55*, 1259–1276. https://doi.org/10.1175/JAMC-D-15-0137.1.

Schraff, C., Reich, H., Rhodin, A., Schomburg, A., Stephan, K., Periáñez, A., & Potthast, R. (2016). Kilometre-scale ensemble data assimilation for the COSMO model (KENDA). *Quarterly Journal of the Royal Meteorological Society, 142*(696), 1453–1472.

Seidel, D. J., Ao, C. O., & Li, K. (2010). Estimating climatological planetary boundary layer heights from radiosonde observations: Comparison of methods and uncertainty analysis. *Journal of Geophysical Research Atmospheres, 115*(D16).

Smet, G., Termonia, P., & Deckmyn, A. (2012). Added economic value of limited area multi-EPS weather forecasting applications. *Tellus A, 64*, 18901.

Smith, E., & Weintraub, S. (1953, August), The constants in the equation for atmospheric refractive index at radio frequencies. *Proceedings of the IRE*, *41*(8), 1035–1037. https://doi.org/10.1109/JRPROC.1953.274297.

Smith, W., & Wessel, P. (1990, March). Gridding with continuous curvature splines in tension. *Geophysics*, *55*(3), 293–305. https://doi.org/10.1190/1.1442837.

Stephan, K., Klink, S., & Schraff, C. (2008). Assimilation of radar-derived rain rates into the convective-scale model COSMO-DE at DWD. *Quarterly Journal of the Royal Meteorological Society, 134*(634), 1315–1326.

Stoev, K., & Guerova, G. (2017). Climatology of the foehn in Sofia for 1975–2014. *International Journal of Climatology*. In review 9/2017. http://suada.phys.uni-sofia.bg/?page_id=3801

Stoycheva, A., & Guerova, G. (2015). Study of fog in Bulgaria by using the GNSS tropospheric products and large scale dynamic analysis. *Journal of Atmospheric and Solar-Terrestrial Physics, 133*, 87–97. https://doi.org/10.1016/j.jastp.2015.08.004.

Stoycheva, A., Manafov, I., Vassileva, K., & Guerova, G. (2017). Study of persistent fog in Bulgaria with Sofi a Stability Index, GNSS tropospheric products and WRF simulations. *Journal of Atmospheric and Solar-Terrestrial Physics, 161*, 160–169. https://doi.org/10.1016/j.jastp.2017.06.011.

Stull, R. (1995). *Meteorology today for scientists and engineers* (385 p). Minneapolis: West Publishing.

Van Malderen, R., Brenot, H., Pottiaux, E., Beirle, S., Hermans, C., De Mazière, M., Wagner, T., De Backer, H., & Bruyninx, C. (2014). A multi-site techniques intercomparison of integrated water vapour observations for climate change analysis. *Atmospheric Measurement Techniques Discussions, 7*, 1075–1151. https://doi.org/10.5194/amtd-7-1075-2014.

Vedel, H., Huang, X. Y., Haase, J., Ge, M., & Calais, E. (2004). Impact of GPS Zenith tropospheric delay data on precipitation forecasts in Mediterranean France and Spain. *Geophysical Research Letters, 31*(2), 2004.

Vey, S., Dietrich, R., Fritsche, M., Rülke, A., Steigenberger, P., & Rothacher, M. (2009, May). On the homogeneity and interpretation of precipitable water time series derived from global GPS observations. *Journal of Geophysical Research Atmospheres*, *114*(D10). https://doi.org/10.1029/2008JD010415.

Wang, J., Zhang, L., & Dai, A. (2005). Global estimates of water-vapour-weighted mean temperature of the atmosphere for GPS applications. *Journal Geophysical Research, 110*, D21101. https://doi.org/10.1029/2005JD006215.

Wang, J., Zhang, L., Dai, A., van Hove, T., & van Baelen, J. (2007, June). A near-global, 2-hourly data set of atmospheric precipitable water from ground-based GPS measurements. *Journal of Geophysical Research Atmospheres*, *112*(D11). https://doi.org/10.1029/2006JD007529.

Wang, X., Barker, Snyder, C., & Hamill, T. M. (2008). A hybrid ETKF–3DVAR data assimilation scheme for the WRF Model. Part I: Observing system simulation experiment. *Monthly Weather Review, 136*, 5116–5131.

Watson, D. (1982). Acord: Automatic contouring of raw data. *Computers and Geosciences, 8*(1), 97–101. https://doi.org/10.1016/0098-3004(82)90039-5.

Wattrelot, E., Caumont, O., & Mahfouf, J. F. (2014). Operational implementation of the 1D+ 3D-Var assimilation method of radar reflectivity data in the AROME model. *Monthly Weather Review, 142*(5), 1852–1873.

Yan, X., Ducrocq, V., Poli, P., Jaubert, G., & Walpersdorf, A. (2008). Mesoscale GPS Zenith delay assimilation during a Mediterranean heavy precipitation event. *Advances in Geosciences, 17*, 71–77.

Yan, X., Ducrocq, V., Poli, P., Hakam, M., Jaubert, G., & Walpersdorf, A. (2009). Impact of GPS zenith delay assimilation on convective-scale prediction of Mediterranean heavy rainfall. *Journal of Geophysical Research, 114*(D03104), 2009.

Zus, F., Bender, M., Deng, Z., Dick, G., Heise, S., Shang-Guan, M., & Wickert, J. (2012). A methodology to compute GPS slant total delays in a numerical weather model. *Radio Science, 47*, RS2018.

Zus, F., Dick, G., Heise, S., & Wickert, J. (2014). A forward operator and its adjoint for GPS slant total delays. *Radio Science, 50*(5), 393–405.

Chapter 5
Use of GNSS Tropospheric Products for Climate Monitoring (Working Group 3)

O. Bock, R. Pacione, F. Ahmed, A. Araszkiewicz, Z. Bałdysz, K. Balidakis, C. Barroso, S. Bastin, S. Beirle, J. Berckmans, J. Böhm, J. Bogusz, M. Bos, E. Brockmann, M. Cadeddu, B. Chimani, J. Douša, G. Elgered, M. Eliaš, R. Fernandes, M. Figurski, E. Fionda, M. Gruszczynska, G. Guerova, J. Guijarro, C. Hackman, R. Heinkelmann, J. Jones, S. Zengin Kazancı, A. Klos, D. Landskron, J. P. Martins, V. Mattioli, B. Mircheva, S. Nahmani, R. T. Nilsson, T. Ning, G. Nykiel, A. Parracho, E. Pottiaux, A. Ramos, P. Rebischung, A. Sá, W. Dorigo, H. Schuh, G. Stankunavicius, K. Stępniak, H. Valentim, R. Van Malderen, P. Viterbo, P. Willis, and A. Xaver

O. Bock (✉) · S. Nahmani · A. Parracho · P. Rebischung · P. Willis
IGN Institut national de l'information géographique et forestière, Paris, France
e-mail: olivier.bock@ign.fr; Samuel.Nahmani@ign.fr; ana.parracho@etu.upmc.fr; paul.rebischung@ign.fr; pascal.willis@ipgp.fr

R. Pacione
e-GEOS/Centro di Geodesia Spaziale-Agenzia Spaziale Italiana, Matera, MT, Italy
e-mail: rosa.pacione@e-geos.it

F. Ahmed
Geodesy and Geospatial Engineering, Institute of Civil Engineering and Environment, University of Luxembourg, Luxembourg City, Luxembourg
e-mail: furqan.ahmed@csr.utexas.edu

A. Araszkiewicz · Z. Bałdysz · J. Bogusz · M. Figurski · M. Gruszczynska · A. Klos · G. Nykiel
Centre of Applied Geomatics, Warsaw Military University of Technology, Warszawa, Poland
e-mail: andrzej.araszkiewicz@wat.edu.pl; zbaldysz@wat.edu.pl; jbogusz@wat.edu.pl; mfigurski@wat.edu.pl; marta.gruszczynska@wat.edu.pl; anna.klos@wat.edu.pl; grzegorz.nykiel@wat.edu.pl

K. Balidakis · R. Heinkelmann · R. T. Nilsson · H. Schuh
GFZ German Research Centre for Geosciences, Potsdam, Germany
e-mail: balidak@gfz-potsdam.de; rob@gfz-potsdam.de; jan.tobias.nilsson@gfz-potsdam.de; harald.schuh@gfz-potsdam.de

C. Barroso · J. P. Martins · P. Viterbo
Instituto Português do Mar e da Atmosfera, Lisbon, Portugal
e-mail: carla.barroso@ipma.pt; joao.p.martins@ipma.pt; pedro.viterbo@ipma.pt

S. Bastin
Université Paris-Saclay, Saint-Aubin, France

Sorbonne Universités, Paris, France
e-mail: sophie.bastin@latmos.ipsl.fr

J. Jones et al. (eds.), *Advanced GNSS Tropospheric Products for Monitoring Severe Weather Events and Climate*, https://doi.org/10.1007/978-3-030-13901-8_5

S. Beirle
Max-Planck-Institute for Chemistry, Mainz, Germany
e-mail: steffen.beirle@mpic.de

J. Berckmans
Royal Meteorological Institute of Belgium, Brussels, Belgium
e-mail: julieb@meteo.be

J. Böhm · D. Landskron · A. Xaver
Department of Geodesy and Geoinformation, TU Wien, Wien, Austria
e-mail: Johannes.Boehm@geo.tuwien.ac.at; szengin@ktu.edu.tr;
Angelika.Xaver@geo.tuwien.ac.at

M. Bos · R. Fernandes · H. Valentim
University of Beira Interior, Covilhã, Portugal
e-mail: machiel@segal.ubi.pt; rmanuel@di.ubi.pt; hugo.valentim@segal.ubi.pt

E. Brockmann
Swiss Federal Office of Topography, Köniz, Switzerland
e-mail: Elmar.Brockmann@swisstopo.ch

M. Cadeddu
Argonne National Laboratory, Lemont, IL, USA
e-mail: mcadeddu@anl.gov

B. Chimani
Central Institute for Meteorology and Geodynamics, Veinna, Austria
e-mail: barbara.chimani@zamg.ac.at

J. Douša
Geodetic Observatory Pecný, RIGTC, Ondřejov, Czech Republic
e-mail: jan.dousa@pecny.cz

G. Elgered
Chalmers University of Technology, Göteborg, Sweden
e-mail: gunnar.elgered@chalmers.se

M. Eliaš
Geodetic Observatory Pecný, Research Institute of Geodesy, Topography and Cartography,
Ondřejov, Czech Republic
e-mail: michal.elias@pecny.cz

E. Fionda
Fondazione Ugo Bordoni, Rome, Italy
e-mail: efionda@fub.it

G. Guerova · B. Mircheva
Physics Faculty, Department of Meteorology and Geophysics, Sofia University “St. Kliment
Ohridski”, Sofia, Bulgaria
e-mail: guerova@phys.uni-sofia.bg; bmircheva@uni-sofia.bg

J. Guijarro
AEMET, Madrid, Spain
e-mail: jguijarrop@aemet.es

C. Hackman
United States Naval Observatory, Washington, DC, USA
e-mail: hackman.christine@usno.navy.mil

J. Jones
Met Office, Exeter, UK
e-mail: jonathan.jones@metoffice.gov.uk

S. Z. Kazancı
Karadeniz Technical University, Trabzon, Turkey

V. Mattioli
Centre of Excellence Telesensing of Environment and Model Prediction of Severe Events, University of L'Aquila, L'Aquila, AQ, Italy
e-mail: vinia.mattioli@diei.unipg.it

T. Ning
The Swedish Mapping, Cadastral and Land Registration Authority, Stockholm, Sweden
e-mail: tong.ning@lm.se

E. Pottiaux
Royal Observatory of Belgium, Brussels, Belgium
e-mail: eric.pottiaux@oma.be

A. Ramos
Instituto Dom Luiz, University of Lisbon, Lisbon, Portugal
e-mail: amramos@fc.ul.pt

A. Sá
Polytechnic Institute of Guarda, Guarda, Portugal

W. Dorigo
Department of Geodesy and Geoinformation, TU Wien, Wien, Austria
e-mail: Wouter.Dorigo@geo.tuwien.ac.at

G. Stankunavicius
Vilnius University, Vilnius, Lithuania
e-mail: gintas.stankunavicius@gf.vu.lt

K. Stępniak
Advanced Methods for Satellite Positioning Laboratory, University of Warmia and Mazury in Olsztyn, Olsztyn, Poland
e-mail: katarzyna.stepniak@uwm.edu.pl

R. Van Malderen
Royal Meteorological Institute of Belgium, Brussels, Portugal
e-mail: roeland@meteo.be

Abstract There has been growing interest in recent years in the use of homogeneously reprocessed ground-based GNSS, VLBI, and DORIS measurements for climate applications. Existing datasets are reviewed and the sensitivity of tropospheric estimates to the processing details is discussed. The uncertainty in the derived IWV estimates and linear trends is around 1 kg m^{-2} RMS and $\pm$ 0.3 kg m^{-2} per decade, respectively. Standardized methods for ZTD outlier detection and IWV conversion are proposed. The homogeneity of final time series is limited however by

changes in the stations equipment and environment. Various homogenization algorithms have been evaluated based on a synthetic benchmark dataset. The uncertainty of trends estimated from the homogenized times series is estimated to ± 0.5 kg m^{-2} per decade. Reprocessed GNSS IWV data are analysed along with satellites data, reanalyses and global and regional climate model simulations. A selection of global and regional reprocessed GNSS datasets and ERA-interim reanalysis are made available through the GOP-TropDB tropospheric database and online service. A new tropo SINEX format, providing new features and simplifications, was developed and it is going to be adopted by all the IAG services.

5.1 Introduction[1]

O. Bock
IGN Institut national de l'information géographique et forestière, Paris, France
e-mail: olivier.bock@ign.fr

R. Pacione
e-GEOS/Centro di Geodesia Spaziale-Agenzia Spaziale Italiana, Matera, MT, Italy
e-mail: rosa.pacione@e-geos.it

5.1.1 Motivation

Water vapour plays a key role in the climate system as it is the dominant greenhouse gas and a strong feedback variable (temperature changes are enhanced typically by a factor of 2–3 by the atmospheric water vapour content). Global warming and hydrological cycle are tightly linked, with a global scaling ratio of 5–7% of IWV per 1 K. Water vapour is also the main resource for precipitation as about 70% results from moisture convergence and a crucial ingredient of moist processes which are responsible for severe weather events such as heavy precipitation and flooding.

Our knowledge of the global water vapour distribution and its long term evolution is limited due to sparsity and inhomogeneity of the global observing system. As a consequence, both global and regional reanalyses suffer from observation system limitations and model uncertainties. Model uncertainties, especially regarding the water cycle, are also limiting the quality climate model simulations.

Strong interest grew in recent years to assess the benefit of ground-based GNSS measurements for climate research, both as a basic observable of the water cycle, e.g. to evaluate IWV trends and variability, and as a validation data for atmospheric

[1]In the following sections material is republished with kind permission: Sects. 5.3.2, 5.3.3, 5.3.4, 5.3.5 and 5.3.6, 5.3.9, 5.3.10 and 5.3.11, 5.4.3, 5.7.1, 5.7.3, 5.7.5 and 5.7.6.

models. Indeed, IWV was recognized as an essential climate variable by GCOS, and global GNSS measurements cover now about 20 years (e.g., IGS and EPN networks include hundreds of stations) which make them an interesting independent observational dataset for climate model validation. Moreover, several global and regional homogeneously reprocessed GNSS datasets were produced in recent years which were not analysed in this respect so far.

5.1.1.1 Context

At the beginning of this COST Action, few studies had investigated the requirements and the potential of ground-based GNSS measurements for climate research.

Accuracy requirements for water vapour profiles in the troposphere for climate monitoring were specified in GCOS-112 (2007) as: precision = 2%, accuracy = 2%, stability = 1% or 0.3% per decade. They were complemented in GCOS-171 (2013) more specifically for satellite IWV measurements as: random error = 5% and systematic error = 3%, but not for stability. If one applies these recommendations for GNSS, the acceptable limits for IWV expressed in kg/m^2 for a 5% systematic error, a 3% random error, and a 0.3% per decade error are: 0.15 kg/m^2, 0.25 kg/m^2, 0.015 kg/m^2per decade for a dry atmosphere of 5 kg/m^2 (polar regions and high mountain sites) and 1.5 kg/m^2, 2.5 kg/m^2, and 0.15 kg/m^2 per decade in a wet atmosphere of 50 kg/m^2 (tropics or temperate climate summer extremal values).

Accuracy and stability, and good spatial and temporal homogeneity and coverage are key features required for a climate data record. GNSS measurements satisfy some these characteristics. Especially, high accuracy and good temporal coverage was demonstrated in many past studies comparing GNSS IWV data to other techniques (especially radiosondes and microwave radiometers) and the all-weather capability is a unique characteristic of GNSS water vapour measurements. Good spatial coverage is achieved thanks to the dense and well documented permanent global and regional networks. Temporal coverage is reasonably well achieved back to the early 1990s, but it is recognized that early measurements (before 1995) are much noisier and more difficult to process because the quality of the equipment was lower. The quality of the IGS satellite products (orbits, clocks, EOPs) is of highest quality after 2000. Inhomogeneities in GNSS ZTD time series are related to processing changes (updates of the reference frame and applied models, implementation of different mapping functions, use of different elevation cut-off angles and any other updates in the processing strategies) and instrumental changes. To reduce processing-related inconsistencies, a homogenous reprocessing of the whole GNSS data set is mandatory and, for doing it properly, well-documented, long-term metadata set is required.

Changes in equipment and subsequent changes in the measurement characteristics are beneficial to most applications as they go along with quality improvement, but they generate a distinct issue for climate monitoring. Indeed, equipment changes are known to introduce small breaks in the observed time series which may mix up with the underlying climate trends and variability. The homogeneity issue is one of

the major unsolved topics of GNSS data analysis for climate research. Activity on this topic was initiated during the course of the Action and is foreseen to continue well after. Improvement of processing and post-processing techniques aiming at retrieving better homogenised GNSS IWV times series will be a central concern of methodological research for the upcoming years.

5.1.1.2 Objectives and Organisation of Activities

The general objectives of WG3 were the following:

- Review and evaluate existing reprocessed long-term GNSS datasets, processing and post-processing methods.
- Establish standards and recommendations for processing and post-processing of GNSS measurements consistent with climate research requirements.
- Establish a database of qualified GNSS IWV data for climate research.
- Cooperate with climate community on the exploitation of GNSS IWV data.

Figure 5.1 illustrates the flow of GNSS data from observation to climate application. The various steps the data typically undergo are identified, with indication of the main options (methods, settings, and necessary auxiliary data and metadata).

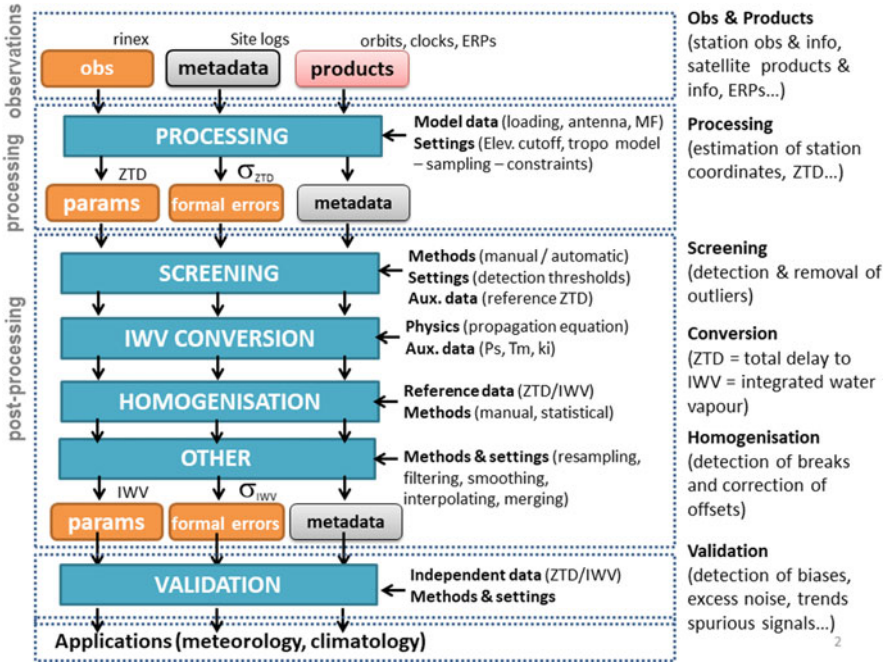

Fig. 5.1 Logical Scheme of GNSS Data Processing from the collection of GNSS data, metadata and products to the validation of the GNSS-estimated ZTD and GNSS-derived IVW

Questions regarding observations (data, metadata, and products), data processing (which software, processing options and products) and dissemination of results (sinex topo format) implied tight cooperation with the geodetic community and WG1. Post-processing (screening, IWV conversion, and homogenization) as well as validation (IWV intercomparisons between GNSS and other techniques) was more at the heart of the activities of WG3 participants and stimulated cooperation with the remote sensing community (e.g. GRUAN, NDACC). Finally, thematic studies on IWV trends and variability with GNSS data and climate models were conducted as well by participants and stimulated collaborations with WG2 and the climate community.

Five work packages were defined at the beginning of the Action to organise more efficiently the activity in the different fields.

WP3.1 Processing: aimed at making an inventory of available reprocessed GNSS datasets, which included DORIS and VLBI as well. Sensitivity studies, tests and evaluations were also conducted on processing options and products.

WP3.2 Post-processing: aimed at developing ZTD screening methods, standardize the ZTD to IWV conversion procedure, and assess the homogeneity of existing GNSS datasets and existing homogenisation methods.

WP3.3 IWV intercomparisons: aimed at making a literature review from previous multitechnique campaigns and stimulate new intercomparison with well qualified IWV data (from GNSS and other techniques).

WP3.4 GNSS and climate research: aimed at conducting studies of IWV trends and variability using GNSS data as well as other observations, reanalyses and climate model simulations.

WP3.5 Database, formats, and dissemination: aimed at providing support to other WPs, develop a GNSS/climate database and update SINEX tropo format in cooperation with IAG, IGS, and EUREF.

It is worth noting that cooperation was established with experts from GRUAN, GEWEX, WMO, ECMWF, previous COST Action HOME, and results were communicated in climate meetings from EGU, AGU, EMS, GEWEX, IAMAS, among others.

At the end of the Action, both a global reference GNSS IWV dataset (1995–2010) and a European reference ZTD dataset (1996–2014) were established.

5.2 Available Reprocessed ZTD and IWV Datasets

5.2.1 Inventory of Available Reprocessed ZTD Datasets

F. Ahmed
Geodesy and Geospatial Engineering, Institute of Civil Engineering and Environment, University of Luxembourg, Luxembourg City, Luxembourg
e-mail: furqan.ahmed@csr.utexas.edu

R. Pacione
e-GEOS/Centro di Geodesia Spaziale-Agenzia Spaziale Italiana, Matera, MT, Italy
e-mail: rosa.pacione@e-geos.it

O. Bock
IGN Institut national de l'information géographique et forestière, Paris, France
e-mail: olivier.bock@ign.fr

At the beginning of the COST action, with updates in the course of the action, an inventory of available GNSS, VLBI and DORIS reprocessed ZTD and IWV datasets was carried out. For each dataset in the inventory the following information is reported:

- Network coverage (global, Europe, other regions, national, campaigns) and number of stations,
- Availability of RINEX data,
- Availability of ZTD, horizontal gradients and IWV estimates,
- Data file format,
- Archive address (url, ftp) & type of access,
- GNSS data processing software,
- Processing Mode (double differences, precise point positioning) and options (GNSS Product used...), elevation cut-off angle, handling of site coordinate, mapping function...).

Information was collected for about 24 GNSS datasets as well as global DORIS and VLBI reprocessed datasets. The global GNSS datasets included IGS repro1 (PPP solution) produced by JPL, IGS repro2 solutions from various Analysis Centres, and TIGA solutions from various ACs. The European GNSS datasets included EPN repro1 (a combined solution) and EPN repro2 from various Analysis Centres. Several regional and national reprocessed datasets are also described (e.g. for Scandinavia, West Africa...).

Some of the datasets have been uploaded to the GOP tropo database (ref. Sect. 5.1).

At the beginning of the Cost Action, several GNSS reprocessed solutions were available. Since a majority of groups had already been using IGS repro1, and this dataset is a global, fully reprocessed dataset, it was adopted by the WG3 participants as a first reference dataset for community activities throughout the course of the Action. This dataset is further described in the next subsection. Other GNSS, VLBI, and DORIS datasets produced and/or used during the course of the Action are described in subsequent subsections, including forthcoming datasets that may be of interest for future studies.

Several long-term (20+ years) reprocessed tropospheric solutions currently exist and are available for climate studies. These time series have been produced using various software and various strategies, and include GNSS stations belonging to various network scale: global (IGS troposphere Repro 1 and TIGA), regional (EPN troposphere Repro 2) and local.

International Reprocessing Activities:

- EUREF Tropospheric 2nd Reprocessing Campaign http://www.epncb.oma.be/_productsservices/troposphere/
- TIGA Reprocessing Campaign http://adsc.gfz-potsdam.de/tiga/index_TIGA.html
- GRUAN Reprocessing Campaign http://www.gfz-potsdam.de/en/section/space-geodetic-techniques/projects/gruan/
- IGS 2nd reprocessing campaign (http://acc.igs.org/reprocess2.html)

More details about some of the reprocessed datasets can be found in the Chap. 3.

5.2.2 IGS Repro1 as First Reference GNSS IWV Dataset

O. Bock
IGN Institut national de l'information géographique et forestière, Paris, France
e-mail: olivier.bock@ign.fr

5.2.2.1 Objectives

The motivations for using a common ZTD and/or IWV dataset are the following:

- Avoid extra uncertainty due to the use of different datasets when the results from a large community are to be intercompared (e.g. compare results from various post-processing methods: screening, ZTD to IWV conversion, homogenisation, trend estimation...),
- Provide a well-documented and validated IWV dataset to the climate community for model verification.

5.2.2.2 Description of the ZTD Dataset

The tropospheric parameters (ZTD and gradients) were produced by JPL as coordinator of the IGS tropo working group in 2010. The dataset actually used here and referred to as repro1 is composed of two streams:

- IGS repro1 (1995/01-2007/12): produced by JPL in May 2010,
- IGS trop_new (2008/01-2010/12): consistently reprocessed by JPL after May 2010.

The reason why two batches are available is that the official IGS repro1 campaign (which aim was to reprocess satellite orbits and clocks mainly) covered the period from 1995/01 to 2007/12 only. However, JPL extended the length of the reprocessed

tropospheric solution beyond that period using consistent operationally produced satellite orbits and clocks (combined final IGS products). Unfortunately, we noticed that in the 2008 and 2009 archive, a few days of the trop_new dataset were not reprocessed for a number of stations. The impact of this mix of old and new tropospheric estimates is small at most sites except in Antarctica which exhibit small ZTD biases (<5 mm) due to the use of different mapping functions (NMF in the old solution, GMF in the new).

The main processing options used to produce the IGS repro1 dataset are summarised below:

- Software: GIPSY-OASIS II in PPP mode,
- Fixed orbits and clocks: IGS Final Re-Analysed Combined (1995–2007), and IGS Final Combined 2008–2011,
- Earth orientation: IGS Final Re-Analysed Combined (1995–2007), and IGS Final Combined (2008–2011),
- Transmit/Receiver antenna phase centre map: IGS Standards (APCO/APCV),
- Elevation angle cutoff: 7 degrees,
- Mapping function (hydrostatic and wet): GMF,
- A priori delay (m): hyd = 1.013*2.27*exp(−0.116*ht) wet = 0.1,
- Data arc: 24 hours = > increased errors at 00:00 UTC,
- Data rate: 5 min,
- Temporal resolution of tropospheric estimates: 5 min,
- Estimated parameters: station position (daily), station clock (white noise), wet zenith delay (3 mm/$h^{1/2}$ random walk), delay gradients (0.3 mm/$h^{1/2}$ random walk), phase biases (white noise) = > smooth tropo solution.

More information and validation results are available in (Byun and Bar-Sever 2009) and in [IGSMAIL-6298].

The dataset includes tropospheric products for 460 stations over the full period. However, not all stations have been operating since 1995. Figure 5.2 shows the sites with more than 10 and 15 years of observations. For climate related studies (e.g. analysis of trends) a subset of 120 stations with more than 15 years of data can be selected (Bock 2016a).

The selected ZTD dataset was screened for outliers and converted to IWV using the following procedures. The screening included a range check and an outlier check for ZTD estimates and their formal errors (σ_{ZTD}) at the highest temporal resolution (5 min sampling):

- range check: ZTD ϵ [1 m, 3 m] and σ_{ZTD} ϵ [0, 6 mm],
- outlier check: ZTD ϵ median (ZTD) $\pm$ 0.5 m and formal error for σ_{ZTD} < 2.5 * median (σ_{ZTD}).

It rejected about 0.08% of all ZTD estimates.

The conversion of ZTD to IWV was done using surface pressure at the GPS sites interpolated from ERA-Interim reanalysis, pressure level data (geopotential), and weighted mean temperature (Tm) also computed from ERA-Interim reanalysis, pressure level data. The reanalysis data were bi-linearly interpolated in the horizontal

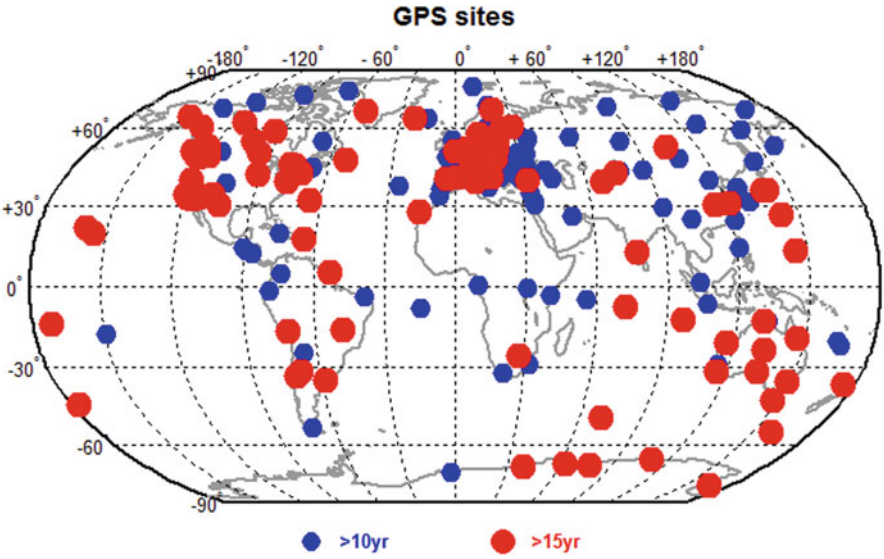

Fig. 5.2 Map of GPS stations from the IGS network for which reprocessed ZTD data are available in the IGS repro1 dataset over the period from January 1995 to December 2010

plane from the 4 grid points surrounding each GPS site. Refractivity constants from Thayer 1974, were used here. More information on the post-processing methods is given in Bock 2016b, c, d, and in Sect. 5.4 of this report.

Temporal averaging was applied to the ZTD data to reduce them from 5 min interval to 1-hourly, with at least 4 values in each 1-h bin. The conversion from ZTD to IWV was performed on the 1-hourly ZTD data at the 6-hour time interval of the reanalysis. The resulting 6-hourly GPS IWV data were further averaged to daily and monthly values. Weighted daily means were computed from the corresponding t = 00:00, 06:00, 12:00, 18:00 and 24:00 UTC estimates with half weights at the edges. The daily values were aggregated to monthly means when at least 15 days were available in a given month.

Validation of the resulting GPS IWV data was done by comparison with ERA-Interim. In order to minimize representativeness differences, the ERA-Interim IWV data were recomputed from the pressure level data at the 4 grid points surrounding each GPS site and then bi-linearly interpolated in the horizontal plane (Bock and Parracho 2019). The vertical integration of specific humidity was performed from the height (altitude) of the GPS station to the top of the atmosphere. Thanks to these precautions, good agreement was found between GPS and ERA-Interim at most sites. Figure 5.3 shows the overall mean difference and standard deviation of difference (in % of IWV) for the daily data. Ten stations are identified in this figure for which the difference is quite large. The number grows up to 14 when absolute differences are analysed. A careful analysis of the time series and comparison with independent DORIS data, helped to understand or hypothesize

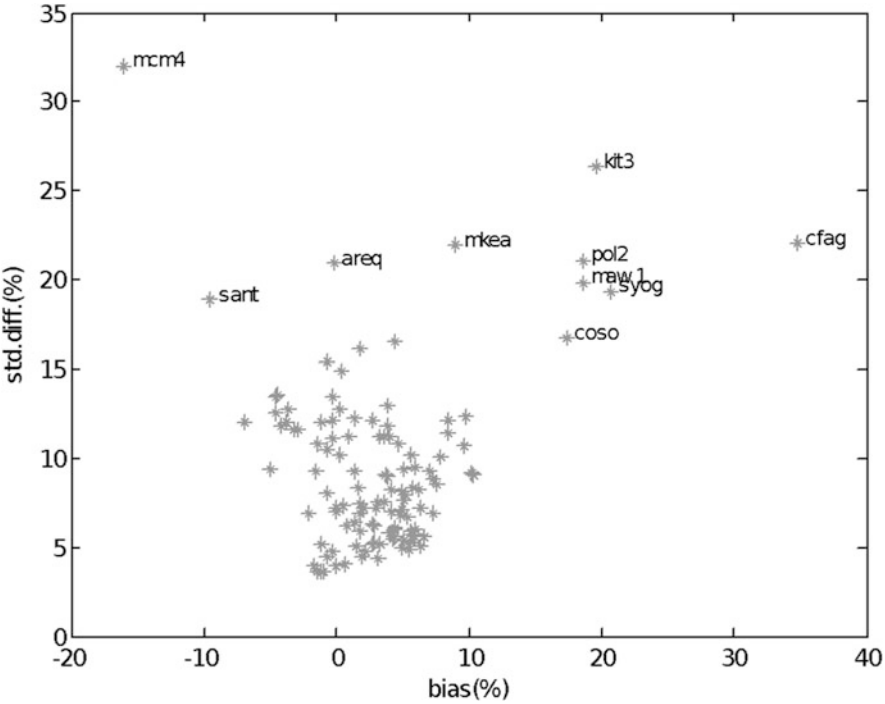

Fig. 5.3 comparison of IGS repro1 GPS IWV data and ERA-Interim reanalysis at 120 global sites: standard deviation of difference as a function of mean difference (both in % of IWV) for the daily data

the origin of the differences. In most cases, representativeness differences are suspected (Bock and Parracho 2019). Indeed, the GPS IWV is representative of a local IWV content while the ERA-Interim values is computed from 4 grid points on a $0.75° \times 0.75°$ mesh. Representativeness differences occur in regions of steep orography and in coastal regions. Absolute differences are magnified in regions and periods of high IWV contents (e.g. in the tropics or in summer), but relative difference can also be large in regions of low differences (e.g. CFAG, SANT, AREQ in the Andes mountains, MCM4, SYOG, MAW1, in Antarctica). Few sites could be detected with evidence of problems in the GPS observations or in the ZTD estimates (e.g. MCM4 in Antarctica) as days with problematic observations they would typically be rejected during the data processing and ZTD outliers by the screening procedure.

Homogeneity issues in the GPS series due to equipment changes do not show up in this figure as they are usually quite small, but they impact more strongly ZTD and IWV trend estimates, as gaps in the time series do. These issues are discussed in Sect. 5.5. Trend estimates are thus a useful diagnostic for the detection of inhomogeneities in the time series and have been used extensively by the community. The

final IWV dataset is publicly available at: ftp://ftp.climserv.ipsl.polytechnique.fr/GPS_IWV_VEGA/cost/

Citable with DOI: 10.14768/06337394-73a9-407c-9997-0e380dac5590

5.2.3 EPN Repro2 GNSS Reprocessing Campaign

R. Pacione
e-GEOS/Centro di Geodesia Spaziale-Agenzia Spaziale Italiana, Matera, MT, Italy
e-mail: rosa.pacione@e-geos.it

In Europe, in the framework of the EPN-Repro2, the second reprocessing campaign of the EPN, five Analysis Centres homogenously reprocessed the EPN network for the period 1996–2014. Both individual and combined tropospheric products (Pacione et al. 2011) along with reference coordinates and other metadata, are stored in SINEX TRO format, Gendt (1997), and are available to the users at the EPN Regional Data Centres (RDC), located at BKG (Federal Agency for Cartography and Geodesy, Germany, https://igs.bkg.bund.de/root_ftp/EPNrepro2/products/).

For each EPN station, plots on ZTD time series, ZTD monthly mean, comparison versus radiosonde data (if collocated), are publicly available at the EPN Central Bureau (Royal Observatory of Belgium, Brussels, Belgium, http://www.epncb.oma.be/_productsservices/analysiscentres/repro2.php).

The evaluation with respect to other sources or products, such as radiosonde data from the E-GVAP and numerical weather reanalysis from the European Centre for Medium-Range Weather Forecasts, ECMWF (ERA-Interim), provides a measure of the accuracy of the EPN-Repro2 ZTD combined products.

The assessment of the EPN Repro1 (Voelksen 2011) and Repro2 with respect to the radiosonde data has an improvement of approximately 3–4% in the overall standard deviation. The assessment of the EPN Repro1 and Repro2 with respect to the ERA-Interim re-analysis showed the 8–9% improvement of the latter over the former in both overall standard deviation and systematic error, which was obvious for the majority of the stations.

The EPN-Repro2 data record can be used as a reference for a variety of scientific applications and has a high potential for monitoring trend and variability in atmospheric water vapour, improving the knowledge of climatic trends of atmospheric water vapour and being useful for regional Numerical Weather Prediction (NWP) reanalyses as well as climate model simulations.

For five EPN stations, among those with the longest time span, GOPE (Ondrejov, Czech Republic, integrated in the EPN since 31-12-1995), METS (Kirkkonummi, Finland, integrated in the EPN since 31-12-1995), ONSA (Onsala, Sweden, integrated in the EPN since 31-12-1995), PENC (Penc, Hungary, integrated in the EPN since 03-03-2096) and WTZR (Bad Koetzting, Germany, integrated in the EPN since 31-12-1995), we have computed ZTD trends using EPN Repro2, EPN Repro1 completed with the EUREF operational products, radiosonde and ERA-Interim data.

All of them are also in the IGS Network, for which IGS Repro1 completed with the IGS operational products are available and extracted from the GOP-TropDB. We have screened all data sets (classical 3 sigma). Then for all GPS ZTD data sets we have estimated and removed shifts related to the antenna replacement. No homogenization has been done for radiosonde data since radiosonde metadata are not available. A LSE method is applied to estimate trends and seasonal component. ZTD trends for all three GPS ZTD data sets are consistent, as soon as the same homogenisation procedure is applied. Then overall RMS is 0.02 mm/year. Among all five ZTD sourced, we find the best agreement for ONSA (RMS = 0.04 mm/year) and WTZR (RMS = 0.02 mm/year). For PENC we have good agreement with respect to ERA-Interim (0.05 mm/year), but a large discrepancy versus radiosonde (−0.31 mm/year). This large discrepancy is probably due to the distance to the radiosonde launch site (40.7 km, radiosonde code 12843) and to the lack of the homogenisation stage. For the five considered stations, the agreement with respect to ERA-Interim (RMS = 0.11 mm/year) is better than that with respect to radiosonde (RMS = 0.16 mm/year) even though the EPN Repro2 does not change significantly the detection of ZTD trends, it has a better agreement with respect to radiosonde and ERA-Interim data than EPN Repro1. It has also the best spatial resolution compared to IGS Repro1 and radiosonde data, which are used today for long-term analysis over Europe. Taking into account the good consistency among trends, EPN Repro2 can be used for trend detection in areas where other data are not available (Fig. 5.4).

The reprocessing activity of the five EPN ACs is a very large effort generating homogeneous products not only for station coordinates and velocities, but also for tropospheric products. The knowledge gained will certainly help for future reprocessing activities which will most likely include Galileo and BeiDou and therefore will be started some years from now after having successfully integrated these new data into the current operational near real-time and daily EUREF products. The consistent use of identical models in various software packages is another challenge for the future to be able to improve the consistency of the combined solution. Prior to any next reprocessing, it was agreed in EUREF to focus on

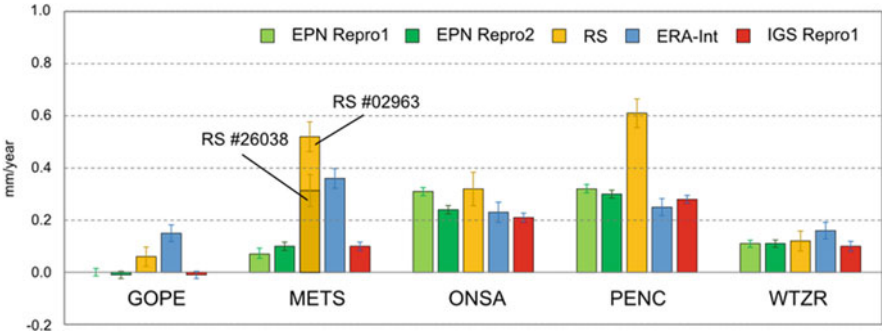

Fig. 5.4 ZTD trend comparisons at five EPN stations. The error bars are the formal error of the trend values

cleaning and documenting data in the EPN historical archive, as it should highly facilitate any future work. For this purpose, all existing information needs to be collected from all the levels of data processing, combination and evaluation which includes initial GNSS data quality checking, generation of individual daily solutions, combination of individual coordinates and ZTDs, long-term combination for velocity estimates and assessments of ZTDs and gradients with independent data sources. A detailed description of the EPN-Repro2 campaign is reported in Pacione et al. (2017).

5.2.4 VLBI Reprocessing Campaign

K. Balidakis
GFZ German Research Centre for Geosciences, Potsdam, Germany
e-mail: balidak@gfz-potsdam.de

R. Heinkelmann
GFZ German Research Centre for Geosciences, Potsdam, Germany
e-mail: rob@gfz-potsdam.de

R. T. Nilsson
GFZ German Research Centre for Geosciences, Potsdam, Germany
e-mail: jan.tobias.nilsson@gfz-potsdam.de

H. Schuh
GFZ German Research Centre for Geosciences, Potsdam, Germany
e-mail: harald.schuh@gfz-potsdam.de

For the sake of comparison and validation of long-term GNSS atmospheric parameters within the EU COST Action GNSS4SWEC zenith total and wet delays (ZTD, ZWD) and gradients (NS, EW) were provided from a GFZ VLBI solution employing VieVS@GFZ software (Nilsson et al. 2015) with high temporal resolution: 10 min for the zenith delays and 1 hour for gradients.

Since all VLBI stations run under IVS (International VLBI Service for Geodesy and Astrometry) are co-located with GNSS, the solution includes all VLBI stations in the common GNSS-VLBI time span: 1995.0–2013.0. Currently the Analysis Centres (AC) of the IVS apply different analysis strategies e.g., mapping functions and meteorological data sets for the analysis of atmospheric parameters what hinders the determination of a homogeneous long-term combined solution.

For the climate applications foreseen in WG3 of this COST action, it is of specific importance to apply consistent models and in particular long-term homogenized meteorological data. Thus, analytical models of this solution largely adhere to IERS Conventions (Petit and Luzum 2010). In principle a long-term homogenized data set of in-situ observed meteorological variables, atmospheric pressure and temperature, would be the best input for climate studies. For the sake of comparison with GNSS,

however, we used GPT2 model values instead because this model is available for GNSS solutions as well.

The data set was uploaded to the Pecný Observatory's ftp server.

5.2.5 *DORIS Reprocessing Campaign*

O. Bock
IGN Institut national de l'information géographique et forestière, Paris, France
e-mail: olivier.bock@ign.fr

P. Willis
IGN Institut national de l'information géographique et forestière, Paris, France
e-mail: pascal.willis@ipgp.fr

A high quality, consistent, global, long-term dataset of ZTD and IWV estimates was produced from Doppler Orbitography Radiopositioning Integrated by Satellite (DORIS) measurements at 81 sites (Bock et al. 2014). The DORIS Doppler observations were processed using GIPSY-OASIS II software package (Zumberge et al. 1997) with the same strategy as the one used by Bock et al. [2010] but over a longer period of time (January 1993 to August 2008). Compared to previous releases, this strategy (referred to as ignwd08 (Willis et al. 2012) uses an improved method for mitigating errors in solar radiation pressure models (Gobinddass et al. 2009) and atmospheric drag corrections (Gobinddass et al. 2010) (Fig. 5.5).

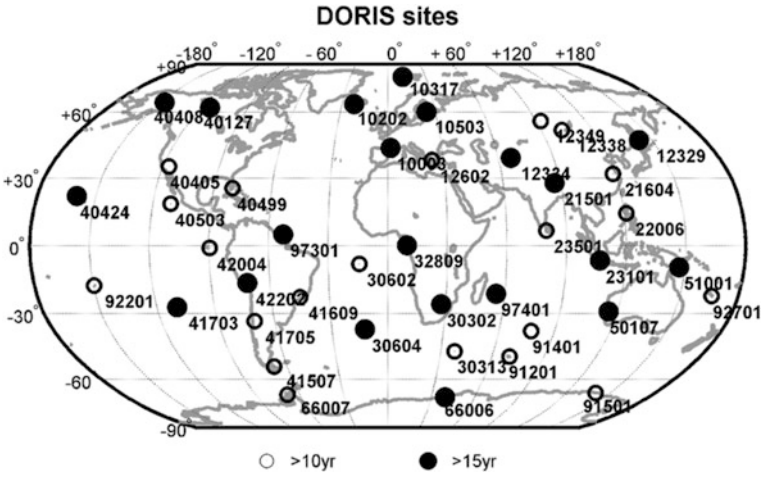

Fig. 5.5 Map showing the locations of DORIS sites with more than 10 years (42 sites) and with more than 15 years (21 sites) over the period from January 1993 to August 2008 used in Bock et al. 2014. The historical DORIS data cover the period from 1990 to present, for which 27 sites have more than 20 years of data

The ZTD dataset was screened using range checks and outlier checks were applied to ZTD and formal error estimates (see Sects. 5.2.2 and 5.4.1). Further quality check and validation was done by comparing DORIS ZTD with ECMWF reanalysis (ERA-Interim) data. The outlier checks rejected 3% of the data, while the ERA-Interim comparison further rejected 1% of data based on a normality test. A linear drift was evidenced in the screened DORIS ZTD data compared to ERA-Interim and to the IGS repro1 GPS ZTD data (Sect. 5.2.2), which was associated to the progressive replacement of Alcatel antennas with Starec antennas at the DORIS sites. The DORIS IWV data was homogenized by applying a bias correction computed from comparison with ERA-Interim data, each time station equipment was changed (mostly for antenna replacement). The homogenized DORIS data showed excellent agreement with the GPS data (correlation coefficient of 0.98 and standard deviation of differences of 1.5 kg/m^2). Comparison with ERA-Interim and satellite IWV data was also quite good (correlation coefficient > 0.95 and standard deviation of differences <2.7 kg/m^2). The agreement with radiosonde data was less good, however. Preliminary results of IWV trends and variability at 31 sites with more than 10 years of data showed good consistency between DORIS, ERA-Interim, and GPS. This study demonstrated the high potential of the DORIS IWV data for climate applications. This DORIS IWV dataset is public available at: http://onlinelibrary.wiley.com/doi/10.1002/2013JD021124/

Later improvements in the DORIS processing procedure are related to zenith tropospheric gradients estimation strategies, for example when estimating such parameters on an hourly basis, instead of once a day as before (Willis et al. 2014; Heinkelmann et al. 2016), to the use of more recent DORIS satellites, such as Jason2 (Willis et al. 2016a), and trying to cope with the effect on the on-board oscillator when passing over the South Atlantic Anomaly region (SAA) around South America, and to the realization of an updated version of the DORIS terrestrial reference frame, known as DPOD2008 (Willis et al. 2016b), and to its newest version (DPOD2014), aligned on the ITRF2014 (Altamimi et al. 2016).

Following the availability from CNES of antenna correction models (corrections in azimuth and elevation) derived from anechoic chamber measurements for the Starec antennas (newer type), we reprocessed the DORIS data, showing a better consistency in ZTD between Starec and Alcatel antennas results. The bias observed in the first results (Bock et al. 2010) was decreased, thanks to this new type of corrections, frequently used for GNSS receivers. For Alcatel antennas (the older ones), as no anechoic measurements could be performed by then, we used phase centre correction models provided by the manufacturers.

Finally, the use of the new DORIS/RINEX format, providing DORIS phase and pseudorange instead of previously destructive integrated Doppler data, for the most recent satellites was investigated using the current JPL software (GIPSY/OASIS II) used for all the above results. New developments are currently on-going to incorporate the DORIS data processing capability to the most recent JPL software package (GipsyX), in addition to the current GNSS data (GPS, GLONASS, Galileo and BeiDou), to the Satellite laser ranging (SLR) data and, in the future to the VLBI data as well as other type of data.

5.3 Sensitivity Studies on GNSS Processing Options

5.3.1 An Overview of the GNSS Data Processing Strategies

K. Stępniak
Advanced Methods for Satellite Positioning Laboratory, University of Warmia and Mazury in Olsztyn, Olsztyn, Poland
e-mail: katarzyna.stepniak@uwm.edu.pl

R. Pacione
e-GEOS/Centro di Geodesia Spaziale-Agenzia Spaziale Italiana, Matera, MT, Italy
e-mail: rosa.pacione@e-geos.it

Ground-based GNSS data can be processed according to the standard technique of network adjustment or in Precise Point Positioning mode (Zumberge et al. 1997). Advantages and disadvantages of both processing techniques are reported in Guerova et al. (2016) and in the next subsection.

In this subsection we describe how GNSS data are processed in the framework of the EUREF (http://www.euref.eu/) Permanent Network (EPN, http://www.epncb.oma.be) (Bruyninx et al. 2012), being the reference for best practices in Europe concerning data management and data processing.

The EPN is a science-driven network of continuously operating GNSS reference stations, covering the European continent, and with precisely known coordinates. All contributions to the EPN are voluntary, with more than 100 European agencies/universities involved and the reliability of the network is based on redundancy. Since 1996, GNSS data collected at approximately 300 operating stations of EPN have been routinely analysed by 16 EPN Analysis Centres (ACs). The strategy to analyse EPN observations is in accordance with the so-called distributed processing approach. Each EPN AC processes the observations of a dedicated sub-network of EPN stations and, in order to guarantee the redundancy of the estimates, the same station is processed by at least 3 ACs. Each AC estimates daily and weekly station coordinates and station zenith tropospheric path delays for its own EPN sub-network that are later combined by the EPN Analysis Centre Coordinator and by the EPN Tropospheric Coordinator in order to deliver the EPN official product. Processing strategies used by all ACs are followed consistent with the general EUREF recommendations included in "Guidelines for the EPN Analysis Centres" prepared by the EPN Coordination Group and the EPN Central Bureau, (http://www.epncb.oma.be/_documentation/guidelines/guidelines_analysis_centres.pdf). The EPN ACs rely on a network approach and 15 over 16 processes data with Bernese GNSS Software v.5.2 (Dach et al. 2015) while only one AC uses GIPSY-OASIS II Software (Webb and Zumberge 1997). All systematic errors are modelled according to IERS Conventions 2010 (Petit and Luzum 2010). For the final solution, in order to obtain the highest precision and accuracy, the IGS final precise satellite orbits, clocks, and earth rotation parameters are applied. Also, azimuth/elevation-

dependent phase centre variations and offsets from IGS, including individual phase centre corrections, are used for ground and satellite antennas. It is also mandatory to include second order of ionospheric corrections and ionospheric ray bending corrections to minimize the impact of ionospheric delays on station estimates. For tropospheric modelling, half of the ACs apply Global Mapping Function (GMF; Boehm et al. 2006a) and the remaining Vienna Mapping Function (VMF1; Boehm et al. 2006b) along with Chen-Herring gradient model (Chen and Herring 1997) for the Bernese solution while in GIPSY-OASIS, gradients are modelled according to Bar-Sever et al. (1998). These mapping functions go along with specific a priori zenith hydrostatic and wet delay models: GPT (an empirical model based on ERA-40 reanalysis, Boehm et al. 2007) is recommended with GMF whereas gridded a priori delay models computed from ECMWF operational analysis are recommended with VMF1 (Boehm et al. 2006b). More recently, the group from the Technical University of Vienna released two updates of the GPT empirical model: GPT2 (Lagler et al. 2013) and GPT2w (Böhm et al. 2015).

At the last EPN Analysis Centres (AC) Workshop held in Brussels in October 2017, it was agreed that all EPN must use the Vienna Mapping Function. In the Bernese software, the ZTD parameters are modelled as piecewise linear functions of time and usually estimated at 1-hourly intervals and the tropospheric gradients are estimated every 24 hours, with absolute and relative constraints of 5 m. In GIPSY-OASIS II software wet zenith delay is modelled with a sampling rate of 5 min as random walk with unconstrained a priori and a random walk sigma. In processing strategies of some ACs, ambiguity resolution is performed by using the quasi-ionosphere-free (QIF) strategy in conjunction with regional TEC information. However, most of ACs follow the recommended procedure with Bernese software which applies several methods depending on the length of baselines. Ambiguities are resolved in a baseline-by-baseline mode, fixed to integer values and introduced in the final network solution. In most of ACs in the network processing, independent baselines are defined by the criterion of maximum common observations. More details can be found at: http://www.epncb.oma.be/_productsservices/analysiscentres/LAC.php.

5.3.2 *Software Agreement*[2]

R. Pacione
e-GEOS/Centro di Geodesia Spaziale-Agenzia Spaziale Italiana, Matera, MT, Italy
e-mail: rosa.pacione@e-geos.it

The agreement among different GNSS SW package has been investigated in the framework of the second EPN Reprocessing Campaign where the three main GNSS

[2]Parts from this section were previously published in Pacione et al. (2017).

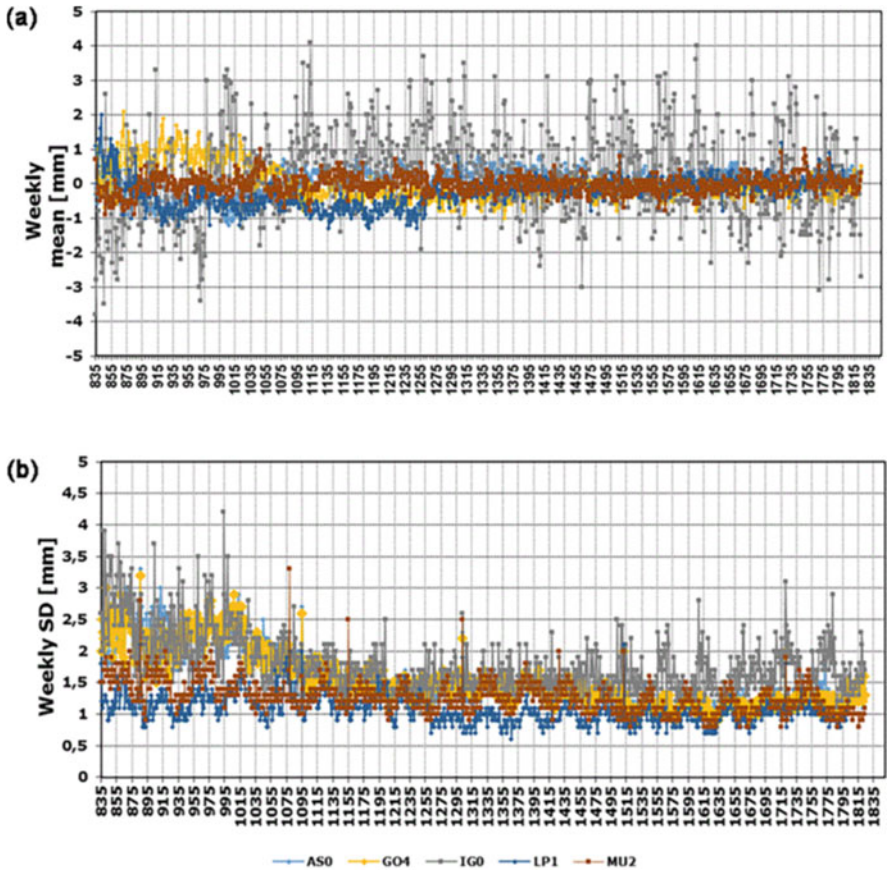

Fig. 5.6 Weekly mean ZTD biases (**a**) and standard deviations (**b**) of each contributing solution with respect to the final EPN-Repro2 combination

software packages, Bernese (Dach et al. 2015), GAMIT (King et al. 2010) and GIPSY-OASIS II (Webb and Zumberge 1997), have been used to reprocess the whole EPN network.

The agreement in terms of the standard deviation with respect to the combination (see Figure below) is below 3 mm before GPS week 1055 (26 March 2000) and 2 mm thereafter. This is related to the worse quality of data and products during the first years of the EPN/IGS activities (Fig. 5.6).

All the details about the combination procedure are reported in Pacione et al. (2011) and Pacione et al. (2017).

5.3.3 PPP vs. DD Processing Modes[3]

K. Stępniak
Advanced Methods for Satellite Positioning Laboratory, University of Warmia and Mazury in Olsztyn, Olsztyn, Poland
e-mail: katarzyna.stepniak@uwm.edu.pl

Two approaches of GNSS data processing can be used to estimate ZTD: relative and precise point positioning (PPP). Relative processing mode uses double-difference observations from a network of stations, while PPP uses zero-difference observations from a single station. Relative processing is usually considered as being more precise, but not necessarily more accurate and more stable. Indeed, the network configuration (extent and geometry of the baselines) can have a significant impact on estimated parameters in double-difference processing. PPP is an absolute technique since there is no propagation of errors between stations. However, the accuracy of data processing in PPP mode depends strongly on the quality of external products: satellite orbits and clocks. It should be noted that currently very accurate products are not available in real time (e.g. for now-casting weather applications). This is one of reasons why most of E-GVAP analysis centres use double-difference processing where the dependency on the clock products is much smaller. Data processing in PPP mode is a faster method than the DD solution, because only the observations for the stations of interest are processed while in relative processing additional stations are required to form long baselines and reduce the correlation between tropospheric parameters.

Many researches have used tropospheric delay estimates from DD and PPP strategies in the context of weather and climate studies. Ahmed et al. (2014) observed that for globally distributed stations the RMS of the difference between the ZTD estimates from PPP and DD solutions has a latitude dependence and is largest at the equator and smaller in high latitudes (Fig. 5.7a). A latitude dependence of the bias between the PPP and DD ZTD estimates is shown in Fig. 5.7. It is commonly observed that discrepancies are larger at the equator, where the higher concentration of atmospheric water vapour occurs, than in mid-to-high latitudes.

Stępniak et al. (2016) discussed the impact of network design strategy on the quality and homogeneity of relative (double difference) strategy and comparison to absolute PPP solutions. In order to compare PPP and DD solutions, the ZTD estimates were computed using both processing techniques and the same processing options were set. Figure 5.8 shows long time series of ZTD estimates and formal error of ZTD for DD and PPP strategies and a zoom on a period when ZTD outliers

[3]Parts from this section were previously published in Ahmed et al. (2014).

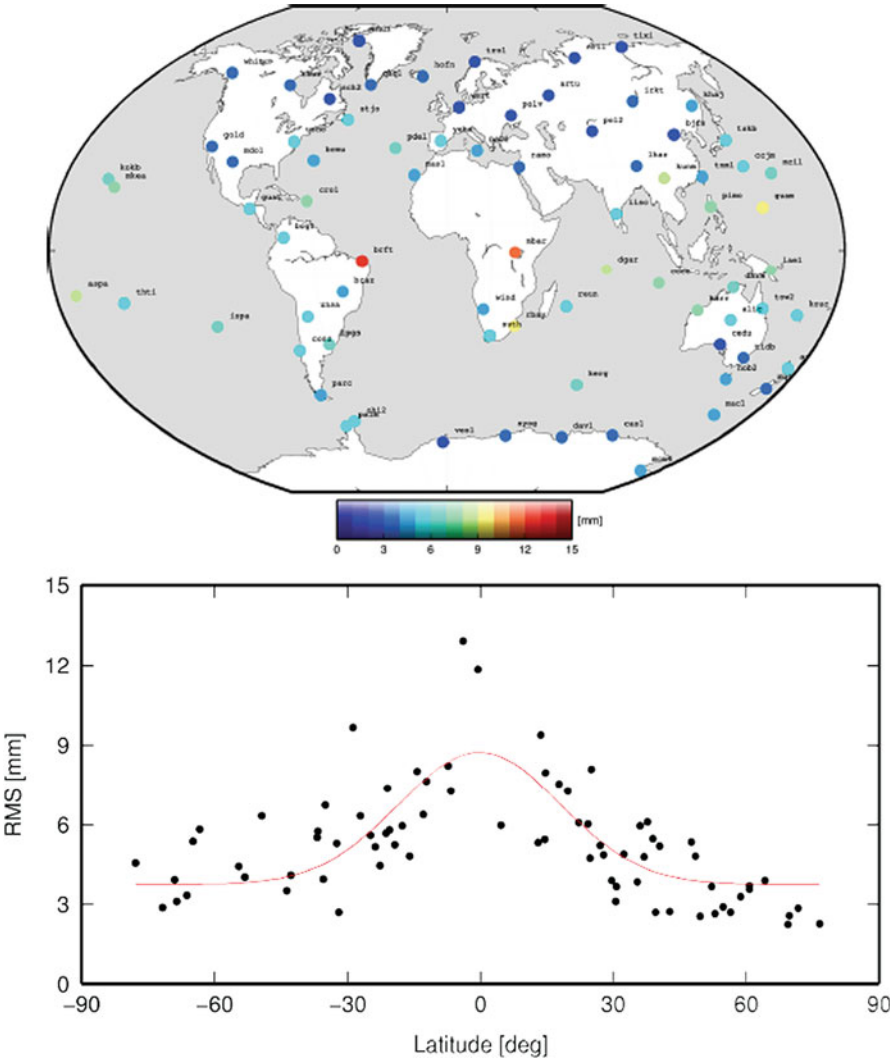

Fig. 5.7 (top) Station-wise RMS of the difference between the ZTD from PPP and DD solutions; (bottom) Distribution of the RMS difference (Gaussian fit in red) with respect to latitude

can be observed in DD solution. These outliers are due to very few observations in common with other stations in baseline and are not seen in PPP ZTD time series. It can be assumed that PPP might be an interesting alternative to prevent outliers arising from defects in the baseline geometry in a double-difference processing.

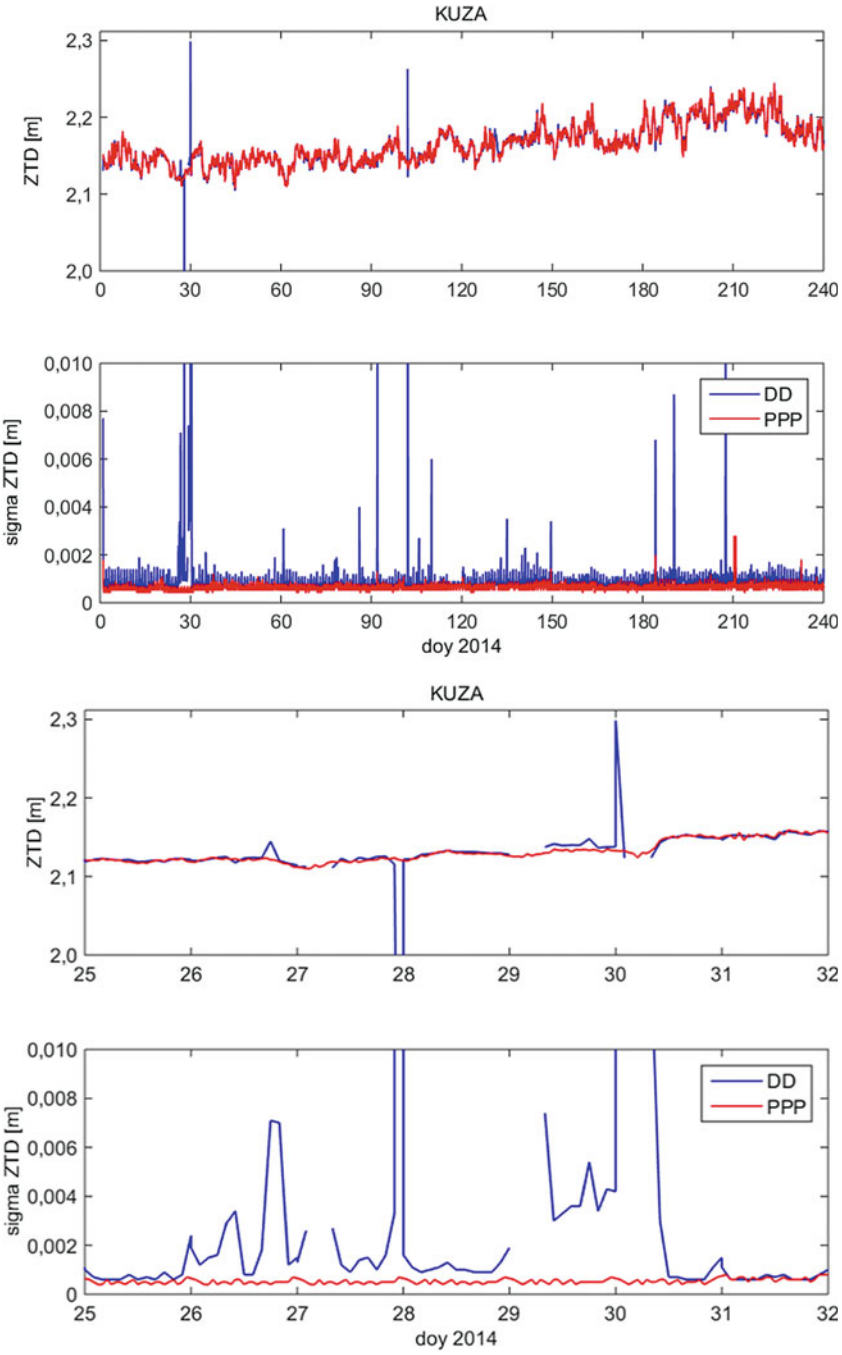

Fig. 5.8 Comparison of ZTD estimates and formal error for the DD and PPP solutions; (top) all year 2014 (bottom) Zoom on a period (end of January 2014) when the DD solution has outliers due the geometry of the network

5.3.4 *Baseline Strategy in DD Processing*[4]

K. Stępniak
Advanced Methods for Satellite Positioning Laboratory, University of Warmia and Mazury in Olsztyn, Olsztyn, Poland
e-mail: katarzyna.stepniak@uwm.edu.pl

The baseline design strategy in a double-difference network processing has a strong impact on the quality and continuity of ZTD time series. Stępniak et al. (2017) show that ZTD outliers are most of the time caused by sub-daily data gaps at reference stations which provoke disconnections of clusters of stations from the reference network and common–mode biases due to the strong correlation between stations in short baselines. Outliers can reach a few centimetres and more in ZTD and coincide usually with a jump in formal errors. The magnitude and sign of these biases are impossible to predict, because they depend on different errors in the observations and on the geometry of the baselines. Therefore, an alternative baseline strategy for GNSS data from moderate-size network (e.g. national scale) was developed that ensures that all the stations remain connected to the main reference network (Stępniak et al. 2017). The main ingredients of this strategy are: apply a selection of the reference stations based on results from an initial processing, connect the other stations only to stations of the reference network and not between them, and introduce redundancy in the baselines. As an example, the results of this new processing strategy are compared to the standard one and to obs-max in Table 5.1. In the standard solution, a pre-defined network is composed of a skeleton of reference stations to which secondary stations are connected in a star-like structure; in the second variant the same network was processed using Bernese obs-max strategy; and the third variant is the alternative/new baseline strategy. Columns 3 and 4 in Table 5.1 report the numbers of stations for which the standard deviation

Table 5.1 Statistics of ZTD estimates and formal errors for three processing variants computed over 104 common stations, one year of GPS data

No.	Solution	Times Max STD(ZTD)	Times Max STD(sigma)	Rejected data	Used data	Mean STD (ZTD)	Mean STD (sigma)
1	Pre-defined	54	84	1453	466,487	0.0129 m	0.00040 m
2	Obs-max	43	18	696	**470,824**	0.0127 m	0.00031 m
3	New	**7**	**2**	**668**	468,705	**0.0124 m**	**0.31 m**

Column 2 (resp. 3) gives the number of stations for which the standard deviation of ZTD (resp. sigma) is maximal among the three solutions (e.g. STD (ZTD) of the pre-defined solution is maximal 54 times out of 104)

[4]Parts from this section were previously published in Stepnaik et al. (2017).

of ZTD and formal error are the largest among all: the new solution has the largest ZTD variations at only 7 sites, whereas obs-max has the largest number at 43 sites and the pre-defined solution at 54 sites. The number of rejected ZTDs (and thus the number of used ZTDs) are very similar between the new and obs-max strategies (columns 5 and 6), and the mean standard deviations of ZTD and formal errors (columns 7 and 8) are slightly smaller for the new/alternative solution, i.e. this solution is more stable and more accurate. The only spikes remaining in the ZTD series in the new solution are due to small number of observations or short gaps at sub-regional stations. Therefore, it is still necessary to apply a post-processing screening procedure to provide a clean ZTD dataset.

This study shows that many outliers can be avoided using the new baseline strategy. The strategy is well adapted to post-processing when the network can be optimized by successive processing tests, e.g. to get the most stable time series (what is important for climate applications), but also for NRT applications when e.g. national networks are processed in DD – then adopting the star design would help avoiding the disconnections and large outliers.

5.3.5 Mapping Functions[5]

5.3.5.1 Tests with DD and PPP Processing of GNSS Data

Z. Bałdysz
Centre of Applied Geomatics, Warsaw Military University of Technology, Warszawa, Poland
e-mail: zbaldysz@wat.edu.pl

G. Nykiel
Centre of Applied Geomatics, Warsaw Military University of Technology, Warszawa, Poland
e-mail: grzegorz.nykiel@wat.edu.pl

M. Figurski
Centre of Applied Geomatics, Warsaw Military University of Technology, Warszawa, Poland
e-mail: mfigurski@wat.edu.pl

Mapping function plays a key role in GNSS observations processing. It delivers a priori ZTD value, which is often identified as a ZHD value. This results from the fact that the hydrostatic part of the atmosphere is subject to relatively minor changes in time and therefore is easy to model. Consequently, in GNSS processing, next to the humidity delay, also correction to this value is estimated. Therefore, no matter what kind of mapping function would be applied, the final ZTD value should be the same

[5]Parts from this section were previously published in Bałdysz et al. (2016).

for all solutions, through proper estimation of these corrections. Nowadays, the most common used mapping functions are GMF (Global Mapping Function) (Boehm et al. 2006a) and VMF1 (Vienna Mapping Function1) (Boehm et al. 2006b). For some time, also an extension of NMF (Niell Mapping Function) (Niell 1996), IMF (Isobaric mapping Function) (Niell 2000), was used. As it was mentioned, theoretically all functions should return the same ZTD value, which practically does not happen in reality. Vey et al. (2006) has verified this by comparing results from NMF and IMF. On the basis of one year of data, the mean ZTD difference between these two functions was at the level of 5 mm. Steingerberger et al. (2009) have analysed GMF and VMF1. They focused mostly on coordinates, however they found out that an improper estimation of a priori ZHD value translates also into discrepancies in coordinate solutions. Bałdysz et al. (2016) have shown that they are also differences in long-term changes between consecutive reprocessings of EPN, which inter alia may result from using various mapping functions. To verify the possible impact of mapping functions on short and long time changes of ZTD parameter, an additional reprocessing of EPN was conducted.

Firstly, in Bernese 5.2 software we reprocessed 18 years of data both in DD and PPP mode. Each of these approaches was conducted two times, with applying only one change in the processing scheme: the mapping function. In the first one GMF was used, whereas in the second one VMF1 was used. In term of short-time changes like annual and semi-annual amplitudes, only negligible changes occurred between the compared solutions, as it can be seen on the Fig. 5.9 (annual amplitudes) and Table 5.2.

From the point of view of climate monitoring the most important parameters are the long–time changes, which will be described here by a linear trend. Therefore, for our 18-years time span of data, we also calculated the linear trend values. Similar to

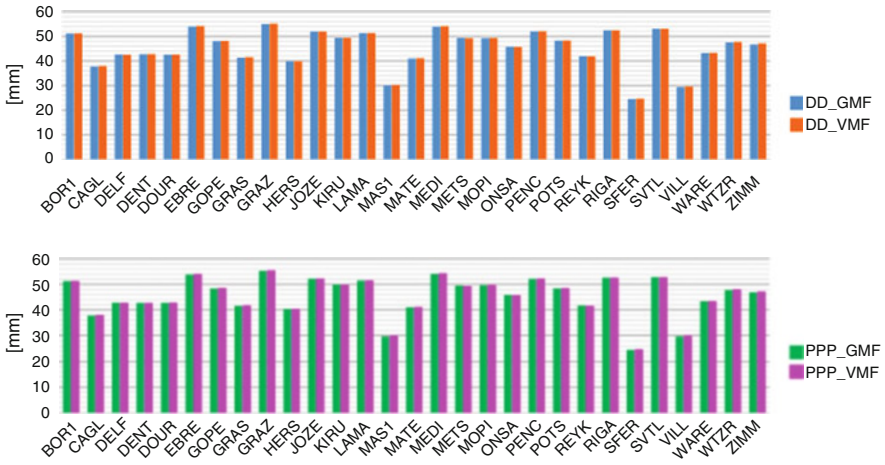

Fig. 5.9 Comparison of annual amplitude between GMF and VMF1 for double difference (top) and precise point positioning (bottom) modes

Table 5.2 Statistics of ZTD annual amplitude, semi-annual amplitude and trends differences between GMF and VMF in DD and PPP mode

	Annual amplitude [mm]		Semi-annual amplitude [mm]		Linear trend [mm/year]	
Statistics	DD_GMF-DD_VMF	PPP_GMF-PPP_VMF	DD_GMF-DD_VMF	PPP_GMF-PPP_VMF	DD_GMF-DD_VMF	PPP_GMF-PPP_VMF
Min	−0,45	−0,31	−0,40	−0,42	−0,03	−0,02
Max	0,12	0,19	0,30	0,34	0,02	0,01
Mean	−0,09	−0,07	−0,17	−0,16	0,00	0,00
SD	0,12	0,13	0,16	0,17	0,01	0,01

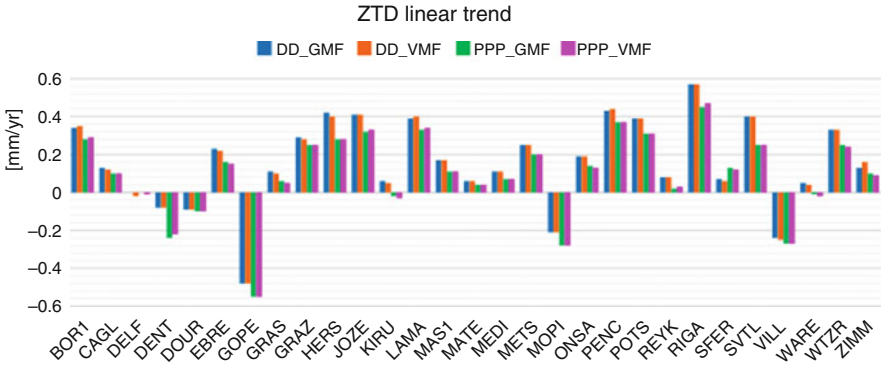

Fig. 5.10 Linear trend values from 18-years ZTD time series and four analysed strategies, obtained in Bernese software

the annual amplitude, the trend differences between the solutions obtained from these two mapping functions were very small. This was true both for DD and PPP approaches. We can therefore state that in case of Bernese software, using GMF or VMF1 both in DD and PPP mode does not introduce large differences in the obtained results. This is despite the fact that there are differences between these both approaches, as it can be found on Fig. 5.10.

In Table 5.2 there is a statistical summary of differences in seasonal components between DD and PPP solutions, as well as differences in linear trend values. As can be noted, discrepancies in annual and semi-annual amplitudes were less than 0.5 mm. In case of the PPP approach, standard deviations of both these components was only slightly higher than in DD solutions, but at the same time, its absolute mean values were smaller. Differences in linear trends were negligible, as both the mean value of differences and its standard deviations were the same in DD and PPP approach.

5.3.5.2 Tests for EPN Repro2 at GOP

J. Douša
Geodetic Observatory Pecný, RIGTC, Ondřejov, Czech Republic
e-mail: jan.dousa@pecny.cz

Douša et al. (2017a, b) compared two solutions with different mapping functions for 172 stations in Europe: GO0 (legacy repro1 using GMF, 3°) and GO1 (repro2 using VMF, 3°). GO1 improves slightly the coordinate repeatability. The change in mean ZTD is about −0.36 mm (GO1 ZTD estimates are slightly lower) and the standard deviation of differences is about 2.0 mm. In terms of ZTD trends, the mean difference is about 0.36 mm/decade, with extreme values of −1.18 mm/decade and 0.45 mm/decade.

5.3.5.3 Tests with VLBI Data

K. Balidakis
GFZ German Research Centre for Geosciences, Potsdam, Germany
e-mail: balidak@gfz-potsdam.de

We tested the impact of mapping functions and a priori zenith delay data on VLBI-derived baseline length, tropospheric parameters and derived products (e.g. IWV trends) using the Potsdam Mapping Factor (PMF) concept (Zus et al. 2014) and a new a priori zenith delay empirical model called GFZ-PT (Balidakis et al. 2018). The PMF coefficients have been estimated based on 6-hourly 0.5° ERA Interim reanalysis fields. In contrast to VMF1 where only the "a" coefficients are calculated epoch-wise, PMF provides "b" and "c" coefficients in addition, thus improving the elevation-dependent fit. The change in height estimates between the VMF1 and PMF is in the range − 2 to +2 mm, globally.

GFZ-PT is an empirical model for pressure, temperature, relative humidity, zenith delays, mapping function coefficients (a, b, c), gradient components of first and second order, and water vapour-weighted mean temperature. In essence, it is a fit at annual, semi-annual, inter-annual, diurnal, semi-diurnal, and inter-diurnal frequencies – linear trend included – to ray-tracing products as well as other parameters. The seasonal signals and trend stem from ERA Interim, and the high-frequency signals are estimated from hourly ERA5.

Owing to its more rigorous parametrization, PMF is slightly more accurate than VMF1, in terms of the assembled slant delays. Despite the fact that changing the mapping function affects the scale of the geodetic networks from the different VLBI analysis set-ups (mm level), no significant relative errors appear in the estimated IWV rates. Therefore, PMF, GFZ-PT or VMF1 may be used interchangeably in this regard (Fig. 5.11).

The ZHD is mainly a function of pressure and as such is prone to inhomogeneities in the related observations. We have addressed the impact of using several different

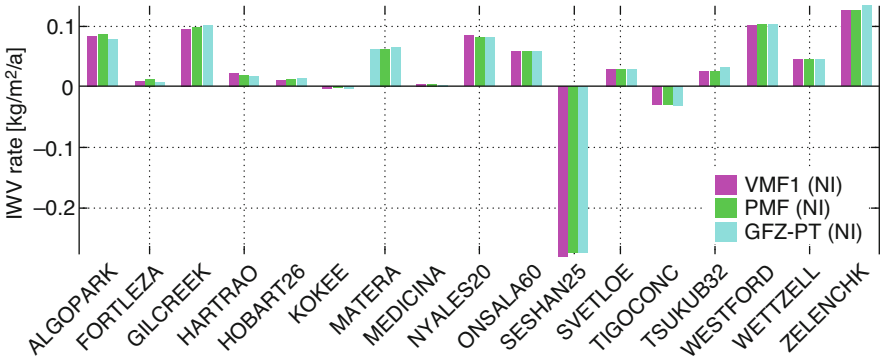

Fig. 5.11 IWV rates from the VLBI solutions where the mapping functions were alternated. NI stands for numerical integration, which was used to obtain the water vapour-weighted mean temperature. Shown are the stations with long observation record and statistically significant trends

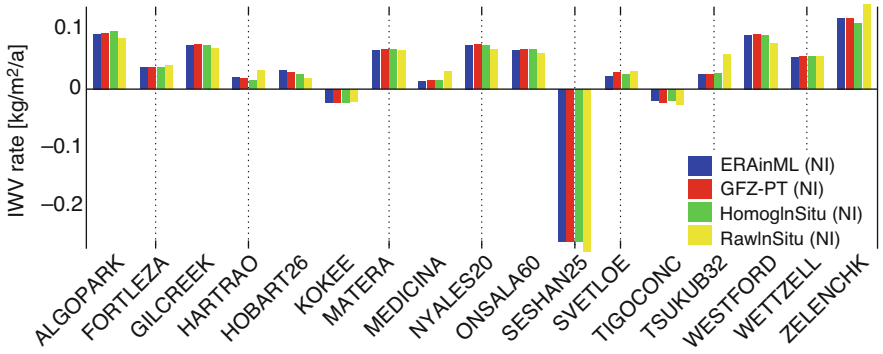

Fig. 5.12 IWV rates from the VLBI solutions where the meteorological data were alternated. NI stands for numerical integration, which was used to obtain the water vapour-weighted mean temperature. Shown are the stations with long observation record and statistically significant trends

pressure and ZHD datasets on the VLBI results: raw in-situ meteorological observations recorded at VLBI stations, the same observations but homogenized, ERA Interim reanalysis, and GFZ-PT. The raw in-situ meteorological observations have been homogenized employing the penalized maximal t-test and series from the model levels of ERA Interim reanalysis (ERAinML) as a reference (Balidakis et al. 2018) (Fig. 5.12).

Using meteorological data homogenized in such a manner for VLBI analysis improves the baseline length repeatability due to improved a priori zenith delays (mainly) and thermal deformation (secondary). However, more appropriate ZHD applied a-posteriori, compensate for most cases.

5.3.6 Trends in the IWV Estimated from Ground-Based GPS Data: Sensitivity to the Elevation Cutoff Angle[6]

T. Ning
The Swedish Mapping, Cadastral and Land Registration Authority, Stockholm, Sweden
e-mail: tong.ning@lm.se

G. Elgered
Chalmers University of Technology, Göteborg, Sweden
e-mail: gunnar.elgered@chalmers.se

The observations acquired from the ground-based GNSS stations may contain the inconsistencies due to effects of signal multipath, which are highly elevation dependent. The multipath effects are worse for observations at low elevation angles. Therefore, the selection of the elevation cutoff angle used in the GNSS data processing can have a significant impact on the resulting trend in the atmospheric integrated water vapour content (IWV). Using 14 years of data from 12 GPS sites in Sweden and Finland, Ning and Elgered (2012) found that a higher elevation cutoff angle (25°) gives the best agreement between the GPS-derived IWV trends and the ones obtained from profiles measured by radiosondes at nearby launching sites.

In a more recent study (Ning et al. 2017) the problem was readdressed by using 20 years of GPS data from 13 sites in Sweden and Finland, and applying two different elevation cutoff angles, 10° and 25°, to estimate the atmospheric IWV. The estimated linear trends in the IWV were compared to the corresponding trends from radiosonde data at 7 nearby (< 120 km) sites and the trends given by the European Centre for Medium-Range Weather Forecasts (ECMWF) reanalysis data (ERA-Interim).

The results show that due to the larger formal errors of the individual IWV estimates a larger standard deviation is seen in the IWV difference between the GPS elevation 25° solution and the other two techniques. However, such larger formal error is not the limiting factor for the uncertainty of the estimated IWV trend. Figure 5.13 shows similar correlation coefficients of 0.74 and 0.71 when comparing the trends obtained from the GPS elevation cutoff angle 25° and 10° solutions with the ones obtained from the radiosonde data. A significantly higher correlation is seen for the GPS 25° solution compared to the 10° solution when the two are compared to the IWV trends given by the ERA-Interim data. The study indicates that using different elevation cutoff angles is a valuable diagnostic tool that can be used for the validation purpose and detection of possible multipath impacts. When using GPS data to monitor the long-term change of the IWV, e.g. as linear trends, it is recommended to apply at least two significantly different elevation cutoff angles

[6]Parts from this section were previously published in Douša et al. (2017a, b), Balidakis et al. (2018) and Ning et al. (2017).

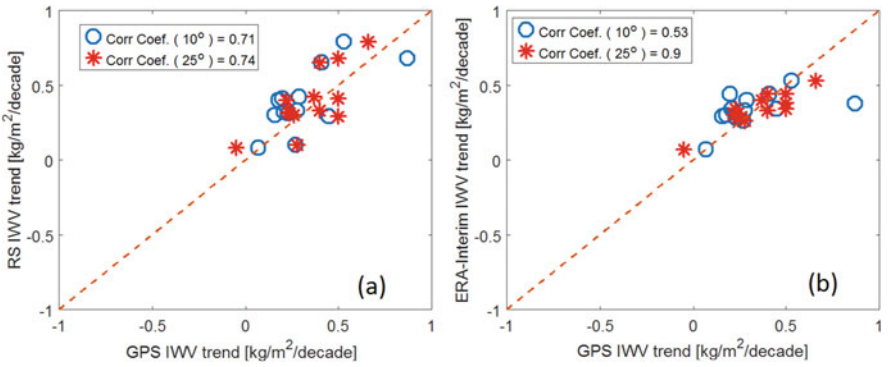

Fig. 5.13 Correlations between the IWV trends from the GPS and the radiosonde data (**a**), and the ERA-Interim data (**b**) for 10° and 25° elevation cutoff angles, from Ning et al. (2017)

in the data processing. Ideally the IWV trends obtained from the two solutions should be the same if there is no significant multipath, or any other elevation dependent phenomena in addition to the atmosphere, that affects the observations.

5.3.7 Improving Stochastic Tropospheric Model for Better Estimates During Extreme Weather Events

S. Nahmani
IGN Institut national de l'information géographique et forestière, Paris, France
e-mail: Samuel.Nahmani@ign.fr

P. Rebischung
IGN Institut national de l'information géographique et forestière, Paris, France
e-mail: paul.rebischung@ign.fr

O. Bock
IGN Institut national de l'information géographique et forestière, Paris, France
e-mail: olivier.bock@ign.fr

Developing and evaluating advanced tropospheric products for monitoring severe weather events and climate was one of the main objectives of the ESSEM COST Action ES1206. Zenithal Wet Delays (ZWD) are estimated during GNSS data processing and used to retrieve Integrated Water Vapour (IWV) with a usual precision around 1–2 kg/m^2. During the GNSS data processing, the temporal evolution of ZWD is generally modelled as a random walk ($ZWD(t + dt) = ZWD(t) + \varepsilon(t)$), where the variance of $\varepsilon(t)$ equals $q_{rw}{}^2.dt$ with dt the sampling rate and q_{rw} the parameter of the random walk. Depending on the software, qrw is fixed to 3 mm.h$^{-1/2}$ with uniform weighting (with $\sigma = 10$ mm) in GIPSY-OASIS (Bar-Sever et al. 1998) or 20 mm.h$^{-1/2}$ with elevation-dependent weighting in GAMIT (King and

Bock 2005). As for the temporal evolution model of tropospheric gradients, it is common to use a random walk whose parameter qtgrd is ten times smaller than that of ZWD in GIPSY-OASIS (Bar-Sever et al. 1998). More recently, Selle and Desai (2016) reassessed the parameterization of the random walk and the weighting function in GIPSY-OASIS using water vapour radiometer measurements as a reference. They confirmed the [3, 0.3] $mm.h^{-1/2}$ random walk parameters when using a uniform weighting (UNIF) of the observations, and suggested [8.4, 0.84] $mm.h^{-1/2}$ as random walk parameters if $\sigma = a/\sin(elev.)$ (SINE) is used as a weighting function for the observations. Fixing these random walk parameters regardless of the location of the station and of local weather conditions is one limitation for the accuracy of GNSS-derived IWV, especially during extreme weather events.

Nahmani and Bock (2014) demonstrated the sensitivity of GPS tropospheric estimates during mesoscale convective system (MCS) events in West Africa to the random walk parameters used to constrain the temporal evolution of ZWD and tropospheric gradients. As an example, Fig. 5.14 shows tropospheric estimates obtained with different random walk parameters and weighting functions of the GPS observations during the MCS over Niamey (Niger) on August 11, 2006.

- An unsuitable parameterization of the random walk and the weighting function leads to an underestimation of ZWD and tropospheric gradients during severe weather events (dotted green curves). This is the case for the model using [3, 0.3] $mm.h^{-1/2}$ with SINE weighting included in Fig. 5.14 only to illustrate the unrealistic results provided by an inaccurate parameterization.
- Both standard GIPSY-OASIS parameterizations proposed by Selle and Desai (2016) allow observing the sudden increase of ZWD induced by the passage of the MCS (red and cyan curves), even if the shapes of both curves are not exactly the same. The estimated tropospheric gradients, however, are clearly different: The East/West displacement of the MCS is clearly reflected in the East component of the tropospheric gradient estimated using the [3, 0.3] $mm.h^{-1/2}$ parameters with UNIF weighting, which is not the case with the [8.4, 0.84] $mm.h^{-1/2}$ parameters with SINE weighting. The random walk parameter for tropospheric gradients fixed at 0.84 $mm.h^{-1/2}$ is not suitable for this case study.

Selle and Desai (2016) advise increasing the random walk parameters in order to track high variability events, but without specifying which values to use. In the rare cases where a radiometer or LIDAR is collocated with the GPS station, the measurements obtained are of poor quality during an intense meteorological event, which makes it impossible to have an external evaluation of the stochastic parameters to be used.

Nahmani and Bock (2014) carried out some tests to set the random walk parameters to be used in the Niamey MCS case study (Fig. 5.14) by increasing them to [10, 1] $mm.h^{-1/2}$ and [20, 2] $mm.h^{-1/2}$ with UNIF weighting, and to [20, 2] $mm.h^{-1/2}$ and [40, 4] $mm.h^{-1/2}$ with SINE weighting. These different parameterizations lead to different conclusions about the studied MCS:

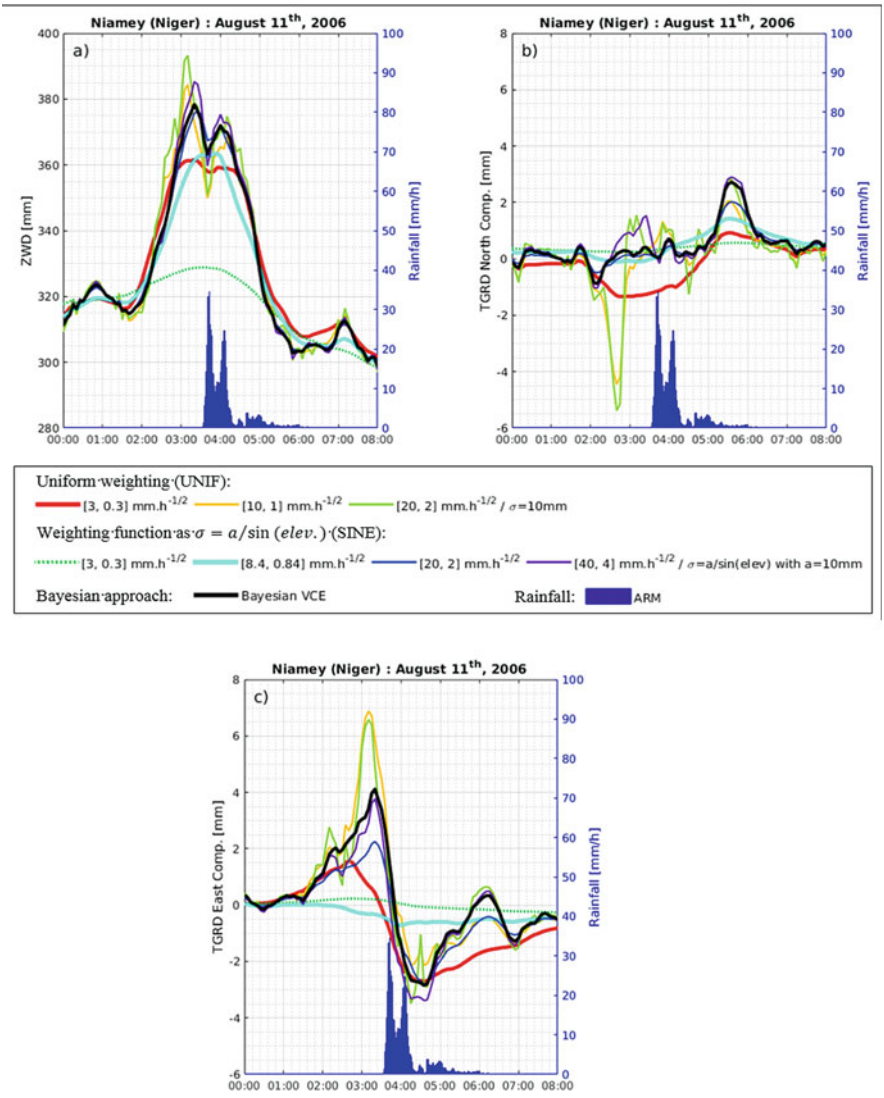

Fig. 5.14 Tropospheric estimates from GISPY-OASIS during the mesoscale convective system of August 11th, 2016 at Niamey (Niger): Zenithal Wet Delay [mm] (**a**), North (**b**) and East (**c**) components of tropospheric gradients (TGRD) [mm] retrieved using different random walk parameters [qzwd, qtgrd] to constrain their temporal evolution. Rainfall data are retrieved from ARM Mobile Facility (Miller and Slingo 2007)

- The time series of ZWD (Fig. 5.14) can have one or two local maxima interspersed with a more or less emphasized local minimum. The ZWD differences at these extrema can reach 35 mm, corresponding to IWV differences of around 5 kg/m^2.

- The North component of the tropospheric gradient consistently shows a peak between 5:00 and 6:00 am, which is, however, more or less emphasized depending on the parameterization used. Other features appear for certain parameterizations only, like the sharp peaks between 2:15 and 3:00 am of the curves from [10, 1] $mm.h^{-1/2}$ and [20, 2] $mm.h^{-1/2}$ with UNIF weighting.
- The East component of the tropospheric gradient globally reflects the East/West displacement of the MCS when the stochastic constraints are not too tight (i.e. except the curves from [3, 0.3] $mm.h^{-1/2}$ and [8.4, 0.84] $mm.h^{-1/2}$ with SINE weighting). The increase from 1:30 am on corresponds to the approach of the MCS near the station. However, the local maximum has more or less stressed amplitude, between 1.5 mm ([3, 0.3] $mm.h^{-1/2}$ – UNIF) and almost 7 mm ([10, 1] $mm.h^{-1/2}$ – UNIF) and is more or less delayed, between 2:30 and 3:15 am. It is followed by a steep fall to a local minimum around −2 to −3 mm between 4:00 and 5:00 am with a zero crossing indicating the presence of the MCS above the GPS station.

Thus, an empirical approach to set the parameters of the random walks to be used during extreme weather events is not appropriate: the tropospheric estimates indeed differ significantly depending on the stochastic constraints and the weighting of the GPS observations used.

Using simulated data, Nahmani et al. (2017) showed the potential interest of using a Bayesian approach to overcome this problem. For a given dataset, the evidence (probability of a model given the observations) can be computed for different models and used to select the most appropriate modelling. One can thus decide whether ZWD should rather be modelled as a random walk or as a step or piecewise linear function. One can also discriminate between different weighting functions of the GPS observations. Using the Bayesian Variance Component Estimation (VCE) technique, it is also possible to determine optimal random walk parameters for the ZWD and tropospheric gradients, as well as the optimal variance of GPS observations. To apply this approach to real GPS data, it is mandatory to get observation equations from GPS data processing software, which is not possible with the standard version of GIPSY-OASIS software. Nahmani et al. (2017) extracted observation equations from ESA NAPEOS software for the case study of the MCS over Niamey (Niger) on August 11, 2006. They first demonstrated that it is preferable to choose an elevation-dependant weighting function as $\sigma = a/\sin(\text{elev.})$ rather than a uniform weighting of the GPS observations. Then, applying the Bayesian VCE, they estimated a standard deviation of $a = 3.9$ mm for zenith GPS observations, and the random walk parameters [$q_{zwd} = 10.5$, $qt_{grd} = 1.3$] $mm.h^{-1/2}$. Those parameters were finally used to process the GPS data again with the GIPSY-OASIS software. The final estimates of ZWD and tropospheric gradients are shown in Fig. 5.14 as the solid black curves. It can be concluded that:

- The two peaks on ZWD are confirmed.
- The North component of the gradient is mostly weak, except between 5:00 and 6:00 am indicating the passage of a small cell in the North of the station.

- The East component of the gradient shows a strong and clear signal: the increase starts at 1:30 am to reach a maximum around 4 mm at 3:18 am. It then drops quickly, crossing zero at 3:48 am, and reaches a minimum around −2.7 mm at 4:36 am.

The Bayesian VCE approach is relevant to validate the stochastic parameterization of GPS data processing and better estimate tropospheric parameters during severe weather events. It opens the way to an adaptive processing of GPS data according to the location of the station and the local weather conditions. One could even consider using a time-varying stochastic parameterization. In the case of the Niamey MCS, at least three sets of stochastic parameters would indeed be required to take into account the physics of the phenomenon: one set before, one during and one after the passage of the MCS. Nahmani et al. (2016) indeed demonstrated that this specific modelling has higher evidence than when using a single stochastic parameterization. The Bayesian approach is thus particularly promising, but it remains to be assessed more thoroughly before a software implementation for operational use can be considered.

5.3.8 Multi-GNSS Data Processing

E. Brockmann
Swiss Federal Office of Topography, Köniz, Switzerland
e-mail: Elmar.Brockmann@swisstopo.ch

GLONASS observations have been available since 2003 but only from 2008 onwards, the amount of GLONASS data is significant. In the framework of the second EPN Reprocessing Campaign (Pacione et al. 2017), the impact of GLONASS observations has been evaluated in terms of raw differences between ZTD estimates as well as on the estimated linear trend derived from the ZTD time series. Two solutions were prepared and compared, using the same software and the same processing characteristics, but different observation data: one with GPS and GLONASS, and one with GPS data only. The difference in ZTD trends between a GPS-only and a GPS + GLONASS solution shows no significant rates for more than 100 stations (rates usually derived from more than 100 000 ZTD differences). This indicates that the inclusion of additional GLONASS observations in the GNSS processing has a neutral impact on the ZTD trend analysis. Satellite constellations are continuously changing over time due to satellites being replaced and newly added for all systems. For instance, in the near future the inclusion of additional Galileo and BeiDou data will become operational in the GNSS data processing. These data will certainly improve the quality of the tropospheric products and this study points out that the ZTD trends might be determined independently of the satellite systems used in the processing, and therefore multi-GNSS data processing might not introduce systematic changes in terms of ZTD trends.

5.3.9 *Impact of IGS Type Mean and EPN Individual Antenna Calibration Models*[7]

A. Araszkiewicz
Centre of Applied Geomatics, Warsaw Military University of Technology, Warszawa, Poland
e-mail: andrzej.araszkiewicz@wat.edu.pl

According to the processing options listed in the EPN guidelines for the Analysis Centre (http://www.epncb.oma.be/_documentation/guidelines/guidelines_analysis_centres.pdf), EPN individual antenna calibration models have to be used instead of IGS type mean calibration models, when available. Currently, individual antenna calibration models are available at about 70 EPN stations. However, in the second EPN Reprocessing campaign, there are individual solutions carried out with IGS type mean antenna calibration models only (Schmid et al. 2016) while others use IGS type mean plus EPN individual antenna calibration models. Therefore, for the same station, there are contributing solutions obtained by applying different antenna models. To evaluate the impact of using these different antenna calibration models on the ZTD, two solutions were prepared and compared using the same software and the same processing, but different antenna calibration models. The first solution used the IGS type mean models only, and the second one used the individual calibrations whenever it was possible and the IGS type mean for the rest of the antennas.

An example of the time series of the ZTD differences obtained by applying individual and type mean antenna calibration models for the EPN station KLOP (Kloppenheim, Frankfurt, Germany) is shown in Fig. 5.15.

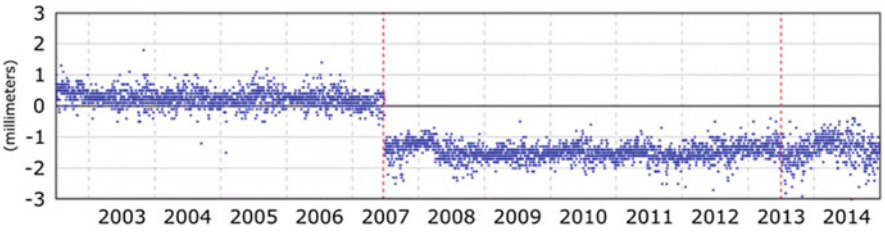

Fig. 5.15 EPN station KLOP (Kloppenheim, Frankfurt, Germany) ZTD differences time series between solutions processed with individual and type mean antenna calibration models. Two instrumentation changes occurred at the station (marked by vertical dashed red lines): the first in 27 June 2007, when the previous antenna was replaced with a TRM55971.00 and a TZGD radome, and the second in 28 June 2013 with the installation of a TRM57971.00 and a TZGD radome

[7]Parts from this section were previously published in Araszkiewicz and Voelksen (2017) and Pacione et al. 2017).

Switching between phase centre corrections from type mean to individual (or vice versa) causes a disagreement in the estimated up component of the stations, as was mentioned by Araszkiewicz and Voelksen (2017), and therefore in their ZTD time series. Depending on the antenna model, the offset at station KLOP in the up component (vertical displacement) is -5.2 ± 0.5, 8.7 ± 0.6 and 5.6 ± 0.8 mm with a corresponding offset in the ZTD of 0.2 ± 0.5, -1.5 ± 0.5, -1.4 ± 0.8 mm, respectively. Similar values were obtained between solutions calculated for all stations/antennas for which individual calibration models are available. The corresponding offset in the ZTD has the opposite sign for the antennas with an offset in the up component larger than 5 mm (16 antennas) and, generally, does not exceed 2 mm. Such inconsistencies in the ZTD time series are not large enough to be captured during the combination process upon which the official EPN product is based, where a 10 mm threshold in the ZTD bias (about 1.5 kg/m^2 IWV) is set in order to flag problematic ACs or stations. The detailed analysis is reported in Pacione et al. (2017).

5.3.10 Impact of Non-Tidal Atmospheric Loading Models[8]

A. Araszkiewicz
Centre of Applied Geomatics, Warsaw Military University of Technology, Warszawa, Poland
e-mail: andrzej.araszkiewicz@wat.edu.pl

Non-tidal atmospheric loading models are not yet considered as Class 1 models by the IERS (Petit and Luzum 2010), indicating that there are currently no standard recommendations for data reduction. To evaluate their impact, two solutions, one with and one without a non-tidal atmospheric loading model, have been compared for the year 2013. In the solution with the model, the National Centres for Environmental Prediction (NCEP) model is used at the observation level during data reduction (Tregoning and Watson 2009). Dach et al. (2010) have already found that the repeatability of the station coordinates improves by 20% when applying the non-tidal atmospheric loading correction directly on the data analysis and by 10% when applying a post processing correction to the resulting weekly coordinates. However, the effect on the ZTDs seems to be negligible. Generally, it causes a difference below 0.5 mm with a standard deviation not larger than 0.3 mm. The detailed analysis is reported in Pacione et al. (2017).

[8]Parts from this section were previously published in Pacione et al. (2017).

5.3.11 *Using Estimated Horizontal Gradients as a Tool for Assessment of GNSS Data Quality*[9]

T. Ning
The Swedish Mapping, Cadastral and Land Registration Authority, Stockholm, Sweden
e-mail: tong.ning@lm.se

G. Elgered
Chalmers University of Technology, Göteborg, Sweden
e-mail: gunnar.elgered@chalmers.se

J. Douša
Geodetic Observatory Pecný, RIGTC, Ondřejov, Czech Republic
e-mail: jan.dousa@pecny.cz

5.3.11.1 Background

It is a common view that because the basic observable in GNSS is the time of arrival the system is well suited for climate monitoring of the atmospheric water vapour content. This is obtained via the estimates of the total equivalent zenith delay and the delay due to water vapour. It is also common practice to estimate two-dimensional horizontal linear gradients for each site in the GNSS data processing because it improves the reproducibility of estimated geodetic parameters, see e.g. Bar-Sever et al. (1998). We have addressed the question if also these estimated gradients are useful in climate research, i.e. if they can detect any long term systematic changes. While doing so it became clear that first of all estimating horizontal linear gradients is a tool to assess the quality of the observations of the GNSS signals. It was also early recognised, using GPS data from Sweden, that no significant long-term trends were detected for the horizontal gradients.

In this subsection, we first give a short background on the cause of horizontal gradients in the atmosphere, then we show a comparison between gradients estimated using data from two collocated GNSS stations and one microwave radiometer. Thereafter we study if the GNSS gradients contain any information about the atmosphere by comparing them to gradients estimated from the ERA-Interim analyses from the ECMWF. Finally, we give some conclusions related to the present and future use of linear horizontal gradients.

[9]Parts from this section were previously published in Forkman et al. (2017).

5.3.11.2 Cause of Horizontal Gradients

The refractivity in the atmosphere is determined mainly by the total pressure, the temperature and the partial pressure of water vapour. Pressure gradients exist mainly over global scales and regional scales (e.g. mesoscale weather systems). Temperature and especially water vapour exists also over local scales. The large local gradients over a GNSS site have spatial scales ranging from hundreds of metres to a few kilometres. For example, during the passage of a weather front the gradients can be significant, especially for distinct cold fronts. Other specific weather phenomena that can cause horizontal variability are sea breeze (Munn 1966), cloud rolls (Brown 1970) and convection processes in general. We note that none of the known processes is expected to be strictly linear, but the strength in the geometry and the data quality do not provide the option to determine additional atmospheric parameters.

5.3.11.3 Gradients from Two Collocated GNSS Sites

Two GNSS sites have been operating continuously at the Onsala Space Observatory, on the west coast of Sweden for many years. The primary site, ONSA, was established already in the late 1980s and the other site, ONS1, was taken into operation in 2011. The two sites are shown in Fig. 5.16. The antennas of these

Fig. 5.16 The two GNSS stations ONSA (left) and ONS1 (right) at the Onsala Space Observatory

two sites are located within 100 m from each other and should observe similar gradients.

We have used 4 years of GPS data (2013–2016) from these two sites and estimated the horizontal gradients in the east and the north directions every 5 min. The analysis follows the same lines as described by Ning et al. (2013). We have also included a comparison with the microwave radiometer Konrad that has been observing the sky continuously, in a sky mapping mode, during most of the time during these 4 years. Correlation plots are shown in Fig. 5.17 and show a much higher correlation between the gradients from the two GNSS sites compared to when the GNSS gradients are correlated with the gradients from the microwave radiometer. This is expected because GNSS is estimating the gradients in the total refractivity

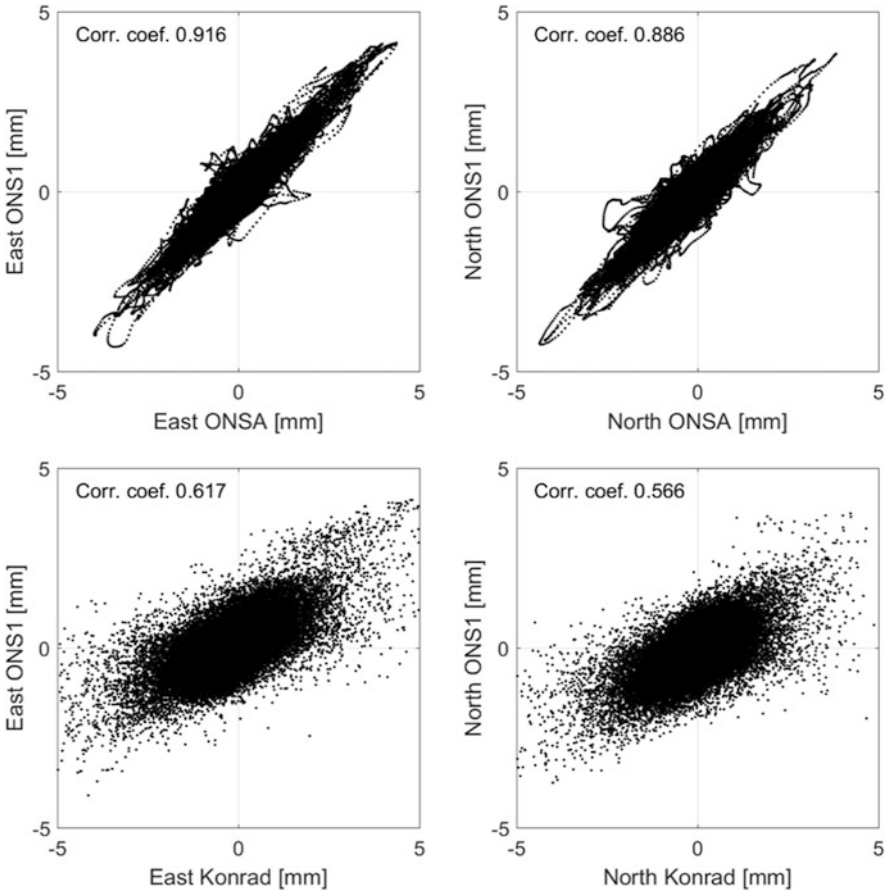

Fig. 5.17 Comparisons of the total east and north gradients estimated from the ONSA and ONS1 stations with a temporal resolution of 5 min (top). Below is a corresponding comparison between the gradients from the microwave radiometer Konrad (wet gradients only) and ONS1 (total gradients), here using a temporal resolution of 15 min, from Forkman et al. (2017)

whereas the radiometer is only sensitive to gradients in the water vapour. Also, the directions of the observations are towards the same satellites using GNSS but the radiometers observation are evenly spread of the sky. More details on this study have been given by Forkman et al. (2017).

5.3.11.4 Comparison Between Gradients from GNSS Data and the ERA Interim Analyses

We have searched for any systematic changes in the horizontal gradients using 17 years (1997–2013) of estimated gradients from GPS data for 21 sites in Sweden. The temporal resolution of the originally estimated gradients was 5 min. Based on these data we formed average values of 1 hour, 1 day, and 1 month. The ECMWF data (see e.g. Boehm and Schuh 2007) that were available while doing this study were from the mid of 2005, resulting in a subset of almost 9 years of data.

The results, in terms of correlation coefficients, are shown in Table 5.3. The correlations seen in all cases confirm that an atmospheric signal in terms of gradients is detected by the GPS observations. We note that the correlation coefficients increase for longer averaging time periods. Our interpretation for that is that we compare a larger fraction of the gradient that is caused by large scale temperature and pressure gradients, which is better modelled by the ERA Interim analysis. Another result worth noting is that the two sites with the highest correlation coefficients for the monthly averages are ONSA and SPT0. These two sites are the only ones that are equipped with ECCOSORB® material below the antenna. This could reduce the impact from unwanted multipath effects. The phenomenon calls for further studies.

In the future, we also plan to subtract the hydrostatic gradients calculated using the ECMWF data in order to study the estimated wet gradients from GPS only. Unfortunately, the temporal resolution of the ECMWF data is not sufficiently high to resolve many of the short lived small-scale gradients. In order to carry out comparisons we are therefore turning to microwave radiometer data.

Table 5.3 Correlation coefficients for the total east-west (EW) and north-south (NS) linear horizontal gradients estimated from GPS data and compared to ERA Interim data

	Hourly averages		Daily averages		Monthly averages	
	EW	NS	EW	NS	EW	NS
Kiruna (KIR0)	0.57	0.53	0.77	0.76	0.76	0.81
Mårtsbo (MAR6)	0.61	0.52	0.71	0.75	0.85	0.82
Onsala (ONSA)	0.62	0.55	0.78	0.78	0.95	0.90
Borås (SPT0)	0.58	0.53	0.75	0.76	0.91	0.90
Visby (VIS0)	0.54	0.51	0.72	0.74	0.89	0.79

5.3.11.5 On Estimating Trends Based on Estimated Horizontal Gradients from VLBI Data

Given that horizontal gradients in general are small and that the larger values typically occur for a short time we expect that any long-term trends would be very small and therefore also difficult to detect. An estimated gradient has a direction and from a time series we estimate trends for the east and the north gradients. Combining these two trends will give a change in the average gradient at the site. There is also a second possibility and that is to estimate a trend in a time series with absolute values of the gradients. Such a positive trend will occur if there is an increase in the variability at the site, which can happen even if there are no trends in the east and north gradients.

We have estimated trends for the two VLBI sites Wettzell and Onsala for the time period 1997–2014. The resulting 17 years long time series is then the base for estimating linear trends. To be sensitive to the short-term variability we used gradients with a temporal resolution of 1 h. The results are shown in Table 5.4. We note that there are no indications of change in the absolute values at any of the two sites. There are small trends detected in the east and north gradients. Preliminary results using ECMWF data from the period 2005–2014 suggest that these trends may be caused by systematic changes in the hydrostatic and the wet horizontal gradients. Such changes will occur randomly over time periods of a few years due to the motion of mesoscale weather systems and is already well known from existing meteorological observation networks. We conclude that no trends related to small scale variability in the water vapour has been detected. Because no trends are seen in the absolute value of the gradients we have at the same time an indication that the two sites had a stable electromagnetic environment during the studied time period.

5.3.11.6 GNSS Tropospheric Gradients and Problems with Low-Elevation Data Quality

When developing a new interactive web interface over tropospheric parameter comparisons within the GOP-TropDB (Győri and Douša 2016), we could easily observe large systematic behaviour in GNSS-derived tropospheric gradients from the GOP European second reprocessing (Douša et al. 2017a, b) during specific years at several stations of the EUREF Permanent network (EPN). We can estimate only total tropospheric horizontal gradients from GNSS data, i.e. without being able to distinguish between dry and wet contributions. The former is mostly due to horizontal asymmetry in atmospheric pressure, and the latter is due to asymmetry in the

Table 5.4 Estimated trends for linear horizontal gradients

Site	East gradient (mm/year)	North gradient (mm/year)	Absolute gradient (mm/year)
Wettzell	0.008	0.028	0.000
Onsala	0.010	0.010	0.000

water vapour content being more variable in time and space than the former (Li et al. 2015). However, mean wet gradients should be close to zero, whereas dry gradients may tend to point slightly to the equator, corresponding to latitudinal changes in atmosphere thickness (Meindl et al. 2004). Similarly, orography-triggered horizontal gradients can appear due to the presence of high mountain ranges in the vicinity of the station (Morel et al. 2015). Such systematic effects can reach the maximum sub-millimetre level, while a higher long-term gradient (i.e. that above 1 mm), is likely more indicative of issues with site instrumentation, the environment, or modelling effects.

Therefore, in order to clearly identify these systematic effects, we compared GOP gradients with those calculated from the ERA Interim data during period 1996–2014. During the study, we could observe a strong impact in the most extreme case identified at the MALL station (Mallorca, Spain). The monthly differences in gradients steadily increased from 0 mm up to −4 mm and 2 mm for the east and north gradients, respectively, within the period of June 2003–October 2008, Fig. 5.16. Such large differences were not realistic and were attributed to data processing because long-term increasing biases dropped down to zero on November 1, 2008, immediately after the antenna and receiver were changed at the station. During the same period, also yearly mean ZTD differences to ERA-Interim steadily changed from about 3 mm to about −12 mm and immediately dropping down to −2 mm in 2008 after the antenna change, see Fig. 5.18.

The EPN Central Bureau (http://epncb.oma.be), operating at the Royal Observatory of Belgium (ROB), provides a web service for monitoring GNSS data quality and includes monthly snapshots of the tracking characteristics of all stations. The sequence of plots displayed in Fig. 5.19, representing the interval of interest (2002, 2004, 2006 and 2008), reveals a slow but systematic and horizontally asymmetric degradation of the capability of the antenna to track low-elevation observations at the station. Therefore, we analysed days of the year (DoY) 302 and 306 (corresponding to October 28 and November 1, 2008) with the in-house G-Nut/Anubis software (Václavovic and Douša 2016) and observed differences in the sky plots of these 2 days. The left-hand plot in Fig. 5.20 depicts the severe loss of dual-frequency observations up to a 25° elevation cut-off angle in the South-East direction (with an

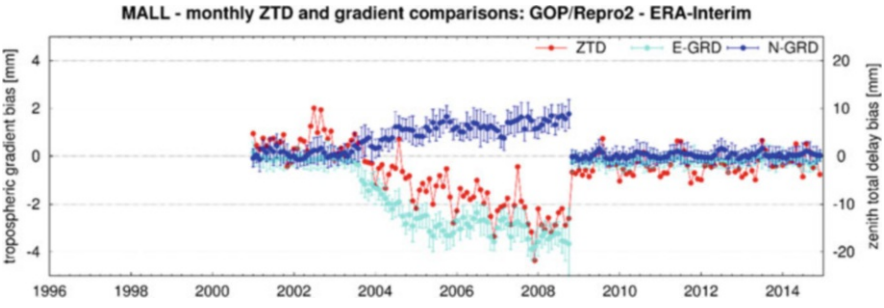

Fig. 5.18 MALL station – monthly mean differences in GNSS tropospheric horizontal gradients vs ERA Interim data

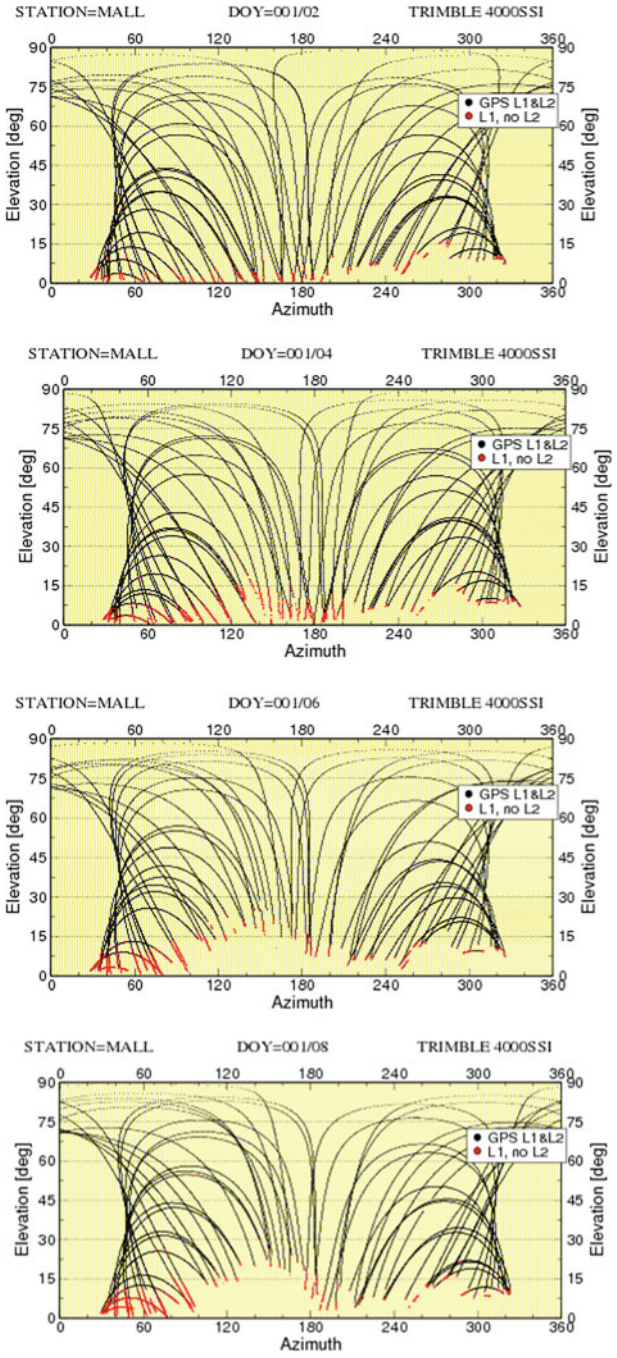

Fig. 5.19 Low-elevation tracking problems at the MALL station during the period of 2003–2008. From left-top to right-bottom: January 2002, 2004, 2006 and 2008 (courtesy of the EPN Central Bureau, ROB)

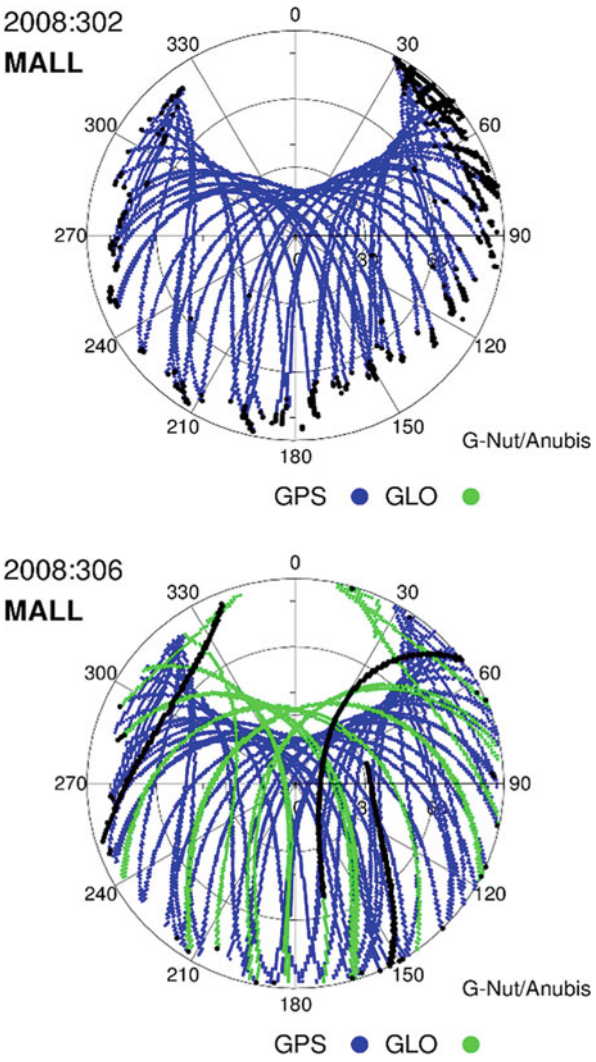

Fig. 5.20 Sky plots before (top) and after (bottom) replacing the malfunctioning antenna at the MALL site (Oct. 30, 2008). Black dots indicate single-frequency observations available only

azimuth of 90°–180°), which cause the tropospheric linear gradient of approximately 5 mm to point in the opposite direction. The figure also demonstrates that an increasing loss of second frequency observations appears to occur in the East (represented as black dots). The right-hand plot in this figure demonstrates that both of these effects fully disappeared after the antenna was replaced on October 30, 2008 (DoY 304), resulting in the appearance of normal sky plot characteristics and a GLONASS constellation with one satellite providing only single frequency observations (represented as black lines).

This situation demonstrates the high sensitivity of the estimated gradients on data asymmetry, particularly at low-elevation angles. The systematic behaviour of these monthly mean gradients, their variations from independent data and a profound progress over time, seem to be useful indicators of instrumentation-related issues at permanent GNSS stations. It has to be noted that the strategy of elevation-dependent weighting plays a significant role here, as the main impact is due to an asymmetry and poor quality of low-elevation observations. It is also considered that gradient parameters can be valuable method as a part of ZTD data screening procedure (Bock 2016b).

Although the station MALL represented an extreme case, biases at other stations were observed too, e.g. GOPE (1996–2002), TRAB (1999–2008), CREU (2000–2002), HERS (1999–2001), GAIA (2008–2014) and others. Site-specific, spatially or temporally correlated biases suggest different possible reasons such as site-instrumentation effects including the tracking quality and phase centre variation models, site-environment effects including multipath and seasonal variation (e.g. winter snow/ice coverage), edge-network effects when processing double-difference observations, spatially correlated effects in reference frame realization and possibly others.

5.3.11.7 Conclusions

The gradients estimated from GPS data are clearly reflecting the atmospheric conditions since there is a significant correlation with ERA-Interim results. However, the very small-scale water vapour variability seems, as expected, not to be captured by the ERA-Interim model. We also noted that long-term trends in estimated gradients from GPS data are insignificant given the uncertainties involved. Statistics of gradient time series can be a valuable tool to search for problems in the GPS data, such as sudden changes in the electromagnetic environment of the GNSS antenna and this calls for further more detailed case studies.

5.3.12 Conclusions and Recommendations on Processing Options

R. Pacione
e-GEOS/Centro di Geodesia Spaziale-Agenzia Spaziale Italiana, Matera, MT, Italy
e-mail: rosa.pacione@e-geos.it

O. Bock
IGN Institut national de l'information géographique et forestière, Paris, France
e-mail: olivier.bock@ign.fr

While standards for GNSS processing for positioning devted to geodetic and geodynamic applications (e.g. Reference frame realization, tectonics, GIA monitoring…) are well established, nothing similar is available for long ZTD/IWV time series devoted to climate applications (e.g. monitoring seasonal to decadal trends and variability). The results reported in this subsection are a quite comprehensive overview of the sensitivity of ZTD time series to the most important processing options from which we can draw some first conclusions.

In general, the main scientific GNSS software packages used by the geodetic community for data processing agree at 5–6 mm ZTD level (~1 kg/m^2 IWV) for instantaneous estimates, or about ~ 2 mm ZTD (0.3 kg/m^2 IWV) for weekly estimates, and about 0.15–0.30 kg/m^2 per decade for IWV trends.

Both widely used processing modes based either on double-difference (DD) combination of observations or using undifferenced observations in a PPP processing are consistent at the level of ~1 kg/m^2 IWV and 0.30 kg/m^2 per decade for IWV trends. For the retrieval of long time series, the quality of satellite orbits and clock corrections are of prime importance and may be a significant source of uncertainty in PPP for the early GPS period (before 2001). Processing in a double-difference mode is much less impacted by the uncertainty in the external products but suffers from network effects, e.g. changes in the baseline design over time might induce spurious trends and gaps in data have been shown to be a major source of outliers in the ZTD time series.

The details of the tropospheric delay modelling (mapping functions and a priori zenith delay corrections, deterministic vs. stochastic model for ZTD parameters) in the GNSS processing software has a direct impact on the properties of the derived ZTD parameters, e.g. unconstrained ZTD parameters are prone to become outliers in case of gaps or errors in the observations (at the station or at nearby stations in case of DD processing). Similarly, over-constrained ZTD parameters may hide the true ZTD variability in case of strong short-lived events (e.g. convective systems passing over the station). Optimal approaches for better constraining the tropospheric models are foreseen as an active area of investigation in the near future.

For tropospheric modelling mapping functions play a key role. Nowadays two mapping functions are mainly used: GMF and VMF1. Althought it is recommended to use VMF1, from the point of view of climate monitoring (that is in terms of linear trends) the differences between these two mapping functions are very small.

The selection of the elevation cut-off angle used in the GNSS data processing can have a significant impact on the resulting IWV biases and trends. This result is explained by the well known sensivitiy of GNSS ZTD estimates to elevation dependent errors (e.g. due to signal multipath, tropospheric model, antenna model, etc.). For linear trend estimation, it is recommended to apply a cutoff test using at least two different elevation cut-off angles in the data processing and compare the results. In case the difference in ZTD trends obtained from the two solutions is above the acceptable level (ca 0.5 mm/decade), the underlying elevation-dependent error source should be tracked and reduced.

As the GNSS satellite constellations are growing, the impact of using observations from different systems in the recent years compared to GPS-only in the older ones was

questionable for trend monitoring. Tests conducted in the framework of the second EPN Reprocessing campaign helped to investigate this question. It was shown that the impact of GLONASS observations on linear ZTD trends wes not significant.

To improve the site coordinates repeatability, it is a common practice to estimate two-dimensional horizontal linear gradients for each site in the GNSS data processing and the estimated gradients are clearly reflecting the asymmetry in the atmospheric refractivity. The question whereas the gradient parameters contain some interesting signature for climate research has been investigated. However, so far, analysis of long time series of gradient parameters did reveal any significant signal (e.g. trends in gradients are insignificant given the uncertainties involved). However, gradient parameters have been shown toresponds strongly to the presence of problems in the GNSS data (e.g. degradation of antenna pattern).

The sensitivity studies on GNSS data modelling and processing settings devoted to climate applications that were initiated during the COST Action have pointed to the most important areas of uncertainty that shall be futher investigated in the future.

5.4 Standardisation of ZTD Screening and IWV Conversion

5.4.1 ZTD Screening

O. Bock
IGN Institut national de l'information géographique et forestière, Paris, France
e-mail: olivier.bock@ign.fr

Screening is the process of inspecting data for errors and correcting them prior to doing data analysis[10] (Bock 2016b). In GNSS data processing software, outliers in phase and code observations are typically rejected based on both a priori and a posteriori statistical tests (e.g. Sect. 5.2 "Pre-processing on the RINEX Level" and Section 5.6 "Screening of Post–Fit Residuals" in Dach et al. 2015). In NWP assimilation systems, as well, observations have to pass several quality checks and statistical tests to be actually used (Järvinen and Undén 1997). One of the main reasons for the necessity of screening is that most processing algorithms rely on the assumption that input data have well behaved statistical properties. This is obviously not the case for most observational data, which can include outliers (gross errors) due to equipment malfunctioning or mishandling, or simply due to a human operator's typing errors.

Despite the precautions taken with the use of efficient screening algorithms at the observation level, it is often observed that processing results contain discontinuities and outliers. This is the case for GNSS coordinate time series (Klos et al. 2015) and

[10] http://www.businessdictionary.com/definition/data-screening.html

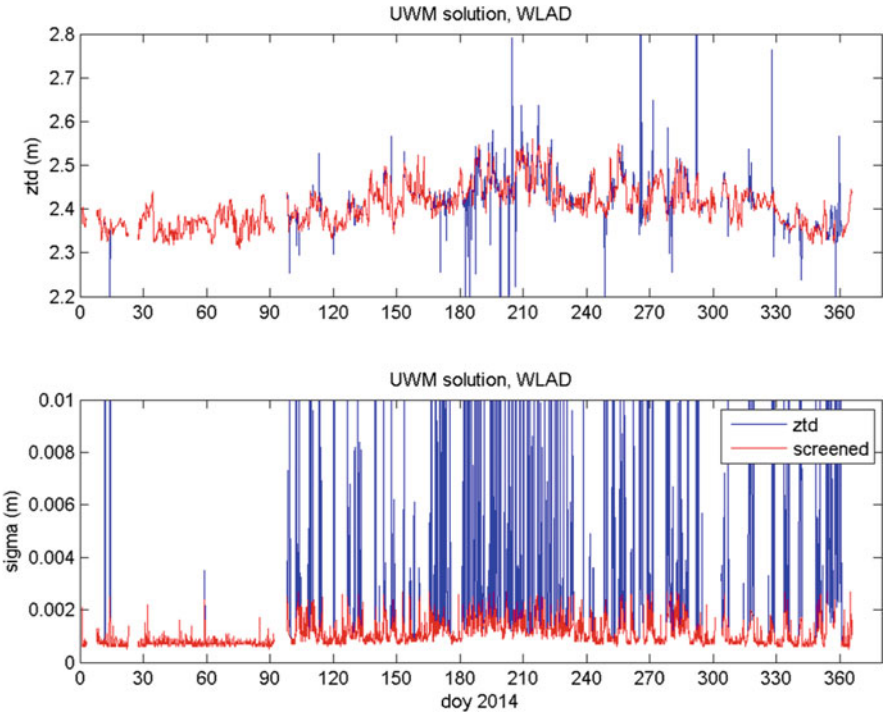

Fig. 5.21 Time series of ZTD estimates (upper) and corresponding formal errors (lower) for GNSS station WLAD (Poland) over year 2014 as resulting from a regular post-processing procedure with Bernese GNSS software (Stepniak et al. 2017)

ZTD time series (Stepniak et al. 2017). Figure 5.21 below shows a typical example of ZTD time series and their corresponding formal errors produced with Bernese software in double-difference mode. Outliers in the original ZTD estimates can be clearly detected visually. Stepniak et al. 2017, identified several causes for ZTD outliers in a double-difference mode processing: (1) deficiencies in the baseline strategy that lead to temporary disconnections of a station from the main network due to observation gaps in connecting baseline, (2) short observation gaps at the station that lead to poorly determined ZTD estimates, (3) other causes (e.g. incorrect ambiguity fixing, increased measurement noise, etc.). The latter two impact also PPP. All three causes lead usually also to an increase in formal error as can be seen in the lower plot of Fig. 5.21.

According to Fig. 5.21, one has the impression that spikes in formal error are much more frequent than spikes in ZTD estimates. This is due to the fact that ZTD natural fluctuations due to changing weather conditions are quite large and not easy to distinguish from small outliers and erroneous fluctuations due to measurement noise.

5.4.1.1 Screening Based on GNSS Results Only

If we want to detect erroneous ZTD values based on a simple range-check (comparison with fixed upper and lower limits for all stations), we need to use an interval large enough to accommodate for extremal natural variations encountered at all stations of interest. This interval can be determined from the physical basis of natural ZHD and ZWD variations due to variations in surface pressure and IWV. Monthly data from ERA-Interim reanalysis yield ZHD variations in the range [1.20, 2.41] m and ZWD in the range [0.00, 0.54] m, globally. A reasonable range check interval for ZTD would thus be [1.00, 3.00] m. If a regional network is considered, this interval can be further reduced.

The range-check on ZTD values alone is not sufficient. It can be complemented with an outlier check (comparison with station-dependent upper and lower limits). The choice of interval limits is not trivial because ZTD values don't follow a known empirical probability distribution function (PDF). Nevertheless, it is common to use an interval such as the mean $\pm$ 3, 4, or 5 standard deviations (Kouba 2003; Wang et al. 2007a, b, c). In the case of a normal PDF, these limits correspond to a fraction between 0.0027 and $5.7 \cdot 10^{-7}$ of the data. In the case of real data, the fraction of rejected data is much higher because of several reasons: the PDF of ZTD data is not normal, the mean and standard deviation estimates are not robust (i.e. they are biased when outliers are included), outliers in the data yield larger deviations from the mean than expected for a normal PDF (this is what we want to detect). As an example, the ZTD data from the IGS repro1 solution (Sect. 5.2.2) for year 1996 give a fraction of rejected data between 0.0065 (mean $\pm$ 3σ) and $1.6\ 10^{-5}$ (mean $\pm$ 5σ) over all available stations. Inspection of results station by station reveals that only a small number of stations contain a significant number of outliers. For these stations, a rejection rate of 0.01 (i.e. 1%) is achieved when the limits are taken at the mean $\pm$ 3.5σ. We thus recommend to use the latter interval.

Because formal errors are very sensitive to changes in the quality of ZTD estimates, we can improve the screening procedure by applying a range check and an outlier check on the formal errors. Inspection of empirical PDFs and percentiles of the formal errors from various reprocessed ZTD datasets showed that the PDFs of stations with no or only few outliers resemble a Chi distribution and that the 95, 98, and 99% percentiles can be used to detect stations with large numbers of outliers (Bosser and Bock 2016). However, the results are highly dependent on the processing options, especially the constraints on the temporal evolution of the estimated ZTDs (see Sect. 5.3). Hence, the 95% percentile for a global dataset such as the IGS repro1 solution produced with GIPSY OASIS II (one ZTD parameter estimated every 5 min with a random walk model constraint of 3 mm $h^{-1/2}$) ranges between 2.0 mm (good stations) and 4.0 mm (bad stations), while for a EPN repro2 solution with Bernese software (one ZTD parameter estimated every 2 h and no constraints) the range is extended to between 1.2 mm (good stations) and 9.0 mm (bad stations).

We thus recommend to use range check limits matched to the data processing options. An upper limit for the formal error of 10 or 15 mm is adequate to unconstrained tropospheric models (e.g. Bernese EPN repro2), while a limit of 5 to 6 mm seems more reasonable in case of a constrained model (e.g. IGS repro1).

The range check on formal errors should be station-specific (thus implicitly processing specific). We tested two estimators for the upper limit: median + $k \times \sigma$ and $p \times$ median. The former yields good results with $k = 3$ or $k = 3.5$, but σ is not a robust scale estimator. The latter yields good results with $p = 2$ or $p = 2.5$ and is more robust to outliers because it does not use the standard deviation. A trial and error approach is suggested here to examine the results from different parametrizations.

Note that for the tests of both ZTD and formal errors, it is important to apply both the range check and the outlier check. Even if the range check might appear unnecessary because it is more permissive than the outlier check, its role is mainly to eliminate the largest outliers before data-dependent limits are computed for the range checks.

When the screening is applied to long (multi-annual) time series, the limits for outlier checks should account for the variation in observation and processing quality over time. We suggest to update the limits yearly.

5.4.1.2 Screening Based on Comparison with Reference ZTD Data

Because the ZTD data can have large temporal variability, it is necessary to set the limits for the range check and outlier check quite far apart. It is hence impossible to distinguish between small outliers and large natural variations based on the ZTD values alone. Only the comparison to a predicted ZTD value, or first guess, used as reference can help reducing the detection interval. This procedure is commonly used in data assimilation systems for the screening of observations (Järvinen and Undén 1997). Short-range forecast from the NWP model are used as a reference to compute background departures (observation minus background). In this procedure, the square of the normalized background departure is considered suspect when it exceeds its expected variance more than a predefined multiple.

Such a procedure can be applied offline to GNSS ZTD data using e.g. a NWP model such as ERA-Interim reanalysis. We will refer to it as a model departure quality control (MDQC). The reference ZTD values can be computed from the model IWV and ZHD/pressure data by following the reverse procedure as used for the conversion of GNSS ZTD into IWV (see next subsection). The ZTD differences (GNSS minus model) are expected to follow a normal PDF. A normality test can thus be applied to detect the anomalous values (outliers). Various tests have shown that it is most efficient to check the data station-wise in yearly batches using as limits the median $\pm 3\sigma$. According to the normal PDF, the fraction of values outside of this range should be smaller than 0.0027. Because σ is sensitive to outliers we suggest to use a robust scale estimator such as $\sigma^* =$ (84th – 16th percentile)/2. In addition, if we don't want to be too strict we can allow a higher fraction than the theoretical one,

e.g. 2×0.0027, and apply the test iteratively. In brief, the recommended procedure is the following:

- Form ZTD differences: GNSS – model (e.g. Reanalysis),
- Do the normality test: if the number of values outside the interval median $\pm$ 3 $\sigma > 2 \times 0.0027$ then reject all these values; a robust estimate for σ is $\sigma^* =$ (84th – 16th percentile)/2,
- Do up to 10 iterations (usually 2 or 3 are enough).

The performance of the MDQC depends on the spatial and temporal resolution of the model at hand. Using e.g. ERA-Interim with 0.75° x 0.75° horizontal resolution might be problematic for stations in mountainous regions because of representativeness differences (Bock and Parracho 2019). Most model archives have also limited temporal resolution, e.g. from 6-hourly data it will be difficult to compute accurate departures for 5-min resolution GNSS ZTD data.

Other reference datasets or approaches might be interesting to screen GNSS ZTD data, e.g. comparison ZTD data from collocated GNSS, DORIS or VLBI stations can be realized at a number of sites.

5.4.1.3 Conclusions

Screening the ZTD data is a mandatory step before they can be further used for a scientific purpose.

Two approaches have been described in this subsection: (1) a method based on GNSS results only, composed of range checks (with fixed limits) and outlier checks (with station and time-dependent limits) applied to ZTD and formal errors; (2) a method based on comparison with reference ZTD data (e.g. NWP model or reanalysis) inspired from the background departure quality control using in data assimilation systems. Both approaches can be used independently and yield consistent results (Bock 2015; Stepniak et al. 2015). Higher efficiency is however gained when both methods are applied sequentially.

Reduction of outlier in the GNSS ZTD data would also be achieved by a more careful screening at observation level and improved processing options (e.g. optimized baseline design and constraints on ZTD parameters, Stepniak et al. 2017).

5.4.2 ZTD to IWV Conversion

O. Bock
IGN Institut national de l'information géographique et forestière, Paris, France
e-mail: olivier.bock@ign.fr

At the beginning of the COST Action, a survey on the conversion methods used by the community was organized with the WG3 participants (Pacione et al. 2014b; Bock and Pacione 2014). Thirteen contributions were received which revealed that

there was no established methodology. Debate at the Munich workshop confirmed that there was no clear consensus and it was decided to review the state of the art methods, try to highlight their limits and uncertainties, and come up with recommendations, distinguishing between real-time (now-casting) and offline applications (climate monitoring).

The specification of the conversion method recovers three different aspects: the conversion formulas, the constants, and the auxiliary data (Bock 2016c).

5.4.2.1 Conversion Formulas

The most commonly admitted formulas are presented below:

Definition		Application to GPS ZTD conversion	
$ZTD = ZHD + ZWD$	5.1a	$ZTD_{GPS} = ZHD_{ap} + ZWD_{estim}$	5.1b
$ZTD = 10^{-6} k_1 R_d \frac{P_s}{g_m}$	5.2a	ZHD_{GPS} computed from Equation 5.2a with pressure at GPS stations P_s	
$ZWD = 10^{-9} R_v \int_0^\infty \rho_v(z) \left[k'_2 + \frac{k_3}{T(z)}\right] dz$	5.3a	$ZWD_{GPS} = (ZTD_{GPS} - ZHD_{GPS})$	5.3b
$IWV = \int_0^\infty \rho_v(z) dz$	5.4a	$IWV_{GPS} = \kappa(T_m) \times ZWD_{GPS}$	5.4b
$k(T_m) = \frac{1}{10^{-6} R_v \left[k'_2 + \frac{k_3}{T_m}\right]}$	5.5a	$\kappa(T_m)$ computed from T_m	
$T_m = \frac{\int_0^\infty \rho_v(z) dz}{\int_0^\infty \frac{\rho_v(z)}{T(z)} dz}$	5.6a	T_m computer from...	
$g_m = \frac{\int_0^\infty \rho(z) g(z) dz}{\int_0^\infty \rho_v(z) dz}$	5.7a	$gm = 9.784\ [1 - 0.00266 \cos(2\lambda) - (2.8 \cdot 10^{-7}) \times H]$	5.7b

The definitions of ZTD, ZHD, ZWD, and g_m as in Eqs. 5.1a, 5.2a, 5.3a, 5.7a and 5.7b follow the formalism from Saastamoinen (1972) and Davis et al. (1985).

It is important to note that the GPS ZWD quantity that should be used in Eq. 5.4b is the one defined by Eq. 5.3b and not the estimated ZWD which may be biased if the a priori ZHD used in the processing is biased (e.g. when an empirical a priori delay model such as GPT is used). Indeed, the estimated ZWD would compensate for an a priori ZHD bias. However, the total delay ZTD obtained from the sum of a priori ZHD and the estimated ZWD (see Eq. 5.1b) is correct. For the computation of ZWD, a better ZHD estimate must be used such as computed from Eq. 5.2a.

Note also that ZHD is sometimes computed as an integral of the total density of the air (see the definition in Davis et al. 1985). We do not recommend this approach as it is likely to introduce numerical errors depending on the limited vertical resolution and extent of the air density profile. Under hydrostatic equilibrium, the

integral expressed as in Eq. 5.1a can be computed with much higher accuracy from the surface pressure Ps either from observations or a Numerical Weather Prediction model.

The definition of κ(Tm) and Tm in Eqs. 5.5a and 6.6a are from Askne and Nordius (1987) and Bevis et al. (1992). These authors proposed empirical formulas for Tm depending on the surface temperature, Ts, only (Bevis et al. 1994), and on additional scaling parameters (Askne and Nordius 1987). The most commonly used formulation is Tm = 70.2 + 0.72Ts, from Bevis et al. (1994), where the coefficients were derived from a linear regression of radiosonde data over the USA. Other linear formulations have been proposed for different regions of the globe but all empirical formulations have limited accuracy in representing the spatial and temporal variations of Tm (Wang et al. 2005). NWP models offer an interesting alternative for the computation of Tm by numerical integration of Eq. 5.6a as they are available at any place globally and any time with high temporal resolution (e.g. 6-hourly) in almost real-time.

5.4.2.2 Constants

The calculation of ZHD and κ(Tm) involve specific gas constants for dry air Rd. = 287.04 ± 0.02 J K^{-1} kg^{-1} (ICAO 1993) and water vapour Rv = 461.522 ± 0.008 J K^{-1} kg^{-1} (Kestin et al. 1984), and refractivity coefficients k_1, k_2 and k_3 with $k'_2 = k_2 - k_1 \times (Rd/Rv)$.

Many authors published coefficient values from experimental work performed from the 1950s to the 1970s. Smith and Weintraub (1953) compiled and averaged the early measurements, and Hasegawa and Stokesberry (1975) compiled and characterized a significantly larger number of experimental results. Thayer (1974) developed an alternative and hybrid approach which includes measurements extrapolated from optical frequencies. Bevis et al. (1994) revisited the data used by Hasegawa and Stokesberry (1975) and determined a new set of average values and associated uncertainties. Finally, Rueger (2002) proposed a new set of 'best average' coefficients after reassessing the dataset used by Bevis et al. (1994). While there has been a broad consensus on the value of k_1 from previous authors, Rueger's new k_1 coefficient is 0.115% larger than the standard value. The impact on ZHD computed from Eq. 5.2a is an increase of about 2.6 mm at mean sea level (i.e. a bias of IWV =0.4 kg/m^2). The impact is also significant on the determination of bending angles from GNSS radio-occultation measurements (Healy 2011). Healy (2011) examined the reasons of increase in Rueger's k_1 estimate and identified two obvious reasons: a numerical inconsistency in the value of 0° = 273 K instead of 273.15 K and the inclusion or not of CO2 in the gas mixture composing the dry air by the previous authors. Rueger's estimate of k_1 includes 0.0375% of CO2, while the values reported by Hasegawa and Stokesberry (1975) and Bevis et al. (1994) are for dry CO2 free air. Healy (2011) highlights that though Rueger's estimate of k_1 appears to be more robust and defendable than the standard value, it does not account for non-ideal gas effects. This point requires further discussion and clarification because it is unclear in some of the older literature how and when non-ideal gas effects were included.

Finally, this study reinforces the need for new measurements of refractivity constants taking all these aspects into account.

Note that in Eq. 5.2a, it is the product of Rd. k_1 that appears. Hence the Rd. value used should be consistent in CO2 concentration with k_1. The value Rd = 287.04 J K^{-1} kg^{-1} from ICAO (1993) assumes a 0.0314% of CO2.

As for the other coefficients, the values for k2 from Bevis et al. (1994) and Rueger (2002) are fairly consistent. The values for k_3 differ by -0.01563 10^5 K^2 hPa^{-1} leading to a small fractional change in IWV of -0.42% (or 0.21 kg/m^2 in a high humidity content of IWV = 50 kg/m^2).

According to the significant work done by Rueger (2002) in re-assessing past measurements and re-evaluating the refractivity coefficients we recommend to use his results after correction for the non-ideal gas effects, as suggested by Healy (2011). Using the compressibility factors given by Owens (1967), i.e. 1/Zd = 1.000588 for dry air at 273.15 K and 1013.25 hPa, and 1/Zw = 1.000698 for water vapour at 293.15 K and a partial pressure of 13.33 hPa (the conditions of measurements of refractivity use by Rueger, 2002), Rueger's 'best average' coefficients become:

$$k_1 = 77.643 \pm 0.0094 \text{ K hPa}^{-1}\, k_2 = 71.2455 \pm 1.3 \text{ K hPa}^{-1}\, k_3$$
$$= (375.201 \pm 0.76) \times 10^3 \text{K}^2\text{hPa}^{-1} \quad (5.8)$$

Which should be used with an updated value of the specific gas constant for dry air including 0.0375% of CO2, Rd = 287.027 J K^{-1} kg^{-1}.

Note that the uncertainties of the refractivity coefficients indicated in Eq. 5.8 are those given by Rueger (2002).

5.4.2.3 Auxiliary Data

The computation of ZHD from Eq. 5.2a requires surface pressure at the GPS station. However, surface pressure is not often observed at GPS stations. Only a small number of IGS stations are equipped with pressure sensors and Wang et al. (2007a, b, c) and Heise et al. (2009) have pointed out inaccuracies in these data. On the other hand, surface pressure observations are available from the World Meteorological Organization (WMO) surface synoptic network (SYNOP) at about 8500 sites globally, with mostly 1- to 6-hourly reports. The main issues that arise with these data are related to sensor calibration, which has not been performed in a consistent manner across all stations over time, and height correction when reduced to mean sea level pressure (Ingleby 1995). Parracho (2017) compared ERA-Interim and SYNOP data over Europe and observed that altitude changes larger than 10 m are not uncommon in this dataset and that the update of station altitudes in the WMO and national weather services can be delayed by several months, hence introducing spurious biases and breaks in the observed pressure data. Recalibration of sensors, relocations of stations, equipment changes and changes in data processing, produce inhomogeneity in the times series which are detrimental to the analysis of climate

trends. NWP model outputs, such as operational analysis/forecasts or reanalysis, offer again an interesting alternative to sparse and inhomogeneous observational data.

Keeping in mind that an error of 1 hPa in Ps leads to an error of 2.3 mm in ZHD and an error of 0.35 kg/m^2 in IWV, it is important to choose the most accurate pressure data available (e.g. with an error < 1 hPa) compliant with the specific space and time scales of the application.

Whatever pressure data is used, a vertical adjustment is usually required to correct for the height difference between the barometer or the model topography and the location of the GPS antenna. A modified version from the Berg (1948) formula is commonly used to relate pressure between the two heights z1 and z2: P2 = P1 (1–0.0000226(z2−z1))5.225. Unfortunately, this formula assumes a standard temperature profile with T0 = 288 K at mean sea level and a lapse rate of – 6.5 K km^{-1} (Parracho 2017). A primary limitation of this formulation is with the constant mean sea level temperature which can induce a large bias when used globally (note that the lapse rate effect is only of second order). Instead, we recommend to use the ICAO (1993) formula:

$$P_2 = P_1 \left(\frac{T_2}{T_1} \right)^{-g_0/\alpha R_d} \tag{5.9a}$$

$$T_2 = T_1 + \alpha (z_2 - z_1) \tag{5.9b}$$

where α is the temperature lapse rate (in K km^{-1}), and P_1 and T_1 are the pressure and temperature at the initial height z_1, R_d=287.04 J K^{-1} kg^{-1} and g_0=9.80665 m s^{-2}. This formulation assumes the temperature varies linearly within the layer. With no other indication of the lapse rate, one can use α= − 6.5 K km^{-1}.

Pressure data in NWP models are usually available at the model surface (orography), at model levels (usually from a few meters above the surface up to a constant pressure level in the stratosphere, e.g. 0.01 hPa or 80 km for the current ECMWF operational model), or at a predetermined number of standard pressure levels (e.g. 37 pressure levels going from 1000 to 1 hPa with ERA-Interim). Extrapolation from the nearest model level can be done using Eq. 5.9a + 5.9b in the case when only data on the surface are available or when the final height is below the lowest model level. When the final height is between two model levels or pressure levels then it might be interesting to interpolate the temperature and pressure data from the two adjacent levels rather than doing a pure extrapolation based on a single level. Linear interpolation can be used with temperature and the logarithm of pressure.

When 3D gridded model data are available, it can be interesting to interpolate also data in horizontal dimension from the nearest grid points if the horizontal resolution is not too coarse. However, in regions of complex topography (mountains) or with transition from land to sea, horizontal interpolation is questionable as the adjacent grid points may have significant representativeness (Bock and Parracho 2019).

Wang et al. (2017) compared ERA-Interim pressure level data on a 0.75° by 0.75° grid, GPT2w (an empirical model derived from ERA-Interim on a 1° by 1° grid with annual and semi-annual oscillations, Böhm et al. 2015), and pressure measurements at 99 GPS stations, globally. They showed that the 6-hourly pressure data from

ERA-Interim have a RMSE compared to observations <2 hPa (to a few exceptions), with no clear benefit from horizontal interpolation using 4 grid points versus nearest grid point. The empirical model is shown to be unable to represent properly the temporal variations at short time scales (6-hourly and even monthly) with the required accuracy and furthermore does not include trends in surface pressure. If pressure trends in ERA-Interim and in reanalyses in general are correct merits further discussion.

The sensitivity of IWV errors to errors in Tm is about 0.069 kg/m^2 per K (Parracho 2017). The spatial and temporal variation of Tm, evaluated from the Earth surface to the top of the atmosphere, is in the range 220–300 K, globally. Hence, to guarantee an accuracy at the 0.2 kg/m^2 (resp. 1%) level, Tm should be determined with an error < 3 K (resp. < 1% or 2.2 K).

Estimates of Tm can be computed from Eq. 5.6a when vertical profiles of temperature and specific humidity are available. Radiosonde data are sometimes used to derive local or regional empirical models for that purpose but may not be adequate for applications requiring high accuracy (at 1–2 K level) and high temporal resolution (e.g. resolving the diurnal cycle and/or seasonal variations). Empirical Tm models derived from NWP data (e.g. GPT2w) have similar limitations. When high spatial and temporal resolutions are required, e.g. for climate applications, numerical integration of NWP model data is the best option (Wang et al. 2005, 2016b).

When Tm values are provided on a reference height, a vertical adjustment is required which can be computed from the following formula:

$$T_m = T_{m0} + \alpha_m (z_s - z_0) \tag{5.10}$$

where αm is the lapse rate for Tm, and Tm0 is the reference Tm value valid at height and z0, and zs is the final height. If no other information is available, a standard value $\alpha m = -5.4\ \mathrm{K\ km^{-1}}$ can be used (Parracho 2017).

Ready to use gridded data for ZHD and Tm are provided for example by the Technical University of Vienna (TUV). The data can be accessed from:

http://ggosatm.hg.tuwien.ac.at/DELAY/GRID/STD/ for ZHD,

http://ggosatm.hg.tuwien.ac.at/DELAY/ETC/TMEAN/ for weighted mean temperature,

http://ggosatm.hg.tuwien.ac.at/DELAY/GRID/orography for the model orography.

The data are distributed on global grid with a horizontal resolution of 2° latitude and 2.5° longitude, and 6-hourly temporal resolution, and are valid on the model orography. A vertical correction using Eq. 5.9a, 5.9b + 5.2a and 5.10 is usually required to extrapolate them to the altitude of the GNSS antenna.

The TUV data are computed from the ERA-40 reanalysis until 2002 and ECMWF operational analysis afterwards. While their use is fine for short term studies, their use for trend analysis is questionable, however, since the switch from ERA-40 to operational data and subsequent changes in the operational model may induce small inhomogeneities. In order to minimize such discontinuities, the conversion data should be better computed from a reanalysis (e.g. ERA-Interim). Though the homogeneity of current reanalyses is not guaranteed either (Thorne and Vose 2010), they nevertheless are the best and most stable representation of the atmospheric state.

5.4.2.4 Recommendations

As of the end of this COST Action, the recommended methodology and datasets for the conversion of GNSS ZTD data to IWV are the following:

- Use set of conversion equations presented in this subsection: Eq. 5.1a to 5.7b
- Use the set of 'best average' refractivity constants published by Rueger (2002) adjusted for non-ideal gas and updated for a CO_2 concentration of 0.0375%: Eq. 5.8
- Use NWP model data for the calculation of surface pressure and Tm at the station, e.g. provided by TUV or, better, recomputed from ERA-Interim pressure-level data
- Apply a vertical adjustment for Ps (or ZHD) and Tm if these data are not valid at the altitude of the GNSS station: Eqs. 5.9a, 5.9b and 5.10

5.4.3 *The Uncertainty of the Atmospheric Integrated Water Vapour Estimated from GNSS Observations*[11]

T. Ning
The Swedish Mapping, Cadastral and Land Registration Authority, Stockholm, Sweden
e-mail: tong.ning@lm.se

All GNSS measurements are subject to error sources that influence the uncertainty of the estimated IWV. Those errors can be random or systematic, or more commonly a mixture of both, depending on the timescale studied. Since the expected (mean) value of random errors is zero, the impact of such errors is reduced as the number of measurements increases. Systematic errors cannot be averaged out as the time series becomes longer. They can however change at a specific time epoch. For example, a change of the GNSS antenna or its environment may introduce such an offset.

In order to obtain the total uncertainty, all relevant error sources in GNSS-derived IWV are essential to be investigated. This work was initially motivated by GCOS (Global Climate Observing System) Reference Upper-Air Network (GRUAN) (Bodeker et al. 2016) and was at the same time highly relevant for the COST action. The results were reported by Ning et al. (2016a, b) and are summarised here.

A theoretical analysis was carried out where the uncertainties associated with the input variables in the estimations of the IWV were combined in order to obtain the total uncertainty of the IWV. We calculated the IWV uncertainties for several sites, used by the GRUAN, with different weather conditions. Table 5.5 below is taken from Ning et al. (2016a, b) which summarises the calculated total IWV uncertainties

[11]Parts from this section were previously published in Ning et al. 2016a, b).

Table 5.5 Summary of the calculated total IWV uncertainties for the GRUAN sites: LDBO, LDRZ, and NYA2

					Corresponding IWV uncertainty								
Input variable	LDBO	LDRZ	NYA2	uncertainty	LDBO			LDRZ			NYA2		
					[kg/m^2]	[%]	[%][e]	[kg/m^2]	[%]	[%][e]	[kg/m^2]	[%]	[%][e]
ZTD [mm]	2487	2376	2434	3.8, 3.7, 3.3[a]	0.59	3.2	79.9	0.58	4.8	82.2	0.49	6.1	77.0
Ground pressure P_0[hPa]	1000.1	968.7	1005.6	0.2[b]	0.07	0.4	1.2	0.07	0.6	1.3	0.07	0.9	1.5
Constant[f]	2.2767	2.2767	2.2767	0.0015	0.23	1.3	12.2	0.22	1.8	11.9	0.23	2.9	17.0
Mean temperature T_m [K]	274.6	270.8	262.3	1.1[c]	0.13	0.7	3.8	0.1	0.8	2.5	0.09	1.1	2.6
k_2'[K/hPa]	22.1	22.1	22.1	2.2[d]	0.05	0.3	0.6	0.04	0.3	0.5	0.03	0.4	0.3
k_3[$10^5 \times$ K^2/hPa]	3.739	3.739	3.739	0.012[d]	0.10	0.6	2.3	0.08	0.7	1.6	0.07	0.9	1.6
IWV [kg/m^2]	18	12	8										
Conversion factor Q	6.4	6.5	6.7										
Total IWV uncertainty					0.66	3.7		0.64	5.3		0.56	7.0	

[a]The values are given by the mean ZTD uncertainty calculated from one year of data for LDBO, LDRZ, and NYA2, respectively
[b]For GRUAN sites equipped with surface barometers which are calibrated routinely
[c]Taken from Wang et al. (2005) based on the comparison between ECMWF reanalysis and radiosonde data
[d]Taken from Table 1 in Bevis et al. (1994)
[e]Percentage of the total IWV uncertainty
[f]The constant given in Equation (23)

for three GRUAN sites: LDBO, LDRZ, and NYA2. For each site, the GPS data acquired from the year 2014 were processed using a Precise Point Positioning (PPP) strategy to obtain ZTD time series. The corresponding total ZTD uncertainties were then determined after taking both random and systematic errors into account. The estimated ZTD was converted to the IWV using the measured ground pressure and the mean temperature obtained from the ECMWF reanalysis data, ERA-Interim. In Table 5.5, the corresponding absolute values for IWV, ZTD, ground pressure, and mean temperature are given using the mean values of the year 2014 for each site. The table shows a similar relative importance of all uncertainty contributions where the uncertainties in ZTD dominate the error budget of the IWV, contributing over 75% of the total IWV uncertainty. The impact of the uncertainty associated with the conversion factor between the IWV and the ZWD is proportional to the IWV and increases slightly for moist weather conditions.

5.5 ZTD/IWV Homogenisation

R. Van Malderen
Royal Meteorological Institute of Belgium, Brussels, Belgium
e-mail: roeland@meteo.be

M. Eliaš
Geodetic Observatory Pecný, Research Institute of Geodesy, Topography and Cartography, Ondřejov, Czech Republic
e-mail: michal.elias@pecny.cz

E. Pottiaux
Royal Observatory of Belgium, Brussels, Belgium
e-mail: eric.pottiaux@oma.be

A. Klos
Centre of Applied Geomatics, Warsaw Military University of Technology, Warszawa, Poland
e-mail: anna.klos@wat.edu.pl

M. Gruszczynska
Centre of Applied Geomatics, Warsaw Military University of Technology, Warszawa, Poland
e-mail: marta.gruszczynska@wat.edu.pl

J. Bogusz
Centre of Applied Geomatics, Warsaw Military University of Technology, Warszawa, Poland
e-mail: jbogusz@wat.edu.pl

O. Bock
IGN Institut national de l'information géographique et forestière, Paris, France
e-mail: olivier.bock@ign.fr

B. Chimani
Central Institute for Meteorology and Geodynamics, Veinna, Austria
e-mail: barbara.chimani@zamg.ac.at

J. Guijarro
AEMET, Madrid, Spain
e-mail: jguijarrop@aemet.es

S. Zengin Kazancı
Karadeniz Technical University, Trabzon, Turkey
e-mail: szengin@ktu.edu.tr

T. Ning
The Swedish Mapping, Cadastral and Land Registration Authority, Stockholm, Sweden
e-mail: tong.ning@lm.se

This section is partly a summary of "Van Malderen R., Pottiaux E., Klos A., Bock O., Bogusz J., Chimani B., Elias M., Gruszczynska M., Guijarro J., Zengin Kazancı S. and Ning T.," "Homogenizing GPS integrated water vapour time series: methodology and benchmarking the algorithms on synthetic datasets" in Proceedings of the Ninth Seminar for Homogenization and Quality Control in Climatological Databases and Fourth Conference on Spatial Interpolation Techniques in Climatology and Meteorology, Budapest, Hungary, 2017, WMO, WCDMP-No. 845, edited by T. Szentimrey, M. Lakatos, L. Hoffmann, pp. 102–114 (http://www.wmo.int/pages/prog/wcp/wcdmp/wcdmp_series/WCDMP_85.pdf)".

5.5.1 Introduction

As water vapour is an important greenhouse gas and is responsible for the strongest positive feedback effect, estimating the long-term trends in water vapour is important for climate monitoring. However, the potential temporal shifts in the IWV time series obtained from GNSS can change the resulting trends significantly. In order to obtain realistic and reliable climate signals a homogenization of the IWV time series is necessary. In earlier work (Vey et al. 2009, Ning et al. 2016a, b) the time series of the differences between the GPS-derived IWV and the one obtained from the ERA-Interim model (Dee et al. 2011) are used for the data homogenization. Ning et al. (2016a, b) used a statistical test, the penalized maximal t test modified to account for first-order autoregressive noise in time series (PMTred, see Sect. 5.5.5), to identify the possible mean shifts (change points) in the difference time series. This approach allows for identification of the change points not only in the GPS IWV time series but also in ERA-Interim. After the correction of the mean shifts for the GPS data, an improved consistency in the IWV trends is evident between nearby sites, while a better agreement is seen between the trends from the GPS and ERA-Interim

data on a global scale. In addition, the IWV trends estimated for 47 GPS sites were compared to the corresponding IWV trends obtained from nearby homogenized radiosonde data. The correlation coefficient of the trends increases significantly by 38% after using the homogenized GPS data.

Within the COST action, a homogenization activity was also set up, targeting the following objectives: (i) select one or two long-term reference datasets, (ii) apply different homogenization algorithms on these reference datasets, and build up a list of commonly identified inhomogeneities based on statistical detection and metadata information, and (iii) come up with an homogenized version of the reference dataset that can be re-used to study climate trends and time variability by the entire community.

As a first reference dataset, we decided to focus on the existing first tropospheric product given by the data reprocessing of the International GNSS Service (IGS) network, named hereafter IGS repro 1. This homogeneous reprocessing (one single strategy) of the data results from a set of 120 GPS stations distributed worldwide providing continuous observations from 1995 until the end of 2010, see Fig. 5.22. The retrieved ZTDs estimated from the GNSS receiver observations at the stations have been screened, and the outliers have been removed as described in Bock (2015) and in Sect. 5.4.1. To convert those ZTD measurements in IWV, the surface pressure at the station location and a weighted mean temperature are needed, which are taken or calculated from ERA-interim (or ERAI), see Bock (2016a, b, c, d) and Sect. 5.4.2.

5.5.2 *Methodology*

As in the previously mentioned studies (Vey et al. 2009; Ning et al. 2016a, b), for a particular GNSS station, we chose to use the ERA-interim IWV time series at this GNSS site location as the reference series for the candidate IGS repro 1 IWV time

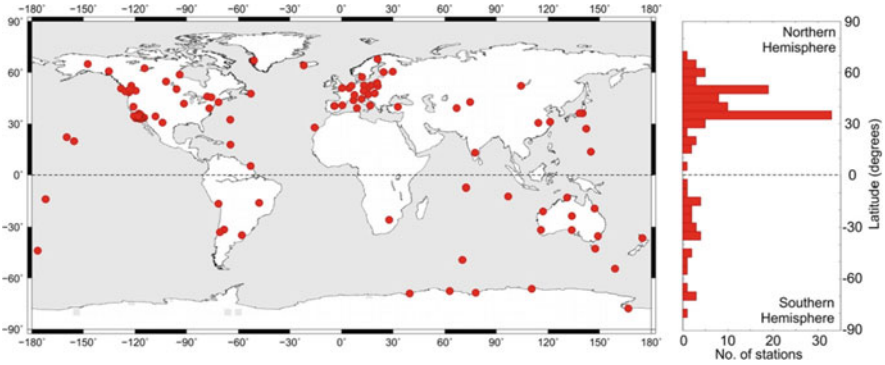

Fig. 5.22 Distribution of the 120 IGS repro 1 stations with data available from 1995 until the end of 2010

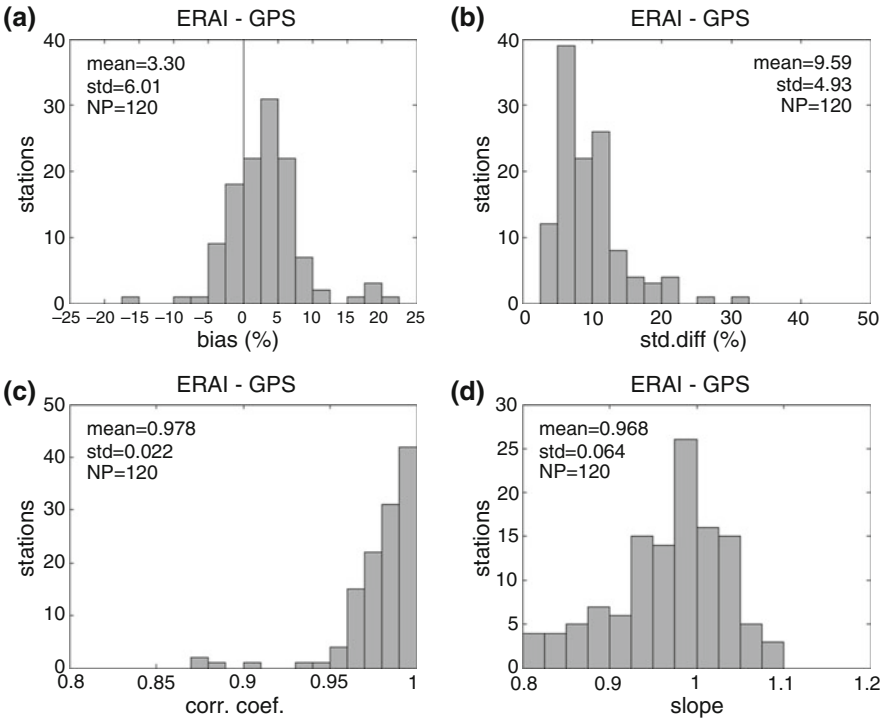

Fig. 5.23 Histograms of the relative biases (**a**), relative standard deviations (**b**), correlation coefficients (**c**), and linear correlation slope coefficients (**d**) between the IGS repro 1 and ERA-interim IWV time series for our sample of 120 GNSS stations

series. As can be seen in Fig. 5.23, for the large majority of the sites, the IGS repro 1 and ERA-interim IWV time series are highly correlated; the lower correlations are ascribed to a bad spatial representation by the model at those sites (e.g. large differences in orography in adjacent pixels). It should however be mentioned that the IGS repro 1 and ERA-interim IWV time series are not completely independent from each other: ERA-interim is used in the ZTD screening process and, as has been noted already above, the surface pressure and weighted mean temperature values, needed for the IGS repro 1 ZTD to IWV conversion, are taken from ERA-interim as well.

Most of the inhomogeneities in the GNSS-derived IWV time series due to antenna or radome changes and changes in the observation statistics (= events) are characterized by jumps in the IWV time series (Vey et al. 2009). Therefore, for each site, we calculate differences time series between the IGS repro 1 and ERA-interim IWV datasets, and we will look for the epochs of those events causing offsets in the difference time series.

5.5.3 Assessment of the Homogeneity of ERA-Interim

Although ERA-interim is used as reference dataset in our activity, ERA-interim might have inhomogeneities of its own, e.g. when new satellite datasets are introduced in the data assimilation system (see e.g. Ning et al. 2016a, b; Schröder et al. 2016). ERA-interim is also used for the development of tropospheric blind models which includes the temporal modelling of the model parameters. Therefore, Eliaš et al. (2019) tried to detect potential change-points that may occur in the ERA-Interim ZHD and ZWD time series.

They applied a statistical method that is based on the maximum value of two-sample t-statistics. More than 64.000 original time series for both products are then analysed, whereas the time span of the series included the years 1990–2015 with a time resolution of 6 h.

The epochs and the offsets of the detected change points for the ERA-interim ZWD time series are presented in Fig. 5.24. The regions in which change points are detected are mostly located near the equator, such as in the Pacific, but also in the Amazonia region, in Africa, and in Indonesia. Another interesting area is in the North Pacific. The average offset values are approximately around 20 mm. Those ERA-interim ZWD time series strongly depend on satellite humidity observations in areas such as oceans and deserts, which might introduce inhomogeneities due to changes in satellite missions and their calibrations. Overall a change point was identified in more than 12% of the total amount of the node profiles. Eliaš et al. (2019) did not detect change points for the ZHD series from the ERA-Interim reanalysis. This can be explained by the fact that the ZHD is related strongly with the atmospheric pressure, a rather smooth variable, which is easily observed and modelled.

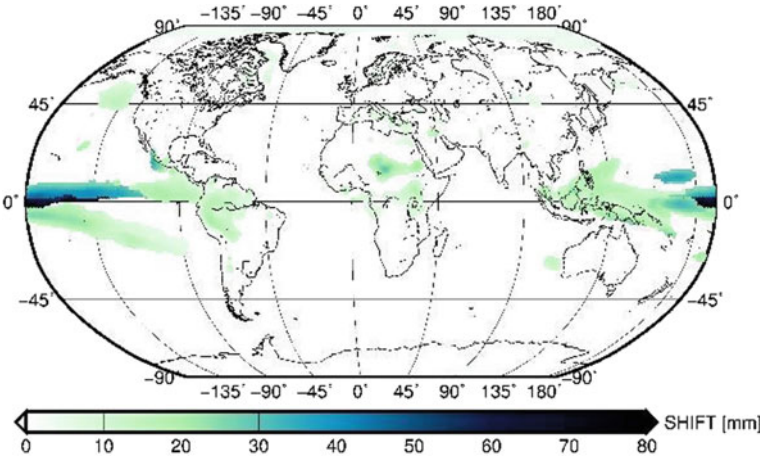

Fig. 5.24 The epochs in MJD (**a**) and offsets in mm (**b**) of the detected change points in the ERA-interim ZWD time series

5.5.4 Synthetic Gataset Generation

We tested different homogenization algorithms on the ERAI-IGS repro 1 differences, and compared their lists of identified epochs of offsets with a list of manually detected breakpoints from the metadata information. At some sites, breakpoints were detected in the metadata and by visual inspection, but not by any of the algorithms. In other cases, breakpoints were detected by a number of (or all) statistical tools, but no metadata information was available for the considered epoch. Therefore, we decided to first generate synthetic time series, with known inserted offsets, on which the different homogenization tools could be blindly applied and assessed. Additionally, we undertook a sensitivity analysis of the performance of the homogenization algorithms on varying characteristics of the synthetic time series.

It should be noted here that we generated synthetic time series of IWV differences directly, based on the characteristics of the real IGS repro 1 and ERA-interim IWV differences. By considering the differences, seasonal variability will be removed and the complexity of the noise will be reduced, making the generation of synthetic time series an easier task. First, we characterized the properties of the offsets (typical number per site and amplitudes) in the real IWV differences, based on the manual detection of 1029 events of instrumental changes, reported in the metadata files of the stations. Of those 1029 events, about 164 epochs were confirmed by visual inspection, and 57 new epochs were added. We derived the amplitudes of the offsets arising at those epochs and these are used for a first-order correction of the real IWV differences at those 221 identified epochs. Subsequently, we analysed the significant frequencies, the noise model, the presence of a linear trend and gaps in those corrected IWV differences with a Maximum Likelihood Estimation (MLE) in the Hector Software (Bos et al. 2013). As it is illustrated for the KOSG station in Fig. 5.25, we found that the most adapted noise model is given by the combination of white noise (WN) plus autoregressive noise of the first order (AR (1)), characterised by the amplitudes of white noise (with median value 0.35 mm) and autoregressive noise (median value 0.81 mm), the fraction and coefficient of AR (1), with respective median values 0.71 and 0.50. Another important finding is the presence of trends (of the order of ± 0.05 kg/m^2/year) in the IWV differences series.

So, based on the characteristics of the IWV differences series at each site separately, we generated for every site a synthetic time series of daily values that includes a number of offsets in the mean. As a matter of fact, to test the sensitivity of the performance of the homogenization tools on the complexity of the time series, 3 datasets of 120 synthetic daily IWV differences time series have been created, with increasing complexity:

- "easy" dataset: includes seasonal signals (annual, semi-annual, inter- and quarter-annual, if present for a particular station) + offsets + white noise (WN)
- "less-complicated" dataset: same as "easy" + autoregressive process of the first order (noise model = AR (1) + WN)

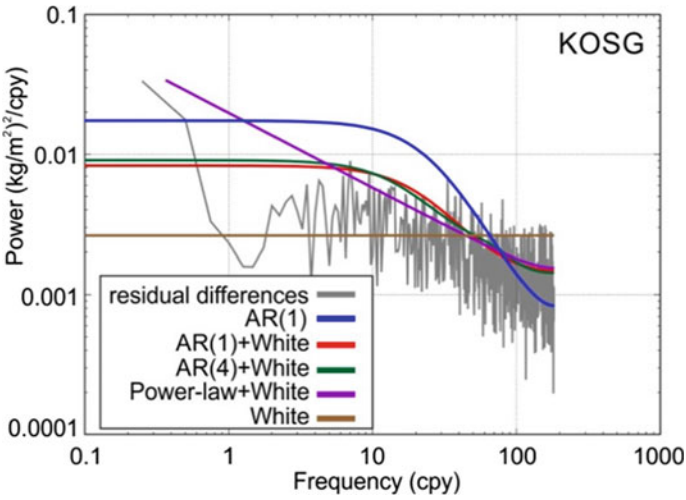

Fig. 5.25 Power spectrum of the IGS repro 1 and ERA-interim IWV residual differences at the site KOSG (Kootwijk, the Netherlands, 52.18°N, 5.81°E). The colour lines denote different noise models that we tested to decide on the noise model and that best characterize the IWV residuals

- "fully-complicated" dataset: same as "less-complicated" + trend + gaps (up to 20% of missing data). This dataset is closest to the real IWV differences.

These sets of synthetic time series were made available to the community for a blind testing of homogenization algorithms in use. The inserted offsets of the easy dataset are available to be revealed, if asked for by a participant, for fine-tuning of the algorithm on the use of IWV differences.

5.5.5 Involved Homogenization Algorithms

In this subsection, we give a small summary of the homogenization algorithms that participated so far in the blind homogenization of at least one of the variants of the synthetic time series. Those homogenization tools have been applied on daily and/or monthly values of the synthetic datasets.

5.5.5.1 Two-Sample t Test (Operator: M. Elias)

The procedure applied for the purpose of breakpoint detection is based on hypothesis testing. In this study we used a test statistic that is of so-called "maximum type" (see Jaruskova 1997). Within the field of mathematical statistics, the problem can be solved by testing the null hypothesis that claims that there is no change in the distribution of the series, against the alternative hypothesis that claims that the

distribution of the series changed at the time k. The null hypothesis is then rejected if at least one of the estimated statistics is larger than the corresponding critical value. Approximate critical values are obtained by the asymptotic distribution (see Yao and Davis 1986). Two ways of time series proceedings and method application were discussed; (i) the proposed method was applied to the uncorrected original series of IGS repro 1 and ERA-interim IWV differences and (ii) the method was applied to corrected difference series when the seasonality was removed and also the gaps were filled in the series before the breakpoint detection, for instance. The method of breakpoint detection is applicable on both monthly and daily time series. A confidence interval for the detected breakpoint is also possible to estimate.

5.5.5.2 PMTred (operator: T. Ning)

The rationale of this adapted *t* test is based on Wang et al. (2007a, b, c), which describes this penalized maximal *t* test (PMT) to empirically construct a penalty function that evens out the U-shaped false-alarm distribution over the relative position in the time series. Another modification, named the PMTred test, accounts for the first-order autoregressive noise and it was this test that was used for the homogenization. The critical values (CVs) of the PMTred test were obtained by Monte Carlo simulations running for 1,000,000 times as a function of the sample length N (monthly data, might have to be redone for daily data). In addition, the CVs were calculated for the lag-1 autocorrelation from 0 to 0.95 with an interval of 0.05 and for the confidence levels of 90%, 95%, 99%, and 99.9% (see Ning et al. 2016a, b). This test runs on monthly and daily values, but the critical values are calculated based on monthly data. The detection of multiple breakpoints is achieved by applying the test to the remaining segments.

5.5.5.3 HOMOP (Operator: B. Chimani)

The homogenization code HOMOP is a combination of PRODIGE (for detection, Caussinus and Mestre 2004), SPLIDHOM (adjustment, Mestre et al. 2011), an adapted interpolation (Vincent et al. 2002), and improved by some additional plots for facilitating the decision of the homogenisation and extended with some uncertainty information by using different reference stations as well as bootstrapping methods (HOMOP, Gruber et al. 2009). The approach is neighbour-based, and in the particular case of our synthetic datasets, a lower limit of 0.6 for the correlation coefficients was imposed for selecting potential reference stations. Break detection is done at annual or seasonal base.

5.5.5.4 CLIMATOL (Operator: J. Guijarro)

Another neighbour-based homogenization algorithm is CLIMATOL, which performs a form of orthogonal regression known as Reduced Major Axis (RMA, Leduc 1987) between the standardized anomalies (x-μx)/σx and (y- μy)/σy of the two distributions. Orthogonal regression is adjusted by minimizing the perpendicular distance of the scatter points to the regression line, instead of minimizing the vertical distance to that line as in Ordinary Least Squares regression (OLS). In the case of our synthetic datasets, it was imposed that the only reference time series at the site is the ERA-interim time series. The Standard Normal Homogeneity Test (SNHT, Alexandersson 1986) is applied to find shifts in the mean of the anomaly series in two stages. The code incorporates a filling in of missing data and outlier removal. The adjustment of the identified offsets can be done with a varying amplitude: by including e.g. σx in the standardization, you might include seasonality in the amplitudes. As in the other algorithms described so far, the detection of multiple breakpoints is done by applying the test to the remaining segments. CLIMATOL can be applied to any time scale data, but it is advised to detect the breakpoints at the monthly scale, and then use the break dates to adjust the daily series. This algorithm does not provide the amplitudes of breaks, as they are time varying. We might obtain the amplitudes by differencing the non-homogenized series with the homogeneous series.

5.5.5.5 Non-parametric Tests (Operator: R. Van Malderen)

In this case, the used statistical tests are non-parametric distributional tests that utilize the ranks of the time series to find breakpoints (or more general to test the equality of the medians of two distributions). Because such tests are based on ranks, there are not adversely affected by outliers and can be used when the time series has gaps. On the other hand, the significance of the test statistic cannot be evaluated confidently within 10 points of the ends of the time series and those tests show an increased sensitivity to breakpoints in the middle of the time series, when a clear trend is present (Lanzante 1996). We used two of such non-parametric tests: The Mann-Whitney (-Wilcoxon) test and the Pettitt (−Mann-Whitney) test, nicely described in Lanzante (1996). As an additional reference, the CUSUM test, based on the sum of the deviations from the mean, is also used. We developed an iterative procedure to detect multiple breakpoints: if 2 out of those 3 tests identify a statistical significant breakpoint, the time series is corrected (by adjustment of the oldest segment with the detected amplitude of the offset) and the 3 tests are applied again on the complete corrected time series. These tests have been applied on both the monthly and daily values.

5.5.5.6 Pettitt Test (Operator: S. Zengin Kazancı)

The Pettitt test (Petitt 1979) has been applied by another operator on the ranks of the daily values, together with the von Neumann ratio (von Neumann 1941) to determine if there is a breakpoint in the time series. If the series is homogeneous, the von Neumann ratio is equal to 2, for lower values of this ratio the series has a breakpoint (Wijngaard et al. 2003). The Pettitt test statistic is related to the Mann-Whitney statistic (see above).

5.5.6 Assessment of the Performance of the Tools on the Synthetic Datasets

In this subsection, we will assess the performance of the different homogenization tools on the synthetic datasets on two different aspects: (i) the identification of the epochs of the inserted breakpoints (+ sensitivity analysis) in the synthetic datasets, and (ii) the estimation of the trends that were or were not imposed to the 3 sets of synthetic IWV differences.

5.5.6.1 Identification of the Breakpoints

To assess whether or not the breakpoint given by a statistical detection tool coincides with the inserted, known, epoch of the break depends on the choice of the time window. Some homogenization algorithms give a confidence interval for the detected breakpoints, but other tools do not. To treat those different methods in a consistent manner, a proper, fixed time window for successful detection has to be set. A sensitivity study revealed that an adopted time window of 2 months is a good compromise.

Then we calculate for every breakpoint detection tool the statistical scores: the true positives (TP, "hits"), true negatives (TN: no breaks inserted, no break found), false positives (FP, "false alarms"), and false negatives (FN, "misses"). More details on how to calculate these scores can be found in e.g. Venema et al. (2012). To visualize the performance of the different tools in terms of those different statistical scores, we adapted the ternary graph representation from Gazeaux et al. (2013), shown in Fig. 5.26, for the fully complicated dataset. It depicts the ratios of the statistical detection scores (TP + TN, FP, and FN) by their position in an equilateral triangle, highlighting the trade-off between those. A perfect solution would appear on the bottom right corner of the triangle (see blue lines in the figure). From a glance on this figure, it can be directly noted that the involved homogenization tools do not perform very well for the fully complicated dataset: especially the number of false positives are too high. Fortunately, the probabilities of true detection are also high. Some methods nearly detect all the inserted breakpoints, but at the cost of a high

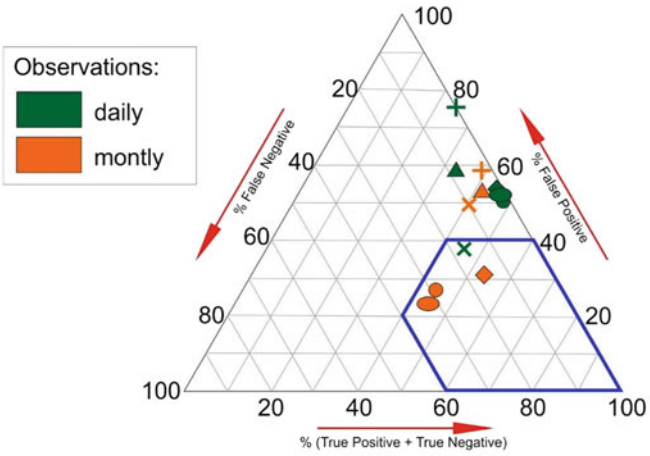

	Method 1	Method 2	Method 3	Method 4	Method 5	Method 6	Method 7
Symbol	● ⬭	▲	+	×	◆	▼	-
Operator	M. Elias	R. Van Malderen	R. Van Malderen	J. Guijarro	T. Ning	S. Zengin	B.Chimani
Method / SW	2-sample t-test	2 of 3	PMW	CLIMATOL	PMTred	Pettitt	HOMOP
Daily/Monthly	D+M	D+M	D+M	D+M	D+M	D	X
Easy/Less/Full	E+L+F	E+L+F	E+L+F	L+F	E+L+F	E+L+F	E+F

Fig. 5.26 Ternary graph representing the ratio between three performance measures of the breakpoint detection solutions (TP + TN, FP, and FN). The performance increases with decreasing numbers of false positives and false negatives and increasing numbers of true positives and negatives, so that a perfect solution is located in the lower right corner, marked by the blue area. The different solutions are marked with the symbols and colours outlined in the legend and in the table

number of false alarms, while other methods are more conservative in detecting breakpoints, resulting in low scores for both true detection and false alarms.

So far, we only discussed the results on the breakpoint detection on the fully complicated dataset. It should however be noted that a good performance of the tools is achieved for the majority of the participating methods on the easy and less complicated datasets, especially due to a lower amount of false positives. So, we can conclude that the performance decreases for almost all the tools when adding gaps and a trend in the benchmark time series; adding autoregressive noise of the first order has less impact.

Some of the homogenization algorithms also provided the (constant) amplitudes of the detected offsets. These were compared with the amplitudes of the offsets that were put in the synthetic time series. The result, again for the fully complicated dataset, is shown in Fig. 5.27. From this figure, it could be seen that some methods tend to underestimate the number of offsets with small amplitudes relatively (e.g. ME1 and ME2), while other methods on the contrary overestimate the amount of those offsets (e.g. RVM 2of3 D), but on the other hand underestimate the number

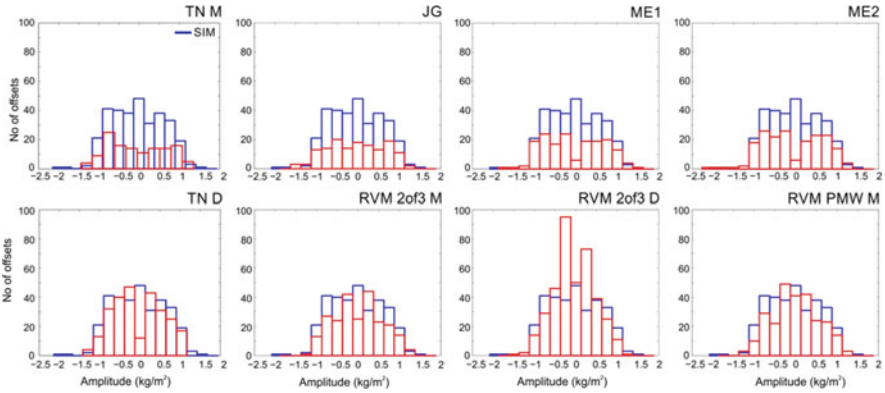

Fig. 5.27 The histograms of the amplitudes of the detected offsets by the different methods (in red in all figures), compared to the amplitude distribution of the inserted offsets in the fully complicated synthetic dataset of IWV differences (in blue)

of offsets with large amplitudes. Clearly, the different methods have a different sensitivity to the amplitudes of the offsets, and some fine-tuning on the statistical thresholds might be advised for some methods. For the other variants of the synthetic datasets, the amplitude distribution of the detected offsets more closely follows the amplitude distribution of the true inserted offsets.

5.5.6.2 Trend Estimation for the Homogenized Datasets

Only in the fully complicated dataset, a trend was inserted in the IWV differences series, and the homogenized time series by the different time series should hence reveal the same trend. However, for some stations, trends as large as 0.1 kg/m^2 (or mm) per year arise after correcting for the detected offset by some methods. Overall, for the fully complicated synthetic datasets, most trends differ within $\pm$0.05 kg/m^2 per year. As one of the main goals of our homogenization activity is the provision of a homogenized dataset of GNSS IWV time series for use in trend analysis, special care should be taken not to introduce spurious trends in the time series after correction. In this sense, the impact of homogenization on the estimated trend uncertainties should also be further elaborated.

5.5.7 Conclusions and Outlook

In this contribution, we described the current activity in homogenizing a world-wide dataset of IWV measurements retrieved from observations made at ground-based GNSS stations. As the distances between those 120 stations are large and

correlations are generally low (lower than 0.6 for distances larger than 1°), we used the ERA-interim reanalysis IWV fields at those station locations as the reference time series for relative statistical homogenization. Based on the characteristics of the IWV differences series between the GNSS dataset and ERA-interim and the properties of manually checked instrumental change events reported in the metadata of the GNSS sites, we generated three variants of 120 synthetic IWV difference time series with increasing complexity: we first added autoregressive noise of the first order and subsequently trends and gaps. Those synthetic time series enable us to test the performances of six participating breakpoint detection algorithms and their sensitivity to this increasing dataset complexity.

We found that the performances of those algorithms in identifying the epochs of the inserted offsets especially decreases when adding trends and gaps to the synthetic datasets, due to a larger number of false alarms. On the other hand, the hit rates of most tools are rather good, even when applied on daily values instead of on monthly values. Different tools show a different sensitivity for detecting different ranges of amplitudes of offsets, especially for the most complex (fully complicated) synthetic time series: some tools overestimate (underestimate) the number of small-amplitude (large-amplitude) offsets, while the opposite is true for other breakpoint detection algorithms. After eliminating differences due to different calculation methodologies, we found trend differences mostly within ± 0.05 kg/m^2 per year between the inserted trends and trends calculated from the different homogenization solutions.

Owing to the fact that metadata on instrumental changes are available for the GNSS stations, we primarily focused on the identification of the epochs of offsets until now. At the end, we would like to combine the outcome of statistical breakpoint detection with these metadata. However, we will also assess the performances of the different tools by comparing the final solutions for the time series given by different tools with the original time series (e.g. calculating Centred Root Mean Square errors as in Venema et al. (2012), calculating trends directly from the final solutions, etc.).

Of course, we highly welcome contributions from other groups running homogenization tools, and in the future, our benchmark will already be extended with few more contributions. After providing solutions for the synthetic time series, the participants will get the opportunity to fine-tune their methods on the specifications of the datasets with the help of the knowledge of the true inserted offsets and their amplitudes. Thereafter, a second round of blind homogenization on a newly generated synthetic dataset of IWV values (probably with simulated metadata information) will be held. Based on the performance of the statistical homogenization tools on these synthetic datasets, we will develop a methodology for combining the results of good performing homogenization tools with metadata information. This methodology and those tools will then be applied on the IGS repro 1 dataset of retrieved GPS IWV time series, resulting in a homogenized dataset, which will be validated by other sources of IWV time series and finally made available to the community for assessing the time variability of IWV and for validation of climate model IWV outputs.

5.6 IWV Intercomparisons

5.6.1 A Literature Overview

R. Van Malderen
Royal Meteorological Institute of Belgium, Brussels, Belgium
e-mail: roeland@meteo.be

5.6.1.1 Introduction

Already in 1992 demonstrated Bevis et al. the potential of GNSS ground-based receivers for measuring the IWV amount in the zenithal column of the atmosphere (Bevis et al. 1992). Summing up the uncertainties of the individual contributions (the uncertainties of the ZTD estimations, the ZHD modelling, and the conversion from ZWD to IWV) to the GNSS IWV retrieval, the estimated total uncertainty is generally less than 2 mm (e.g. Wang et al. 2007a, b, c; Van Malderen et al. 2014). Ning et al. (2016a, b) calculated, from a theoretical point of view, the total IWV uncertainty from the individual uncertainties of each of the input variables, according to the rule of uncertainty propagation for uncorrelated errors (see also Sect. 5.4.3. The results show a similar relative importance of all uncertainty contributions where the uncertainties in the ZTD dominate the error budget of the IWV, contributing over 75% of the total IWV uncertainty. Alternatively, in the same paper, a statistical analysis is proposed to evaluate the uncertainty of the GNSS-derived IWV if independent estimates are available from at least three co-located techniques, measuring the same true variability of the IWV.

Clearly, one of the aims of IWV intercomparison studies is to assess the quality, consistency, accuracy, and stability of different techniques measuring IWV, with respect to each other or a chosen reference. This can be on a local, regional, or global scale, and considering only a short time period or on a decadal time scale, when the usability of the different techniques for long-term climate research is investigated. Examples of intercomparison analyses focusing on one of those different aspects can be found in the inventory of past studies in the literature, which has been built up in the course of the COST action (http://www.meteo.be/IWVintercomp). Whereas in the beginning of the GNSS (GPS) era, the accuracy of GNSS retrieved IWV was evaluated through comparison studies with radiosonde (RS) and microwave radiometer (MWR) IWV measurements, the focus of recent IWV intercomparison studies involving GNSS is the validation of the satellite IWV retrievals and (climate) model IWV output with GNSS as reference.

Recent reports or papers overviewing IWV inter-technique comparisons hang up a rather pessimistic view of the consistency of the results between those different studies, or to cite Buehler et al. (2012): “A literature survey reveals that reported systematic differences between different techniques are study-dependent and show

no overall consistent pattern." Also Guerova et al. (2016) conclude that "it is, however, not possible to draw final conclusions regarding the absolute accuracies of the instruments and techniques. All techniques suffer from systematic errors at different timescales meaning that case studies using specific sensors, at specific locations, at different times, will give different comparison results, often presented as biases and root mean square (RMS) differences. For example, an error appearing as a bias in a 2-week long comparison may present itself as a random error over a period of many years." Additionally, the Global Energy and Water Cycle Experiment Data and Assessments Panel (GDAP) has found that assessment activities should not be viewed as static but rather as dynamic activities that need to be repeated every 5–10 years. In this contribution, we will nevertheless try to distillate some general findings from the inventory of the IWV intercomparison studies, but, of course, taking into account that those studies cover different instruments, sites, periods, methodologies, etc.

5.6.1.2 Datasets and Methods in Past IWV Intercomparisons

We compiled an online inventory of past IWV intercomparisons involving GNSS: http://www.meteo.be/IWVintercomp, which will be regularly updated. As can be seen from this inventory, the GNSS IWV retrievals have been compared with a wide range of other techniques. Each instrument has its own specific sensing properties, which have to be taken into account when giving an overview of different inter-technique analyses.

5.6.1.3 Differences in Instruments

There are numerous techniques measuring IWV, from ground-based devices, in-situ (radiosondes) and from space on board satellites. Remote sensing techniques can be divided into 3 categories: (1) differential time of arrival measurements, like GNSS, Very Long Baseline Interferometry (VLBI) and Doppler Orbitography Radio Positioning Integrated by Satellite (DORIS), (2) active techniques like LIght Detection And Ranging (LIDAR) and RAdio Detection And Ranging (RADAR) (3) passive techniques based on emission/absorption measurements (Guerova et al. 2016). Among ground-based emission/absorption measurements there are microwave radiometers, photometers (with the sun, the moon or a star as light source), and Fourier-Transform Infrared Spectroscopy (FTIR). Also space measurements of IWV make advantage of different parts of the electromagnetic spectrum of the Earth's atmosphere: microwave (AMSU-B, AMSR-E, SSM/I, SSMIS, HSB, etc.), visible (OMI, GOME, GOME-2, SCIAMACHY, etc.), near-infrared (MODIS) and thermal infrared (MODIS, AIRS, SEVIRI, IASI, ISCCP (TOVS), etc.).

Those different techniques have some specific constraints on the capability of measuring the IWV: the opacity of clouds makes the measurements in the visible or (near) infrared spectral range unreliable under cloudy sky conditions. When data in

the visible or near infrared range are analysed, measurements are also restricted to daytime, which is the case for e.g. GOME, SCIAMACHY, GOME-2 and of course for a ground-based sun photometer. For passive microwave nadir sensors (like SSM/I, AMSU-A), the large variability of the surface emissivity over land and sea ice makes the retrievals generally more difficult than over the ocean where the emissivity is well known. The operational products retrieved from those sensors provide therefore only data over the oceans (Urban 2013). Microwave radiometers from the ground cannot observe during rain or snow. The GNSS technique, on the other hand, can be used under all weather conditions and therefore has no weather bias as some of the other techniques. This weather bias, and in particular the presence of clouds, might have an impact on the comparison of the IWV measurements between two instruments. For instance, the IWV linear regressions at Brussels between (i) a sun photometer and GNSS and (ii) satellite retrievals and GNSS have different properties when comparing clear sky and partly cloudy scenes (see Figs. 6 and 9 respectively in Van Malderen et al. 2014).

Furthermore, the instruments have a different horizontal representativeness of the IWV field they measure. The satellite devices use mostly nadir techniques for the IWV measurements, but depending on their orbits, the horizontal resolution vary between 1 × 1 km (MODIS) to 40 × 320 km (GOME). On the other hand, ground-based techniques like MWR and Lidar measure in the zenith, while a sun photometer traces the water vapour amount in the solar slant. The GNSS IWV is retrieved in a cone, representative for about 100 km^2, and the radiosonde is drifted away from the launch site during its ascent. The disadvantage of ground-based techniques with respect of satellite retrievals is that the coverage of stations is quite often not sufficient to represent the high spatial variability of water vapour. Satellite observations can cover the whole planet in 1–2 days.

Water vapour has also a high temporal variability, and instruments on board of low Earth orbiting satellites, cannot adequately sample e.g. the diurnal cycle of IWV, as at most one or two measurements a day are available at a given location. Sun photometers have a temporal resolution of about 15 min, but of course can only measure during daytime and at clear skies in the direction of the sun. Microwave radiometers and GNSS measure continuously and hence are the devices with the highest temporal resolutions. In practice, GNSS IWV retrievals are available at time scales of 5 min to 1 hour, depending on the processing options but also on the time resolution of the auxiliary meteorological variables required to convert ZTD into IWV.

So, due to the different characteristics of the different techniques, the agreement between IWV retrievals by different techniques will not be perfect. Moreover, Buehler et al. (2012) also showed that systematic differences between subsets of the same technique (e.g. FTIRa/FTIRb) at one site may exceed differences between different techniques (as demonstrated by their Figure 9) at this site.

5.6.1.4 Differences in Methodology

Given the high spatial and temporal variability of the integrated water vapour and because the different instruments have a different horizontal representativeness and different spatial and temporal samplings, co-location and coincidence criteria have to be chosen in IWV inter-technique analyses. Starting with the temporal separation, past studies have used only concurrent time stamped data, others have interpolated data to the time of other measurements, and others have used the temporally nearest data point within a certain time limit, ranging from less than 10 min to less than 2 hours, depending on the temporal resolutions of the compared techniques. Spatial co-location is achieved by imposing an upper limit for the distance between two sites (ranging from on site to more than 150 km, e.g. Torres et al. 2010) or between the site and the satellite ground pixel centre or by demanding that the site lies in the satellite ground pixel. Of course, due to the large differences in horizontal resolutions between the satellite samplings, those site-satellite co-location criteria will impact the IWV agreement to a large extent, even when comparing with satellite instruments that make use of the same wavelength range for the IWV retrieval (e.g. GOME and SCIAMACHY).

To prevent the presence of a systematic bias between two datasets of IWV measurements, the vertical separation between sites should be taken into account and corrected for. This can be most easily done when vertical profile measurements of temperature and humidity are present (by radiosonde measurements), e.g. Buehler et al. (2012) found for the Arctic station Esrange a relative bias ΔIWV/IWV of -3.5% per 100 m altitude difference. However, the actual scaling factors seem to depend on location, as Bock et al. (2007) found a value of -4.0% per 100 m for Africa, and might therefore not generally applicable. Other possible corrections rely on the assumption of a constant temperature lapse rate, a constant dew point depression with height (Deblonde et al. 2005) or a constant relative humidity with height (Hagemann et al. 2003). In this context, it should also be noted that a vertical correction is also required for the surface temperature and pressure measurements needed to convert ZTD into IWV, if an altitude difference exists between the GNSS station and the co-located meteorological station or reanalysis grid pixels that provide the surface measurements.

Finally, past studies also use different statistical parameters to describe the agreement between two (or more) IWV datasets. The most commonly used variables are the (absolute and relative) bias and the standard deviation, but also the median of the differences, the mean bias error, RMS, RMSE, the linear regression slope and the linear regression offset are widely used. Vaquero-Martinez et al. (2017a) calculated the pseudo median and the interquartile range of the relative differences as estimators for the accuracy and the precision respectively of their satellite data with respect to ground-based GNSS data.

Discussion of "Common" Results from Past Intercomparison Studies

5.6.1.5 General Overview

The range of values reported for the most common statistical parameters, with the GNSS IWV retrievals as reference, are summarized in Table 5.6 for the IWV intercomparison studies present in the inventory http://www.meteo.be/IWVintercomp. A first thing to note is the very wide range of biases (GNSS – instrument), even within one technique, except for the MWR and FTIR. But only 3 different studies compared GNSS and FTIR IWV retrievals. The highest variability in the statistical parameters is obtained in the GNSS-model and GNSS-satellite comparisons. In those cases, the possible large differences in spatial representativeness of the IWV field between the GNSS station and the grid pixel(s) surrounding this station might cause large disagreements, especially in stations located in regions with large topographical variability (e.g. coastal stations, mountain areas, etc.). But several other factors are likely to affect the observed biases (see Buehler et al. 2012): for the radiosonde, important factors are the sensor type (see e.g. Fig 6. in Wang et al. 2007a, b, c), launching procedures and the local time, as some sensors suffer from a radiation dry bias. For the GNSS, the exact antenna characteristics play a role, including the characteristics of a radome covering the antenna, and the presence or absence of microwave absorber material around the antenna. Ning et al. (2011) reported that the addition of absorber material decreased the GNSS IWV bias by 1.3 kg/m^2, and the addition of a radome made a difference of 0.4 kg/m^2. How strongly these hardware differences actually affect the IWV data also depends on the data analysis, particularly how slant wet delays are mapped to the zenith and what satellite elevation angle cut-offs are applied (Ning et al. 2011).

The ranges shown in Table 5.6 are of course study-dependent and also vary from region to region. We however note that the ranges become narrower when applying a uniform methodology for different sites and different instruments. We also believe that the range of the slopes reflects the presence of a weather bias in the instruments: the all-weather devices like RS and MWR have higher minimal regression slope coefficients with respect to GNSS, and the low upper limit of the regression slope coefficients for SPM and FTIR is believed to be caused by the weather observation bias of these instruments. We will come back to this point later.

Table 5.6 Ranges of the bias (mm), standard deviation (mm), linear regression slope and offsets of IWV retrievals by different instruments, with GNSS taken as reference

Instrument	N	Bias	Stdev	Slope	Offset
RS	45	−8.01 – 8.00	0.21–7.29	0.82–1.47	−25.95 – 11.66
MWR	18	−1.66 – 0.50	1.02–4.18	0.82–1.21	−1.46 – 4.60
SPM	21	−3.58 – 5.90	0.80–3.07	0.63–1.03	−3.37 – 5.70
FTIR	3	−0.09 – 0.61	0.73–1.02	0.95–1.06	−0.78 – 0.40
Satellite	31	−7.05 – 1.50	0.35–7.04	0.75–2.33	−2.92 – 8.89
Models	23	−8.70 – 5.30	0.64–8.08	0.66–2.00	−31.90 – 9.70

The values have been taken from all intercomparison studies present in the inventory. *SPM* Sun photometer

5.6.1.6 IWV Dependence of the Differences

Despite the differences between the techniques and the different applied methodologies, some general properties could be observed in the past studies. It turns out that the IWV bias and standard deviation of the differences between GNSS and other instruments both show a dependency on the IWV value measured (see e.g. the plots in Vaquero-Martínez et al. (2017a, b, c) for GNSS-satellite, and in Campanelli et al. (2017) for GNSS-SPM). Because the IWV values are higher in summer than in winter, past studies have mentioned the same dependency indirectly by pointing to a seasonal behaviour of the GNSS-RS IWV bias (Ohtani and Naito 2000; Basili et al. 2001; Deblonde et al. 2005; Kwon et al. 2007; Van Malderen et al. 2014), the GNSS IWV MWR bias (Sohn et al. 2012), the GNSS-SPM IWV bias (Nyeki et al. 2005; Morland et al. 2006; Prasad and Singh 2009; Van Malderen et al. 2014, Pérez-Ramírez et al. 2014), the GNSS-model IWV bias (NCEPNCAR reanalysis: Prasad and Singh 2009; Vey et al. 2010; AMPS: Vázquez and Grejner-Brzezinska 2013), the GNSS-satellite IWV bias (AIRS: Prasad and Singh 2009; Van Malderen et al. 2014; MODIS: Prasad and Singh 2009; Bennouna et al. 2013; Joshi et al. 2013; GOMESCIA: Van Malderen et al. 2014, GOME-2: Román et al. 2015, OMI: Wang et al. 2016a, b), the GNSS-MWR IWV standard deviation (Basili et al. 2001; Sohn et al. 2012), and the GNSS-satellite standard deviation (MODIS: Joshi et al. 2013; Ningombam et al. 2016; OMI: Wang et al. 2016a, b). Also, Ning et al. (2012) noted a seasonal behaviour in the GNSS–RS/ECMWF/MWR standard deviations of the ZWD. Additionally, because the IWV is higher for lower latitudes, global IWV inter-technique analyses observed a latitudinal dependency of the GNSS-NCEP IWV biases (Vey et al. 2010), the GNSS-GOME-2 IWV biases (Kalakoski et al. 2016), the GNSS-HIRLAM ZTD biases (Haase et al. 2003), the GNSS- RS/SPM/AIRS/GOMESCIA IWV standard deviations (Van Malderen et al. 2014), and the GNSS-DORIS ZTD standard deviations (Bock et al. 2010).

In the literature, several causes have been addressed for this IWV dependency of the differences (bias and SD) of several techniques with GNSS. Let us first concentrate on the IWV dependency of the biases with GNSS. This seems related to the fact that the different techniques and GNSS have different sensitivities: under dry conditions, the GNSS data are known to be less precise (Wang et al. 2007a, b, c) and therefore underestimates the IWV values (Schneider et al. 2010) or satellite retrievals tend to overestimate the low IWV values (Bennouna et al. 2013; Van Malderen et al. 2014; Kalakoski et al. 2016; Vaquero-Martínez et al. 2017c), whereas at large IWV values, a weather observation bias (clear sky) or sampling bias (Bennouna et al. 2013) might lead to an IWV underestimation by other techniques (Prasad and Singh 2009; Van Malderen et al. 2014). In particular, several studies comparing IWV satellite retrievals with ground-based measurements noted an underestimation of satellite (large) IWV values (AIRS, GOME, MODIS, GOMESCIA, see e.g. Van Malderen et al. 2014 Román et al. 2015, and Vaquero-Martínez et al. 2017c) with increasing cloud fraction. This can be due to the so called shielding effect (Román et al. 2015): clouds can hide the water vapour under them.

In this context, we also mention that several studies found a solar zenith angle (SZA) dependency of the GNSS-satellite IWV differences (and of the GNSS-MWR IWV difference, see Pérez-Ramírez et al. 2014), which is also linked with the seasonal variation of the IWV differences: small SZA exclusively arise in summer, large SZA exclusively in winter. For GOME-2, Antón et al. (2015) suggested that the SZA dependency (increasing biases with increasing SZA) could be related to inaccuracies in the geometrical correction factor applied in the GOME-2 retrieval algorithm to determine the air mass factor (AMF) of the water vapour. The SZA dependency of the GOME-2/GNSS differences may be also affected by other factors like cloudiness and albedo conditions (Román et al. 2015). But a SZA dependency of the GNSS-satellite biases is also present for other satellites (OMI, MODIS-Aqua, SEVIRI-daytime show the same dependency as GOME-2, see Vaquero-Martínez et al. 2017c). Another reason for the different sensitivities of satellites and GNSS to different IWV regions is given by those same authors (and phrased as "all satellites tend to homogenize water vapour: low IWV tends to be overestimated, while high IWV tends to be underestimated"): the spatial resolution of satellites is much lower than GNSS ground-based stations, and thus the IWV measurement is somehow averaged over the whole pixel. Other explanations for the IWV dependency of biases are uncertainties in the spectroscopic data base used for the MODIS retrieval, so that large differences with large amount of water vapour are caused by uncertainties in the calculation of the atmospheric transmittance for water vapour (Joshi et al. 2013), the RS day-night humidity bias, which scales with humidity (Haase et al. 2003; Kwon et al. 2007), deficiencies in the water vapour modelling due to e.g. assimilation of dry biased radiosondes (Vey et al. 2010) or insufficient model resolution or physics parameterization (Haase et al. 2003), uncertainties in the RS measurements, which are used as reference data for the MWR IWV estimation algorithm or from influences of protecting film of the scanning mirror (Sohn et al. 2012), the variation of the GNSS station position caused by ocean tidal loading (Ohtani and Naito 2000) and the seasonal change of the mapping function, which varies as the height scale of the atmosphere changes (Ohtani and Naito 2000; Nyeki et al. 2005), and a GNSS antenna phase centre mis-calibration or the lack of proper calibration parameters (Vázquez and Grejner-Brzezinska 2013).

The tendency for the GNSS–RS SD to increase with IWV was attributed (Ohtani and Naito 2000; Basili et al. 2001; Haase et al. 2003; Deblonde et al. 2005) in part to stronger humidity gradients that can exist between dry and moist air when moister air is involved. In the presence of strong gradients, the location and sampling differences between GNSS and RS can be more significant than for lower IWV conditions. In addition, Ohtani and Naito (2000) claimed that the presence of strong horizontal gradients in atmospheric properties can have a negative impact on the ZTD accuracy due to a breakdown of the azimuthal symmetry assumption. Other authors point to the fact that uncertainties of some techniques are dependent on the absolute measured value (e.g. RS accuracy of 4%, Ning et al. 2012), on the number of measurements and the number of satellites simultaneously in view (e.g. for DORIS, Bock et al. 2010). The standard deviations between GNSS and MODIS

IWV retrievals during summer and autumn (monsoon) seasons in India are due to large variation of the daily PWV data at the site. Such large variation in values may be attributed to larger uncertainties associated in the MODIS retrieval algorithm particularly during monsoon season (Prasad and Singh 2009; Joshi et al. 2013; Ningombam et al. 2016).

5.6.1.7 Conclusions

Due to its high accuracy and precision, growing coverage, long-term stability and all weather observing capability, the GNSS technique for IWV retrieval is recently been used more frequently as reference device for e.g. the validation of IWV satellite retrievals. Also the validation of the IWV time series from climate models is an emerging field. Assessing the long-term stability and homogeneity of GNSS IWV datasets is therefore of great importance. However, past IWV inter-technique studies including GNSS (http://www.meteo.be/IWVintercomp) concluded that the results of those studies are hard to intercompare, because study and time dependent to a large extent.

Here, we summarized some of the most important characteristics of the different instruments and we described major differences between the past studies. Because IWV is highly variable in space and time, we also want to highlight the need for spatial co-location and temporal coincidence criteria that reflect the horizontal representativeness of the different instruments. Additionally, when comparing ground-based devices, a correction for the vertical separation between sites is indispensable. The ranges of IWV biases and standard deviations and linear regression coefficients of one technique with respect to GNSS, extracted from the inventory of IWV intercomparison studies (http://www.meteo.be/IWVintercomp), are very broad, but we believe that, when applying a uniform methodology for different sites, those could be narrowed down.

A general property that has been observed by many past studies is the IWV dependence of the IWV differences with GNSS (both the bias and the standard deviation). Apart from some specific deficiencies in the IWV retrieval methodology, the fact that GNSS is an all-weather technique and other techniques clearly show an observation bias (partially clear sky or low cloud cover), with a clear dependence on the cloud cover, will certainly be a role in this feature. Also the SZA dependence of some techniques is clearly linked. Of course, sampling issues between satellite retrieved IWV and GNSS might, at least for some sites, be partly responsible. This IWV dependence of the IWV differences with GNSS is mimicked by a seasonal or latitudinal variation of the IWV differences.

5.6.2 *A Comparison of Precipitable Water Vapour Products Over the Iberian Peninsula*

J. P. Martins
Instituto Português do Mar e da Atmosfera, Lisbon, Portugal
e-mail: joao.p.martins@ipma.pt

P. Viterbo
Instituto Português do Mar e da Atmosfera, Lisbon, Portugal
e-mail: pedro.viterbo@ipma.pt

C. Barroso
Instituto Português do Mar e da Atmosfera, Lisbon, Portugal
e-mail: carla.barroso@ipma.pt

R. Fernandes
University of Beira Interior, Covilhã, Portugal
e-mail: rmanuel@di.ubi.pt

H. Valentim
University of Beira Interior, Covilhã, Portugal
e-mail: hugo.valentim@segal.ubi.pt

M. Bos
University of Beira Interior, Covilhã, Portugal
e-mail: machiel@segal.ubi.pt

A. Ramos
Instituto Dom Luiz, University of Lisbon, Lisbon, Portugal
e-mail: amramos@fc.ul.pt

J. Jones
Met Office, Exeter, UK
e-mail: jonathan.jones@metoffice.gov.uk

A. Sá
Polytechnic Institute of Guarda, Guarda, Portugal
e-mail:

5.6.2.1 Abstract

This work compares GNSS PWV estimates over Iberia with independent sources of the parameter such as the clear-sky TPW estimate based on SEVIRI observations provided by the NWC-SAF, ECMWF forecasts and local radiosondes. A general quality assessment of the products is performed and the biases between datasets are discussed.

5.6.2.2 Introduction

A team from the Instituto Português do Mar e da Atmosfera (IPMA) and the Space & Earth Geodetic Analysis Laboratory (SEGAL) – who already demonstrated the usefulness of GNSS PWV retrievals for weather and climate purposes (Adams et al. 2011), developed an operational scheme to produce these estimates for the Iberian Peninsula. The main objective of this work is to validate GNSS PWV by comparison with other standard datasets for this region, which are used routinely at IPMA for nowcasting of extreme precipitation events.

5.6.2.3 Data and Methods

The GNSS PWV is estimated operationally for a set of receivers located over Portugal and Spain using the GIPSY software, maintained by NASA JPL, every 5 min with a 2 h delay (Bevis et al. 1992, 1994; Calori et al. 2016; Duan et al. 1996). The inputs used in this method include: 1) the raw GNSS observations from 146 GNSS receivers located over Central and Western Iberia, collected every hour, from the Portuguese networks SERVIR and ReNEP (59 stations) and the Spanish networks ANDALUCIA, CASTILLA, EXTREMADURA and IGN (88 stations); 2) surface pressure and temperature, provided in advance by IPMA, from the hourly ECMWF forecasts initialized at least 12 h before a given measurement to avoid the model spin-up and so that the operational GNSS-PWV scheme is not limited by the timeliness of these data. A height correction is performed, assuming hydrostatic equilibrium for pressure and a dry lapse rate for temperature; 3) GNSS satellite orbits, provided by the NASA Jet Propulsion Laboratory (JPL).

An independent estimate of PWV is provided by the Spinning Enhanced Visible and Infrared Imager (SEVIRI) instrument on-board the Meteosat Second Generation (MSG), for clear sky pixels only. For the retrieval of the data, the iSHAi software (Martínez and Calbet 2016) is used, developed by the European Organisation for the Exploitation of Meteorological Satellites (EUMETSAT) Satellite Application Facility on support to Nowcasting and Very Short-Range Forecasting (SAF-NWC). The algorithm is based on an optimal estimation approach, and uses the SEVIRI brightness temperatures (BTs) of the channels 6.2 μm, 7.3 μm, 8.7 μm, 10.8 μm, 12.0 μm, and 13.4 μm, with ECMWF forecast profiles of temperature and specific humidity for the first guess of the iterative algorithm. The used radiative transfer model is RTTOV (Radiative Transfer for TOVS – https://nwpsaf.eu/site/software/rttov/).

A third PWV estimate is given by the operational ECMWF hourly forecast (9 km resolution). In this work, the ECMWF PWV time series is extracted from the forecasts using time steps 12 to 23 from the forecasts initialized at 0:00 UTC and 12:00 UTC, so that hourly values may be used.

Finally, radiosondes launched daily (mostly around 12:00 UTC but there are a few that were launched at 00:00, 06:00 and 18:00 UTC) at the Lisboa – Gago

Coutinho station were used to calculate the PWV. This station uses RS292-SGP Vaisala radiosondes.

5.6.2.4 Results

In Fig. 5.28, all the different estimates of PWV are compared for the Lisboa – Gago Coutinho station from December 2016 to March 2017. There is a good overall agreement between the 4 analysed datasets, but the GNSS estimates being wetter than the other techniques for most of the observing period. Part of the mismatch between estimates is likely attributable to errors in colocation.

The scatter plots between GNSS and the other data sets are shown in Fig. 5.29. A Hampel filter was used for outlier removal (Liu et al. 2004). The comparison with the SAF-NWC shows the lowest RMSE, of about 1.3 mm, and lowest bias (SAF-NWC-GNSS) of about −0.7 mm. However, this is also the comparison with the lowest

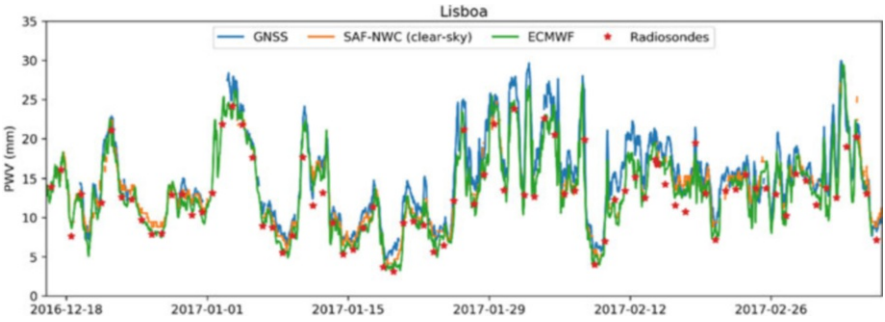

Fig. 5.28 Time series of the PWV for Lisboa – Gago Coutinho, using GNSS (blue), the SAF-NWC (orange), the ECMWF (green) and the radiosondes (red dots)

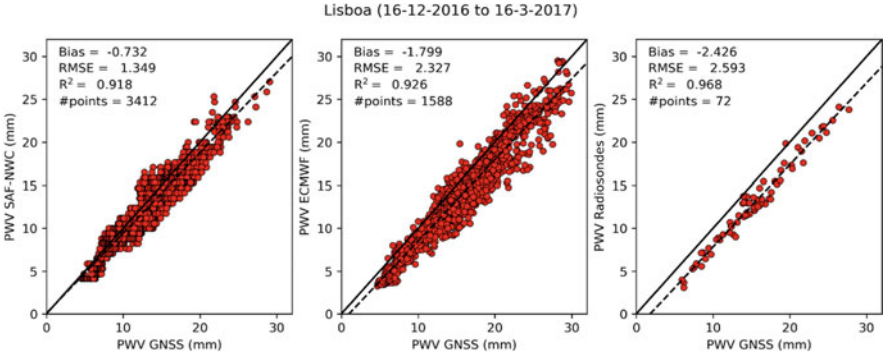

Fig. 5.29 Comparison of GNSS estimates to the remaining data sets (SAF-NWC on the right, ECMWF in the centre and radiosondes in the right)

correlation coefficient ($R^2 = 0.918$). Note that this comparison only reflects clear sky conditions, as the SAF-NWC product is not produced over cloudy pixels. A major source of uncertainty of this clear sky product is introduced by the possibility of a cloud not being detected by the cloud mask algorithm. In this case the brightness temperatures measured by SEVIRI correspond to energy emitted mainly by the cloud top and not by the surface, as is assumed by the iSHAi algorithm. In such cases a negative bias will arise.

When compared to the ECMWF PWV, the GNSS shows a bias of +1.8 mm and a RMSE of 2.3 mm. The correlation coefficient is similar to the previous comparison ($R^2 = 0.926$). This overall slightly worse comparison could be due to the inclusion of cloudy pixels and also the forecast errors in the model. The comparison to radiosondes is the one showing the highest correlation coefficient ($R^2 = 0.968$) but also a significant bias of −2.4 mm, which may be indicating that some systematic error (the known daytime radiation dry bias in the RS92 radiosondes) is affecting the comparison (currently under investigation). The RMSE is therefore quite high (around 2.6 mm).

The error statistics (bias, RMSE, R^2, number of observations) for each GNSS receiver are illustrated in Fig. 5.30 (SAFNWC-GNSS on top and ECMWF-GNSS in the bottom). The positive bias of GNSS versus ECMWF and SAFNWC (negative values in the leftmost panels) is confirmed for the bulk of the stations, which should be investigated in closer detail. The RMSEs are generally below 2 mm for most of the stations, with some exceptions that include the Lisboa – Gago Coutinho. The correlation coefficients are generally substantially above 0.90, especially vs ECMWF, except for a few stations that need further attention. Also shown is the number of data points used for each statistic. Major limitations are the 1 h time sample of ECMWF, the number of cloud masked cases of SAF-NWC (which has a time sampling of 15 min), and the failure of the GNSS networks to deliver their estimates on time.

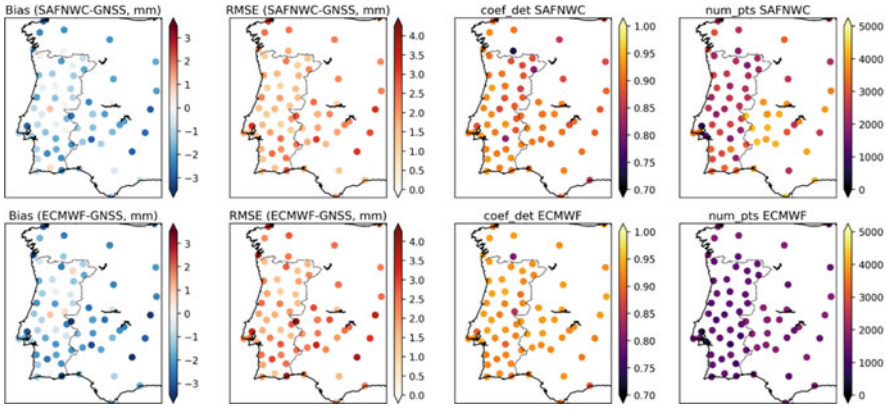

Fig. 5.30 Error statistics for all the GNSS locations with valid measurements

5.6.2.5 Conclusions

A GNSS-based operational Precipitable Water Vapour product was developed for nowcasting support by the SEGAL/IPMA team. The product is available every 5 min with a 2 h delay for 146 stations from 6 GNSS receiver networks over Portugal and Spain. The estimates of ZTD are computed using the GIPSY software and then converted into PWV estimates using surface temperature and temperature data from ECMWF forecasts.

The GNSS PWV product was compared to other high-availability products such as SAF-NWC (clear-sky), ECMWF hourly forecast, and the Lisboa – Gago Coutinho radiosondes. Although slightly biased positively against other products, the GNSS shows good performance and allows a comprehensive spatial and temporal coverage, all-weather observations (in contrast with the SAF-NWC product, for example) and high frequency variability sampling. Despite the systematic biases that were identified, the correlation with the other high frequency datasets is encouraging and suggests that simple corrections could be applied in order to make the products more comparable, e.g. the orographic correction proposed by Bock et al. (2007).

There is still room for fine-tuning of the product, namely through proper identification of outliers, development of a quality flag for the retrievals, reducing timeliness and increasing station availability. Given the high annual variability of the PWV over Iberia, using a more extended period, as well as comparison to more data sources could also provide a more complete validation – this is ongoing work. A measure of the product uncertainty is also key and it is envisaged to the near future so that the product usage can be expanded for applications such as data assimilation by limited area numerical weather forecast models.

5.6.3 Comparing Precipitable Water from Remote Sensing and Space Geodetic Techniques with Numerical Weather Models

D. Landskron
Department of Geodesy and Geoinformation, TU Wien, Wien, Austria
e-mail: daniel.landskron@geo.tuwien.ac.at

A. Xaver
Department of Geodesy and Geoinformation, TU Wien, Wien, Austria
e-mail: Angelika.Xaver@geo.tuwien.ac.at

J. Böhm
Department of Geodesy and Geoinformation, TU Wien, Wien, Austria
e-mail: Johannes.Boehm@geo.tuwien.ac.at

W. Dorigo
Department of Geodesy and Geoinformation, TU Wien, Wien, Austria
e-mail: Wouter.Dorigo@geo.tuwien.ac.at

Space geodetic applications such as GNSS and VLBI open new possibilities in obtaining tropospheric water vapour. GNSS has proven to be ideally suited for deriving meteorological parameters such as PW and is currently further gaining in importance. Less well known is the ability to determine water vapour through observations of radio waves from quasars billions of light years away using the space geodetic technique VLBI. The presence of water vapour and water particles in the troposphere decelerates these signals similarly to those from GNSS satellites, which enables accurate estimations of their amount. Some VLBI stations make observations for almost 40 years now, yielding fairly long time series of water vapour. Another dataset stems from microwave radiometry by remote sensing satellites as, e.g., combined and provided by the GlobVapour product by the European Space Agency (ESA). In GlobVapour, data of several Earth observation missions (MERIS, GOME, SSM,) was combined with the aim of providing global and consistent time series of IWV, which, in simplified terms, can be equated with PW.

In this study, we analyse the correlation between all these datasets and compare them with NWM data from the European Centre for Medium-Range Weather Forecasts (ECWMF). Eventually we draw conclusions about possible synergies and the dataset's ability and performance in describing the amount and variation of water vapour in the troposphere.

As to derive more information from the datasets, all observations are plugged into a least squares fitting for Eq. 5.11 below, the so-called seasonal fit. This outputs information about seasonal variations as well as long-term changes in the data.

$$\begin{aligned} \mathrm{b(mjd)} = {} & \mathrm{A0} + \mathrm{A1}\cos(\mathrm{mjd}365.252\pi) + \mathrm{B1}\sin(\mathrm{mjd}365.252\pi) + \mathrm{A2}\cos(\mathrm{mjd}365.254\pi) \\ & + \mathrm{B2}\sin(\mathrm{mjd}365.254\pi) + \mathrm{k\ mjd} \end{aligned} \tag{5.11}$$

In Eq. 5.11, *b(mjd)* denotes the respective output quantity dependent on the modified Julian date *mjd*, A_0 the mean value, A_1 and B_1 the annual terms, A_2 and B_2 the semi-annual terms, and k the linear trend. Figure 5.31 shows an example of how the fitting affects the data.

The seasonal fits are determined for the whole data at all 18 globally distributed VLBI/GNSS stations which are considered in this study. The temporal resolution of the datasets is slightly different:

- NWM: 1995–2016 (6-hourly)
- VLBI: 1995–2014 (6-hourly)
- GNSS: 1995–2007 (6-hourly)
- GlobVapour: 1996–2008 (weekly)

In Fig. 5.32, the comparison of IWV from all four datasets is shown for station MATERA in Italy.

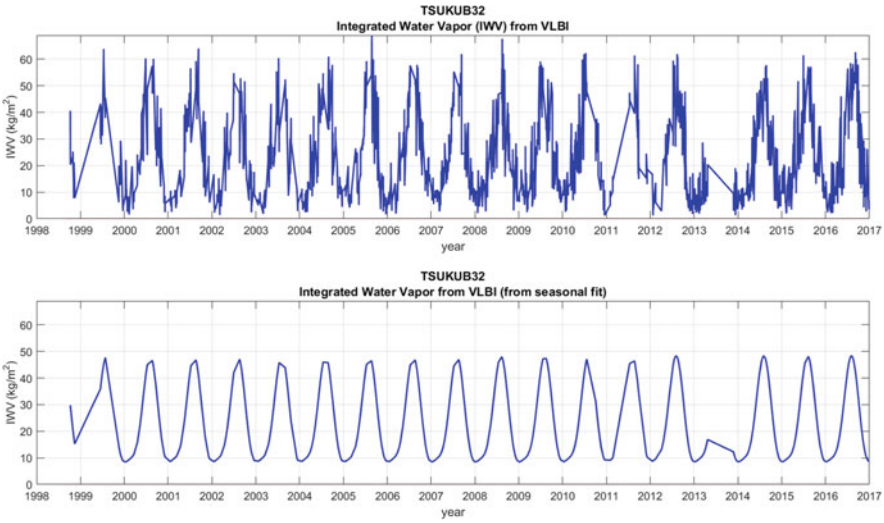

Fig. 5.31 IWV from VLBI at station WETTZELL in southern Germany. Top: the observed IWV. Bottom: the IWV resulting from application of the seasonal fit

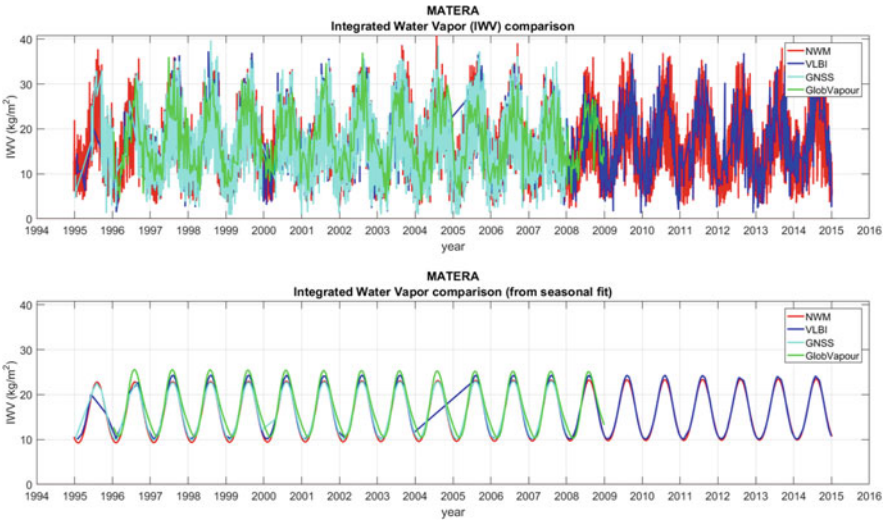

Fig. 5.32 IWV from all four techniques at station MATERA in Italy. Top: the observed IWV. Bottom: the IWV resulting from application of the seasonal fit

Figure 5.32 proves that the datasets in general fit quite well to each other. Averaging the IWV from all 18 considered stations yields the main results of this study (Table 5.7).

Table 5.7 Statistical evaluation of the different datasets regarding correlation coefficient (column 1), bias (column 2) and standard deviation (column 3) through forming pairs

	Corr. Coeff.	Bias (kg/m^2)	StD (kg/m^2)
NWM/VLBI	0.87	0.2	3.9
NWM/GNSS	0.91	0.3	3.5
NWM/GlobVapour	0.67	0.7	6.9
VLBI/GNSS	0.97	−0.4	1.9
VLBI/GlobVapour	–	–	–
GNSS/GlobVapour	0.62	0.3	7.6

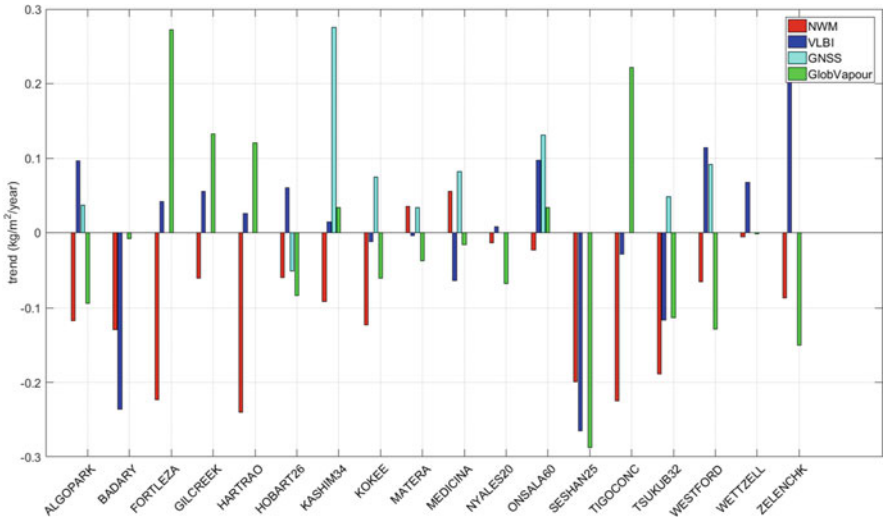

Fig. 5.33 The IWV linear trends k of all four datasets, as resulting from the seasonal fit

Highest correlation is reached between IWVs from VLBI and GNSS, with the NWM data yielding very high correlation coefficients with VLBI and GNSS as well. The GlobVapour data, on the other hand, does not correlate that well with the other datasets, although a correlation coefficient between 0.6 and 0.7 is not bad either. A comparison between GlobVapour and VLBI is not possible, as they have too few identical epochs. The biases of the dataset pairs are generally very small, which means that none of the datasets is systematically higher or lower than the others. The standard deviation is inversely proportional to the correlation coefficient; a high correlation coefficient is therefore accompanied by a low standard deviation, and vice versa. Furthermore, we also took a look at the linear trends *k*, that is, the long-term changes of the respective IWVs (Fig. 5.33).

Unfortunately, no clear systematics can be derived whether the IWV increases or decreases at the considered stations, as all datasets provide contradicting results. Only at one single station, SESHAN25 in China, the datasets agree about the algebraic sign of the gradient. As a result, no safe statements can be made about

long-term changes of IWV from this study. The reason is most likely that the considered time spans are too short.

In summary we can conclude that the considered datasets agree very well with each other. VLBI turns out to be a very appropriate technique for deriving long time series of IWV as well. The GlobVapour data is highly beneficial, in particular because it is available globally and not bound to terrestrial stations such as GNSS and VLBI, however its performance suffers from the fairly low temporal resolution compared to the other techniques. In further research we will consider longer time spans, more sample stations and more remote sensing products, as to derive even more meaningful results.

5.6.4 *Inter-Comparison Analysis of Tropospheric Parameters Derived from GPS and RAOB Data Observed in Sodankylä, Finland*

E. Fionda
Fondazione Ugo Bordoni, Rome, Italy
e-mail: efionda@fub.it

M. Cadeddu
Argonne National Laboratory, Lemont, IL, USA
e-mail: mcadeddu@anl.gov

V. Mattioli
Centre of Excellence Telesensing of Environment and Model Prediction of Severe Events, University of L'Aquila, L'Aquila, AQ, Italy
e-mail: vinia.mattioli@diei.unipg.it

R. Pacione
e-GEOS/Centro di Geodesia Spaziale-Agenzia Spaziale Italiana, Matera, MT, Italy
e-mail: rosa.pacione@e-geos.it

This study compares tropospheric parameters derived from GPS and radiosondes (RAOB) data at Sodankylä (GRUAN and EPN site, at the Arctic Research Centre of the Finnish Meteorological Institute, 67°37'N, 26°65′E) These entire databases were processed to estimate ZTD, ZWD, and IWV. Using the Sodankylä RAOB database collected from 1999 to 2013, synthetic climatic and radiometric parameters were calculated by applying the microwave radiative transfer equation (RTE) together with a cloud model. This allowed the generation of simulated long-term ZTD, ZWD and IWV. The radiosonde station is located near the EPN GPS permanent station. From that GPS ground-receiver homogeneously reprocessed ZTD time series (1999–2013) (Pacione et al. 2014a), carried out in the framework of the EPN Repro2 campaign (hereafter AS0), and combined ZTD Near-Real time time-series (2008-present) (Pacione et al. 2011) derived in the E-GVAP framework (hereafter

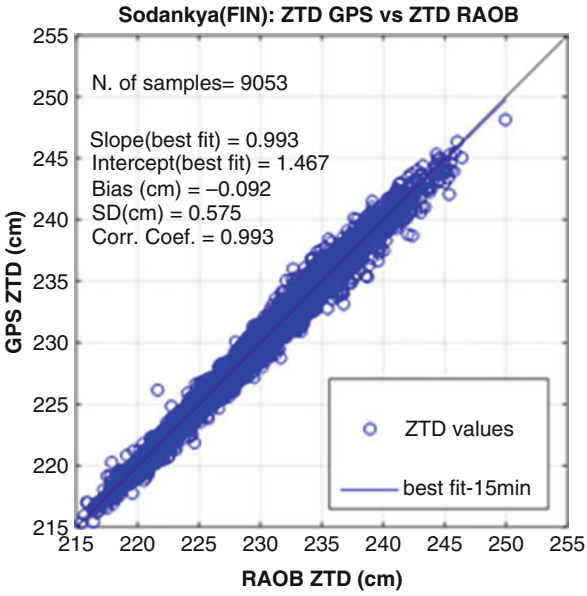

Fig. 5.34 Scatterplot of ZTD computed at Sodankylä (1999–2013) from GPS versus RAOB. The solid line represents the linear correlation

ASIC), were utilized in the present analysis. To derive ZTD from GPS the AS0 solution characterized by a 5-min sampling was applied and GPS data were averaged over 15 min. A scatter plot of GPS and RAOB-derived ZTD for the entire dataset is shown in Fig. 5.34.

A relatively small bias and standard deviation (SD) of −0.092 cm and 0.575 cm respectively, with a correlation coefficient of 0.993 were found. The bias value highlights a slight underestimation of GPS-derived ZTD. However, the scatter plot in Fig. 5.34 shows a good agreement between GPS and RAOB over a large ZTD range covering a long-term observation period in the Arctic climatic region. Figure 5.35 shows the yearly trends of bias and SD from 1999 to 2013. The bias on the right hand side displays three anomalous values in 2001, 2005 and 2011. The 2005 anomaly could be correlated with the use of the RS80-15 L radiosonde, however the anomalous values in 2001 and 2011 are so far unexplained. Interestingly, Fig. 5.35 (left) shows that until 2004, when RS90 radiosondes were in use, the GPS-derived ZTD is less than the RAOB-derived ZTD. After 2004 when the radiosondes were changed to RS92 the GPS-derived ZTD is generally higher than the RAOB-derived. Except for the year 2005 (when the RS80-15 L radiosonde were used) the SD values shown on the right hand panel of Fig. 5.35 display a pronounced and constant decreasing trend probably due to the improvement of the RS92 radiosonde data quality. From 1999 to 2013, the SD decreases from 0.671 to 0.435 cm with an average value of 0.575 cm. The bias has a long-term average value of −0.092 cm.

Using the same database, yearly bias and SD between GPS and ZTD RAOB were computed for all corresponding values at 00:00 UTC and 12:00 UTC and are shown

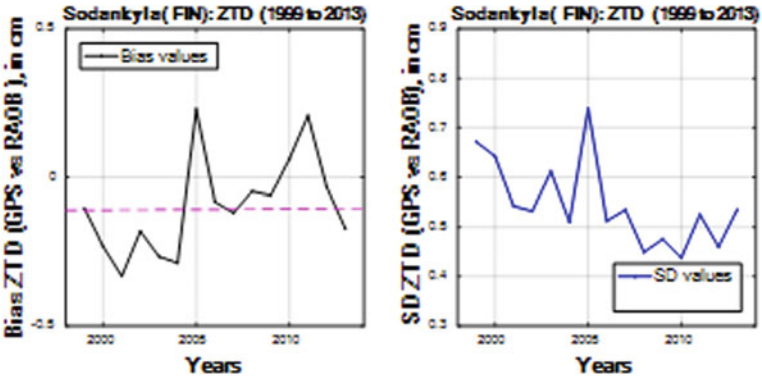

Fig. 5.35 (Left): Yearly ZTD Bias (GPS – RAOB) and (Right) error standard deviation (SD) at Sodankylä from 1999 to 2013

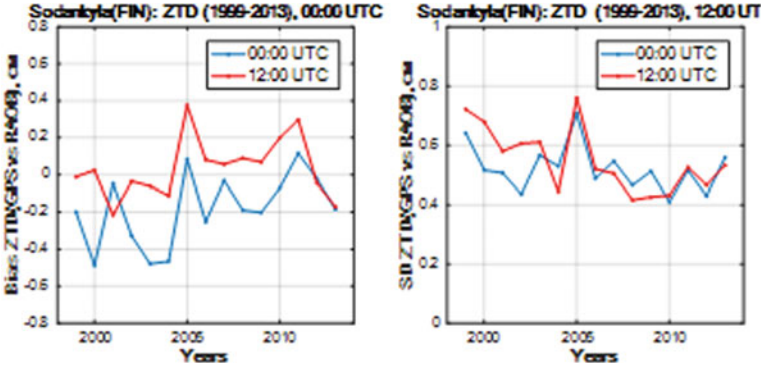

Fig. 5.36 Same as Fig. 5.35 but at 00:00 and 12:00 UTC time using 30-min averaged data

in Fig. 5.36. The results are consistent with those shown in Fig. 5.35, although the magnitudes of the day-time (red points) and night-time (blue points) biases appear to be different.

As part of the analysis the GPS data collected at Sodankylä from 2008 to 2013 were processed using the ASIC and ASO solutions. The ZTD GPS values from the ASIC solution have a sampling time of 15 min, while the corresponding values referred to the AS0 solution have a sampling time of 5 min. Fig. 5.37 shows the bias and SD of the ZTD obtained with the two methodologies with respect to the RAOB. The GPS ASIC solution produces a considerably higher positive bias than the AS0 solution. On the contrary, the AS0 solution lead to smaller bias values that however show a slight seasonal dependence: slightly negative in summer and almost zero during colder months. The monthly SDs associated with the two GPS solutions have a similar seasonal behaviour, but with slight better performance of the AS0 solution. The overall better performance of AS0 solution w.r.t. ASIC is expected. As AS0 is a

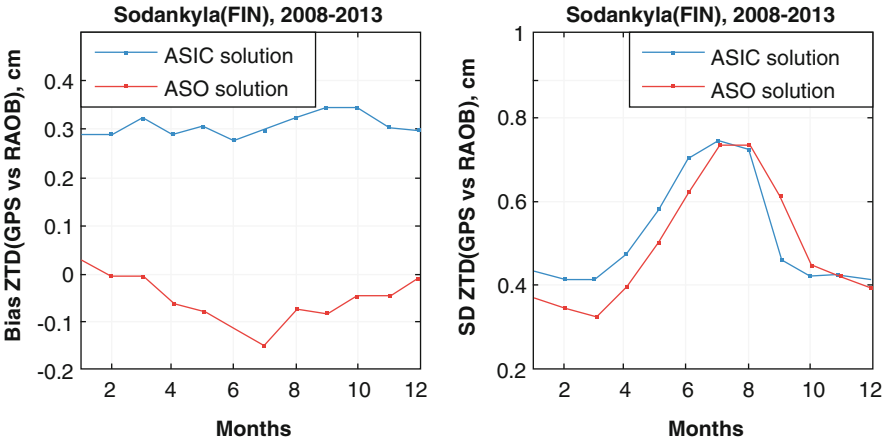

Fig. 5.37 (Left): Monthly ZTD bias and standard deviation (SD) (right) for the ASIC (blue) and AS0 (red) GPS solutions with respect to the corresponding RAOB. Data are 30-min averages from Sodankylä (period 2008–2013)

homogeneously reprocessed ZTD solution, not affected by inconsistencies due to updates of reference frame or applied models, it might be suitable for long-term analysis, while ASIC is mainly devoted to NWP data assimilation and quality control of the contribution solution.

We can conclude that ZTD inter-comparison performed on 14 years (1999–2013) of concurrent GPS and RAOB values collected at Sodankylä showed a small bias, that was radiosonde-dependent and decreasing trend of standard deviations. Considering all the data, the bias and SD assumed values of −0.092 cm and 0.575 cm respectively. Results also showed that the GPS ASO solution performs better that than the ASIC solution.

5.7 IWV Trends & Variability from GNSS Data and Atmospheric Models[12]

5.7.1 Analysis of IWV Trends and Variability from GNSS and Re-Analyses

A. Parracho
IGN Institut national de l'information géographique et forestière, Paris, France
e-mail: ana.parracho@etu.upmc.fr

[12]Parts from this section were previously published in Parracho et al. (2018).

O. Bock
IGN Institut national de l'information géographique et forestière, Paris, France
e-mail: olivier.bock@ign.fr

S. Bastin
Université Paris-Saclay, Saint-Aubin, France
e-mail: sophie.bastin@latmos.ipsl.fr

Water vapour plays a key role in the climate system. However, its short residence time in the atmosphere and its high variability in space and time make it challenging when it comes to study trends and variability. In this work, IWV estimated from GPS ZTD observations reprocessed by JPL (repro1) at 104 stations of the IGS network (see Sect. 5.2.2) was intercompared with data from two atmospheric reanalyses: ECMWF's ERA-Interim (Dee et al. 2011) and NASA's MERRA-2 (Gelaro et al. 2017). Monthly and seasonal (December–January-February and June–July-August) means, inter-annual variability, and linear trends were analysed and compared for the 1995–2010 period (period with GPS data).

5.7.1.1 Means and Variability

Figure 5.38a, b show the mean ERA-Interim fields superposed with the GPS mean values (as points) corrected to the ERA-Interim model height. Globally, the mean IWV is strongest in the tropics where strong evaporation occurs from the warm oceans and land surface and where trade winds transport moisture to the Intertropical Convergence Zone (ITCZ). Lower IWV is observed at mid to high latitudes, where lower evaporation occurs due to the cooler oceans and land surface, and over arid regions (e.g. Sahara, Arabic peninsula, south-eastern Africa, Australia), where lack of water limits evaporation. IWV is also lower at higher altitudes (e.g. the Himalayas and the Andes cordillera) due to the rapid decrease of water vapour saturation pressure with altitude as predicted by Clausius–Clapeyron equation. Figure 5.38a, b also show a strong seasonal variation is driven by the movement of the incoming solar radiation from one hemisphere to the other and back along the course of the year, resulting in a global swinging of the trade winds and ITCZ across the Equator.

In general, there is good agreement between ERA-Interim and GPS, with ERA-Interim reproducing the spatial variability well, including the sharper gradients in IWV (e.g. northern and southern flanks of the ITCZ in both seasons, and in the regions of steep orography). ERA-Interim is slightly moister on average than GPS. The median bias is 0.51 kg/m^2 (6.2%) in DJF and 0.52 kg/m^2 (2.7%) in JJA, and the standard deviation of the bias across the network amounts to 0.83 kg/m^2 (6.9%) in DJF and 0.95 kg/m^2 (7.8%) in JJA. There is some spatial variation in the mean difference, namely a negative mean difference in the tropics (ERA-Interim < GPS) which is compensated in the global median by the larger number of stations in the extra-tropics which have a positive difference (ERA-Interim > GPS). A paired two-sample t-test detected 20 stations with significant differences in the mean

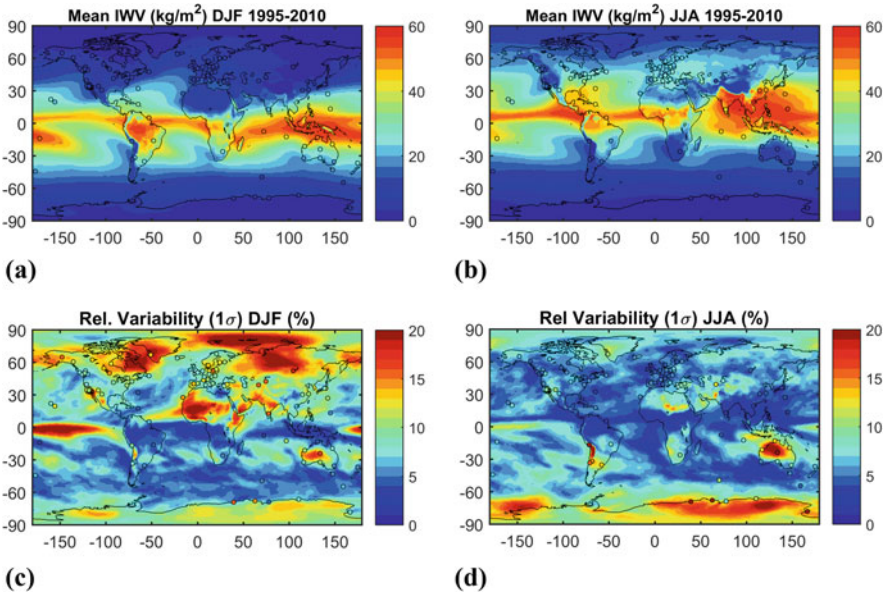

Fig. 5.38 (**a**) Mean value of IWV from ERA-Interim between 1995 and 2010 for JJA. Filled circles correspond to IWV retrieved by GPS. (**b**) same as **a**) for DJF. (**c**) relative variability (standard deviation of the IWV series divided by its mean) for JJA, between 1995 and 2010. (**d**) Same as **c**) for DJF

IWV values at 0.01 confidence level in DJF and 17 in JJA. These sites are located in coastal regions and/or regions with complex topography, and representativeness errors are suspected to be the cause of these biases (Bock and Parracho 2019).

The inter-annual variability was computed as the relative standard deviation of the seasonal IWV time series (i.e. standard deviation of seasonal time series divided by its mean value), and is presented for ERA-Interim (fields) and GPS sites (points), for DJF and JJA, in Fig. 5.38c, d. In DJF (Fig. 5.38c), strong inter-annual variability (> 15%) is found for northern high-latitude regions (north-eastern Canada and eastern Greenland, polar Artic area, and a large part of Russia and north-eastern Asia) and for the tropical arid regions (Sahara, Arabic peninsula, central Australia). Some correlation was found between the seasonal IWV anomalies and the North Atlantic Oscillation (NAO) index (Barnston and Livezey 1987) over Siberia ($r = 0.5$) and Greenland ($r = -0.5$) (not shown). Noticeable variability is also seen in the central tropical Pacific in DJF but this is due to the extremely large variability in absolute IWV contents (up to 6 kg/m^2) associated with the El Niño Southern Oscillation (ENSO). Linear correlation coefficients between the seasonal IWV anomalies and the Multivariate ENSO Index (MEI; Wolter and Timlin 1993, 1998) in this region reach $r = 0.80$ (not shown). In JJA, large inter-annual variability is observed mainly over Antarctica and Australia (Figure 1d). Locally enhanced variability is also seen over the Andes cordillera, but this is mainly due to the very low IWV values at high altitudes.

Most of the marked regional features of inter-annual variability are also confirmed by GPS observations (Fig. 5.38c, d), with a median difference between ERA-Interim and GPS close to zero for both DJF and JJA with a standard deviation across the stations of 1.7% in DJF and 4.1% in JJA. One can especially notice the good representation of the relative variability over Australia or South America, both in DJF and JJA, and in the northern high latitudes, where the gradients are strong and well captured. However, a few stations show different values compared to the ERA-Interim background. These are located in Antarctica and Hawaii, where representativeness errors are again expected, due to the large variability in the IWV values of the surrounding grid points connected with large variations in the altitudes (> 500 m). In the case of Hawaii, the error is due to the limited imprint of Mauna Kea Island on the 0.75° resolution grid of ERA-Interim. In the case of MCM4 and SYOG (in Antarctica), the time series of monthly mean IWV and IWV differences reveal variations in the means which coincide with GPS equipment changes and processing changes and unexplained variations in the amplitude of the seasonal cycle resulting in a marked oscillation in the monthly mean differences (ERAI – GPS). Variations in the means introduce a spurious component of variability in the GPS IWV series.

Finally, in addition to representativeness differences and errors in the GPS data, errors in the reanalysis data (expected in data-sparse regions and regions where the performance of model physics and dynamics are poor) can also be responsible for differences in the IWV means and variability. These can be diagnosed by comparing several reanalyses based on different models and different observational data or hypothesized by eliminating the other causes.

5.7.1.2 Linear Trends

The linear trends were computed using the Theil-Sen method (Theil 1950; Sen 1968) applied to the anomalies obtained by removing the monthly climatology from the monthly data. The statistical significance of the monthly and seasonal trends was assessed using a modified Mann-Kendall trend test (Hamed and Rao 1998), which is suitable for auto-correlated data, at a 10% significance level.

Results from ERA-Interim based on the full monthly time series (Fig. 5.39a) showed generally significant positive trends over the ocean (over most of the tropical

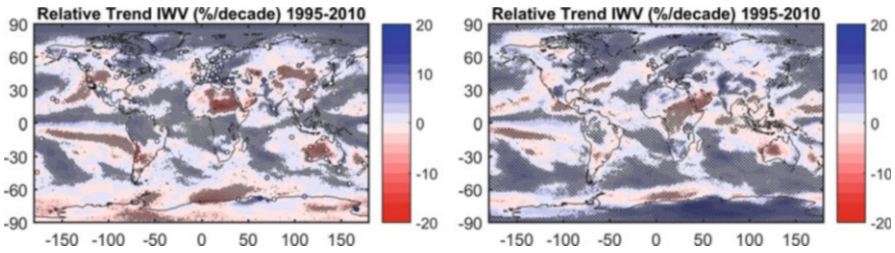

Fig. 5.39 Relative trends in IWV in ERA-Interim (left) and MERRA-2 (right) reanalysis for 1995–2010

oceans and over the Arctic). Significant negative trends were observed in south-tropical eastern Pacific region, west of the United States and generally south of 60°S. The dipole structure in the south-eastern tropical Pacific area is consistent with the findings of Mieruch et al. (2014) and is due to the different ENSO phases for this time period, as reported by Trenberth et al. (2005). Over land, significant positive trends were observed in the equatorial region along the ITCZ, especially in northern South America, Central Africa, and Indonesia, and in the northern hemisphere, especially over northern North America, Greenland, most of Europe and Siberia. Significant negative trends over land are observed over North Africa, Australia, Antarctica, central Asia, south of South America, and most of the USA. In general, there is continuity between oceanic and continental trends (e.g. North and South America, Central Africa), suggesting a trend in air mass advections. However, the magnitudes of the larger trends (e.g. -3.5 kg/m^2 per decade or -17% per decade over northern Africa) are questionable. Comparison to GPS observations, when they are available, helps to address this question.

In general, the monthly trends computed at the GPS stations are in good agreement with ERA-Interim even in areas of marked gradients (e.g. between western Canada and the USA, or from central to Western Europe). However, there are a number of GPS stations where the trend estimates are large and of opposite sign compared to ERA-Interim. For some of these stations, the discrepancy is due to gaps and/or inhomogeneities (due to equipment changes) in the GPS time series which corrupt the trend estimates (e.g. CCJM station, south of the Japanese home islands). Representativeness differences are also suspected at mountainous and coastal sites. Finally, some sites also show more gradual drifts in the times series which do not seem connected with known GPS equipment changes (e.g. MAW1, in Antarctica). At such sites, drifts in the reanalysis, due to changes in the data assimilated by the reanalysis over time, are plausible.

Therefore, a second reanalysis, MERRA-2, was used to complement ERA-Interim and GPS, namely in regions of high uncertainty in these datasets (e.g. *Antarctica*) or in regions where few or no GPS data are available (e.g. Africa, Asia, the global oceans). The monthly IWV trends computed for MERRA-2 (Fig. 5.38b) are in good agreement with ERA-Interim for most regions. They describe consistent global moistening/drying dipoles along the inter-tropical Pacific Ocean, across Australia, South America and between eastern and western USA, and general moistening over the Arctic and Europe. However, there appears to be also significant differences over several parts of the globe, in particular over Indonesia and the Indian Ocean, central Africa, western (coastal) and northern Africa, Central Asia and Antarctica.

To better understand the trends, we separated them by seasons (DJF or JJA), which are presented for ERA-Interim in Figure 3a and b. The seasonal trends have a larger magnitude than the monthly trends, which emphasizes the role of atmospheric circulation (which is largely changing between seasons) on IWV trends. On the other hand, trends of opposite signs between winter and summer can be observed in western Antarctica, central South America, South Africa, Eastern Europe, and off the West coast of the USA. A strong drying occurs over Antarctica in JJA and over

central Asia during JJA and DJF (though not exactly at the same location). Western Europe shows a drying in winter (DJF) and a moistening in summer, leading to weak trend when considering the full time series. Over Australia, according to ERA-Interim, the drying is stronger in DJF, i.e. when associated with a decrease of the intensity of the moist flow during the monsoon period. Another area likely sensitive to the intensity of the monsoon flow is northern Africa, where the drying is occurring in JJA over eastern Sahel, in a band covering Chad, Sudan and Eritrea. Overall, the seasonal trends estimated from the GPS data are in good agreement with ERA-Interim. The sites with largest differences in the seasonal estimates include: KIRU in Sweden, COCO in the Indian Ocean, IRKT in Russia, and ANKR in Turkey. However, trend estimates at some of these sites might be inaccurate due to the enhanced impact of time gaps for the short seasonal time series (based on 16 years at best).

The seasonal trends computed from MERRA-2 (Figs. 5.40c, d) show quite good agreement with ERA-Interim and GPS in DJF (e.g. dipole in the trends over Antarctica, strong drying trend over Siberia, the Arabic peninsula, western Australia, western Europe, and most of the USA; and the strong moistening over the Arctic). In JJA, there are considerable differences between the reanalyses, with opposite trends seen in Indonesia and in most of southern Asia, north and central Africa, Antarctica, and in the eastern Arctic region. These differences emphasize the uncertainty of reanalyses in data sparse regions.

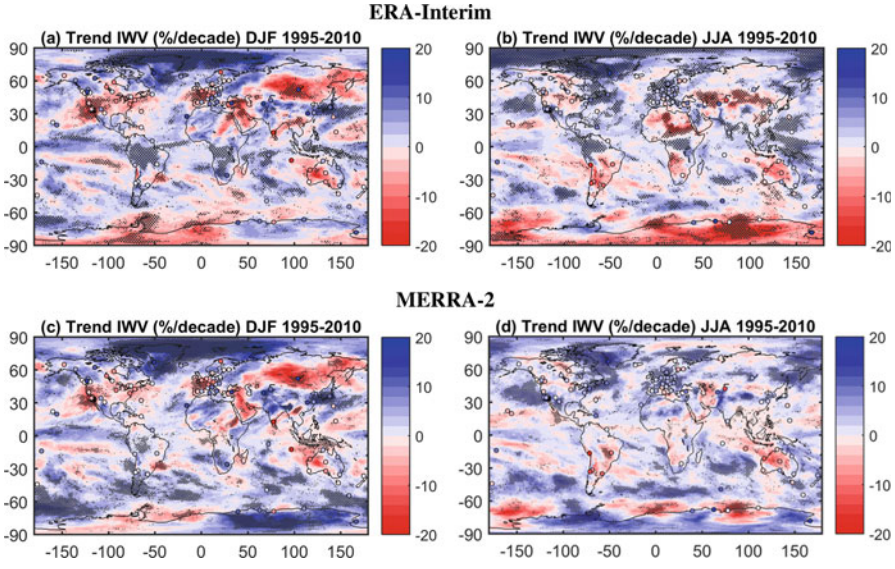

Fig. 5.40 Relative trends in IWV in ERA-Interim (top) and MERRA-2 (bottom) reanalysis for the 1995–2010 period for DJF (**a**, **c**) and JJA (**b**, **d**). The statistically significant trends are highlighted by stippling

5.7.1.3 Conclusions

GPS data proves to be useful in the study of IWV trends and variability. In spite of some differences at handful of stations, there is a general good agreement between GPS and ERA-Interim IWV means, variability and trends. The main drawback of GPS is the lack of long term data in certain regions where ERA-Interim shows intense IWV trends. To curb this issue in regions lacking in GPS data or regions of disagreement, MERRA-2 reanalysis was used. The IWV means, variability, and trends in both reanalyses agree well in most regions. However, the comparison of seasonal trends in both reanalyses also highlighted areas where the reanalyses disagree. These differences emphasized the uncertainty of reanalyses in data sparse regions, and the uncertainty of trend estimation for such a limited time period. A more detailed analysis over two of these regions, Western Australia and North Africa, as well as an extension of the trend analysis to a longer period (1980–2016) is presented in Parracho et al. (2018).

5.7.2 Analysis of IWV Trends and Variability from GNSS and Satellite Data

R. Van Malderen
Royal Meteorological Institute of Belgium, Brussels, Belgium
e-mail: roeland@meteo.be

E. Pottiaux
Royal Observatory of Belgium, Brussels, Belgium
e-mail: eric.pottiaux@oma.be

S. Beirle
Max-Planck-Institute for Chemistry, Mainz, Germany
e-mail: steffen.beirle@mpic.de

G. Stankunavicius
Vilnius University, Vilnius, Lithuania
e-mail: gintas.stankunavicius@gf.vu.lt

The IGS repro 1 dataset and ERA-Interim have been compared to satellite IWV data. In this analysis, a long (1995–2014), homogenized, global dataset of monthly mean IWV data was retrieved from three VIS measuring satellite instruments: GOME, SCIAMACHY, and GOME-2 (Beirle et al. 2018), hereafter named GOMESCIA.

5.7.2.1 Frequency Distributions

We first looked at the histograms of all available IWV data for both IGS repro 1 and ERA-interim (with time resolution of 6 h, which for IGS repro 1 depends

additionally on the ZTD availability). We found that almost all stations of our sample follow a lognormal distribution for their IWV field, in consistency with Foster et al. (2006). The traditional lognormal distribution is found for every station at the Australian continent, and is commonly found in Scandinavia and USA (except at the entire west coast). A reversed lognormal form is found for some tropical island or coastal sites. Other tropical sites are characterized by distinct bimodal lognormal distributions, which might be explained by the impact of the monsoon. The remaining stations or regions (in particular the USA west coast and Europe) have mainly a standard lognormal distribution, but with a clear, secondary lognormal distribution which is responsible for an additional peak (or "shoulder") in the histogram, at the higher IWV range. The frequency distribution is hence composed by a winter and summer IWV distribution. Apart from some site to site exceptions, this geographical distribution is similar for both IGS repro 1 and ERA-interim.

5.7.2.2 Seasonal Variability

Now we study how the seasonal cycle is represented (geographically) by the different IWV datasets. We therefore plot harmonic functions through the IWV time series and compare the amplitudes and phases of those functions, see Fig. 5.41. Overall, we found that the seasonal cycle and its geographical variability

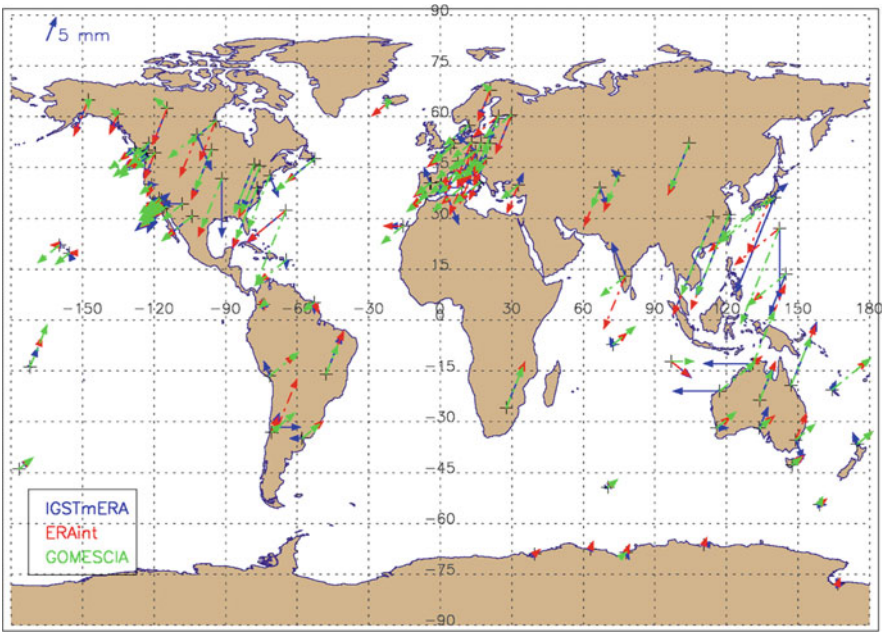

Fig. 5.41 Phase and amplitude of the seasonal cycle of the IWV time series of the different datasets (coloured) at the locations of the IGS Repro 1 sites. The direction of the arrow denotes the month of the maximum IWV value (1 h = Jan, 2 h = Feb, etc.); the arrow length gives an idea of the amplitude of the seasonal cycle

are similarly depicted by all datasets. GOMESCIA underestimates the number of sites with small amplitudes of the seasonal cycle (< 4 mm), especially with respect to ERA-interim, and the phase of the maximum in the seasonal cycle also peaks one month later in the Northern Hemisphere in the GOMESCIA dataset. Additionally, the GOMESCIA time series also more often contain higher order periodic signals (e.g. 6 months) than the IGS Repro 1 and ERA-interim datasets.

5.7.2.3 Linear Trends

From the IWV monthly anomalies, we calculated linear trends for the different datasets. These are shown in Fig. 5.42 for IGS Repro 1 and GOMESCIA. Overall, we found that IGS Repro 1 has the highest number of sites with (statistically significant) positive trends in IWV: about two third of the sites have positive trends. GOMESCIA on the other hand, has the highest number of sites with negative trends in IWV. The sign of the trend is hence dependent on the dataset used, and only above Europe (moistening) and West Australia (drying) a consistent geographical pattern is achieved among the three considered datasets here (ERA-interim not shown). We also want to note that the ERA-interim IWV trends can, at least from a qualitative point of view, nicely be explained by the ERA-interim surface temperature trends.

5.7.2.4 Stepwise Multiple Linear Regression

To gain insight in the processes responsible for the IWV time variability present in the 3 datasets, we tried to fit the monthly mean time series with a linear regression that uses explanatory variables as the surface temperature, surface pressure, tropopause pressure, but also teleconnection patterns like ENSO, NAO, etc. The approach is stepwise: first, we include all the explanatory variables in the linear regression and rank them according to the explained variability; then we include the explanatory variables one by one, according to this ranking, and only the explanatory variables that explain a statistically significant part of the variability are retained in the regression. An example of a fit is given in Fig. 5.43.

One important outcome of the analysis is that a large fraction of the variability, and for the majority of the sites, can be explained by the surface temperature, of course after accounting for the seasonal cycle by the use of long term means or harmonic functions. Given the already mentioned qualitative agreement between the ERA-interim trends in IWV and surface temperature, this is not very surprising and this might be explained by the link between the time variability of both parameters through the Claussius-Clapeyron equation. Another explanation might be that the surface temperature accounts for some remaining seasonality in the IWV time series, even after accounting for it by using the long term means or harmonics. Another important explanatory variable is the surface pressure, so that it should not be a surprise that the IWV time series of ERA-interim can be best fitted by the linear regression (the surface pressure and temperature time series are

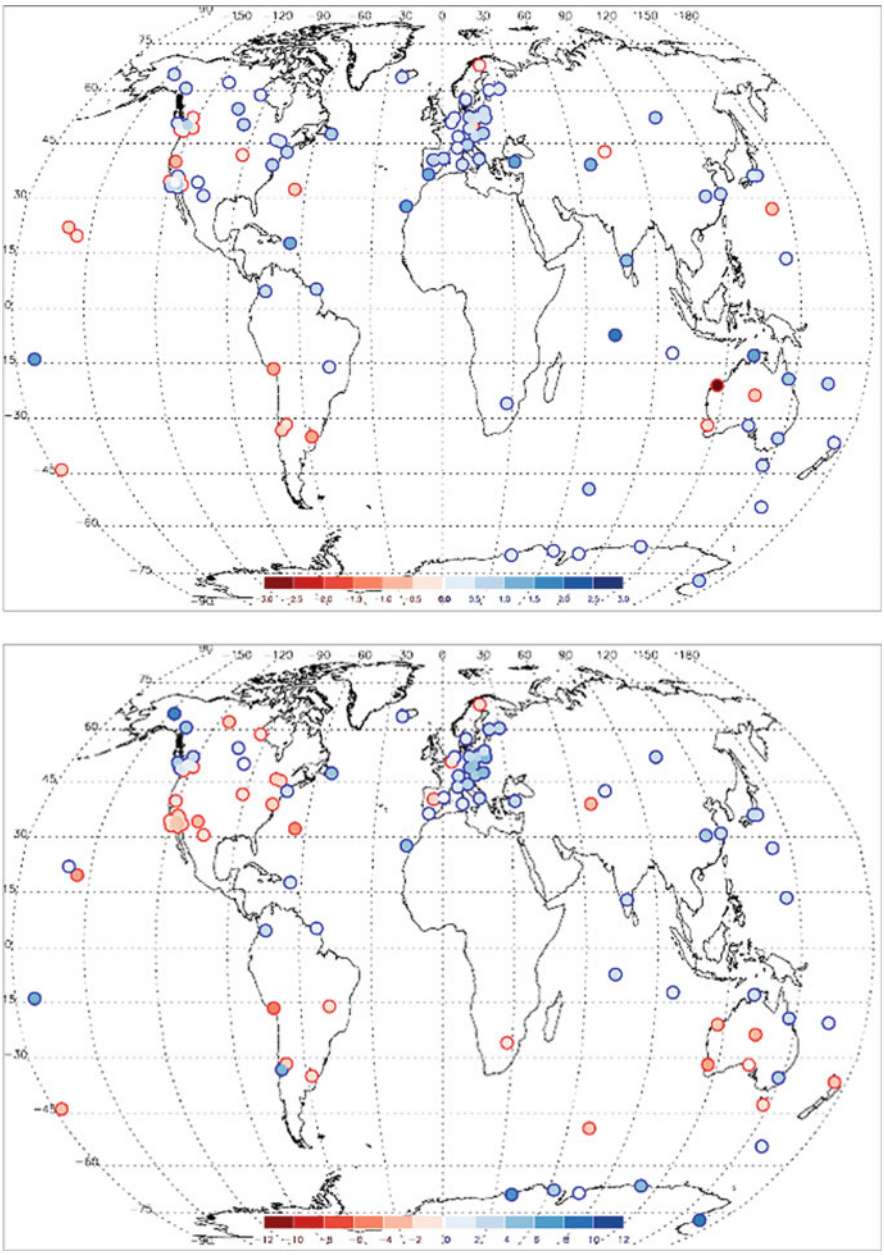

Fig. 5.42 IWV linear trends [%/decade] calculated for the period 1996–2010 for IGS Repro 1 (top) and GOMESCIA (bottom)

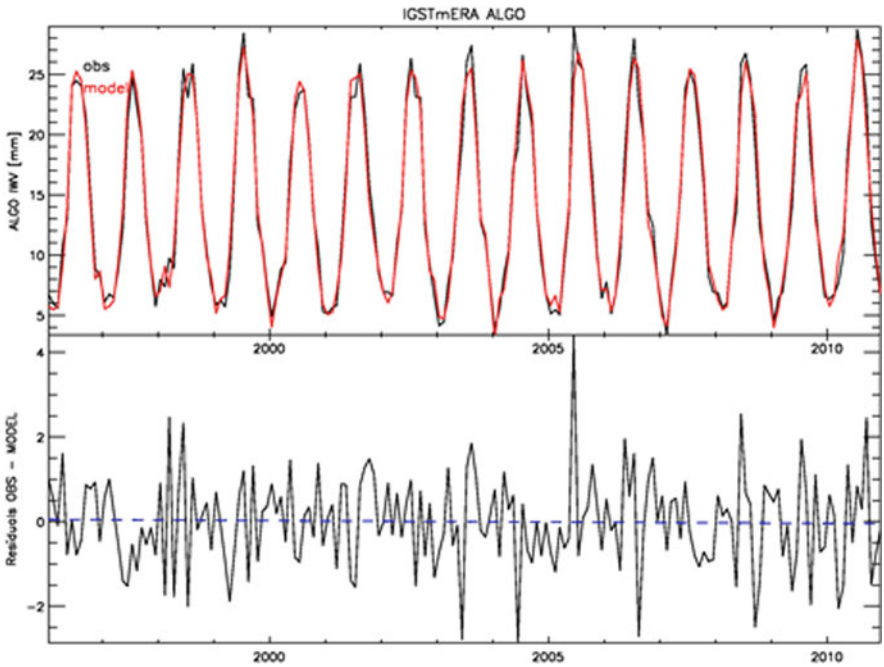

Fig. 5.43 Linear regression fit (in red) for the IGS Repro-1 time series of the site ALGO (Canada). The explanatory variables used are the long-term means, the surface temperature, the tropopause pressure, the EP flux, the Tropical/Northern Hemisphere pattern, East Atlantic/West Russia pattern (4 months leading), Polar/Eurasia pattern, and the Pacific Transition pattern. About 97.9% of the variability is explained by the fit and the correlation coefficient equals 0.989

calculated from ERA-interim). The GOMESCIA IWV time series are fitted worst by the linear regression. The highest explained variabilities are achieved for European and USA sites (except at the southern part of the west coast), but this might be due to the large number of NH teleconnection patterns that were included in the regression. There is certainly some regional consistency in the use of explanatory variables (ENSO in Australia, NAO in USA/Canada, East Atlantic in Europe), but not always (e.g. Arctic Oscillation in Antarctica, Pacific/North America pattern in Australia), so some more work is needed to guide the selection process of the explanatory variables.

Only for a few sites, a linear trend was retained as explanatory variable. Furthermore, the residuals between the IWV time series and the linear regression fit only show for a very limited number of sites a significant trend. The stepwise multiple linear regression fits are hence able to capture the (overall positive) trend in IWV.

5.7.2.5 Conclusions

We examined three completely different IWV datasets (GNSS, ERA-interim and GOMESCIA satellite retrievals) to study the IWV variability of a set of 120 global IGS Repro 1 sites. Although every used dataset might have its own remaining issues like homogeneity, spatial representativeness, etc.), we can conclude that combining the analysis results of the three of them, has the potential to characterize and understand the IWV time variability from a geographical consistent point of view.

5.7.3 Evaluation of IWV Diurnal Variation in Regional Climate Models using GPS[13]

T. Ning
The Swedish Mapping, Cadastral and Land Registration Authority, Stockholm, Sweden
e-mail: tong.ning@lm.se

Given the ability of operating under all weather conditions and the long-term stability, the GPS technique has a superiority to measure long time series of the IWV with a temporal resolution as high as several minutes. Therefore, the GPS data are valuable to study the diurnal cycle of atmospheric IWV. In addition, in difference to the radiosonde data, the ground-based GPS data have not yet been assimilated into the climate reanalysis products, meaning that they offer an independent data set suitable for the evaluation of climate models.

GPS measurements acquired at 99 European sites were processed to estimate the atmospheric IWV time series for a period of 14 years (January 1997 to December 2010). The GPS-derived IWV were used to evaluate the simulations obtained from the regional Rossby Centre Atmospheric climate model (RCA) driven at the boundaries by ECMWF reanalysis data (ERA-Interim). The comparison was first made using the monthly mean values. Averaged over the domain and the 14 years covered by the GPS data, IWV differences of 0.47 kg/m^2 and 0.39 kg/m^2 are obtained for RCA–GPS and ECMWF–GPS, respectively. The RCA–GPS standard deviation is 0.98 kg/m^2 whereas it is 0.35 kg/m^2 for the ECMWF–GPS comparison.

Figure 5.44 depicts the diurnal cycles of IWV for the summer months, June, July, and August, as a function of the local solar time (LST) averaged for all sites using data from GPS, RCA, and ECMWF. The RCA captures the diurnal cycle reasonably well but with a slightly later phase, especially for the minimum, and a smaller amplitude. The mean peak time is at 18 LST compared to the mean peak time of

[13]Parts from this section were previously published in Ning et al. (2013).

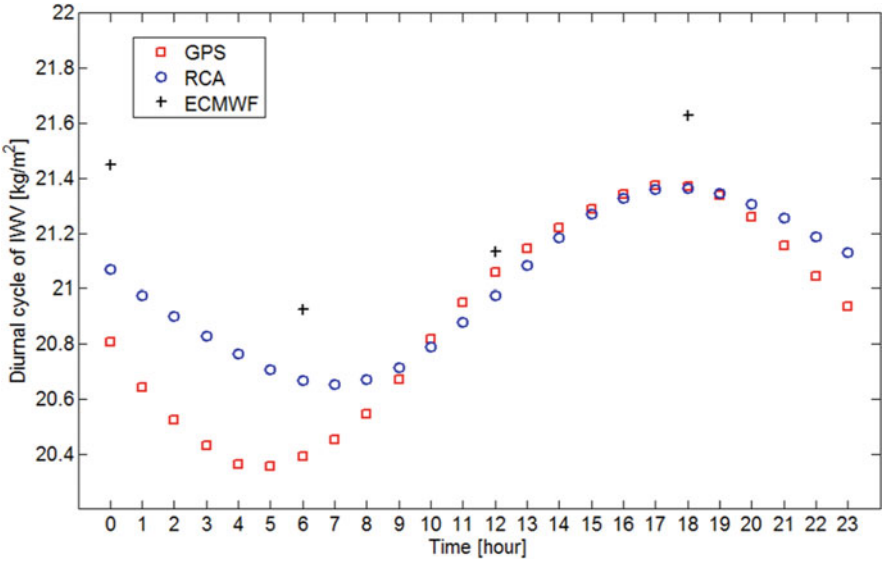

Fig. 5.44 Diurnal cycles of IWV as a function of local solar time for the summer months (JJA) obtained from the data for all sites and all years, from Ning et al. (2013)

the GPS at 17 LST. The amplitude and phase differences may partly be explained by the fact that the model value is an average over 50 × 50 km and a time step of 30 min whereas the GPS data represent one point with a time step of 5 min. The differences in amplitude and phase may, however, also be due to errors in the convective and surface parameterizations, as found by Jeong et al. (2011) investigating the RCA diurnal cycle of precipitation. For ECMWF, we only have values every 6 h, but as for RCA, the IWV amplitude is smaller and the mean value is higher both for the night and the day compared to the GPS data. The variation of the peak time of the diurnal cycle for each site for the summer months is shown in Fig. 5.45 where a clear positive correlation is seen between GPS and RCA. The peak varies from 16 to 19 LST for the GPS data while there is a dominant peak at 18 LST for the RCA data. The RCA captures the geographical variations from west to east, with later peaks in the afternoon further east, and the late night and early morning peaks along the east coast of Sweden. These coastal IWV outliers may be related to the observed and modelled peaks in precipitation in early morning at 4–7 LST, found by Jeong et al. (2011), which they suggested could be linked to deep convection development over the Baltic Sea. Future studies using a model with a higher horizontal resolution of 2–3 km will enable a study of these local effects and also help to investigate the differences in the GPS and modelled IWV.

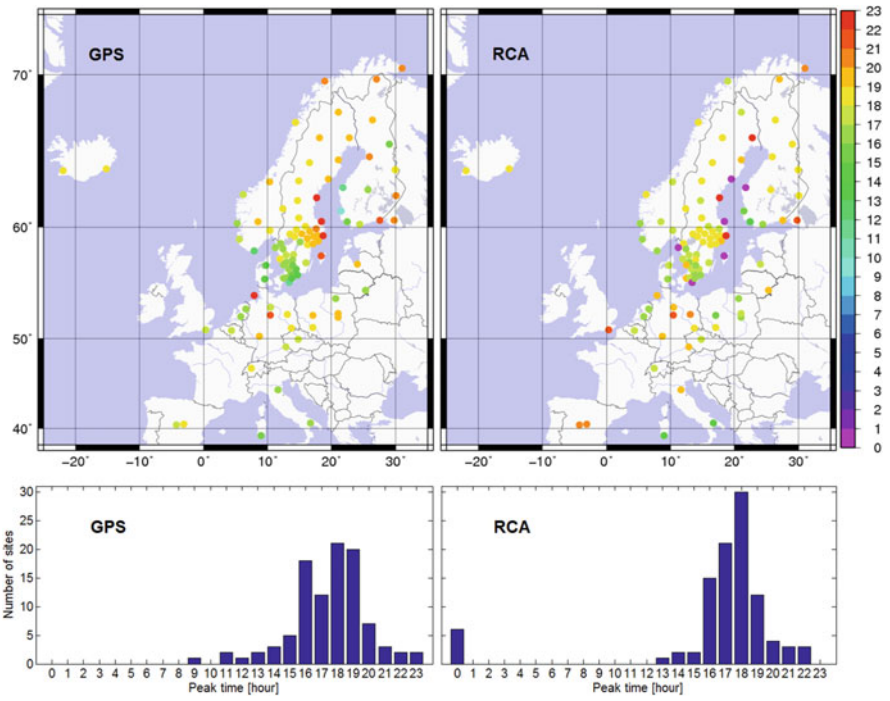

Fig. 5.45 The peak time of the diurnal cycle of the IWV, for the summer months (JJA), obtained from the GPS data and the RCA simulation for each GPS site (upper panels) and histograms of the peak time (lower panels). The hour is in local solar time (LST), from Ning et al. (2013)

5.7.3.1 Some More Recent Results by Ning et al.

We have analysed 17 years (from January 1997 to December 2013) of the GPS data from 123 sites in Europe and obtained time series of IWV in the atmosphere. We selected in total 69 sites for which we have data from a period longer than 10 years. Again, we calculated diurnal cycles of IWV for the summer months, June, July, and August.

We investigated the diurnal signal by calculating the mean IWV for each hour (local solar time). The result shows that it is reasonable to model the variation in the diurnal signal using a sine function, although significant deviations are seen for some sites. Thereafter we studied the stability of the diurnal signal over the years where we calculated the amplitude and the phase averaged over periods of 1, 3, and 5 years. The result is shown for four example sites in Figure 3. It is clear that both the amplitude and the phase averaged over only 1 year are highly variable and, as can be expected, the results are more stable for longer averaging time periods (Fig. 5.46).

Figure 5.47 summarises the results of the amplitude of the diurnal signal for all 69 sites with data covering at least 10 years. The estimated amplitude varies from

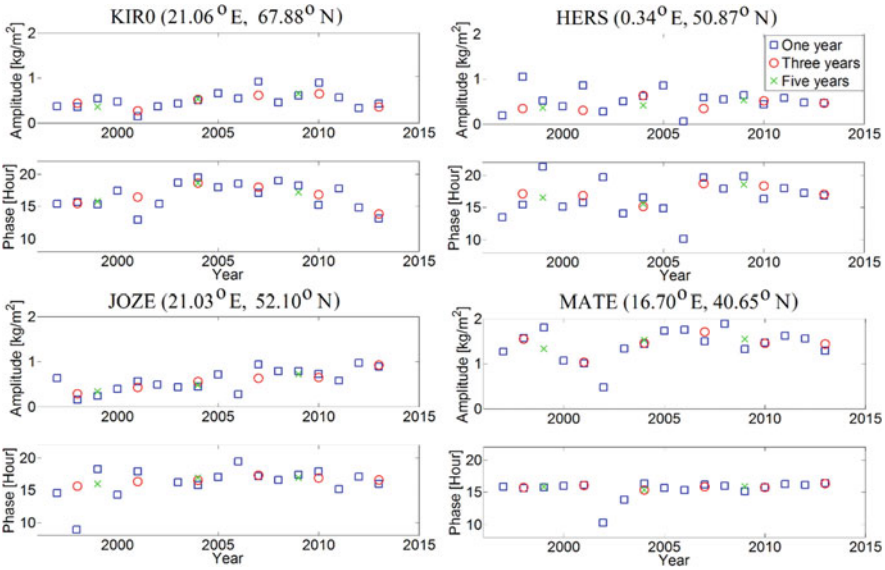

Fig. 5.46 The amplitude and the phase of the diurnal cycle estimated for the summer months (JJA) and averaged over 1, 3, and 5 years for four example sites

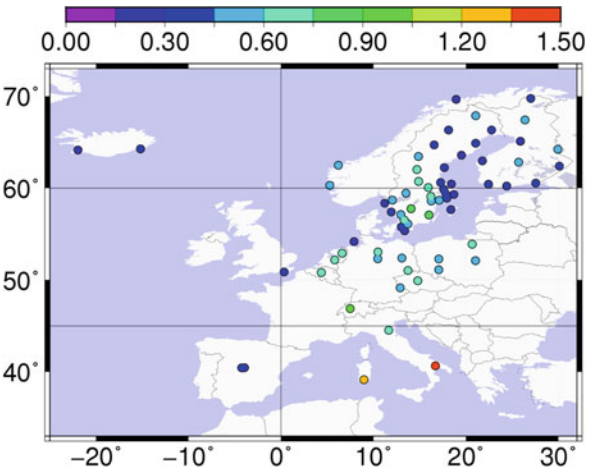

Fig. 5.47 Estimated amplitudes of the diurnal cycle in the IWV at the 69 sites with more than 10 years of data, the unit of the colour bar is kg/m^2

0.16 kg/m^2 to 1.46 kg/m^2. In general, an increase of the amplitude is seen when the latitude decreases. Fig. 5.48 depicts the peak time of the hourly IWV mean. Similar to the results shown in Ning et al. (2013) the peak time of the hourly IWV mean is varying from 16 to 20 local solar time for most of the sites. In addition, it shows a systematic variation from west to east over the Scandinavian peninsula.

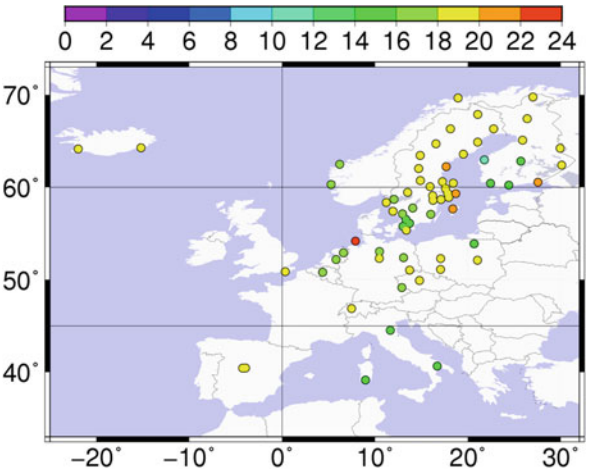

Fig. 5.48 The peak of the hourly mean of the IWV in local solar time (same sites and time periods as in Fig. 4)

5.7.4 Validation of the Regional Climate Model ALARO-SURFEX by EPN Repro2

J. Berckmans
Royal Meteorological Institute of Belgium, Brussels, Belgium
e-mail: julieb@meteo.be

The use of ground-based observations is suitable for the assessment of atmospheric water vapour in climate models. We used IWV observations at 100 European sites to evaluate the regional climate model ALARO coupled to the land surface model SURFEX (Berckmans et al. 2017), driven by the European Centre for Medium-Range Weather Forecasts (ECMWF) Interim Re-Analysis (ERA-Interim) data. The selected stations provide data for a minimum of 10 years, resulting from the second reprocessing campaign of EPN (EPN Repro2, Pacione et al. 2017).

The yearly cycle of the IWV for the 19-year period from 1996 to 2014 reveals that the model simulates well the seasonal variation. The intra-annual variability is higher than the inter-annual variability. Although the model overestimates IWV during winter and spring, it is consistent with the driving field of ERA-Interim. However, the results for summer demonstrate an underestimation of the modelled IWV and a larger standard deviation, which is not present in ERA-Interim (Fig. 5.49). The dry bias in summer can be explained by fewer evaporation by the model, hence an underestimation of the IWV.

The spatial variability among the sites is high and varies between -1.4 kg/m^2 and + 4.6 kg/m^2 in winter and between -2.0 kg/m^2 and 4.9 kg/m^2 in summer. The standard deviation shows a latitudinal dependence with increasing values towards the south of the domain. Overall, these findings are in agreement with the distribution of the cold and wet bias by the model in winter, and the cold and mixed dry and wet bias in summer.

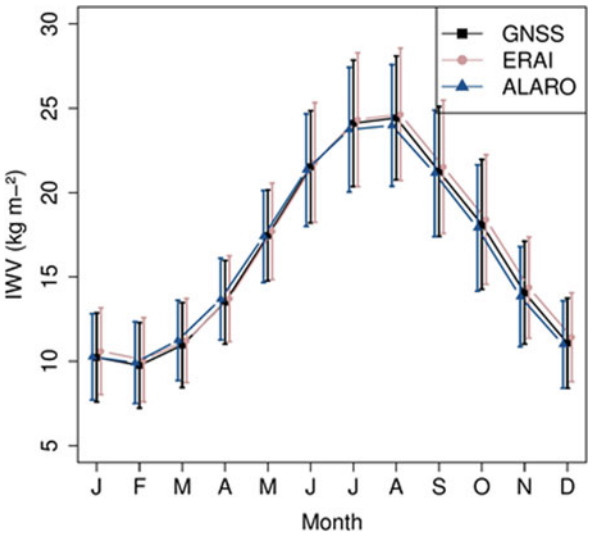

Fig. 5.49 Monthly averaged Integrated Water Vapour (IWV, kg/m^2) values averaged over the 19-year period of 1996–2014 and all stations from EPN-Repro2 in a Western European domain and corresponding grid points modelled by ERA-Interim and ALARO-SURFEX. The vertical bars represent the standard deviations

In summary, the model ALARO-SURFEX performed better for the simulation of water vapour in autumn and winter than for spring and summer. The underestimation of the IWV in summer by the model could be related to an underestimation of the evaporation. This mechanism was most pronounced in summer as land-atmosphere feedbacks are strongest in summer. The spatial distribution demonstrated a high variability of the IWV. We recommend to investigate the relations between stations with similar characteristics.

5.7.5 *Evaluation of IWV Trends and Variability in a Global Climate Model*[14]

A. Parracho
IGN Institut national de l'information géographique et forestière, Paris, France
e-mail: ana.parracho@etu.upmc.fr

O. Bock
IGN Institut national de l'information géographique et forestière, Paris, France
e-mail: olivier.bock@ign.fr

S. Bastin
Université Paris-Saclay, Saint-Aubin, France
e-mail: sophie.bastin@latmos.ipsl.fr

[14]Parts from this section were previously published in Parracho (2017).

Water vapour is responsible for the most important positive feedback in climate change. Globally, as temperatures increase, evaporation and the water-holding ability of the atmosphere also increase, leading to an increase in atmospheric water vapour. Because water vapour is a powerful greenhouse gas, its increase leads to a further rise in temperature, creating a vicious cycle. Although the water vapour feedback is a robust feature across all climate models (Soden et al. 2005), simulated water vapour variabilities have been found to differ from observations (Pierce et al. 2006). Uncertainties in convective and turbulent parameterizations, cloud microphysics, land surface/atmosphere interactions in climate models lead to uncertainties in the accuracy of simulated water vapour and, ultimately, to uncertainties in climate predictions. An effort has been made to improve model representation of clouds and water vapour, guided by different types of observation (e.g. Jiang et al. 2012).

In this subsection, the trends and variability in IWV in the IPSL-LMDZ model (at a $1.9° \times 3.75°$ resolution, for the 1995–2009 period) were compared with those obtained from GPS observations and ERA-Interim. Two versions of model were used: LMDZ5A (Hourdin et al. (2013a)), used within the Coupled Model Intercomparison Project 5 (CMIP5) under the name IPSL-CM5A and LMDZ5B (Hourdin et al. (2013b)), used within CMIP5 as IPSL-CM5B model. LMDZ5A uses similar physical parametrizations to LMDZ4, a previous version of the model used in the CMIP3, described in Hourdin et al. (2006), while LMDZ5B uses different parameterizations of turbulence, convection and clouds. In addition, for each physics, two runs were performed: a free run and a run that is nudged towards ERA-Interim wind fields every 6 hours, so that the large-scale dynamics is very close to that of ERA-Interim. In the following, the four simulation runs will be referred to as CM5A (LMDZ5A free run), CM5An (LMDZ5A nudged), CM5B (LMDZ5B free run), and CM5Bn (LMDZ5B nudged).

GPS data from 104 globally-distributed stations with over 15 years of data was used. In order to solve the problem of breaks in the GPS data, the time series were homogenized using ERA-Interim as a reference. In this case, the GPS IWV means were bias corrected to be consistent with ERAI means for each and every segment of time delimited by equipment or processing changes (in the rare case when no change occurred, the overall bias was simply corrected). Although the means of the corrected GPS data and the ERA-Interim data were strictly equal, the variability and trends could still differ slightly.

The ERA-Interim data used was filtered and interpolated to the model grid. As in Sect. 5.7.1, the analysis was done in terms of mean IWV, inter-annual variability, and linear trends, and divided into two seasons: December–January-February (DJF) and June–July-August (JJA).

5.7.5.1 Means and Variability

In terms of the mean IWV, both the free and nudged simulations show a consistent global pattern with the one seen previously for ERA-Interim (presented in Sect. 5.7.1). However, there are differences in the magnitude of mean IWV and the free

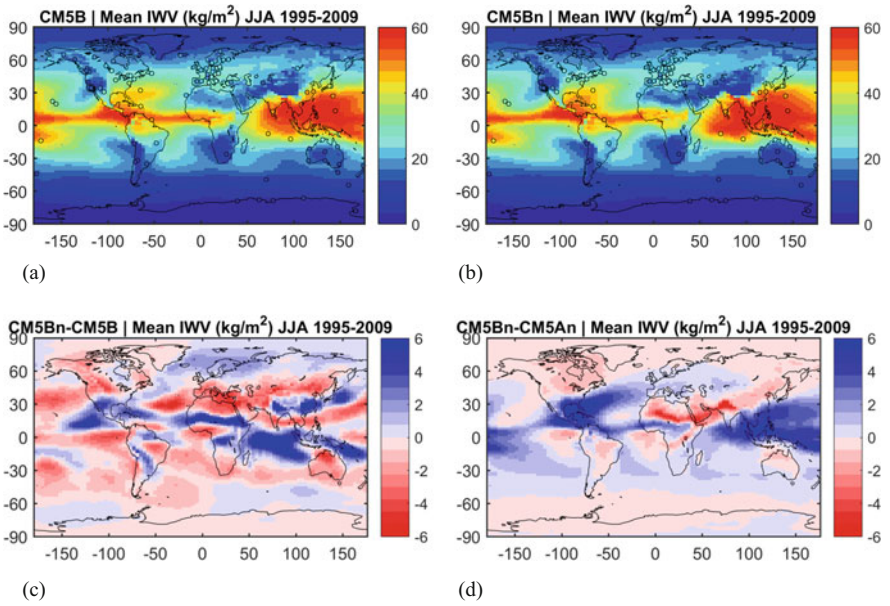

Fig. 5.50 Mean IWV for JJA, for CM5B and CM5B nudged (**a**, **b**). Difference in mean IWV between nudged and free run of the new physics (**c**). Difference in mean IWV between physics (both nudged) (**d**)

runs of the model have difficulty in representing regional features such as the monsoon flows over West Africa and India in JJA (Fig. 5.50a). This is improved in the nudged simulations (Fig. 5.50b), as the nudging improves the water advection in both regions and allows the monsoon to penetrate further north. This is observed in the dipole structure over both regions in the difference fields between nudged and free simulations (Fig. 5.50c). For the mean IWV, nudging and difference in physics (Fig. 5.50d) have an impact of the same order of magnitude, with differences between models of up to around 6 kg/m^2. From Fig. 5.50d it is also noticeable that the new physics is moister in general over the tropics. Comparison between the model and ERA-Interim (not shown) also highlighted a moist bias in the new physics (both free and nudged) for the tropical oceans in both seasons, which is also seen in the comparison between the model and the GPS stations in the region.

The free runs of the model have difficulty in reproducing the inter-annual variability in IWV, especially in the winter hemisphere. For DJF (Fig. 5.51) the inter-annual variability of IWV is noticeably different in the free and nudged simulations. The nudged simulations have well-defined regions of higher variability over the Arctic and Siberia, West Africa, India, Australia and the tropical Pacific Ocean around the Equator, whereas the free configurations have maximum values over Canada and Alaska. In comparison with GPS, it is clear that the nudged simulations are better at representing the IWV inter-annual variability for DJF. Although there are no GPS stations over the Arctic and Siberia, the stations over

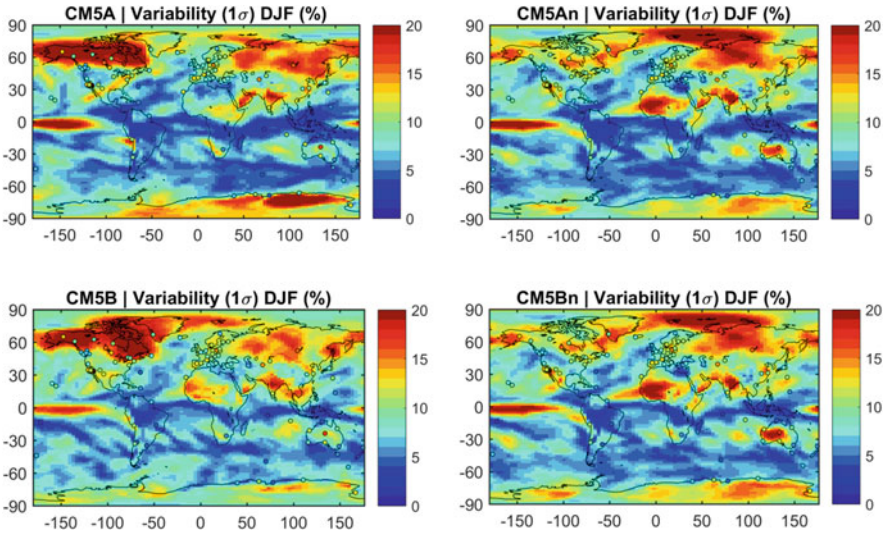

Fig. 5.51 Variability in IWV fields in model with GPS variability as points for DJF

Canada and Alaska have lower variability than the free simulations (around 10%, as opposed to over 20% in CM5A and CM5B). They are in better agreement with nudged simulations, but some stations still indicate an overestimation of inter-annual variability in CM5An and CM5Bn (e.g. Alaska, Greenland).

On the other hand, over Australia, GPS station ALIC presents higher variability, which is once again better captured by the nudged simulations than by the free ones. This can be observed in more detail in the time-series at the ALIC station for CM5A and CM5An (in Fig. 5.52). From the time series for CM5A it is observed that higher (lower) IWV events for DJF in 2000 (2005) are not well captured by the model. The nudged simulations are also in better agreement with ERA-Interim (not shown), with differences of between −5% and 5%, in contrast with differences of up to 15% in the free simulations.

For JJA (Fig. 5.53), the inter-annual variability in IWV shows more similar patterns across the four models. There is a maximum of variability over Antarctica, which appears to be overestimated in the model in comparison with GPS, especially for CM5A and with the exception of the easternmost station. There is also strong variability over Australia, which is slightly underestimated in all models, in comparison with the GPS station ALIC (in the centre of Australia). For the nudged simulations, the differences in variability with ERA-Interim (not shown) are relatively small (mostly within 2%) and similar between the two physics, which highlights the importance of the large-scale dynamics in the IWV inter-annual variability. Over the variability, the difference in model physics has a smaller impact than the nudging (about one half of the magnitude).

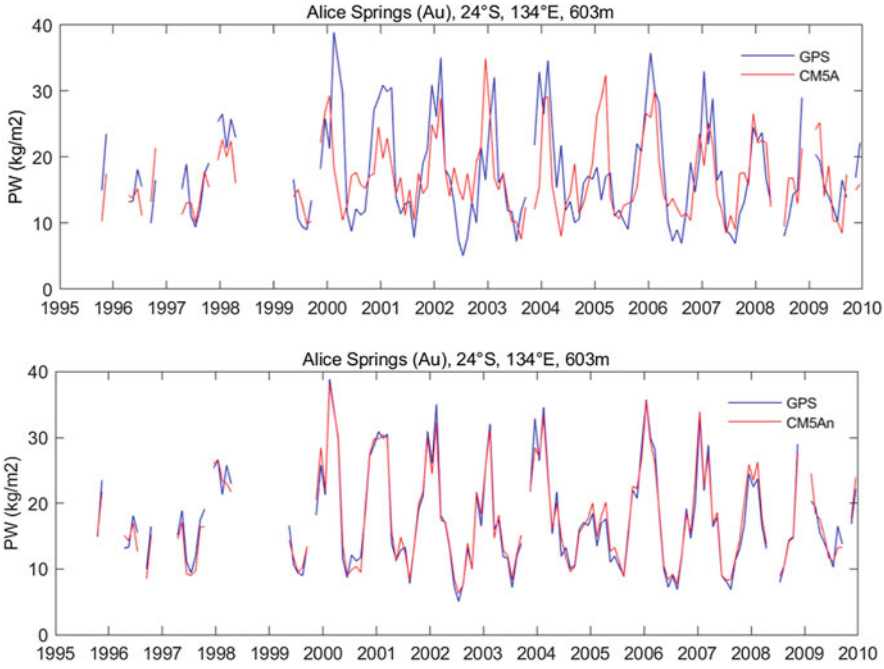

Fig. 5.52 Time series of GPS IWV at the ALIC (Alice Springs in Australia) site and IWV for CM5A and CM5An at the GPS site

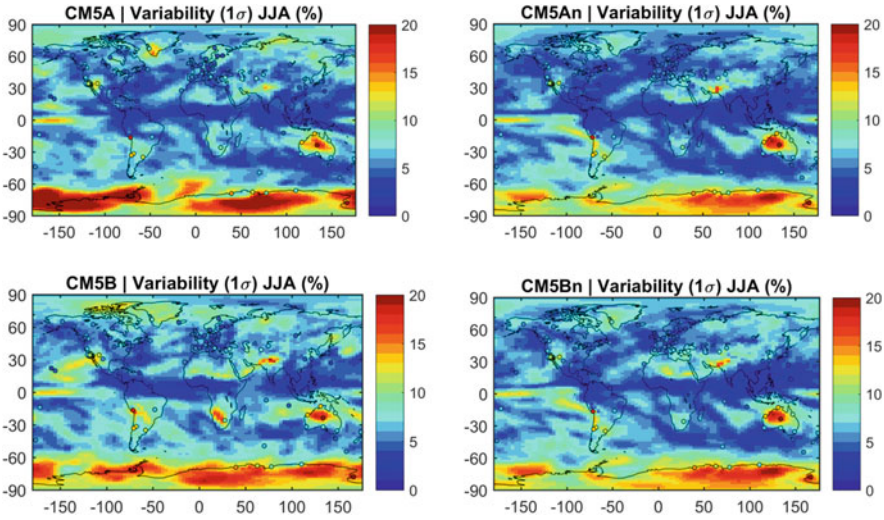

Fig. 5.53 Variability in IWV fields in model with GPS variability as points for JJA

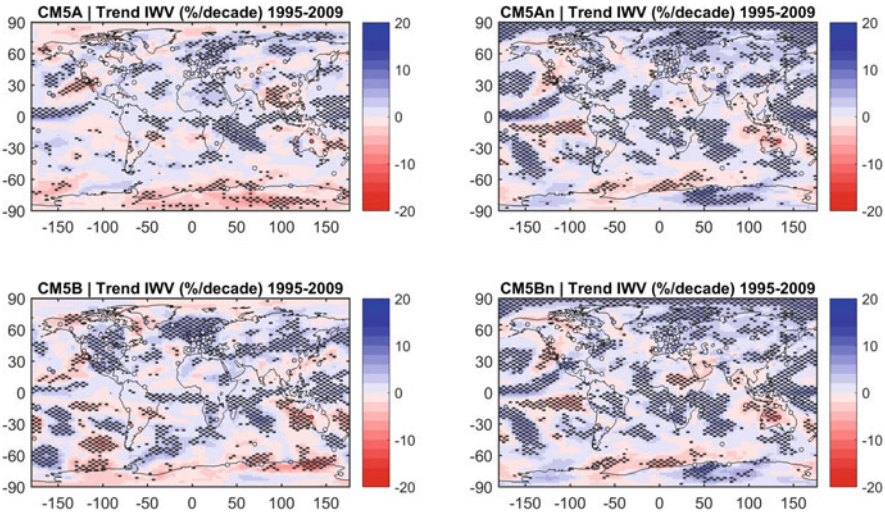

Fig. 5.54 Trends in IWV fields in model with GPS trends as points

5.7.5.2 Linear Trends

The monthly trends are shown for the four configurations of the model in Fig. 5.54. Although there are differences in the computed trends, especially when it comes to the free and nudged simulations, there are trend structures that are consistent in all four configurations. These include a moistening over Northern Europe and Siberia, western coast of North America, the Western Pacific, and over part of the Indian Ocean; and a drying over the Western United States and off the coast into the Pacific. On the other hand, the drying over Western Australia and the moistening over southern Africa are observed for CM5An, CM5B and CM5Bn (but not CM5A) and are consistent with the trends computed at the GPS stations over these regions. Furthermore, CM5B is also able to reproduce the dipole structure in IWV trends in the tropical Pacific, which had been observed for ERA-Interim (Sect. 5.7.1), and which is a result of the strong 1997/98 El Niño event. This structure is not as significant in CM5A. On the other hand, there are significant trends which are only present in the nudged simulations, such as the moistening over Eastern Antarctica, which is in agreement in sign with the GPS stations, and most of South America; and the drying in Eastern Sahel, which is more significant in CM5Bn.

For the seasonal trends in both seasons, there is poorer agreement between the trend patterns observed for the free and nudged simulations, although the nudged simulations show similar trend patterns. For DJF in particular (Fig. 5.55), the nudged simulations show strong moistening over the Arctic and Northern Europe, Antarctica, China and South America; and strong drying over the West and East coasts of North America, the Arabian Peninsula, and Eastern Siberia. Some of these strong trends are confirmed by the GPS observations (e.g. some stations over Antarctica,

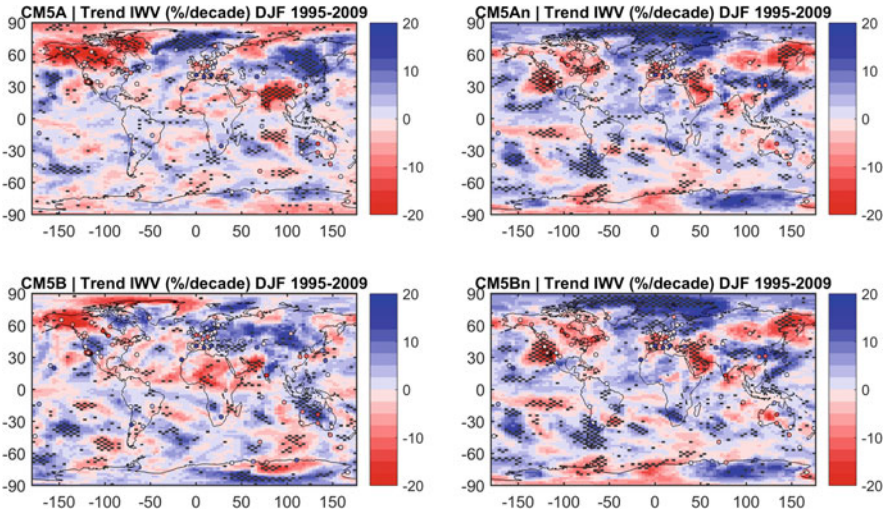

Fig. 5.55 Trends in IWV fields in model with GPS trends as points for DJF

and North America), but there are notable exceptions, such as the two stations over China and the station over Sweden, which register a drying (instead of moistening). However, overall, the trends observed at the GPS sites are in better agreement with the nudged simulations.

This confirms the importance of dynamics over the trends in IWV. The impact of the difference in physical parametrizations is much lighter. While the impact of nudging is in the 20% range, the impact of the physics is in the 5% range.

Most of the conclusions found for DJF are also seen for the JJA season, although for this season, there are trend structures that are observed in all four simulations. In Fig. 5.56, a few same sign significant trends are observed for Australia (drying), Western Europe (moistening), and the Indian Ocean (mostly positive, but partly negative in the eastern part, which is confirmed by the two GPS stations in the area. More results can be found in Parracho (2017).

5.7.5.3 Conclusions

The four configurations of the model are able to represent the global mean IWV patterns seen in ERA-Interim and at the majority of GPS stations, although some regional features such as the monsoon flows are only well represented when the model is nudged with wind fields. In addition to the important impact of the nudging over the means, the differences between physics are of the same order of magnitude, and denote a moist bias for the new physics over the tropical oceans.

The free runs have difficulty in representing the trends and variability in IWV. For the variability, the impact of nudging outweighs the impact of the difference in

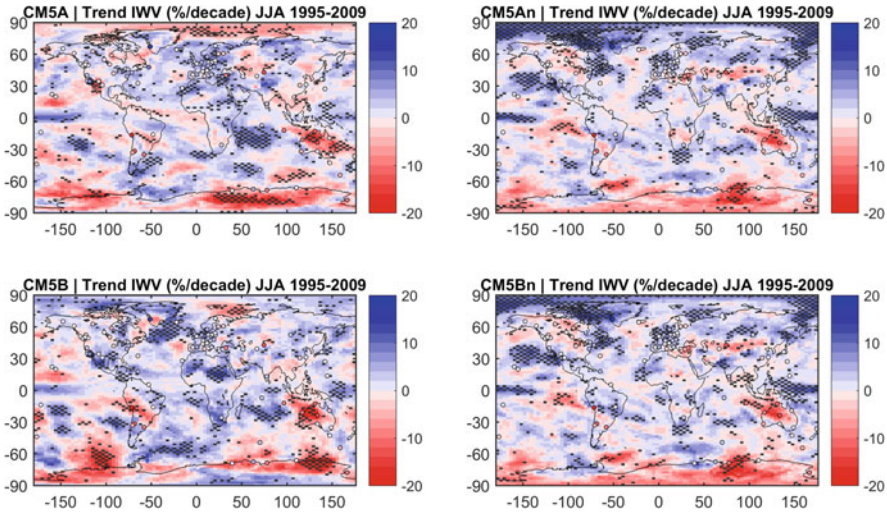

Fig. 5.56 Trends in IWV fields in model with GPS trends as points for JJA

physics. In fact, when the simulations are nudged, the variability follows that observed for ERA-Interim more closely, and the agreement with GPS is improved. The same is observed for the IWV trends to some extent, although some regions still show relatively high differences between the model and GPS and ERA-Interim, even when the model is nudged (e.g. North Africa, Australia and Antarctica).

Finally, the fact that nudging significantly improves the results, demonstrates that dynamics (moisture transport) controls IWV variability and trends at both global and regional scales.

5.7.6 Anomalies of Hydrological Cycle Components During the 2007 Heat Wave in Bulgaria[15]

G. Guerova
Physics Faculty, Department of Meteorology and Geophysics, Sofia University "St. Kliment Ohridski", Sofia, Bulgaria
e-mail: guerova@phys.uni-sofia.bg

B. Mircheva
Physics Faculty, Department of Meteorology and Geophysics, Sofia University "St. Kliment Ohridski", Sofia, Bulgaria
e-mail: bmircheva@uni-sofia.bg

[15]Parts from this section were previously published in Mircheva et al. (2017).

5.7.6.1 Motivation

Heat waves have large adverse social, economic and environmental effects including increased mortality, transport restrictions and a decreased agricultural production. The estimated economic losses of the 2007 heat wave in South-east Europe exceed 2 billion EUR with 19,000 hospitalisations in Romania only. Understanding the changes of the hydrological cycle components is essential for early forecasting of heat wave occurrence. Valuable insight of two components of the hydrological cycle, namely IWV and Terrestrial Water Storage Anomaly (TWSA), is now possible using observations from GNSS and Gravity Recovery And Climate Experiment (GRACE) mission. In this work the IWV is derived from the GNSS station in Sofia (SOFI), which is processed within the first reprocessing campaign of the International GNSS Service.

5.7.6.2 Main Results

In 2007, positive temperature anomalies are observed in January (5 °C), February (3.4 °C) and July (2.1 °C). There is a negative IWV and precipitation anomalies in July 2007 (−2.7, −56 mm) that coincide with the heat wave in Bulgaria. TWSAs in 2007 are negative in January, May and from July to October being largest in August. Long-term trends of 1) temperatures have a local maximum in March 2007, 2) TWSA local minimum in May 2007, 3) IWV has a local minimum in September 2007, and 4) precipitation has a local maximum in July 2007. In Fig. 5.57 are shown the long-term time series of temperature (red line), precipitation (blue line), IWV (green line) and TWSA (black line) for the 2003–2010 period. There is an increase visible in the values of the four parameters for the studied period. Clearly is seen that there is a local maximum for the temperature early in 2007. Values of TWSA start from −94 mm in July 2003 and rise to 121 mm in December 2010. However, the trend is nonlinear and there is a local minimum of −30 mm in the summer of 2007. In the first months of

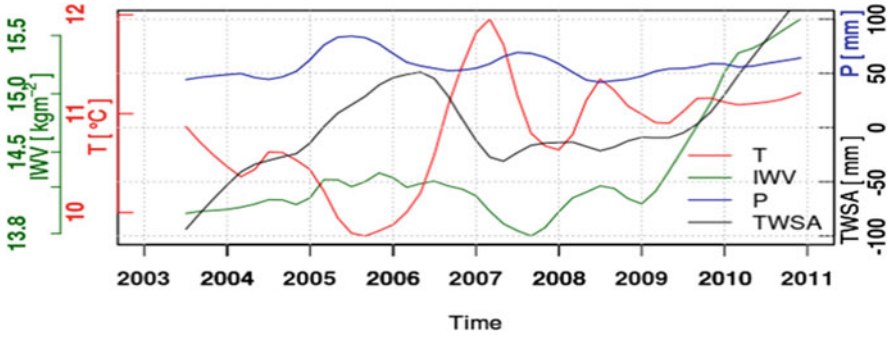

Fig. 5.57 Long-term time series of monthly temperature (red line), precipitation (blue line), IWV (green line) and TWSA (black line) for the 2003–2010 period

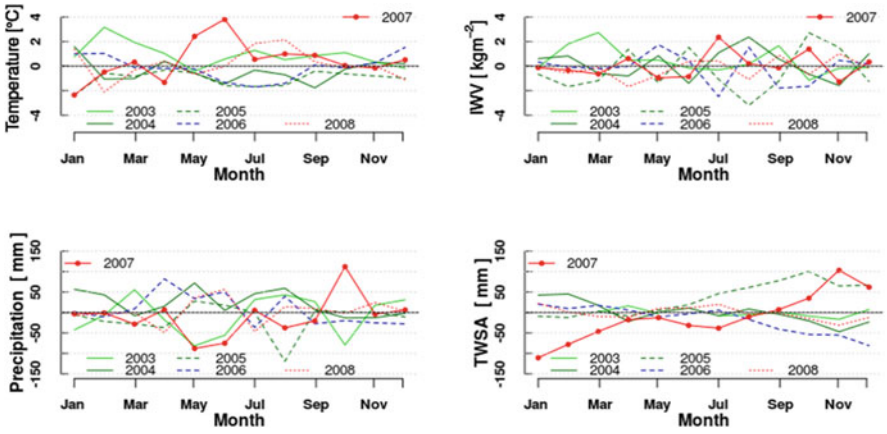

Fig. 5.58 Monthly anomaly (ALADIN-Climate minus observed) of: (**a**) temperature, (**b**) IWV, (**c**) precipitation and (**d**) TWSA

2007 downward trends of precipitation, IWV and TWSA are observed. The combination of above average temperatures and negative anomalies of IWV, precipitation and TWSA characterize the extreme hot weather situation in Bulgaria during the 2007 summer (Mircheva et al. 2017). To analyse the differences between the observed SYNOP, GNSS and GRACE anomalies are compared with ALADIN-Climate model simulations for period 2003–2008 and particularly for 2007. In Fig. 5.58 are shown anomaly differences (model minus observed) of monthly pairs of 1) temperature (top left), 2) IWV (top right), 3) precipitation (bottom left) and 4) TWSA (bottom right). Plotted are anomaly differences for each month of the years from 2003 to 2008. The heat wave year (2007) is plotted with a solid red line with dots. Positive and negative values correspond respectively with overestimation and underestimation of the computed RCM monthly anomalies against observations. The following features stand out for the distribution of monthly temperature anomaly differences (Fig. 5.58 top left): (1) mean monthly distribution range is generally in the interval $\pm$ 2 ° C and (2) there are two positive outliers in 2007 (May and June) and one in 2003 (February), indicating model overestimation with more than 2 °C. One negative outline in 2007 (January) shows underestimation of about 2 °C. The monthly IWV anomaly differences (figure 2 top right) are: 1) generally in the range $\pm$ 2, 2) negative in August 2003 and July 2006 and 3) positive in March 2003, August 2004, October 2005 and July 2007. The precipitation anomaly difference (bottom left panel of figure 12) is generally in the range $\pm$ 50 mm. There are large model underestimations in May and October 2003, August 2005 and May 2007. The model strongly overestimates the precipitation in October 2007 (112 mm) and April 2006 (88 mm). The TWSA differences are also generally in the range $\pm$ 50 mm with good agreement between the model and GRACE data sets from March to August (Fig. 5.58 bottom right). In winter months of 2007 TWSA observations and model data differ strongly. The largest positive anomaly differences are observed in November (103 mm) and December (62 mm) while the negative anomaly differences are in January (111 mm) and February (82 mm). It is

noteworthy that TWSA anomalies for winter months of 2007 are modelled less well than every other time period. The computed cross-correlation coefficients of 2007 anomalies between observations and the ALADIN-Climate model indicates: 1) high correlation for temperature and IWV data pairs (over 0.7) and 2) no correlation for precipitation anomalies and TWSA data pairs (0.3).

5.7.6.3 Future Work

In the near future the remotely sensed data sets like GRACE and GNSS observations are likely to have large impact in regions like Bulgaria where in situ data are sparse. Future work will include comparison of the studied observation with long term climate data. Also the results will be used to analyse the changes of the hydrological cycle components and its relation with the heat wave and flood occurrence in Bulgaria.

5.8 Database, Formats and Dissemination

5.8.1 GOP-TropDB – Comparison Tropospheric Database

J. Douša
Geodetic Observatory Pecný, RIGTC, Ondřejov, Czech Republic
e-mail: jan.dousa@pecny.cz

C. Hackman
United States Naval Observatory, Washington, DC, USA
e-mail: hackman.christine@usno.navy.mil

J. Böhm
Department of Geodesy and Geoinformation, TU Wien, Wien, Austria
e-mail: Johannes.Boehm@geo.tuwien.ac.at

The system for a long-term evaluation of the tropospheric parameters estimated as a product of space geodetic data analyses (GNSS, VLBI, DORIS), numerical weather model (NWM) analyses or in situ observations (radiometers, radio sounding) has been implemented within the frame of IGS Troposphere Working Group (TWG). The initial goal aimed at improving the accuracy and usability of GNSS-based tropospheric parameters through the inter-comparison to the independent observation techniques. For this purpose, GOP developed a Postgres database system GOP-TropDB (Douša and Győri 2013; Győri and Douša 2016) which was completed with a web graphic user interface for interactive view of the inter-comparison results. GOP also performed comparison of tropospheric parameters from a variety of IGS and EUREF solutions and implemented service for online user calculation of tropospheric, meteorological and other auxiliary parameters from a NWM

re-analysis. USNO coordinated the effort within the TWG and developed new portal linking all these services together. The GOP-TropDB can also serve for the assessment of NWM or climate models. Finally, the development of inter-technique troposphere comparison services, the provision of the NWM-based online tropospheric service and recent study on optimal modelling of tropospheric ties contributed to the IAG Joint Working Group 'Tropospheric ties' (Douša et al. 2017a, b). The service is available at the http://twg.igs.org.

5.8.1.1 Comparisons of Tropospheric Parameters

The GOP-TropDB was extensively used for evaluating results of the 2nd EUREF reprocessing including solutions provided by individual ACs (Pacione et al. 2017), variants of troposphere modelling performed at GOP (Douša et al. 2017a, b, subsection 3.5.2) and results of the 1st/2nd IGS reprocessing (Douša et al. 2014, 2016). Differences between various GNSS solutions as well as NWM and radiosondes products were calculated for both ZTDs and tropospheric gradients (when available). The time series of differences were analysed by performing monthly, yearly and total statistics which have been provided for each station or as a mean over all stations. Figure 5.59 shows an example of the visualization of ZTD statistics for the EUREF 2nd reprocessing vs. ERA-Interim reanalysis.

Assessment of the global IGS tropospheric products with respect to the ERA-Interim (Dee et al. 2011) has been performed for the IGS 1st reprocessing and the 2nd reprocessing from CODE and GFZ analysis centres. Table 5.8 shows summary statistics for all stations and the differences of ZTD and tropospheric gradients (GRD) between GNSS product and ERA-Interim reanalysis over the period 1996–2014.

Figure 5.60 shows comparisons of two CODE reprocessing solutions, namely 3-day (CO2) and 1-day (CF2), indicating the impact of combining tropospheric parameters at the daily boundaries on ZTD parameters. The mean standard deviation of ZTD differences is 0.8 mm over a day, but almost 1.8 mm at the day boundaries and about 2–3 larger dispersion characterized by 1-sigma over all stations. Actual differences in ZTD could even be larger, because of necessary approximations used to compute statistics from low-resolution product when close to the day boundaries.

5.8.1.2 GOP TropDB Visualization Tools

In order to facilitate browsing and interpreting huge statistical data sets from the GOP-TropDB, a new interactive web-based visualization tool was developed too. It is configurable for plotting data in spatial and temporal scopes for user selection of parameters, stations, products etc. Optionally, spatio-temporal statistics can be viewed using the animation of a single selected parameter. With adaptable value ranges, users can plot parameters of site metadata, statistical values and original data; the last one for a limited period only.

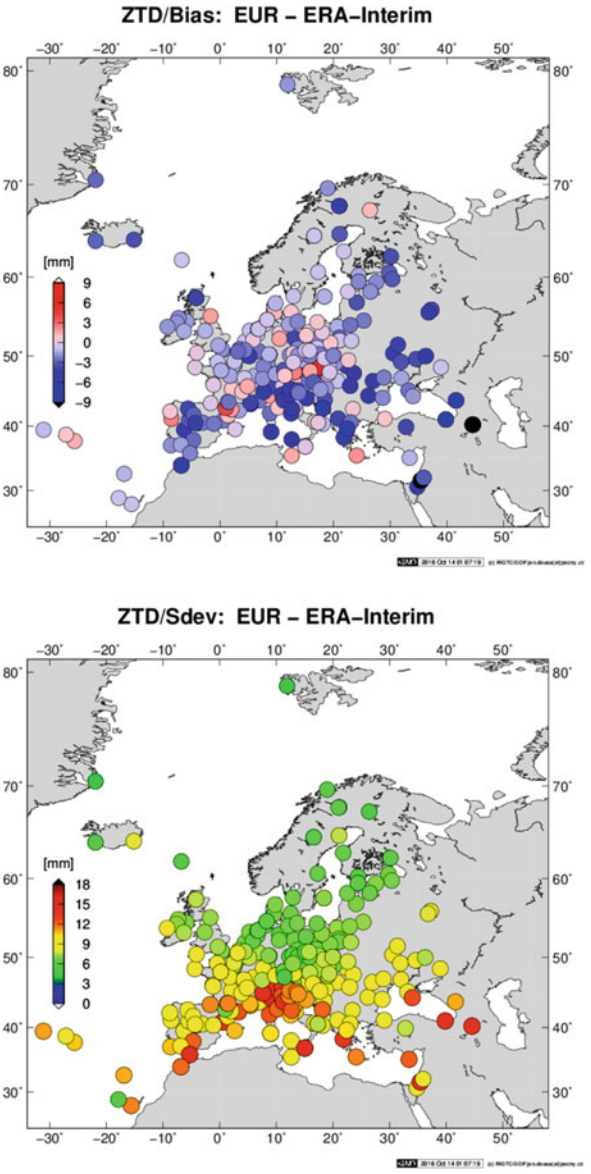

Fig. 5.59 Summary statistics for ZTD from EUREF second reprocessing and ERA-Interim reanalysis (1996–2014)

Figure 5.61 shows an example of metadata viewing page with selecting different data sources (or source groups), filtering data by station name or through a user spatial domain. Similarly, Fig. 5.62 shows the statistical results on a geographical map. Wheather a single station or a group of stations, an individual solution or a group of products, the time series can be plotted in the optional bottom panel when selecting a particular parameter. The time series can be zoomed in and the graph can be switched for plotting individual values or average (+dispersion) over all the values.

Table 5.8 Summary statistics for ZTD, gradients from global reprocessing vs. ERA-Interim reanalysis (1996–2014)

AC solution	Processing strategy	ZTD [mm]		N-GRD [mm]		E-GRD [mm]	
		mean	sdev	mean	sdev	mean	sdev
CO2 Repro2	BSW (network), 3-day solution (Steigenberger et al. 2014) piece-wise linear model: ZTD (2 h), GRD(24 h)	−2.01	8.37	−0.03	0.31	0.00	0.34
CF2 Repro2	BSW (network) 1-day solution (Steigenberger et al. 2014) piece-wise linear model: ZTD (2 h), GRD(24 h)	−2.04	8.37	−0.03	0.32	0.00	0.37
GFZ Repro2	EPOS (PPP), 1-day solution (Ning et al. 2016a, b) piece-wise constant model: ZTD (1 h), GRD(24 h)	−1.44	10.73	0.06	0.58	0.35	0.78
IGS Repro1 + operation	BSW (PPP), 1-day solution (Byram et al. 2011) piece-wise constant model: ZTD (5 min), GRD (5 min)	−2.28	9.94	−0.01	0.44	0.00	0.52

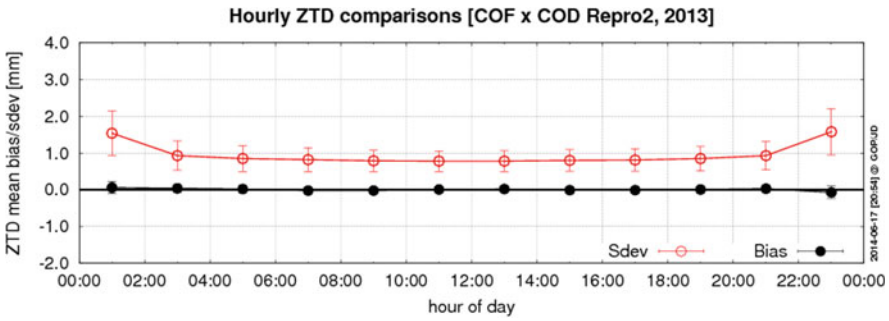

Fig. 5.60 Mean bias and standard deviation between two CODE reprocessing solutions (all stations over year 2013)

5.8.1.3 GOP TropDB Online Service

The online service makes it possible for a user to calculate tropospheric, meteorological or other interesting parameters (e.g. mean temperature and its lapse rate, scale heights, vertical reduction rates) on request using 3D data from a historical NWM archive, currently the ERA-Interim reanalysis, but in the future possibly others too.

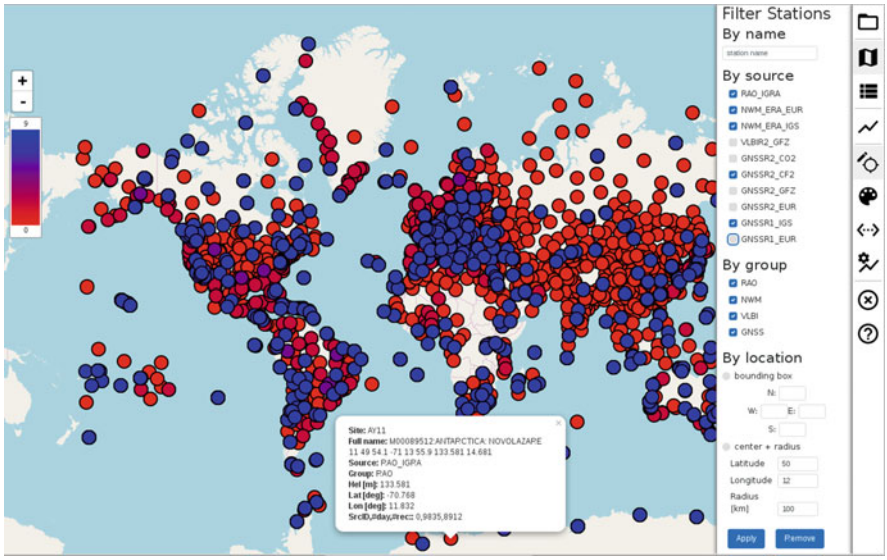

Fig. 5.61 Web interactive visualization of station metadata with various tropospheric products

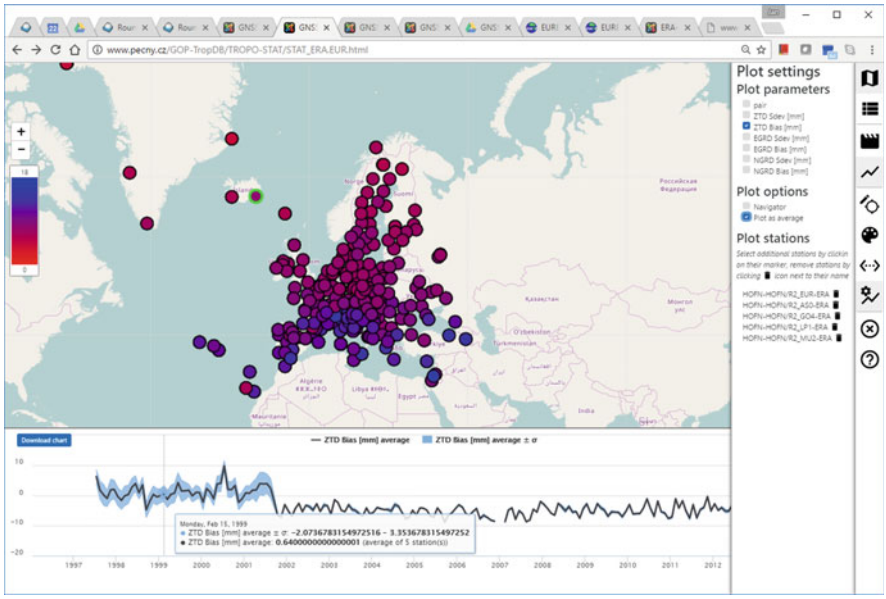

Fig. 5.62 Web interactive visualization of statistics from troposphere parameter comparisons

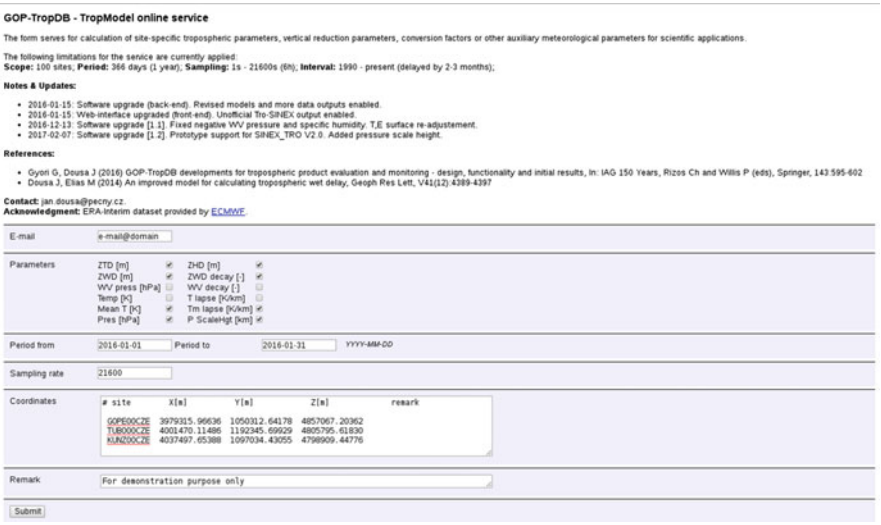

Fig. 5.63 Web service for user-specific calculation of tropospheric, meteorological and other parameters

The service can be used for calculating: (1) ZTD, ZWD and ZHD values at different positions (not limited to Earth's surface), (2) mean temperature for converting ZWD to IWV, (3) tropospheric ties for space-geodetic inter-technique comparisons/combinations, or for other purposes.

Figure 5.63 shows the web form where a user may request up to 100 locations for which parameters are calculated with requested sampling. Although the ERA-Interim reanalysis contains data at 00, 06, 12 and 18 hours, any higher time resolution is supported by using spline interpolations. Currently, requests are ordered in a processing queue, and results files, each of which limited to 1 year in length are provided in TRO_SINEX v2.0 (Pacione and Douša 2017) or in a plain-text column format. The user can download the results from a temporary storage location after being informed by e-mail about the completed job.

5.8.2 Tropo SINEX Format

R. Pacione
e-GEOS/Centro di Geodesia Spaziale-Agenzia Spaziale Italiana, Matera, MT, Italy
e-mail: rosa.pacione@e-geos.it

J. Douša
Geodetic Observatory Pecný, RIGTC, Ondřejov, Czech Republic
e-mail: jan.dousa@pecny.cz

The effort to standardize the exchange format for tropospheric products has started in early 1997 by a number of IGS participants (Gendt 1997). In November 2010 [IGSMAIL-6298] SINEX_TRO format was slightly expanded to accommodate the addition of gradients. This expanded format has never been officially accepted and adopted. Due to the lack of the standardization, different software packages and organizations have started to use different field names referring to the same variables ad-hoc supporting optional and mandatory metadata, output files with different naming conventions and overall data contents. As a result, the format cannot be handled with a unique decoder.

According to further developments, new demands arose on the format for exchanging tropospheric parameters, in particular supporting:

(a) Parameters from different sources than space geodetic techniques such as numerical weather prediction models and re-analyses, radiosondes and water vapour radiometers,
(b) Long station names (9 characters) in concordance with RINEX 3 data format,
(c) Products including slant tropospheric delays,
(d) Parameters corresponding to long-term time series of individual stations.

This was the driver to develop a unique format to be adopted within all the IAG services and by all the techniques dealing with tropospheric parameters. However, because of difficulties in supporting all legacy and new features, it was decided to revise the format without keeping a full compatibility with any previous SINEX_TRO unofficial version. In this way new features, such as long station names or time series data support, could be introduced much easier while simplifying the format definition and usage.

The SINEX-TRO v2.00 format description is reported in Appendix D.

The SINEX-TRO v2.00 format has been officially presented at the IGS Workshop (July 3–7, 2017, 2017), at the Unified Analysis Workshop (July 10–12, 2017, Paris), at the EPN Analysis Centre Workshop (October, 25–26, 2017 Brussels).

Tropospheric zenith total delay and precipitable water vapour delivered in the framework of the NASA SESES– MEaSUREs project are in SINEX-TRO v2.00 format, (https://cddis.nasa.gov/Data_and_Derived_Products/GNSS/SESES_time_series_products.html).

References

Adams, D. K., Fernandes, R. M. S., & Maia, J. M. F. (2011). GNSS precipitable water vapour from an Amazonian rain forest flux tower. *Journal of Atmospheric and Oceanic Technology, 28*(10), 1192–1198. https://doi.org/10.1175/JTECH-D-11-00082.1.

Ahmed F., Teferle N., Bingley R., & Hunegnaw A. (2014). A comparative analysis of tropospheric delay estimates from network and precise point positioning processing strategies. Presented at IGS Workshop 2014, 23–27.06.2014, Pasadena, California, USA.

Alexandersson, H. (1986). A homogeneity test applied to precipitation data. *Journal of Climatology, 6*, 661–675.

Altamimi, Z., Rebisching, P., Metivier, L., & Collilieux, X. (2016). ITRF2014: A new release of the International Terrestrial Reference Frame modelling nonlinear station motions. *Journal of Geophysical Research – Solid Earth, 121*(8), 6109–6131. https://doi.org/10.1002/2016JB013098.

Antón, M., Loyola, D., Román, R., & Vömel, H. (2015). Validation of GOME-2/MetOp-A total water vapour column using reference radiosonde data from the GRUAN network. *Atmospheric Measurement Techniques*, *8*, 1135–1145. https://doi.org/10.5194/amt-8-1135-2015

Araszkiewicz, A., & Voelksen, C. (2017). The impact of the antenna phase centre models on the coordinates in the EUREF Permanent Network. *GPS Solutions, 21*, 747–757. https://doi.org/10.1007/s10291-016-0564-7.

Askne, J., & Nordius, H. (1987). Estimation of tropospheric delay for microwaves from surface weather data. *Radio Science, 22*(3), 379–386. https://doi.org/10.1029/RS022i003p00379.

Bałdysz Z, Nykiel G, Araszkiewicz A, Figurski M, Szafranek K (2016) Comparison of GPS tropospheric delays derived from two consecutive EPN reprocessing campaigns from the point of view of climate monitoring. *Atmospheric Measurement Techniques, 9*(9), 4861–4877. https://doi.org/https://doi.org/10.5194/amt-9-4861-2016 (licensed under CC BY 3.0, https://creativecommons.org/licenses/by/3.0/).

Balidakis, K., Nilsson, T., Zus, F., Glaser, S., Heinkelmann, R., Deng, Z., & Schuh, H. (2018). Estimating integrated water vapour trends from VLBI, GPS and numerical weather models: sensitivity to tropospheric parameterization. *Journal of Geophysical Research: Atmospheres, 123*, 6356–6372. https://doi.org/10.1029/2017JD028049.

Barnston, A. G., & Livezey, R. E. (1987). Classification, seasonality and persistence of low-frequency atmospheric circulation patterns. *Monthly Weather Review, 115*(6), 1083–1126. https://doi.org/https://doi.org/10.1175/1520-0493(1987)115<1083:CSAPOL>2.0.CO;2

Bar-Sever, Y. E., Kroger, P. M., & Borjesson, J.A. (1998). Estimating Horizontal Gradients of Tropospheric Path Delay with a Single GPS Receiver. *Journal of Geophysical Research, 103*, 5019–5035.

Basili, P., Bonafoni, S., Ferrara, R., Ciotti, P., Fionda, E., & Arnbrosini, R. (2001). Atmospheric water vapour retrieval by means of both a GPS network and a microwave radiometer during an experimental campaign in Cagliari, Italy. In *1999, Geoscience and Remote Sensing, IEEE Transactions on*, Vol. 39, No.11, pp. 2436–2443. https://doi.org/10.1109/36.964980

Beirle, S., Lampel, J., Wang, Y., Mies, K., Dörner, S., Grossi, M., Loyola, D., Dehn, A., Danielczok, A., Schröder, M., & Wagner, T. (2018). The ESA GOME-Evolution "Climate" water vapor product: a homogenized time series of H_2O columns from GOME, SCIAMACHY, and GOME-2. *Earth System Science Data, 10*, 449–468. https://doi.org/10.5194/essd-10-449-2018.

Bennouna, Y. S., Torres, B., Cachorro, V. E., Ortiz de Galisteo, J. P., & Toledano, C. (2013). The evaluation of the integrated water vapour annual cycle over the Iberian Peninsula from EOS-MODIS against different ground-based techniques. *Quarterly Journal of the Royal Meteorological Society, 139*, 1935–1956. https://doi.org/10.1002/qj.2080.

Berckmans, J., Giot, O., De Troch, R., Hamdi, R., Ceulemans, R., & Termonia, P. (2017). Reinitialised versus continuous regional climate simulations using ALARO-0 coupled to the land surface model SURFEXv5. *Geoscientific Model Development, 10*, 223–238.

Berg, H. (1948). *Allgemeine meteorologie*. Bonn: Dümmler's Verlag.

Bevis, M., Businger, S., Herring, T. A., Rocken, C., Anthes, R. A., & Ware, R. H. (1992). GPS meteorology: remote sensing of atmospheric water vapour using the global positioning system. *Journal of Geophysical Research, 97*(D14), 15787–15801.

Bevis, M., Businger, S., Chiswell, S., Herring, T. A., Anthes, R. A., Rocken, C., & Ware, R. H. (1994). GPS meteorology: Mapping Zenith wet delays onto precipitable water. *Journal of Applied Meterology, 33*(3), 379–386. https://doi.org/https://doi.org/10.1175/1520−0450(1994)033<0379:GMMZWD>2.0.CO;2

Bock, O. (2015, May) *ZTD assessment and screening*. COST ES1206 GNSS4SWEC Workshop, Thessaloniki, Greece, 11–13 May 2015.

Bock, O. (2016a). *A reference IWV dataset combining IGS repro1 and ERA-Interim reanalysis for the assessment of homogenization algorithms.* 3rd COST ES1206 Workshop, 8–11 March 2016, Reykjavik, Island.

Bock, O. (2016b). Post-processing of GNSS ZTD, COST ES1206 GNSS4SWEC Summer School, 29–31 August 2016, GFZ, Potsdam, Germany. Available at: ftp://ftp.gfz-potsdam.de/pub/GNSS/workshops/gnss4swec/Summer_School/D2/3_Bock_PostProc.pdf

Bock, O. (2016c). Conversion of GNSS ZTD to IWV, COST ES1206 GNSS4SWEC Summer School, 29–31 August 2016, GFZ, Potsdam, Germany. Available at: ftp.gfz-potsdam.de/pub/GNSS/workshops/gnss4swec/Summer_School/D3/2_Bock_Homogenization.pdf

Bock, O. (2016d). Screening and validation of new reprocessed GNSS IWV data in Arctic region, COST ES1206 GNSS4SWEC Workshop, Potsdam, Germany, 31 August–2 September 2016.

Bock O., & Pacione, R. (2014). *ZTD to IWV conversion, COST action ES1206 – GNSS4SWEC*. 2nd WG meeting, Varna, Bulgaria, 11–12 September, 2014.

Bock, O., Bouin, M.-N., Walpersdorf, A., Lafore, J. P., Janicot, S., Guichard, F., & Agusti-Panareda, A. (2007). Comparison of ground-based GPS precipitable water vapour to independent observations and NWP model reanalyses over Africa. *Quarterly Journal of the Royal Meteorological Society, 133*, 2011–2027. https://doi.org/10.1002/qj.185.

Bock, O., P. Willis, M. Lacarra, & P. Bosser (2010) An inter-comparison of zenith tropospheric delays derived from DORIS and GPS data, *Advances in Space Research, 46*(12), 1648–1660. https://doi.org/10.1016/j.asr.2010.05.018

Bock, O., Willis, P., Wang, J., & Mears, C. (2014). A high-quality, homogenized, global, long-term (1993-2008) DORIS precipitable water dataset for climate monitoring and model verification. *Journal of Gephysics Research Atmosphere, 119*(12), 7209–7230. https://doi.org/10.1002/2013JD021124.

Bock O., & Parracho, A. C. (2019) Consistency and representativeness of integrated water vapour from ground-based GPS observations and ERA-Interim reanalysis, Atmos. Chem. Phys. Discuss., https://doi.org/10.5194/acp-2019-28

Bodeker, G. E., Bojinski, S., Cimini, D., Dirksen, R. J., Haeffelin, M., Hannigan, J. W., Hurst, D. F., Leblanc, T., Madonna, F., Maturilli, M., Mikalsen, A. C., Philipona, R., Reale, T., Seidel, D. J., Tan, D. G. H., Thorne, P. W., Vömel, H., and Wang, J. (2016) Reference upper-air observations for climate: From concept to reality, *Amer Meteorological Society, 123–135*. https://doi.org/10.1175/BAMSD-14-00072.1

Boehm, J., & Schuh, H. (2007). Troposphere gradients from the ECMWF in VLBI analysis. *Journal of Geodesy, 81*, 403–408. https://doi.org/10.1007/s00190-0144-2.

Boehm, J., Niell, A., Tregoning, P., & Schuh, H. (2006a). Global Mapping Function (GMF): A new empirical mapping function based on numerical weather model data. *Geophysical Research Letters, 33*, L07304. https://doi.org/10.1029/2005GL025546.

Boehm, J., Werl, B., & Schuh, H. (2006b). Troposphere mapping functions for GPS and very long baseline interferometry from European Centre for Medium-Range Weather Forecasts operational analysis data. *Journal of Geophysical Research, 111*, B02406. https://doi.org/10.1029/2005JB003629.

Boehm, J., Heinkelmann, R., & Schuh, H. (2007). Short Note: A global model of pressure and temperature for geodetic applications. *Journal of Geodesy, 81*(10), 679–683. https://doi.org/10.1007/s00190-007-0135-3.

Böhm, J., Möller, G., Schindelegger, M., Pain, G., & Weber, R. (2015). Development of an improved empirical model for slant delays in the troposphere (GPT2w). *GPS Solutions, 3*, 433–441.

Bos, M. S., Fernandes, R. M. S., Williams, S. D. P., & Bastos, L. (2013). Fast Error Analysis of Continuous GNSS Observations with Missing Data. *Journal of Geodesy, 87*(4), 351–360. https://doi.org/10.1007/s00190-012-0605-0.

Bosser, P., & Bock, O. (2016). *Screening of GPS ZTD estimates*. 3rd COST ES1206 Workshop, 8–11.03.2016, Reykjavik, Island.

Brown, R. A. (1970). A secondary flow model for the planetary boundary layer. *Journal of the Atmospheric Sciences, 27*, 742–757.

Bruyninx, C. H., Habrich, W., Söhne, A., Kenyeres, G., & Stangl, V. C. (2012). *Enhancement of the EUREF Permanent Network Services and Products*. Geodesy for Planet Earth, IAG Symposia Series, Vol. 136, pp. 27–35. https://doi.org/10.1007/978-3-642-20338-1_4.

Buehler, S. A., Östman, S., Melsheimer, C., Holl, G., Eliasson, S., John, V. O., Blumenstock, T., Hase, F., Elgered, G., Raffalski, U., Nasuno, T., Satoh, M., Milz, M., & Mendrok, J. (2012). A multi-instrument comparison of integrated water vapour measurements at a high latitude site. *Atmospheric Chemistry and Physics, 12*, 10925–10943. https://doi.org/10.5194/acp-12-10925-2012.

Byram S., Hackman C., & Tracey J. (2011). Computation of a high-precision GPS-based troposphere product by the USNO. In *Proceedings of ION GNSS*.

Byun, S. H., & Bar-Sever, Y. E. (2009). A new type of troposphere zenith path delay product of the International GNSS Service. *Journal of Geodesy, 83*(3–4), 1–7.

Calori, A., Santos, J. R., Blanco, M., Pessano, H., Llamedo, P., Alexander, P., & de la Torre, A. (2016). Ground-based GNSS network and integrated water vapour mapping during the development of severe storms at the Cuyo region (Argentina). *Atmospheric Research, 176–177*, 267–275. https://doi.org/10.1016/j.atmosres.2016.03.002.

Campanelli, M., Mascitelli, A., Sanò, P., Diémoz, H., Estellés, V., Federico, S., Iannarelli, A. M., Fratarcangeli, F., Mazzoni, A., Realini, E., Crespi, M., Bock, O., Martìnez-Lozano, J. A., & Dietrich, S. (2017). Precipitable water vapour content from ESR/SKYNET Sun-sky radiometers: Validation against GNSS/GPS and AERONET over three different sites in Europe. *Atmospheric Measurement Techniques Discussions*, 1–27. https://doi.org/10.5194/amt-2017-221,. in review.

Caussinus, H., & Mestre, O. (2004). Detection and correction of artificial shifts in climate series. *Journal of the Royal Statistical Society, Series C, 53*, 405–425.

Chen, G., & Herring, T. A. (1997). Effects of atmospheric azimuthal asymmetry on the analysis of space geodetic data. *Journal of Geophysical Research, 102*, 20489–20502. https://doi.org/10.1029/97JB01739.

Dach, R., Böhm, J., Lutz, S., Steigenberger, P., & Beutler, G. (2010). Evaluation of the impact of atmospheric pressure loading modelling on GNSS data analysis. *Journal of Geodesy, 85*, 75–91. https://doi.org/10.1007/s00190-010-0417-z.

Dach, R., Lutz, S., Walser, P., & Fridez, P. (2015). *User manual of the Bernese GNSS Software, Version 5.2*. University of Bern, Bern Open Publishing. https://doi.org/10.7892/boris.72297.

Davis, J. L., Herring, T. A., Shapiro, I. I., Rogers, A. E., & Elgered, G. (1985). Geodesy by radio interferometry: Effects of atmospheric modelling errors on estimates of baseline length. *Radio Science, 20*, 1593–1607.

Deblonde, G., Macpherson, S., Mireault, Y., & Heroux, P. (2005). Evaluation of GPS precipitable water over Canada and the IGS network. *Journal of Applied Meteorology, 44*, 153–166. https://doi.org/10.1175/JAM-2201.1

Dee, D. P., Uppala, S. M., Simmons, A. J., Berrisford, P., Poli, P., Kobayashi, S., Andrae, U., Balmaseda, M. A., Balsamo, G., Bauer, P., & Bechtold, P. (2011). The ERA-Interim reanalysis: Configuration and performance of the data assimilation system. *Quarterly Journal of the Royal Meteorological Society, 137*(656), 553–597. https://doi.org/10.1002/qj.828.

Douša, J., & Győri, G. (2013). Database for tropospheric product evaluations – implementation aspects. *Geoinformatics, 10*, 39–52.

Douša, J., Byram, S., Győri, G., Böhm, O., Hackman, C., & Zus, F.. (2014). *Development towards inter-technique troposphere parameter comparisons and their exploitation.* 2014 IGS Workshop, Pasadena, CA.

Douša, J., Böhm, O., Byram, S., Hackman, C., Deng, Z., Zus, F., Dach, R., & Steigenberger, P. (2016). *Evaluation of GNSS reprocessing tropospheric products using GOP-TropDB*. Presentation at IGS Workshop 2016, Sydney, March 8–10.

Douša, J., Heikelmann, R., & Balidakis, K. (2017a). *Tropospheric ties for inter-technique comparisons and combinations, Presentation at IAG – IASPE, July 30 – August 4, 2017*. Japan: Kobe.

Douša, J., Václavovic, P., & Elias, M. (2017b). Tropospheric products of the second GOP European GNSS reprocessing (1996–2014). *Atmospheric Measurement Techniques, 10*, 3589–3607. https://doi.org/10.5194/amt-10-3589-2017 (licensed under CC BY 3.0, https://creativecommons.org/licenses/by/3.0/).

Duan, J., Bevis, M., Fang, P., Bock, Y., Chiswell, S., Businger, S., Rocken, C., Solheim, F., van Hove, T., Ware, R., McClusky, S., Herring, T. A., & King, R. W. (1996). GPS meteorology: Direct estimation of the absolute value of precipitable water. *Journal of Applied Meteorology, 35*(6), 830–838. https://doi.org/https://doi.org/10.1175/1520-0450(1996)035<0830:GMDEOT>2.0.CO;2.

Eliaš, M., Douša, J., & Jarušková, D. (2019). *An assessment of method for change-point detection applied in tropospheric parameter time series given from numerical weather model* (submitted to Acta Geodyn Geomater).

Forkman, P., Elgered, G., & Ning, T. (2017). Accuracy assessment of the two WVRs, Astrid and Konrad, at the Onsala Space Observatory. In *Proceedings of the 23rd European VLBI Group for Geodesy and Astrometry Working Meeting*, Chalmers University of Technology, Gothenburg, Sweden (pp. 65–69).

Foster, J., Bevis, M., & Raymond, W. (2006). Precipitable water and the lognormal distribution. *Journal of Geophysical Research, 111*, D15102. https://doi.org/10.1029/2005JD006731.

Gazeaux, J., et al. (2013). Detecting offsets in GPS time series: First results from the detection of offsets in GPS experiment. *Journal of Geophysical Research – Solid Earth, 118*, 2397–2407. https://doi.org/10.1002/jgrb.50152.

GCOS-112. (2007, April). *GCOS Reference Upper-Air Network (GRUAN): Justification, requirements, siting and instrumentation options*. April 2007. WMO Tech. Doc. No. 1379, WMO.

GCOS-171. (2013, March). *The GCOS Reference Upper-Air Network (GRUAN) GUIDE*. GCOS-171, Version 1.1.0.3, March 2013, WIGOS Technical Report No. 2013–03.

Gelaro, R., McCarty, W., Suárez, M. J., Todling, R., Molod, A., Takacs, L., Randles, C. A., Darmenov, A., Bosilovich, M. G., Reichle, R., & Wargan, K. (2017). The modern-era retrospective analysis for research and applications, version 2 (MERRA-2). *Journal of Climate, 30* (14), 5419–5454. https://doi.org/10.1175/JCLI-D-16-0758.1.

Gendt, G. (1997). *SINEX TRO – solution (Software/technique) independent exchange format for combination of TROpospheric estimates Version 0.01*, 1 March 1997. Available at: https://igscb.jpl.nasa.gov/igscb/data/format/sinex_tropo.txt. (Last access 29 April 2017).

Gobinddass, M. L., Willis, P., Sibthorpe, A., Zelensky, N. P., Lemoine, F. G., Ries, J. C., Ferland, R., Bar-Sever, Y. E., de Viron, O., & Diament, M. (2009). Improving DORIS geocenter time series using an empirical rescaling of solar radiation pressure models. *Advances in Space Research, 44*(11), 1279–1287. https://doi.org/10.1016/j.asr.2009.08.004.

Gobinddass, M. L., Willis, P., Menvielle, M., & Diament, M. (2010). Refining DORIS atmospheric drag estimation in preparation of ITRF2008. *Advances in Space Research, 46*(12), 1566–1577. https://doi.org/10.1016/j.asr.2010.04.004.

Gruber C., Auer I., & Böhm R. (2009). *Endberichte HOM-OP Austria Aufbau und Installierung eines Tools zur operationellen Homogenisierung von Klimadaten mit 3 Annexen*.

Guerova, G., Jones, J., Douša, J., Dick, G., de Haan, S., Pottiaux, E., Bock, O., Pacione, R., Elgered, G., Vedel, H., & Bender, M. (2016). Review of the state of the art and future prospects of the ground-based GNSS meteorology in Europe. *Atmospheric Measurement Techniques, 9*, 5385–5406. https://doi.org/10.5194/amt-9-5385-2016.

Győri, G., & Douša, J. (2016). GOP-TropDB developments for tropospheric product evaluation and monitoring – Design, functionality and initial results. *IAG Symposia Series, Springer, 143*, 595–602.

Haase, J., Ge, M., Vedel, H., & Calais, E. (2003). Accuracy and variability of GPS tropospheric delay measurements of water vapour in the Western Mediterranean. *Journal of Applied Meteorology, 42*(11), 1547–1568.

Hagemann, S., Bengtsson, L., & Gendt, G. (2003). On the determination of atmospheric water vapour from GPS measurements. *Journal of Geophysical Research, 108*(D21), 4678. https://doi.org/10.1029/2002JD003235.

Hamed, K. H., & Rao, A. R. (1998). A modified Mann-Kendall trend test for autocorrelated data. *Journal of Hydrology, 204*(1–4), 182–196. https://doi.org/10.1016/S0022-1694(97)00125-X.

Hasegawa, S., & Stokesberry, D. (1975). Automatic digital microwave hygrometer. *The Review of Scientific Instruments, 46*, 867–873. https://doi.org/10.1063/1.1134331.

Healy, S. B. (2011). Refractivity coefficients used in the assimilation of GPS radio occultation measurements. *Journal of Geophysical Research, 116*, D01106. https://doi.org/10.1029/2010JD014013.

Heinkelmann, R., Willis, P., Deng, Z., Dick, G., Nilsson, T., Soja, B., Zus, F., Wickert, J., & Schuh, H. (2016). The effect of the temporal resolution of atmospheric gradients on atmospheric parameters. *Advances in Space Research, 58*(12), 2758–2773. https://doi.org/10.1016/j.asr.2016.09.023.

Heise, S., Bender, M., Beyerle, G., Dick, G., Gendt, G., Schmidt, T., & Wickert, J. (2009). *Integrated water vapor from IGS ground-based GPS observations: Initial results from a global 5-minute data set*. (Geophysical Research Abstracts, Vol. 11, EGU2009-5330), General Assembly European Geosciences Union (Vienna, Austria 2009).

Hourdin, F., Musat, I., Bony, S., Braconnot, P., Codron, F., Dufresne, J. L., et al. (2006). The LMDZ4 general circulation model: Climate performance and sensitivity to parametrized physics with emphasis on tropical convection. *Climate Dynamics, 27*(7–8), 787–813.

Hourdin, F., Foujols, M. A., Codron, F., Guemas, V., Dufresne, J. L., Bony, S., et al. (2013a). Impact of the LMDZ atmospheric grid configuration on the climate and sensitivity of the IPSL-CM5A coupled model. *Climate Dynamics, 40*(9–10), 2167–2192.

Hourdin, F., Grandpeix, J. Y., Rio, C., Bony, S., Jam, A., Cheruy, F., et al. (2013b). LMDZ5B: The atmospheric component of the IPSL climate model with revisited parameterizations for clouds and convection. *Climate Dynamics, 40*(9–10), 2193–2222.

ICAO. (1993). *Manual of the ICAO standard atmosphere, Doc 7488/3* (3rd ed.). International Civil Aviation Organisation, Montreal.

IGSMAIL-6298, Reprocessed IGS Trop Product now available with Gradients. (2012, November 11). http://igscb.jpl.nasa.gov/pipermail/igsmail/2010/007488.html

Ingleby, N. B. (1995). Assimilation of station level pressure and errors in station height. Weather and Forecasting 10: 172-182.

Jaruskova, D. (1997). Some problems with application of change-point detection methods to environmental data. *Environmetrics, 8*(5), 469–483.

Järvinen, J. and Undén, P. (1997) Observation screening and background quality control in the ECMWF 3D Var data assimilation system. Technical memorandum of the European Centre for Medium-Range Weather Forecasts, 1997, Vol. 236.

Jeong, J.-H., Walther, A., Nikulin, G., Chen, D., & Jones, C. (2011). Diurnal cycle of precipitation amount and frequency in Sweden: Observation versus model simulation. *Tellus A, 63*, 664–674. https://doi.org/10.1111/j.1600-0870.2011.00517.x.

Jiang, J. H., Su, H., Zhai, C., Perun, V. S., Del Genio, A., Nazarenko, L. S., et al. (2012). Evaluation of cloud and water vapour simulations in CMIP5 climate models using NASA "A-Train" satellite observations. *Journal of Geophysical Research: Atmospheres, 117*(D14).

Joshi, S., Kumar, K., Pande, B., & Pant, M. C. (2013). GPS-derived precipitable water vapour and its comparison with MODIS data for Almora, Central Himalaya, India. *Meteorology and Atmospheric Physics, 120*, 177–187. https://doi.org/10.1007/s00703-013-0242-z.

Kalakoski, N., Kujanpää, J., Sofieva, V., Tamminen, J., Grossi, M., & Valks, P. (2016). Validation of GOME-2/Metop total column water vapour with ground-based and in situ measurements. *Atmospheric Measurement Techniques, 9*, 1533–1544. https://doi.org/10.5194/amt-9-1533-2016.

Kestin, J., Sengers, J. V., Kamgar-Parsi, B., & Sengers, J. L. (1984). Thermophysical properties of fluid H2O. *Journal of Physical and Chemical Reference Data, 13*(1), 175–183.

King, R. W., & Bock, Y. (2005). *Documentation for the GAMIT GPS processing software release 10.2*. Massachusetts Institute of Technology, Cambridge.

King, R., Herring, T., & Mccluscy, S. (2010). *Documentation for the GAMIT GPS analysis software 10.4*. Technical Report. Massachusetts Institute of Technology, Cambridge, MA, USA.

Klos, A., Bogusz, J., Figurski, M., & Kosek, W.. (2015) On the handling of outliers in the GNSS time series by means of the noise and probability analysis. In C. Rizos, & P. Willis (Eds.), *IAG 150 Years*. International Association of Geodesy Symposia (Vol. 143). Cham: Springer.

Kouba J (2003) *A guide to using International GPS Service (IGS) products*. Pasadena: IGS Central Bureau (available at http://igscb.jpl.nasa.gov/igscb/resource/pubs/GuidetoUsingIGSProducts.pdf)

Kwon, H-. T., Iwabuchi, T., & Lim, G. –H. (2007). Comparison of precipitable water derived from ground-based GPS measurements with radiosonde observations over the Korean Peninsula. *Journal of the Meteorological Society of Japan Series II*, *85*(6), 733–746.

Lagler, K., Schindelegger, M., Böhm, J., Krásná, H., & Nilsson, T. (2013). GPT2: Empirical slant delay model for radio space geodetic techniques. *Geophysical Research Letters, 40*, 1069–1073. https://doi.org/10.1002/grl.50288.

Lanzante, J. (1996). Resistant, robust and non-parametric techniques for the analysis of climate data: Theory and examples, including applications to historical radiosonde station data. *International Journal of Climatology, 16*, 1197–1226.

Leduc, D. J. (1987). A comparative analysis of the reduced major axis technique of fitting lines to bivariate data. *Canadian Journal of Forest Research, 17*, 654–659.

Li, X., Zus, F., Lu, C., Ning, T., Dick, G., Ge, M., Wickert, J., & Schuh, H. (2015). Retrieving high-resolution tropospheric gradients from multiconstellation GNSS observations. *Geophysical Research Letters, 42*(10), 4173–4181.

Liu, H., Shah, S., & Jiang, W. (2004). On-line outlier detection and data cleaning. *Computers and Chemical Engineering, 28*(9), 1635–1647. https://doi.org/10.1016/j.compchemeng.2004.01.009.

Martínez, M. A., & Calbet, X. (2016). *Algorithm theoretical basis document for the clear air products processor of the NWC/GEO*. [online] Available from: http://www.nwcsaf.org/AemetWebContents/ScientificDocumentation/Documentation/GEO/v2016/NWC-CDOP2-GEO-AEMET-SCI-ATBD-ClearAir_v1.1.pdf

Meindl, M., Schaer, S., Hugentobler, U., & Beutler, G. (2004). Tropospheric gradient estimation at CODE: Results from global solutions. *Journal of the Meteorological Society of Japan, 82*, 331–338.

Mestre, O., Gruber, C., Prieur, C., Caussinus, H., & Jourdain, S. (2011). SPLIDHOM: A method for homogenization of daily temperature observations. *Journal of Applied Meteorology and Climatology, 50*, 2343–2358.

Mieruch, S., Schröder, M., Noël, S., & Schulz, J. (2014). Comparison of decadal global water vapour changes derived from independent satellite time series. *Journal of Geophysical Research – Atmospheres, 119*(22), 12489–12499. https://doi.org/10.1002/2014JD021588.

Miller, M. A., & Slingo, A. (2007). The arm mobile facility and its first international deployment: Measuring radiative flux divergence in West Africa. *Bulletin of the American Meteorological Society, 88*, 1229–1244. https://doi.org/10.1175/BAMS-88-8-1229.

Mircheva, B., Tsekov, M., Meyer, U., & Guerova, G. (2017). Anomalies of hydrological cycle components during the 2007 heat wave in Bulgaria. *Journal of Atmospheric and Solar-Terrestrial Physics, 165-166*, 1–9. https://doi.org/10.1016/j.jastp.2017.10.005.

Morel, L., Pottiaux, E., Durand, F., Fund, F., Follin, J. M., Durand, S., Bonifac, K., Oliveira, P. S., van Baelen, J., Montibert, C., Cavallo, T., Escaffit, R., & Fragnol, L. (2015). *Global validity and*

behaviour of tropospheric gradients estimated by GPS. Presentation at the 2nd GNSS4SWEC Workshop held in Thessaloniki, Greece, May 11–14.

Morland, J., Liniger, M. A., Kunz, H., Balin, I., Nyeki, S., Mätzler, C., & Kämpfer, N. (2006). Comparison of GPS and ERA40 IWV in the Alpine region, including correction of GPS observations at Jungfraujoch (3584 m). *Journal of Geophysical Research, 111*, D04102. https://doi.org/10.1029/2005JD006043.

Munn, R. E. (1966). *Descriptive micrometeorology*. New York: Academic Press.

Nahmani, S., & Bock, O. (2014). *Sensitivity of GPS measurements and estimates during extreme meteorological events: The issue of stochastic constraints used for ZWD estimation in West Africa*. Joint ES1206 MC and MC meeting, Golden Sands Resort, 11/09/2014 to 12/09/2014, Varna, Bulgaria.

Nahmani, S., Rebischung, P., & Bock, O. (2016). *Statistical modelling of ZWD in GNSS processing*. 3rd ES1206 Workshop, Rugbrauðsgerdin, 08-03-2016 to 10-03-2016, Reykjavik, Iceland.

Nahmani, S., Rebischung, P., & Bock, O. (2017). *Bayesian approach to apply optimal constraints on tropospheric parameters in GNSS data processing: Implications for meteorology*. ES1206 Final Workshop, ESTEC, 2017-02-21 to 2017-02-23. Noordwijk, Netherlands.

Niell, A. E. (1996) Global mapping functions for the atmospheric delay at radio wavelengths, Journal of Geophysical Research, 101(B2), doi: https://doi.org/10.1029/95JB03048, 1996, pp 3227–3246.

Niell, A. E. (2000). Improved atmospheric mapping functions for VLBI and GPS. *Earth Planet Sp, 52*, 699–702. https://doi.org/10.1186/BF03352267.

Nilsson, T., Soja, B., Karbon, M., Heinkelmann, R., & Schuh, H. (2015). Application of Kalman filtering in VLBI data analysis. *Earth, Planets and Space, 67*(136), 1–9. https://doi.org/10.1186/s40623-015-0307-y.

Ning, T., & Elgered, G. (2012). Trends in the atmospheric water vapour content from ground-based GPS: the impact of the elevation cutoff angle. *IEEE J-STARS, 5*(3), 744–751. https://doi.org/10.1109/JSTARS.2012.2191392.

Ning, T., Elgered, G., & Johansson, J. (2011). The impact of microwave absorber and radome geometries on GNSS measurements of station coordinates and atmospheric water vapour. *Advances in Space Research, 47*, 186–196.

Ning, T., Haas, R., Elgered, G., & Willén, U. (2012). Multi-technique comparisons of 10 years of wet delay estimates on the west coast of Sweden. *Journal of Geodesy, 86*, 565–575. https://doi.org/10.1007/s00190-011-0527-2.

Ning, T., Elgered, G., Willén, U., & Johansson, J. M. (2013). Evaluation of the atmospheric water vapour content in a regional climate model using ground-based GPS measurements. *Journal of Geophysical Research, 118*, 1–11. https://doi.org/10.1029/2012JD018053.

Ning, T., Wang, J., Elgered, G., Dick, G., Wickert, J., Bradke, M., Sommer, M., Querel, R., and Smale, D. (2016a) The uncertainty of the atmospheric integrated water vapour estimated from GNSS observations, Atmospheric Measurement Techniques, 9, 79–92, doi:https://doi.org/10.5194/amt-9-79-2016 (licensed under CC BY 3.0, https://creativecommons.org/licenses/by/3.0/).

Ning, T., Wickert, J., Deng, Z., Heise, S., Dick, G., Vey, S., & Schöne, T. (2016b). Homogenized Time Series of the Atmospheric Water Vapour Content Obtained from the GNSS Reprocessed Data. *Journal of Climate, 29*, 2443–2456. https://doi.org/10.1175/JCLI-D-15-0158.1.

Ning, T., Elgered, G., & Heise, S. (2017). Trends in the atmospheric water vapour estimated from two decades of ground-based GPS data: Sensitivity to the elevation cutoff angle. In *Proceedings of 6th international colloquium scientific and fundamental aspects of the Galileo programme*, Valencia, Spain, 25–27 October 2017.

Ningombam, S. S., Jade, S., Shrungeshwara, T. S., & Song, H.-J. (2016). Validation of water vapour retrieval from Moderate Resolution Imaging Spectro-radiometer (MODIS) in near infrared channels using GPS data over IAO-Hanle, in the trans-Himalayan region. *Journal of Atmospheric and Solar-Terrestrial Physics, 137*, 76–85,. ISSN 1364-6826. https://doi.org/10.1016/j.jastp.2015.11.019.

Nyeki, S., Vuilleumier, L., Morland, J., Bokoye, A., Viatte, P., Mätzler, C., & Kämpfer, N. (2005). A 10-year integrated atmospheric water vapour record using precision filter radiometers at two high-alpine sites. *Geophysical Research Letters, 32*, L23803. https://doi.org/10.1029/2005GL024079.

Ohtani, R., & Naito, I. (2000). Comparisons of GPS-derived precipitable water vapors with radiosonde observations in Japan. *Journal of Geophysical Research, 105*(D22), 26917–26929. https://doi.org/10.1029/2000JD900362.

Owens, J. C. (1967). Optical Refractive Index of Air: Dependence on Pressure, Temperature and Composition. *Applied Optics, 6*(1), 51–59.

Pacione R., & Douša J. (2017). SINEX-TRO V2.00 format description, COST Action 1206 Final Report, J. Jones et al eds.

Pacione, R., Pace, B., de Haan, S., Vedel, H., Lanotte, R., & Vespe, F. (2011). Combination methods of tropospheric time series. *Advances in Space Research, 47*, 323–335. https://doi.org/10.1016/j.asr.2010.07.021.

Pacione, R., Pace, B., & Bianco, G.. (2014a). Homogeneously reprocessed ZTD long-term time series over Europe, EGU GA 2014. http://meetingorganizer.copernicus.org/EGU2014/EGU2014-2945.pdf

Pacione, R., O. Bock, & Douša, J. (2014b). *GNSS atmospheric water vapor retrieval methods.* COST Action ES1206 – GNSS4SWEC, 1st Workshop, Munich, 26–28 February 2014.

Pacione, R., Araszkiewicz, A., Brockmann E., & Douša J. (2017). EPN-Repro2: a reference tropospheric data set over Europe, *Atmospheric Measurement Techniques, 10*, 1689–1705, https://doi.org/10.5194/amt-10-1689-2017 (licensed under CC BY 3.0, https://creativecommons.org/licenses/by/3.0/)..

Parracho, A. (2017). *Study of trends and variability of atmospheric integrated water vapour with climate models and observations from global GNSS network.* PhD report from Université Pierre et Marie Curie, Paris, France.

Parracho, A. C., Bock, O., & Bastin, S. (2018). Global IWV trends and variability in atmospheric reanalyses and GPS observations, *Atmospheric Chemistry and Physics Discussions*. https://doi.org/10.5194/acp-2018-137, in review (licensed under CC BY 4.0, https://creativecommons.org/licenses/by/4.0/).

Pérez-Ramírez, D., Whiteman, D. N., Smirnov, A., Lyamani, H., Holben, B. N., Pinker, R., Andrade, M., & Alados-Arboledas, L. (2014). Evaluation of AERONET precipitable water vapour versus microwave radiometry, GPS, and radiosondes at ARM sites. *Journal of Geophysical Research – Atmospheres, 119*, 9596–9613. https://doi.org/10.1002/2014JD021730.

Petit, G., & Luzum, B. (2010). IERS Conventions, 2010. *IERS Technical Note No. 36*. Frankfurt am Main: Verlag des Bundesamts für Kartographie und Geodäsie, ISBN 3-89888-989-6.

Pettitt, A. N. (1979). A nonparametric approach to the change-point problem. *Applied Statistics, 28*, 126–135. https://doi.org/10.2307/2346729.

Pierce, D. W., Barnett, T. P., AchutaRao, K. M., Gleckler, P. J., Gregory, J. M., & Washington, W. M. (2006). Anthropogenic warming of the oceans: Observations and model results. *Journal of Climate, 19*(10), 1873–1900.

Prasad, A. K., & Singh, R. P. (2009). Validation of MODIS Terra, AIRS, NCEP/DOE AMIP-II Reanalysis-2, and AERONET Sun photometer derived integrated precipitable water vapour using ground-based GPS receivers over India. *Journal of Geophysical Research, 114*, D05107. https://doi.org/10.1029/2008JD011230.

Román, R., Antón, M., Cachorro, V. E., Loyola, D., Ortiz de Galisteo, J. P., de Frutos, A., & Romero-Campos, P. M. (2015). Comparison of total water vapour column from GOME-2 on MetOp-A against ground-based GPS measurements at the Iberian Peninsula. *Science of the Total Environment, 533*, 317–328,. ISSN 0048-9697. https://doi.org/10.1016/j.scitotenv.2015.06.124.

Rüeger, J. (2002) *Refractive index formulae for electronic distance measurements with radio and millimetre waves*. Unisurv Rep. 109, pp. 758–766, Univerity of New South Wales, Sydney, Australia.

Saastamoinen, J. (1972). Atmospheric correction for the troposphere and stratosphere in radio ranging of satellites. The use of artificial satellites for geodesy, American Geophysics Union. *Geophysics Monograph Series, 15*, 274–251.

Schmid, R., Dach, R., Collilieux, X., Jäggi, A., Schmitz, M., & Dilssner, F. (2016). Absolute IGS antenna phase center model igs08.atx: status and potential improvements. *Journal of Geodesy, 90*, 343–364. https://doi.org/10.1007/s00190-015-0876-3.

Schneider, M., Romero, P. M., Hase, F., Blumenstock, T., Cuevas, E., & Ramos, R. (2010). Continuous quality assessment of atmospheric water vapour measurement techniques: FTIR, Cimel, MFRSR, GPS, and Vaisala RS92. *Atmospheric Measurement Techniques, 3*, 323–338. https://doi.org/10.5194/amt-3-323-2010.

Schröder, M., Lockhoff, M., Forsythe, J. M., Cronk, H. Q., Vonder Haar, T. H., & Bennartz, R. (2016). The GEWEX water vapour assessment: Results from intercomparison, trend, and homogeneity analysis of total column water vapour. *Journal of Applied Meteorology and Climatology, 55*, 1633–1649. https://doi.org/10.1175/JAMC-D-15-0304.1.

Selle, C. & Desai, S. (2016). *Optimization of tropospheric delay estimation parameters by comparison of GPS-based precipitable water vapour estimates with microwave radiometer measurements.* IGS Workshop 2016, 8–12 February 2016, Sydney, NSW, Australia.

Sen, P. K. (1968). Estimates of the regression coefficient based on Kendall's tau. *Journal of the American Statistical Association, 63*(324), 1379–1389,. JSTOR 2285891, MR 0258201. https://doi.org/10.2307/2285891.

Smith, E., & Weintraub, S. (1953). The constants in the equation for atmospheric refractive index at radio frequencies. *Proceedings of the IRE, 41*, 1035–1037.

Soden, B. J., Jackson, D. L., Ramaswamy, V., Schwarzkopf, M. D., & Huang, X. (2005). The radiative signature of upper tropospheric moistening. *Science, 310*(5749), 841–844.

Sohn, D.-H., Park, K.-D., Won, J., Cho, J., & Roh, K.-M. (2012). Comparison of the characteristics of precipitable water vapour measured by Global Positioning System and microwave radiometer. *Journal of Astronomy Space Science, 29*, 1–10. https://doi.org/10.5140/JASS.2012.29.1.001.

Steigenberger, P., Boehm, J., & Tesmer, V. (2009). Comparison of GMF/GPT with VMF1/ECMWF and Implications for Atmospheric Loading. *Journal of Geodesy, 83*, 943–951. https://doi.org/10.1007/s00190-009-0311-8.

Steigenberger, P., Lutz, S., Dach, R., Schaer, S., & Jäggi, A. (2014). CODE repro2 product series for the IGS. Published by Astronomical Institute, University of Bern. URL: http://www.aiub.unibe.ch/download/REPRO_2013; https://doi.org/10.7892/boris.75680.

Stepniak, K., Bock, O., & Wielgosz, P. (2015). *Assessment of ZTD screening methods and analysis of water vapour variability over Poland*. 2nd COST GNSS4SWEC Workshop, Thessaloniki, Greece, 11–14 May 2015.

Stepniak, K., Bock, O., & Wielgosz, P. (2016). *Improved methods for reprocessing of GNSS data for climate monitoring over Poland.* Presented at 3rd ES1206 Workshop, 8–11.03.2016, Reykjavik, Iceland.

Stepniak, K., Bock, O., & Wielgosz, P. (2017). Reduction of ZTD outliers through improved GNSS data processing and screening strategies. Atmospheric Measurement Techniques Discussions. https://doi.org/10.5194/amt-2017-371, 2017 (licensed under CC BY 4.0, https://creativecommons.org/licenses/by/4.0/).

Thayer, G. (1974). An improved equation for the refractive index of air. *Radio Science, 9*(10), 803–807. https://doi.org/10.1029/RS009i010p00803.

Theil, H. (1950). A rank-invariant method of linear and polynomial regression analysis, I, II, III, Nederl. *Akad Wetensch Proceedings, 53*, 386–392, 521–525, 1397–1412, MR 0036489. https://doi.org/10.1007/978-94-011-2546-8_20.

Thorne, P. W., & Vose, R. S. (2010). Reanalyses suitable for characterizing long-term trends: Are they really achievable? *Bulletin of the American Meteorological Society, 91*(3), 353–361.

Torres, B., Cachorro, V. E., Toledano, C., Ortiz de Galisteo, J. P., Berjón, A., de Frutos, A. M., Bennouna, Y., & Laulainen, N. (2010). Precipitable water vapour characterization in the Gulf of

Cadiz region (southwestern Spain) based on Sun photometer, GPS, and radiosonde data. *Journal of Geophysical Research, 115*, D18103. https://doi.org/10.1029/2009JD012724.

Tregoning, P., & Watson, C. (2009). Atmospheric effects and spurius signals in GPS analyses. *Journal of Geophysical Research, 114*. https://doi.org/10.1029/2009JB006344.

Trenberth, K. E., Fasullo, J., & Smith, L. (2005). Trends and variability in column-integrated atmospheric water vapour. *Climate Dynamics, 24*(7–8), 741–758. https://doi.org/10.1007/s00382-005-0017-4.

Urban, J. (2013). Satellite sensors measuring atmospheric water vapour. In *Monitoring Atmospheric Water Vapour*, ISSI Scientific Report Series, 10, Kämpfer, N. https://doi.org/10.1007/978-1-4614-3909-7_9.

Václavovic, P., & Douša, J. (2016) G-Nut/Anubis – Open-source tool for multi-GNSS data monitoring. In Ch. Rizos, & P. Willis (Eds.), *IAG 150 Years. IAG Symposia Series* (Vol. 143, pp. 775–782). Springer.

Van Malderen, R., Brenot, H., Pottiaux, E., Beirle, S., Hermans, C., De Mazière, M., Wagner, T., De Backer, H., & Bruyninx, C. (2014). A multi-site intercomparison of integrated water vapour observations for climate change analysis. *Atmospheric Measurement Techniques, 7*, 2487–2512. https://doi.org/10.5194/amt-7-2487-2014.

Vaquero-Martínez, J., Antón, M., Pablo Ortiz de Galisteo, J., Cachorro, V. E., Costa, M. J., Román, R., & Bennouna, Y. S. (2017a). Validation of MODIS integrated water vapour product against reference GPS data at the Iberian Peninsula. *International Journal of Applied Earth Observation and Geoinformation, 63*, 214–221,. ISSN 0303-2434. https://doi.org/10.1016/j.jag.2017.07.008.

Vaquero-Martínez, J., Antón, M., Pablo Ortiz de Galisteo, J., Cachorro, V. E., Wang, H., Abad, G. G., Román, R., & Costa, M. J. (2017b). Validation of integrated water vapour from OMI satellite instrument against reference GPS data at the Iberian Peninsula. *Science of the Total Environment, 580*, 857–864,. ISSN 0048-9697. https://doi.org/10.1016/j.scitotenv.2016.12.032.

Vaquero-Martínez, J., Antón, M., de Galisteo, J. P. O., Victoria E. Cachorro, Álvarez-Zapatero, P., Román, R., Loyola, D., Costa, M. J., Wang, H., Abad, G. G., & Noël, S. (2017c) Intercomparison of integrated water vapour from satellite instruments using reference GPS data at the Iberian Peninsula. *In Remote Sensing of Environment*. ISSN 0034-4257. https://doi.org/10.1016/j.rse.2017.09.028

Vázquez B, G. E., & Grejner-Brzezinska, D. A. (2013). GPS-PWV estimation and validation with radiosonde data and numerical weather prediction model in Antarctica. *GPS Solutions, 17*, 29–39. https://doi.org/10.1007/s10291-012-0258-8.

Venema, V. K. C., Mestre, O., Aguilar, E., Auer, I., Guijarro, J. A., Domonkos, P., Vertacnik, G., Szentimrey, T., Stepanek, P., Zahradnicek, P., Viarre, J., Müller-Westermeier, G., Lakatos, M., Williams, C. N., Menne, M. J., Lindau, R., Rasol, D., Rustemeier, E., Kolokythas, K., Marinova, T., Andresen, L., Acquaotta, F., Fratianni, S., Cheval, S., Klancar, M., Brunetti, M., Gruber, C., Prohom Duran, M., Likso, T., Esteban, P., & Brandsma, T. (2012). Benchmarking homogenization algorithms for monthly data. *Climate of the Past, 8*, 89–115. https://doi.org/10.5194/cp-8-89-2012.

Vey, S., Dietrich, R., Fritsche, M., Rülke, A., Rothacher, M., & Steigenberger, P. (2006). Influence of mapping functions parameters on global GPS network analyses: Comparison between NMF and IMF. *Geophysical Research Letters, 33*, L01814. https://doi.org/10.1029/2005GL024361.

Vey, S., Dietrich, R., Fritsche, M., Rülke, A., Steigenberger, P., & Rothacher, M. (2009). On the homogeneity and interpretation of precipitable water time series derived from global GPS observations. *Journal of Geophysical Research, 114*, D10101. https://doi.org/10.1029/2008JD010415.

Vey, S., Dietrich, R., Rülke, A., Fritsche, M., Steigenberger, P., & Rothacher, M. (2010). Validation of precipitable water vapour within the NCEP/DOE reanalysis using global GPS observations from one decade. *Journal of Climate, 23*, 1675–1695. https://doi.org/10.1175/2009JCLI2787.1.

Vincent, L. A., Zhang, X., Bonsal, B. R., & Hogg, W. D. (2002). Homogenization of daily temperatures over Canada. *Journal of Climate, 15*, 1322–1334. https://doi.org/10.1175/1520-0442(2002)015<1322:HODTOC>2.0.CO;2.

Voelksen, C. (2011). *An update on the EPN reprocessing project: Current achievements and status*. Presented at EUREF 2011 symposium, 25–28 May 2011, Chisinau, Republic of Moldova. Available at: http://www.epncb.oma.be/_documentation/papers/eurefsymposium2011/an_update_on_epn_reprocessing_project_current_

Von Neumann, J. (1941). Distribution of the ratio of the mean square successive difference to the variance. *Annals of Mathematical Statistics, 13*, 367–395.

Wang, J., Zhang, L., & Dai, A. (2005). Global estimates of water-vapour-weighted mean temperature of the atmosphere for GPS applications. *Journal of Geophysical Research: Atmosphers, 110*(D21).

Wang, J., Zhang, L., Dai, A., Van Hove, T., & Van Baelen, J. (2007a). A near-global, 2-hourly data set of atmospheric precipitable water from ground-based GPS measurements. *Journal of Geophysical Research, 112*, D11107. https://doi.org/10.1029/2006JD007529.

Wang, X. L., Wen, Q. H., & Wu, Y. (2007b). Penalized maximal t test for detecting undocumented mean change in climate data series. *Journal of Applied Meteorology and Climatology, 46*, 916–931. https://doi.org/10.1175/JAM2504.1.

Wang, J., Zhang, L., Dai, A., Van Hove, T., & Van Baelen, J. (2007c). A near-global, 2-hourly data set of atmospheric precipitable water from ground-based GPS measurements. *Journal of Geophysical Research, 112*, D11107. https://doi.org/10.1029/2006JD007529.

Wang, H., Gonzalez Abad, G., Liu, X., & Chance, K. (2016a). Validation and update of OMI total column water vapour product. *Atmospheric Chemistry and Physics, 16*, 11379–11393. https://doi.org/10.5194/acp-16-11379-2016.

Wang, X., Zhang, K., Wu, S., Fan, S., & Cheng, Y. (2016b). Water vapour-weighted mean temperature and its impact on the determination of precipitable water vapour and its linear trend. *Journal of Geophysical Research – Atmospheres, 121*, 833–852. https://doi.org/10.1002/2015JD024181.

Wang, X., Zhang, K., Wu, S., He, C., Cheng, Y., & Li, X. (2017). Determination of zenith hydrostatic delay and its impact on GNSS-derived integrated water vapour. *Atmospheric Measurement Techniques, 10*, 2807–2820. https://doi.org/10.5194/amt-10-2807-2017.

Webb, F. H. and Zumberge, J. F. (1997) *An introduction to GIPSY/OASIS II, Jet Propulsion Laboratory Document JPL D-11088*. California Institute of Technology.

Wijngaard, J. B., Klein Tank, A. M. G., & Können, G. P. (2003). Homogeneity of 20th century European daily temperature and precipitation series. *International Journal of Climatology, 23*, 679–692. https://doi.org/10.1002/joc.906.

Willis, P., Gobinddass, M.-L., Garayt, B., & Fagard, H. (2012). Recent improvements in DORIS data processing in view of ITRF2008, the ignwd08 solution. *IAG Symposium, 136*, 43–49. https://doi.org/10.1007/978-3-642-20338-1_6.

Willis, P., Bock, O., & Bar-Sever, Y. E. (2014). DORIS tropospheric estimation at IGN: current strategies, GPS intercomparisons and perspectives. *IAG Symposium, 139*, 11–18. https://doi.org/10.1007/978-3-642-37222-3_2.

Willis, P., Heflin, M. B., Haines, B. J., Bar-Sever, Y. E., Bertiger, W. B., & Mandea, M. (2016a). Is the Jason2 DORIS oscillator still affected by the South Atlantic Anomaly? *Advances in Space Research, 58*(12), 2617–2627. https://doi.org/10.1016/j.asr.2016.09.015.

Willis, P., Zelensky, N. P., Ries, J. C., Soudarin, L., Cerri, L., Moreaux, G., Lemoine, F. G., Otten, M., Argus, D. F., & Heflin, M. B. (2016b). DPOD2008, A DORIS-oriented terrestrial reference frame for precise orbit determination. *IAG Symposium, 143*, 175–181. https://doi.org/10.1007/1345_2015_125.

Wolter, K., & Timlin, M. S. (1993) Monitoring ENSO in COADS with a seasonally adjusted principal component index. In *Proceedings of the 17th climate diagnostics workshop* (Vol. 5257).

Wolter, K., & Timlin, M. S. (1998). Measuring the strength of ENSO events: How does 1997/98 rank? *Weather, 53*(9), 315–324. https://doi.org/10.1002/j.1477-8696.1998.tb06408.x.

Yao, Y.-C., & Davis, R. A. (1986). The asymptotic behaviour of the likelihood ratio statistic for testing a shift in mean in a sequence of independent normal variates. *Sankhya, 48*, 339–353.

Zumberge, J. F., Heflin, M. B., Jefferson, D. C., & Watkins, M. M. (1997). Precise point positioning for the efficient and robust analysis of GPS data from large networks. *Journal of Geophysical Research – Solid Earth, 102*, 5005–5017.

Zus, F., Dick, G., Douša, J., Heise, S., & Wickert, J. (2014). The rapid and precise computation of GPS slant total delays and mapping factors utilizing a numerical weather model. *Radio Science, 49*, 207–216. https://doi.org/10.1002/2013RS005280.

Chapter 6
National Status Reports

Guergana Guerova, G. Möller, E. Pottiaux, H. Brenot, R. Van Malderen, H. Haralambous, F. Tymvios, J. Douša, M. Kačmařík, K. Eben, H. Vedel, K. Rannat, R. Kivi, A.-M. Harri, O. Bock, J. F. Mahfouf, J. Wickert, G. Dick, R. Potthast, S. Crewell, C. Pikridas, N. Zinas, A. Ganas, R. Szabolcs, M. Mile, S. Thorsteinsson, B. G. Ófeigsson, Y. Reuveni, S. Krichak, R. Pacione, G. Bianco, R. Biondi, G. Stankunavicius, F. N. Teferle, J. Bosy, J. Kaplon, K. Szafranek, R. Fernandes, P. Viterbo, A. Sá, J. Hefty, M. H. Igondova, E. Priego, G. Elgered, M. Lindskog, M. Ridal, U. Willén, T. Ning, E. Brockmann, K. Wilgan, A. Geiger, C. Mekik, J. Jones, Z. Liu, B. Chen, C. Wang, S. Masoumi, M. Moore, and S. MacPherson

G. Guerova (✉)
Physics Faculty, Department of Meteorology and Geophysics, Sofia University "St. Kliment Ohridski", Sofia, Bulgaria
e-mail: guerova@phys.uni-sofia.bg

G. Möller
Department of Geodesy and Geoinformation, TU Wien, Wien, Austria
e-mail: gregor.moeller@geo.tuwien.ac.at

E. Pottiaux
Royal Observatory of Belgium, Brussels, Belgium
e-mail: eric.pottiaux@oma.be

H. Brenot
Royal Belgian Institute for Space Aeronomy, Uccle, Belgium
e-mail: hugues.brenot@oma.be

R. Van Malderen
Royal Meteorological Institute of Belgium, Brussels, Belgium
e-mail: roeland@meteo.be

H. Haralambous
Frederick University, Limassol, Cyprus
e-mail: eng.hh@frederick.ac.cy

F. Tymvios
Cyprus Department of Meteorology, Nicosia, Cyprus
e-mail: f.tymvios@cyi.ac.cy

J. Douša
Geodetic Observatory Pecný, RIGTC, Ondřejov, Czech Republic
e-mail: jan.dousa@pecny.cz

J. Jones et al. (eds.), *Advanced GNSS Tropospheric Products for Monitoring Severe Weather Events and Climate*, https://doi.org/10.1007/978-3-030-13901-8_6

M. Kačmařík
Institute of Geoinformatics, VŠB Technical University of Ostrava, Ostrava, Czech Republic
e-mail: michal.kacmarik@vsb.cz

K. Eben
Czech Institute of Computer Science, Academy of Sciences, Praha, Czech Republic
e-mail: eben@cs.cas.cz

H. Vedel
Danish Meteorological Institute, Copenhagen, Denmark
e-mail: hev@dmi.dk

K. Rannat
Tallinn University, Tallinn, Estonia
e-mail: kalev.rannat@ttu.ee

R. Kivi · A.-M. Harri
Finnish Meteorological Institute, Helsinki, Finland
e-mail: Rigel.Kivi@fmi.fi; ari-matti.harri@fmi.fi

O. Bock
IGN Institut national de l'information géographique et forestière, Paris, France
e-mail: olivier.bock@ign.fr

J. F. Mahfouf
Météo-France, Paris, France
e-mail: jean-francois.mahfouf@meteo.fr

J. Wickert
GFZ German Research Centre for Geosciences, Potsdam, Germany
e-mail: wickert@gfz-potsdam.de

G. Dick
GFZ German Research Centre for Geosciences, Helmholtz Centre Potsdam, Potsdam, Germany
e-mail: dick@gfz-potsdam.de

R. Potthast
Deutscher Wetterdienst, Offenbach, Germany
e-mail: roland.potthast@dwd.de

S. Crewell
University of Cologne, Cologne, Germany
e-mail: crewell@meteo.uni-koeln.de

C. Pikridas
Aristotle University of Thessaloniki, Thessaloniki, Greece
e-mail: cpik@topo.auth.gr

N. Zinas
Tekmon Geomatics, Ioánnina, Greece
e-mail: nzinas@tekmon.gr

A. Ganas
National Observatory of Athens, Athens, Greece
e-mail: aganas@gein.noa.gr

R. Szabolcs
Budapest University of Technology and Economics, Budapest, Hungary
e-mail: szrozsa@agt.bme.hu

M. Mile
Hungarian Meteorological Service, Budapest, Hungary
e-mail: mile.m@met.hu

S. Thorsteinsson · B. G. Ófeigsson
The Icelandic Meteorological Institute, Reykjavík, Iceland
e-mail: siggi@vedur.is; bgo@vedur.is

Y. Reuveni
Interdisciplinary Centre (IDC) Herzliya, Herzliya, Israel
e-mail: yuvalr@ariel.ac.il

S. Krichak
Tel Aviv University, Tel Aviv, Israel
e-mail: shimonk@post.tau.ac.il

R. Pacione
e-GEOS/Centro di Geodesia Spaziale-Agenzia Spaziale Italiana, Matera, MT, Italy
e-mail: rosa.pacione@e-geos.it

G. Bianco
Centro di Geodesia Spaziale/Agenzia Spaziale Italiana contrada Terlecchia Matera, Rome, Italy
e-mail: giuseppe.bianco@asi.it

R. Biondi
Abdus Salam International Centre for Theoretical Physics, Trieste, Italy
e-mail: riccardo.biondi@uni-graz.at

G. Stankunavicius
Vilnius University, Vilnius, Lithuania
e-mail: gintas.stankunavicius@gf.vu.lt

F. N. Teferle
University of Luxembourg, Luxembourg, Luxembourg
e-mail: norman.teferle@uni.lu

J. Bosy · J. Kaplon · K. Wilgan
Wrocław University of Environmental and Life Sciences, Wrocław, Poland
e-mail: jaroslaw.bosy@up.wroc.pl; jan.kaplon@igig.up.wroc.pl;
karina.wilgan@igig.up.wroc.pl

K. Szafranek
Centre of Applied Geomatics of the Warsaw Military University of Technology, Warsaw, Poland
e-mail: kszafranek@wat.edu.pl

R. Fernandes
University of Beira Interior, Covilhã, Portugal
e-mail: rmanuel@di.ubi.pt

P. Viterbo
Instituto Português do Mar e da Atmosfera, Lisbon, Portugal
e-mail: pedro.viterbo@ipma.pt

A. Sá
Polytechnic Institute of Guarda, Guarda, Portugal
e-mail: andre_sa@ipg.pt

J. Hefty · M. H. Igondova
Slovak University of Technology, Bratislava, Slovakia
e-mail: jan.hefty@stuba.sk; miroslava.igondova@stuba.sk

E. Priego
Universidad Politécnica de Valencia, Valencia, Spain
e-mail: epriego@cgf.upv.es

G. Elgered
Chalmers University of Technology, Gothenburg, Sweden
e-mail: gunnar.elgered@chalmers.se

M. Lindskog · M. Ridal · U. Willén
Swedish Meteorological and Hydrological Institute, Gothenburg, Sweden
e-mail: Magnus.Lindskog@smhi.se; Martin.Ridal@smhi.se; Ulrika.Willen@smhi.se

T. Ning
The Swedish Mapping, Cadastral and Land Registration Authority, Gävle, Sweden
e-mail: tong.ning@lm.se

E. Brockmann
Swiss Federal Office of Topography, Wabern, Switzerland
e-mail: Elmar.Brockmann@swisstopo.ch

A. Geiger
ETH Zurich, Zürich, Switzerland
e-mail: alain.geiger@geod.baug.ethz.ch

C. Mekik
Bulent Ecevit University, Zonguldak, Turkey
e-mail: cetinmekik@beun.edu.tr

J. Jones
Met Office, Exeter, UK
e-mail: jonathan.jones@metoffice.gov.uk

Z. Liu · B. Chen
Hong Kong Polytechnic University, Hung Hom, Hong Kong
e-mail: lszzliu@polyu.edu.hk; yeary124@csu.edu.cn

C. Wang · S. Masoumi · M. Moore
Geoscience Australia, Canberra, Australia
e-mail: Carl.Wang@ga.gov.au; Salim.Masoumi@ga.gov.au; Michael.Moore@ga.gov.au

S. MacPherson
Environment Canada, Gatineau, QC, Canada
e-mail: stephen.macpherson@canada.ca

Abstract In this section a summary of the national progress reports is given. GNSS4SWEC Management Committee (MC) members provided outline of the work conducted in their countries combining input from different partners involved. In the COST Action paticipated member from 32 COST countries, 1 Near Neighbour Country and 8 Intrantional Partners from Australia, Canada, Hong Kong and USA. The text reflects the state as of 1 January 2018.

6.1 COST Countries

6.1.1 Austria

G. Möller
Department of Geodesy and Geoinformation, TU Wien, Wien, Austria
e-mail: gregor.moeller@geo.tuwien.ac.at

GNSS-Met activities at TU Wien: Atmospheric monitoring is an active research field at the Department of Geodesy and Geoinformation at TU Wien. Fostered by various nationally funded projects but also due to the excellent exchange within the COST action GNSS4SWEC, significant progress can be reported in research fields like GNSS tomography, multi-GNSS data analysis, atmospheric modelling or tropospheric mapping (see Möller et al. 2015; Möller 2017 or Landskron and Böhm 2017).

Within COST action GNSS4SWEC, TU Wien actively contributed to the real-time demonstration campaign. Therefore, the PPP software developed within the research project PPPserve (Hinterberger 2016) was further modified for estimation of real-time tropospheric parameters. Since March 2017, TU Wien acts as an analysis centre for near real-time GNSS data processing. Near real-time ZTDs are provided on a routine basis for selected GNSS reference sites in Austria and neighbouring countries to the ZAMG (https://www.zamg.ac.at) and EGVAP (http://egvap.dmi.dk/) for data assimilation purposes. For more details, the reader is referred to Chap. 3.

GNSS-Met activities at ZAMG; ZAMG was invited to participate in the homogenisation activity of this COST action, due to the experience gathered during the COST action ES0601 on the homogenization of surface data. Homogenisation is an essential topic for climate research and different methods are available and used in different countries. At ZAMG the software HOMOP (Gruber et al. 2009), combining PRODIGE (Caussinus and Mestre 2004), SPLIDHOM (Mestre et al. 2011) and INTERP (Vincent et al. 2002), is used for daily homogenization. It's a relative homogenization method, therefore relying on highly correlated reference series. Break detection is done on an annual/seasonal basis. For the calculation of adjustments, a homogeneous sub period of about 5 years is usually recommended.

The dataset available on integrated water vapour are very different to the time series usually homogenized in climate research: The stations are sparsely distributed over the whole globe and the time series are of short duration only. Therefore, it is necessary to use reference stations, which are not located within the same climate zone and have low correlation. This is somehow circumvented by using differences between model output and stations data under the assumption that the model shows the same skill over the whole globe. Moreover, a higher precision of break detection would be of advantage. Workshops helped to understand the problems of the GNSS-community and supported the exchange of experience gathered by the two groups (ES0601 and ES1206) on homogenization. The testing of different homogenization methods initiated in the framework of the COST action ES1206 is still work in progress.

6.1.2 Belgium

E. Pottiaux
Royal Observatory of Belgium, Brussels, Belgium
e-mail: eric.pottiaux@oma.be

H. Brenot
Royal Belgian Institute for Space Aeronomy, Uccle, Belgium
e-mail: hugues.brenot@oma.be

R. Van Malderen
Royal Meteorological Institute of Belgium, Brussels, Belgium
e-mail: roeland@meteo.be

Belgium partners from the Royal Observatory of Belgium (ROB), the Royal Belgium Institute for Space Aeronomy (BIRA), and the Royal Meteorological Institute of Belgium (RMI) have contributed to most topics addressed by the WG1, WG2 and WG3 during the whole period of the COST action ES1206 (GNSS4SWEC). Their main contributions are listed below and refer to the proper section in this final report.

Contributions to WG1:

- Contribution to advanced GNSS processing techniques by BIRA and ROB (Chap. 3; Pottiaux et al. 2014; Douša et al. 2015, 2016a, 2017).
- Contribution to Benchmark campaign by BIRA and ROB (Sect. 3.2.1; Dick et al. 2016; Douša et al. 2016b).
- Contribution to the Real-time PPP demonstration campaign by ROB (Sects. 3.2.2; Douša et al. 2016c).
- State-of-the-art of GNSS meteorology by BIRA and ROB (Sect. 2.1, Brenot et al. 2015; Guerova et al. 2016).
- Coordination of sub-WG1 ASYM by BIRA and contribution to ASYM by ROB (Sect. 3.3).
- Comparison of horizontal gradients and investigation on their information content and physical meaning by ROB (Sect. 3.3.2; Morel et al. 2015a, b).
- Investigation of the use of residuals and implementation of new indicator of tropospheric activity by BIRA (Sect. 3.3.4; Brenot et al. 2014a).
- Contribution STD validation by BIRA and ROB (Sect. 3.3.5; Kačmařík et al. 2017).
- Investigation of the use of residuals and their information content to reconstruct STD by ROB (Sect. 3.3.5; Kačmařík et al. 2017).
- Multi-GNSS troposphere modeling for improved monitoring and forecasting of severe weather by ROB (Pottiaux et al. 2014).
- Assessment of GNSS ZTD errors and correlations using UKV model by ROB (Bennitt et al. 2017).
- Development and evaluation of ultra-fast tropospheric products (sub-hourly and real-time) and their dissemination by ROB (Sects. 3.4.4 and 3.7.4, Pottiaux et al. 2015).

- Development of new solutions contributing to E-GVAP (sub-hourly and worldwide solutions) by ROB (Sect. 3.7.4; Pottiaux and Bruyninx 2016).
- GNSS tropospheric products for climate by ROB (Sect. 3.6.3; Pottiaux and Pacione 2016; Pacione et al. 2017a, b).
- STSM at ROB of Pavel Václavovic on developing a processing prototype for real-time tropospheric products over dense network in Belgium (Chap. 7).

Contributions to WG2:

- Co-chairing of WG2 by ROB (Chap. 4; Jones et al. 2014, 2015a, b, c, d, e, 2016a, b, c, 2017a, b, c).
- Development of a GNSS-based toolbox for non-numerical nowcasting and severe weather in Belgium by ROB (Sect. 4.2.4).
- Improvement of forecast skill of the GLAMEPS Model based on data assimilation of GNSS products by RMI and ROB (Sect. 4.3.3).
- Contribution to sub-WG TOMO (Sect. 4.4):
  - GNSS tomography using of dense network by BIRA (Brenot et al. 2014b).
  - Cross-validation of GNSS tomography models by BIRA (Brenot et al. 2018).
  - Optimal geometrical setting of water vapour density tomography retrievals by BIRA and RMI (Brenot et al. 2014c).
  - Interest of GNSS tomography for nowcasting by BIRA (Brenot et al. 2017b).
  - STSM at BIRA of Riccardo Biondi (INGV) in summer 2014 about GNSS atmospheric water vapour detection for extreme events using GNSS tomography and radio occultations (Chap. 7).
- Contribution to the 1st GNSS4SWEC Summer School in Varna by ROB, BIRA and RMI with lectures about Extreme weather & Interactive session about Nowcasting.
- Characterisation of tropical cyclones in the South Indian Ocean by BIRA (Nogherotto et al. 2017).
- Monitoring of water cycle with reflectometry, contribution by ROB (Simeonov et al. 2017).

Contributions to WG3:

- Coordination of sub-WG3 IWV intercomparison by RMI (Sect. 5.6).
- Literature study of past IWV intercomparison studies (Sect. 5.6.1).
- Multi-site inter-comparison of IWV observations for climate change analysis by RMI, BIRA, and ROB (Sect. 5.6; Van Malderen et al. 2014).
- STSM at BIRA of Karina Wilgan (ETHZ) in summer 2016 about the implement of lookup tables of refractivity coefficients using 10 year of outputs from ERA-Interim (Chap. 7).
- GNSS tropospheric products for climate by ROB (Sect. 4.5.3; Pottiaux and Pacione 2016; Pacione et al. 2017a, b).
- Using GNSS to validate climate model runs used for climate impact studies in the CORDEX.be project by ROB (Sect. 4.5.3; Gobin et al. 2016; Termonia et al. 2016, 2018; Van Schaeybroeck et al. 2017a, b).

- Coordination of homogenisation activity of GNSS IWV time series by RMI and ROB (Bogusz et al. 2016; Klos et al. 2017a, b; Van Malderen et al. 2017a, b, Sect. 5.5)
- World-wide analysis of the time variability of IWV by RMI, ROB and BIRA (Sect. 5.7.2), Van Malderen et al. 2017c).
- GPS water vapour and its comparison with radiosondes and ERA-Interim reanalysis in Algeria by RMI, IRA and ROB (Namaoui et al. 2017).
- Validation of climate model IWV fields by reprocessed European GNSS dataset EPN Repro 2 (Sect. 5.7.4; Berckmans et al. 2017).
- STSM at ROB and RMI of Anna Klos (MUT) on the homogenisation and characterisation of IWV time series from IGS repro1 and its comparison to ERA-Interim (Sect. 5.5 and Chap. 7).

Eric Pottiaux (ROB) and Roeland Van Malderen (RMI) are editors of the Special Issue "Advanced Global Navigation Satellite Systems tropospheric products for monitoring severe weather events and climate (GNSS4SWEC) (AMT/ACP/ANGEO inter-journal SI)".

6.1.3 Bulgaria

G. Guerova
Physics Faculty, Department of Meteorology and Geophysics, Sofia University "St. Kliment Ohridski", Sofia, Bulgaria
e-mail: guerova@phys.uni-sofia.bg

Application of GNSS tropospheric products in Bulgaria/Southeast Europe was initiated in 2011 with the project titled "Exploitation of ground-based Global Navigation Satellite Systems (GNSS) for Meteorology and Climate studies in Bulgaria/Southeast Europe" (2011–2014, http://cordis.europa.eu/result/rcn/164029_en.html). Within this project the Sofia University Atmospheric Data Archive (SUADA, http://suada.phys.uni-sofia.bg) was developed and used to study short and long-term variation of Water Vapour (WV) in the region. The GNSS4SWEC was very beneficiary for sustaining and further advancing the GNSS meteorology in Bulgaria. A summary of the GNSS4SWEC work in Bulgaria is given below.

Contribution WG1: A collaboration with University of Luxembourg resulted in establishment of the Sofia University GNSS Analysis Centre (SUGAC). SUGAC is the first Analysis Centre in Southeast Europe targeting atmospheric monitoring with the tropospheric products from the ground-based GNSS networks. The SUGAC first processing campaign took place in 2014 with processing seven Bulgarian GNSS stations for 1 year and deriving tropospheric products with very high temporal resolution (5 min). Further detail is available in Chap. 3.

Contribution WG2: In collaboration with the Operational Weather Prediction department of the National Institute of Meteorology and Hydrology case studies of fog, foehn, convective and frontal precipitation and hails storms in Bulgaria were conducted (see Chap. 3). A comparison of diurnal cycle of GNSS derived WV and WRF model simulations for Bulgaria indicate a negative model bias in the range 0.5–1.5 kg/m^2 (Simeonov et al. 2016). Collaboration with Aristotle University of Thessaloniki resulted in production of two dimensional WV map covering Bulgaria and Greece.

Contribution WG3: In collaboration with Hungarian Meteorological Service the WV anomalies from GNSS, regional climate model (ALADIN-Climate) and ERA-Interim reanalysis during the 2007 heat wave in Bulgaria were compared. The observed with GNSS (black line in Fig. 6.1) annual WV cycle at Sofia was found to be well captured in the ERA-Interim reanalysis (blue line in Fig. 6.1) while the ALADIN-Climate model peak in 2007 was 1 month earlier (red and green line in Fig. 6.1).

The early career researchers from Bulgaria participated actively in the GNSS4SWEC working group meetings and workshops. In total six MSc and five PhD students from Sofia University attended the GNSS4SWEC summer schools (2014, 2016). In 2014 the GNSS4SWEC summer school and WG meeting took place in Bulgaria (http://suada.phys.uni-sofia.bg/?page_id=2466). One early career researcher (Tzvetan Simeonov) conducted a STSM to the University of Luxembourg. Peter Szabo from the Hungarian Meteorological Service visited Sofia

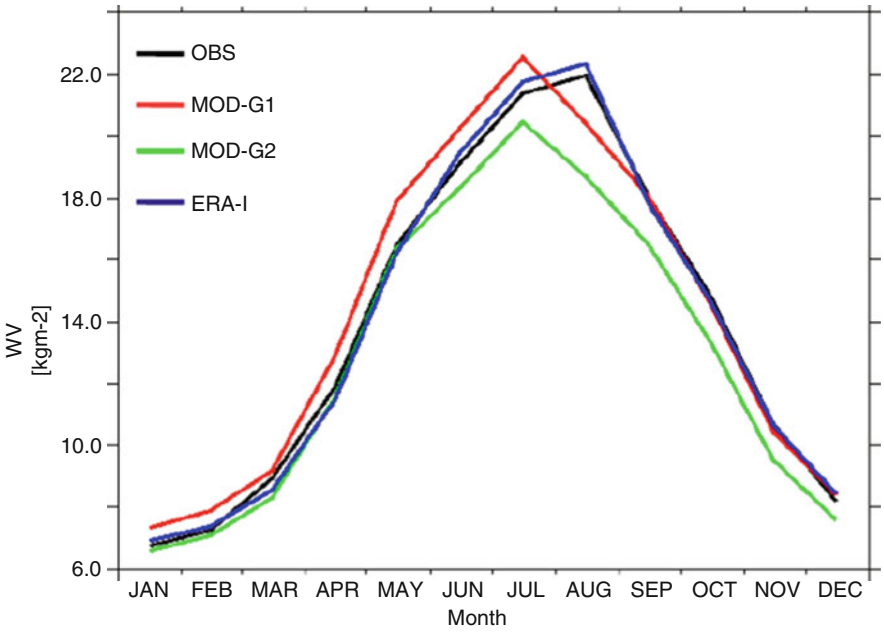

Fig. 6.1 Monthly mean WV for 2007 from GNSS (black line), ERA-Interim (blue line) and ALADIN-Climate (green and red line) at Sofia, Bulgaria. (Courtesy to P. Szabo)

University for a STSM. Published were four peer-review journal papers and two papers are in preparation. Established was close collaborations with colleagues from Cyprus and Greece, which will continue in the framework of the regional project "BalkanMed real time severe weather service" (BeRTISS, 2017–2019).

6.1.4 Cyprus

H. Haralambous
Frederick University, Limassol, Cyprus
e-mail: eng.hh@frederick.ac.cy

F. Tymvios
Cyprus Department of Meteorology, Nicosia, Cyprus
e-mail: f.tymvios@cyi.ac.cy

Cyprus has not been particularly active on GNSS meteorology in recent years. This has been partly due to a lack of an operational GNSS network on the island. Although the situation has improved in recent years with the deployment of the CYPOS network (seven GNSS stations), activities related to GNSS meteorology did not change until last year when the Frederick Research Centre (Cyprus) along with two more countries from the COST Action GNSS4SWEC (Greece and Bulgaria) submitted a joint proposal in the frame of the Transnational Cooperation Programme (TNCP) "Balkan-Mediterranean 2014–2020". The proposal BeRTISS "BalkanMed real time severe weather service" was successfully evaluated and its 2-year implementation started in September 2017. The geographical scope of the related existing network is shown in Fig. 6.2 and the network under deployment in Fig. 6.3.

The objective of the project is to develop and implement a pilot transnational severe weather service based on GNSS tropospheric products for the Balkan-Mediterranean area to improve the safety and quality of life and the protection of the environment, through the timely information regarding severe weather events and the long-term monitoring of climate change in the region.

In particular, the technical aims of the project are:

1. Integration of national networks of GNSS stations located in the three countries in a united system
2. Collection, processing and analysis of GNSS tropospheric data through the establishment of GNSS Analysis Centres,
3. Calculation of the meteorological parameter PWV for more accurate short-term prediction of severe weather events, following the innovative approach of exploiting GNSS satellite products
4. Creation of a dedicated website to provide in real-time the National Meteorological Services and the public with PWV data and warnings of severe weather events.

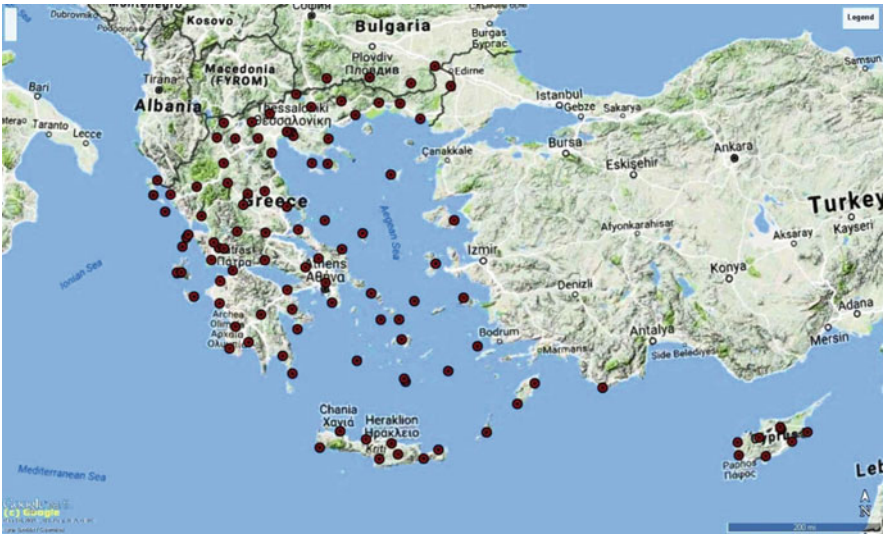

Fig. 6.2 Existing stations involved for the delivery of ZTD parameters in the frames of the BeRTISS project

Fig. 6.3 Stations to be deployed for the delivery of ZTD in the frame of the BeRTISS project

6.1.5 Czech Republic

J. Douša
Geodetic Observatory Pecný, RIGTC, Ondřejov, Czech Republic
e-mail: jan.dousa@pecny.cz

M. Kačmařík
Institute of Geoinformatics, VŠB Technical University of Ostrava, Ostrava, Czech Republic
e-mail: michal.kacmarik@vsb.cz

K. Eben
Czech Institute of Computer Science, Academy of Sciences, Praha, Czech Republic
e-mail: eben@cs.cas.cz

Three institutions participated actively in the COST Action, namely

- Geodetic Observatory Pecný (GOP), Research Institute of Geodesy, Topography and Cartography (RIGTC)
- Institute of Geoinformatics, Technical University of Ostrava (VŠB)
- Institute of Computer Science (ICS), Academy of Sciences of the Czech Republic (AS CR)

A long-term engagement of GOP in the ground-based GNSS troposphere monitoring for meteorological applications and related activities exists since 1999. GOP participated in COST-716 (2000–2003), contributed to the first NRT Demonstration campaign since the beginning in 2001, participated in EU TOUGH project (2003–2006) Targeting Optimal Use of GPS Humidity Measurements in Meteorology, and from the beginning contributed to the E-GVAP (2003–present). On a continuous basis, GOP provides several products including the first global, GPS + GLONASS combined and real-time solutions. The above experience lead to an active GOP participation during the planning, preparation and co-organization of this COST Action during which all three institutions were actively contributed to all three working groups summarized below.

Contributions to WG1:

- Chairing the working group (GOP), leading several WG1 tasks (GOP, VŠB), co-organizing workshops, group meetings, summer schools, external presentations (GOP)
- WG1 Benchmark campaign (GOP and VŠB)
  - Planning, design, coordination, data collection and provision
  - Provision and assessment of reference GNSS & NWM products
  - Assessment of tropospheric gradients in denes regional network
  - Optimizing strategy for real-time tropospheric production in simulated real-time mode

- New products for tropospheric anisotropy monitoring (GOP and VŠB)
  - Inter-comparison of slant delays retrieved from GNSS, NWM and WVR
  - Extensive comparisons of GNSS & NWM tropospheric gradients
  - Development and assessment of a fully consistent strategy for estimating ZTDs, gradients and slant-delays in (near) real-time
  - Impact of the forward filtering and the backward smoothing processing method on horizontal gradients and slant delays
  - Impacts of observation elevation weighting, gradient mapping function and multi-GNSS processing on troposheric gradients
- Ultra-fast product development (GOP and VŠB)
  - Development of in-house G-Nut/Tefnut for real-time ZTD and gradient estimation, routine provision of RT solutions since 2013
  - Development of new all-in-one strategy for a unique and optimal NRT and RT estimation of all tropospheric parameters
  - Contribution to RT Demonstration campaign with G-Nut/Tefnut software (GOP) and RTKlib software (VŠB) solutions
  - Long-term assessment of IGS RTS orbit and clock corrections
- Real-time demonstration campaign (GOP)
  - Design and coordination of the RT demonstration campaign
  - Campaign monitoring: http://www.pecny.cz/COST/RT-TROPO
  - Provision of NWM-forecasted ZTDs in RT demonstration
- Tropospheric correction models for GNSS positioning (GOP)
  - Development of accurate tropospheric parameter vertical scaling
  - Development of combined GNSS+NWM tropospheric model
  - Development and long-term assessment of tropospheric correction models in various user modes
- NWM-based data in GNSS positioning (GOP)
  - Impact of exploiting various external tropospheric corrections on hot-air baloon positioning, correlation study, multi-GNSS etc.
  - Impact of tropospheric corrections on PPP convergence time, re-convergence and pseudo-kinematic processing
  - Impact of NWM forecast length on derivation of ZTD parameters
- Support for setting up new analysis centres, transfer-of-knowledge (GOP)
  - Establishing new ACs: Trabzon (Turkey), Thessaloniki (Greece), Zolgundak (Turkey), Reykjavik (Iceland), Bucharest (Romania)
  - Development and provision of the TropNET system and transfer-of-knowledge (Poland, Netherlands, Slovakia, China).
  - Processing of national networks from Latvia and Slovakia
  - Monitoring of TropNET: http://www.pecny.cz/COST/TropNET

Contributions to WG2:

- Development of ensemble assimilation techniques (ICS)
  - Contribution to background covariance modelling
  - Initial twin experiment of assimilation of ZTD into WRF model
- Preparation of NWP data field for geodetic application (ICS, GOP)
  - Co-operation on WRF data encoding for input to PPP
  - GNSS kinematic experimental campaign supported with NWM
  - Monitoring ZTD predictions from WRF-ICS in RT-Demo

Contributions to WG3:

- GNSS re-analysis, done partly within WG1 (GOP)
  - Contribution to the EUREF GNSS 2nd reprocessing (1996–2014)
  - Assessment of seven processing variants in terms of coordinate repeatability, ZTD and tropospheric horizontal gradient estimates
  - Impact of re-processing strategy and models on ZTD trends
  - Impact of GNSS data quality on tropospheric gradients
- GOP-TropDB development and community support (GOP)
  - Evaluation of global IGS reprocessing products
  - Evaluation of individual AC + combined EUREF Repro2 solutions
  - Provision of NWM parameters for GNSS product evaluations
  - Interactive visualization of comparison statistics at the portal of the IGS Tropospheric WG: twg.igs.org/Tropo_Comp_Site
  - Online NWM-based calculation service for selected tropospheric and meteorological parameters: http://www.pecny.cz
- GNSS ZTD time-series analysis (GOP)
  - Development of the tools for time-series analysis, data cleaning, homogenization, variation and trend estimation
  - Developments and comparisons of data homogenization
  - Assessment of reference time-series from ERA-Interim
- SINEX_TRO V2.0 format design and implementation (GOP)

Finally, GOP acknowledges the national support of the Ministry of Education, Youth and Sports towards various contributions to the COST Action 1206 (LD14102, LH14089, LO1506, LM2015079).

GOP also acknowledge the Czech Hydrometeorological Institute for providing and consulting data for the Benchmark campaign.

6.1.6 Denmark

H. Vedel
Danish Meteorological Institute, Copenhagen, Denmark
e-mail: hev@dmi.dk

Ground-based GNSS meteorological activities at DMI: DMI has been active in ground-based GNSS meteorology since 1998, partaking in, among other things, EU project MAGIC, EU Cost action 716, EU project TOUGH, and being part of the E-GVAP (egvap.dmi.dk) team since the start of E-GVAP in 2005, with the role of coordinator.

The first GNSS research work at DMI was related to validation of GNSS derived IWV using NWP. But most research has concentrated on the use of GNSS delays in NWP, refining assimilation algorithms and doing impact experiments. The experiments showed an increase in NWP skill from using GNSS delays. Following assimilation became operational, but stopped when access to Nordic data ceased for a period. It is now being tested again, but not yet operational. The number of GNSS sites providing ZTDs within the DMI NWP areas has increased significantly in the meantime, and the primary NWP model has changed to a non-hydrostatic model, calling for the determination of new bias corrections, observation error estimates, etc.

DMI runs a rapid update NWP model with special focus on the forecast of local, convective precipitation. These systems use 3DVar data assimilation of standard observations + additional nudging assimilation of certain types of observations obtained many times an hour and of importance for precipitation, like radar 2D precipitation estimates and satellite images of clouds. Similarly, we will consider methods enabling usage of more GNSS delay data than 3DVar, which is restricted to one observation per site per assimilation cycle.

In addition, DMI extracts radiosonde data for validation of European GNSS delays, they are made available through E-GVAP. And do statistics of the E-GVAP ZTDs wrt. UK Met Office Global model NWP ZTDs, as part of the monitoring of E-GVAP data.

GNSS4SWEC has been a big benefit to DMI. Directly, enabling us to meet other GNSS meteorological researchers, learning from them and help drive the research in directions useful to DMI. And not the least indirectly, through a very effective spread of GNSS meteorological expertise in Europe. This has both increased the rate of progress in the field regarding both GNSS data processing for NWP and climate, and use of GNSS data in NWP. And it has resulted in a much better geographical coverage as regards the GNSS observation network, which is beneficial to European meteorology at large.

Other GNSS meteorological activities at DMI: DMI is leading the EUMETSAT ROM SAF (www.romsaf.org), which process GNSS RO measurements from the EUMETSATs Metop satellites for usage in meteorology and climate monitoring.

GNSS RO data from Metop and COSMIC are assimilated into the operational AROME NWP models.

Other GNSS meteorological activities in Denmark: Two other public institutions working with GNSS, DTU Space (Danish Technical University, research oriented), and "Geodatastyrelsen" (national mapping agency, Danish reference frame), exist. None of them are active in traditional ground-based GNSS meteorology, except that the Danish GNSS ZTDs available in E-GVAP (processed by NGA and ROB) are based on RINEX data delivered by Geodatastyrelsen to DMI. That is of the order ten sites. Potentially about 50 more sites, belonging to two private networks could be included, but currently they are not available to us. DTU is involved in experiments on Greenland, testing the ability to measure sea level and ice from reflected GNSS signals. DTU operates a number of GNSS sites on Greenland that could potentially be included in the E-GVAP processing.

6.1.7 Estonia

K. Rannat
Tallinn University, Tallinn, Estonia
e-mail: kalev.rannat@ttu.ee

In frame of COST ES1206, the Estonian team (based on Tallinn University of Technology and University of Tartu) has participated in WP2 and WP3. The works under WP2 were targeted to the case studies – extreme weather events at coastal areas of the Northern Baltic Sea (Estonia and Finland). Extreme snowfalls in Merikarvia in January 2016 and its connections to the large scale water vapour transport to the Northern Europe were studied. The activities under WP3 were targeted to investigations of GNSS IPW trend analysis and issues related to harmonisation of meteorological time series. The interest in GNSS-meteorology remains basically academic. Scientific collaboration has started with FMI (modelling and analysis of extreme snow events) and the Israeli Meteorological Service. In general, there are 27 permanent GPS stations in Estonia, of what 18 were installed in 2014–2015. Thus, the possibilities in using GNSS-data for regional analysis have increased remarkably due to installation of ESTPOS RTK-network (2014–2016), owned by the Estonian Land Board (ELB). It could be a good possibility to start negotiations with ELB about delivering data (tropospheric products) for E-GVAP. The ELB has capabilities to process GNSS-data on regular basis also. Additionally, many sites are equipped with Vaisala AWS (no need for interpolating meteorological data, meteo RINEXes are archived).

6.1.8 Finland

R. Kivi
Finnish Meteorological Institute, Helsinki, Finland
e-mail: Rigel.Kivi@fmi.fi

A.-M. Harri
Finnish Meteorological Institute, Helsinki, Finland
e-mail: ari-matti.harri@fmi.fi

Finnish Meteorological Institute has participated in COST Action ES1206 WGs and MC. Main activities are listed below.

- GRUAN site Sodankylä (Fig. 6.4) provided measurements by multiple techniques, including GNSS, RS92, MWR, FTS, AERONET sun photometer data. Sodankylä is involved in several relevant networks, e.g. GNSS networks, GRUAN, NDACC, TCCON, AERONET. GRUAN data are available regarding the RS92 SGP post processing.
- SODF is a new GNSS station, established in 2015 during the COST Action. IWV data processing has been organized in cooperation with GFZ in Potsdam, Germany and GRUAN Lead centre in Lindenberg, Germany.

Fig. 6.4 Two GNSS systems at Sodankylä, Finland, 97 m vertical difference, 12 km apart. Left panel: antenna installed at Sodankylä Tähtelä. Right panel: antenna installed at Sodankylä Pittiövaara

- Detection of possible discontinuities in the ZTD and IWV time series due to changes in instrumentation (Fig. 6.5).
- Inclusion of radiosonde data from long-term operation at the GRUAN site.
- Quality control of RS data set.
- Quality control of other available IWV data sets.
- Comparison of IWV values from redundant measurements.
- Collaboration with other COST countries has included study of Severe Weather using GNSS data (Fig. 6.6).

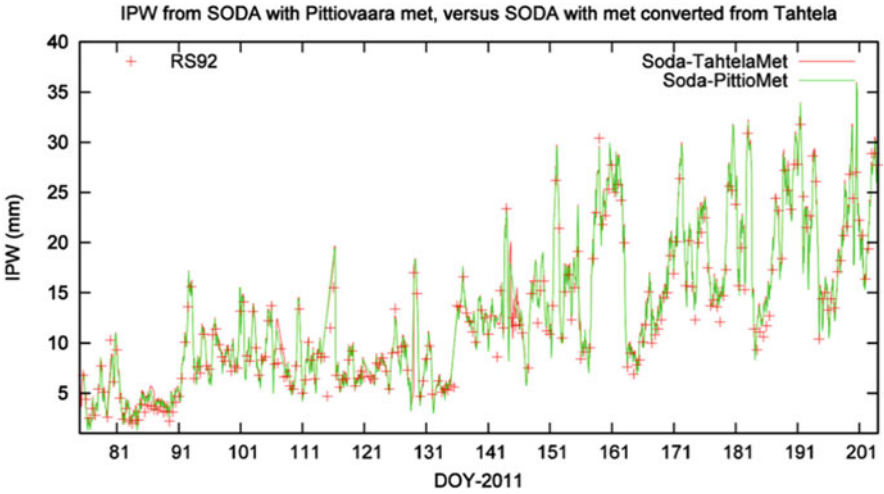

Fig. 6.5 GPS-PW from two stations in Sodankylä

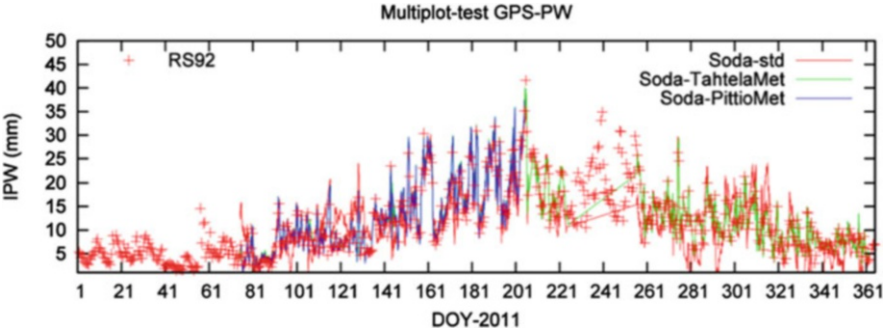

Fig. 6.6 PW in Sodankylä for the year 2011

6.1.9 France

O. Bock
IGN Institut national de l'information géographique et forestière, Paris, France
e-mail: olivier.bock@ign.fr

J. F. Mahfouf
Météo-France, Paris, France
e-mail: jean-francois.mahfouf@meteo.fr

IGN's operational geodetic and levelling service (SGN) is maintaining the French national GNSS network (RGP) comprising more than 450 stations. The network includes a small core of geodetic reference stations as well as a large number of stations from private and public operators. The rinex data from all the stations are publicly available at a central data centre hosted by IGN. The data are processed with Bernese GNSS software in different batches using near real time (NRT), rapid, and final IGS products, with 1-hourly, daily and weekly updates, respectively. One of the NRT batches is dedicated to operational GNSS meteorology as IGN has been an official E-GVAP Analysis Centre since 2001. Similarly, one of the weekly batches is dedicated to maintain the European terrestrial reference frame (EUREF). The main activities of IGN/SGN during the course of the GNSS4SWEC project were: the inclusion of new stations, both over the metropolitan zone and overseas (namely in the Caribbean region), the switch from GPS only to GPS + GLONASS solutions, and the participation in the EUREF repro2 reprocessing campaign.

Research activities were conducted by IGN/LAREG (Laboratoire de Recherche en Géodésie), in collaboration between several partners from the Action: ENSTA, France, LATMOS, France, AgroParisTech, France, RMI, Belgium, UWM, Poland, MUT, Poland. They covered the following topics:

1. The signature of Mesoscale convective systems passing over GPS stations in West Africa was investigated in ZTD, gradients, and phase residuals, and a stochastic model parametrization method based on Bayesian model selection was proposed to optimally tune the GNSS data processing options in case of such extreme events (Nahmani and Bock 2014; Nahmani et al. 2016, 2017).
2. The impact of baseline strategy on ZTD estimates in double-difference processing of GNSS networks was investigated and a methodology was proposed to significantly reduce the number of ZTD outliers by an improved network design (Stepniak et al. 2018).
3. ZTD post-processing screening strategy has been developed to detect ZTD outliers and has been proposed as a standard method for GNSS meteorology (Bock 2016b; Bosser and Bock 2016). The method is based on range-checks and outlier checks and comprises two options: one using GNSS-results only (ZTD and formal error data) and one using an independent dataset as a reference (e.g. NWP reanalysis). It can be used both for operational and post-processed data.

4. ZTD to IWV conversion methods have been reviewed, including the uncertainty due to refractivity constants and various sources of auxiliary data (Parracho 2017). Recommendations are provided in the Final Report (WG3).
5. A reference long-term reprocessed GNSS IWV dataset was prepared for homogenization activities in WG3 (Bock 2016a; Klos et al. 2017a, b; Van Malderen et al. 2017a, b, c). It is based on IGS repro1 ZTD data, screened and converted to IWV using the aforementioned methods and ERA-Interim as auxiliary data (for surface pressure and Tm).
6. Global IWV trends and variability have been analysed based on the aforementioned GNSS IWV dataset and on reanalysis data from ERA-Interim and MERRA (Parracho et al. 2018) as well as from global climate model simulations (Parracho 2017) and regional climate model simulations Med-CORDEX project (Bastin et al. 2017).
7. Satellite IWV data from three instruments (MODIS, SCIAMACHY, and AIRS) have been evaluated against GPS IWV data in the Arctic region for the period 2001–2014 (Alraddawi et al. 2017). It was shown that surface albedo and cloudiness (in cloud-cleared data) are not enough well modelled in current satellite retrieval algorithms with MODIS and SCIAMACHY and introduce spurious seasonal and inter-annual variability in IWV retrievals.
8. Existing homogenization methods were tested for the detection of breaks in the GNSS IWV time series and it was shown that due to the non-stationarity of noise in the GNSS observations, the performance of homoscedastic and heteroscedastic methods breaks down (Ahmed et al. 2015). New methods are currently being developed in collaboration with AgroParisTech.

6.1.10 Germany

J. Wickert
GFZ German Research Centre for Geosciences, Potsdam, Germany
e-mail: wickert@gfz-potsdam.de

G. Dick
GFZ German Research Centre for Geosciences, Helmholtz Centre Potsdam, Potsdam, Germany
e-mail: dick@gfz-potsdam.de

R. Potthast
Deutscher Wetterdienst, Offenbach, Germany
e-mail: roland.potthast@dwd.de

S. Crewell
University of Cologne, Cologne, Germany
e-mail: crewell@meteo.uni-koeln.de

GNSS Meteorology at GFZ: GNSS Meteorology is an integrative part of the GFZ research activities in the Helmholtz Association's Research Field "Earth and Environment" Programme "Atmosphere and Climate" (ATMO). The related scientific

work was initiated in 2000 with the GPS Atmosphere Sounding Project (GASP). GNSS ground-based observations of global networks as IGS and TIGA, of EUREF and the German SAPOS (SAtelliten-POSitionierungsdienst), as well as campaign-type networks (all-together around 1300 stations) are used for operational atmospheric sounding. The data are analysed in near-real time for the assimilation to weather models and consistently re-processed for climatological investigations in the framework of the Global Climate Observing System (GCOS). Recent investigations at GFZ focus on exploiting the potential of real-time multi-GNSS observations for atmospheric data products with improved accuracy, higher spatio-temporal resolution and immediate availability. Additional tasks like the derivation of 3D water vapour distributions and GNSS applications for climate research are also included into the GFZ developments.

GFZ contribution to GNSS4SWEC: GFZ significantly contributed to all three Working Groups of the COST Action GNSS4SWEC and especially to the Working Group 1 by the development of the next-generation data products with improved impact to forecasts in close cooperation with German Weather Service (DWD). The international cooperation within the COST action was extremely useful for these investigations. Multi-GNSS tropospheric products in real time (Fig. 6.7) were one of the main focuses of the GFZ contributions. GRDs (Fig. 6.8) and STDs were other investigation areas. Operational retrieval of slants was established at GFZ for the first time and the STDs were continuously provided to DWD for forecast experiments (Fig. 6.9) after intense validation with water vapour radiometer data. The new assimilation operator for slants was developed in close cooperation of DWD with GFZ.

Operational Weather Forecast: The application of operational atmospheric products to improve regional and global weather forecasts is an integral part of the scientific development work in GNSS Meteorology at GFZ and a significant contribution to the Working Group 2 of GNSS4SWEC. Figure 6.9 exemplarily shows a regional precipitation forecast study by the German Weather Service (DWD). More than 20% improvement was reached by additional use of the GNSS slant total delays from GFZ.

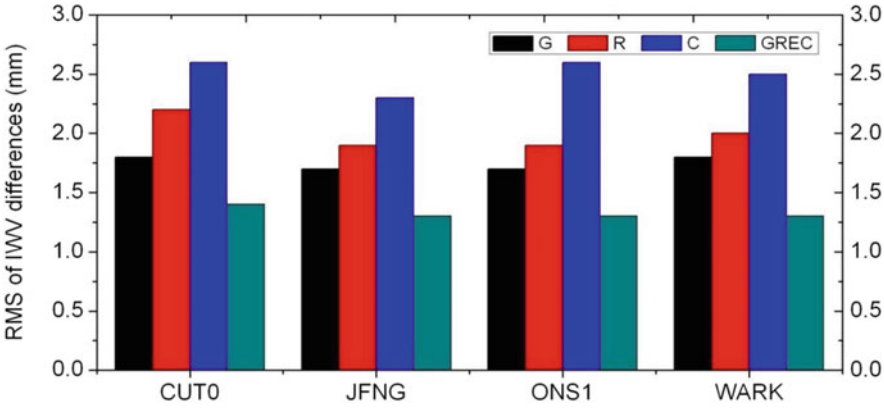

Fig. 6.7 Multi-GNSS IWV in simulated real time: Validation with radiosondes data. Results are presented for: G – GPS only, R – GLO only, C – BDS only, and GREC – all four satellite systems GPS + GLO + GAL+BDS. Time period: January–July, 2014

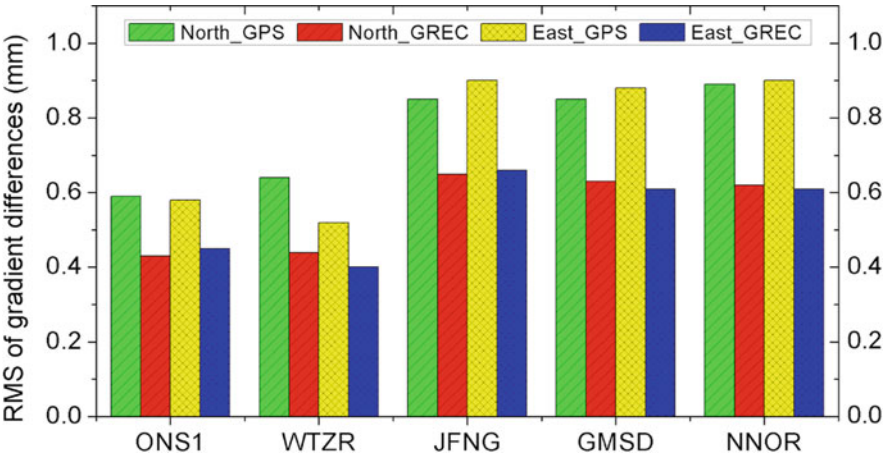

Fig. 6.8 Multi-GNSS (GREC-GPS + GLO + GAL+BDS) high-resolution tropospheric gradients compared to horizontal delay gradients from a NWM refractivity field (ECMWF analysis)

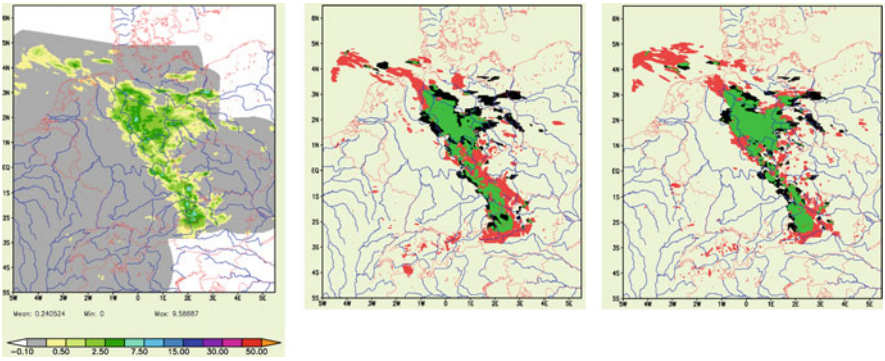

Fig. 6.9 Results of a DWD forecast experiment using GNSS slant delays from the German network on May 28, 2014, during a strong precipitation event. Left: radar observation (mm/hour; truth), middle: forecast without GNSS and right: forecast with GNSS. Green/red colour indicates good/bad agreement of forecast and radar data. The assimilation of GNSS slant data improves the forecast more than 20% indicated by larger green and smaller red areas. (Figures provided by K. Stephan, DWD)

Climatological Investigations: GFZ contributed to the Working Group 3 with re-processing of GNSS data of about 800 globally distributed stations within IGS TIGA project. Precise trends of water vapour can be derived from such long-term data sets (Fig. 6.10).

An additional contribution is GFZ's activity within the GCOS Reference Upper Air Network (GRUAN, www.gruan.org) of the World Meteorological Organization (WMO). GFZ was selected as the central GRUAN GNSS Data Processing Centre of WMO.

GNSS Meteorology activities at DWD: The Data Assimilation Group of DWD has integrated the assimilation of GNSS ZTD data into the global ICON model (13 km resolution) and its two-way nested area over Europe (6.5 km resolution),

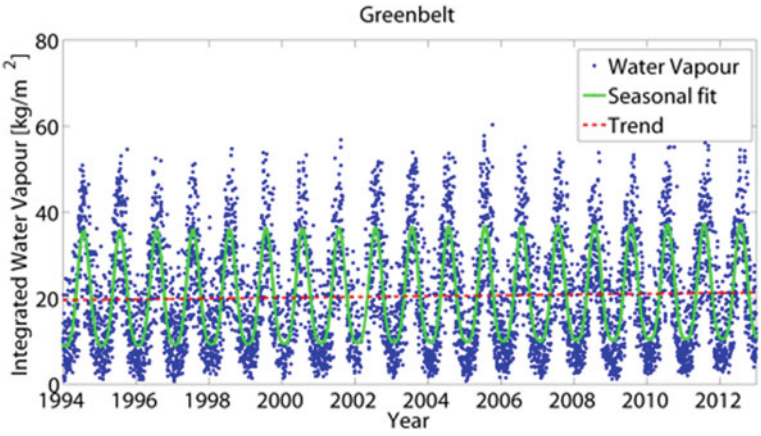

Fig. 6.10 Integrated water vapour at the GNSS station Greenbelt (U.S.). Trend of 0.94 mm/year was derived, based on the re-processed data set of ~800 TIGA stations for 20 years

based on the Local Ensemble Transform Kalman Filter (LETKF) and Ensemble Variational Data Assimilation EnVAR. The assimilation of ZTD shows a slightly positive impact on upper air verification in the global forecasting system. However, the GNSS data lead to some spin-up effect on precipitation in the ICON model for the first 24 h, which is under investigation currently. ZTD assimilation is in preoperational testing state waiting for the remaining issues to be resolved. For the convection-permitting COSMO-DE and COSMO-DE-EPS the assimilation of GNSS STD has been developed based on the Kilometre-Scale Ensemble Kalman Filter (KENDA), with a sophisticated GNSS-STD forward operator includes ray tracing (Bender et al., in preparation). Initial experiments (compare Fig. 6.9) show a positive effect on the localization of precipitation. More intense testing is being carried out currently, with the need of careful tuning of localization and thinning in the LETKF to reduce the influence of correlated errors and spurious correlations in the 40 member KENDA ensemble. We expect to enter a preoperational state for the KENDA-STD system in the near future.

GNSS Meteorology activities at University Cologne: Near-real time IWV estimates from GFZ are used as at University of Cologne to investigate the performance of a new high-resolution reanalysis (Bollmeyer et al. 2015) with 6 km resolution (COSMO-REA6) on the European scale and 2 km over Germany (COSMO-REA2). Their suitability for this for temporal scales of 15 min and longer has been shown Steinke et al. (2015) using comprehensive instrument comparisons and high resolution modelling during the HOPE campaign (Macke et al. 2017). The comparison of reanalyses revealed the benefit of the high resolution which show standard deviation with observed of about 1.5 mm and thus significantly lower than ERA-Interim (2.5). This improvement compared to global reanalysis also holds for daily mean IWV values but disappears than monthly means are considered. Figure 6.11 shows that the improved standard deviation is observed over all seasons and that both bias and standard deviation differ much less between different stations than for ERA-Interim.

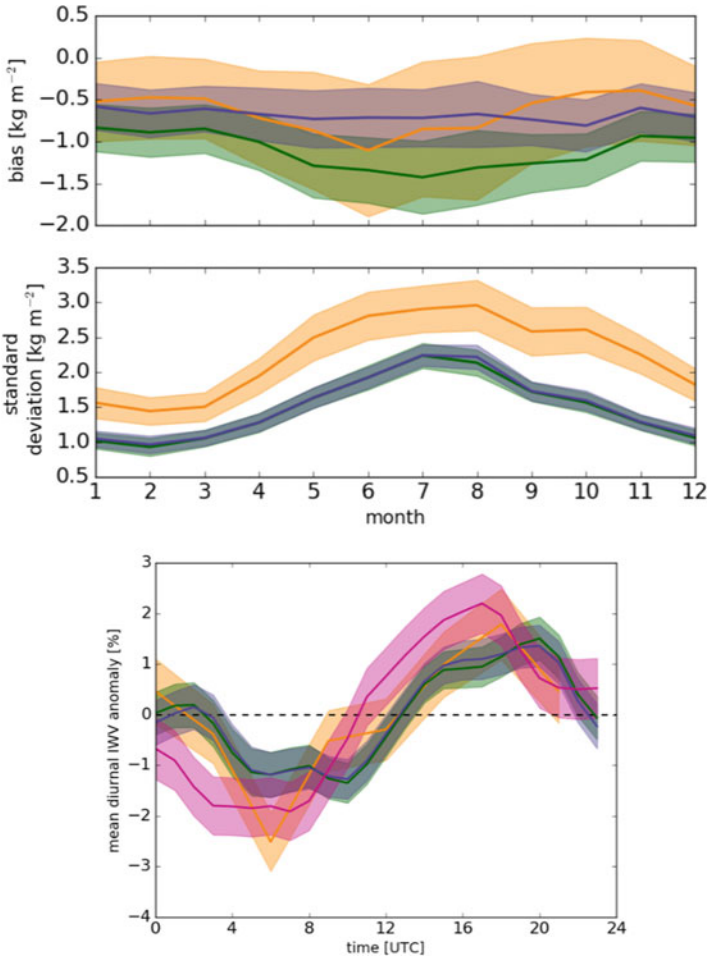

Fig. 6.11 IWV monthly mean of bias (top) and standard deviation (bottom) simulated with COSMO-REA2 (green), COSMO-REA6 (purple) and ERA-Interim (orange) compared to 133 GPS station observations for 2007–2013. The standard deviation of the respective error is shaded

A major improvement of COSMO-REA compared to ERA-Interim which only is available every 6 h (forecasts every 3 h) is the availability to resolve the diurnal cycle of IWV. In general COSMO-REA reproduces the observed diurnal cycle (Fig. 6.11) but shows some phase shift and reduced amplitude. This evaluation already helped to identify an issue with the surface vegetation information in COSMO-REA which will be fixed in later versions. Because the surface is the source for water vapour and the water vapour content of the boundary layer contributes roughly half of the total IWV, the observations are well suited to analyse land surface exchange processes and could reveal differences in the diurnal cycle for different circulation weather types and surface elevations (not shown).

6.1.11 Greece

C. Pikridas
Aristotle University of Thessaloniki, Thessaloniki, Greece
e-mail: cpik@topo.auth.gr

N. Zinas
Tekmon Geomatics, Ioánnina, Greece
e-mail: nzinas@tekmon.gr

A. Ganas
National Observatory of Athens, Athens, Greece
e-mail: aganas@gein.noa.gr

In the frame of a Short Term Scientific Mission on October 2014, a new analysis centre (AC) for near real-time GNSS tropospheric monitoring in Greece was established at the Department of Surveying Engineering of the Aristotle University of Thessaloniki (AUTh). Since then the AUTh Analysis Centre contributes to the EGVAP hourly ZTDs from over 90 permanent GNSS stations in Greece using the Trop-NET Engine. The AC provides a unique contribution of tropospheric products to the meteorological community for the E-GVAP project that cover the whole of Greece. Also as a direct result of Greece's participation in this COST action, in collaboration with two other COST participating countries, Bulgaria and Cyprus, the AUTh Research team received funding under the frame of the European Territorial Cooperation Programme "Interreg V-B Balkan-Mediterranean 2014–2020" for the project BeRTISS (Balkan-Meditteranean Real Time Severe weather Service). More information on the new AC activities in Greece can be found in Sect. 3.6.7 of this report.

6.1.12 Hungary

R. Szabolcs
Budapest University of Technology and Economics, Budapest, Hungary
e-mail: szrozsa@agt.bme.hu

M. Mile
Hungarian Meteorological Service, Budapest, Hungary
e-mail: mile.m@met.hu

Within the frame of the project the Budapest University of Technology and Ecomics (BME), the Hungarian Meteorological Service (HMS) and the Satellite Geodetic Observatory of the Institute for Geodesy, Cartography and Remote Sensing (SGO) worked closely together to improve the coverage of the near-realtime ZTD estaimations in central and eastern Europe.

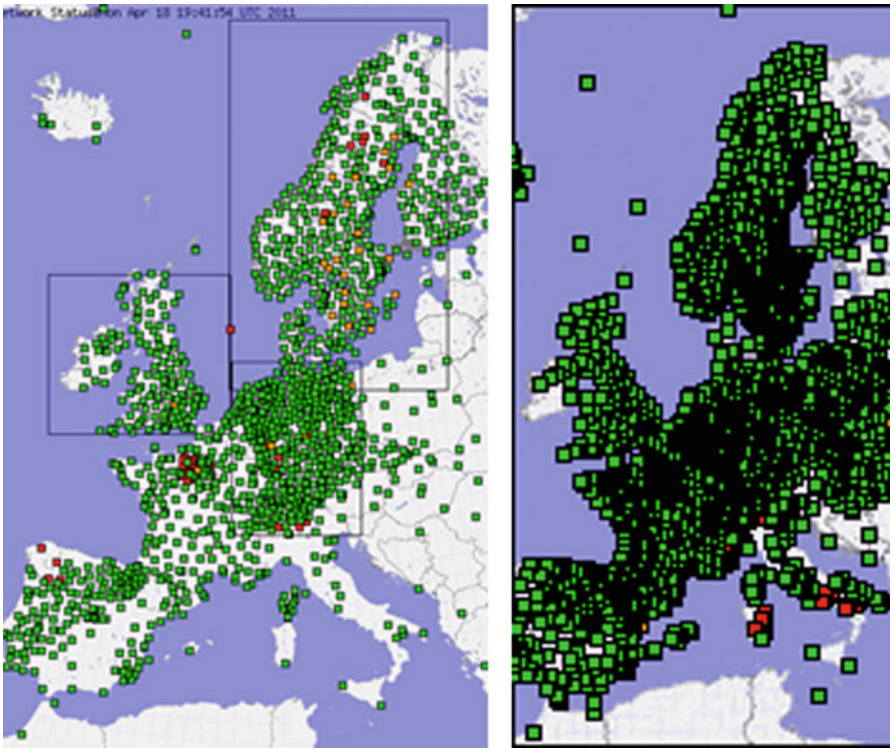

Fig. 6.12 The E-GVAP coverage in 2011 (left) and 2013 (right). Observe the significant improvement in Central and Eastern-Europe

In order to achieve this goal, a new near real-time GNSS processing centre has been established with the cooperation of BME and SGO and the estimations were automatically transferred to the E-GVAP data centre for testing and validation purposes. The centre (SGOB) processed the following GNSS stations:

- Hungarian GNSS network (GNSSNet.hu)
- additional GNSS stations from the neighbouring countries including E-GVAP supersites for validation
- As a result of this activity altogether 54 new Hungarian and Central-European GNSS stations were added to the E-GVAP coverage (see Fig. 6.12).

Since the GNSS observations must be processed within the premises of the SGO due to legal restrictions, the SGOB processing centre has been transformed to the SGO1 processing centre by the Satellite Geodetic Observatory and the original SGOB centre has been abandoned.

After the validation of the ZTD estimates, some preliminary tests were done in the assimilation of ZTD data in numerical weather models. The colleagues at the Hungarian Meteorological Service assimilated the near real-time ZTD estimates in

a test run of the AROME 3DVar numerical weather model. The tests were done with the pre-selection of the GNSS ZTDs from SGO1 E-GVAP network. The estimates were tested and tuned with static and variational bias correction in 3DVar. The preliminary results showed promising impact on the ARTOME analyses and forecasts. The RMSE and the bias of the parameters MSLP and Rh2m of the analysis and the forecasts are depicted on Fig. 6.13. It can be seen that the bias of both of the parameters were significantly improved by the assimilation of the ZTDs in the model runs. Moreover, the RMSE of the short-term forecasts of these parameters improved, too.

6.1.13 Iceland

S. Thorsteinsson
The Icelandic Meteorological Institute, Reykjavík, Iceland
e-mail: siggi@vedur.is

B. G. Ófeigsson
The Icelandic Meteorological Institute, Reykjavík, Iceland
e-mail: bgo@vedur.is

There are approximately 100 GNSS sites in Iceland (Fig. 6.14), mainly for geodetic purpose. Jan Douša and Benedikt established the IMO processing centre in March 2016 with approximately 60 ZTD processed stations. There were just two ZDT processed stations in Iceland before that. Then IMO became one of the analysis centres in E-GVAP and is in charge of the data processing for the GNSS stations in Iceland. Benedikt extended it with six well spread coast stations (GUSK, ISAF, SIFJ, HEID, AKUR, MYVA) in January 2017. One near real-time ZTD product (IMOA) is currently provided. The IMOA product is obtained from using the GOP's Trop-NET system (http://www.pecny.cz/gop/index.php/trop-net) which utilizes BSW52 software. The time resolution is 60 min.

Sigurdur has started and plans to continue to do assimilation impact studies with the above mentioned GNSS ZTD data as well as from four GNSS sites in Greenland gotten from EGVAP in HARMONIE on the 2.5 km IGB grid domain. New decision regarding the common operational system between IMO and the Danish Meteorological Institute (DMI) is to extend the domain to cover the whole Greenland and Iceland and its surrounding islands, termed IGB domain.

The HARMONIE tools and the Icelandic processing GNSS ZTD centre that we have developed in COST ES1206 to monitor convective clouds and severe weather conditions will become useful for IMO.

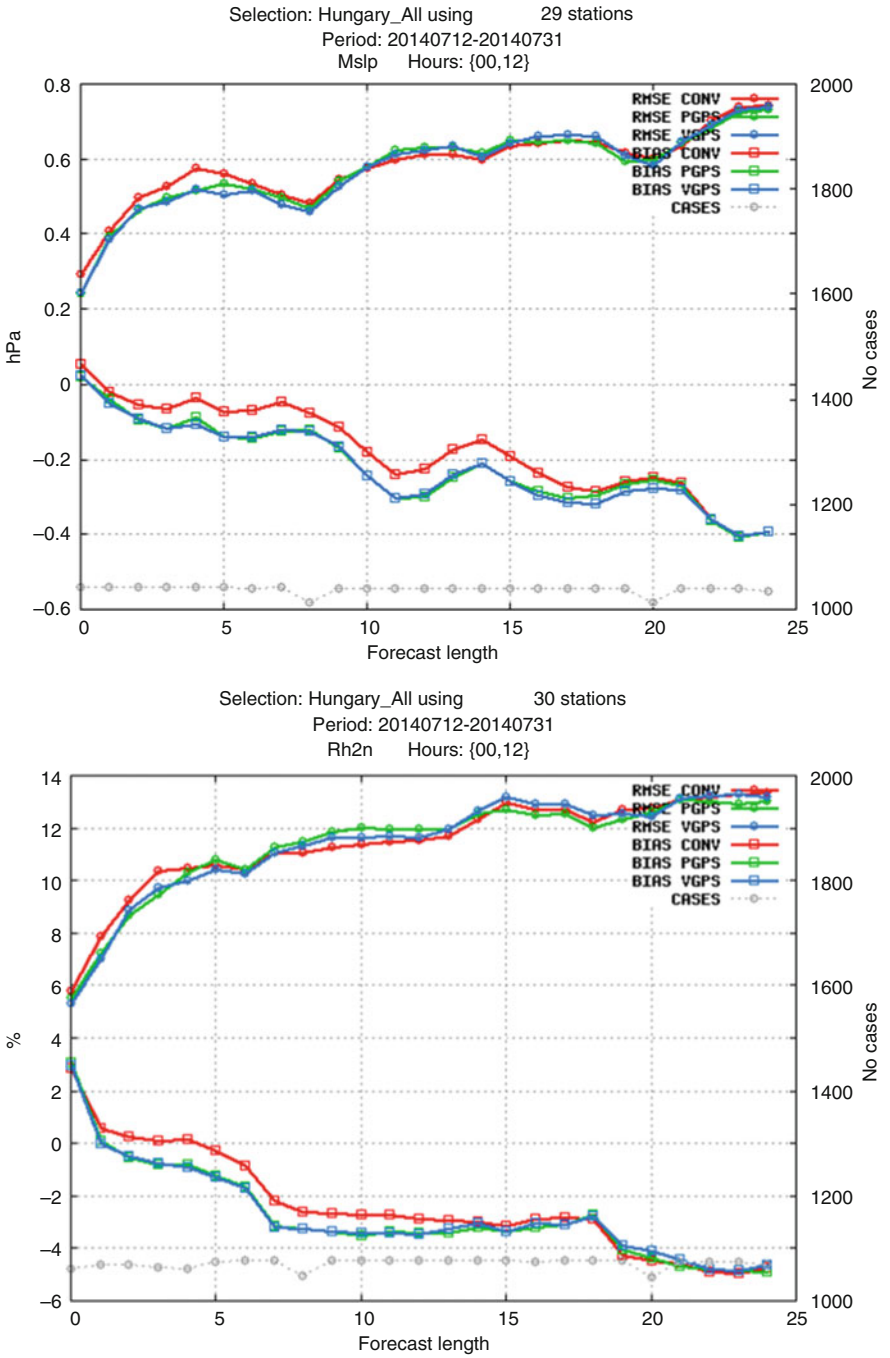

Fig. 6.13 The RMSE and the bias of MSLP and Rh2m parameters of the model runs. (AROME CONV: operational AROME model run without ZTD assimilation; AROME PGPS: operational AROME model with ZTD assimilation using static bias correction; AROME VGPS: operational AROME model with ZTD assimilation using variable bias correction)

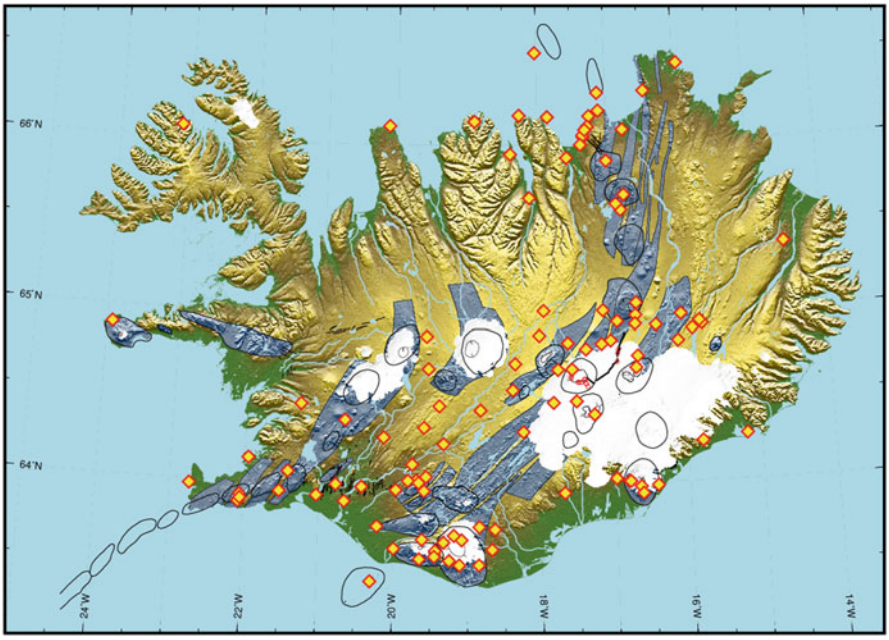

Fig. 6.14 Approximately 100 GNSS sites are in Iceland, mainly for geodetic purpose. So far we ZTD process approximately 60 of these stations

6.1.14 Israel

Y. Reuveni
Interdisciplinary Centre (IDC) Herzliya, Herzliya, Israel
e-mail: yuvalr@ariel.ac.il

S. Krichak
Tel Aviv University, Tel Aviv, Israel
e-mail: shimonk@post.tau.ac.il

The operational GPS network in Israel is consisted of 24 permanent stations and is operated by the Survey of Israel (SOI). Currently, we have near real-time RINEX data from all the stations, while hopefully in the near future SOI will partner with E-GVAP to allow real-time access with 1-h latency. Other data sources which are being used for on-going GNSS-meteorology R&D in Israel are METEOSAT-10 real time data (mainly 7.3 and 10.8 μm channels), IMS radiosondes and surface temperature data from about 80 permanent stations. We have presented for the first time the use of Israel's dense regional GPS network for extracting tropospheric zenith path delays combined with near-real time METEOSAT-10 Water Vapour (WV) and surface temperature pixel intensity values (7.3 and 10.8 μm channels, respectively) in order to assess if it is possible to obtain absolute IWV (kg/m^2) distribution. The

results show good agreement between the absolute values obtained from our triangulation strategy based solely on GPS ZTDs and METEOSAT-10 surface temperature data compared with available radiosonde IWV absolute values. The presented strategy can provide high temporal and special IWV resolution, which is required as part of the accurate and comprehensive observation data integrated in modern data assimilation systems, and is required for increasing the accuracy of regional Numerical Weather Prediction (NWP) systems forecast. Furthermore, constructing WV maps using only interpolated GPS zenith wet delay (ZWD) estimations has a main disadvantage: it doesn't take into account clouds, which are situated outside the integrated GPS paths when interpolating the IWV estimations from a network of GPS stations. Recently, we have developed a new and upgraded strategy, which combines our initial approach for WV estimations by using the mathematical dependency between GPS ZWD and Meteosat-10 in order to estimate the IWV amount, while also taking into account the spatio-temporal cloud distribution when performing the interpolation between adjacent GPS station inside our network. This modified approach increases the accuracy of the estimated regional IWV maps distribution and could potentially increase the accuracy of regional NWP platforms.

6.1.15 Italy

R. Pacione
e-GEOS/Centro di Geodesia Spaziale-Agenzia Spaziale Italiana, Matera, MT, Italy
e-mail: rosa.pacione@e-geos.it

G. Bianco
Centro di Geodesia Spaziale/Agenzia Spaziale Italiana contrada Terlecchia Matera, Rome, Italy
e-mail: giuseppe.bianco@asi.it

R. Biondi
Abdus Salam International Centre for Theoretical Physics, Trieste, Italy
e-mail: riccardo.biondi@uni-graz.at

GNSS-Met activities at ASI/CGS: ASI/CGS is active in the GNSS-Met field since 1999 participating to several European projects:

- MAGIC (1999–2001), one of the first projects being set up to develop and test the capacity for meteorological organizations to benefit from GPS as new data source;
- COST-716 (2001–2003), a NRT demonstration campaign;
- TOUGH (2003–2006) Targeting Optimal Use of GPS Humidity Measurements in Meteorology;

- E-GVAP (2005–present), towards operational use and establishing a GPS delay observing system.

In the E-GVAP framework, ASI/CGS is participating as Analysis Centre and Combination Centre delivering four tropospheric solutions:

1. Near Real Time ZTD (Operational): every hour, 15′ ZTD estimates with a 1h45′ latency for a European network of more than 200 sites;
2. Near Real Time Combined ZTD (Operational): every hour, the 15′ ZTD estimates from the contributing E-GVAP Analysis Centres are combined and made available to the project, using a combination scheme outlined in Pacione et al. (2011);
3. Near Real Time ZTD (Test): the aim of this solution is to evaluate IGS RT products in hourly PPP for NWP application;
4. Sub-hourly ZTD (Test): the aim of this solution is to test RT GNSS observation and products in sub-hourly PPP for now-casting application.

During the present COST Action, we increased the number of GNSS stations in Italy including several regional networks in the operational solution delivered to E-GVAP. Since 1996 ASI/CGS has been an EPN Analysis Centre, producing on a routine basis the requested solutions for the European Reference Frame definition and maintenance and tropospheric applications.

In 2014, at the EUREF Symposium in Vilnius, ASI/CGS was appointed as EPN Tropospheric coordinator with the task of monitor the EPN Analysis Centres troposphere solutions, generate the combined EPN station zenith path delay solutions and processes inter-technique tropospheric solutions.

On the long-term, a reprocessing was carried out in 2014. The whole EPN Network was analysed in a homogeneous way using the latest available models for the period 1996–2014 (Pacione et al. 2014). GNSS data have been analysed with GIPSY-OASIS II 6.2 in PPP mode applying the state-of-the-art models and the JPL reprocessed products. As a result, homogeneous time series of site coordinates as well as of ZTD and horizontal gradient parameters were generated.

The reprocessing efforts is part of the second EPN reprocessing campaign ‘EPN-Repro2’ organized in the framework of the special EUREF project ‘EPN reprocessing’ where the individual contributions of five EPN Analysis Centres are combined in order to provide the official EPN reprocessed products (Pacione et al. 2017a, b). For each EPN station, plots on ZTD time series, ZTD monthly mean, comparison versus Radiosonde data (if collocated), are available at the EPN Central Bureau (http://www.epncb.oma.be/_productsservices/sitezenithpathdelays/). EPN-Repro2 data can be used as a reference dataset over Europe for a variety of scientific applications and has a high potential for monitoring trend and variability in atmospheric water vapour, improving the knowledge of climatic trends of atmospheric water vapour and being useful for regional Numerical Weather Prediction (NWP) reanalyses as well as climate model simulations.

ASI/CGS has been also involved in the standardization and development of a unique format to exchange tropospheric and meteorological parameters. This format should be adopted within all the IAG services and by all the techniques dealing with

tropospheric parameters. The SINEX-TRO v2.00 format has been officially presented at the IGS Workshop (July 3–7, 2017, 2017), at the Unified Analysis Workshop (July 10–12, 2017, Paris), at the EPN Analysis Centre Workshop (October, 25–26, 2017 Brussels).

GNSS-Met activities at International Centre for Theoretical Physics: Within the STSMs of Riccardo Biondi and Rita Nogherotto, we have collected several severe weather cases in Europe and Indian Ocean (all the tropical cyclones passing over Ile de La Reunion), and archived the data and info into the Met Office server as planned during the meeting in Wroclaw 2015. The study first focused on severe events in Belgium and United Kingdom by using ground based GNSS measurements for the ZTD and IWV estimation, and GNSS Radio Occualtions (RO) for atmospheric vertical profiles, and it was then expanded to Italy. The combination of ground based measurements and RO has been used for developing the tomography of the single events (Brenot et al., in preparation). The focus work on Italy (Bonafoni and Biondi 2015), has analysed several precipitation events occurred exploiting the potential of the two GNSS techniques (i.e. ground-based and space-based GNSS receivers) showing a typical decrease of IWV with the rain and an increase of the cloud top altitude with the rain rate. From ground-based receivers, time series of IWV were produced at specific locations with the purpose of analysing the water vapour behaviour during precipitation events. From LEO receivers, the profiling potential was exploited to retrieve the cloud top altitude of convective events, taking into account that although GNSS RO could capture the dynamics of the atmosphere with high vertical resolution, the temporal resolution is not enough to continuously monitor such an event in a local area. A detailed analysis of all the tropical cyclone Bejisa (2013–2014) has been done with three ground based stations - REUN (Ile de La Reunion), ABPO (Madagascar) and VACS (Mauritius Island) – and collocated ROs. A statistical analysis has been done by using all the tropical cyclones´ tracks in the period of data availability (2007–2016) highlighting a specific trend of IWV before the cyclone overpass and a typical cyclone thermal structure.

For these analyses new collaborations were established within the COST member countries:

- H. Brenot (BIRA, Belgium) and J. Le Clair de Bellevue (Meteo France) for the study of tropical cyclones;
- H. Brenot (BIRA, Belgium), M. Kačmařík (Univ. Ostrava, Czech Republic) and W. Rohm (Wroclaw University, Poland) for the tomography models by using ground based GNSS and ROs.

Brenot, H., et al. (2018). Cross-validation of GNSS tomography models and methodological improvements using CORS network, AMT, in preparation for AMT.

Pacione, R., et al. (2011). Adv. Space Res., 47, 323–335, doi: https://doi.org/10.1016/j.asr.2010.07.021.

Pacione, R., et al. (2014). EGU GA 2014 http://meetingorganizer.copernicus.org/EGU2014/EGU2014-2945.pdf

6.1.16 Lithuania

G. Stankunavicius
Vilnius University, Vilnius, Lithuania
e-mail: gintas.stankunavicius@gf.vu.lt

Vilnius University (Lithuania) as participating partner of COST Action ES1206 became at the end of 2013. In December 2014 we signed an agreement with Lithuanian Positioning System (LitPOS - the network of permanent reference GNSS stations) administration, for open data accessibility from their 25 GNSS stations for the needs of the COST activity. LitPOS is a state company and a part of EUPOS® for territory of Lithuania. EUPOS® provides high-quality differential GNSS information for high-precision positioning and navigation usable in a large field of applications.

RINEX format hourly data started to be processed in September 2015 by Jan Kaplon from the Institute of Geodesy and Geoinformatics, Wroclaw University of Environmental and Life Sciences, Wroclaw, Poland (WUEL). The processed data since autumn 2015 are also available on the E-GVAP network. These data also are stored in ftp server of the Department of Hydrology & Climatology, Institute of Geosciences, Vilnius University: ftp://158.129.144.65/incoming/.

Vilnius University signed agreement concerning data availability also with other large GNSS reference station network in Lithuania – Leica SmartNet LT. This is the private company operational since 2006 and manages the reference network consisting of 16 stationary GPS stations located at identical distances. Unlike the LitPOS the Leica SmartNet LT gave access to RINEX files only via http and these data still remain unprocessed.

The national MC member Dr Gintautas Stankunavicius participated in all Action ES1206 organised meetings since February 2014: February 2014, Munich, Germany; May 2015, Thessaloniki, Greece; September 2015, Wroclaw, Poland; March 2016, Reykjavik, Iceland; September 2016, Potsdam, Germany and February 2017, ESTEC, Noordwijk, Netherlands (in some meetings together with other national representatives).

The processed Lithuanian GNSS data already started to be used in educational process in Vilnius University – mainly for students' coursework but still wasn't used for extreme weather and regional climate research. Despite these shortages the processed GNSS data were used in common research with other GNSS4SWEC partners: WUEL and Royal Meteorological Institute of Belgium (RMI). Research results were presented in two international conferences: EGU 2016, Vienna and EMS Annual Meeting 2017, Dublin. Presentations are described below:

Kapłon J., Stankunavicius G. (2016) Effect of densifying the GNSS GBAS network on monitoring the troposphere zenith total delay and precipitable water vapour content during severe weather events. European Geosciences Union General Assembly 2016, Vienna, Austria, 18–22.04.2016 (poster), pp. Posters G5.2/

AS4.17/CL2.22 http://meetingorganizer.copernicus.org/EGU2016/EGU2016-12883.pdf

Van Malderen R., Pottiaux E., Stankunavicius G., Beirle S., Legrand J., Brenot H., Wagner T., De Backer H., Bruyninx C. (2017). A world-wide analysis of the time variability of Integrated Water Vapour, based on ground-based GNSS and GOMESCIA satellite retrievals, and with reanalyses as auxiliary tools.

European Meteorological Society Annual Meeting 2017, 04–08/09/2017, Dublin, Ireland.

https://meetingorganizer.copernicus.org/EMS2017/presentations/

6.1.17 Luxembourgh

F. N. Teferle
University of Luxembourg, Luxembourg, Luxembourg
e-mail: norman.teferle@uni.lu

Through various projects the University of Luxembourg (ULX) was able to contribute to the objectives of the COST Action. The main activities at ULX revolved about the establishment of two near real-time GPS ZTD processing systems, the establishment of several real-time GPS and multi-GNSS ZTD processing systems and the use of a long-term GPS ZTD processing system as provided by the IGS TIGA Working Group Analysis Centre at ULX for benchmarking. ULX also hosted three STSMs and one ULX researcher visited MétéoFrance under the same scheme. In 2017 ULX established in collaboration with MétéoLux, the national meteorological service of Luxembourg, a new continuous GNSS station at the meteorological site Findel (WMO ID 06590). Besides the inputs from Norman Teferle the contributions came from one PhD candidate (Furqan Ahmed) and two post-doctoral researchers (Wenwu Ding, Addisu Hunegnaw) at ULX and the three STSM visitors (Tzvetan Simeonov, Anna Klos and Tomas Hadaś). Besides numerous presentations at COST Action workshops and international conferences the small team also published six peer-reviewed papers on the related subjects and Furqan Ahmed completed his PhD thesis.

6.1.17.1 Near Real-Time GPS Processing Systems

Two near real-time (NRT) GPS processing systems for ZTD estimation have been developed at ULX. The first one provides hourly NRT solutions with 15-min ZTD estimates and has contributed to the EUMETNET EGVAP program (http://egvap.dmi.dk/) as solution UL01. The second one provided 15-min NRT solutions with 15-min ZTD estimates. This solution was abandoned due to the newly developed real-time processing systems. The NRT system UL01 is based on BSW50 and uses double differencing to process a Europe-wide network (Fig. 6.15). With the support for BSW50 by the University of Berne ceasing in 2017, the system could no longer

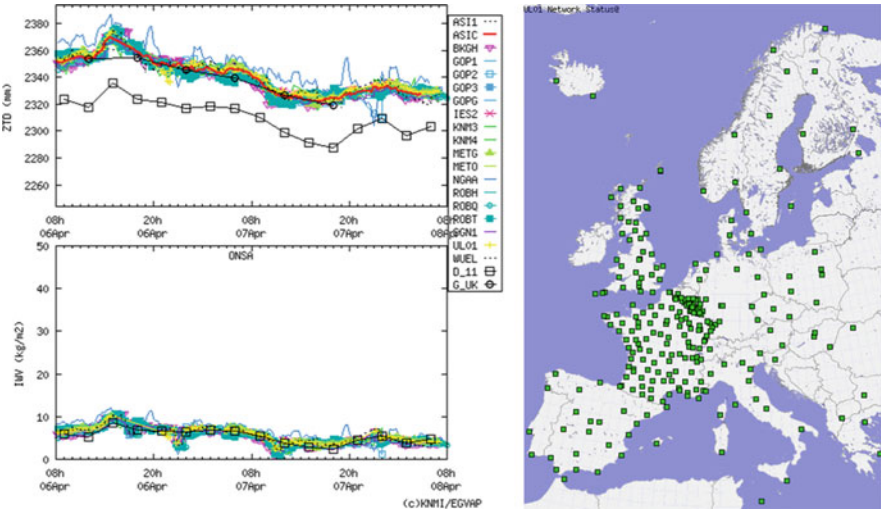

Fig. 6.15 Network of the GNSS stations processed by UL01 (right panel) and evaluation of the UL01 solution (yellow line) by EGVAP (left panel). (Reproduced from egvap.dmi.dk)

be supported. The update of the system to BSW52 is underway and will also allow the inclusion of GLONASS beside that of GPS.

6.1.17.2 Real-Time GPS/Multi-GNSS Processing Systems

The work on the real-time (RT) processing systems involved a comparison of various RT PPP software capable of producing ZTD estimates from GNSS data streams. From this evaluation the software PPP-Wizard was selected to go forward for modifications to develop a multi-GNSS PPP processing system for ULX. Using products from the Centre National d'Études Spatiales (CNES) the system is capable of producing PPP ambiguity resolved solutions with ZTD estimates every few second. ULX contributed to the RT Demonstration Campaign with two solutions based on these systems. In future the RT system can be employed for severe weather monitoring over Luxembourg.

6.1.17.3 Outcomes

Besides the establishment of the various processing systems which can be used for further research and development, the most important outcome for Luxembourg is the fact that it was possible to show that the assimilation of NRT ZTD estimates from UL01 in the AROME numerical weather prediction model of MétéoFrance positively impacts the model output with the potential to improve weather forecasts for Luxembourg and the Greater Region (Fig. 6.16). Using objective forecast skill

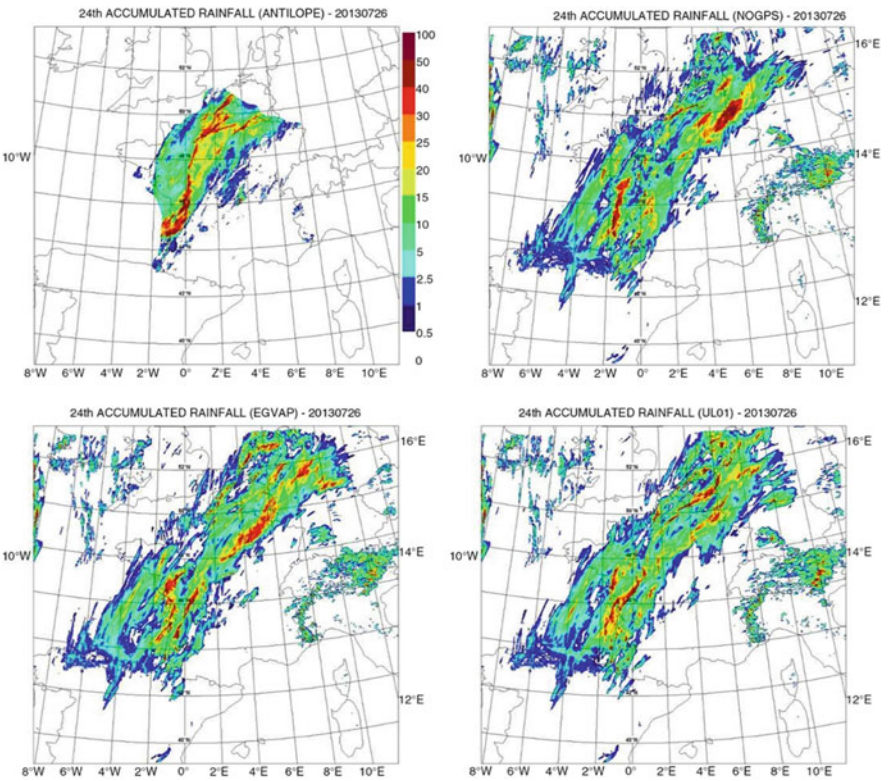

Fig. 6.16 Daily accumulated precipitation in mm as analysed by ANTILOPE and simulated by the AROME model starting from different atmospheric analyses on 26 July 2013: analysis (upper left), experiment NOGPS (upper right), experiment EGVAP (lower left), experiment UL01 (lower right). (Reproduced from Mahfouf et al. 2015)

scores, a small positive benefit has been noticed both on screen-level relative humidity and 24-h precipitation accumulations. The categorical scores are systematically improved when the UL01 data are assimilated on top of EGVAP ZTD observations. When examining case studies, it has been confirmed that GPS ZTD observations affect the predicted location and intensity of rainy systems that generally improves the quality of the numerical forecasts. For such specific situations the additional ZTD data processed by ULX significantly modify rainfall patterns with, most of the time, a better location and intensity of precipitating cells.

Gaining on importance in the future are the results from the long-term GPS processing system when changes in atmospheric water vapour from GNSS are analysed for climate trends. Through the STSM of Anna Klos the ZTD time series of the reprocessed solution from the IGS TIGA analysis centre at ULX were analysed in order to investigate the noise characteristics of these as there may be an impact on the uncertainties associated with the trend estimates. The study showed

that a combination of an autoregressive process with white noise needs to be taken into account when aiming at the estimation of secular trends from ZWD, ZTD or IWV time series. If a proper stochastic model is not employed, one will obtain results that should not be interpreted in terms of climate change as the trend uncertainties may be underestimated by a factor of 5–14 compared to the white noise only assumption. Moreover, a global comparison was performed between the ZTD derived from the ERA-Interim and that derived from ground-based GPS. It was found that the ability of ERA-Interim to predict the ZTD degrades with the increase in the amount of atmospheric water vapour, and vice versa. This comparison was based on a 5-years long dataset comprising of 406 globally distributed GPS stations. The ERA-Interim data was provided by Jan Douša of GOP.

Acknowledgments
Furqan Ahmed and Wenwu Ding were funded by the Fonds National de la Recherche, Luxembourg through projects PWVLUX (Reference No. 1090247) and POSILUX (Reference No. 6823109). Addisu Hunegnaw was funded through the competitive ULX research projects GSCG and SGSL. Besides the IGS and EUREF special acknowledgment is given to the GNSS data provides Walcors, SPSLux and BIGF, who provided real-time streams and hourly RINEX files for the various processing systems at ULX. The Administration des Services Techniques de l'Agriculture (ASTA) and MétéoLux of the Administration de la Navigation Aérienne (ANA) for the provision of meteorological data from Luxembourg and the latter for advise on meteorological aspects and its continued support of ULX GNSS meteorology activities. MétéoFrance is acknowledged for collaboration and the hosting of the STSM of Furqan Ahmed. Finally, Nottingham Geospatial Institute and the UK Met Office are thanked for their support with the near real-time GPS processing systems.

6.1.18 Poland

J. Bosy
Wrocław University of Environmental and Life Sciences, Wrocław, Poland
e-mail: jaroslaw.bosy@up.wroc.pl

J. Kaplon
Wrocław University of Environmental and Life Sciences, Wrocław, Poland
e-mail: jan.kaplon@igig.up.wroc.pl

K. Szafranek
Centre of Applied Geomatics of the Warsaw Military University of Technology, Warsaw, Poland
e-mail: kszafranek@wat.edu.pl

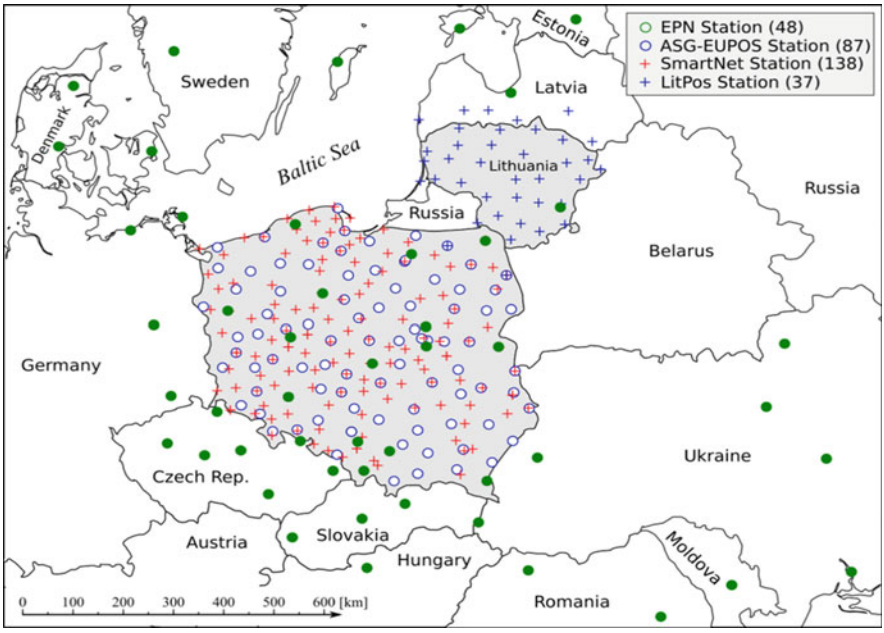

Fig. 6.17 WUEL and WLIT (E-GVAP) networks stations processed for troposphere state estimation at WUELS

ZTD/IWV estimation in Poland: Analysis centre held at Institute of Geodesy and Geoinformatics GNSS&Meteo Working Group of Wrocław University of Environmental and Life Sciences (WUELS) is participating in ZTD/IWV estimation from GNSS data in Poland, Lithuania (in cooperation with Vilnius University) as well as in Victoria state in Australia (in cooperation with RMIT University in Melbourne). ZTD estimates including horizontal gradients from Polish and Lithuanian stations are submitted hourly to the E-GVAP database in COST-716 format. Except of near real-time GNSS data processing, WUELS is also developing ultra-fast ZTD estimation services, estimating troposphere products each 15 min. The pilot implementation of processing engine at Wroclaw Centre of Networking and Supercomputing (WCSS) was developed in 2017. The ultra-fast processing is now optimized to process GNSS data from 50 stations (15 EPN + 35 selected from Leica SmartNet, Fig. 6.17).

The details of WUELS GNSS data processing activities for troposphere study are as follows:

- WUEL network (submitted to E-GVAP): since 2012, 225 stations (EPN + ASG-EUPOS+SmartNet),
- WLIT network (submitted to EGVAP): since 2016, 50 stations (EPN + LitPOS),
- VICNET network (Australia): since 2015, 149 stations (IGS + APREF+GPSNet).

- Ultra-fast processing (each 15 min) for EPN and SmartNet stations in Poland (50 stations).

WG1 tasks: Except of ZTD/IWV estimation the GNSS&METEO research group at WUELS is working on real-time ZTD multi-GNSS (GPS/GLO/GAL/BDS) PPP service, tropospheric refractivity and slant path delays estimation from NWP models and GNSS data as well as real-time precise point positioning augmented with high-resolution NWP models. Research group at Advanced Methods for Satellite Positioning Laboratory University of Warmia and Mazury in Olsztyn (UWM) is working on exploitation of NWP-derived tropospheric products in RTK positioning and GNSS-derived IWV vs. microwave radiometer data analysis.

WG2 tasks: Two Polish research groups were working on WG2 tasks including GNSS RO processing and raytracing in NWP WRF model domain (WUELS), GNSS tomography TOMO2 software development (WUELS), assimilation of GNSS data from local dense GNSS networks in NWP WRF model (WUELS) and Centre of Applied Geomatics of the Military University of Technology in Warsaw (MUT).

WG3 tasks: The research on noise characteristics in ZTD from homogeneously reprocessed GPS time series was performed at MUT as well as the investigation of the influence of adopted GNSS processing strategy on ZTD parameter, including e.g. various mapping functions, elevation mask, troposphere alignment or software. The same group was working on the influence of incorrectly modelled vertical position on tropospheric delay parameters and uncertainties of ZTD linear trend estimation process.

MUT contributed significantly with synthetic benchmark datasets for homogenization of IWV time series retrieved by GPS delivered to the GNSS4SWEC community. WUELS group investigated on refractivity coefficients obtained from ERA-Interim data.

Research group at UWM analysed the influence of troposphere modelling on the realization of the ETRS89 by the reference stations of the Polish national Ground Based Augmentation System (GBAS) network – ASG-EUPOS, and also on the tropospheric parameters. In addition, the influence of the network design strategy on the estimated coordinates of permanent stations, ZTD and gradients time series was investigated, especially in the context of GNSS meteorology and climate studies (Stepniak et al. 2018). Other goal of UWM study was to test and compare of relative and precise point positioning (PPP) techniques to determine which processing is most suited for achieving high accuracy, stability, and homogeneity in the estimated tropospheric parameters.

6.1.19 Portugal

R. Fernandes
University of Beira Interior, Covilhã, Portugal
e-mail: rmanuel@di.ubi.pt

P. Viterbo
Instituto Português do Mar e da Atmosfera, Lisbon, Portugal
e-mail: pedro.viterbo@ipma.pt

A. Sá
Polytechnic Institute of Guarda, Guarda, Portugal
e-mail: andre_sa@ipg.pt

6.1.19.1 Areas of Research

(a) GPS data processing for tropospheric products using GIPSY-OASIS; Improvement on the solutions testing different parameterization.
(b) Development of new software using parallelized Algebraic Reconstruction Techniques (ART) for the water vapour tomography.
(c) Analysis of the influence of a-priori values on the derived ZTD solutions. The daily boundary problem.
(d) Correlation between (ocean and atmospheric) loading and PWV.
NUVEM – New methods to Use GNSS Vapour Estimates for Meteorology of Portugal.

NUVEM is using 146 GNSS stations (Fig. 6.18) from six GNSS receiver networks over Portugal and Spain. NUVEM is operational (http://nuvem.di.ubi.pt) and the implemented processing in shown in Fig. 6.19. The water vapour tropospheric tomography has been one of the areas with strong research. A tomographic software (SWART – SEGAL GNSS Water Vapour Reconstruction Image Software) to estimate the 3D field of tropospheric water vapour in a region, in order to evaluate its high spatial-temporal variability in a 4D reference (spatial 3D plus time) was developed from scratch at SEGAL (UBI/IDL) and applied to a set of case studies. In respect of the COST action, SWART was used in an intercomparison study for cross-validation concerning the potential of GNSS tomography for meteorological applications and for tomographic methodological improvements.

The periodic Ocean Tide Loading (OTL) effects in tropospheric delays have been also studied. OTL corrections are not perfect, especially at coastal sites where OTL is several cm and mismatches between predicted and actual OTL can reach the cm level. Using the latest ocean tide models and an improved elastic model of the Earth, better OTL and therefore better ZTD estimates will be produced for selected coastal sites (Fig. 6.20).

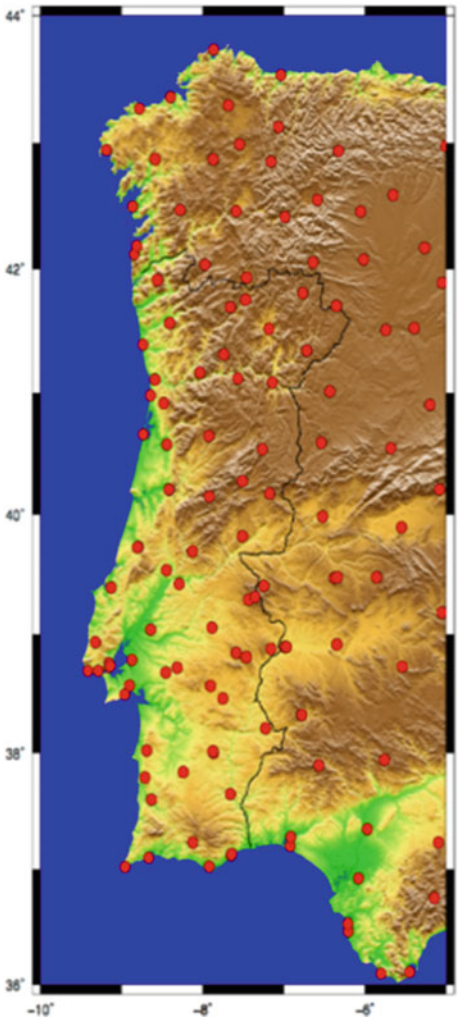

Fig. 6.18 NUVEM GNSS stations

6.1.20 Slovakia

J. Hefty
Slovak University of Technology, Bratislava, Slovakia
e-mail: jan.hefty@stuba.sk

M. H. Igondova
Slovak University of Technology, Bratislava, Slovakia
e-mail: miroslava.igondova@stuba.sk

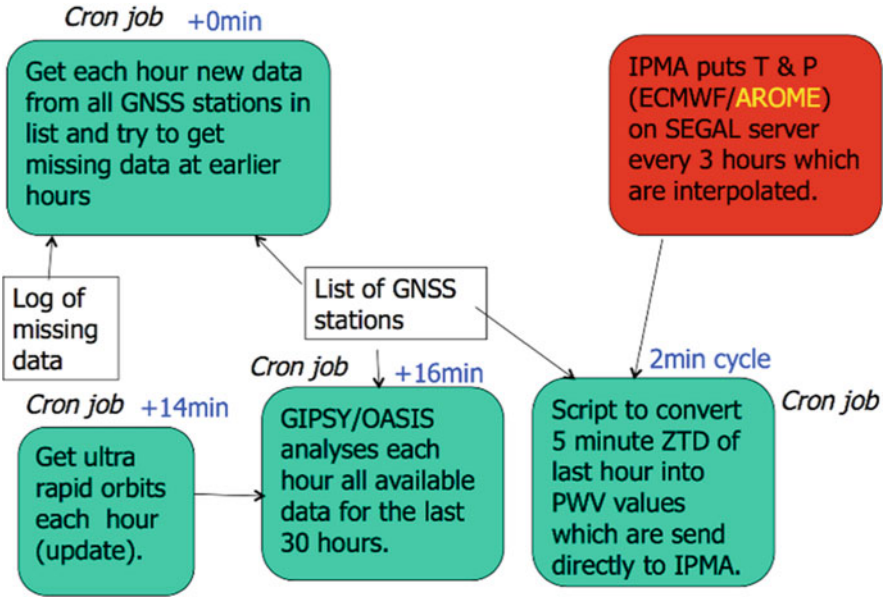

Fig. 6.19 NUVEM implemented structure

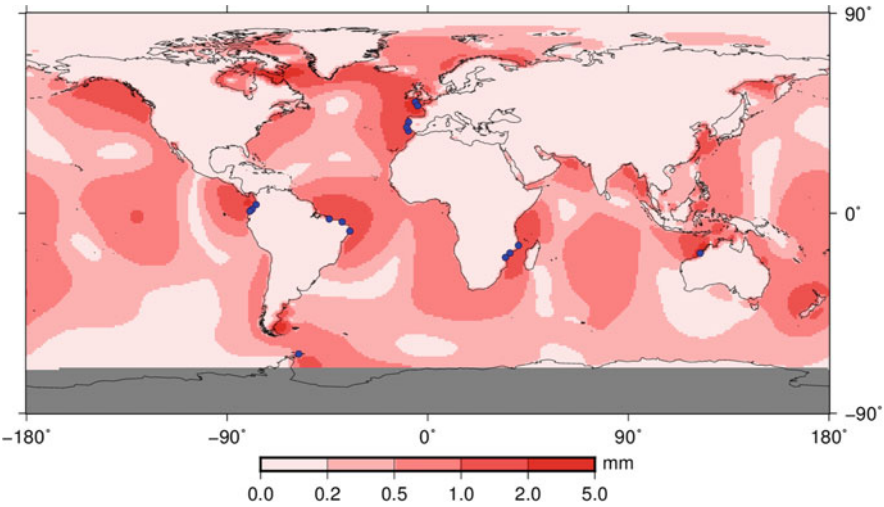

Fig. 6.20 Difference in vertical ocean tide loading (computed using tide model FES2004, harmonic M2) using the standard PREM and modified PREM elastic Earth model. The blue dots represent GNSS stations

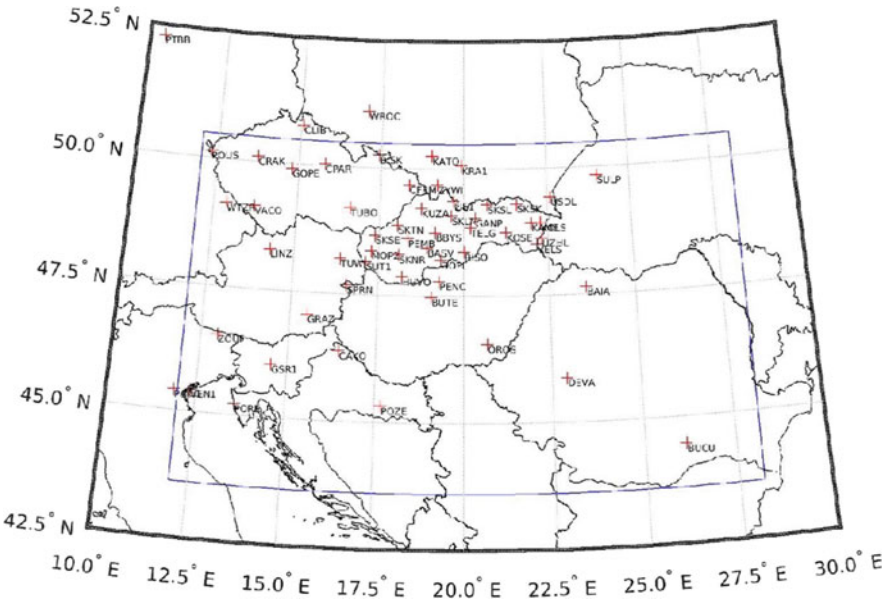

Fig. 6.21 GNSS station network

In last 4 years we have achieved at Slovak University of Technology (SUT) in Bratislava significant progress in Global Navigation Satellite Systems (GNSS) meteorology. There was developed a routine hourly processing system based on BSW52, which is computing ZTDs from network of selected national permanent GNSS stations extended by stations from neighbouring countries. Our processed network recently consists in full constellation from 59 permanent stations (Fig. 6.21). Twenty-two of them are from Slovak National Network of GNSS stations, maintained by Slovak University of Technology, Department of Theoretical Geodesy, and by Geodetic and Cartographic Institute in Bratislava. We have established beneficial cooperation with Slovak Hydro-Meteorological Institute (SHMU) in Bratislava. SHMU is providing us pressure, temperature and relative humidity at all Slovak GNSS permanent stations from numerical weather prediction model ALADIN. With these meteorological data we are able to transform ZTD at permanent stations to PWV and visualize ZTD and PWV maps over Slovakia. Selected results are available online at http://space.vm.stuba.sk/pwvgraph/. Files of ZTD for direct assimilation to numerical weather prediction model are generated every 6 h.

We assimilate our estimated ZTD to non-hydrostatic spectral mesoscale AROME model with three-dimensional data assimilation system. At this state we are able to apply ZTD from 53 stations. Static bias correction of ZTD, estimated from statistics of first guess departures between AROME and ZTD at station, is used to correct ZTD before assimilation. In last year we have performed several impact studies of

ZTD assimilation to accumulated rainfall, relative and specific humidity and others atmospheric parameters. This impact studies were made on interesting meteorological situations like heavy rainfall or strong wind. More data assimilation studies and technical work will be necessary until we will be fully prepared to assimilate ZTD into operational numerical weather prediction model. For more information, please contact responsible researcher from SUT Martin Imrisek via e-mail martin.imrisek@stuba.sk.

6.1.21 Spain

E. Priego
Universidad Politécnica de Valencia, Valencia, Spain
e-mail: epriego@cgf.upv.es

Spain's participation in this action is based on the work of three organisations: National Geographic Institute (IGN), Spanish Meteorological Agency (AEMET), Polytechnic University of Valencia (UPV) and Public University of Navarra (UPN).

Firstly, National Geographic Institute manages a network of about 85 GNSS permanent stations, 26 of them integrated in international networks such as EUREF and IGS (Fig. 6.22).

Fig. 6.22 IGN GNSS permanent stations network (ERGNSS)

IGN GNSS permanent stations network (ERGNSS): IGN is a EUREF Local Analysis Centre (LAC) since 2001, processing a subnetwork of 75 EPN stations and therefore submitting troposphere files for the project "Troposphere Parameter Estimation" where ZPD series and other products are being elaborated since 2001. On the other hand, this institution is an E-GVAP Analysis Centre since 2008, providing ZTD from about 340 stations for Spain and Portugal in near real time. For this purpose, 1 h GNSS data files are downloaded every hour from 22 regional networks servers and immediately after the download, the processing starts, submitting to EUMETNET partner agencies files containing ZTD every 15 min in cost2.2 format. The processing is run with BSW52 and it takes 5 min. About 300 of the processed stations are located in the Iberian Peninsula, about 70 IGS or EPN stations and 10 E-GVAP "supersites" in order to check the ZTD quality estimation. The standard deviation for the ZTD estimation use to be about 7–8 mm.

IGN, as EUREF LAC, has participated in the second reprocessing of the EPN, carried out in 2015 (Fig. 6.23). Thanks to this project, a new set of homogeneous ZPD have been obtained from the combination of individual LAC solutions in the whole EPN network. IGN processed a subnet of 125 EPN stations from 1996 to 2014.

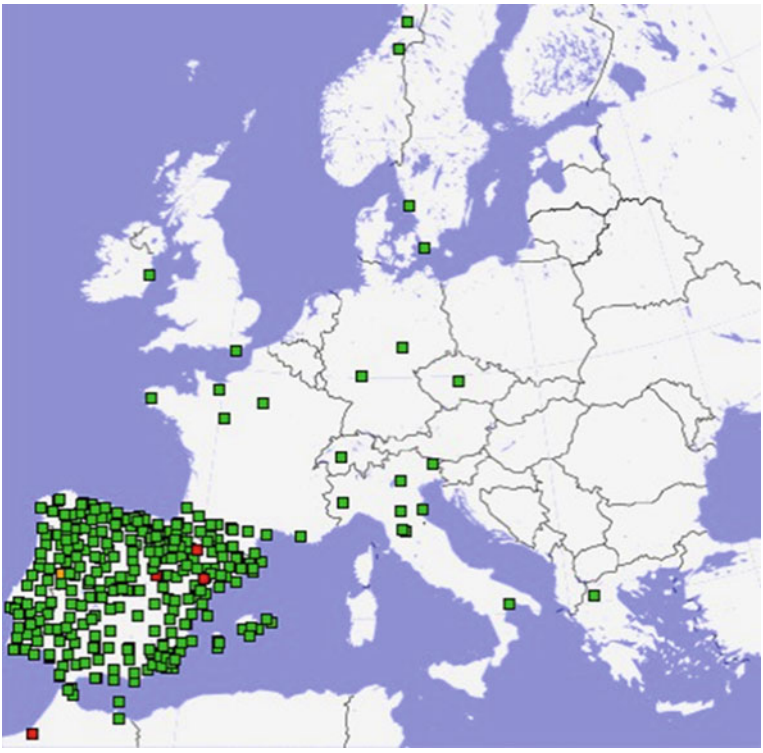

Fig. 6.23 GNSS network processed by IGN in EGVAP project (from http://egvap.dmi.dk)

Secondly, the Spanish Meteorological Agency (AEMET) started in 2001 with the assimilation of GNSS ZTD observations in HIRLAM and HARMONIE-AROME high resolution models in the framework of other European projects like COST717 and TOUGH. During this Action ES126, AEMET has also participated in the HyMeX project, assimilating GNSS ZTD observations together with data targeting of radiosondes on a series of experiments over the Mediterranean area. At the beginning of the Action, AEMET prepared the HARMONIE-AROME km scale data for assimilation of GNSS ZTD observations. A three-dimensional variational data assimilation was applied and the importance of using an extensive observation handling was pointed out, and in particular the benefit of using an adaptive so called variational bias correction for these observations. Currently, AEMET is assimilating operationally more than 200 GNSS sites over Iberian Peninsula and Canary Islands domains together with conventional and ATOVS observations due to the good impact found on the assimilation of this humidity source. A daily monitoring of the availability and quality of the data is therefore performed over the two domains.

And thirdly, the Polytechnic University of Valencia and the Public University of Navarra have been several research on the analysis of local rainfalls with ZTD GNSS. In 2013, the first experiments were focused in the relationship between rain occurrence and atmospheric pressure and atmospheric water vapour content (PW-GNSS estimated). The available 9 years' time series in Pamplona of each variable were analysed. It allowed to state the existence of three rain patterns and monthly differences in the pressure and precipitable water combinations.

Later, it was analysed all the cases of heavy rain over 15 years in Valencia city (Fig. 6.24). In all of these cases, it exists an apparent link between pressure drops at times of high levels of IWV with severe precipitation events. In 2017, additional case studies are being developed to quantify this apparent link and it might be the basis for a future severe weather warning system.

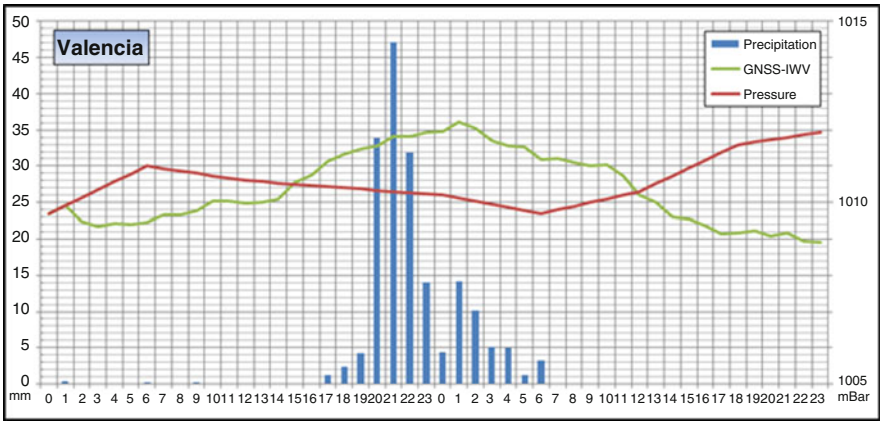

Fig. 6.24 Time evolution of IWV and atmospheric pressure along with the amount of rainfall registered

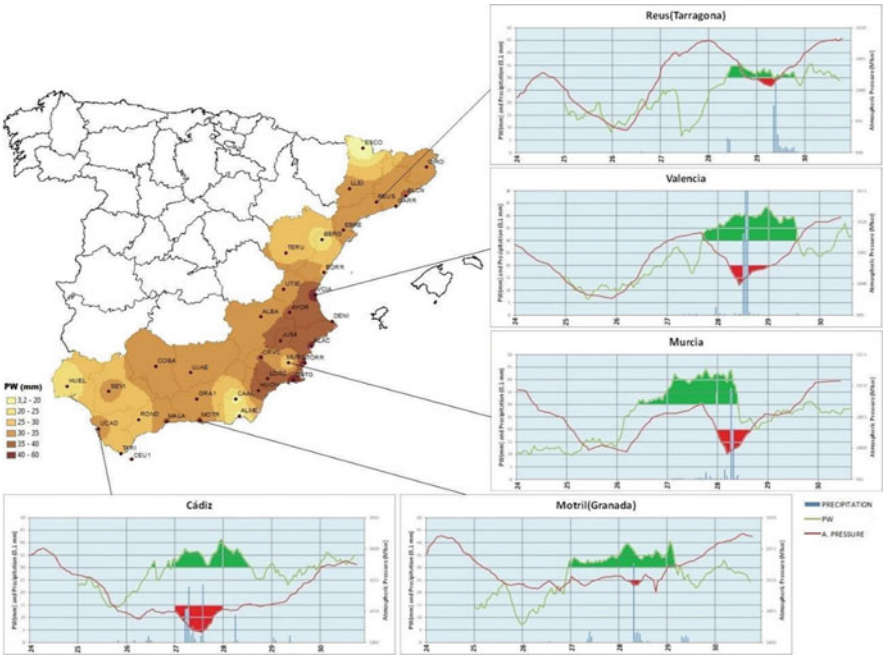

Fig. 6.25 Spatial distribution of IWV along the Spanish Mediterranean coast

Apart from that, several monitoring ZTD GNSS during some heavy rainfall event have been conducted (Fig. 6.25). Those analyses are being done in the Spanish Mediterranean area, where Precipitable Water values are higher, due to the contribution of moisture from the Mediterranean Sea. All GNSS stations show a quick and clear increase in IWV a few hours before the onset of precipitation.

The results of all of this research have been published in four papers of different journals (Appendix 4).

6.1.22 Sweden

G. Elgered
Chalmers University of Technology, Gothenburg, Sweden
e-mail: gunnar.elgered@chalmers.se

M. Lindskog
Swedish Meteorological and Hydrological Institute, Gothenburg, Sweden
e-mail: Magnus.Lindskog@smhi.se

M. Ridal
Swedish Meteorological and Hydrological Institute, Gothenburg, Sweden
e-mail: Martin.Ridal@smhi.se

U. Willén
Swedish Meteorological and Hydrological Institute, Gothenburg, Sweden
e-mail: Ulrika.Willen@smhi.se

T. Ning
The Swedish Mapping, Cadastral and Land Registration Authority, Gävle, Sweden
e-mail: tong.ning@lm.se

Since June 2016 Lantmäteriet (Swedish Mapping, Cadastre and Land Registration Authority) became one of the analysis centres in E-GVAP and is in charge of the data processing for the GNSS stations in Sweden, Finland, Norway, Denmark, and some IGS stations, in total approximately 700 (Fig. 6.26). Two near real-time (NRT) ZTD products (NGA1 and NGA2) are currently provided. The NGA1 product is obtained from the BSW52 network solution, while the NGA2 is from the GIPSY/OASIS II v.6.2 data processing using the Precise Point Positioning (PPP) strategy.

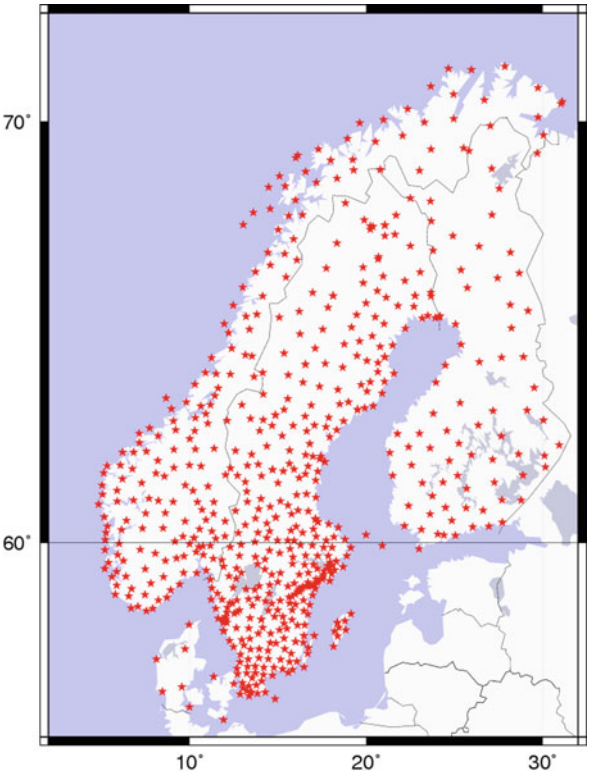

Fig. 6.26 GNSS stations processed by Swedish mapping, cadastre and land registration authority

The NGA1 product is obtained from a BSW hourly data processing. We use the ultra-rapid GPS orbit products provided by CODE (ftp.unibe.ch). The ocean tide loading correction (FES2004) and the antenna PCV absolute calibration are implemented. The tropospheric estimates are updated every 15 min and a 10° elevation cut-off angle is used with a GMF. The NGA1 product is currently under the operational status with a time delay of 45 min.

The NGA2 product from the GIPSY NRT data processing where the GPS data were analysed by GIPSY-OASIS v6.2 using the PPP strategy. Currently we use the ultra-rapid GPS orbit and clock products provided by JPL. The same set-ups are used for the GIPSY data processing, i.e., FES2004 model, antenna PCV absolute calibration, a 10° elevation cut-off angle, and a GMF. The tropospheric estimates are updated every 5 min. In addition, the single receiver phase ambiguity resolution is also implemented. The NGA2 product is now under a test mode due to a longer time delay of about 1.5 h for fetching the JPL ultra-rapid orbit and clock products.

The benefit of using GNSS ZTD in the state-of the art HARMONIE-AROME km-scale data assimilation and forecasting system has been demonstrated in cooperation with colleagues from Spain, Norway and Iceland (Sánchez Arriola et al. 2016). A three-dimensional variational data assimilation was applied and the importance of using an extensive observation handling was pointed out, and in particular the benefit of using an adaptive so called variational bias correction. Based on the research GNSS ZTD is now used operationally in the Nordic MetCoOp HARMONIE-AROME numerical weather prediction system (Muller et al. 2017). The system has been further optimized through sensitivity experiments and the benefit of utilizing GNSS ZTD processed by the newly re-vitalised NGAA processing centre has been demonstrated (Lindskog et al. 2017). GNSS ZTD data from the NGAA processing centre is recently assimilated operationally in the Nordic MetCoOp HARMONIE-AROME numerical weather prediction system, in addition to GNSS ZTD processed by the Met Office processing centre in the UK (METO) and by the Royal Observatory of Belgium (ROBH).

The uncertainty of the IWV estimated from GNSS observations needs to be thoroughly assessed as required by climate applications. All relevant error sources in GNSS-derived IWV are therefore essential to be investigated. A theoretical analysis was carried out where the uncertainties associated with the input variables in the estimations of the IWV were combined in order to obtain the total uncertainty of the IWV. We calculated the IWV uncertainties for several sites, used by the Global Climate Observing System (GCOS) Reference Upper-Air Network (GRUAN), with different weather conditions. The results show a similar relative importance of all uncertainty contributions where the uncertainties in the ZTD dominate the error budget of the IWV, contributing over 75% of the total IWV uncertainty. The impact of the uncertainty associated with the conversion factor between the IWV and the ZWD is proportional to the amount of water vapour and increases slightly for moist weather conditions (Ning et al. 2016a).

Estimated horizontal gradients were used as a tool for assessment of GNSS data quality**.** We have searched for any systematic changes in the horizontal gradients using 17 years (1997–2013) of estimated gradients from GPS data for 21 sites in

Sweden. We conclude that estimated gradients from GPS data are not only of an atmospheric origin. Statistics of long term time series can be a valuable tool to search for problems in the GPS data, such as sudden changes in the electromagnetic environment of the GPS antenna. Long-term trends estimated in the IWV are important for climate monitoring as an independent data source. However, potentially unwanted temporal shifts in the IWV time series from the different techniques can change the trends significantly. In order to obtain reliable climate signals a homogenization of the IWV time series is necessary. The time series of the differences between the GPS-derived IWV and the one obtained from the ERA-Interim model was used for the data homogenization. A statistical test, the penalized maximal t test, modified to account for first-order autoregressive noise (PMTred), is used to identify possible sudden mean shifts in the time series. Different tunings are also carried out in the PMTred test in order to find the optimal set up for the data homogenization (Ning et al. 2016b).

A 17-year long time series (1997–2013) of IWV obtained from homogenously reprocessed ground-based GNSS data was produced. The GNSS data were acquired at 123 European sites located between the latitudes 39°N and 79°N, and between the longitudes −69°E and + 31°E. The IWV data set was used for evaluation of the atmospheric water vapour content in a regional climate model, both in terms of a comparison of monthly means and for diurnal components (amplitude and phase) (Ning et al. 2013).

Climate models overestimate the positive feedback from the greenhouse effect of water vapour for ENSO (Chen et al. 2013). Therefore, it is important to evaluate observations of water vapour and the relation to global phenomena as El Niño/Southern Oscillation (ENSO) and other climate processes. We used monthly means of water vapour data, from GPS and ERA-Interim reanalysis, to investigate global inter-annual water vapour climate variability by calculating the correlations with climate indices representing ENSO and the North Atlantic Oscillation (NAO). The GPS IWV data came from reprocessed ZTD solutions from the IGS network, we used 120 stations worldwide for the time-period 1995–2010. The ERA-Interim IWV was extracted for the four closest grid-points to the GPS station and vertically adjusted to the station height using ERA-Interim temperature and humidity fields on pressure levels and thereafter horizontally interpolated to the station. The climate indices ENSO Nino3.4 and NAO were obtained from NOAA. We find that GPS and ERA-Interim IWV correlates with the ENSO and NAO indices on global and regional scales, the pattern resembles corresponding patterns for surface temperature and precipitation for both ENSO and NAO as expected. The GPS and ERA-Interim IWV correlations with the indices are fairly similar except for ENSO over Antarctic. The study will be continued after the COST project including other climate processes and indices on seasonal and monthly scales, for evaluation of the Swedish global climate model EC-Earth and other CMIP5 and CMIP6 models. A main benefit of the GPS IWV data, compared to reanalysis data is the high temporal resolution, as shown by Bock et al. (2007). Investigating water vapour variability on shorter time scales than 2 days could show the benefit of using GPS data for climate process evaluations.

6.1.23 Switzerland

E. Brockmann
Swiss Federal Office of Topography, Wabern, Switzerland
e-mail: Elmar.Brockmann@swisstopo.ch

K. Wilgan
Wrocław University of Environmental and Life Sciences, Wrocław, Poland
e-mail: karina.wilgan@igig.up.wroc.pl

A. Geiger
ETH Zurich, Zürich, Switzerland
e-mail: alain.geiger@geod.baug.ethz.ch

GNSS-Meteo activities at Swisstopo: Swisstopo is active in the GNSS-Meteo field since 2000 and contributed to the COST-716 project as well as to the EUMETNET E-GVAP projects until today. There are important synergies between geodetic applications and meteorological applications. In the near real-time field, hourly solutions are computed to validate the stability of the reference points. As an added-value results of ZTD parameters are determined and submitted to MeteoSwiss and to UK Met Office for numerical weather prediction applications. Figure 6.27 shows the monitoring status of the network consisting of about 200 stations. On the long-term, a reprocessing was carried out in 2014. Data of about 200 stations, covering a time span starting 1996, were analysed with various options in a homogeneous way using the BSW52. Since 2004, also GLONASS observations were used. As a result, homogeneous series of coordinates as well as for ZTD parameters

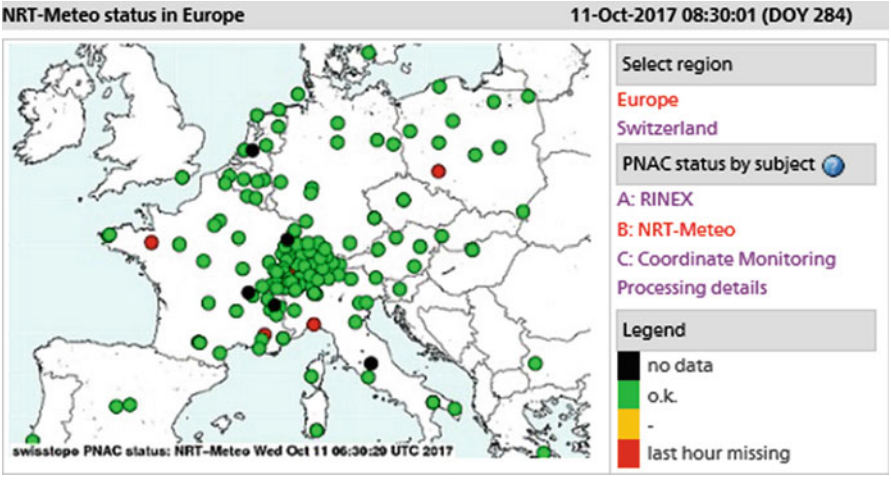

Fig. 6.27 Near real-time status of the hourly Swisstopo processing for the delivery of ZTD parameters (October 11, 2017). Hourly updates at http://pnac.swisstopo.admin.ch/

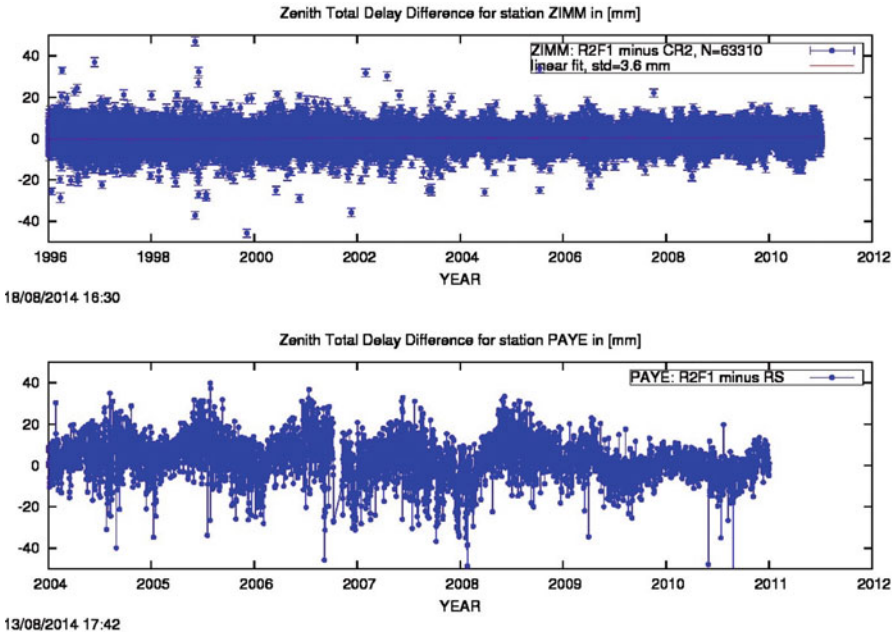

Fig. 6.28 Swisstopo Repro2 compared with CODE Repro2 for station ZIMM (upper diagram) and with radiosonde derived ZTD estimates for station PAYE (lower diagram)

were generated. Overlapping 3-day solutions were generated to optimize the ZTD estimates at midnight. The long-term ZTD parameters were compared to other post-processing results as well compared to radiosonde data (Fig. 6.28). The impact of additional GLONASS observations on the long-term was especially analysed in this project. Fortunately, the impact of the additional GLONASS observations is negligible when analysing ZTD trends.

In 2015, the complete Swiss GNSS network AGNES was enhanced with GPS + GLO + GAL+BDS capable receivers. In 2016, most operational computations are based on Multi-GNSS already. The complete data flow was switched from RINEX-2 to RINEX-3 and the analysis is performed on a Multi-GNSS development version BSW5.3 (Fig. 6.29).

Many tools, developed to analyse the reprocessing results within the COST GNSS4SWEC project, are applied in the operational processing scheme. Routinely, various validations of the complete time series, consisting of reprocessing results till end 2014 and operational solutions till today, are calculated and made available on the Swisstopo web. These type of plots are available:

- ZTD differences at 30 double stations (nine in Switzerland),
- ZTD differences to radiosondes (61 stations),
- ZTD estimation details (including estimated formal RMS values, spectral analyses and estimation of an approximated mean ZTD model; Fig. 6.30).

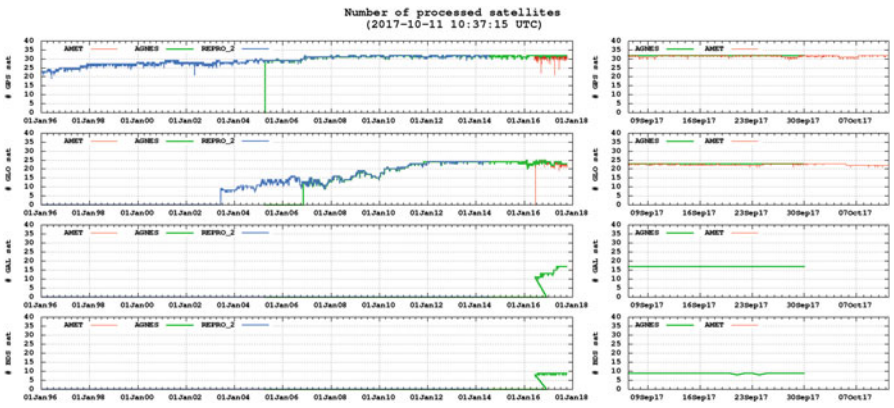

Fig. 6.29 Number of satellites used in the various processing chains (GAL+BDS processing since June 2016)

GNSS-Meteo activities at ETHZ: The Mathematical and Physical Geodesy chair, former Geodesy and Geodynamics Lab at ETH Zurich has developed a software package COMEDIE (Collocation of Meteorological Data for Interpretation and Estimation of Tropospheric Path delays) to interpolate and extrapolate meteorological and tropospheric parameters, especially zenith path delays, from the real measurements to the arbitrary locations. The method used in the software is the least-squares collocation technique, where each observation is divided into a deterministic part, a regular stochastic part (signal) and an irregular stochastic part (noise). The selected parameters from different data sources are estimated simultaneously in the least-squares sense taking into account the two kinds of errors. Using the obtained model coefficients, it is possible to reconstruct the value of considered parameter at any time and place. Originally, the software was used to interpolate the meteorological parameters: air pressure, temperature and humidity, but currently also the models of refractivity and tropospheric delays are implemented. The input data source in the software can be ZTD from Swisstopo or meteorological parameters from ground-based stations, radiosondes or numerical weather model (NWM). The tropospheric models calculated with COMEDIE can be used in any measuring technique where a microwave signal is delayed in the atmosphere, especially for GNSS Precise Point Positioning (PPP). Currently at ETHZ, the COSMO-1 model from MeteoSwiss along with ZTDs from Swisstopo processing are used as a base of building the tropospheric correction's model for space-borne Synthetic Aperture Radar Interferometry (InSAR), In a regional scale, it is possible to also use the relative ZTDs from a network of permanent GPS stations operated in the Matter Valley (Swiss Alps) since winter 2010/2011 in the framework of the interdisciplinary project X-Sense. Currently there are 32 stations equipped with low-cost L1 GPS receivers. The major goal of the X-Sense project is the monitoring of alpine mass movements such as rock glaciers.

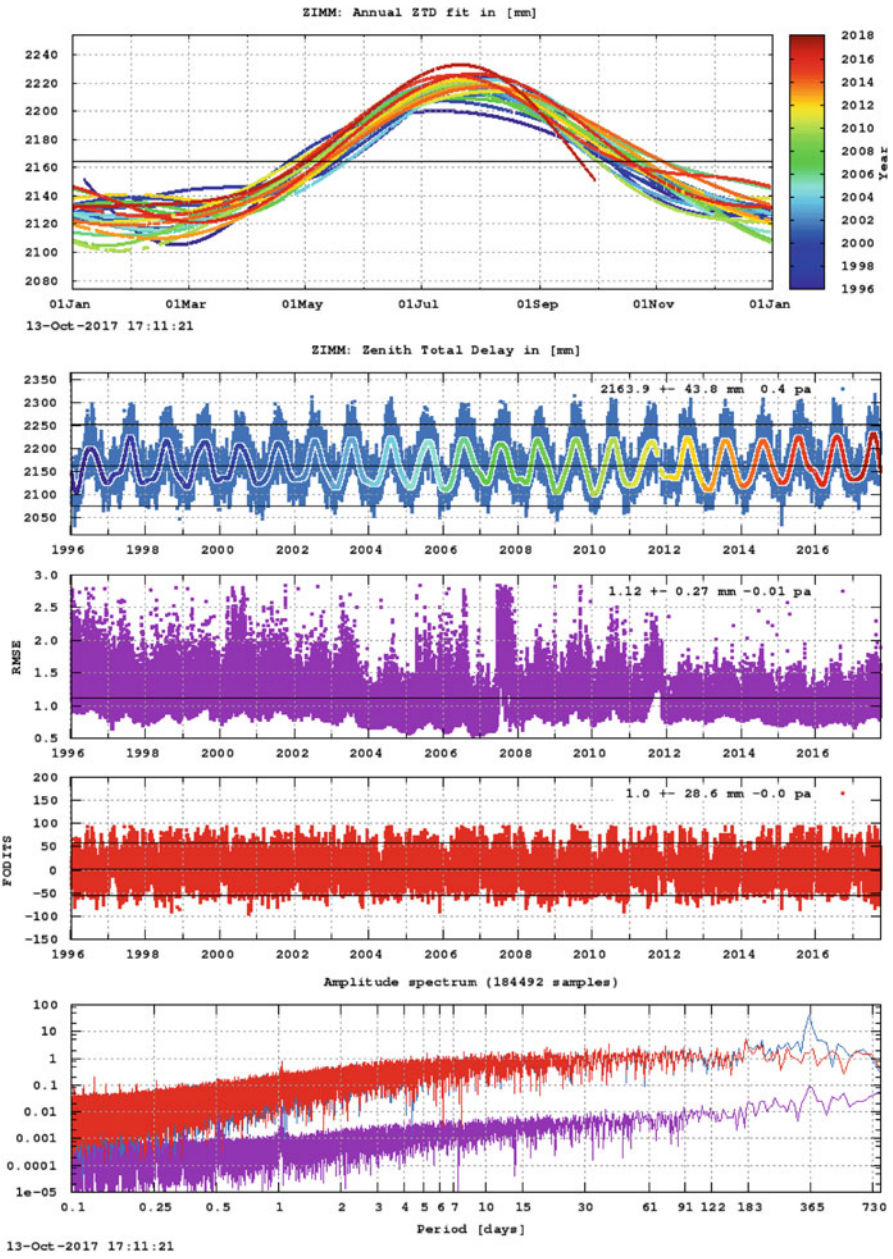

Fig. 6.30 Details of the ZTD estimates (Repro till end 2014, then continued with operational) for station ZIMM. Mean annual model (upper graph) and various other information (lower graph)

In the context of environmental and climate research, ETH develops the applications of GNSS in reflectometric methods for the determination of snow depth and snow water equivalents. The meteorological data which is used in the studies described above is mostly provided by MeteoSwiss (http://www.meteoswiss.admin.ch). The SwissMetNet network of ground-based meteorological stations consists of about 160 automatic monitoring stations. Standard stations record temperature, humidity, atmospheric pressure, solar radiation and the volume of precipitation as well as the wind direction and speed with 10 min resolution. The only aerological sounding station is located at the Payerne regional centre of MeteoSwiss. The measurements are taken twice a day at midnight and 12:00 UTC. The balloons are tracked up to an altitude of 30–35 km. The radiosondes measures wind speed and direction, air pressure, temperature and humidity. MeteoSwiss uses two radiometer types to measure temperature (TEMPRO, HATPRO) and humidity profiles (HATPRO) which provide vertical profiles from ground up to approximately 6 km every 10 min. The average vertical resolution is around 500 m. The temperature profiles allow to detect certain patterns in the atmosphere like temperature inversions in the troposphere. The temperature and humidity radiometers are also used in the meteorological surveillance tool of nuclear power plants (CN-MET).

MeteoSwiss uses the COSMO (Consortium for Small-scale Modelling) NWM. There are currently three configurations of COSMO models:

- COSMO-1: High-resolution model for short-range weather forecast for current and next day; grid size: 1.1 km, area: the entire Alpine region
- COSMO-E: This ensemble model calculates a probabilistic forecast based on 21 individual model runs.; grid size 2.2 km, area: the entire Alpine region
- COSMO-7: Lower-resolution model with forecasts for 3 days ahead; grid size: 6.6 km; area: central and western Europe.

6.1.24 Turkey

C. Mekik
Bulent Ecevit University, Zonguldak, Turkey
e-mail: cetinmekik@beun.edu.tr

Recent studies on GNSS Meteorology in Turkey: The Project titled "The Estimation of Atmospheric Water Vapour Using GPS "is supported by The Scientific and Technological Research Council of Turkey (TUBITAK) (May 2013–October 2015). Aims of this project are to determine the total zenith delays and the precipitable water vapour accurately and reliably from TUSAGA-Active (CORS-TR), and to produce the numerical models based on time and position In this context, the weighted mean temperature model ($T_m = 48.55 + 0.80T_s$) and the conversion factor model (QBEU = 5.7053–0.0067 (Ts [K]-287.7620) + 0.0130 θ [°] + 0.0833 H [km] + 0.0709sin (2πtD365) +0.1195 cos(2πtD365)) are developed by analysing 8 radiosonde stations in Turkey (4103 radiosonde profiles for the year of 2011).

PWV are estimated from a year of observations at the Ankara and Istanbul RS-GNSS stations (PWV_{GNSS}) and later they are compared with PWV derived from radiosonde observations (PWV_{rad}). Standard deviations of the differences of PWV_{GNSS} from PWV_{rad} are consistent with Haase et al. (2003) (7 ± 12 mm), (-2.8 ± 4.1 mm).

Since May 2013, the ZTDs and PWVs have been being estimated using regional or global networks at Bulent Ecevit University, Geomatics Engineering Department. As a result of studies conducted until 2015, Turkey finally started to take steps to join near real-time activities exploiting the meteorological aspects of the dense CORS-TR (Continuously Operating Reference Station called TUSAGA-active) network of 146 reference stations operated by General Command of Mapping and Organization of the General Directorate of Land Registry and Cadastre in Turkey for positioning applications. However, at the moment several permanent GNSS stations belong to Bulent Ecevit University (BEU) and Bursa Water and Sewerage Administration (BUSAGA Network) are actively being used for computation of NRT-ZTDs. It has been initiated to include the CORS-TR stations in the NRT-ZTD estimation processes. The hourly observations of 18 Turkish permanent GNSS stations belong to BEU (Bulent Ecevit University), ISKI-UKBS and BUSAGA Network are processed. This network is extended beyond the country to cover about 40 stations covering Europe. The data analysis is being carried out using the BSW52 GPS data processing software with the help of powerful computer obtained through the grant of TUBITAK (The Scientific and Technological Research Council of Turkey) project no. 112Y350.

The tropospheric estimates have been obtained from the Analysis Centre (AC) at the Bulent Ecevit University which has been established with the help of Jan Douša from GOP (Geodetic Observatory Pecny) using Trop-NET software package, and routinely estimating ZTD's since July 2015. This analysis centre called BEU1, has been joined E-GVAP (GNSS Water Vapour Programme of the Network of European Meteorological Services, EUMETNET) and thus continuously sending results to E-GVAP system.

6.1.25 United Kingdom

J. Jones
Met Office, Exeter, UK
e-mail: jonathan.jones@metoffice.gov.uk

6.1.25.1 History of GNSS Meteorology at the UK Met Office

The Met Office has had an interest in GNSS as far back as 1998, when a small number of Ashtech Z-XII receivers and choke-ring antennae were purchased and installed at locations in the UK collocated with other meteorological remote sensing equipment, such as at operational radiosonde sites. At this time, the main purpose of

the GPS receivers was experimental (was there additional, useful information which could be obtained from GNSS?), primarily for validation of radiosonde humidity data. Between 1998 and 2003, the Met Office sent raw GNSS data to the Geodetic Observatory Pecny, Czech Republic (http://www.pecny.cz/gop/) for processing. Data would then be send on CD-ROM back to the Met Office for comparison against radiosonde humidity data. It was soon evident that not only was GNSS useful for radiosonde validation but was of sufficient quality to be assimilated operationally. A number of case studies were carried out using GNSS data to identify radiosonde dry humidity bias cause by solar heating of the radiosonde sensor, and following this assessment, it was deemed that GNSS was in fact more reliable than radiosonde for retrieving an integrated total column water vapour observation.

In 2003, the Met Office invested in GNSS-meteorology by determining that it needed its own operational processing capability and partnered with the Institute of Engineering, Surveying and Space Geodesy (IESSG), Nottingham University (now the Nottingham Geospatial Institute – https://www.nottingham.ac.uk/ngi/) to develop an robust 24/7 processing system, and awarded IESSG an R&D contracts to develop and deliver such a system to the Met Office.

In 2004, the Met Office took delivery of a prototype system based around Bernese v4.0 in double-difference mode, processing around 100 IGS and EUREF sites in near real-time. Over time, the system was upgraded to a Bernese v5 system processing over 200 sites from a European domain to feed the North-Atlantic and European (NAE) NWP model, which culminated in April 2007 with operational assimilation of GNSS ZTD data into the Met Office NAE model. At the time, the UK Met Office was the first national met service in the world to be processing and assimilating GNSS data (Fig. 6.31).

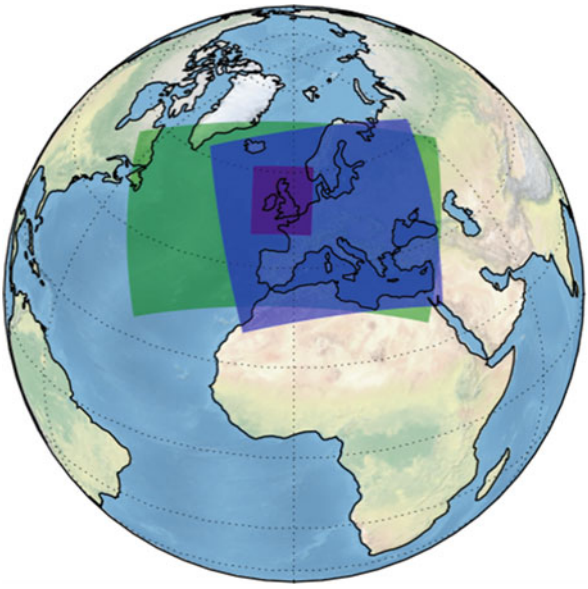

Fig. 6.31 2016 Met Office NWP model domains. No colour = global model (17 km resolution, 4D-Var DA). Blue = old NAE model (retired). Green = EURO4 model (4 km model, no DA). Purple = UKV model (1.5 km, 3D-Var)

6.1.25.2 Agreements with National Mapping Agencies

Whilst the Met Office has, since 1998, owned and operated its own network of GPS receivers, to provide the maximum benefit to both forecasting and NWP communities, additional raw data was required. In 2006 The Met Office signed a Memorandum of Understanding (MoU) with Ordnance Survey GB, stating that Ordnance Survey GB could install a number of GNSS equipment on Met Office sites around the UK, and in return Ordnance Survey would grant the Met Office access to data from their network of around 150 GNSS sensors in the UK, free of charge. Additionally, another MoU on the same basis was signed in 2006 between the Met Office and the Ordnance Survey of Northern Ireland.

In 2007, a 3-party MoU was signed between the Met Office (acting on behalf of the EIG EUMETNET E-GVAP Programme) and the Ordnance Survey of Ireland (OSi) and Met Eireann, whereby Osi would provide raw GNSS data to the Met Office, who, would process the data and provide processed data to Met Eireann for NWP assimilation of forecaster visualisation.

6.1.25.3 Tropospheric GNSS Processing at the UK Met Office

The original Met Office processing system (METO) was designed (in terms of data quality, timeliness and size and orientation of network processed) to best meet the needs of the NAE model. Positive benefit of GNSS ZTD assimilation was demonstrated (Bennitt and Jupp 2012) and other, internal assimilation impact experiments. From this work, it was decided that GNSS data would most likely be of benefit to the other Met Office NWP models such as the global model, and more recently the UKV 1.5 km UK-specific model. To meet the observational requirements of these models, additional GNSS processing systems were established, namely METG (global, hourly processing system) and METR (UK-specific, 15 min processing system). Both additional systems were again developed in partnership with the University of Nottingham under R&D contracts. In 2012, the Met Office started operational assimilation of GNSS data into the global model from a limited number of European ACs processing global networks of stations (METG and GOPG the global product from the Geodetic Observatory, Pecny, Czech Republic).

The Met Office process raw GNSS data on behalf of some countries who do not have the facility to process data themselves. In 2006 a 3-party Memorandum of Understanding was established between the Ordnance Survey of Ireland, Met Eireann and the UK Met Office, whereby the UK Met Office (acting on behalf of E-GVAP), would process raw GNSS data provided my OSi and make the products (ZTD and IWV) available to E-GVAP member Met Eireann for operational NWP assimilation or forecaster use. This service has been ongoing since and the Met Office is in the process of updating the system to provide Met Eireann with sub-hourly rather than hourly ZTD/IWV products. Similar, albeit less formal, arrangements (i.e. no MoU) are in place where the Met Office (again, acting on

behalf of E-GVAP) processes data on behalf of the Icelandic and soon to be, Canadian Met Services.

6.1.25.4 Data Use

NWP Data Assimilation

Operational GNSS data assimilation began in April 2007 in the NAE model, and, as mentioned in 2012 into the global model. When we look at the total Impact of observations in the global model for example for Sept. 2017 (Fig. 6.32), Ground GNSS is relatively low in terms of overall impact. When we consider the small number of observations in each assimilation cycle (as compared with traditional meteorological satellite observations for example), it is not surprising. However, when the impact per observation is assessed for the same time period (Fig. 6.33), ground-based GNSS observations of ZTD actually have the second highest impact per observation. Additionally, when the fraction of observations which have a beneficial effect on NWP is assessed (this time for July 2016) it can also be seen that GNSS is again one of the highest. This is shown in Fig. 6.34.

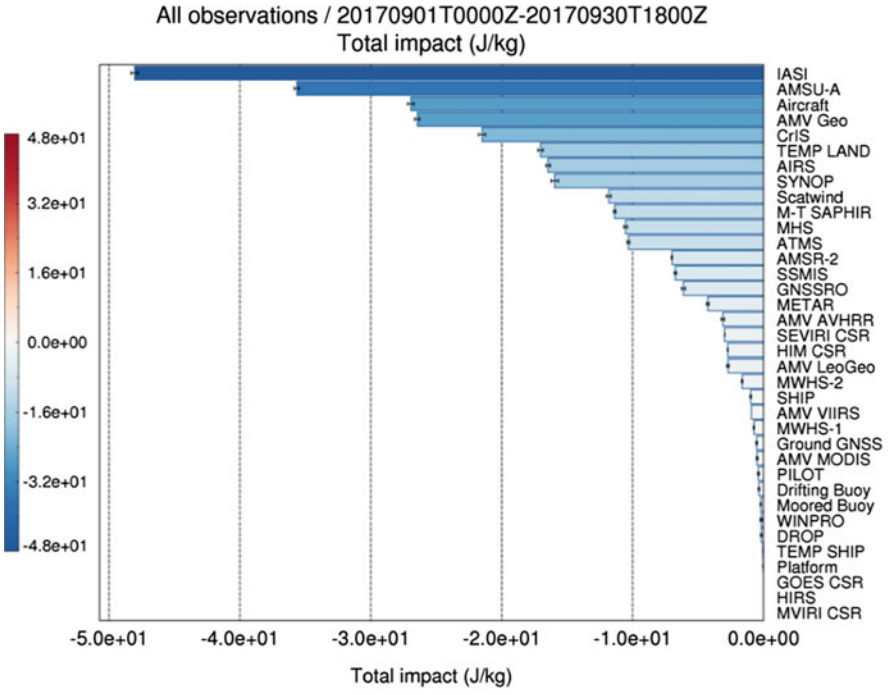

Fig. 6.32 Total impact per observation type in the Met Office Global NWP model, Sept. 2017

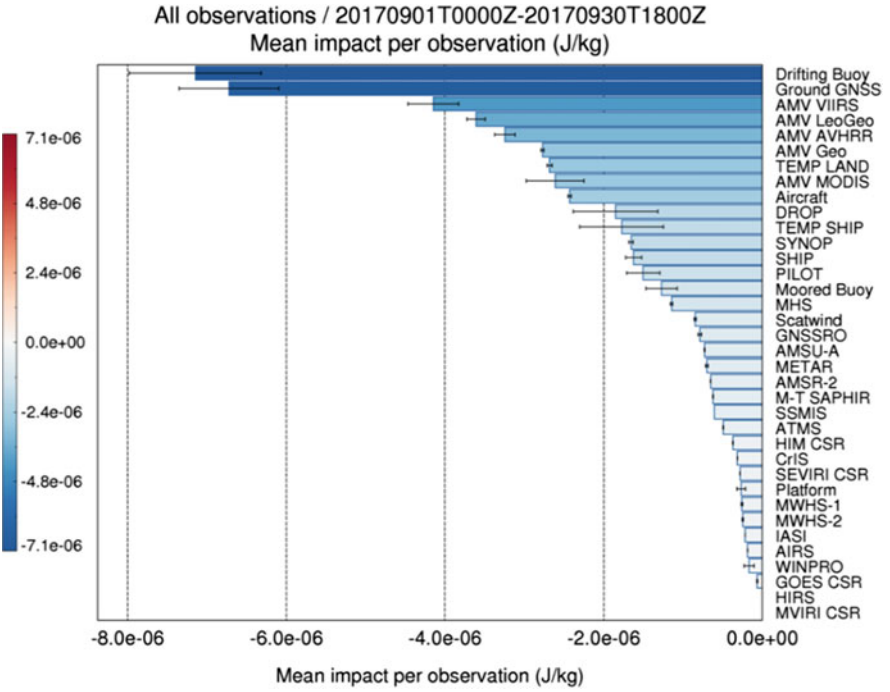

Fig. 6.33 NWP model impact per observation in the Met Office Global NWP model, Sept. 2017

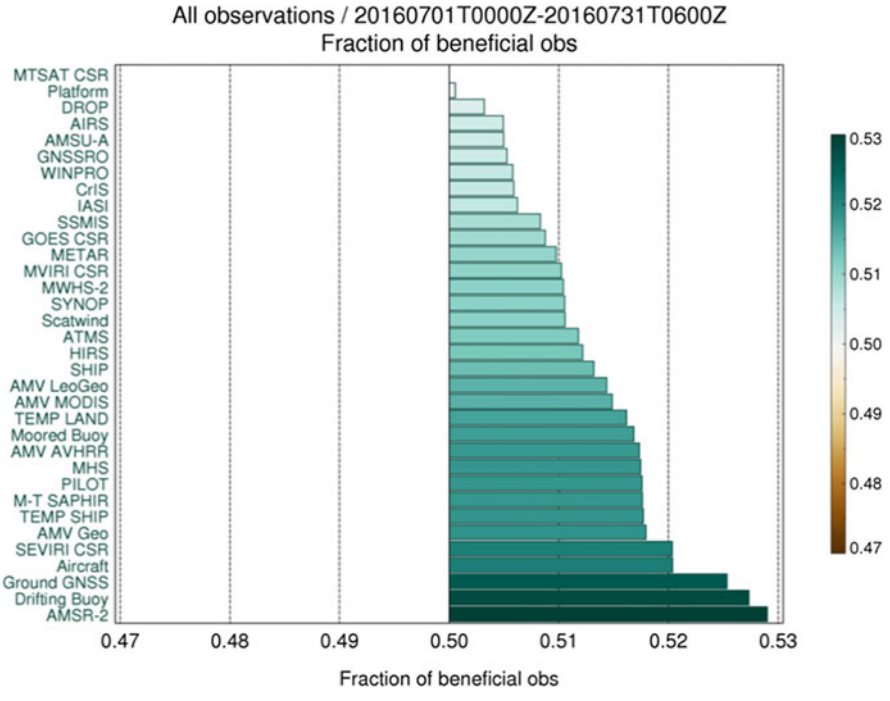

Fig. 6.34 Fractional benefit of all observations in the global NWP model, July 2016

From Figs. 6.32, 6.33 and 6.34, we can see that whilst the overall impact from GNSS in the global model is relatively low, this appears to be due to the very low number of observations actually assimilated in any one model run. Figures 6.33 and 6.34 clearly demonstrate high impact per observation, thus suggesting additional GNSS processing and assimilation (particularly of remote sites) will have a direct, measurable positive impact on NWP scores.

6.1.25.5 Forecaster Use

Whilst the primary use of GNSS data in the UK Met Office is for NWP data assimilation, ZTD is also converted to IWV using nearby synoptic pressure and temperature observations and 2D maps and animations of water vapour fields are produced for operational forecaster use. A number of case studies were developed to aid forecaster understanding of humidity field evolution.

Ongoing forecaster evaluation is underway to determine which conditions are best suited to the use of IWV imagery from ground-based GNSS and thus aid operational forecasting, particularly of severe weather.

6.1.25.6 Climate

The Met Office has been actively involved the assimilation of high-quality reprocessed ZTDs (i.e. EUREF Repro2 products) in the regional climate reanalysis system (UERRA, http://www.uerra.eu/). This work is ongoing.

6.2 COST International Partner Countries

6.2.1 Hong Kong

Z. Liu
Hong Kong Polytechnic University, Hung Hom, Hong Kong
e-mail: lszzliu@polyu.edu.hk

B. Chen
Hong Kong Polytechnic University, Hung Hom, Hong Kong
e-mail: yeary124@csu.edu.cn

Abstract Apart from the well-known positioning, navigation and timing applications, GNSS (Global Navigation Satellite System) is now an established important atmospheric water vapour observing system. GNSS nowadays has been developed with capability to retrieve atmospheric water vapour with high spatial and temporal resolutions. In China, the application of GNSS in meteorology started at the last few

years of the twentieth century and today it is a well-established research field. This paper makes a review of the GNSS meteorology situation in China over the last 5 years from 2013 to 2017. Review includes the GNSS data processing for retrieving tropospheric products, advances in GNSS water vapour tomography, application of GNSS water vapour products for weather prediction and the GNSS raw data used in each study. In the last 5 years, GNSS meteorology in China has achieved abundant outcomes and attracted more attentions from other communities to this field.

Introduction Water vapour has always been a focus of research interest for many atmosphere-related studies, such as in climatology, meteorology, space geodesy, and satellite navigation. This is due to its important role in many atmospheric processes. Water vapour is the dominant natural greenhouse gas in the atmosphere and it provides the largest feedback on surface temperature among various climate feedbacks (Held and Soden 2000). Water vapour is also a precursor of precipitation and it provides the fuel for thunderstorms as a considerable amount of latent heat releases during the condensation process. Although the atmosphere contains only 0.001% of the total amount of water on the earth, water vapour takes an important part in the water cycle of the earth (Troller 2004). Due to the variations in water vapour concentration and in latent heat release, a small amount of water vapour may cause severe weather changes (Mohanakumar 2008). When the radio signal travels through the atmosphere, it will be refracted by the presence of water vapour and thus introducing an equivalent excess path length to the primary observable (Davis et al. 1985; Mendes 1998). Therefore, water vapour also acts as a major error source in range measurements of space geodetic applications. Over the years, many techniques have been developed to improve the atmospheric water vapour observation, including both ground-based observation systems and satellite-borne remote sensing sensors (Elgered et al. 1991; Niell et al. 2001). Among various platforms, Global Navigation Satellite System (GNSS) has been regarded as a potent approach to retrieve atmospheric water vapour with high spatial and temporal resolutions. In addition, GNSS also has the advantages of low operational cost and all-weather capability when compared to other traditional techniques. The strengths of GNSS in atmospheric sounding have significantly facilitated the development of GNSS meteorology, which has become a focus of multidisciplinary research in the fields of meteorology and space geodesy. This summary reviews the research work in GNSS meteorology in China over the last 5 years (2013–2017).

GNSS Meteorology in China: In mainland China, researchers from the Wuhan University have done many studies on GNSS meteorology over the last 5 years. Shi et al. (2015) investigated real-time GPS precise point positioning (PPP)-based PWV estimation and its potential for rainfall monitoring and forecasting. They compared the real-time PPP-derived PWV values with the post-processed counterparts at the IGS station WUHN, yielding a RMS error of 2.4 mm and a correlation coefficient of 0.99. By comparing the real-time PWVs with ground rainfall records during severe rainfall events, they demonstrated the feasibility of real-time GPS PPP-derived PWV for rainfall monitoring. The Chinese BeiDou Navigation Satellite System (BDS) is under progressive development and now can provide regional

Positioning, Navigation and Timing (PNT) services over the Asia–Pacific region since December 2012. Li et al. (2015) presented a study on PWV estimation using ground-based BDS observations using PPP technique. In their study, BDS and GPS data collected from ten stations located at the Asia–Pacific and West Indian Ocean regions during the year 2013 were processed using the PANDA (Position and Navigation Data Analyst) software package that was developed by the Wuhan University, China. BDS derived PWVs were compared to GPS PWVs at ten stations. The mean bias and StDev of their differences at ten stations are 0.78 mm and 1.77 mm, respectively. Their study indicates that the BDS is ready for the high precision meteorological applications in the Asia–Pacific and West Indian Ocean regions. Xu et al. (2013) from the Liaoning Technical University, China, estimated ZTD using BDS observations to assess its capacity for troposphere remote sensing. They used BDS data for the period 5–8 November 2012 collected from a local network with six stations in Hebei province. BDS data were processed in both network and PPP modes. Compared with the IGS ZTD products, results showed that the bias and the StDev of the ZTD differences are about 2 mm and 5 mm, respectively. More studies have been carried out for retrieving the water vapour fields with tomographic techniques. Xia et al. (2013) proposed a combined iterative and non-iterative method for reconstructing the water vapour field using tomographic technique. In this method, the non-iterative reconstruction algorithm is first applied to retrieve water vapour field using COSMIC RO data as a priori water vapour information. Then the estimates from non-iterative reconstruction are used as initial data in the iterative reconstruction method. They evaluated this combined method using 10-day GPS data in Hong Kong and COSMIC profiles. Evaluation results showed that water vapour density retrieved from the combined method has a good agreement with radiosonde data at altitudes above 2.5 km. The average RMS value of their differences above 2.5 km is 0.44 g m^{-3}. Jiang et al. (2014) developed a near real-time four-dimensional water vapour tomographic system. Sliding time window strategy and double-difference network solution are used to retrieve the GPS water vapour data. In order to improve the distribution of observations in the lowest layers of tomographic grid, they also assimilated the surface relative humidity data into the tomographic system. They tested this tomographic system by using the GPS data collected from the 12 stations of Hong Kong network in the year of 2010. Compared with the radiosonde profiles, this tomographic system achieved overall bias of 0.13 g m^{-3} and RMS error of 1.28 g m^{-3}. In the study reported by Ye et al. (2016), the water vapour tomography was optimized with the aid of radiosonde and COSMIC historical data. They first optimized the regional ZHD model by compensating the estimates from the Saastamoinen model. Second, the regional conversion factor of converting the ZWD to PWV is refined by improving the quality of the atmospheric weighted mean temperature. They developed a method for discretizing the tomography grid with an uneven voxel height and a varying water vapour top layer. They also proposed a Gaussian exponential vertical interpolation method for better reflecting the vertical variation characteristic of water vapour. The optimized tomography was assessed by using 1-month GPS data of February 2014 collected in Hong Kong. Compared with tomographic results

without optimization, the optimized method improved the tomographic water vapour results by 15% and 12% for layers below 3.75 km and above 3.75 km, respectively. Yao and Zhao (2016) presented a method to maximally use GNSS signals that penetrate the tomography area. They studied the possibility of selecting a reasonable tomography boundary and using signals entering the tomography area from side face. Based on 40-year radiosonde data, they determined the tomography boundary in Hong Kong. For the signals passing through the side face, they introduced a scale factor to determine the proportion of the signal that belongs within the tomography area. GNSS data from the 12 stations of Hong Kong over the period of 4–30 May 2013 were adopted to validate the proposed method. Comparisons showed that the utilization rate of signals is improved by 30.32% and the number of voxels crossed by rays is enhanced by 12.62% when considering the signals passing through the side. A comparison of radiosonde, ECMWF, and tomography showed that the RMS errors of the proposed method (1.23 and 2.12 g/m^3, respectively) are superior to those of the previous method (1.60 and 2.43 g/m^3, respectively). To fully use the GNSS signals passing through the tomographic region, Yao et al. (2016) also proposed an approach to use both signals that pass the side and top of a research area of the tomography. This method can enhance the utilization of GNSS data and increase the number of voxels crossed by satellite signals. They validated this approach by using GNSS data from 10 GNSS stations of the CORS network of Zhejiang Province, China from 1 to 31 May 2015. Compared with radiosonde profiles, they showed that the proposed approach is feasible and effective. In the study presented by Guo et al. (2016), an optimal weighting method was proposed to reasonably determine the weights of three types of tomography equations including the observation equation, the horizontal constraint equation, and the vertical constraint equation. Based on a GPS network consisting of seven stations in Wuhan, China, they demonstrated that the proposed method can adaptively adjust the weights for various equations and enable the posterior unit weight variances for the three types of equations that achieve statistically equal. Zhang et al. (2017) proposed an improved tomography method based on adaptive Laplacian smoothing (ALS) and ground meteorological observations. They tested this tomography approach in Hong Kong during a heavy rainy period and a rainless period. Results showed that the ALS method got better results than the constant Laplacian smoothing (CLS) method. They also found that the assimilation of ground meteorological data into tomography can solve the perennial problem of resolving the wet refractivity in the lower troposphere.

Wang et al. (2014) from the Nanjing University of Information Science and Technology, China, proposed two new statistical parameters to improve the deficiencies of existing accuracy evaluation parameters in algebraic reconstruction techniques (ART). The new statistical parameters, i.e. bias and RMS, are calculated from wet refractivity of the total voxels. Simulations showed that Gaussian constraints can be applied to update the value of voxels without ray-crossings and the new method can improve the overall accuracy, especially in a poor grid model with a lot of empty voxels.

Another group from the China University of Mining and Technology proposed a new GPS tomographic parameterization approach based on IDW (inverse distance weighted) interpolation (Ding et al. 2017). The proposed algorithm can avoid the use of horizontal constraints to smooth voxels without ray-crossings. They also applied a prime number decomposition (PND) access order scheme to minimize correlation between SWD observations. They carried out several tomographic experiments by using 14 days (dry days from 2 to 8 August 2015 and rainy days from 9 to 15 August 2015) of data from the Hong Kong GPS network. The new method was proved to have better performance under stable weather conditions than unstable weather (e.g., rainy days).

In Hong Kong, GNSS meteorology related work is mainly carried out at the Micro-Laboratory of Atmospheric Research and Geomatics Engineering (Micro-LARGE) at the Department of Land Surveying & Geo-Informatics, the Hong Kong Polytechnic University (PolyU). As the leader of Micro-LARGE, Dr Zhizhao Liu has conducted various studies on atmospheric water vapour retrieval using GNSS technology. Based on GNSS Precise Point Positioning (PPP) technique, Micro-LARGE developed the first PWV Real-Time Monitoring System (PWVRMS) for the Pearl-River-Delta region of China (Liu and Li 2013). The processed GNSS data are collected from three networks in Pearl-River-Delta region: Hong Kong SatRef GNSS network, Macao MoSRef GNSS network and Guangdong CORS network. In data processing, PWVRMS directly uses IGS predicted precise satellite orbit while the GPS satellite clock error is estimated in real-time. This PWVRMS system provides the PWV data with a temporal resolution of 10 min. Evaluation results by radiosonde showed that PWV data estimated by PWVRMS have an accuracy better than 2 mm. This PWVRMS system can provide real-time water vapour data to meteorological agency such as Hong Kong Observatory for weather forecasting service and research (Liu and Li 2013).

The Micro-LARGE has also done many studies in retrieving the three-dimensional atmospheric water vapour distribution with the use of tomographic technique. Micro-LARGE group developed a new method to optimize the discretization of the tomographic model (Chen and Liu 2014). Using this method, the tomographic voxel of Hong Kong region was optimized towards both high accuracy and high spatial resolution of the tomographic solutions. This tomographic voxel optimization method includes top boundary determination, vertical layer discretization, and horizontal boundary optimization. Unlike the traditional tomography, the horizontal boundary of the tomographic model is no longer fixed. For different tomographic period, predicted GPS satellite orbits are used to predefine the optimal horizontal boundary. The horizontal boundary optimization is achieved by moving the voxel location in latitude and longitude directions until the maximum number of voxels with ray crossings is reached. By using the observations collected from 12 Hong Kong GPS stations, extensive experiments were carried out to determine the optimal discretization of the tomographic model for Hong Kong region.

The Micro-LARGE developed and performed a multi-sensor tomographic method using water vapour data derived from GPS, radiosonde, WVR (water vapour

radiometer), NWP (numerical weather prediction), sun photometer, and synoptic observations in Hong Kong (Chen and Liu 2016). Based on extensive tomographic tests covering a 6-month period of May to October 2013, the multi-sensor tomography achieved obvious better performance than that using GPS data only. In the evaluation by radiosonde profiles, the multi-sensor tomography yielded an overall accuracy of 7.13 mm/km. For different vertical layers, RMS error generally decreased with altitude from 11.44 mm/km at the lowest layer (0–0.4 km) to 3.30 mm/km at the uppermost layer (7.5–8.5 km).

The Micro-LARGE applied the tomographic results to investigate the evolution of water vapour during three heavy precipitation events occurred in Hong Kong (Chen et al. 2017). They investigated the variability of the total ZWD and ZWDs at five different vertical layers (below 1 km, 1~2 km, 2~3 km, 3~5 km and above 5 km) during the three events. It was observed that the fluctuations (increase or decrease) in the total ZWD largely came from the water vapour variations in the layers above 3 km. The remarkable increase or decrease of water vapour in the vertical layers can be seen as precursors to detect heavy precipitations as they reflect the instability of the atmosphere. This study demonstrated that the tomographic water vapour fields can reveal water vapour accumulation, saturation, and condensation.

Conclusions In the future, it is expected that GNSS meteorology will gain more attentions and great development opportunities in China due to three reasons. First, an increasing number of cities and provinces are developing their own GNSS network for various applications including precise positioning, real-time positioning and navigation, urban plan, land surveying, cadastral management and environment monitoring, etc. The increasing number of GNSS stations will contribute to a better implementation of GNSS meteorology. Especially for water vapour tomography, denser ground GNSS stations could produce water vapour field with higher accuracy and spatial resolution. Second, with the rapid development of Chinese BeiDou system, the number of satellites visible to any location at any time will increase significantly. The increase of GNSS satellites implies more possible signals penetrating through the troposphere. The developing multi-GNSS constellations has the potential to provide more accurate high-resolution PWV and tropospheric gradient products. In addition, multi-GNSS will improve the geometry of observations in the tomographic modelling and thus have a positive impact on the accuracy of the tomographic solutions. Third, continued climate change will trigger more extreme weather events in China. This demands an improvement in the capability of short-term weather forecasting. GNSS meteorology products including PWV, tropospheric gradient and water vapour field, closely linked to strong humidity variations accompanying severe weather phenomena, are considered as new important data for meteorological applications, e.g., nowcasting of severe rainfall events.

6.2.2 *Australia*

C. Wang
Geoscience Australia, Canberra, Australia
e-mail: Carl.Wang@ga.gov.au

S. Masoumi
Geoscience Australia, Canberra, Australia
e-mail: Salim.Masoumi@ga.gov.au

M. Moore
Geoscience Australia, Canberra, Australia
e-mail: Michael.Moore@ga.gov.au

Since 2016 Geoscience Australia (GA) has produced two 'trial' Zenith Troposphere Delay (ZTD) products. They are currently being delivered to the Australian Bureau of Meteorology (BoM) and the E-GVAP in COST format. The first product is available in 'near-real-time' with a latency of approximately 40 min. The second, 'rapid' product, has a latency of approximately 18 h, and includes a much denser set of observations obtained from over 700 stations obtained mainly from the Asia Pacific Region.

Both products are derived using a Precise Point Positioning (PPP) based approach to estimate the ZTD. We found that there are a number of operational advantages to using a PPP based approach compared to a double-differenced approach. The PPP approach takes less compute resources to obtain a solution; in addition, the PPP solutions provides position and ZTD estimates that are consistent with the global reference frame. The software and models applied are detailed in Table 6.1.

Near-real time products: The near-real-time-product was put together with the aim of improving short range weather forecasting with latencies of 12 h and under. The processing system utilizes the GNSS network run and operated by GA. This consists of approximately 150 Continuously Operating Reference Stations (CORS), which span Australia, the South Pacific, and Antarctica. These stations stream real-time data directly back to GA's data centre. In addition to this network, a set of stations owned and operated by the Victorian State Government department to aid in the densification of the near-real-time ZTD estimates in Victoria, as well as data streams provided to the IGS by Land Information New Zealand (LINZ) are also utilised. The distribution of GNSS stations used for the near-real-time system is shown in Fig. 6.35.

Compute infrastructure: The data collection and processing system is based on infrastructure provided by Amazon Web Services (AWS). Moving to a cloud infrastructure has significantly improved the reliability of the compute infrastructure, and provided a straightforward pathway to increasing the scale of the processing system as required (Fig. 6.36).

Table 6.1 Processing details

Model/parameter	Type	Solution	Notes
Processing software	BSW52	NRT and rapid	
Processed observation	Ionosphere free	NRT and rapid	
Ambiguity resolution	No	NRT and rapid	Float solution only
GPS data	RTCM 3	NRT	Rolling 24 h window updated every hour
	RINEX 2.1	Rapid	24 h of observation based on UTC day
Elevation mask	10	10	
Clock products	'IGS02' – real time clocks	NRT	
	IGS rapid	Rapid	
Orbit products	IGS ultra rapid	NRT	observed and predicted
	IGS rapid	Rapid	
Earth-rotation parameters	IGS ultra-rapid	NRT	
	IGS rapid	Rapid	
Antenna model PCO and PCV	Latest IGS ANTEX igs14.atx	NRT and rapid	
DCB	CODE	NRT and rapid	
Atmosphere (Dry)	GMF	NRT and rapid	
Mapping function	GPT	NRT and rapid	
Atmosphere (wet)	Estimated	NRT and rapid	ZTD estimate provided for every hour of observed data processed

Rapid products: The 'rapid product' is primarily used as a quality control system for the GPS data aggregated by Geoscience Australia, with the aim of screening out poor or inconsistent meta data before the final geodetic processing is attempted. The rapid solution is also used to monitor the performance of the near-real-time ZTD estimates. Each day we compare the results obtained from the rapid product with the near-real-time product. Figure 6.37 below shows a yearly comparison of the ZTD estimates obtained from the IGS station MOBS, located at the Melbourne Observatory, Melbourne, Australia. Two ZTD comparison plots are viewable for each station processed (to view another station replace the four-char ID MOBS, with the four char ID of the station of interest):

1. Yearly comparison https://s3-ap-southeast-2.amazonaws.com/gnss-analysis/status/rapid/ztd/yearly_MOBS_ztd.png

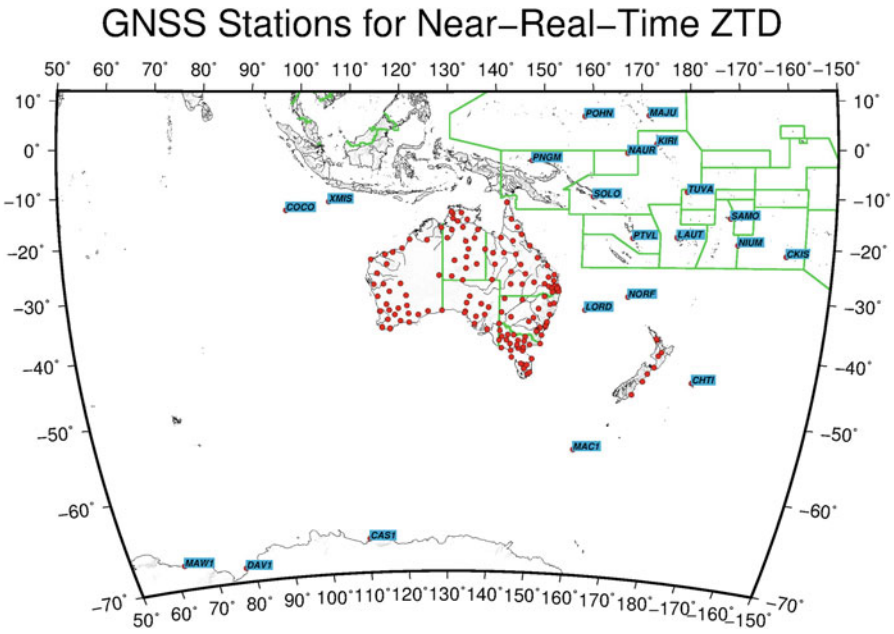

Fig. 6.35 The distribution of GNSS stations used for the near-real-time zenith delay estimates

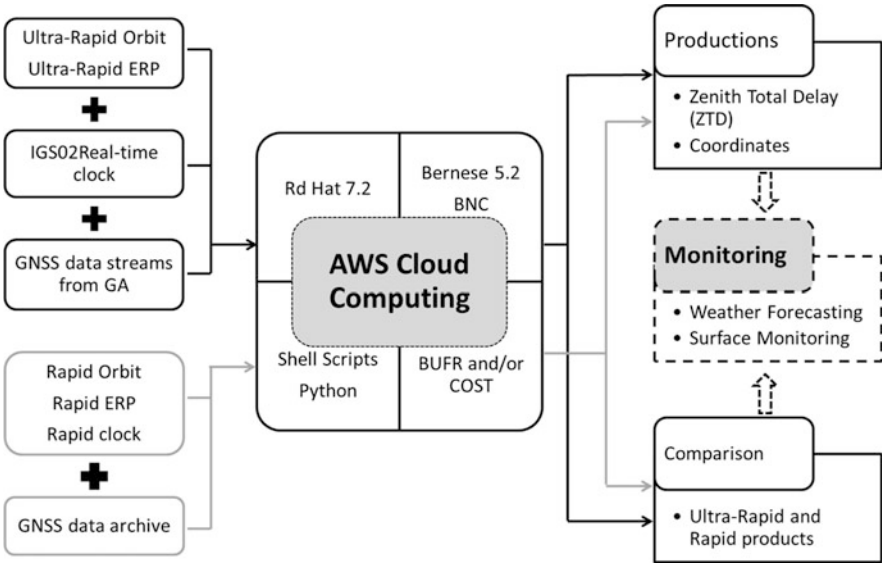

Fig. 6.36 The structure and flowchart of the Australian ZTD estimation system

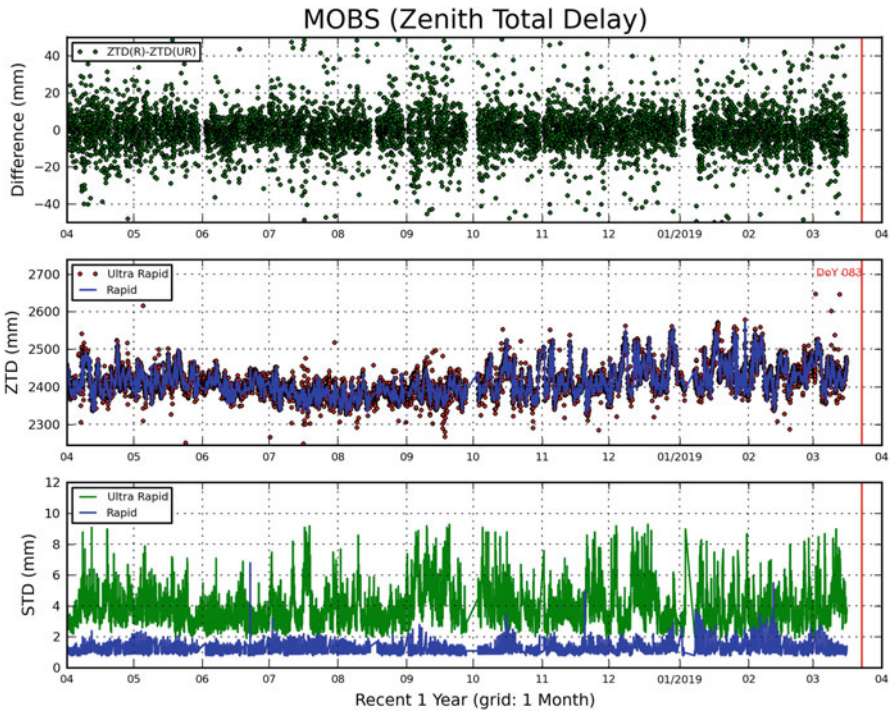

Fig. 6.37 An example plot of the comparison of the near-real-time and rapid processing result obtained from the IGS station located at Melbourne Observatory (MOBS). The top plot shows a time series of the difference between the near-real-time and rapid product, the middle plot shows the estimates obtained from both solutions, and the bottom plot is the standard deviation for each of the solutions

2. Weekly comparison https://s3-ap-southeast-2.amazonaws.com/gnss-analysis/status/rapid/ztd/weekly_MOBS_ztd.png

The distribution of GNSS stations used for the rapid system is shown in Fig. 6.38 below.

Current and future focus: Currently the Australian BoM is trialling the near-real-time product in their test assimilation models. Initial results look promising and it is likely to be included into operation forecasts in the near future. Once the product has been accepted into operational forecast then we will start increasing the number of stations used to create the near-real-time product. We will be also looking at ways we can decrease the latency of the NRT product through tuning of the compute infrastructure, processing procedures and observation window length used. GA is also currently developing its own in-house real-time GNSS processing software package, and we will also assess the applicability of using this to provide ZTD

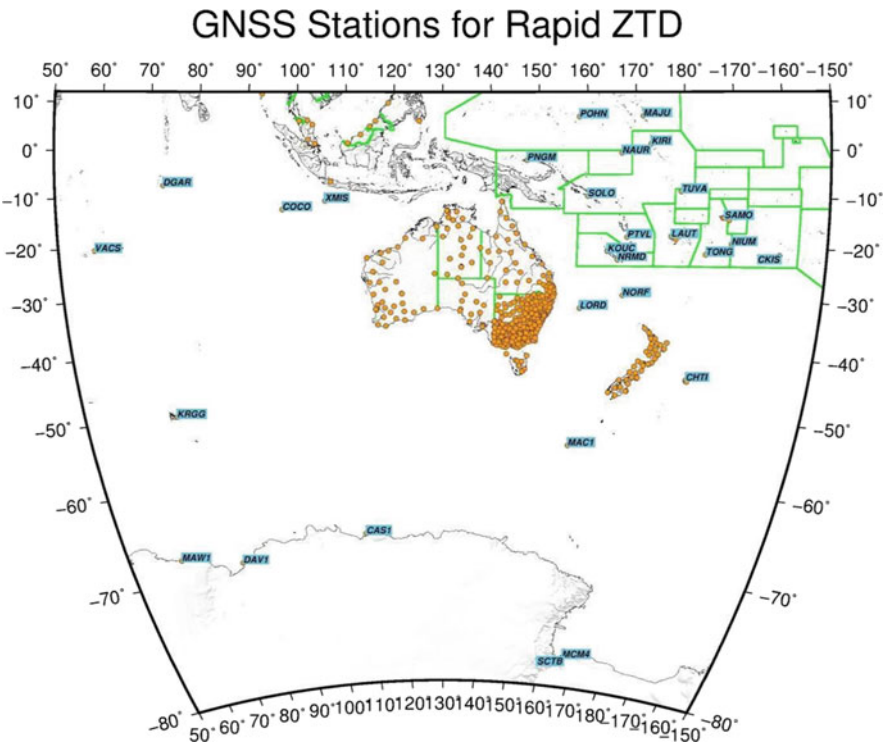

Fig. 6.38 GNSS stations used in the Asia Pacific Region for the rapid product (global stations not shown here)

estimates as the package matures. To help improve real-time positioning in Australia we are also looking at utilizing the ZTD estimates obtained from ray tracing of forecasted weather models. Currently we are trialling unassimilated ACCESS weather models to aid positioning for PPP-RTK applications.

6.2.3 Canada

S. MacPherson
Environment Canada, Gatineau, QC, Canada
e-mail: stephen.macpherson@canada.ca

At Environment and Climate Change Canada (ECCC), we assimilate ZTD observations from the E-GVAP network that are available on the GTS. ZTD observations over North America from the NOAA GPS-IPW network were assimilated until December 2016 when free access to the data was cut off. The data are assimilated in our global and regional deterministic NWP systems. Recent research activities

related to ground-based GNSS include the diagnosis of ZTD observation errors and their temporal correlations. We plan to submit a paper on this research in the near future. GNSS IWV and ZTD observations are also used in one of our forecast verification systems. We are currently exploring ways to restore/replace the lost North American data and to obtain data from more GNSS sites in Canada. Options include obtaining data from UCAR, working with Natural Resources Canada geodetic division to provide ZTD for sites that they have access to, and producing ZTD data ourselves from raw GNSS receiver data.

References

Ahmed, F., Gazeaux, J., Lebarbier, E., & Bock, O. (2015). Development of new segmentation algorithms for the homogenisation of GNSS IWV data. COST ES1206, 3rd WG meeting, Wroclaw, Poland, 29–30 September 2015.

Alraddawi, D., Sarkissian, A., Keckhut, P., Bock, O., Noël, S., Bekki, S., Irbah, A., Meftah, M., & Claud, C. (2017). Comparison of total water vapour content in the Arctic derived from GPS, AIRS, MODIS and SCIAMACHY. *Atmospheric Measurement Techniques Discussions*. https://doi.org/10.5194/amt-2017-195, in review.

Bastin, S., Bock, O., Chiriaco, M., Bosser, P., Ahrens, B., Gallardo, C., Dominguez-Alonso, M., Roehrig, R., Li, L., Drobinski, P., & Parracho, A. (2017). Representation of integrated water vapor at different time scales and its impact on precipitation in MED-CORDEX simulations. 10th HyMeX workshop, 4–7 July 2017, Barcelona, Spain.

Bennitt, G. V., & Jupp, A. (2012). Operational assimilation of GPS zenith total delay observations into the met Office numerical weather prediction models. *Monthly Weather Review*, 140(8), 2706–2719.

Bennitt, G. V., Johnson, H. R., Weston, P. P., Jones, J., & Pottiaux, E. (2017). An assessment of ground-based GNSS Zenith total delay observation errors and their correlations using the Met Office UKV model. *Quarterly Journal of Meteorological Society, 143*(707), 2436–2447.

Berckmans, J., Van Malderen, R., Pottiaux, E., & Pacione, R. (2017). Evaluation of the atmospheric water vapor content in the regional climate model ALARO-0 using GNSS observations from EPN Repro2, EMS2017-736, oral, EMS.

Bock, O. (2016a). A reference IWV dataset combining IGS repro1 and ERA-Interim reanalysis for the assessment of homogenization algorithms. 3rd COST ES1206 workshop, 8–11 March 2016, Reykjavik, Island.

Bock, O. (2016b). Post-processing of GNSS ZTD, COST ES1206 GNSS4SWEC Summer School, 29–31 August 2016, GFZ, Potsdam, Germany. Available at: ftp://ftp.gfz-potsdam.de/pub/GNSS/workshops/gnss4swec/Summer_School/D2/3_Bock_PostProc.pdf

Bock, O., Bouin, M. N., Walpersdorf, A., Lafore, J. P., Janicot, S., Guichard, F., & Agusti-Panareda, A. (2007). Comparison of ground-based GPS precipitable water vapour to independent observations and NWP model reanalyses over Africa. *Quarterly Journal of the Royal Meteorological Society: A journal of the atmospheric sciences, applied meteorology and physical oceanography, 133*(629), 2011–2027.

Bogusz, J., Klos, A., Teferle, N., Bock, O., Pottiaux, E., & Van Malderen, R. (2016). Autoregressive processes in homogenization of GNSS tropospheric data, G31B-1067, poster, AGU.

Bollmeyer, C., Keller, J., Ohlwein, C., Wahl, S., Crewell, S., Friederichs, P., Hense, A., Keune, J., Kneifel, S., Pscheidt, I., Redl, S., & Steinke, S. (2015). Towards a high-resolution regional reanalysis for the European CORDEX domain. *Quarterly Journal of the Royal Meteorological Society, 141*(686), 1–15.

Bonafoni, S., & Biondi, R. (2015). The usefulness of the Global Navigation Satellite Systems (GNSS) in the analysis of precipitation events. *Atmospheric Research, 167*, 15–23. https://doi.org/10.1016/j.atmosres.2015.07.011.

Bosser, P., & Bock, O. (2016). Screening of GPS ZTD estimates. 3rd COST ES1206 workshop, 8–11 March 2016, Reykjavik, Island.

Brenot, H., Wautelet, G., Warnant, R., Nemeghaire, J., & Van Roozendael, M. (2014a). *GNSS meteorology and impact on NRT position*. Proceedings of the European navigation conference (ENC), Rotterdam, The Netherlands.

Brenot, H., Walpersdorf, A., Reverdy, M., van Baelen, J., Ducrocq, V., Champollion, C., Masson, F., Doerflinger, E., Collard, P., & Giroux, P. (2014b). A GPS network for tropospheric tomography in the framework of the Mediterranean hydrometeorological observatory Cévennes-Vivarais (southeastern France). *Atmospheric Measurement Techniques, 7*, 553–578. https://doi.org/10.5194/amt-7-553-2014.

Brenot, H., Errera, Q., Champollion, C., Verhoelst, T, Kumps, N., Van Malderen, R., & Van Roozendael M. (2014c). GNSS tomography and optimal geometrical setting to retrieve water vapour density of the neutral atmosphere, EGU2014-12204, oral, EGU.

Brenot, H., Jones, J., Biondi, R., Clarisse, L., Delobbe, L., Clerbaux, N., & Van Roozendael, M. (2015). Propagation delays induced in GNSS signals during extreme conditions of the neutral atmosphere, G43C-03, invited oral, AGU.

Brenot, H., Rohm, W., Kačmařík, M., Möller, G., Sá, A., Tondás, D., Rapant, L., Biondi, R., Manning, T., & Champollion, C. (2017a). Cross-validation of GNSS tomography models and methodological improvements using CORS network, EGU2017-7078, poster, EGU.

Brenot, H., Caumont, O., Bosser, P., Biondi, R., Bock, O., Ducrocq, V., & Van Roozendael, M. (2017b). Interest of GNSS tomography for nowcasting in the frame of HyMeX, EGU2017-6979, poster, EGU.

Brenot, H., Rohm, W., Kačmařík, M., Möller, G., Sá, A., Tondaś, D., Rapant, L., Biondi, R., Manning, T., & Champollion, C. (2018). Cross-validation of GPS tomography models and methodological improvements using CORS network. *Atmospheric Measurement Techniques Discussions*. https://doi.org/10.5194/amt-2018-292. (in review, 2018).

Caussinus, H., & Mestre, O. (2004). Detection and correction of artificial shifts in climate series. *Journal of the Royal Statistical Society: Series C (Applied Statistics), 53*, 405–425. https://doi.org/10.1111/j.1467–9876.2004.05155.x.

Chen, B., & Liu, Z. (2014). Voxel-optimized regional water vapour tomography and comparison with radiosonde and numerical weather model. *Journal of Geodesy, 88*, 691–703. https://doi.org/10.1007/s00190-014-0715-y.

Chen, B., & Liu, Z. (2016). Assessing the performance of troposphere tomographic modelling using multi-source water vapour data during Hong Kong's rainy season from May to October 2013. *Atmospheric Measurement Techniques, 9*, 5249–5263. https://doi.org/10.5194/amt-9-5249-2016.

Chen, L., Yu, Y., & Sun, D.-Z. (2013). Cloud and water vapour feedbacks to the El Niño warming: Are they still biased in CMIP5 models? *Journal of Climate, 26*, 4947–4961.

Chen, B., Liu, Z., Wong, W.-K., & Woo, W.-C. (2017). Detecting water vapour variability during heavy precipitation events in Hong Kong using the GPS tomographic technique. *The Journal of Atmospheric and Oceanic Technology, 34*, 1001–1019. https://doi.org/10.1175/JTECH-D-16-0115.1.

Climate indices. http://www.esrl.noaa.gov/psd/data/climateindices/list/

Davis, J. L., Herring, T. A., Shapiro, I. I., Rogers, A. E. E., & Elgered, G. (1985). Geodesy by radio interferometry: Effects of atmospheric modelling errors on estimates of baseline length. *Radio Science, 20*, 1593–1607.

Dick, G., Douša, J., Kačmařík, M., Pottiaux, E., Zus, F., Brenot, H., Möller, G., Kaplon, J., Morel, L., & Hordyniec, P. (2016). Benchmark campaign of the COST action GNSS4SWEC: Main goals and achievements, G43C-04, invited oral, AGU.

Ding, N., Zhang, S., & Zhang, Q. (2017). New parameterized model for GPS water vapour tomography. *Annales de Geophysique, 35*, 311–323. https://doi.org/10.5194/angeo-35-311-2017.

Douša, J., Dick, G., Zus, F., Kačmařík, M., Václavovic, P., Brenot, H., Szafranek, K., Deng, Z., Brockmann, E., Teferle, N., Rohm, W., Santos, M., Zinas, N., Wielgosz, P., Nahmani, S., & Morel, L. (2015). Activities of GNSS4SWEC Working Group 1: Advanced GNSS processing techniques, EMS2015-455, poster, EMS.

Douša, J., Dick, G., Kačmařík, M., Václavovic, P., Pottiaux, E., Zus, F., Brenot, H., Möller, G., Hinterberger, F., Pacione, R., Stuerze, A., Eben, K., Teferle, N., Ding, W., Morel, L., Kaplon, J., Hordyniec, P., & Rohm, W. (2016a). Achievements of GNSS4SWEC Working Group 1: Advanced GNSS processing techniques, EMS2016-705, poster, EMS.

Douša, J., Dick, G., Kačmařík, M., Brožková, R., Zus, F., Brenot, H., Stoycheva, A., Möller, G., & Kaplon, J. (2016b). Benchmark campaign and case study episode in central Europe for development and assessment of advanced GNSS tropospheric models and products. *Atmospheric Measurement Techniques, 9*, 2989–3008. https://doi.org/10.5194/amt-9-2989-2016.

Douša, J., Václavovic, P., Pottiaux, E., Hinterberger, F., Pacione, R., Kačmařík, M., Stuerze, A., & Teferle, N. (2016c). GNSS4SWEC real-time demonstration campaign: Development and assessment of future tropospheric products. IAG Commission 4th symposium, 4–7 September 2016, Wroclaw, Poland.

Douša, J., Dick, G., Kačmařík, M., Václavovic, P., Pottiaux, E., Zus, F., Brenot, H., Möller, G., Hinterberger, F., Pacione, R., Stuerze, A., Eben, K., Teferle, N., Ding, W., Morel, L., Kaplon, J., Hordyniec, P., & Rohm, W. (2017). Working Group 1 "advanced GNSS processing techniques" of the COST Action GNSS4SWEC: Overview of main achievements, EGU2017-8440, oral, EGU.

Elgered, G., Davis, J. L., Herring, T. A., & Shapiro, I. I. (1991). Geodesy by radio interferometry: Water vapour radiometry for estimation of the wet delay. *Journal of Geophysical Research – Solid Earth 1978–2012, 96*, 6541–6555.

Gobin, A., Van Schaeybroeck, B., Termonia, P., Willems, P., Van Lipzig, N., Marbaix, P., van Ypersele, J.-P., Fettweis, X., De Ridder, K., Stavrakou, T., Luyten, P., & Pottiaux, E. (2016). Climate impacts on agricultural biomass production in the CORDEX.be project context, EGU2016-13711, poster, EGU.

Gruber, C., Auer, I., & Böhm, R. (2009). Endbericht HOM-OP Austria, Aufbau und Installierung eines Tools zur operationellen Homogenisierung von Klimadaten mit Annexen: Gruber C., Auer I, 2009: Description of a procedure for the homogenization of daily temperature time series, Annex zu Endbericht HOM-OP-Austria.

Guerova, G., Jones, J., Douša, J., Dick, G., de Haan, S., Pottiaux, E., Bock, O., Pacione, R., Elgered, G., Vedel, H., & Bender, M. (2016). Review of the state of the art and future prospects of the ground-based GNSS meteorology in Europe. *Atmospheric Measurement Techniques, 9*, 5385–5406. https://doi.org/10.5194/amt-9-5385-2016.

Guo, J., Yang, F., Shi, J., & Xu, C. (2016). An optimal weighting method of Global Positioning System (GPS) troposphere tomography. *The IEEE Journal of Selected Topics in Applied Earth Observations and Remote Sensing, 9*(12), 1–8. https://doi.org/10.1109/JSTARS.2016.2546316.

Haase, J., Ge, M., Vedel, H., & Calais, E. (2003). Accuracy and variability of GPS tropospheric delay measurements of water vapor in the western Mediterranean. *Journal of Applied Meteorology, 42*(11), 1547–1568.

Held, I. M., & Soden, B. J. (2000). Water vapour feedback and global warming. *Annual Review of Energy and the Environment, 25*, 441–475.

Hinterberger, F. (2016). Influence of GPS satellite orbits and clock corrections on the estimation of single difference uncalibrated phase delays. Dissertation, Department of Geodesy and Geoinformation, TU Wien. http://repositum.tuwien.ac.at/obvutwhs/id/1553637

Jiang, P., Ye, S. R., Liu, Y. Y., Zhang, J. J., & Xia, P. F. (2014). Near real-time water vapour tomography using ground-based GPS and meteorological data: long-term experiment in Hong Kong. *Annales de Geophysique, 32*, 911–923. https://doi.org/10.5194/angeo-32-911-2014.

Jones, J., Guerova, G., Douša, J., de Haan, S., Bock, O., Dick, G., Pottiaux, E., & Pacione, R. (2014). COST Action ES1206: Advanced Global Navigation Satellite Systems tropospheric products for monitoring severe weather events and climate (GNSS4SWEC), EGU2014-14097, poster, EGU.

Jones, J., Guerova, G., Douša, J., Dick, G., de Haan, S., Pottiaux, E., Bock, O., & Pacione, R. (2015a). COST Action ES1206: GNSS for severe weather and climate (GNSS4SWEC), EGU2015-9, poster, EGU.

Jones, J., Guerova, G., Douša, J., Dick, G., de Haan, S., Pottiaux, E., Bock, O., & Pacione, R. (2015b). COST Action ES1206: GNSS for severe weather and climate (GNSS4SWEC), EMS2015-323, poster, EMS.

Jones, J., Guerova, G., Douša, J., Dick, G., de Haan, S., Pottiaux, E., Bock, O., & Pacione, R. (2015c). COST Action ES1206: Advanced GNSS tropospheric products for monitoring severe weather events and climate (GNSS4SWEC), G31B-1050, poster, AGU.

Jones, J., Guerova, G., Douša, J., Dick, G., De Haan, S., Pottiaux, E., Bock, O., & Pacione, R. (2015d) Satellite systems tropospheric products for monitoring severe weather events and climate (GNSS4SWEC). 5th international colloquium scientific and fundamental aspects of the Galileo Programme, 27–29 October 2015, Braunschweig, Germany.

Jones, J., Guerova, G., Douša, J., Dick, G., De Haan, S., Pottiaux, E., Bock, O., & Pacione, R. (2015e). COST Action ES1206: Advanced Global Navigation Satellite Systems tropospheric products for monitoring severe weather events and climate (GNSS4SWEC) International Union of Geodesy and Geophysics, General Assembly, 22 June to 2 July 2015, Prague, Czech Republic.

Jones, J., Guerova, G., Douša, J., Dick, G., de Haan, S., Pottiaux, E., Bock, O., & Pacione, R. (2016a). COST Action ES1206: Advanced GNSS tropospheric products for monitoring severe weather events and climate (GNSS4SWEC), EGU2016-2615, poster, EGU.

Jones, J., Guerova, G., Douša, J., Dick, G., de Haan, S., Pottiaux, E., Bock, O., & Pacione, R. (2016b). COST Action ES1206: Advanced GNSS tropospheric products for monitoring severe weather events and climate (GNSS4SWEC), G31B-1050, poster, AGU.

Jones, J., Guerova, G., Douša, J., De Haan, S., Bock, O., Dick, G., Pottiaux, E., & Pacione, R. (2016c). Advanced GNSS tropospheric products for monitoring severe weather events and climate (GNSS4SWEC), IGS Workshop, 8–12 February 2016, Sydney, Australia.

Jones, J., Guerova, G., Douša, J, Dick, G., de Haan, S., Pottiaux, E., Bock, O., & Pacione R. (2017a). COST Action ES1206: Advanced GNSS tropospheric products for monitoring severe weather events and climate (GNSS4SWEC), EGU2017-96, poster, EGU.

Jones, J., Guerova, G., Douša, J., Dick, G., de Haan, S., Pottiaux, E., Bock, O., & Pacione, R. (2017b). COST Action ES1206: Advanced GNSS tropospheric products for monitoring severe weather events and climate (GNSS4SWEC), EMS2017-51, oral, EMS.

Jones, J., Guerova, G., Douša, J, Dick, G., de Haan, S., Pottiaux, E., Bock, O., & Pacione R. (2017c). COST Action ES1206: The current status and future of GNSS-meteorology in Europe, G31D-0933, poster, AGU.

Kačmařík, M., Douša, J., Dick, G., Zus, F., Brenot, H., Möller, G., Pottiaux, E., Kapłon, J., Hordyniec, P., Václavovic, P., & Morel, L. (2017). Inter-technique validation of tropospheric slant total delays. *Atmospheric Measurement Techniques, 10*, 2183–2208. https://doi.org/10.5194/amt-10-2183-2017.

Klos, A., Pottiaux, E., Van Malderen, R., Bock, O., & Bogusz, J. (2017a). Study on homogenization of synthetic GNSS-retrieved IWV time series and its impact on trend estimates with autoregressive noise, EGU2017-11706, poster, EGU.

Klos, A., Van Malderen, R., Pottiaux, E., Bock, O., Bogusz, J., Chimani, B., Elias, M., Gruszczynska, M., Guijarro, J., Zengin Kazanci, S., & Ning, T. (2017b). Performance of various homogenization tools on a synthetic benchmark dataset of GPS and ERA-interim IWV differences. IAG-IASPEI Joint Scientific Assembly 2017, July 30–August 4, 2017, Kobe, Japan.

Landskron, D., & Böhm, J. (2017). VMF3/GPT3: Refined discrete and empirical troposphere mapping functions. *Journal of Geodesy*. https://doi.org/10.1007/s00190-017-1066-2.

Li, M., Li, W., Shi, C., Zhao, Q., Su, X., Qu, L., & Liu, Z. (2015). Assessment of precipitable water vapour derived from ground-based BeiDou observations with Precise Point Positioning approach. *Advances in Space Research, 55*, 150–162. https://doi.org/10.1016/j.asr.2014.10.010.

Lindskog, M., Ridal, M., Thorsteinsson, S., & Ning, T. (2017). Data assimilation of GNSS zenith total delays from a Nordic Processing Centre. *Chemical Physics, 17*, 13983–13998. https://doi.org/10.5194/acp-17-13983-2017.

Liu, Z., & Li, M. (2013). The first PPP-based GPS Water Vapour Real-Time Monitoring System in Pearl-River-Delta Region, China. In J. Sun, W. Jiao, H. Wu, & C. Shi (Eds.), *China satellite navigation conference (CSNC) 2013 proceedings* (pp. 71–87). Berlin/Heidelberg: Springer.

Macke, A., Seifert, P., Baars, H., Barthlott, C., Beekmans, C., Behrendt, A., Bohn, B., Brück, M., Bühl, J., Crewell, S., Damian, T., Deneke, H., Düsing, S., Foth, A., Di Girolamo, P., Hammann, E., Heinze, R., Hirsikko, A., Kalisch, J., Kalthoff, N., Kinne, S., Kohler, M., Löhnert, U., Madhavan, B. L., Maurer, V., Muppa, S. H., Schween, J., Serikov, I., Siebert, H., Simmer, C., Späth, F., Steinke, S., Träumner, K., Trömel, S., Wehner, B., Wieser, A., Wulfmeyer, V., & Xie, X. (2017). The HD(CP)2 observational prototype experiment HOPE – An overview. *Atmospheric Chemistry and Physics, 17*, 4887–4914. https://doi.org/10.5194/acp-17-4887-2017.

Mahfouf, J-F., Ahmed, F., Moll, P., & Teferle, F.N. (2015). Assimilation of zenith total delays in the AROME France convective scale model: a recent assessment. Tellus A, [S.l.], ISSN 1600-0870. https://doi.org/10.3402/tellusa.v67.26106. Available at: http://www.tellusa.net/index.php/tellusa/article/view/26106. Accessed 9 Dec 2016.

Mendes, V. B. (1998). Modeling the neutral-atmosphere propagation delay in radiometric space techniques. Ph.D. dissertation, University of New Brunswick, Fredericton, NB, Canada.

Mestre, O., Gruber, C., Prieur, C., Caussinus, H., & Jourdain, S. (2011). SPLIDHOM, a method for homogenization of daily temperature observations. *Journal of Applied Meteorology and Climatology, 50*, 2343–2358. https://doi.org/10.1175/2011JAMC2641.1.

Mohanakumar, K. (2008). *Stratosphere troposphere interactions: An introduction*. New York: Springer.

Möller, G. (2017). Reconstruction of 3D wet refractivity fields in the lower atmosphere along bended GNSS signal paths. Dissertation, Department of Geodesy and Geoinformation, TU Wien. http://repositum.tuwien.ac.at/obvutwhs/id/2268559

Möller, G., Wittmann, C., Yan, X., Umnig, E., Joldzic, N., & Weber, R. (2015). 3D ground based GNSS atmospheric tomography. Final report, FFG project GNSS-ATom (ID:840098).

Morel, L., Pottiaux, E., Durand, F., Fund, F., Boniface, K., de Oliveira, P. S., Jr., & Van Baelen, J. (2015a). Validity and behaviour of tropospheric gradients estimated by GPS in Corsica. *Advances in Space Research, 55*(1), 135–149. https://doi.org/10.1016/j.asr.2014.10.004.

Morel, L, Pottiaux, E., Durand, F., Fund, F., Follin, J.-M., Durand, S., Boniface, K., de Oliveira Jr, P. S., & Van Baelen, J. (2015b). Global validity and behaviour of tropospheric gradients estimated by GPS. International Union of Geodesy and Geophysics, General Assembly, 22 June–2 July 2015, Prague, Czech Republic.

Muller, M., Homleid, M., Ivarsson, K.-I., Koltzow, M., Lindskog, M., Midtbo, K.-H., Andrae, U., Aspelien, T., Berggren, L., Bjorge, D., Dahlgren, P., Kristiansen, J., Randriamampianina, R., Ridal, M., & Vigne, O. (2017). AROME-MetCoOp: A Nordic convective-scale operational weather prediction model. *Weather and Forecasting, 32*, 609–627. https://doi.org/10.1175/WAF-D-16-0099.1.

Nahmani S., & Bock, O. (2014). Sensitivity of GPS measurements and estimates during extreme meteorological events: The issue of stochastic constraints used for ZWD estimation in West Africa. Joint ES1206 MC and MC meeting, Golden Sands Resort, 11–12 September 2014, Varna, Bulgaria.

Nahmani S., Rebischung, P., & Bock, O. (2016). Statistical modelling of ZWD in GNSS processing. 3rd ES1206 workshop, Rugbrauðsgerdin, 8–10 March 2016, Reykjavik, Iceland.

Nahmani S., Rebischung, P., & Bock, O. (2017). Bayesian approach to apply optimal constraints on tropospheric parameters in GNSS data processing: Implications for meteorology. ES1206 final workshop, ESTEC, 21–23 February 2017, Noordwijk, Netherlands.

Namaoui, H., Kahlouche, S., Belbachir, A.-H., Van Malderen, R., Brenot, H., & Pottiaux, E. (2017). GPS water vapour and its comparison with radiosondes and ERA-Interim reanalysis in Algeria. *Advances in Atmospheric Sciences, 34*(5), 623–634.

Niell, A. E., Coster, A. J., Solheim, F. S., Mendes, V. B., Toor, P. C., Langley, R. B., & Upham, C. A. (2001). Comparison of measurements of atmospheric wet delay by radiosonde, water vapour radiometer, GPS, and VLBI. *The Journal of Atmospheric and Oceanic Technology, 18*, 830–850.

Ning, T., Elgered, G., Willén, U., & Johansson, J. M. (2013). Evaluation of the atmospheric water vapour content in a regional climate model using ground-based GPS measurements. *Journal of Geophysical Research, 118*. https://doi.org/10.1029/2012JD018053.

Ning, T., Wang, J., Elgered, G., Dick, G., Wickert, J., Bradke, M., Sommer, M., Querel, R., & Smale, D. (2016a). The uncertainty of the atmospheric integrated water vapour estimated from GNSS observations. *Atmospheric Measurement Techniques, 9*, 79–92. https://doi.org/10.5194/amt-9-79-2016.

Ning, T., Wickert, J., Deng, Z., Heise, S., Dick, G., Vey, S., & Schone, T. (2016b). Homogenized time series of the atmospheric water vapour content obtained from the GNSS reprocessed data. *Journal of Climate, 29*, 2443–2456. https://doi.org/10.1175/JCLI-D-15-0158.1.

Nogherotto, R., Biondi, R., Leclair de Bellevue, J, & Brenot, H. (2017). Characterization of tropical cyclones in the South Indian Ocean by using GNSS observations, EGU2017-3287, poster, EGU.

Pacione, R., Pace, B., de Haan, S., Vedel, H., Lanotte, R., & Vespe, F. (2011). Combination methods of tropospheric time series. *Advances in Space Research, 47*, 323–335. https://doi.org/10.1016/j.asr.2010.07.021.

Pacione, R., Pace, B., & Bianco G. (2014). Homogeneously reprocessed ZTD long-term time series over Europe, EGU GA. http://meetingorganizer.copernicus.org/EGU2014/EGU2014-2945.pdf

Pacione, R., Araszkiewicz, A., Brockmann, E., & Dousa, J. (2017a). EPN-Repro2: A reference tropospheric data set over Europe. *Atmospheric Measurement Techniques, 10*, 1689–1705. https://doi.org/10.5194/amt-10-1689-2017. (licensed under CC BY 3.0, https://creativecommons.org/licenses/by/3.0/).

Pacione, R., Pottiaux, E., & The IAG JWG 4.3.8 Team. (2017b). GNSS tropospheric products for climate: Objectives and future plans, EGU2017-8332, poster, EGU.

Parracho, A. (2017). Study of trends and variability of atmospheric integrated water vapour with climate models and observations from global GNSS network. PhD report from Université Pierre et Marie Curie, Paris, France.

Parracho, A. C., Bock, O., & Bastin, S. (2018). Global IWV trends and variability in atmospheric reanalyses and GPS observations. *Atmospheric Chemistry and Physics Discussions, 18*, 16213–16237. https://doi.org/10.5194/acp-2018-137, in review.

Pottiaux, E., & Bruyninx, C. (2016). GNSS-meteorology and GNSS-climate activities at ROB: Contribution to national projects, E-GVAP and COST Action ES1206 (GNSS4SWEC). 4th E-GVAP III joint expert team meeting, 6–0 December 2016, Copenhagen, Denmark.

Pottiaux, E., & Pacione, R. (2016). The IAG Joint Working Group 4.3.8: GNSS tropospheric products for climate. IAG Commission 4th Symposium, 4–7 September 2016, Wroclaw, Poland.

Pottiaux, E., Berckmans, J., & Bruyninx, C. (2014). Advanced multi-GNSS troposphere modeling for improved monitoring and forecasting of severe weather, EGU2014-11730, poster, EGU.

Pottiaux, E., Douša, J., Václavovic, P., & Bruyninx, C. (2015). First results of the real-time multi-GNSS troposphere parameters demonstration campaign at the royal observatory of Belgium. International Union of Geodesy and Geophysics, General Assembly, 22 June–2 July 2015, Prague, Czech Republic.

Sánchez Arriola, J., Lindskog, M., Thorsteinsson, S., & Bojarova, J. (2016). Variational bias correction of GNSS ZTD in the HARMONIE modeling system. *Journal of Applied Meteorology and Climatology, 55*, 1259–1276. https://doi.org/10.1175/JAMC-D-15-0137.

Shi, J., Xu, C., Guo, J., & Gao, Y. (2015). Real-time GPS precise point positioning-based precipitable water vapour estimation for rainfall monitoring and forecasting. *IEEE Transactions on Geoscience and Remote Sensing, 53*, 3452–3459. https://doi.org/10.1109/TGRS.2014.2377041.

Simeonov, T., Sidorov, D., Teferle, F. N., Milev, G., & Guerova, G. (2016). Evaluation of IWV from the numerical weather prediction WRF model with PPP GNSS processing for Bulgaria. *Atmospheric Measurement Techniques Discussions*. https://doi.org/10.5194/amt-2016-152.

Simeonov, T., Vey, S., Alshawaf, F., Dick, G., Guerova, G., Güntner, A., Hohmann, C., Lopez, E., Pottiaux, E., Trost, B., & Wickert, J. (2017). Monitoring of water cycle elements using GNSS geodetic receivers in North-East Germany at sub-daily resolution, EMS2017-28, poster, EMS.

Steinke, S., Eikenberg, S., Loehnert, U., Dick, G., Klocke, D., Di Girolamo, P., & Crewell, S. (2015). Assessment of small-scale integrated water vapour variability during HOPE. *Atmospheric Chemistry and Physics, 15*, 2675–2692. https://doi.org/10.5194/acpd-14-22837-2014.

Stepniak, K., Bock, O., & Wielgosz, P. (2018). Reduction of ZTD outliers through improved GNSS data processing and screening strategies. *Atmospheric Measurement Techniques, 11*, 1347–1361. https://doi.org/10.5194/amt-11-1347-2018.

Termonia, P., Van Schaeybroeck, B., De Ridder, K., Fettweis, X., Gobin, A., Luyten, P., Marbaix, P., Pottiaux, E., Stavrakou, T., Van Lipzig, N., van Ypersele, J.-P., & Willems, P. (2016). CORDEX.be: COmbining regional climate downscaling EXpertise in Belgium, EGU2016-12252, EGU, poster.

Termonia, P., Van Schaeybroeck, B., De Cruz, L., De Troch, R., Caluwaerts, S., Giot, O., Hamdi, R., Vannitsem, S., Willems, P., Tabari, H., Van Uytven, E., Hosseinzadehtalaei, P., Van Lipzig, N., Wouters, H., Vanden Broucke, S., van Ypersele, J.-P., Marbaix, P., Villanueva-Birriel, C., Fettweis, X., Wyard, C., Scholzen, C., Doutreloup, S., De Ridder, K., Gobin, A., Lauwaet, D., Stavrakou, T., Bauwens, M., Müller, J.-F., Luyten, P., Ponsar, S., Van den Eynde, D., & Pottiaux, E. (2018). The CORDEX.be initiative as a foundation for climate services in Belgium. Submitted to *Climate Services 11*, 49–61.

Troller, M. (2004). *GPS based determination of the integrated and spatially distributed water vapour in the troposphere*. Zurich: Swiss Federal Institute of Technology Zurich.

Van Malderen, R., Brenot, H., Pottiaux, E., Beirle, S., Hermans, C., De Mazière, M., Wagner, T., De Backer, H., & Bruyninx, C. (2014). A multi-site intercomparison of integrated water vapour observations for climate change analysis. *Atmospheric Measurement Techniques, 7*, 2487–2512. https://doi.org/10.5194/amt-7-2487-2014.

Van Malderen, R., Pottiaux, E., Klos, A., Bock, O., Bogusz, J., Chimani, B., Elias, M., Gruszczyńska, M., Guijarro, J., Zengin Kazancı, S., & Ning, T. (2017a). The homogenization of GPS Integrated Water Vapour time series: Methodology and benchmarking the algorithms on synthetic datasets, EMS2017-496, oral, EMS.

Van Malderen, R., Pottiaux, E., Klos, A., Bock, O., Bogusz, J., Chimani, B., Elias, M., Gruszczynska, M., Guijarro, J., Zengin Kazancı, S., & Ning, T. (2017b). Homogenizing GPS integrated water vapour time series: Methodology and benchmarking the algorithms on synthetic datasets. *Proceedings of the ninth seminar for homogenization and quality control in climatological databases and fourth conference on spatial interpolation techniques in climatology and meteorology*, Budapest, Hungary, 2017c, WMO, WCDMP-No. 845, edited by T. Szentimrey, M. Lakatos, L. Hoffmann, pp. 102–114 (http://www.wmo.int/pages/prog/wcp/wcdmp/wcdmp_series/WCDMP_85.pdf) pp. 104–116.

Van Malderen, R., Pottiaux, E., Stankunavicius, G., Beirle, S., Legrand, J., Brenot, H., Wagner, T., De Backer, H., & Bruyninx, C. (2017c). A world-wide analysis of the time variability of integrated water vapour, based on ground-based GNSS and GOMESCIA satellite retrievals, and with reanalyses as auxiliary tools, EMS2017-547, oral, EMS.

Van Schaeybroeck, B., Termonia, P., De Ridder, K., Fettweis, X., Gobin, A., Luyten, P., Marbaix, P., Pottiaux, E., Stavrakou, T., Van Lipzig, N., van Ypersele, J.-P., & Willems, P. (2017a). The foundation for climate services in Belgium: CORDEX.be, EGU2017-6855, PICO, EGU.

Van Schaeybroeck, B., Termonia, P., De Ridder, K., Fettweis, X., Gobin, A., Luyten, P., Marbaix, P., Pottiaux, E., Stavrakou, T., Van Lipzig, N., van Ypersele, J.-P., & Willems, P. (2017b). The foundations for climate services in Belgium: CORDEX.be, EMS2017-414, poster, EMS.

Vincent, L. A., Zhang, X., Bonsal, B. R., & Hogg, W. D. (2002). Homogenisation of daily temperatures over Canada. *Journal of Climate, 15*, 1322–1334.

Wang, X., Dai, Z., Zhang, E., Ke, F., Cao, Y., & Song, L. (2014). Tropospheric wet refractivity tomography using multiplicative algebraic reconstruction technique. *Advances in Space Research, 53*, 156–162. https://doi.org/10.1016/j.asr.2013.10.012.

Xia, P., Cai, C., & Liu, Z. (2013). GNSS troposphere tomography based on two-step reconstructions using GPS observations and COSMIC profiles. *Annales de Geophysique, 31*, 1805–1815. https://doi.org/10.5194/angeo-31-1805-2013.

Xu, A., Xu, Z., Ge, M., Xu, X., Zhu, H., & Sui, X. (2013). Estimating zenith tropospheric delays from BeiDou Navigation Satellite System observations. *Sensors, 13*, 4514–4526. https://doi.org/10.3390/s130404514.

Yao, Y., & Zhao, Q. (2016). Maximally using GPS observation for water vapour tomography. *IEEE Transactions on Geoscience and Remote Sensing, 54*, 7185–7196. https://doi.org/10.1109/TGRS.2016.2597241.

Yao, Y. B., Zhao, Q. Z., & Zhang, B. (2016). A method to improve the utilization of GNSS observation for water vapour tomography. *Annales de Geophysique, 34*, 143–152. https://doi.org/10.5194/angeo-34-143-2016.

Ye, S., Xia, P., & Cai, C. (2016). Optimization of GPS water vapour tomography technique with radiosonde and COSMIC historical data. *Annales de Geophysique, 34*, 789–799. https://doi.org/10.5194/angeo-34-789-2016.

Zhang, B., Fan, Q., Yao, Y., Xu, C., & Li, X. (2017). An improved tomography approach based on adaptive smoothing and ground meteorological observations. *Remote Sensing, 9*, 886. https://doi.org/10.3390/rs9090886.

Chapter 7
STSM Reports

Guergana Guerova

Abstract In this section are presented the Short Term Scientific Mission (STSM). STSM is a very efficient tool for knowledge transfer between the network partner. Based on submitted and evaluated application funding is provided for a visit between 1 week up to 3 months. GNSS4SWEC funded 22 STSM, which took place in the period 2013–2017.

STSM Applicant: *Mr Furqan Ahmed, University of Luxembourg, Luxembourg (LU),* furqan.ahmed@uni.lu

STSM Topic: *Impact of Assimilating GNSS-derived ZTD from Luxembourg and the Greater Region into NWP model AROME*

Host: *Jean-Francois Mahfouf, Meteo-France, Toulouse (FR),* jean-francois.mahfouf@meteo.fr

The main objective of this short-term scientific mission (STSM) under COST Action ES1206 was to investigate whether the densification of the GNSS network over Luxembourg and the Greater Region would show an improvement in the weather forecasts for this region based on MétéoFrance's regional NWP model AROME. It also addressed the question if there would be any benefits for MétéoFrance to include ZTDs from these additional GNSS stations in future.

Methodology The hourly NRT ZTD solution generated at the UL, namely UL01, contains ZTD estimates from a European network of GNSS stations, which include stations belonging to IGS, the EPN and the Reseau GNSS Permanent (RGP). To densify the network over Luxembourg and the Greater Region, six stations from SPSLux (Luxembourg) and 22 from WALCORS (Wallonie, Belgium) were also processed. In total the GNSS network approaches 200 stations. A dataset containing

G. Guerova (✉)
Physics Faculty, Department of Meteorology and Geophysics, Sofia University "St. Kliment Ohridski", Sofia, Bulgaria
e-mail: guerova@phys.uni-sofia.bg

J. Jones et al. (eds.), *Advanced GNSS Tropospheric Products for Monitoring Severe Weather Events and Climate*, https://doi.org/10.1007/978-3-030-13901-8_7

ZTD (and IWV) estimates from UL01 for a period of approximately 1 month (July 17–August 20, 2013) was prepared in the form of 1-hourly COST-716 format files and was then converted into the BUFR format. Please note that the term "GNSS" will imply only the Global Positioning System (GPS) in this summary.

Followed by the generation of the GNSS-derived NRT ZTD dataset, forecast experiments were conducted using the 3D-variational (3D-VAR) data assimilation system of the AROME NWP model. For the period of July 17–August 20, 2013, three forecast experiments were conducted using the AROME 3D-VAR NWP model:

i. One experiment without any GNSS ZTD observations
ii. One experiment with GNSS ZTD from the operational EGVAP solutions assimilated
iii. One experiment with GNSS ZTD from UL01 in addition to operational EGVAP solutions assimilated

Results and Conclusions As a result of the assimilation of the GNSS-derived ZTD, the AROME 3D-VAR short-range forecasts were found to be closer to the observations that are sensitive to humidity which implies that through the assimilation of GNSS-derived ZTD, the 3-h prediction of the humidity field by AROME becomes closer to the truth. The investigation of the impact on objective forecast skill scores revealed a small positive impact on screen-level relative humidity and the 24-h precipitation accumulations. The categorical scores were found to be systematically improved when the UL01 data were assimilated in addition to the operational EGVAP ZTD observations. Examination of three precipitation case studies confirmed that the GNSS-derived ZTD observations affect the predicted location and intensity of rain systems that generally improved the quality of the numerical forecasts. It was found that the additional ZTD data provided by UL01 significantly modified rainfall patterns with, most of the time, a better location and intensity of precipitating cells. Furthermore, this STSM was the first instance when the ZTD from SPSLux stations was compared to a non-GNSS reference ZTD. As one of the results of this STSM, it was found that the ZTD from the SPSLux stations have a significant bias. Therefore, after this STSM, the reason for this bias in the ZTD estimates from SPSLux stations was investigated and the biases were mitigated.

Recommendations It is of high interest that a similar set of experiments, as performed in this STSM, be performed again with the new SPSLux data after the removal of the biases. This will further help understanding the impact of NRT ZTD from Luxembourg on the quality of AROME 3D-VAR forecasts for Luxembourg.

Furthermore, the results of this STSM suggested that the E-GVAP Test Solution UL01 should be made an E-GVAP Operational Solution to routinely benefit NWP activities.

Publication of Results The results from this study were published in a peer reviewed journal with an impact factor of 2.518 (Mahfouf et al. 2015).

STSM Applicant: Dr Kalev Rannat, Tallinn University of Technology, Tallinn (EE), kalev.rannat@dcc.ttu.ee

STSM Topic: Improved processing and use of GNSS Zenith Total Delay and Integrated Water Vapour data for Climatology.

Host: Jens Wickert, GFZ German Research Centre for Geosciences, Potsdam (DE), wickert@gfz-potsdam.de

The purpose of this STSM was to initiate a long-term study on quantifying the impact of GNSS data quality and collocation issues for inter-comparison experiments supporting climatological investigations. In general, this study consists of two tasks – one is related to GNSS data processing and the IWV derivation from the ZTD data and another is related to quantifying the effects of distances (both horizontal and vertical shifts) between different GNSS instrumentation used during inter-comparison experiments at collocated sites. The motivation for this STSM was to get additional information and to improve expertise in organizing raw GNSS observation data flow and routine quality check for meteorological purposes. This expertise will be used for preparing the GRUAN (GCOS Reference Upper Air Network) network operational (i.e., by working out technical requirements for sending GNSS data from GRUAN sites to the GNSS Data Processing Centre (GFZ) for offering GRUAN IWV product to end users).

The STSM started at GFZ Potsdam and lasted 5 days. The work was planned on the following subtopics:

- acquisition of raw data and the methods for data quality control, practical issues by using data from collocated sites (use cases, where the ground level meteorological data and GNSS-observational data does not come from the same site, but from some kilometres afar);
- reprocessing of some data samples taken from Sodankylä (GRUAN site), using different processing methods (PPP and DD), comparing and analysing the results with those, calculated earlier (by using GAMIT);
- investigating the possibilities for improving the quality of raw data and the final product (GNSS IWV) using reprocessing results and the expertise from GFZ.

One of the main results was introducing personal contacts with researchers of GFZ and finding common interests in further research. A lot of practical experience and know-how was collected (from numerous personal communications) during this STSM. Common interests were found in experimental work planned to Sodankyla and dedicated to collocation issues. This work will support both COST ES1206 efforts and GRUAN scientific part and will last for years. For quantifying the effects of distances (both horizontal and vertical shifts) between different instrumentation (incl. GNSS and Radiosondes) during inter-comparison experiments the collocated sites from Sodankyla have been chosen - Pittiövaara (SODA) and Tahtela (SOD1), hosted by FMI. To validate the effect of distances and heights while using surface meteorological data from radius of 20 km, extra RS will be launched at Pittiövaara (using a mobile RS launcher). Resulting IWV time series derived from RS and GNSS will be compared (additionally with MWR and FTIR if possible). These experiments need to follow meteorological conditions (e.g. wind speed and direction), to estimate the impact of balloon drift on the results of IWV time series

obtained by different techniques. GFZ can process GNSS data both with PPP and DD methods (EPOS software). It gives an independent proof for planned intercomparison results from Sodankyla.

The work will not end with this STSM. It will continue in frames of GRUAN scientific activities and the ongoing COST ES1206, by using data sets from many sites. The aim is to help GRUAN GNSS-sites to support GRUAN data analysis with the best available and continuous observational data. Additionally, it supports COST ES1206 WG3 efforts in validating IWV time series for trends' analysis. The results of intercomparison experiments from Sodankyla are planned to be published as an ISI journal article.

STSM Applicant: *Mr Tomasz Hadaś, Wroclaw University of Environmental and Life Sciences, Wroclaw (PL),* tomasz.Hadaś@up.wroc.pl
STSM Topic: *Neutral atmosphere delay model for Precise Point Positioning*
Host: *Marcelo Santos, University of New Brunswick, Fredericton (CA),* msantos@unb.ca

The purpose of this STSM was to investigate the application of neutral-atmospheric delay models in real-time Precise Point Positioning (PPP). Grantee used his original GNSS positioning software GNSS-WARP and developed it by implementing UNB3 neutral atmosphere delay model and VMFs. Both models can be used alternatively, as well as jointly e.g. by taking zenith delay values from UNB3 and mapping functions from VMF. The resulting kinematic coordinates were compared with true, static coordinates of station WROC (plot 'dNEU'), and the error of coordinates component were provided from covariance matrix (plot 'mNEU'). One can see (Fig. 7.1) that generally the coordinates are accurate and precise at the level of 10 cm for horizontal components and 20 cm for vertical component after about 45 min of convergence. Unfortunately, there are regular picks in both plots, that are related with IODE mismatching between RTS stream and ephemeris data. This bug requires additional checking to be implemented in the software.

The performance of the program was initially verified by comparing the exemplary results with the one obtained by GAPS, when the same set of data was processed, both in kinematic and static positioning. For this purpose, a basic module for RINEX files processing was also implemented. The differences in coordinates between two software are below centimetre level. Even though, the sources of differences have been identified, which is the basis for further development of the GNSS-WARP software. The grantee and the host institution declared a future collaboration related with the development of the GAPS. The grantee can share his experience on using the IGS RTS products and help further development of the software, to become multi-GNSS real-time software as well.

STSM Applicant: *Dr Witold Rohm, Wroclaw University of Environmental and Life Sciences, Institute of Geodesy and Geoinformatics, Wroclaw (PL),* witold.rohm@igig.up.wroc.pl
STSM Topic: *Application of GNSS tomography for severe weather studies*
Host: *Jonathan Jones, Met Office, Exeter (UK),* jonathan.jones@metoffice.gov.uk

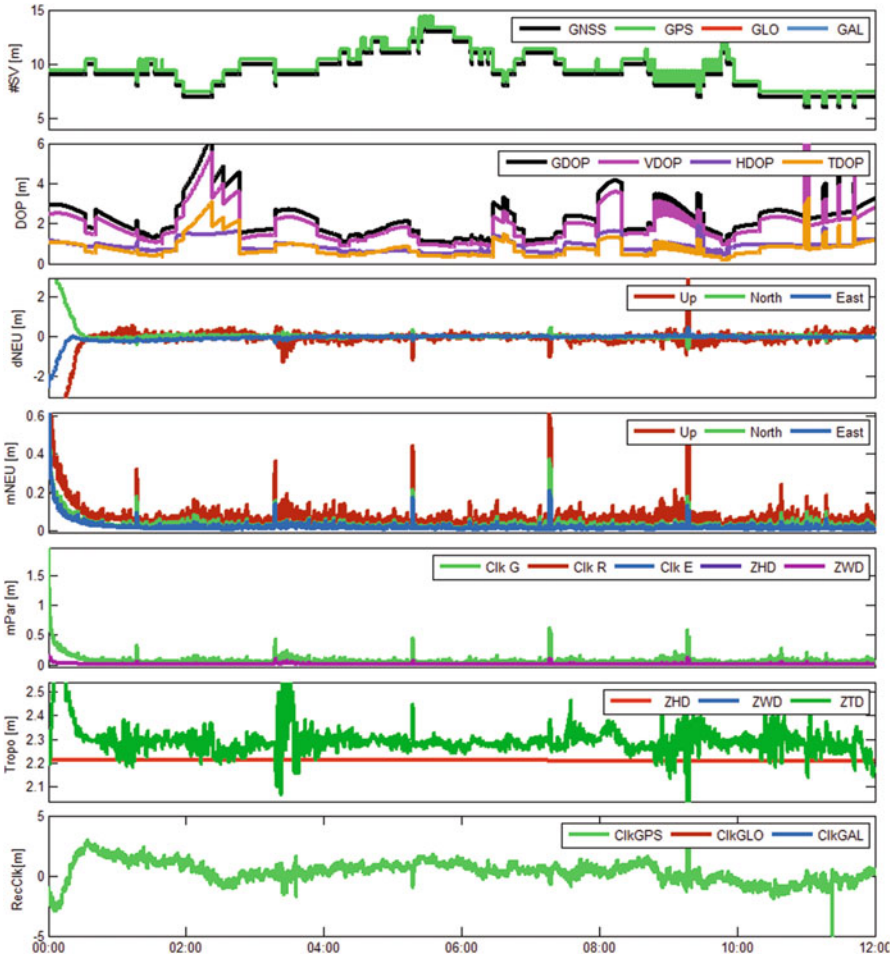

Fig. 7.1 Exemplary performance of GNSS-WARP during 12 h of fully-kinematic data processing for station WROC (IGS RTS IGS03 stream, 1 s sampling, a priori troposphere: Vienna Mapping Functions, elevation cut-off angle: 5°)

Numerical weather prediction (NWP) models are commonly used by all meteorological agencies to forecast short-, mid- and long- term variation of troposphere. Models are based on seven governing fundamental equations of: motion (three directions), continuity, conservation of mass, energy and mixing ratio. The NWP models in general has two major functional parts Data Assimilation (to set up boundary condition, initial conditions and subsequently add observations) and forecasting part that is govern by a number of partial differential equations describing 3D motion of air masses.

One of the important data source for DA is GNSS. The GNSS provides instantaneous, all-weather and precise position all-round the world. However, as signal

propagates through the atmosphere it is refracted and bended. The magnitude of these effects are directly linked, at least in the troposphere, with: temperature, pressure and water vapour content. As GNSS community is interested mostly in the positioning the atmosphere effects were considered to be a nuisance parameter, estimated and removed from the solution. Nowadays, as the distribution and variability of water vapour is of great interest to all members of NWP community and become valuable product that can be assimilated in weather models.

This short-term scientific mission (STSM) aims to improve the understanding of Data Assimilation in NWP models in GNSS community and stimulate development of new more meteorology-oriented GNSS products. It also brings some advanced GNSS processing techniques such as GNSS tomography for NWP community consideration. The selected region of interest is located in the south of England and covers four receivers CHIO, POOL, SANO, SOTN, data are available through the E-GVAP ftp repository. The test stations are located on different heights (~60 m height difference) with inter-station distance of 20–35 km. The investigated case study covers the heavy rain period, between 3rd and 13th of February 2014, the south and south west of UK was flooded along Thames basin. Time resolution of GNSS ZTD is 15 min, therefore the GNSS tomography profile is also available every 15 min.

The preliminary results show that in the normal weather conditions GNSS tomography retrieves the profile quite well i.e. the initial profile from deterministic models (such as GPT or UNB3M are used to initialise TOMO2 model) is shifted to the correct location (the bias of deterministic models is removed). The bottom part of the profile as there are limited number of intersecting rays in the surface layer and it will translate to the problems in retrieving bottom part of the troposphere. The inversion profile has not been reproduced well as it is located in the troposphere region that is barely scanned by the GNSS observations. Further investigations with synthetic data are required to assess whether the quality of the retrieved profile could be improved. Moreover, synthetic simulations should be performed to study minimal requirements for "tomography towers" in the advent of introducing new satellite systems and new, more precise, retrievals of Slant Total Delays.

The forward model for GNSS tomography H has not been fully constructed yet. The concept is quite straight forward; the NWP model variables converted to the wet refractivities at the nodes should be merge (averaged) together to obtain tomography equivalent scale of the model element. The observation errormatrix is available from Kalman filtering as a covariance matrix of the filtered state. However, before assimilating the tomography outputs, more synthetic and real case studies have to be run to assess whether the strict quality requirements imposed by Met Office could be achieved.

STSM Applicant: *Mr Pavel Václavovic, Research Institute of Geodesy, Topography and Cartography, Zdiby (CZ),* pavel.Václavovic@pecny.cz

STSM Topic: *Developing of ultra-fast tropospheric products*

Host: *Eric Pottiaux, Royal Observatory of Belgium, Brussels (BE),* e.pottiaux@oma.be

One topic which the STSM was aimed at was implementation of tropospheric gradients estimation into the G-Nut/Tefnut software (Vaclavovic and Dousa 2013) developed at the Geodetic Observatory Pecný in Czech Republic. The increasing demands for real time and near real time tropospheric products being used for Numerical Weather Prediction (NWP) nowcasting or severe weather monitoring were motivations for improving such new software focused on the troposphere monitoring. As long as observations at low elevation (below 10°) are processed, the troposphere asymmetry must be considered to improve the repeatability of station coordinates and also the precision of other parameters.

The adjustment procedure in the PPP is the Kalman filter coping with various parameter dynamics. Ambiguities are estimated as float values and thus they require a certain time to converge. A backward smoothing algorithm can be applied for reaching estimated parameters with same precision during the entire processing interval. The algorithm can be exploited in the offline or in the near real time processing. The mentioned algorithms were tested and enhanced.

Results The software G-Nut/Tefnut was significantly improved and tested during the STSM. Two approaches for tropospheric gradients modelling were implemented: (1) tilting atmosphere, (2) algorithms provided by (Chen and Herring 1997). Both techniques were tested using data from the dense Belgian permanent stations network.

Statistics of the G-Nut/Tefnut ZTD results was determined for the daily solution (20th September 2012) of the ANTW station with respect to the results from the BSW. Table 7.1 summarizes biases and standard deviations.

Table 7.1 shows lower standard deviation for the smoothed ZTDs which corresponds with the expectation. On the one hand, the improved precision is due to avoiding the convergence period. On the other hand, the backward smoothing exploited data from the entire interval and the standard deviation is better than that of the simple forward filter even when parameters from the convergence period were rejected.

The STSM started very close collaboration between GOP and ROB. The software is being developed at GOP and seriously tested using the dense Belgian network data at the ROB. The collaboration consists of the user feedback and software developments according to potential requirements.

STSM Applicant: *Mr Tzvetan Simeonov, Department of Meteorology and Geophysics, Sofia University, Sofia (BG),* simeonov@phys.uni-sofia.bg

Table 7.1 Biases and standard deviations for ZTD with respect to the BSW solution

Estimation procedure	Data description	Bias [m]	std [m]
Forward filter	All data	0.001	0.010
	Without convergence period	0.000	0.009
Backward smoothing	All data	0.001	0.006
	Without convergence period	0.000	0.006

STSM Topic: *Tropospheric products processing for Bulgarian ground-based GNSS network*

Host: *Felix Norman Teferle, University of Luxembourg, Luxembourg(LU),* Norman.Teferle@uni.lu

The Sofia University GNSS Analysis Centre (SUGAC) is the first AC in South-East Europe with a focus on deriving atmospheric products from ground-based GNSS networks The SUGAC uses the NAPEOS GNSS software for this purpose. The mission was foreseen for gaining experience with the software while a license from ESA is granted. A comparison with the BSW is envisaged as a next step. The SUGAC is established in collaboration with the Bulgarian network, contributing to EUPOS. The stations, chosen for initial processing are from East to West: Varna (VARN), Burgas (BURG), Shumen (SHUM), Stara Zagora (STAR), Lovech (LOVE), Rozhen peak (ROZH) and Montana (MONT).

NAPEOS has several key features:

- Multi-GNSS processing, incorporating GPS, GLONASS and the European GALILEO
- Includes processing of undifferenced and double-differenced data, although the latter has not been maintained for some time
- User-friendly interface
- The license is free of charge

The analysis centre at the Research Unit in Engineering Science of the University of Luxembourg (Uni. Luxembourg) uses NAPEOS since 2011. The tropospheric products processed during the STSM were be used for comparison with the numerical weather prediction model (WRF) for Bulgaria. The GNSS derived water vapour proved to have very high correlation with the WRF model (above 0.9) for the whole period for the complete dataset. GNSS IWV from this processing has a positive systematic bias, compared to the model simulations. The results of this work are included in Sect. 3.7.2 "Supporting new analysis centres, new networks, transfer of knowledge" of the WG1 report for the COST action. The work from this STSM will be continued with the establishment of autonomous near real-time processing of the regional ground-based GNSS network in Southeast Europe in support of the EUMETNET E-GVAP.

STSM Applicant: *Mr Peter Szabo, Climate Modelling Group, Hungarian Meteorological Service, Budapest (HU),* szabo.p@met.hu

STSM Topic: *Tropospheric products from GNSS and ALADIN-Climate regional climate model for East-Southeast Europe*

Host: *Assoc. Prof Guergana Guerova, Department of Meteorology and Geophysics, Sofia University, Sofia (BG),* guerova@phys.uni-sofia.bg

Methodology and Data The STSM aims to intercompare GNSS tropospheric products with the ALADIN-Climate regional climate model. This version (5.2) of ALADIN-Climate used at the Hungarian Meteorological Service (HMS) has a horizontal resolution of 50 km integrated over the whole European continent. The

simulation used in this study has the lateral boundary conditions derived from ERA-Interim reanalysis fields, which means it can also capture main weather patterns in Europe. Water vapour path is computed in ALADIN-Climate by subtracting solid and liquid phase from total amount of water in the atmosphere.

Regarding observations, Sofia station from IGS-repro1 GNSS data-set was used. The station is located in the Plana mountain about 20 km from Sofia and is equipped with an AR25 Leica antenna.

Activities and Results Firstly, the conversion of ZTD to IWV was checked for the observations–due to different literature, also to calculate ZTD in the model. After that, we could intercompare IWV and ZTD (besides pressure and temperature). Evaluation of ERA-Interim was not considered at this stage.

Calculated were correlations between G1/G2 model grid points (two closest points) and observation, variance and mean, coefficient of variation, diurnal cycle, annual cycle, different thresholds in the distribution. We also looked into detail of different weather situations, e.g. the IWV model simulations during the 2007 heatwave over Bulgaria. Some findings:

- Since G1 is at lower altitude, it overestimates IWV values by 0.36 mm as annual bias while at G2 by 1 mm. Diurnal IWV cycle is relatively well simulated (Fig. 7.2). The simulated IWV minimum is at 00:00 UTC for G1 and G2, while the observed minimum is at 06:00 UTC. The magnitude of the diurnal cycle is higher in the observation than in the model.
- Temperature correlation with the observation is very high in both model grid points, with no significant difference in them (Fig. 7.3). Modelled ZTD and IWV correlation with their observed values are lower (0.67–0.75), and they are the best at 12:00 UTC. Pressure values correlate better at G1 with observation, while both ZTD and IWV have higher values at G2.
- Annual IWV cycle is fairly captured in the model in both lower and higher altitude points (Fig. 7.4). Simulated IWV peaks in July, while the observed one in August. Since G1 is at altitude 250 m below G2, IWV values are always mm higher than at G2. Somehow in the 2nd half of the year, the simulated IWV at G2 is underestimating the observed one and values are closer at G1.
- Zooming in the data, big differences at some time steps can appear (Fig. 7.5). During the heatwave of July 2007, modelled IWV values happen to overestimate by 10–15 mm the observed ones. Regional climate models with the boundary conditions of reanalyses cannot capture all weather events at all times, but they supposed to capture these synoptic-scale events better.
- Percentage of different thresholds (5, 15, 25, 35 mm) of the distribution shows that at no single times occurred values above 35 mm in Sofia (not shown). At G1 the probability of very high values is 0.26%, while at G2 it is virtually zero. Except the threshold of above 15 mm, G2 captures better the values for the selected 4 thresholds than G1.

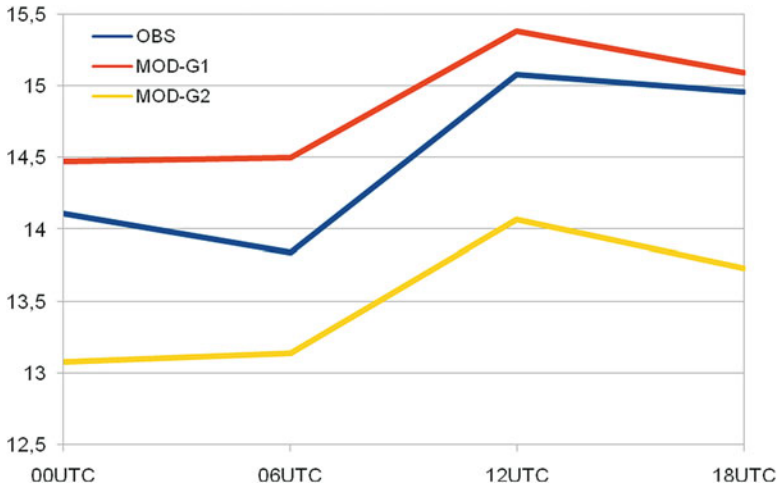

Fig. 7.2 Diurnal cycle of the averaged IWV (mm) in the observation and model grid points

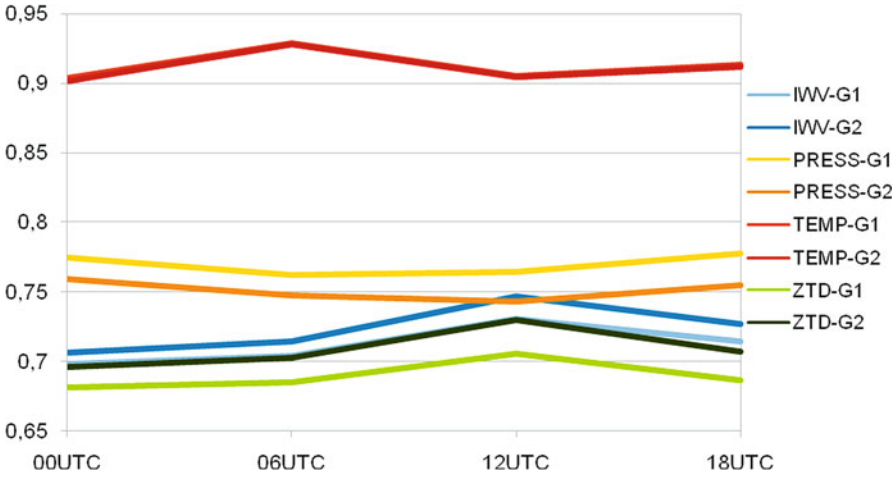

Fig. 7.3 Correlation of observed and modelled (G1/G2) values for IWV, PRESS, TEMP and ZTD

Further Plans We would like to investigate more GNSS sites with available meteorological variables, to include more years (availability from 1995 to 2007), a more homogeneous period and smoother orography, also, stations with different climates in order to test ALADIN-Climate over Europe.

STSM Applicant: *Dr Douša Jan, Research Institute of Geodesy, Topography and Cartography, Ustecka 98 (CZ),* jan.Douša@pecny.cz

STSM Topic: *Installing new analysis centre for near real-time GNSS troposphere monitoring in Turkey*

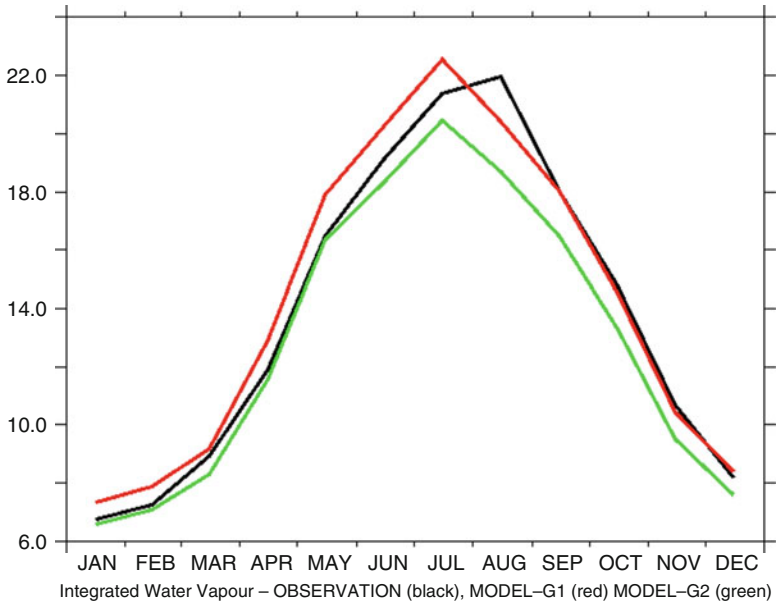

Fig. 7.4 Annual cycle of IWV (mm) for the observation (black) and model grids (G1-red, G2-green)

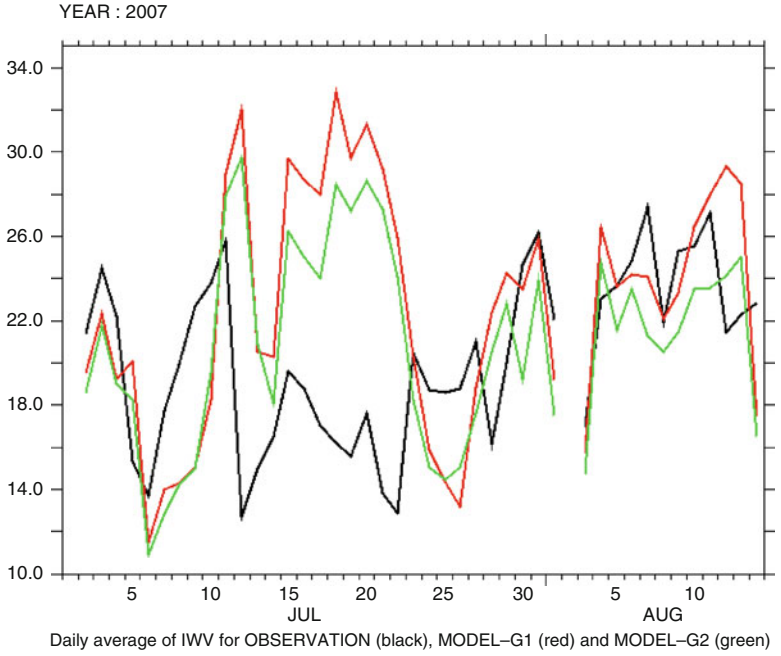

Fig. 7.5 Daily averaged IWV (mm) for the observation (black) and model grids (G1-red, G2-green) over 2007

Host: Emine *Tanir Kaykci, Karadeniz Technical University, Dept. of Geomatics Engineering, Trabzon (TR),* etanir@ktu.edu.tr

STSM Topic: *Installing new analysis centre for near real-time GNSS troposphere monitoring in Greece*

Host: *Christos Pikridas, Aristotle University of Thessaloniki, Dept. of Geodesy and Surveying, Thessaloniki (EL),* cpik@topo.auth.gr

STSM Topic: *Installing new GNSS analysis centre for troposphere monitoring in Iceland*

Host: *Benedikt Gunnar Offeigson, Icelandic Meteorological Service, Reykjavík (IS),* bgo@vedur.is

Three short-term (4–5 days) STSMs have supported the transfer of knowledge aimed at exploiting the developments and long-term expertise in GNSS near real-time (NRT) analyses for the troposphere monitoring. The main goal was to establish four new analysis centres of the EUMETNET GNSS Water Vapour Programme (E-GVAP, http://egvap.dmi.dk) with the support of Geodetic Observatory Pecný (GOP), Czech Republic. For this purpose, GOP offered the TropNET system developed and completed for an easy setting and maintenance of all necessary activities associated with the NRT tropospheric parameter estimates. Four agencies were ready to install the system for setting up an analysis centre contributing with new data to the E-GVAP service:

- AUT – Aristotle University of Thessaloniki (Greece)
- BEU – Bulent Ecevit University in Zolgundak (Turkey)
- KTU – Karadeniz Technical University in Trabzon (Turkey)
- IMO – Icelandic Meteorological Office (Iceland)

The Trop-NET system has been developed as a set of modules and utilities which include data and product downloads and conversions, archiving and cleaning, provides data processing in a fully self-sufficient operation including estimates of precise station coordinates tied to the realization of the international terrestrial reference frame, perform the quality control and validation of all input data and products, reports errors and warnings from the operation, provide quality control of the tropospheric products, their conversion, evaluation and submission to the E-GVAP. The GNSS data analysis uses the BSW and for different installations it supported versions 5.0/5.2. All the STSMs included several tasks from which only some were necessarily performed at the facilities of the new analysis centres:

- hardware consultation and preparation, Linux environment installation and settings, BSW installation and testing,
- installation of GOP' Trop-NET processing system from the shared repository maintained by GOP, system adaptations specific to each individual analysis centre,
- station meta data preparation, repository organization including the mirror of observations from the EUREF reference stations, precise IGS orbit products and processing models,

- testing the functionality of the system modules – data download, data processing, tropospheric products evaluation,
- initial backward processing of 1–2 months followed by operational near real-time processing,
- the system and product education and training,
- support in preparing submissions to E-GVAP,
- product validations in GOP-TropDB and the online monitoring service provided by GOP at http://www.pecny.cz/COST-TropNET.

Over past 1–2 years, all four analysis centres have contributed operationally to the E-GVAP providing 220+ new stations and stable basis for further extensions. More analysis centres were also supported remotely by consultations, by sharing the TropNET system and by processing data in the GOP solution.

STSM Applicant: *Ms Gokhan Gurbuz, Bulent Ecevit University, Zonguldak (TR),* gokhanngurbuz@gmail.com

STSM Topic: *GNSS Processing for tropospheric delay. Develop a near real-time GNSS processing system for the Turkish GNSS stations (Istanbul and Ankara).*

Host: *Szabolcs Rozsa, Budapest University of Technology and Economics, Budapest (HU),* rozsa.szabolcs@epito.bme.hu

My STSM carried out by the hosting of Dr. Szabolcs Rozsa from the Budapest University of Technology and Economics (BME), Hungary. The purpose of the STSM was the realization of the near real time GNSS processing system of the Turkish GNSS stations and relating research activities. The STSM began with a meeting on how to proceed in STSM and discussion of the work plan. BSW50 on UNIX platform is installed while information about the software, processing techniques, adjustment of a network, tropospheric parameter estimations, and near-real time processing has been answered by Dr. Rozsa. He also shared invaluable knowledge of GNSS processing, especially about near real time GNSS processing.

With the help of Dr. Rozsa, we installed and set up a near real time GNSS processing scheme for BSW50 using a network based on EUREF and IGS stations in the vicinity of Turkey. The processing scheme was tested on a data set of 3 weeks. Dr. Rozsa shared the knowledge of automated processing in BSW50 and how to write the appropriate scripts in UNIX environment. Thanks to that information now I am able to write any scripts, which helps me with GNSS processing. I learned how to update the script provided by the colleagues in Budapest. To conclude the STSM a short project was carried out to process ground based GNSS data during a severe weather event happened in Istanbul. The estimated ZTDs were converted to PWV using local surface meteorological observations. The PWV estimations were compared to radiosonde reference values, too. I would like to greatly thank the COST Office for allowing me to visit Budapest University of Technology and Economics.

STSM Applicant: *Ms Karina Wilgan, Wroclaw University of Life and Environmental Sciences, Wroclaw (PL),* karina.wilgan@igig.up.wroc.pl

STSM Topic: *Parameterized refractivity models and GNSS path delays in view of GNSS Severe Weather Monitoring*

Host: *Alain Geiger, Institute of Geodesy and Photogrammetry, ETH Zurich, Zurich (CH),* alain.geiger@geod.baug.ethz.ch

During this STSM a study on parameterized refractivity models and GNSS path delays was conducted. The refractivity values as well as ZTD can be expressed as a functions of meteorological parameters. For various applications, it is necessary to know the values of tropospheric parameters at locations that do not coincide with actual measurement locations. The Geodesy and Geodynamics Lab at ETH Zurich has developed a software package COMEDIE (Collocation of Meteorological Data for Interpretation and Estimation of Tropospheric Path delays) to interpolate and extrapolate meteorological parameters from real measurements to the arbitrary locations. The collocation algorithms were used to calculate the total refractivity field over a western part of Switzerland. The grantee has also implemented the ZTD horizontal gradients models into the software to investigate if they bring any improvements for the interpolation of the refractivity.

The tropospheric parameters were calculated from two main data sources: ground-based meteorological measurements (air pressure, temperature and water vapour used to calculate total refractivity) and GNSS (ZTD and horizontal gradients). From those data sources, different datasets of input data were constructed: ZTD/Ntot, ZTD/Ntot/GRAD and Ntot only. Using the particular input dataset, the total refractivity profiles over Payerne were calculated to assess which dataset has the best agreement with the reference radiosonde measurements. The dataset with the best performance of total refractivity interpolation was ZTD/Ntot with the absolute biases from 0 to 6 ppm and standard deviations 3–10 ppm. Excluding the ZTDs from the collocation results in worsening the interpolation above the 2 km by over 10 ppm. Introducing the horizontal gradients was presumed to improve the interpolation, but for the vertical interpolation at Payerne the refractivity field from the dataset with gradients was worse by about 0.5 ppm than the interpolation without gradients. Another way to assess the refractivity models obtained using COMEDIE is to compare them with ground-based data from all meteorological stations at the surface level. Except for two stations, the absolute biases of the residuals were at the level of 0–4 ppm with 7–8 ppm standard deviations for both datasets - including and excluding the gradients. The interpolation with gradients was unfortunately worse than without, but only by about 0.1 ppm.

STSM Applicant: *Dr Riccardo Biondi, International Centre for Theoretical Physics (ICTP), Trieste (IT),* riccardo@biondiriccardo.it

STSM Topic: *GNSS atmospheric water vapour detection for extreme events*

Host: *Hugues Brenot, Belgian Institute for Space Aeronomy, Brussels (BE),* Hugues.Brenot@oma.be

Within the project CONSYDER FP7-PEOPLE-IEF “Convective systems detection and analysis using radio occultation” I am analysing GPS RO profiles from different missions (COSMIC, METOP, GRACE, CHAMP and SACC) to understand if severe storms leave a significant signature in RO profiles. The combined use of GNSS ground based receivers for measuring the atmospheric water vapour

content and the GNSS RO profiles is a big challenge for forecasting and monitoring such kind of extreme events.

The experience of Dr. Brenot on GNSS water vapour detection and atmospheric water vapour tomography together with my experience on GNSS RO profiling will lead in a short-term period to structure a new collaboration and hopefully new proposals for studying, detecting and monitoring extreme events and in long-term period to the development of a new algorithm for understanding the 3D structure of strong convective systems.

Research Activity We have selected some specific case with extreme weather events in Belgium in August 2010 and August 2011 and a long wet period in United Kingdom from October 2013 to February 2014 and we have decided to focus our work on these events. We also started to collect meteorological parameters such as wind speed and rain rate at the ground for evaluating the storm's strength. The short term objective is to initialize and validate the IWV tomography by using co-located RO profiles. The long term objective is to relate the IWV trend before the rain and the storm's thermal structure to the storm intensity. The GPS RO profiles were downloaded from two different data centres (UCAR and Wegener Centre) which provide water vapour in different units (water vapour pressure in mbar and water vapour in Kg/Kg respectively) and with different tangent point reference. The first step was to create a homogeneous dataset for being compared to the IWV in terms of units, vertical and horizontal resolution.

Belgium Extreme Events We have found about 30 RO profiles co-located with the two extreme events in Belgium but unfortunately just two of them were suitable for this study: 15th of August 2010 (not shown) and 18th of August 2011 (Fig. 7.6). The reasons of such small number are different: the short temporal range of the events (just a few days); the technical problems for retrieving the RO water vapour profile below 10 km of altitudes; the Belgium area is comparable with the GPS RO horizontal resolution. Due to this very small number of available occultations we have decided to work in a wider area and a large temporal range, so we selected all the GPS RO in United Kingdom in the period October 2013–February 2014.

United Kingdom Wet Winter We have found in total about 5000 RO profiles on UK area during the period October 2013–February 2014. We report here a specific case of selected extreme weather event in November 2013. The event passed over UK the 12th of November moving South East the day after. Several GPS ROs were co-located with this event as reported in Fig. 7.6. In both cases it is evident the decrease of IWV just before the event (Fig. 7.7, we just show the UK case).

The study has been deepened with the tomography of the single events (to be published soon) and with the STSM of Rita Nogherotto with the study of tropical cyclones at La Reunion.

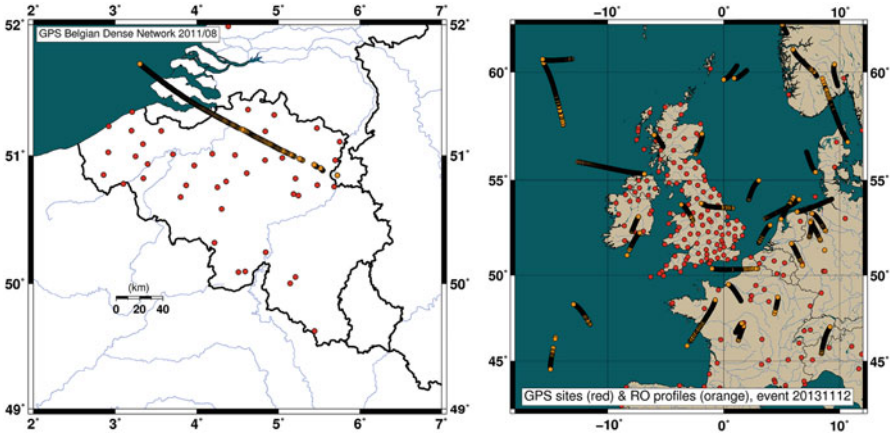

Fig. 7.6 (Right) GPS RO co-located with the extreme event over Belgium the 18th of August 2011. (Left) GPS ROs co-located with the extreme event over UK the 12th of November 2013. Red dots are the ground based GPS stations of the Belgian network. Orange dots are the GPS RO tangent points coordinates

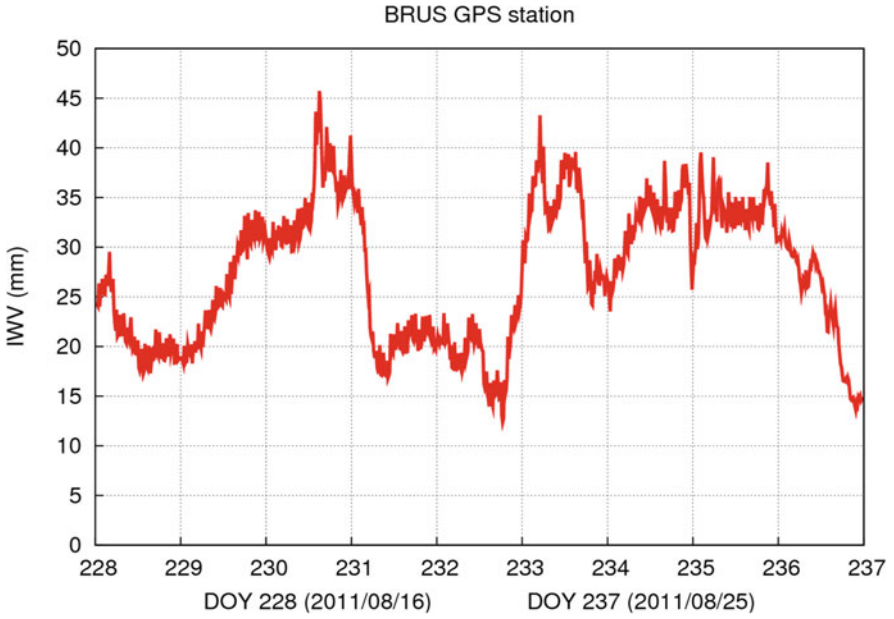

Fig. 7.7 Integrated Water Vapour (IWV) from the 16th of August 2011 to the 25th of August 2011. We can see the IWV dropping down before the extreme event the 19th (DOY 231)

STSM Applicant: *Mr André Sá, Polytechnic Institute of Guarda, Rua do Milagre das Rosas, Lote 36°, 3dt°, Coimbra (PT),* andregvsa@gmail.com
STSM Topic: *Tomography as a tool for atmospheric studies*
Host: *Witold Rohm, Wroclaw University of Environmental and Life Sciences, Wroclaw(PL),* witold.rohm@igig.up.wroc.pl

A tomographic software for water vapour reconstruction based on Global Navigation Satellite Systems (GNSS) observations was developed at Space & Earth Analysis Laboratory (SEGAL – Laboratory of University of Beira Interior). This software is designated SEGAL GNSS Water Vapour Reconstruction Image Software (SWART) and uses parallelized Algebraic Reconstruction Techniques (ART) for the inversion. The research objectives of the STSM were: (a) to validate the quality of tomography retrievals for SWART and; (b) apply the model to investigate severe weather/deep convection events. During the STSM, SWART was analysed and improved (introduction of initialization values/a priori conditions and stop criteria convergence). As an outcome SWART is now being used to produce a COST paper "Cross-validation of GNSS tomography models and methodological improvements using CORS networks".

STSM Applicant: *Ms Katarzyna Stepniak, University of Warmia and Mazury in Olsztyn, Olsztyn (PL),* k-stepniak@wp.pl
STSM Topic: *Impact of processing parameters on the ZTD estimates and adaptation of ZTD screening methods*
Host: *Olivier Bock, IGN – LAREG, Paris (FR),* Olivier.Bock@ign.fr

The main scientific objective of the STSM was performance assessment of tropospheric ZTD screening methods and analysis of the IWV variability over Poland. During the STSM, the estimated ZTDs were compared (1) to ZTD estimated from several EPN analysis centres, (2) to ZTD computed from ERA-Interim reanalysis. Moreover, the adaptation of the screening method developed by Dr. Bock for ZTD data produced with the Gipsy software to those I produced myself with BSW was carried out. The ZTD screening method, based on the analysis of formal errors of ZTD and coordinate estimates, was tested. Subsequently, I learnt about the ZTD to IWV conversion methods developed in Working Group 3 and applied them to the ZTD data for Poland.

STSM Applicant: *Dr Michal Kacmarik, Institute of Geoinformatics, Technical University of Ostrava, Ostrava (CZ),* michal.kacmarik@vsb.cz
STSM Topic: *Validation of GNSS Slant Delays*
Host: *Galina Dick, Helmholtz-Centre Potsdam – GFZ German Research Centre for Geosciences, GPS/Galileo Earth Obs, Potsdam (DE),* dick@gfz-potsdam.de

The main purpose of the STSM at GFZ Potsdam was to initiate an extensive validation of STD from independent measurement techniques - GNSS, Water Vapour Radiometer (WVR) and Numerical Weather Prediction (NWP) models ray-tracing. Hosting institution GFZ Potsdam has a long-term experience with

GNSS slant delays estimation, NWP model ray-tracing, WVR operation and GNSS meteorology products validation.

Firstly, two tools were developed by the recipient. A set of scripts called WVR_POTS_STD, which serves for (pre-) processing of observations from WVR operated by GFZ Potsdam. Its main purpose is a conversion of original slant integrated water vapour (SIWV) values to STDs needed for the validation with an effort to minimally distort the original SIWV observations. The second tool suits for an automatic validation of STDs delivered in a new TRO-SINEX format including generation outputs in a form of tables and figures.

Secondly, an initial validation of STDs was realized. There was a logical decision to use the Benchmark dataset prepared within COST ES1206 Action (Douša et al. 2016) for this purpose. It covers a 56-day long period in May and June 2013 which included severe weather events. In total, a subset of ten GNSS reference stations located at six different places were selected for the validation. Within them three collocated stations can be found which compromise of two or three individual GNSS reference stations situated very close to each other. Three institutions delivered slant total delays from their GNSS processing using different software and strategies for this initial validation (GFZ Potsdam, GO Pecný, VSB-Technical University Ostrava). Moreover, STDs from WVR located at GFZ Potsdam as well as STDs from ray-tracing via NWP models NCEP GFS and ECMWF ERA-Interim delivered by GFZ Potsdam entered the initial validation.

Results of comparisons within individual sources of STDs, over both whole Benchmark period and individual days, at original elevation angles of STDs as well as in the simulated zenith direction were presented in the full version of the STSM report and are not mentioned here due to their preliminary value and considerable extent. Detailed results of the extensive STD validation which was kicked off by this STSM can be found in a paper published by Kačmařík et al. (2017).

STSM Applicant: *Ms Rita Nogherotto, The Abdus Salam International Centre for Theoretical Physics, Trieste (IT),* rnoghero@ictp.it

STSM Topic: *Tropical cyclone intensification, water vapour distribution and GNSS measurements*

Host: *Jimmy LECLAIR DE BELLEVUE, Laboratoire de l'Atmosphère et des Cyclones – CNRS 8105 Universitie de La Reunion, Saint-Denis (FR),* jimmy.leclair-de-bellevue@univ-reunion.fr

The mission aimed at studying the tropical cyclone Bejisa occurred in the South-western Indian Ocean in January 2014 by using:

- Integrated Precipitable Water Vapour (PW) from ground-based GNSS measurements (provided by the *Laboratoire* de l'Atmosphère et des Cyclones LACy-CNRS, Reunion Island (France))
- RO profiles (provided by the Wegener Centre for Climate and Global Change, Graz (Austria))
- Weather stations measurements (provided by different meteorological institutes)
- and models (the new high resolution *model AROME* (Météo-France)).

The purpose was to co-locate the storms best track (from Meteo-France) with GNSS stations and derive the *Integrated Precipitable Water Vapour* PW.

Another goal was to use the RO profile to determine the cloud top altitude and to find the relationship between cloud top altitude, storm intensity and PW variation.

Bejisa cyclone event was also used for a first evaluation of the numerical prediction model AROME, operational at Météo-France.

GPS observed PW anomalies in the three analysed stations (VACS, in Mauritius islands, ABPO in Madagascar and REUN in Reunion island) respect to the period 2008–2015, show that it is an observable general trend that PW starts to increase before the cyclone, reaches its maximum during the closest approach of the cyclone, decreases to a minimum immediately after its passage, and finally recovers to its nominal value a few days later.

AROME model was able to represent well the trend of the PW but behaving differently according to the station: for VACS we found that the bias and the RMSPE assumed almost the same value, indicating that a significant part of the error in the model was due solely to the persistent bias of ~1 cm. For ABPO and REUN the results were remarkable as both the bias and the RMSPE were very low (3% and 15% the bias and 9% and 21% the RMSPE).

For the RO study we analysed the bending angle anomalies and the temperature anomalies respect to the climatological value in the same area. The cyclone's thermal structure presents a warmer core and a cold cloud top confirming results of previous studies.

STSM Applicant: *Dr Tomasz Hadaś, Wroclaw University of Environmental and Life Sciences, Wroclaw (PL),* tomasz.Hadaś@up.wroc.pl

STSM Topic: *Optimization of real-time GNSS troposphere delay estimation algorithms*

Host: *Felix Norman Teferle, University of Luxembourg, Luxembourg (LU),* Norman.Teferle@uni.lu

The purpose of this mission was to optimize ZTD stochastic modelling (random walk setting). In GNSS data processing the station height, receiver clock and tropospheric delay (ZTD) are highly correlated to each other. Although the ZHD of the troposphere can be provided with sufficient accuracy, ZWD has to be estimated, which is usually done in a random walk process. Since ZWD temporal variation depends on the water vapour content in the atmosphere, it seems to be reasonable that ZWD constraints in GNSS processing should be geographically and/or time dependent. We propose to take benefit from numerical weather prediction models to define optimum random walk process noise. In the first approach we used archived VMF1-G data to calculate a grid of yearly and monthly means of the difference of ZWD between two consecutive epochs divided by the root square of the time lapsed, which can be considered as a random walk process noise. Alternatively, we used the Global Forecast System (GFS) model from National Centres for Environmental Prediction (NCEP) to calculate random walk process noise dynamically in real-time. We performed two representative experimental campaigns with 20 globally distributed IGS stations and compared real-time ZTD estimates with the

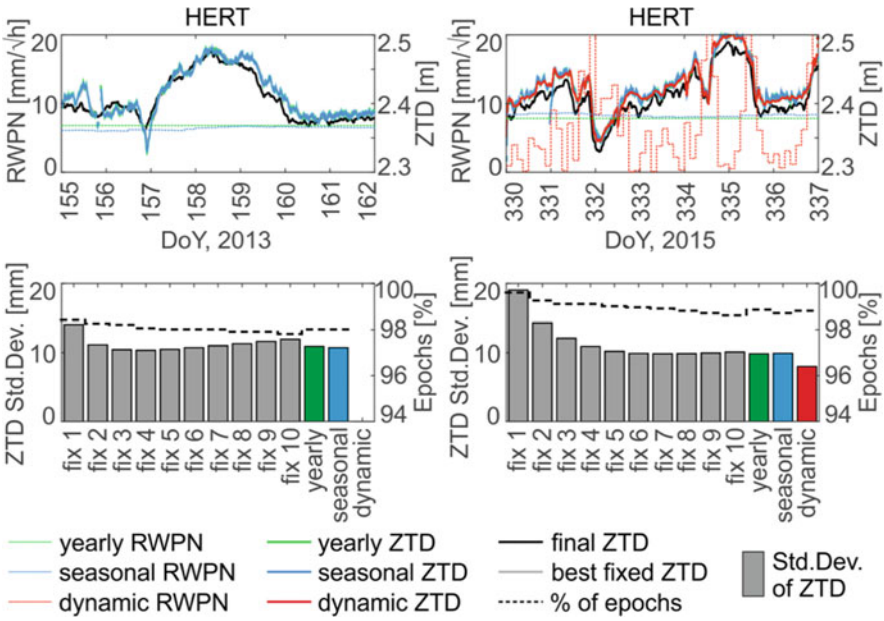

Fig. 7.8 Comparison of wet RWPN, ZTD time series, standard deviations of real-time ZTD residuals with respect to the final ZTD and solution availability among variants for station HERT

official ZTD product from the IGS. With both our approaches, we obtained an improvement of up to 10% in accuracy of the ZTD estimates compared to any uniformly fixed random walk process noise applied for all stations (Fig. 7.8). The results are published in Hadaś et al. (2017).

STSM Applicant: Ms Katarzyna Stepniak, University of Warmia and Mazury in Olsztyn, Olsztyn (PL), katarzyna.stepniak@uwm.edu.pl

STSM Topic: Improved methods for reprocessing of GNSS data for climate monitoring over Poland

Host: Olivier Bock, IGN – LAREG, Paris (FR), Olivier.Bock@ign.fr

The goal of the work was to determine the most accurate and homogeneous processing strategy to reprocess ground-based GNSS data for climate monitoring applications. We investigated impact of network design strategy on the quality and homogeneity of relative (double difference) strategies and afterwards, compared to standard BSW obs-max solution. We found out that the strategies have limitations and are prone to ZTD outliers and gaps. Investigation of various case studies helped to identify the weaknesses of these strategies. We proposed and tested an alternative baseline strategy that overcomes the most severe limitations and yields ZTD time series with much less outliers and gaps. We also described an efficient outlier detection method for the final screening of the reprocessed ZTD time series and assess the quality of final ZTD data by comparison with ERA-Interim reanalysis. The new strategy is recommended by us to use to estimate ZTD time series for

meteorology and climate monitoring applications in moderate-size networks (e.g. national scale).

STSM Applicant: *Ms Anna Klos, Military University of Technology, Warsaw (PL),* anna.klos@wat.edu.pl

STSM Topic: *Analysis of ZTD time series from reprocessed GPS solutions*

Host: *Felix Norman Teferle, University of Luxembourg, Luxembourg (LU),* Norman.Teferle@uni.lu

The Short Term Scientific Mission (STSM) titled: "Analysis of Zenith Total Delay Time Series from Reprocessed GPS Solutions" was hosted by University of Luxembourg and supervised by prof. Felix Norman Teferle. Within and thanks to the funds of COST ES1206 Action, I performed an analysis of ZTD time series obtained by BLT (British Isles continuous GNSS Facility and University of Luxembourg Tide Gauge Benchmark Monitoring (TIGA) Analysis Centre) as one of its activities as IGS analysis centre. The analysis included 44 globally distributed stations situated in 5 different climate zones. The ZTD series were sampled every 1 h. Series varied in length between 1995 and 2015. We modelled the ZTD data as the sum of trend, seasonal signals and breaks. The seasonal signals can reflect seasonal changes with periods of tropical year and its harmonics along with diurnal and semi-diurnal changes. Stochastic part or so-called residua is a misfit between real data and deterministic model of initial value, trend, seasonal component and breaks. We made a deep search through climate literature and found out that climatologists describe noise in all climate time series as autoregressive model (AR), mainly being of 1st order (e.g. Mann and Lees 1996; Matyasovszky 2013). If ZTD series are analysed in terms of climate changes it should show similar noise character to climate time series. We examined few different noise models to be fitted into residuals: white noise, power-law plus white noise and different kinds of autoregressive model. The analysis was performed with the Maximum Likelihood Estimation (MLE) approach. We found that 4th order of autoregressive model is a preferred one to describe the ZTD residuals. We computed the ratios between ZTD trend uncertainty estimated with white and autoregressive noise model. We found, that up until now, the uncertainties of ZTD trends were underestimated by a factor of up to 10. This means, that some trends, used to the analysis of climate change might have been insignificant.

Conclusions In this research, we aimed at evaluation of uncertainty of ZTD trend. To date, all analyses were performed with the assumption of white noise. This is not a proper one, when one concerns on climate implications. We recommend that an autoregressive noise model is used, when ZTD trend is going to be estimated with a high accuracy.

STSM Applicant: *Mr Kamil Kazmierski, Wroclaw University of Environmental and Life Sciences, Wroclaw (PL),* kamil.kazmierski@igig.up.wroc.pl

STSM Topic: *Real-time troposphere delay gradient estimation with multi-GNSS PPP*

Host: *Marcelo Santos, University of New Brunswick, Fredericton (CA),* msantos@unb.ca

The main purpose of this mission was to implement real-time tropospheric gradient estimation module into GNSS-WARP software. This visit was a perfect opportunity to improve GNSS-WARP software, implement additional modules and exchange experience connected with Precise Point Positioning. At the very beginning of my stay I had an opportunity to get to know how GAPS performs PPP calculation, as well as which parameters are estimated during the processing and in what way. After that I was able to make an implementation of tropospheric gradient estimation module into GNSS-WARP software. During the implementation work Chen & Herring linear horizontal gradient formulation was used. Additionally, two parameters were added as extra parameters into the last square adjustment and then estimated in each observation epoch (according to RINEX file interval).

In order to validate the obtained results COST Benchmark data were used. Only one Analysis Centre, Agenzia Spaziale Italiana (ASI), provided information about tropospheric gradients stored in COST format. The second source of reference data came directly from Rosa Pacione who works with ASI. Those results were obtained from PPP processing and provided data in 5 min intervals. As a testing period the dates between 4 and 11 June 2013 (155-161 DoY) were selected. During processing RINEX files served as sources of observations. The real-time data available for this period were provided by IGS and covered both orbit and clock corrections for GPS. Eight European stations were selected as a test stations set (BRST, BRUX, BUCU, NICO, ONSA, SFER, WROC, ZIMM). For the selected stations tropospheric gradients and their statistics were calculated.

The mean BIAS for tropospheric gradients with reference to Rosa Pacione data is smaller than −0.30 mm for NS direction and + 0.20 mm for EW direction. Standard deviation and root mean square error (RMS) equal about 0.6 mm and 0.7 mm, respectively. The results obtained from comparison with COST benchmark data are comparable. The results obtained for tropospheric gradients for NS direction are biased negatively and for EW direction they are biased positively in most cases.

Additionally, during my stay at UNB multi-GNSS positioning function was implemented. As additional systems GALILEO and BeiDou were implemented. We have still some problems connected with appropriate corrections joining for BeiDou ephemeris. In real-time stream decoded by BKG Ntrip Client (BNC) v.2.12 the parameter IOD is recalculated in order to eliminate mistakes during processing. We have still some problems with appropriate BeiDou IOD calculation and at this moment BeiDou is excluded from the precise solution.

During STSM the main aims were achieved and the presented results are promising. Conducted works shown that tropospheric gradient estimation using real-time products estimation performs well. The results are not highly accurate in comparison with the reference data. It may be connected with the quality of real-time products. The differences may occur due to the different strategies in GPISY and in GNSS-WARP. In the near future we hope to finish the work connected with operating BeiDou during processing.

The grantee and the host institution declared future collaboration connected with the development of GNSS-WARP as well as GAPS software. The host confirms the above execution and benefits of this STSM, considering it as successful.

STSM Applicant: *Ms Karina Wilgan, Wroclaw University of Environmental and Life Sciences, Wroclaw (PL),* karina.wilgan@igig.up.wroc.pl

STSM Topic: *Lookup tables of refractivity coefficients for the conversion from zenith path delays to integrated water vapour*

Host: *Hugues Brenot, Department of Atmospheric Composition, Royal Belgian Institute for Space Aeronomy, Brussels (BE),* hugues.brenot@oma.be

The purpose of this STSM was to conduct a study on the refractivity coefficients obtained from ERA-Interim and to test the sensitivity of the different steps to obtain the ZWD from ZTD and IWV from ZWD in the stand-alone GNSS strategy. The refractivity of the atmosphere can be expressed as a function of meteorological parameters with the refractivity coefficients k_1, k_2, k_3. Usually these coefficients are used as constants, but the development of satellite techniques requires re-evaluation of the existing formulas. We calculated new k_1 coefficients based on the hydrostatic formulation of ZHD considering long-term historical outputs of ERA-Interim. The overall plan for k_1 is to calculate ZHD from hydrostatic formula and compare it to ZHD integrated from ERA-Interim using the k_1 parameters at the updated frequency of the GNSS signal. The value of the k_1 from the adjusted formula is latitude dependent, which can be easily presented as a simple function of the latitude. The k_1 coefficient is not time dependent, thus, there is no need to present a look-up table for this coefficient. The simple latitude dependent formula is sufficient. Furthermore, we investigated the behaviour of the k_2 coefficient, which depends on water vapour partial pressure and temperature. The meteorological parameters were again taken from ERA-Interim reanalysis. We calculated the values of the k_2 for every vertical profile (up to 60 km above the ground) and then retrieved the mean value for each profile. The k_2 values are also latitude dependent but not in a less systematic way than k_1 coefficients. Using the ERA-Interim reanalysis we also compared different ways to calculate proportionality factor κ used in the conversion between integrated water vapour and zenith wet delay. The proportionality factor κ values are also latitude and time dependent, thus, we proposed a look-up table for κ based on month of the year and latitude.

STSM Applicant: *Ms Anna Klos, Military University of Technology, Warsaw (PL),* anna.klos@wat.edu.pl

STSM Topic: *Selected Issues of Homogenisation of Synthetic ZTD Data with Noise Characteristic Derived from Reprocessed GPS Solutions*

Host: *Felix Norman Teferle, University of Luxembourg, Luxembourg (LU),* Norman.Teferle@uni.lu

The Short Term Scientific Mission (STSM) titled: “Homogenisation of Synthetic ZTD Data with Noise Characteristic Derived from Reprocessed GPS Solutions” was hosted by University of Luxembourg and supervised by prof. Felix Norman Teferle. Within and thanks to the funds of COST ES1206 Action, I performed an analysis of

synthetic ZTD time series obtained by simulations basing on parameters derived from real changes of ZTD. During the following STSM, the parameters estimated from real ZTD data were used to perform Monte Carlo simulations based on seasonal changes and noise character derived from real data. A set of synthetic series was then subjected to a blind test to detect simulated epochs of breaks. I intended to confirm or deny that simulated breaks can be easily detected when different amplitudes of periodic terms and noise process are being simulated. However, the main thing I had to keep in mind was that most methods, including manual inspection, will not tell whether the estimated epochs of breaks are due to Gaussian behaviour of series, AR regime-like shifts or true breaks. The epochs of breaks are usually reported by individual station, but a manual or statistical inspection is always needed, since few breaks might have been unreported. This reason made me to undertake this research on how one may be misled with reporting the breaks, when the autoregressive process is being assumed. In this case, the breaks reported manually or statistically can result from AR regime-like behaviour of series rather than real changes in ZTDs. In this way, we can artificially change values of trend and misinterpret it. Once the ZTD series were simulated, we made blind tests and used statistic method called STARS (Sequential t-Test and Regime Shifts) at the same time to detect epochs of breaks under different conditions of deterministic parameters.

Conclusions Few points were raised during this STSM and will be discussed and analysed as further cooperation. Breaks are mostly determined with epochs reported by each individual station, but manual inspection is needed. Some statistic methods are used to this task, however, their results have to be carefully checked. We used STARS to indicate on epochs of breaks but this is a semi-automatic method. All results have to be properly checked, as due to regime-like behaviour of AR it is almost impossible for statistical methods to properly detect epochs of breaks. This fact was also reported earlier by climatologists. If reported breaks were not checked carefully before being taken into consideration, they will totally change the character of stochastic part. Also, we need to be aware of regime-like behaviour of noise process.

STSM Applicant: *Ms Anna Klos, Military University of Technology, Warsaw (PL),* anna.klos@wat.edu.pl

STSM Topic: *On the homogenisation and characterisation of IWV time series from IGS repro1 and its comparison to ERA-Interim*

Host: *Eric Pottiaux, Royal Observatory of Belgium, Brussels (BE),* Eric.Pottiaux@oma.be

The short-term scientific mission I attended was hosted by the Royal Observatory of Belgium and the Royal Meteorological Institute of Belgium, under the supervision of Dr. Eric Pottiaux and Dr. Roeland Van Malderen. We examined the properties of the IWV data retrieved from GPS observations and compared these with the IWV values calculated with the ERA-Interim model. The entire analysis was performed for the IGS repro1 dataset of 120 stations, prepared by Dr. Olivier Bock for the purpose of the data homogenisation activities of the sub-WG3 ‘data

Homogenisation'. The differences of IWVs were examined with the Maximum Likelihood Estimation (MLE) approach to estimate the parameters which characterize the dataset, as trend, seasonal signals, breaks and noise character. Thereafter, three synthetic datasets were created basing on the parameters we estimated for real IWV records: 'Easy', 'Less-complicated' and 'Fully-complicated', each containing 120 stations. The datasets differed in a complexity of parameters and noise model. The 'easy' dataset includes only pure white noise, while the 'less-complicated' also includes the autoregressive process of first order in addition to the white noise. Finally, the 'fully-complicated' also includes trends and gaps. In all three variants, seasonal components and breaks of known epoch and amplitude were introduced.

Conclusions The synthetic datasets were used to benchmark the performance of various statistical homogenization tools. These three synthetic datasets were subjected to homogenisation task and shared with the homogenisation activity leaving the epochs of breaks blinded. The synthetic datasets we created within this STSM, will be used to assess the ability of different homogenisation tools to report epochs of breaks when different parameters are found in the series. The tool which performs the best will then be used to homogenise the real IWV dataset before trend is being estimated.

References

Chen, G., & Herring, T. A. (1997). Effects of atmospheric azimuthal asymmetry on the analysis of space geodetic data. *Journal of Geophysical research, 102*(B9), 20489–20502.

Douša, J., Dick, G., Kačmařík, M., Brožková, R., Zus, F., Brenot, H., Stoycheva, A., Möller, G., & Kaplon, J. (2016). Benchmark campaign and case study episode in Central Europe for development and assessment of advanced GNSS tropospheric models and products. *Atmospheric Measurement Techniques, 9*, 2989–3008. https://doi.org/10.5194/amt-9-2989-2016.

Hadaś, T., Teferle, F. N., Kaźmierski, K., Hordyniec, P., & Bosy, J. (2017). Optimum stochastic modelling for GNSS tropospheric delay estimation in real-time. *GPS Solutions*, *21*(3), 1069–1081. Berlin/Heidelberg. https://doi.org/10.1007/s10291-016-0595-0

Kačmařík, M., Douša, J., Dick, G., Zus, F., Brenot, H., Möller, G., Pottiaux, E., Kapłon, J., Hordyniec, P., Václavovic, P., & Morel, L. (2017). Inter-technique validation of tropospheric slant total delays. *Atmospheric Measurement Techniques, 10*, 2183–2208. https://doi.org/10.5194/amt-10-2183-2017.

Mann, M. E., & Lees, J. M. (1996). Robust estimation of background noise and signal detection in climatic time series. *Climatic Change, 33*(3), 409–445.

Matyasovszky, I. (2013). Spectral analysis of unevenly spaced climatological time series. *Theoretical and Applied Climatology, 111*(3–4), 371–378.

Mahfouf, J-F., Ahmed, F., Moll, P., & Teferle, F. N. (2015). *Assimilation of zenith total delays in the AROME France convective scale model: A recent assessment*. Tellus A [S.l.]. ISSN: 1600-0870. http://www.tellusa.net/index.php/tellusa/article/view/26106. Date accessed 9 Dec 2016. https://doi.org/10.3402/tellusa.v67.26106

Vaclavovic, P., & Dousa, J. (2013). G-NUT software library – State of development and first results. *Acta Geodynamica et Geomaterialia, 10*(4), 431–436.

Appendices

List of Meetings and Workshops

- May 2013 – Management Committee (MC) meeting, Brussels, Belgium
- Sep 2013 – Core Team Meeting, Potsdam, Germany
- Oct 2013 – Working Group and MC Meeting, Valencia, Spain
- Dec 2013 – Core Team Meeting, Prague, Czech Republic
- Feb 2014 – Workshop and MC Meeting, Munich, Germany
- Mar 2014 – Dissemination Meeting, Washington D.C., USA
- May 2014 – Core Team Meeting, Vienna, Austria
- Sept 2014 – Training School, Working Group & MC Meeting, Varna, Bulgaria
- Feb 2015 – Core Team Meeting, Paris, France
- May 2015 – Workshop and MC Meeting, Thessaloniki, Greece
- Sept 2015 – Working Group and MC Meeting, Wroclaw, Poland
- Mar 2016 – Workshop and MC Meeting, Reykjavik, Iceland
- Apr 2016 – Homogenisation Workshop, Brussels, Belgium
- Apr 2016 – Core Team Meeting, Vienna, Austria
- Jul 2016–Dissemination Workshop, Beijing, China
- Aug 2016 – Training School, Working Group & MC Meeting, Potsdam, Germany
- Jan 2017–Homogenisation Workshop, Warsaw, Poland
- Feb 2017 – Final Workshop and MC meeting, Nordwijk, Netherlands

J. Jones et al. (eds.), *Advanced GNSS Tropospheric Products for Monitoring Severe Weather Events and Climate*, https://doi.org/10.1007/978-3-030-13901-8

Members of Management Committee and Working Groups

Members of the Management Committee

Christoph Wittmann	Central Institute for Meteorology and Geodynamics	Austria
Robert Weber	Technical University of Vienna	Austria
Hugues Brenot	Belgian Institute for Space Aeronomy	Belgium
Eric Pottiaux	ROB	Belgium
Guergana Guerova	Sofia University	Bulgaria
Damir Bekic	University of Zagreb	Croatia
Filippos Tymvios	Met Cyprus	Cyprus
Haris Haralambous	Frederick University	Cyprus
Jaroslav Resler	Institute of Computer Science AV CR	Czech Republic
Jan Douša	GOP	Czech Republic
Henrik Vedel	DMI	Denmark
Piia Post	University of Tartu	Estonia
Kalev Rannat	Tallinn University of Technology	Estonia
Rigel Kivi	Met Finland	Finland
Ari-Matti Harri	Met Finland	Finland
Olivier Bock	IGN	France
Jean-Francois Mahfouf	Met France	France
Roland Potthast	DWD	Germany
Jens Wickert	GFZ German Research Centre for Geosciencies	Germany
Nicholas Zinas	Tekmon Geomatics	Greece
Athanassios Ganas	National Observatory of Athens	Greece
Szabolcs Rozsa	Budapest University of Technology and Economics	Hungary
Mate Mile	Hungarian Meteorological Service	Hungary
Sigurdur Thorsteinsson	Icelandic Meteorological Institute	Iceland
Igor Kerin	University College Cork	Ireland
Eamon McKeogh	University College Cork	Ireland
Yuval Rueveni	Interdisciplinary Centre (IDC)	Israel
Simon Krichak	Tel Aviv University	Israel
Riccardo Biondi	Abdus Salam Intl. Centre for Theoretical Physics	Italy
Rosa Pacione	e-geos	Italy
Gintautas Stankunavicius	Vilnius University	Lithuania
Inga Dailidiene	Klaipeda University	Lithuania
Norman Teferle	University of Luxembourg	Luxembourg
Charles Galdies	National Meteorological Service	Malta

(continued)

Joseph Schiavone	Malta Airport	Malta
Siebren De Haan	KNMI	Netherlands
Jelena Bojarova	Norwegian Meteorological Institute	Norway
Roger Randriamampianina	Norwegian Meteorological Institute	Norway
Jaroslaw Bosy	Wroclaw Univ. of Environmental and Life Sciences	Poland
Karolina Szafranek	Military University of Technology	Poland
Rui Fernandes	Universidade da Beira Interior	Portugal
Constantin Florin Caruntu	University of Iasi	Romania
Ioan Stefan Sacala	Politehnica University of Bucharest	Romania
Dragan Blagojevic	University of Belgrade	Serbia
Jan Hefty	Slovak University of Technology	Slovakia
Miroslava Haque Igondova	Slovak University of Technology	Slovakia
Enrique Priego De Los Santos	Univ of Valencia	Spain
Andres Seco	Univ of Navarra	Spain
Magnus Lindskog	SMHI	Sweden
Gunnar Elgered	Chalmers University of Technology	Sweden
Elmar Brockmann	SwissTopo	Switzerland
Alain Geiger	ETH Zurich	Switzerland
Cetin Mekik	Karaelmas University	Turkey
Richard Bingley	University of Nottingham	UK
Gemma Bennitt	Met Office	UK
MC Substitutes		**Country**
Mr Gregor Moller	Technical University of Vienna	Austria
Dr Xin Yan	Central Institute for Meteorology and Geodynamics	Austria
Dr Roeland Van Malderen	Meteorological Institute of Belgium	Belgium
Mr Hannes Keernik	University of Tartu	Estonia
Dr Ambrus Kenyeres	Inst. of Geodesy, Cartography and Remote Sensing	Hungary
Dr Cecilia Sciarretta	e-geos	Italy
Egidijus Rimkus	Vilnius University	Lithuania
Lina Davuliene	Institute of Physics	Lithuania
Corneliu Lazar	Technical University Gheorghe	Romania
Mihnea Alexandru Moisescu	Politehnica University of Bucharest	Romania
Ioan Dumitrache	Politehnica University of Bucharest	Romania
Andreea Udrea	Politehnica University of Bucharest	Romania
Oleg Odalovic	University of Belgrade	Serbia
Dr Francisco Javier Gonzalez Matesanz	IGN	Spain
Mr Marcelino Valdes Perez de Vargas	IGN	Spain
Mr Miguel Angel Cano Villaverde	IGN	Spain

Members of the Working Group 1

Kefei Zhang	RMIT	Australia
Robert Weber	Vienna University of Technology	Austria
Gregor Moeller	Vienna University of Technology	Austria
Hugues Brenot	Belgian Institute for Space Aeronomy	Belgium
Eric Pottiaux	Royal Observatory of Belgium, ROB	Belgium
Tzvetan Simeonov	Sofia University	Bulgaria
Marcelo Santos	University of New Brunswick	Canada
Marco Mendonca	University of New Brunswick	Canada
Thalia Nikolaidou	University of New Brunswick	Canada
Jan Douša	Geodetic Observatory Pecny, GOP	Czech Republic
Pavel Václavovic	Geodetic Observatory Pecny, GOP	Czech Republic
Michal Eliaš	Geodetic Observatory Pecny, GOP	Czech Republic
Michal Kačmařík	VŠB – Technical University of Ostrava	Czech Republic
Henrik Vedel	Danish Meteorological Institute, DMI	Denmark
Cédric Champollion	University of Montpellier	France
Pierre Bosser	ENSG IGN	France
Samuel Nahmani	LAREG IGN	France
Laurent Morel	Le CNAM	France
Rana Charara	Trimble	France
Jimmy Leclair de Bellevue	CNRS	France, Reunion
Galina Dick	GFZ German Research Centre for Geosciencies	Germany
Michael Bender	Deutscher Wetterdienst (DWD)	Germany
Florian Zus	GFZ German Research Centre for Geosciencies	Germany
Zhiguo Deng	GFZ German Research Centre for Geosciencies	Germany
Xiaolei Dai	GFZ German Research Centre for Geosciencies	Germany
Cuixian Lu	GFZ German Research Centre for Geosciencies	Germany
Xingxing Li	GFZ German Research Centre for Geosciencies	Germany
Yüksel Altiner	Federal Agency for Cartography and Geodesy	Germany
Wolfgang Söhne	Federal Agency for Cartography and Geodesy	Germany
Andrea Stürze	Federal Agency for Cartography and Geodesy	Germany
Athanassios Ganas	National Observatory of Athens	Greece
Chris Pikridas	Aristotle University of Thessaloniki	Greece
Symeon Katsougiannopoulos	Technical Educational Institute of Serres	Greece

(continued)

Nicholas Zinas	Tekmon Geomatics	Greece
George (Zhizhao) Liu	Hong Kong Polytechnic	Hong Kong
Szabolcs Rózsa	Budapest Univ. of Technology and Economics	Hungary
Ambrus Kenyeres	Inst.of Geodesy, Cartography and Remote Sensing	Hungary
Varga Bálint	Hungarian Meteorological Service, OMSZ	Hungary
Benedikt Gunnar Ofeigsson	Icelandic Met Office	Iceland
Rosa Pacione	E-GEOS	Italy
Brigida Pace	E-GEOS	Italy
Giuseppe Bianco	ASI	Italy
Vincenza Tornatore	DICA Politechnico di Milano	Italy
Eugenio Realini	GReD – Geomatics Research & Development s.r.l.	Italy
Jānis Zvirgzds	Latvian Geospatial Information Agency	Latvia
Didzis Dobelis	Latvian Geospatial Information Agency	Latvia
Furqan Ahmed	University of Luxembourg	Luxembourg
Norman Teferle	University of Luxembourg	Luxembourg
Siebren de Haan	KNMI	Netherlands
Mariusz Figurski	Military University of Technology, Warsaw	Poland
Grzegorz Nykiel	Military University of Technology, Warsaw	Poland
Karolina Szafranek	Military University of Technology, Warsaw	Poland
Pawel Wielgosz	University of Warmia and Mazury in Olsztyn	Poland
Katarzyna Stepniak	University of Warmia and Mazury in Olsztyn	Poland
Jaroslaw Bosy	Wroclaw Univ. of Environmental and Life Sciences	Poland
Jan Kaplon	Wroclaw Univ. of Environmental and Life Sciences	Poland
Witold Rohm	Wroclaw Univ. of Environmental and Life Sciences	Poland
Tomasz Hadaś	Wroclaw Univ. of Environmental and Life Sciences	Poland
Karina Wilgan	Wroclaw Univ. of Environmental and Life Sciences	Poland
Andre Sa	Polytechnic University a Guarda	Portugal
Rui Fernandes	Universidade da Beira Interior	Portugal
Jan Hefty	Slovak University of Technology in Bratislava	Slovakia
Alexandra Muntean	National Institute for Earth Physics (NIEP)	Romania
Nastase Eduard	National Institute for Earth Physics (NIEP)	Romania
Miguel Ángel Cano Villaverde	Instituto Geografico National, IGN	Spain
José Antonio Sánchez Sobrino	Instituto Geografico National, IGN	Spain
Marcelino Valdés Pérez de Vargas	Instituto Geografico National, IGN	Spain
Martin Ridal	Swedish Meteorological and Hydrological Inst.	Sweden
Alain Geiger	ETH Zurich	Switzerland

(continued)

Markus Rothacher	ETH Zurich	Switzerland
Elmar Brockmann	Swiss Federal Office of Topography, SwissTopo	Switzerland
Kamel Naouali	Office of Topography and Cadastre	Tunisia
Emine Tanir Kayikci	Karadeniz Teknik Üniversitesi	Turkey
Gokhan Gurbuz	Bullent Ecevit University, Trabzon	Turkey
Ilke Deniz	Bullent Ecevit University, Trabzon	Turkey
Jonathan Jones	Met Office	UK
Richard Bingley	University of Nottingham	UK
Lei Yang	University of Nottingham	UK

Members of Working Group 2

Kefei Zhang	RMIT	Australia
Christoph Wittmann	Central Inst. for Meteorology and Geodynamics	Austria
Florian Meier	Central Inst. for Meteorology and Geodynamics	Austria
Gregor Moeller	Technical University of Vienna	Austria
Ms. Xin Yan	Central Inst. for Meteorology and Geodynamics	Austria
Robert Weber	Technical University of Vienna	Austria
Eric Pottiaux	ROB	Belgium
Hugues Brenot	Belgian Institute for Space Aeronomy	Belgium
Anastasia Stoycheva	National Institute of Meteorology and Hydrology	Bulgaria
Martin Slavchev	National Institute of Meteorology and Hydrology	Bulgaria
Guergana Guerova	Sofia University	Bulgaria
Nadezhda Yordanova	Sofia University	Bulgaria
Evgenia Egova	Sofia University	Bulgaria
Igor Kerin	University of Zagreb	Croatia
Jaroslav Resler	Institute of Computer Science AV CR	Czech Republic
Krystof Eben	Institute of Computer Science AV CR	Czech Republic
Henrik Vedel	DMI	Denmark
Kalev Rannat	Tallinn University of Technology	Estonia
Cédric Champollion	University of Montpellier	France
Laurent Morel	Le CNAM	France
Mathieu Nuret	MeteoFrance	France
Samuel Nahmani	IGN	France
Florian Zus	GFZ German Research Centre for Geosciencies	Germany
Michael Bender	Deutscher Wetterdienst (DWD)	Germany

(continued)

Roland Potthast	Deutscher Wetterdienst (DWD)	Germany
George (Zhizhao) Liu	HK Polytechnic	Hong Kong
Mile Máté	Met Hungary	Hungary
Sigurður Þorsteinsson	Icelandic Meteorological Institute	Iceland
Riccardo BIONDI	Abdus Salam International Centre for Theoretical Physics	Italy
Siebren de Haan	KNMI	Netherlands
Jelena Bojarova	Met Norway	Norway
Jaroslaw Bosy	Wroclaw University of Env + Life Sciences	Poland
Karolina Szafranek	Military University of Technology	Poland
Krzysztof Kroszczynski	Wroclaw Military University of Technology	Poland
Witold Rohm	Wroclaw University of Env + Life Sciences	Poland
Rui Fernandes	Universidade da Beira Interior	Portugal
Andres Seco	University of Navarra	Spain
Enrique Priego	Valencia Polytechnic University	Spain
Diego Ferragud Trillo	Valencia Polytechnic University	Spain
Francisco Javier Gonzalez Matesanz	IGN	Spain
Jana Sanchez	Met Spain	Spain
Magnus Lindskog	SMHI	Sweden
Alain Geiger	ETH Zurich	Switzerland
Markus Rothacher	ETH Zurich	Switzerland
Gemma Halloran	Met Office	UK
Jonathan Jones	Met Office	UK
Maciej Kryza	Wroclaw Univ. of Environmental and Life Sciences	Poland

Members of Working Group 3

Johannes Boehm	TU Wien	Austria
Barbara Chimani	ZAMG	Austria
Roeland Van Malderen	Met Belgium	Belgium
Hugues Brenot	Institute for Space Aeronomy	Belgium
Eric Pottiaux	Royal Observatory of Belgium	Belgium
Julie Berckmans	Met Belgium	Belgium
Guergana Guerova	Sofia University	Bulgaria
Biliana Mircheva	Sofia University	Bulgaria
Krasimir Stoev	Sofia University	Bulgaria
Christina Oikonomou	Frederick University	Cyprus
Jan Douša	GOP	Czech Republic
Pavel Václavovic	GOP	Czech Republic
Michal Elias	GOP	Czech Republic

(continued)

Henrik Vedel	DMI	Denmark
Piia Post	University of Tartu	Estonia
Kalev Rannat	Tallinn University of Technology	Estonia
Hannes Keernik	University of Tartu	Estonia
Peep Miidla	University of Tartu	Estonia
Rigel Kivi	Finnish Meteorological Institute	Finland
Olivier Bock	IGN	France
Pierre Bosser	IGN	France
Samuel Nahmani	IGN	France
Ana Parracho	IGN	France
Pascal Willis	IGN-IPGP	France
Xavier Collilieux	IGN	France
Sophie Bastin	LATMOS	France
Jimmy Leclair de Bellevue	LaCy-Universite de la Reunion	France
Julien Gazeaux	IPGP	France
Robert Heinkelmann	GFZ German Research Centre for Geosciencies	Germany
Kyriakos Balidakis	GFZ German Research Centre for Geosciencies	Germany
Sybille Vey	GFZ German Research Centre for Geosciencies	Germany
Tzvetan Simeonov	GFZ German Research Centre for Geosciencies	Germany
Fadwa Alshawaf	GFZ German Research Centre for Geosciencies	Germany
Sandra Steinke	University of Cologne	Germany
Tamas Szentimrey	Hungarian Meteorological Service	Hungary
Szabó Péter	Hungarian Meteorological Service	Hungary
Riccardo Biondi	Abdus Salam ICTP	Italy
Rosa Pacione	ASI/CGS	Italy
Ermanno Fionda	Fondazione Bordoni	Italy
Rita Nogherotto	ICTP	Italy
Stefania Bonafoni	Università degli Studi di Perugia	Italy
Furqan Ahmed	University of Luxemburg	Luxembourg
Norman Teferle	University of Luxemburg	Luxembourg
Karina Wilgan	Wroclaw Univ. of Environmental and Life Sciences	Poland
Jan Kaplon	Wroclaw Univ. of Environmental and Life Sciences	Poland
Jaroslaw Bosy	Wroclaw Univ. of Environmental and Life Sciences	Poland
Witold Rohm	Wroclaw Univ. of Environmental and Life Sciences	Poland/Australia
Zofia Baldysz	Military University of Technology	Poland
Karolina Szafranek	Military University of Technology	Poland
Anna Klos	Military University of Technology	Poland
Bogusz Janusz	Military University of Technology	Poland
Katarzyna Stępniak	University of Warmia and Mazury	Poland
Andres Seco	University of Navarra Spain	Spain

(continued)

Eduardo Serna	University of Navarra Spain	Spain
Enrique Priego	University of Valencia	Spain
Jose Guijarro	AEMET	Spain
Gunnar Elgered	Chalmers University of Technology	Sweden
Tong Ning	Chalmers University of Technology	Sweden
Ulrika Willén	Met Sweden	Sweden
Elmar Brockmann	SwissTopo Switzerland	Switzerland
Selma Zengin Kazanci	Karadeniz Teknik Üniversitesi	Turkey
Jonathan Jones	Met Office	UK
Dionne Hansen	University of Nottingham	UK
Kefei Zhang	SPACE Res. Centre, RMIT University	Australia
Xiaoming Wang	SPACE Res. Centre, RMIT University	Australia

Contributors to GNSS4SWEC Final Report by Affiliation

Austria
Department of Geodesy and Geoinformation, TU Wien (http://hg.geo.tuwien.ac.at/)
Johannes Böhm
Daniel Landskron
Gregor Möller
Robert Weber
Angelika Xaver
Wouter Dorigo
Julia Sammer

Central Institute for Meteorology and Geodynamics (ZAMG) (https://www.zamg.ac.at/)
Barbara Chimani
Christoph Wittmann

Belgium
Royal Belgian Institute for Space Aeronomy (http://www.aeronomie.be)
Hugues Brenot

Royal Observatory of Belgium (http://www.astro.oma.be/en/)
Eric Pottiaux
Carine Bruyninx

Royal Meteorological Institute of Belgium (https://www.meteo.be/meteo/view/en/65239-Home.html)
Roeland Van Malderen
Lesley de Cruz

Annelies Duerinckx
Julie Berckmans
B. van Schaeybroeck

Bulgaria
Sofia University 'St. Kliment Ohridski' (http://suada.phys.uni-sofia.bg/)
Guergana Guerova
Tzvetan Simeonov
Biliana Mircheva
Krasimir Stoev
Nikolay Penov

National Institute of Meteorology and Hydrology (http://www.meteo.bg)
Anastasia Stoycheva
Martin Slavchev

Cyprus
Frederick University (http://www.frederick.ac.cy/)
Haris Haralambous

Cyprus Department of Meteorology (http://www.moa.gov.cy/moa/ms/ms.nsf/DMLforecast_en/DMLforecast_en)
Filippos Tymvios

Czech Republic
Geodetic Observatory Pecný, Research Institute of Geodesy, Topography and Cartography,
(http://www.pecny.cz/)
Jan Douša
Pavel Václavovic
Michal Eliaš
Lewen Zhao

Institute of Geoinformatics, VŠB—Technical University of Ostrava (http://gis.vsb.cz/en/institute-of-geoinformatics/)
Michal Kačmařík

Institute of Computer Science, Academy of Sciencies (http://web.cs.cas.cz/Web/web_ics/)
Kryštof Eben
Jaroslav Resler
Pavel Krč

Czech Hydrometeorological Institute (http://www.chmi.cz)
Radmila Brožková

Denmark
Danish Meteorological Institute (http://www.dmi.dk/en/vejr/)
Henrik Vedel

Estonia
Tallinn University, Dept. of Computer Control (https://www.ttu.ee/institutes/department-of-computer-systems/)
Kalev Rannat

Germany
GFZ German Research Centre for Geosciences, Potsdam (https://www.gfz-potsdam.de/en/home/)
Galina Dick
Jens Wickert
Florian Zus
Fadwa Alshawaf
Zhiguo Deng
Cuixian Lu
Xingxing Li
Kyriakos Balidakis
Robert Heinkelmann
Jan Tobias Nilsson
Harald Schuh
Markus Bradke

Deutscher Wetterdienst (https://www.dwd.de/DE/Home/home_node.html)
Roland Potthast
Michael Bender
Michael Sommer

BKG, Federal Agency for Cartography and Geodesy (https://www.bkg.bund.de/EN/Home/home.html)
Yüksel Altiner
Wolfgang Söhne
Andrea Stürze

University of Cologne (https://www.portal.uni-koeln.de/uoc_home.html?&L=1)
Susanne Crewell
Sandra Steinke

Max-Planck-Institute for Chemistry (https://www.mpg.de/153030/chemie)
Steffen Beirle

Greece
Aristotle University of Thessaloniki (https://www.auth.gr/en)

Chris Pikridas

Tekmon Geomatics (https://www.tekmon.gr/)
Nicholas Zinas

National Observatory of Athens (http://www.noa.gr/index.php?lang=en)
Athanassios Ganas

Finland
Finnish Meteorological Institute (http://en.ilmatieteenlaitos.fi/)
Rigel Kivi
Ari-Matti Harri

France
Institut national de l'information géographique et forestière (IGN) (http://www.ign.fr/)
Olivier Bock
Samuel Nahmani
Ana Parracho
Pascal Willis
Paul Rebischung

Météo-France (http://www.meteofrance.com/accueil)
Jean-François Mahfouf

École Supérieure des Géomètres et Topographes (ESGT) (http://www.esgt.cnam.fr/epn-esgt/formation-et-recherche-pour-les-geometres-topographes-960364.kjsp)
Laurent Morel

Université Paris-Saclay, Sorbonne Universités (http://www.sorbonne-universites.fr/)
Sophie Bastin

Hungary
Hungarian Meteorological Service (http://www.met.hu/en/idojaras/)
Mate Mile
Peter Szabo

Department of Geodesy and Surveying, Budapest University of Technology and Economics (https://geod.bme.hu/?language=en)
Szabolcs Rozsa

Iceland
The Icelandic Meteorological Institute (http://en.vedur.is/)
Sigurdur Thorsteinsson
Benedikt G. Ófeigsson

Israel
Interdisciplinary Centre (IDC) Herzliya (https://www.idc.ac.il/en/pages/home.aspx)
Yuval Reuveni

Depatment of Geosciences, Tel Aviv University (https://en-exact-sciences.tau.ac.il/earth)
Simon Krichak

Italy
Abdus Salam International Centre for Theoretical Physics (https://www.ictp.it/)
Riccardo Biondi
Rita Nogherotto

Centro di Geodesia Spaziale/Agenzia Spaziale Italiana contrada Terlecchia Matera (https://www.asi.it/en)
Rosa Pacione
Giuseppe Bianco

Fondazione Ugo Bordoni (http://www.fub.it/)
Ermanno Fionda

Centre of Excellence Telesensing of Environment and Model Prediction of Severe events, L'Aquila, Italy
Vinia Mattioli

Lithuania
Vilnius University (https://www.vu.lt/en/)
Gintautas Stankunavicius

Luxembourg
Geodesy and Geospatial Engineering, Institute of Civil Engineering and Environment, University of Luxembourg (ULX) (https://wwwen.uni.lu/research/fstc/research_unit_in_engineering_sciences_rues/research_areas/civil_environment_engineering_inceen)
Furqan Ahmed
Kibrom Abraha
Wenwu Ding
Addisu Hunegnaw
Norman Teferle

Netherlands
Royal Netherlands Meteorological Institute (KNMI) (http://www.knmi.nl/home)
Siebren de Haan

Poland

The Institute of Geodesy and Geoinformatics GNSS&Meteo Working Group of Wrocław University of Environmental and Life Sciences (WUELS) (http://www.igig.up.wroc.pl/igg/)
Jaroslaw Bosy
Witold Rohm
Jan Kaplon
Tomasz Hadaś
Karina Wilgan
Jan Sierny
Pawel Hordyniec
Kamil Kazmierski
Estera Trzcina

Centre of Applied Geomatics of the Warsaw Military University of Technology (MUT) (http://www.cgs.wat.edu.pl/)
Mariusz Figurski
Karolina Szafranek
Krzysztof Kroszczynski
Grzegorz Nykiel
Zofia, Bałdysz
Anna Kłos
Andrzej Araszkiewicz
Janusz Bogusz
Marta Gruszczynska

Advanced Methods for Satellite Positioning Laboratory of the University of Warmia and Mazury in Olsztyn (UWM) (http://www.uwm.edu.pl/zmps/en/)
Pawel Wielgosz
Jacek Paziewski
Katarzyna Stepniak

Portugal

University of Beira Interior (http://www.ubi.pt/en/)
Rui Fernandes
Machiel Bos
Hugo Valentim

Instituto Português do Mar e da Atmosfera (https://www.ipma.pt/en/)
Joao P. A. Martins
Carla Barroso
Pedro Viterbo

Instituto Dom Luiz, University of Lisbon (http://idl.campus.ciencias.ulisboa.pt/)
Alexandre Ramos

Polytechnic Institute of Guarda (http://www.ipg.pt/relacoes_internacionais/polytechnic.aspx)
André Sá

Slovakia
Slovak University of Technology (https://www.stuba.sk/english.html?page_id=132)
Jan Hefty
Miroslava Haque Igondova

Spain
Universidad Politécnica de Valencia (http://www.upv.es)
Enrique Priego

Universidad Pública de Navarra (http://www.unavarra.es)
Andres Seco

AEMET (http://www.aemet.es)
Jana Sánchez Arriola
José Antonio Guijarro

Sweden
Swedish Meteorological and Hydrological Institute (https://www.smhi.se)
Magnus Lindskog
Martin Ridal
Ulrika Willén

The Swedish Mapping, Cadastral and Land Registration Authority (http://www.lantmateriet.se/)
Tong Ning

Chalmers University of Technology (https://www.chalmers.se)
Gunnar Elgered
Jan M. Johansson

Switzerland
Federal Office of Topography (https://www.swisstopo.admin.ch/)
Elmar Brockmann

ETH Zurich (https://www.ethz.ch/en.html)
Alain Geiger
Fabian Hurter

Turkey
Bulent Ecevit University, Geomatics Engineering Dept. (http://geomatik.beun.edu.tr)
Cetin Mekik
Ilke Deniz
Gokhan Gurbuz

Karadeniz Technical University (http://www.ktu.edu.tr/en)
Selma Zengin Kazanci

United Kingdom
Met Office, UK (https://www.metoffice.gov.uk/)
Jonathan Jones
Gemma Halloran
Owen Lewis

University of Nottingham (https://www.nottingham.ac.uk/ngi/)
Lei Yang
Chris Hill

Australia
Geoscience Australia (http://www.ga.gov.au/)
Carl Wang
Salim Masoumi
Michael Moore

Canada
Environment Canada (https://weather.gc.ca/canada_e.html)
Stephen MacPherson

Hong Kong
Hong Kong Polytechnic University (https://www.polyu.edu.hk/web/en/home/index.html)
Zhizhao Liu
Biyan Chen

New Zealand
National Institute of Water and Atmospheric Research (https://www.niwa.co.nz/)
Richard Querel
Dan Smale

United States
University at Albany (https://www.albany.edu/)
June Wang

United States Naval Observatory (http://www.usno.navy.mil/USNO)

Christine Hackman

Argonne National Laboratory (http://www.anl.gov/)
Maria P. Cadeddu

List of Publications

Publications at COST Action GNSS4SWEC special issue ACP/AMT/ANGEO journals are available on: https://www.atmos-meas-tech.net/special_issue89.html

Austria

G. Möller, R. Weber, J. Böhm: Improved troposphere blind models based on numerical weather data; Navigation – Journal of the Institute of Navigation, 61, 3; S. 203–211, 2014.

J. Böhm, G. Möller, M. Schindelegger, G. Pain, R. Weber: Development of an improved blind model for slant delays in the troposphere (GPT2w); GPS Solutions, Volume 19, Issue 3; S. 433–441, 2015.

G. Möller, C. Wittmann, X. Yan, E. Umnig, N. Joldzic, R. Weber: 3D ground based GNSS atmospheric tomography, Final report, FFG project GNSS-ATom (ID:840098). 2015.

D. Landskron, G. Möller, A. Hofmeister, J. Böhm, R. Weber: Site-Augmentation of Empirical Tropospheric Delay Models in GNSS; Österreichische Zeitschrift für Vermessung und Geoinformation (VGI), 3, S. 128–135, 2016.

D. Landskron, A. Hofmeister, J. Böhm: Refined Tropospheric Delay Models for CONT11; International Association of Geodesy Symposia, S. 1–5, 2016.

- Hofmeister: Determination of path delays in the atmosphere for geodetic VLBI by means of ray-tracing; in Buchreihe "Geowissenschaftliche Mitteilungen Nr. 98", ISSN: 1811-8380, 318 S, 2016.

D. Landskron, Böhm J., 2017, VMF3/GPT3: refined discrete and empirical troposphere mapping functions VMF3/GPT3: refined discrete and empirical troposphere mapping functions, in: J Geod, https://doi.org/10.1007/s00190-017-1066-2, 2017.

G. Möller: Reconstruction of 3D wet refractivity fields in the lower atmosphere along bended GNSS signal paths, Dissertation, TU Wien, Department of Geodesy and Geoinformation, 2017, http://repositum.tuwien.ac.at/obvutwhs/id/2268559, 2017.

Australia

Wang X., Zhang K., Wu S., Fan S., Cheng Y. (2016) Water-vapour-weighted mean temperature and its impact in the determination of precipitable water vapour and climate change analyses, J. Geophys. Res. http://onlinelibrary.wiley.com/doi/10.1002/2015JD024181/full.

Peng, Xiu-Ying, Zang, Jian-Fei, Fan, Shi-Jie, Wu, Su-Qin, Liu, Yan-Xiong and Zhang, Ke-Fei (2015) Validation of Atmospheric Water Vapour Derived from Ship-Borne GPS Measurements in the Chinese Bohai Sea, The journal of Terrestrial, Atmospheric and Oceanic Sciences (TAO), DOI: https://doi.org/10.3319/TAO.2015.11.04.01(A).

Zhang K., Manning T., Wu S., Rohm W., Silcock S. and Choy S. (2015) Capturing the Signature of Severe Weather Events in Australia Using GPS Measurements, IEEE JSTARS, Vol.8, No.4, 1839–1847.

Xiaoming Wang, Cheng Y., Wu S. and Zhang K. (2015) An effective toolkit for the interpolation and gross error detection of GPS time series, Survey Review, DOI: https://doi.org/10.1179/1752270615Y.0000000023.

Norman R., LeMarshall J.; Rohm W., Carter B., Kirchengast G., Alexander S., Liu C. and Zhang K. (2015) Simulating the impact of refractive transverse gradients resulting from a severe troposphere weather event on GPS signal propagation, IEEE JSTARS, 8 (1) 4-18–24.

Liu Z.; Chen B.; Chan S.; Cao Y.; Gao Y.; Zhang K.; Nichol J (2015) Analysis and Modelling of Water Vapour and Temperature Changes in Hong Kong Using 40-year Radiosonde Data: 1973–2012, International Journal of Climatology, Vol.35, Issue 3, pp.462–74.

Li Y., Kirchengast G., Scherllin-Pirscher B., Wu S., Schwaerz M., Fritzer J., Zhang S. Carter B., and Zhang K. (2014) A new dynamic approach for statistical optimization of GNSS radio occultation bending angles for optimal climate monitoring utility, J. Geophys. Res. Atmos., 118, issue 23, pp. 13,022–13,040.

Wang C., Norman R., Yeh T., Zhang K., Choy S. and Tseng T. (2014) Investigation into the Atmospheric Parameters Retrieved from ROPP and CDAAC using GPS Radio Occultation Measurements over the Australian Area, Australian Journal of Earth Sciences, Vol.61, No.6, pp785–792.

Yuan, Y., K. Zhang, W. Rohm, S. Choy, R. Norman, and C.-S. Wang (2014), Real-time retrieval of precipitable water vapour from GPS precise point positioning, J. Geophys. Res. A tmos.,119, 10, 044–10,057, doi:https://doi.org/10.1002/2014JD021486.

Yu K., Rizos C., Burrage D., Dempster A., Zhang K. and Markgraf M. (2014) GNSS Remote Sensing, EURASIP Journal on Advances in Signal Processing, 2014 2014:158, doi:https://doi.org/10.1186/1687-6180-2014-158.

Yu K., Rizos C., Burrage D., Dempster A., Zhang K. and Markgraf M. (2014) An Overview of GNSS Remote Sensing, EURASIP Journal on Advances in Signal Processing, 2014:134, doi:https://doi.org/10.1186/1687-6180-2014-134.

Choy S., Wang C., Zhang K. and Kuleshov Y (2013) GPS sensing of precipitable water vapour during the March 2010 Melbourne storm, Advances in Space Research, Vol 52, Issue 9, Pages 1688–1699.

Manning T, Rohm W., Zhang K, and Wang C (2014) Determining the 4D dynamics of water vapour using GPS tomography in the Australian region, IAG Symp. 139 (CPCI-S indexed, Scopus), "Earth on the Edge: Science for a Sustainable Planet", pp.41–50, Springer-Verlag.

Belgium

Brenot, H., Neméghaire, J., Delobbe, L., Clerbaux, N., De Meutter, P., Deckmyn, A., Delcloo, A., Frappez, L., and Van Roozendael, M.: Preliminary signs of the initiation of deep convection by GNSS, Atmos. Chem. Phys., 13, 5425–5449, doi:https://doi.org/10.5194/acp-13-5425-2013, 2013.

Brenot, H., Walpersdorf, A., Reverdy, M., van Baelen, J., Ducrocq, V., Champollion, C., Masson, F., Doerflinger, E., Collard, P., and Giroux, P.: A GPS network for tropospheric tomography in the framework of the Mediterranean hydrometeorological observatory Cévennes-Vivarais (southeastern France), Atmos. Meas. Tech., 7, 553–578, doi:https://doi.org/10.5194/amt-7-553-2014, 2014.

Brenot, H., G. Wautelet, R. Warnant, J. Nemeghaire, and M. Van Roozendael: GNSS meteorology and impact on NRT position. Proceedings of the European Navigation Conference (ENC), Rotterdam, The Netherlands, 2014a.

Brenot, H., Walpersdorf, A., Reverdy, M., van Baelen, J., Ducrocq, V., Champollion, C., Masson, F., Doerflinger, E., Collard, P., and Giroux, P.: A GPS network for tropospheric tomography in the framework of the Mediterranean hydrometeorological observatory Cévennes-Vivarais (southeastern France), Atmos. Meas. Tech., 7, 553–578, https://doi.org/10.5194/amt-7-553-2014, 2014b.

Van Malderen, R., Brenot, H., Pottiaux, E., Beirle, S., Hermans, C., De Mazière, M., Wagner, T., De Backer, H., and Bruyninx, C.: A multi-site intercomparison of integrated water vapour observations for climate change analysis, Atmos. Meas. Tech., 7, 2487–2512, doi:https://doi.org/10.5194/amt-7-2487-2014, 2014.

Namaoui, H., S. Kahlouche, A.H. Belbachir, R. Van Malderen, H. Brenot, and E. Pottiaux, 2017: GPS Water Vapour and Its Comparison with Radiosonde and ERA-Interim Data in Algeria. Adv. Atmos. Sci., 34(5), 000–000, doi: https://doi.org/10.1007/s00376-016-6111-1.

Termonia, P., Van Schaeybroeck, B., De Cruz, L., De Troch, R., Caluwaerts, S., Giot, O., Hamdi, R., Vannitsem, S., Willems, P., Tabari, H., Van Uytven, E., Hosseinzadehtalaei, P., Van Lipzig, N., Wouters, H., Vanden Broucke, S., van Ypersele, J.-P., Marbaix, P., Villanueva-Birriel, C., Fettweis, X., Wyard, C., Scholzen, C., Doutreloup, S., De Ridder, K., Gobin, A., Lauwaet, D., Stavrakou, T., Bauwens, M., Müller, J.-F., Luyten, P., Ponsar, S., Van den Eynde, D., Pottiaux, E.: The CORDEX.be initiative as a foundation for climate services in Belgium, submitted to Climate Services, 2017.

Van Malderen, R., Pottiaux, E., Klos, A., Bock, O., Bogusz, J., Chimani, B., Elias, M., Gruszczynska, M., Guijarro, J., Zengin Kazancı, S., Ning, T.: Homogenizing GPS Integrated Water Vapour Time Series: Methodology and Benchmarking the Algorithms on Synthetic Datasets, Proceedings of the Ninth Seminar for Homogenization and Quality Control in Climatological Databases and Fourth Conference on Spatial Interpolation Techniques in Climatology and Meteorology, Budapest, Hungary, 2017c, WMO, WCDMP-No. 845, edited by T. Szentimrey, M. Lakatos, L. Hoffmann, pp. 102–114 (http://www.wmo.int/pages/prog/wcp/wcdmp/wcdmp_series/WCDMP_85.pdf) pp. 104–116, 2017b.

Bulgaria

Mircheva B., M. Tsekov, U. Meyer and G. Guerova, 2017. Anomalies of hydrological cycle components during the 2007 heat wave in Bulgaria, Journal of Atmospheric and Solar-Terrestrial Physics, 165–166, 1–9, https://doi.org/10.1016/j.jastp.2017.10.005.

Stoycheva A., I. Manafov, K. Vassileva and G. Guerova, 2017. Study of persistent fog in Bulgaria with Sofia Stability Index, GNSS tropospheric products and WRF simulations. Journal of Atmospheric and Solar-Terrestrial Physics, 161, 160–169, doi: https://doi.org/10.1016/j.jastp.2017.06.011.

Guerova G., J. Jonas, J. Douša, G. Dick, S. de Haan, E. Pottiaux, O. Bock, R. Pacione, G. Elgered, H. Vedel, and M. Bender, 2016, Review of the state-of -the -art and future prospects of the ground-based GNSS meteorology in Europe, Atmos. Meas. Tech., 9, 5385–5406, 2016, https://doi.org/10.5194/amt-9-5385-2016.

Stoycheva A. and G. Guerova, 2015. Study of fog in Bulgaria by using the GNSS tropospheric products and large scale dynamic analysis. Journal of Atmospheric and Solar-Terrestrial Physics, 133, 87–97, doi: https://doi.org/10.1016/j.jastp.2015.08.004.

Manafov I. and G. Guerova, 2015. Numerical simulations of 18 fog case studies at Sofia airport in the period 2011–2014. Annuaire de l'Universite de Sofia "St. Kliment Ohridski", Faculte de Physique, 108, 48–61.

Guerova G., Tzv. Simeonov and N. Yordanova, 2014. The Sofia University Atmospheric Data Archive (SUADA), Atmos. Meas. Tech., 7, 2683–2694, doi:https://doi.org/10.5194/amt-7-2683-2014.

Guerova G., 2014. Water vapour anomaly during the 2003 European summer. Annuaire de l'Universite de Sofia "St. Kliment Ohridski", Faculte de Physique, 107, 58–67.

Simeonov Tzv., K. Vasileva and G. Guerova, 2013. Application of ground-based GNSS meteorology in Bulgaria/Southeast Europe: case study 2007 heat wave. Annuaire de l'Universite de Sofia "St. Kliment Ohridski", Faculte de Physique, 106, 88–100.

Czech Republic

Douša J, Václavovic P, Zhao L, Kačmařík M (2018), New Adaptable All-in-One Strategy for Estimating Advanced Tropospheric Parameters and Using Real-Time Orbits and Clocks. Remote Sens. 2018, 10, 232. doi:https://doi.org/10.3390/rs10020232.

Douša J, Dick G, Kačmařík M, Brožková R, Zus F, Brenot H, Stoycheva A, Möller G, Kaplon J (2016), Benchmark campaign and case study episode in Central Europe for development and assessment of advanced GNSS tropospheric models and products, Atmos. Meas. Tech., 9, 2989–3008, doi:https://doi.org/10.5194/amt-9-2989-2016, 2016, 2016.

Douša J, Eliaš M (2014) An improved model for calculating tropospheric wet delay, Geoph. Res. Lett. V41(12), 4389–4397, doi:https://doi.org/10.1002/2014GL060271.

Douša J, Václavovic P (2014) Real-time zenith tropospheric delays in support of numerical weather prediction applications. Adv Space Res, 53(9):1347–1358, doi: https://doi.org/10.1016/j.asr.2014.02.021.

Douša J, Eliaš M, Václavovic P, Eben K, Krc P, (2018) A two-stage tropospheric correction model combining data from GNSS and numerical weather model. GPS Solut. https://doi.org/10.1007/s10291-018-0742-x.

Douša J, Václavovic P, M. Eliaš (2017), Tropospheric products of the second European GNSS reprocessing (1996–2014), Atmos. Meas. Tech., 10:1–19, doi: https://doi.org/10.5194/amt-10-1-2017.

Douša J, Václavovic P (2016), Evaluation of ground-based GNSS tropospheric products at Geodetic Observatory Pecny, In: IAG 150 Years, Rizos Ch. and Willis P. (eds), IAG Symposia Series, Vol. 143, pp. 759–766, doi:https://doi.org/10.1007/1345_2015_157.

Douša J, Václavovic P, Krč P, Eliaš M, Eben E, Resler J (2015), NWM forecast monitoring with near real-time GNSS products, In: Proceedings of the 5th Scientific Galileo Colloquium, Braunschweig, Germany, October 27–29, 2015.

Douša J, Eliaš M, Veerman H, van Leeuwen S, Zelle H, de Haan S, Martellucci A, Perez OA (2015), High accuracy tropospheric delay determination based on improved modelling and high resolution Numerical Weather Model, Proceedings of the 28th International Technical Meeting of the Satellite Division of the Institute of Navigation, pp. 3734–3744.

Douša J, Gyori G (2013), Database for tropospheric product evaluations – implementation aspects, Geoinformatics, Vol. 10, pp. 39–52, doi:https://doi.org/10.14311/gi.10.4http://geoinformatics.fsv.cvut.cz/pdf/geoinformatics-fce-ctu-2013-10.pdf.

Eliaš M, Douša J (2015), Outlier Detection Using Some Methods of Mathematical Statistic in Meteorological Time-Series, In Proceedings of ICNAAM 2015, Rhodes (Greece).

Eliaš M, Douša J, Jarušková D (2017), An Assessment of Method for Change-Point Detection Applied in Tropospheric Parameter Time Series given from Numerical Weather Model, Adv. Space Res.(submitted).

Gyori G, Douša J (2016), GOP-TropDB developments for tropospheric product evaluation and monitoring – design, functionality and initial results, In: IAG 150 Years, Rizos Ch. and Willis P. (eds), IAG Symposia Series, Springer Vol. 143, pp. 595–602. di:10.1o007/1345_2015_193.

Kačmařík, M.: Retrieving of GNSS Tropospheric Delays from RTKLib in Real-time and Post-Processing Mode, GIS Ostrava 2017, Dynamics in Giscience, Lectures Notes in Geoinformation and Cartography, Springer, 2017.

Kačmařík, M., Douša, J., Dick, G., Zus, F., Brenot, H., Möller, G., Pottiaux, E., Kapłon, J., Hordyniec, P., Václavovic, P., and Morel, L.: *Inter-technique validation of tropospheric slant total delays*, Atmospheric Measurement Techniques, 10, 2183–2208, doi:https://doi.org/10.5194/amt-10-2183-2017, 2017.

Václavovic P, Douša J (2015), Backward smoothing for precise GNSS applications, Advances in Space Research, Volume 56, Issue 8, 15 October 2015, Pages 1627–1634.

Václavovic P, Douša J, Eliaš M, Kostelecký J (2017), Using external tropospheric corrections to improve GNSS positioning of hot-air balloon, GPS Solut. 21 (4):1479–1489, doi:https://doi.org/10.1007/s10291-017-0628-3.

Hackman C, Guerova G, Byram B, Douša J, Hugentobler U (2015), International GNSS Service (IGS) Troposphere Products and Working Group Activities, in: FIG Working Week September 2015, AIP Conf. Proc.2015 Proceedings, Sofia, Bulgaria.

Van Leeuwen S, Douša J (2016), Hopfield revisited: Two-6th Power Tropospheric Zenith Delay Profiles for Correcting GNSS Data, In: Proceedings of the NAVITEC 2016, Dec 14–16, ESTEC, Noordwijk, Netherlands.

Zhao L, Douša J, Václavovic P, Ye S, Xia F (2018) Evaluation of long-term BeiDou/GPS observation quality based on G-Nut/Anubis and initial results, Acta Geodyn. Geomater., Vol. 15, No. 1(189), 77–85, doi:https://doi.org/10.13168/AGG.2018.006.

France

Pollet, A., D., Coulot, O., Bock, S., Nahmani, Comparison of individual and combined Zenithal Tropospheric Delay estimations during CONT08 campaign, J. Geodesy, 88:1095–1112. First online: 30 July 2014. doi:https://doi.org/10.1007/s00190-014-0745-5).

Adler, N. Kalthoff, M. Kohler, J. Handwerker, A. Wieser, U. Corsmeier, C. Kottmeier, D. Lambert, O. Bock (2015) "The variability of water vapour and pre-convective conditions over the mountainous island of Corsica" Q.J. R. Meteorol. Soc. Article first published online: 8 APR 2015, DOI: https://doi.org/10.1002/qj.2545.

Chazette, P., C. Flamant, X. Shang, J. Totems, J.-C. Raut, A. Doerenbecher, V. Ducrocq, O. Bock, and S. Bouffiès-Clocher (2015) A multi-instrument and multi-model assessment of atmospheric moisture variability over the western Mediterranean during HyMeX. Q.J. R. Meteorol. Soc. Article first published online: 11 NOV 2015, DOI: https://doi.org/10.1002/qj.2671.

Khodayar S, Fosser G, Berthou S, Davolio S, Drobinski P, Ducrocq V, Ferretti R, Nuret M, Pichelli E, Richard E, Bock O. A seamless weather-climate multi-model intercomparison on the representation of a high impact weather event in the Western Mediterranean: HyMeX IOP12. Q.J. R. Meteorol. Soc. Article first published online: 2 FEB 2016. DOI: https://doi.org/10.1002/qj.2700.

Bock, O., P. Bosser, R. Pacione, M. Nuret, N. Fourrié, A. Parracho, A high quality reprocessed ground-based GPS dataset for atmospheric process studies, radiosonde and model evaluation, and reanalysis of HyMeX Special Observing Period, Q.J. R. Meteorol. Soc., 2016. Article first published online: 17 FEB 2016. DOI: https://doi.org/10.1002/qj.2701.

Bock O., Willis P., Wang, J., Mears C. (2014), A high-quality, homogenized, global, long-term (1993–2008) DORIS precipitable water dataset for climate monitoring and model verification, Journal of Geophysical Research, Atmospheres, 119(12), 7209–7230, DOI: https://doi.org/10.1002/2013JD021124.

Willis P., Bock O., Bar-Sever Y.E. (2014), DORIS tropospheric estimation at IGN: Current strategies, GPS intercomparisons and perspectives, IAG Symposia Series, 139, 11–18, DOI: https://doi.org/10.1007/978-3-642-37222-3_2.

Teke K., Nilsson T., Boehm J., Hobiger T., Steigenberger P., Garcia-Espada S., Haas R., Willis P. (2013), Troposphere delays from space geodetic techniques, water vapour radiometers, and numerical weather models over a series of continuous VLBI campaigns, Journal of Geodesy, 87(10–12), 981–1001, DOI: https://doi.org/10.1007/s00190-013-0662-z.

Germany

Alshawaf, F., Fersch, B., Hinz, S., Kunstmann, H., Mayer, M., and Meyer, F. J. (2015), Water vapour mapping by fusing InSAR and GNSS remote sensing data and atmospheric simulations, Hydrol. Earth Syst. Sci., 19, 4747–4764, doi: https://doi.org/10.5194/hess-19-4747-2015, 2015.

Alshawaf, F., Hinz, S., Mayer, M., Meyer F. J. (2015), Constructing accurate maps of atmospheric water vapour by combining interferometric synthetic aperture radar and GNSS observations. Journal of Geophysical Research: Atmosphere. 120 (4), pp. 1391–1403.

Alshawaf, F., Fuhrmann, T., Knoepfler, A., Luo, X., Mayer, M., Hinz, S., Heck, B. (2015), Accurate estimation of atmospheric water vapour using GNSS observations and surface meteorological data. Transactions on Geoscience and Remote Sensing. 53 (7), pp. 3764–3771, IEEE Journals & Magazines.

Alshawaf, F., Fuhrmann, T., Heck, B., Hinz, S., Knoepfler, A., Luo, X., Mayer, M., Schenk, A., Thiele, A., Westerhaus, M. (2013), Integration of InSAR and GNSS Observations for the Determination of Atmospheric Water Vapour. In: Krisp JM, Meng L, Pail R, Stilla U (Eds.), Earth Observation of Global Changes (EOGC), Lecture Notes in Geoinformation and Cartography, pp. 147–162, Springer-Verlag Berlin, Heidelberg.

Balidakis, K., F. Zus, J. Douša, T. Nilsson, S. Glaser, B. Soja, M. Karbon, R. Heinkelmann and H. Schuh (2016) On the impact of different mapping functions on geodetic and tropospheric products from VLBI data analysis, In Behrend, D., Baver, K.D. and Armstrong, K. (eds) IVS2016GM Proceedings, pp. 331–335, NASA/CP-2016-219016.

Balidakis, K., R. Heinkelmann, A. Phogat, B. Soja, S. Glaser, T. Nilsson, M. Karbon and H. Schuh (2016) On the impact of inhomogeneities in meteorological data on VLBI data analysis, In Behrend, D., Baver, K.D. and Armstrong, K. (eds) IVS2016GM Proceedings, pp. 356–360, NASA/CP-2016-219016.

Bollmeyer, C., Keller, J., Ohlwein, C., Wahl, S., Crewell, S., Friederichs, P., Hense, A., Keune, J., Kneifel, S., Pscheidt, I., Redl, S., Steinke, S. (2015), Towards a high-resolution regional reanalysis for the European CORDEX domain. Quarterly Journal of the Royal Meteorological Society 141:686, 1–15.

Heinkelmann, R., Willis, P., Deng, Z., Dick, G., Nilsson, T., Soja, B., Zus, F., Wickert, W., Schuh, H. (2016): Multi-technique comparison of atmospheric parameters at the DORIS co-location sites during CONT14, Advances in Space Research, Volume 58, Issue 12, 15 December 2016, pp. 2758–2773, doi: https://doi.org/10.1016/j.asr.2016.09.023.

Heinkelmann, R., Willis, P., Deng Z., Dick, G., Nilsson, T., Soja, B., Zus, F., Wickert, J., Schuh, H., The effect of the temporal resolution of atmospheric gradients on atmospheric parameters, Advances in Space Research, submitted 2017.

Kalthoff, N., Adler, B., Wieser, A., Kohler, M., Traeumner, K., Handwerker, J., Corsmeier, U., Khodayar, S., Lambert, D., Kopmann, A., Kunka, N., Dick, G., Ramatschi, M., Wickert, J., Kottmeier, C. (2013), KITcube – a mobile observation system for convection studies deployed during HyMeX, Meteorologische Zeitschrift, Vol.22, No.6, 633–647, doi: https://doi.org/10.1127/0941-2948/2013/0542.

Labbouz, L., van Baelen, J., Tridon, F., Reverdy, M., Hagen, M. Bender, M., Dick, G., Gorgas, T., and Planche, C. (2013), Precipitation on the lee side of the Vosges Mountains: Multi-instrumental study of one case from the COPS campaign, Meteorologische Zeitschrift, 22 (4), pp. 413–432, doi: https://doi.org/10.1127/0941-2948/2013/0413.

Li, X., Dick, G., Ge, M., Heise, S., Wickert, J., and Bender, M. (2014), Real-time GPS sensing of atmospheric water vapour: precise point positioning with orbit, clock and phase delay corrections, Geophys. Res. Lett., 41(10), 3615–3621, doi: https://doi.org/10.1002/2013GL058721.

Li, X., Zus, F., Lu, C., Ning, T., Dick, G., Ge, M., Wickert, J., and Schuh, H. (2015), Retrieving high-resolution tropospheric gradients from multi-constellation GNSS observations, Geophys. Res. Lett., 42, 4173–4181, doi:https://doi.org/10.1002/2015GL063856.

Li, X., Zus, F., Lu, C., Dick, G., Ning, T., Ge, M., Wickert, J., and Schuh, H. (2015), Retrieving of atmospheric parameters from multi-GNSS in real time: Validation with water vapour radiometer and numerical weather model. J. Geophys. Res. Atmos., Volume 120, Issue 14, pp. 7189–7204, doi: https://doi.org/10.1002/2015JD023454.

Li, X., Dick, G., Lu, C., Ge, M., Nilsson, T., Ning, T., Wickert, J., Schuh, H. (2015), Multi-GNSS meteorology: Real-time retrieving of atmospheric water vapour from BeiDou, Galileo, GLONASS and GPS observations. IEEE Transactions on Geoscience and Remote Sensing, 06/2015; doi:https://doi.org/10.1109/TGRS.2015.2438395.

Lu, C., Li, X., Nilsson, T., Ning, T., Heinkelmann, R., Ge, M., Glaser, S., Schuh, H. (2015), Real-time retrieval of precipitable water vapour from GPS and BeiDou observations. Journal of Geodesy 89(9), 843–856, doi:https://doi.org/10.1007/s00190-015-0818-0.

Lu, C., Li, X., Li, Z., Heinkelmann, R., Nilsson, T., Dick, G., Ge, M., and Schuh, H. (2016), GNSS tropospheric gradients with high temporal resolution and their effect on precise positioning, J. Geophys. Res. Atmos., 121, 912–930, doi:https://doi.org/10.1002/2015JD024255.

Lu, C., X. Li, M. Ge, R. Heinkelmann, T. Nilsson, B. Soja, G. Dick, and H. Schuh (2016), Estimation and evaluation of real-time precipitable water vapour from GLONASS and GPS, GPS Solut., 1–11, doi: https://doi.org/10.1007/s10291-015-0479-8.

Lu, C., F. Zus, M. Ge, R. Heinkelmann, G. Dick, J. Wickert, and H. Schuh (2016), Tropospheric delay parameters from numerical weather models for multi-GNSS precise positioning, Atmos. Meas. Tech., 9(12), 5965–5973, 2016, doi: https://doi.org/10.5194/amt-2016-176.

Lu, C., X. Li, F. Zus, R. Heinkelmann, G. Dick, M. Ge, J. Wickert, and H. Schuh, Improving BeiDou real-time precise point positioning with numerical weather models (2016), J. Geod.

Shangguan, M., Bender, M., Ramatschi, M., Dick, G., Wickert, J., Raabe, A., Galas, R. (2013), GPS Tomography: Validation of Reconstructed 3D Humidity fields with Radiosonde Profiles, Ann. Geophys., 31, 9, 1491–1505, doi: https://doi.org/10.5194/angeo-31-1491-2013.

Shangguan, M., Heise, S., Bender, M., Dick, G., Ramatschi, M., Wickert, J. (2015), Validation of GPS atmospheric water vapour with WVR data in satellite tracking mode, Ann. Geophys., 33, 55–61, 2015, doi: https://doi.org/10.5194/angeo-33-55-2015.

Soja, B., Nilsson, T., Karbon, M., Zus, F., Dick, G., Deng, Z., Wickert, J., Heinkelmann, R., Schuh, H. (2015), Tropospheric delay determination by Kalman filtering VLBI data Earth, Planets and Space 67, 2015, 144, doi: https://doi.org/10.1186/s40623-015-0293-0.

Steinke, S., Eikenberg, S., Loehnert, U., Dick, G., Klocke, D., Di Girolamo, P., Crewell, S. (2015), Assessment of small-scale integrated water vapour variability during HOPE, Atmospheric Chemistry and Physics, 15, 2675–2692, 2015, doi: https://doi.org/10.5194/acpd-14-22837-2014.

Wulfmeyer, V., Hardesty, R. M., Turner, D. D., Behrendt, A., Cadeddu, M. P., Di Girolamo, P., Schlüssel, P., Van Baelen, J., Zus, F. (2015), A review of the remote sensing of lower tropospheric thermodynamic profiles and its indispensable role for the understanding and the simulation of water and energy cycles, *Reviews of Geophysics*, 53, 3, pp. 819—895, doi:https://doi.org/10.1002/2014RG000476.

Zus, F., Dick, G. Douša, J., Heise, S. and Wickert, J. (2014), The rapid and precise computation of GPS slant total delays and mapping factors utilizing a numerical weather model. Radio Science, 49, 2014, 3, pp. 207–216, doi:https://doi.org/10.1002/2013RS005280.

Zus, F., Dick, G., Heise, S., Wickert, J. (2015), A forward operator and its adjoint for GPS slant total delays, Radio Science Volume 50, Issue 5, pp. 393–405, 2015, doi:https://doi.org/10.1002/2014RS005584.

Zus, F., Dick, G., Douša, J., Wickert, J. (2015), Systematic errors of mapping functions which are based on the VMF1 concept. GPS Solutions: Volume 19, Issue 2 (2015), pp. 277–286, doi:https://doi.org/10.1007/s10291-014-0386-4.

Greece

Pikridas C. 2015. The use of GNSS tropospheric products for climate monitoring. A case study in the area of Ioannina Northwestern Greece. South-Eastern European Journal of Earth Observation and Geomatics. Vol 4. ISSN:2241-1224. pp. 82–90.

Katsougiannopoulos S., C. Pikridas, N. Zinas, M. Chatzinikos, S. Bitharis 2015. Analysis of Precipitable Water estimates using permanent GPS station data during the Athens heavy rainfall on 22th February 2013. International Association of Geodesy Symposia-IAG, DOI: https://doi.org/10.1007/1345_2015_16. Springer-Verlag.

Pikridas C. 2014. Monitoring climate changes on small scale networks using ground based GPS and meteorological data. *Jo*urnal of Planetary Geodesy-Artificial Satellites. Vol. 49, No.3. Walter De Gruyter.

Pikridas C., S. Katsougiannopoulos, N. Zinas 2014. A comparative study of zenith tropospheric delay and precipitable water vapour estimates using scientific GPS processing software and web based automated PPP service. Status: *Acta Geodaetica et Geophysica, vol.49, 2,* Springer-Verlag. DOI: https://doi.org/10.1007/s40328-014-0047-7.

Zinas N., S. Kontogiannis, G. Kokonis, C. Pikridas 2013. A novel microclimate forecasting system architecture integrating GPS measurements and meteorological-sensor data. Proceedings of sixth Balkan Conference in Informatics (BCI). 19–21 September, Thessaloniki, Greece.

Hungary

Rozsa S: Uncertainty Considerations for the Comparison of Water Vapour Derived from Radiosondes and GNSS, *INTERNATIONAL ASSOCIATION OF GEODESY SYMPOSIA* 139: *pp. 65–78.* (2014).

Rózsa Sz, Kenyeres A, Weidinger T, Gyöngyösi A Z.: Near real-time estimation of integrated water vapour from GNSS observations in Hungary *INTERNATIONAL ASSOCIATION OF GEODESY SYMPOSIA* 139: *pp. 31–39.* (2014).

Rózsa Sz: Modelling Tropospheric Delays Using the Global Surface Meteorological Parameter Model: GPT2, *PERIODICA POLYTECHNICA-CIVIL ENGINEERING* 58:(4) *pp. 301–308.* (2014).

Italy

Bonafoni S., and R. Biondi, "The usefulness of the Global Navigation Satellite Systems (GNSS) in the analysis of precipitation events", Atmos. Res., 167, 15–23, doi: https://doi.org/10.1016/j.atmosres.2015.07.011, 2015.

Pace, R. Pacione, C. Sciarretta, G. Bianco, "Computation of Zenith Total Delay Correction Fields using Ground-Based GNSS estimates", IAG Symposia Series. Vol 137-2012/ IAGS-D-13-00021.

Pacione, R., Araszkiewicz, A., Brockmann, E., and Douša, J.: EPN Repro2: A reference GNSS tropospheric dataset over Europe, Atmos. Meas. Tech., 10, 1689–1705, doi: https://doi.org/10.5194/amt-2016-369, 2017.

Pacione R and J. Douša: SINEX_TRO – Solution (Software/Technique) INdependent EXchange Format for TROpospheric and meteorological parameters Version 2.00, 2017.

Luxembourg

Ahmed, F., P. Václavovic, F. N. Teferle, J. Douša, R. Bingley and D. Laurichesse (2016). "Comparative analysis of real-time precise point positioning zenith total delay estimates." GPS Solutions 20(2): 187–199.

Ahmed, F., F. N. Teferle, R. M. Bingley and D. Laurichesse (2015). The Status of GNSS Data Processing Systems to Estimate Integrated Water Vapour for Use in Numerical Weather Prediction Models. International Association of Geodesy Symposia. Springer Berlin Heidelberg: 1–7.

Ding, W., F. N. Teferle, K. Kazmierski, D. Laurichesse and Y. Yuan (2017). "An evaluation of real-time troposphere estimation based on GNSS Precise Point Positioning." Journal of Geophysical Research: Atmospheres: 2016JD025727.

Poland

Bałdysz, Z., Nykiel, G., Figurski, M., Szafranek, K., and Kroszczyński, K., Investigation of the 16-year and 18-year ZTD Time Series Derived from GPS Data Processing. Acta Geophys. 63, 1103–1125, DOI: https://doi.org/10.1515/acgeo-2015-0033.

Hadaś T., Bosy J. *IGS RTS precise orbits and clocks verification and quality degradation over time*, GPS Solutions, Vol. 19 No. 1, Berlin Heidelberg 2015, pp. 93–105, DOI: https://doi.org/10.1007/s10291-014-0369-5.

Hadaś T., *GNSS-Warp Software for Real-Time Precise Point Positioning*, Artificial Satellites. Journal of Planetary Geodesy, Vol. 50 No. 2, Warsaw, Poland; Oldenburg, Germany 2015, pp. 59–76, DOI: https://doi.org/10.1515/arsa-2015-0005.

Hordyniec P., Bosy J., Rohm W. Assessment of errors in precipitable water data derived from global navigation satellite system observations, Journal of Atmospheric and Solar-Terrestrial Physics, Vol. 129 No., Amsterdam, the Netherlands 2015, pp. 69–77, DOI: https://doi.org/10.1016/j.jastp.2015.04.012.

Werner M., Kryza M., Skjøth C., Wałaszek K., Dore A., Ojrzyńska H., Kapłon J., (2016). Aerosol-Radiation Feedback and PM10 Air Concentrations Over Poland. Pure and Applied Geophysics. Springer. 2016. pp. 1–18, DOI: https://doi.org/10.1007/s00024-016-1267-2.

Kroszczyński, K., Angular Distributions of Discrete Mesoscale Mapping Functions. Acta Geophys. 63, 1126–1149, DOI: https://doi.org/10.1515/acgeo-2015-0035.

Kroszczyński, K., Investigation of the properties of discrete mesoscale mapping functions. Acta Geophys. (in press).

Paziewski J, Wielgosz P, 2015, Accounting for Galileo-GPS inter-system biases in precise satellite positioning, Journal of Geodesy, Vol. 89(1), pp. 81–93, DOI https://doi.org/10.1007/s00190-014-0763-3.

Paziewski J, Sieradzki R, Wielgosz P, 2015, Selected properties of GPS and Galileo-IOV receiver intersystem biases in multi-GNSS data processing, Measurement Science and Technology 07/2015; 26(9):095008.

Rohm W., Yang Y., Biadeglgne B., Zhang K., Le Marshall J., *Ground-based GNSS ZTD/IWV estimation system for numerical weather prediction in challenging weather conditions*, Atmospheric Research, Vol. 138 No., 2014, pp. 414–426, DOI: https://doi.org/10.1016/j.atmosres.2013.11.026.

Rohm W., Zhang K., Bosy J., *Limited constraint, robust Kalman filtering for GNSS troposphere tomography,* Atmospheric Measurement Techniques, Vol. 7 No. 5, 2014, pp. 1475–1486, DOI: https://doi.org/10.5194/amt-7-1475-2014.

Rzepecka Z., Kalita J., Stępniak K., Wielgosz P., 2015, Time series analysis of radio signals wet tropospheric delays for short-term forecast, Acta Geodynamica et Geomaterialia, V. 12, No. 4(180).

Wilgan K., Zenith total delay short-term statistical forecasts for GNSS Precise Point Positioning, Acta Geodetica et Geomaterialia, Vol. 12 No. 4 (180), Prague, Czech Rep. 2015, pp. 335–343, DOI: https://doi.org/10.13168/AGG.2015.0035.

Wilgan K., Rohm W., Bosy J., Multi-observation meteorological and GNSS data comparison with Numerical Weather Prediction model, Atmospheric Research, Vol. 156 No., Amsterdam, the Netherlands 2015, pp. 29–42, DOI: https://doi.org/10.1016/j.atmosres.2014.12.011.

Hadaś T., Teferle F. N., Kaźmierski K., Hordyniec P., Bosy J. Optimum stochastic modelling for GNSS tropospheric delay estimation in real-time. GPS Solutions, Vol. 21 No. 3, Berlin – Heidelberg 2017, pp. 1069–1081, DOI: https://doi.org/10.1007/s10291-016-0595-0.

Wilgan K., Hadaś T., Hordyniec P., Bosy J. Real-time precise point positioning augmented with high-resolution numerical weather prediction model, GPS Solutions, Vol. 23 No. 3, Berlin – Heidelberg 2017, pp. 1341–1353, DOI: https://doi.org/10.1007/s10291-017-0617-6.

Wilgan K., Hurter F., Geiger A., Rohm W., Bosy J. Tropospheric refractivity and zenith path delays from least-squares collocation of meteorological and GNSS data, Journal of Geodesy, Vol. 91 No. 2, Berlin Heidelberg 2017, pp. 117–134, DOI: https://doi.org/10.1007/s00190-016-0942-5.

Kaźmierski K., Santos M., Bosy J. Tropospheric delay modelling for the EGNOS augmentation system, Survey Review, Vol. 49 No. 357, London, United Kingdom 2017, pp. 399–407, DOI: https://doi.org/10.1080/00396265.2016.1180798.

Spain

Priego, E., Jones, J., Porres, M.J., Seco, A., 2016. Monitoring water vapour with GNSS during a heavy rainfall event in the Spanish Mediterranean area. Geomatics, Natural Hazards and Risk. pp. 1–13. DOI: https://doi.org/10.1080/19475705.2016.1201150.

Priego, E., Seco, A., Jones, J., Porres, M.J., 2016. Heavy rain analysis based on GNSS water vapour content in the Spanish Mediterranean area. Meteorological Applications, 23 (4), pp. 640–649. DOI: https://doi.org/10.1002/met1586.

Arriola, J.S., Lindskog, M., Thorsteinsson, S., Bojarova, J. 2016. Variational bias correction of GNSS ZTD in the HARMONIE modelling system. Journal of Applied Meteorology and Climatology, 55(5), pp. 1259–1276. DOI:https://doi.org/10.1175/JAMC-D-15-0137.1.

Seco, A., Ramírez, F., Serna, E., (...), Miqueleiz, L., Priego, J.E.2012. Rain pattern analysis and forecast model based on GPS estimated atmospheric water vapour content. Atmospheric Environment, 49, pp. 85–93. DOI: https://doi.org/10.1016/j.atmosenv.2011.12.019.

Sweden

Elgered, G., Ground-based GPS networks for remote sensing of the atmospheric water vapour content: a review, 7th Study Conference on BALTEX June 10–14, 2013, Borgholm, Island of Öland, Sweden, 2013.

Forkman, P., G. Elgered and T. Ning (2017) Accuracy assessment of the two WVRs, Astrid and Konrad, at the Onsala Space Observatory. In: R. Haas and G. Elgered (eds.), Proc. 23rd EVGA Working Meeting, Chalmers Univ. Tech., Gothenburg, Sweden, pp. 65–69.

Lindskog, M, Ridal, M, Thorsteinsson, S, Ning, T (2017), Data assimilation of GNSS Zenith Total Delays from a Nordic processing centre, accepted for publication in ACP.

Ning, T., and G. Elgered, A 17-year time series of ground-based GNSS for sensing of atmospheric water vapour, 5th International Colloquium Scientific and Fundamental Aspects of the Galileo Programme, Braunschweig, Germany, 27–29 October, 2015.

Ning, T., Wang, J., Elgered, G., Dick, G., Wickert, J., Bradke, M., and Sommer, M.: The uncertainty of the atmospheric integrated water vapour estimated from GNSS observations, Atmos. Meas. Tech.., 9, 79–92, doi:https://doi.org/10.5194/amt-9-79-2016, 2016.

Ning T., Wickert J., Deng Z., Heise S., Dick G., Vey S., and Schoene T.: Homogenized Time Series of the Atmospheric Water Vapour Content Obtained from the GNSS Reprocessed Data, Journal of Climate, doi: https://doi.org/10.1175/JCLI-D-15-0158.1, 2016.

Ning, T., and G. Elgered, Trends in the atmospheric water vapour estimated from two decades of ground-based GPS data: sensitivity to the elevation cut-off angle, 6th International Colloquium Scientific and Fundamental Aspects of the Galileo Programme, Valencia, Spain, 25–27 October, 2017.

United Kingdom

Bennitt, G. V., Johnson, H.R., Weston, P. P., Jones, J., and Pottiaux, E.: An assessment of ground-based GNSS Zenith Total Delay observation errors and their correlations using the Met Office UKV model, Quarterly Journal of Meteorological Society, 143 issue 707, pp. 2436–2447, 2017.

SINEX-TRO V2.00 Format Description

Detailed Format Description

SINEX_TRO – Solution (Software/Technique) INdependent EXchange
Format for TROpospheric and meteorological parameters
Version 2.00 (October 2017)

R. Pacione, e-GEOS/ASI-CGS, Italy
J. Douša, GOP/RIGTC, Czech Republic

Document History

Date	Notes/Changes
July 2017	Format officially presented and discussed at the IGS Workshop in Paris
October 2017	Add 'TIME SYSTEM' in the TROP/DESCRIPTION Block

Introduction

This document describes the Solution (Software/Technique) Independent Exchange (SINEX) format for TROpospheric and meteorological parameters.

The effort to standardize the exchange format for tropospheric products has started in early 1997 by a number of IGS participants [Gendt 1997]. In November 2010 [IGSMAIL-6298] SINEX_TRO format was slightly expanded to accommodate the addition of gradients. This expanded format has never been officially accepted and adopted. Due to the lack of the standardization, different software packages and organizations have started to use different field names referring to the same variables ad-hoc supporting optional and mandatory metadata, output files with different naming conventions and overall data contents. As a result, the format cannot be handled with a unique decoder.

According to further developments, new demands arose on the format for exchanging tropospheric parameters, in particular supporting:

(a) Parameters from different sources than space geodetic techniques such as numerical weather prediction models and re-analyses, radiosondes and water vapour radiometers,
(b) Long station names (9 characters) in concordance with RINEX 3 data format,
(c) Products including slant tropospheric delays,
(d) Parameters corresponding to long-term time series of individual stations.

This was the driver to develop a unique format to be adopted within all the IAG services and by all the techniques dealing with tropospheric parameters. However, because of difficulties in supporting all legacy and new features, it was decided to revise the format without keeping a full compatibility with any previous SINEX_TRO unofficial version. In this way new features, such as long station names or time series data support, could be introduced much easier while simplifying the format definition and usage.

Previously, the tropospheric products were provided in SINEX_TRO files [Gendt, 1997] along with the standard SINEX files using the corresponding filename. All common blocks (SITE/ID, SITE/ANTENNA, SITE/RECEIVER, SITE/ECCENTRICITY, SITE/COORDINATES etc.) could be then taken from the SINEX product. When tropospheric results were provided only in the SINEX_TRO format, a single file should contain mandatory all the metadata concerning the SITE specification. Newly revised SINEX_TRO format is de-coupled from the official

SINEX as it is impossible to implement important changes, e.g. such as long station names, different timestamp definition and others.

Originally, the SINEX_TRO format was tightly linked to the SINEX developed by the IERS (http://www.iers.org). Because of difficulties of maintaining the SINEX_TRO format along with the SINEX and because of limitations in necessary developments (e.g. a support of long station names, variable length of data lines), the SINEX_TRO format V2.0 is decoupled from the SINEX while keeping a basic philosophy and a similar metadata format description. The most of metadata blocks thus became mandatory in the SINEX_TRO format in order to support a stand-alone and non-ambiguous metadata description in the same way for any file using the format.

Philosophy

The SINEX_TRO has as much as a simple and flexible design following the philosophy of the SINEX format (http://www.iers.org/IERS/EN/Organization/AnalysisCoordinator/SinexFormat/sinex.html) with regards to metadata description and overall data structure. It is aimed at supporting site-specific and time series data stemming from various observing techniques or analyses, such as various space geodetic techniques (DORIS, GNSS, and VLBI), numerical weather prediction models, radiosondes, microwave radiometers, or others. All data and metadata refers to the time period or timestamp in order to support site-specific long-term data storage suitable for a time series analysis or climate research. Specific parameters, such as slant delays, are supported through the introduction of a new dedicated data block. The format supports all the necessary information for the conversion to the COST-716 format (http://egvap.dmi.dk/support/formats/egvap_cost_v22.pdf), so far widely used within GNSS-meteorology applications.

The format is able to accommodate data or products in the following scenarios:

- Parameters at a single site estimated, observed or interpolated in time,
- Parameters at a single site calculated from a vertical profile, using ray tracing or interpolating in space,
- Parameters for more sites coming from a unique source (analysis, method, provider etc.),
- Parameters from a combined solution including additional information from the combination process,
- Parameters from a long period including a full history of metadata,
- Parameters with a consistent temporal resolution (i.e. sampling rate) and representations (interpolation, modelling approach, etc.) while missing values are allowed when reported. Data representation and, optionally, interpolation should be described in the metadata subsection.

Structure

There is no limitation on the number of characters in data lines in SINEX_TRO. The SINEX_TRO file is subdivided into groups of data called blocks. A header and footer line encloses each block. The header and footer line are of 80 ASCII characters. Each block has a fixed format. The metadata blocks contain information on the file, the solution, its inputs and all the sites. Elements within each line are defined and separated by a blank character, at least. A character field without information will have "-" within its field and a missing numerical element will have an undefined value represented by number − 999 (integer) or − 999.000 (float) used always without scaling applied.

Important Note The undefined value should be **written/tested without the parameter scaling** (see TROPO PARAMETER UNITS and SLANT PARAMETER UNITS).

Therefore, the SINEX_TRO file is readable in both forms "column-wise" and "line-wise". Character fields should be left-hand justified whenever applicable.

The first character of each line identifies the type of information that the line contains. Five characters are reserved. They have the following meaning when they are at the beginning of a line, they identify:

- '%' header and footer line,
- '*' comment line within the header and footer line,
- '+' title at the start of a block
- '−' title at the end of a block
- '' (empty space) data line within a block

No other character is allowed at the beginning of a line!
A SINEX_TRO file must start with a header line and end with a footer line.
The following blocks are defined:

FILE/REFERENCE	(Mandatory)
INPUT/FILES	(Combined product only)
CENTERS/INFO_MODEL	(Combined product only)
CENTERS/INFO_SOLUTION	(Combined product only)
SITE/ID	(Mandatory)
SITE/RECEIVE	(Mandatory for GNSS)
SITE/ANTENNA	(Mandatory for GNSS)
SITE/COORDINATES	(Mandatory for GNSS)
SITE/ECCENTRICITY	(Mandatory for GNSS)
TROP/DESCRIPTION	(Mandatory)
TROP/SOLUTION	(Mandatory for values in zenith directions)
SLANT/SOLUTION	(Mandatory for values in slant directions)

These block titles are immediately preceded by a "+" or a "-" as they mark the beginning or the end of a block. The block titles must be in capital letters. After a block has started (+) it must be ended (−) before another block can begin. The general structure is as follows:

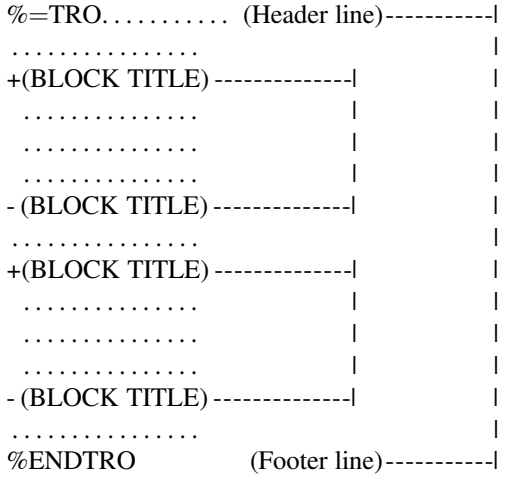

Most fields within a SINEX_TRO line are separated by a single space or a sequence of spaces. In the following subsections, each SINEX_TRO line is defined by its field name, a general description and format using FORTRAN notations.

A comment line (not to be confused with the FILE/COMMENT Block) can be written anywhere between the header and the footer line. All comment lines must start with a "*" in the first column. With the use of this character, information can be hidden from the software reading the file without deleting it from the file. A comment line format definition is provided in the Appendix 1.

Dissemination

Three specific products are foreseen (and distinguished) in various dissemination scenarios supported by the SINEX_TRO format:

1. Individual analysis centre products,
2. Products from the combination centres,
3. Site-specific data time series.

File names

For file naming, it is recommended to use new format convention according to IGS products:

AAAV_PPP_TTT_YYYYDOYHHMM_LEN_SMP.TRO

or

AAAV_PPP_TTT_YYYYDOYHHMM_LEN_SMP_SITENAME.TRO

With:

- '_' used as a separator between all the filename fields except the file extension,
- **AAA** (3-char) –analysis centre acronym,
- **V** (1-char) – version / solution identifier, see VERSION NUMBER (File Reference Block),
- **PPP** (3-char) – project/campaign identification: operational (OPS), demonstration (DEM), testing (TST), re-processing (REP), undefined (UNK),
- **TTT** (3-char) – solution type: final (FIN), rapid (RAP), near real-time (NRT), real-time (RTM), sub-hourly (SUB), unknown (UNK),
- **YYYYDOYHHMM** (11-char) – string representing beginning time of nominal data interval. '00000000000' can be used in case of a long time series storage,
- **LEN** (2-digits+1-char) – file frequency for specifying intended collection period of the file. Three characters are allowed for the format while the last character provides units minutes (xxM), hours (xxH), days (xxD), weeks (xxW), months (xxB), years (xxY), unspecified (00 U). The last (00 U) should be used if the file is used to store cumulative data,
- **SMP** (2-digits+1-char) – frequency for specifying data sampling rate. Three characters are allowed for the format with the last character providing the units: 100 Hertz (xxC), Hertz (xxZ), seconds (xxS), minutes (xxM), hours (xxH), days (xxD), weeks (xxW), months (xxB), years (xxY), unspecified (00 U),
- **SITENAME** (4-char/9-char, optional) – site name consisting of variable length of 4 (old) or 9 (new) characters. New site conventional names according to the RINEX 3 convention are recommended. If a multi-station file is provided, the site name is omitted.
- **CNT** (3-char) – content type TRO,
- **FTM.** (3 char) – file format TRO for troposphere estimates, SUM for summary file (for combined product only).

Examples

GOPG_OPS_NRT_20150301000_01H_05M.TRO
GOP1_DEM_RTM_20150301000_05M_05M_GOPE.TRO
GOP2_TST_SUB_20150301000_15M_05M_GOPE00CZE.TRO
GOP2_OPS_FIN_20150300000_01D_01H.TRO
ASI2_REP_FIN_20150301030_07D_01H.TRO
EUR2_REP_FIN_20150300030_07D_01H.TRO

For the file dissemination, GZIP (.gz) format is recommended. There is no recommendation for using upper or lower cases in filenames. Never mix lower case and upper case.

In case of a very large number of stations, it is recommended to deliver one SINEX_TRO file per station.

Analysis Centre Product

The Analysis Centres of the different IAG services submit, usually on daily or weekly basis, files containing estimated tropospheric parameters from specific site or network processed consistently. Only that information should be given which is directly related to the troposphere estimates. Additional data from other sources are allowed (similar like in time series outputs) until these are homogeneous and properly described in the header. These could be made available in support of information equivalent to the COST-716 format. The corresponding data blocks are:

FILE/REFERENCE	(Mandatory)
SITE/ID	(Mandatory)
SITE/RECEIVER	(Mandatory for GNSS)
SITE/ANTENNA	(Mandatory for GNSS)
SITE/COORDINATES	(Mandatory for GNSS)
SITE/ECCENTRICITY	(Mandatory for GNSS)
TROP/DESCRIPTION	(Mandatory for GNSS)
TROP/SOLUTION	(Mandatory for values in zenith directions)
SLANT/SOLUTION	(Mandatory for values in slant directions)

It is possible that a SINEX_TRO file contains data stemming from more sources, e.g. GNSS analysis completed with meteorological parameters observed in situ or derived from a numerical weather model. In such case, it should be however properly described in the file metadata subsections.

Combination Product

It is necessary to define a combined product in case an IAG service, or any other service, delivers it for a single site or for a network. Besides blocks defined for the Analysis Centre products, the following blocks are added to support information from the combination process:

INPUT/FILES	(Mandatory)
CENTERS/INFO_MODEL	(Mandatory)
CENTERS/INFO_SOLUTION	(Mandatory)

Station Time Series

For the customer, who is interested in time series of tropospheric or other meteorological parameters for a specific location, it is convenient to have a product with separate files for each site.

The Station Time Series products aim at supporting application for which time series analysis is required (e.g. climate research, temporal modelling). A detailed description of a full history of metadata information has to be provided and is supported in the metadata definition since SINEX_TRO V2.0 can handle all metadata including site coordinates defined along with the time period specification.

Tropospheric Models and Other Relations

For the format definition, we need to define basic tropospheric models and other relations useful to exploit the format parameters.

Tropospheric Models

The tropospheric path delay using the standard model and considering a symmetrical troposphere is expressed as follows:

$$d_{trop\_symmetry} = m_h(E)ZHD + m_w(E)ZMD \tag{1}$$

where ZHD and ZWD are zenith hydrostatic and wet delays, E is the elevation angle, m_h and m_w are hydrostatic and wet mapping function.

The tropospheric path delay applying the extended model and considering the first-order asymmetry of the troposphere is defined as:

$$d_{trop\_asymmetry} = m_h(E)ZHD + m_w(E)ZWD + m_g(E)[G_N cos\varphi + G_E sin\varphi] \tag{2}$$

with G_N and G_E horizontal tropospheric gradients in the North and East directions, φ azimuth angle, m_g gradient mapping function.

The ZTD is always defined as a sum of ZHD and ZWD, i.e. independently whether the troposphere asymmetry is modelled or not

$$ZTD = ZHD + ZWD. \tag{3}$$

Total STD is then defined as the delay along the signal path and includes residuals (*res*) to the extended model and excludes potential multipath and other systematic effects (*mpt*). It is expressed with the following relation:

$$STD = mf_h ZHD + mf_w ZWD + mf_g[G_N cos\,\varphi + G_E sin\,\varphi] + res - mpt \tag{4}$$

where mf_h, mf_w and mf_g are mapping factors necessary for an unambiguous reconstruction of all individual model parameters. The mapping factors are float numbers corresponding to the actual observation elevation angles, and they can be calculated from specified mapping function or using a method of meteorological model data ray-tracing.

It is common to consider an approximation that the dry (or hydrostatic) zenith path delay represents the a priori troposphere model in the analysis of data of space geodetic techniques while model parameters estimated in the adjustments corresponds roughly to the wet (non-hydrostatic part).

$$d_{trop\_symmetry} = m_{approx}(E)ZTD_{apriori} + m_{estim}(E)\Delta ZTD_{estim.} \tag{5}$$

Conversion Between ZTD and IWV

The conversion of ZTD estimates to IWV is done in two steps.

Firstly, following the IERS Conventions (2010), ZHD can be estimated by means of the Saastamoinen (1972) model if the surface air pressure P_s is known. Then, ZHD is subtracted from ZTD to form ZWD:

$$ZWD = ZTD - ZHD. \tag{6}$$

Secondly, ZWD is converted to IWV as:

$$IWV = \frac{10^6}{R_v\left(k'_2 + \frac{k_3}{T_m}\right)} ZWD \tag{7}$$

where R_v is the specific gas constant of water vapour, $k'_2[K/hPa]$ and $k_3[K^2/hPa]$ are the refractivity coefficients (Bevis et al. 1994) and T_m is the weighted mean temperature of the atmosphere (Davis et al. 1985)

$$T_m = \frac{\int_H^\infty \frac{e}{T} dh}{\int_H^\infty \frac{e}{T^2} dh}. \tag{8}$$

T_m can be either numerically integrated from the numerical weather/climate model levels, or calculated from the analytical formula given by Askne and Nordius (1987).

Vertical Parameter Scaling

The temperature vertical scaling is usually approximated with the temperature lapse rate β [K/km]

$$T = T_0 - \beta(h - h_0) \tag{9}$$

where T and T_0 [K] are the temperature at height h and h_0 [m], respectively. Notice that the positive sign of the lapse rate is opposite to the U.S. Standard Atmosphere (1976). Similarly, the mean temperature vertical scaling is approximated with the mean temperature lapse rate $\beta_m[K/km]$

$$T_m = T_{m0} - \beta_m(h - h_0) \tag{10}$$

where T_m and T_{m0} [K] are the mean temperature at height h and h_0 [m].

The partial water vapour pressure vertical scaling is approximated using the parameter λ [−] and the formula introduced by Smith (1966) for a vertical approximation of the mixing ratio

$$e = e_0 \left(\frac{P}{P_0} \right)^{\lambda+1} = e_0 \left[1 - \frac{\beta(h - h_0)}{T_0} \right]^{\frac{(\lambda+1)g_m}{R_d \beta}} \tag{11}$$

where P, e and P_0, $e_0[hPa]$ are the atmospheric pressure and partial water vapour pressure at geopotential height h and $h_0[km]$, respectively, and g_m is the standard gravitational acceleration *9.80665 [m.s-2]* defined in the U.S. Standard Atmosphere (1976).

The zenith wet delay is approximated using the ZWD decay parameter, $\Upsilon\,[-]$ and the formula introduced by Douša and Eliaš (2014)

$$ZWD = ZWD_0 \left(\frac{P}{P_0} \right)^{\gamma+1} = ZWD_0 \left[1 - \frac{\beta(h - h_0)}{T_0} \right]^{\frac{(\gamma+1)g_m}{R_d \beta}} \tag{12}$$

where $P\,[hPa]$ and $P_0[hPa]$ are the atmospheric pressure at geopotential height h and $h_0[km]$.

List of Parameter Types

Parameter types are defined specifically for each SINEX_TRO data block.

Parameter Types in Zenith Direction (TROP/SOLUTION)
Different tropospheric parameter types, according to the tropospheric models are summarized in Table D7.1. Parameters can be provided as a product of (1) data analysis, e.g. from data of space geodetic technique, (2) data processing, e.g. from numerical weather model data fields, or radiosounding, or (3) direct observation method, e.g. from water vapour radiometer.

Table D7.1 Tropospheric parameter types in zenith direction

Acronyms	Description	Base unit[a]
TROTOT	tropospheric zenith total delay (ZTD)	m
TROWET	tropospheric zenith wet delay (ZWD)	m
TRODRY	tropospheric zenith dry/hydrostatic delay (ZHD)	m
TGNTOT	tropospheric total gradient – North component (wet + dry parts)	m
TGNWET	tropospheric dry gradient – North direction	m
TGNDRY	tropospheric wet gradient – North direction	m
TGETOT	tropospheric total gradient – East component (wet + dry parts)	m
TGEWET	tropospheric wet gradient – East component	m
TGEDRY	tropospheric dry gradient – East component	m
STDDEV	standard deviation for each estimated value reported in preceding column	
IWV	integrated water vapour	kg/m^2

[a]Base unit is the reference unit for individual parameter scaling (see TROP/DESCRIPTION block).

Table D7.2 Meteorological parameter types

Acronyms	Description	Base unit[a]
PRESS	atmospheric pressure	hPa
EPRESS	partial water vapour pressure	hPa
TEMDRY	dry temperature	K
HUMREL	relative humidity	%

[a]Base unit is the reference unit for individual parameter scaling (see TROP/DESCRIPTION block).

Meteorological parameter types are summarized in Table D7.2 Parameters can be derived from (1) in situ observations, e.g. meteorological sensor, water vapour radiometer, or (2) data processing, e.g. from numerical weather model data fields or radiosounding.

Auxiliary parameter types in zenith direction including parameters for the vertical approximations are summarized in Table D7.3 These could provide (1) additional information about the product quality based on data analysis or, optionally, the differences in height to the reference position, e.g. for long-time series, to enable filtering of GNSS products etc. (2) necessary information for computing tropospheric ties needed for the comparisons at collocated stations.

Parameter Types in Slant Direction (SLANT/SOLUTION)
Slant tropospheric delay parameter types are supported since SINEX_TRO V2.0. The parameters are summarized in Table D7.4 In addition, the following parameter of the TROP/SOLUTION block (see Table D7.1) TROWET, TROHYD, TGNTOT, TGETOT should be provided as well.

Auxiliary parameters for slant directions are supported in order to enable an optimal use of the slant parameters including a full reconstruction of any component of the tropospheric models.

7. YYYY:DDD:SSSSS Time Tags.

Time tags are given in a YYYY:DDD:SSSSS formatted representation:

Table D7.3 Auxiliary parameter types in zenith direction including parameters for the vertical approximations

Acronyms	Description	Base unit[a]
ACOK	number of ACs taken into account for given epoch	–
ACDL	number of ACs deleted for given epoch	–
NSAT	number of satellites	–
GDOP	geometric dilution of precision	–
SCLHGT	pressure scale height	m
TEMLPS	temperature lapse rate	K/m
WVPDEC	water vapour pressure exponential decay	–
ZWDDEC	zenith wet delay exponential decay	–
WMTEMP	weighted mean temperature	K
WMTLPS	weighted mean temperature lapse rate	K/m

[a]Base unit is the reference unit for individual parameter scaling (see TROP/DESCRIPTION block).

Table D7.4 Tropospheric parameter types in slant directions

Acronyms	Description	Base unit[a]
SLTTOT	tropospheric slant total delay (STD)	m
SLTDRY	tropospheric slant dry delay (SHD), i.e. mf_h*ZHD	m
SLTWET	tropospheric slant wet delay (SWD), i.e. mf_w*ZWD	m
SLTGRD	tropospheric slant total delay due to the first-order horizontal gradient	m
SLTTGD	tropospheric slant dry delay due to the first-order horizontal gradient	m
SLTTGW	tropospheric slant wet delay due to the first-order horizontal gradient	m
STDDEV	standard deviation for each estimated value reported in the column preceding	
SLTIWV	tropospheric slant integrated water vapour	kg/m^2

[a]Base unit is the reference unit for individual parameter scaling (see TROP/DESCRIPTION block).

- YYYY = 4- digit year;
- DDD = 3- digit day in year;
- SSSSS = 5- digit seconds in day.

No spaces are allowed within this string.
SINEX_TRO File VERSION 2.00.

Table D7.5 Auxiliary parameter types in slant direction

Acronyms	Description	Base unit[a]
SAT	satellite code: Satellite System Satellite Number Satellite System: G = GPS R = GLONASS E = Galileo C = BeiDou	–
SAT__X	Satellite X-coordinate (Mandatory for Data Assimilation)	m
SAT__Y	Satellite Y-coordinate (Mandatory for Data Assimilation)	m
SAT__Z	Satellite Z-coordinate (Mandatory for Data Assimilation)	m
SATELE	elevation angle	deg
SATAZI	azimuth angle	deg
SATRES	satellite phase residuals	m
SATMPT	satellite multipath	m
FACDRY	dry mapping factor	–
FACWET	wet mapping factor	–
FACGRD	gradient mapping factor	–
FACTGD	gradient mapping factor for dry component	–
FACTGW	gradient mapping factor for wet component	–

[a]Base unit is the reference unit for individual parameter scaling (see TROP/DESCRIPTION block).

Detailed Format Description
In this appendix, the following blocks are described:

1. Header and Footer Lines (Mandatory)
2. Comment line (Optional)
3. FILE/REFERENCE Block (Mandatory)
4. INPUT/FILES (for combined product only)
5. CENTERS/INFO_MODEL Block (for combined product only)
6. CENTERS/INFO_SOLUTION (for combined product only)
7. TROP/DESCRIPTION Block (Mandatory)
8. SITE/ID Block (Mandatory)
9. SITE/RECEIVER Block (Mandatory for GNSS)
10. SITE/ANTENNA Block (Mandatory for GNSS)
11. SITE/COORDINATES Block (Mandatory for GNSS)
12. SITE/ECCENTRICITY Block (Mandatory for GNSS)
13. TROP/SOLUTION Block (Mandatory for values in zenith directions)
14. SLANT/SOLUTION Block (Mandatory for values in slant directions)

Many blocks described in this appendix are in common with SINEX.

Others (as SITE/ID, SITE/RECEIVER, SITE/ECCENTRICITY, SITE/COORDINATES etc.) have a slightly different description/format with respect to what reported in SINEX 2.02.

The last row of each table describing the blocks contains the sum of the characters.

Header and Footer Lines (Mandatory)

The Header line must be the first line in a SINEX_TRO file.
The Footer line must be the last line in a SINEX_TRO file.

Header Line		
Field	Description	Format
File Identifier	% = TRO	A5
Format Version	Four digits indicating the version of SINEX_TRO format used	1X,F4.2
File Agency Code	Identify the agency creating the file	1X,A3
Time	Creation time of this SINEX_TRO file	1X,I4.2,':', I3.3,':',I5.5
	defined as year:day_of_the_year:sec_of_the_day.	
Agency Code	Identify the agency providing the data in the SINEX_TRO file	1X,A3
Start Time	Start time of solution in the this SINEX_TRO file	1X,I4.2,':', I3.3,':',I5.5
	defined as year:day_of_the_year:sec_of_the_day.	
End Time	End time of the solution in the this SINEX_TRO file	1X,I4.2,':', I3.3,':',I5.5
	defined as year:day_of_the_year:sec_of_the_day.	

(continued)

Header Line		
Field	Description	Format
	Technique(s)/Source used to generate the SINEX_TRO.	1X,A1
Observation Code	In case of a space geodetic technique, the code should be consistent with the IERS convention.	
	C – Combined techniques used	
	D – DORIS	
	P – GNSS	
	R – VLBI	
	For non-space geodetic techniques, the following code are defined:	
	W – water vapour radiometer	
	S – radiosounding	
	F – numerical weather forecast	
	N – numerical weather re-analysis	
	M – climate model	
Solution Contents	Marker name if this is a combined solution file and contains only one site or 'MIX' if it is a submission file containing more than one site	1X,A4
		58

Footer Line		
Field	Description	Format
File Identifier	% = ENDTRO	A8
		8

Comment Line (Optional)

A comment line can be placed anywhere, i.e. within or out from any block, as long as it is between the Header and Footer lines.

It is limited to 80 characters in total with the starting '*' character of the line. The definition is following:

Field	Description	Format
Comment	Any general comment relevant to the SINEX_TRO file.	1H*,A79

File/Reference Block (Mandatory)

This block provides information on the Organization, point of contact, software and hardware involved in the generation of the estimates.

File Reference		
Field	Description	Format
Information Type	Describes the type of information present in the next field. May take on the following values	1X, A18
	'DESCRIPTION' – Organization(s) gathering/altering the file contents	1X, 3I
	'OUTPUT' – Description of the file contents	
	'CONTACT' – Address of the relevant contact e-mail	
	'SOFTWARE' – Software used to generate the file	
	'HARDWARE' – Computer hardware on which above software was run	
	'INPUT' – Brief description of the input used to generate this solution	
	'VERSION NUMBER' – Unique (3-digits) identifier of the product specific to a certain processing strategy which matches that as seen in the V in the filename. It must be updated, and never reused, if the processing is modified in a way that might lead to a different error characteristics of the product. Mandatory for space geodetic techniques.	
Information	Relevant information for the type indicated by the previous field	1X, A60
		84

Input/Files (for Combined Product Only)

This block contains the list of the contributing solutions used in the combined product.

Input/Files		
Field	Description	Format
Files	Name of contributing solutions	1X,A79

Centres/Info_Model Block (for Combined Product Only)

This block contains the information about the parameters used by the contributing Analysis Centres.

Centre/Info_Model		
Field	Description	Format
Analysis Centre	Name of Analysis Centre	1X,A3
Observation Code	Observation technique used	1X,A1
Cut-off angle	Elevation cut-off angle used (degrees)	1X,I3
Data rate	Sampling rate for used data	1X,I4
Trop rate	Sampling rate for ALL trop estimates	1X,I4

(continued)

Centre/Info_Model		
Field	Description	Format
Trop. Mapping function	TROP Hydrostatic and Wet Mapping functions used	1X,A29
Grad. Mapping function	GRAD Mapping functions used	1X,A29
		80

Centres/Info_Solution (for Combined Product Only)

This block contains for the site in the combined product file the information about the data and biases for the contributing Analysis Centres.

Centre/Info_Solution		
Field	Description	Format
Site Code	Call sign for a site	1X,A9
Analysis Centre	Name of Analysis Centre	1X,A3
# of days	Number of days used by the AC	1X,I2
Day Code	Flag for each day (0 if not available, 1 otherwise)	1X,7I1
# of bias	Number of biases for the interval (1 = weekly; 7 = daily)	1X,I2
Biases	Biases for each day in [mm]	7(1X,F6.1)
		77

Trop/Description Block (Mandatory)

This block gives important parameters from the analysis and defines the fields in the block 'TROP/SOLUTION' and in the block 'SLANT/SOLUTION'.

Trop/Description		
Field	Description	Format
Information Type	Describes the type of information present in the next field. May take one of the following values:	1X,A29
		n(1X,A6)
	'TROPO PARAMETER NAMES': Names of fields in trop solution (see Tables D7.6, D7.2, and D7.3) – mandatory with TROP/SOLUTION	n(1X,A6)
	'TROPO PARAMETER UNITS': Units applied for individual fields in trop solution (see Table D7.1, D7.2 and D7.3). Values reported in TROP/SOLUTION Block should be divided by the related TROPO UNITS to get the base units – mandatory with TROP/SOLUTION	n(1X,A6)
		n(1X,A6)
	'TROPO PARAMETER WIDTH': Width of fields in trop solution (see Tables D7.7, D7.2 and D7.3) – mandatory with TROP/SOLUTION	n(1X,A6)
	'SLANT PARAMETERS': Names of fields in slant solution (see Tables D7.4 and D7.5) – mandatory with SLANT/SOLUTION	

(continued)

Trop/Description		
Field	Description	Format
	'SLANT PARAMETER UNITS': Units applied for individual fields in slant solution (see Tables D7.4 and D7.5) – mandatory with SLANT/SOLUTION. Values reported in SLANT/SOLUTION Block should be divided by the related SLANT UNITS to get the base units.	n(1X,A6) 1X,I22
	'SLANT PARAMETER WIDTH': Width of fields in slant solution (see Tables D7.4 and D7.5) – mandatory with SLANT/SOLUTION	1X,A22
	'DATA SAMPLING INTERVAL': GNSS data Sampling Rate [sec]	1X,A22
	'TROPO MODELING METHOD': (For GNSS only) Tropospheric estimation method: Filter, Smoother, Least Square, Piece Wise Linear Interpolation	
	'GNSS SYSTEMS': (For GNSS only) Observation from GNSS system used (string concatenating system characters (G = GPS, R = GLONASS, E = Galileo, C=BeiDou)	1X,A22
	'TIME SYSTEM': The time tags specified in the TROP/SOLUTION and in the SLANT/SOLUTION blocks have to be given in a common time system. Possible time systems are:	1X, F5.2, 1X, F5.2, 1X, F8.1
	RINEX GNSS system (flag 'G')	1X,A22
	Coordinated Universal Time (flag 'UTC')	
	Mandatory information.	
	'REFRACTIVITY COEFFICIENTS': Factors used during conversion from ZPD into IWV.	
	'SOURCE OF MET/DATA': source of the surface meteorological observations used, it can be:	
	OBS/LOCAL for on-site (local) meteo sensor	
	OBS/NEARBY for nearby meteo data is used (with pressure adjusted for any GNSS site height difference)	
	OBS/INTERPOLATED: meteo data has been interpolated from a network of nearby stations	1X,A22
	NWP/cccctt data is from an NWP model where cccc is the (3–10 character) ID code for the NWP centre (e.g. ECMWF for ECMWF, METO for the Met Office, KNMI for KNMI, DWD for DWD, etc) and tt is the forecast lead time, e.g. 06 for a T + 6 hr. forecast, 00 for an analysis).	1X,A22 1X,A22
	NONE: not available	1X,I22
	'OCEAN TIDE LOADING MODEL': (For GNSS only) Ocean tide loading model applied	1X,I22
	'ATMOSPH TIDE LOADING MODEL': (For GNSS only) Atmospheric tide loading model applied	1X,A22 1X,A22
	'GEOID MODEL': Geoid model name for undulation values	1X,A22
	Only for individual analysis centre submissions:	1X,F22

(continued)

Trop/Description		
Field	Description	Format
	'TROPO SAMPLING INTERVAL': Tropospheric parameter sampling interval [sec] – mandatory with TROP/SOLUTION	12X,I5,X,I5
	'SLANT SAMPLING INTERVAL': Slant data sampling interval [sec] – mandatory with SLANT/SOLUTION	1X,F22
	'A PRIORI TROPOSPHERE': A priori tropospheric model used	
	'TROPO MAPPING FUNCTION': Name of mapping function used for mapping hydrostatic and wet delay	
	'GRADS MAPPING FUNCTION': Name of mapping function used for mapping horizontal gradients.	
	'ELEVATION CUTOFF ANGLE': Elevation cut-off [deg]	
	Only for combined solution:	
	'BIAS FROM INTERVAL': Begin and end of interval for bias computation [yyddd]	
	'DELETE FACTOR': Limit (factor*sigma) for editing of trop estimates	
	The above fields may be in any order	
Information	Relevant information for the type indicated by the previous field	format is type-dependent
		Variable

Site/ID Block (Mandatory)

This block provides general information for each site containing estimated parameters.

For **NWP Data Assimilation it is mandatory** to provide the coordinates of the observing site used to estimate the tropospheric parameters reported in the TROP/SOLUTION and/or in the SLANT/SOLUTION Block. The reported ellipsoid height and geoid height shall contain the antenna height in the SITE/ECCENTRICITY Block. These are the coordinates to be used for BUFR (Binary Universal Format for the Representation of data (WMO 2001)).

Site/ID		
Field	Description	Format
Site Code	Call sign for a site	1X,A9
Point Code	Physical monument used at a site	1X,A2
Unique Monument Identification	Unique alpha-numeric monument identification. For ITRF purposes it is a nine character DOMES/DOMEX number (five/six digits, followed by the single letter 'M' or 'S', followed by four/three digits)	1X,A9
Observation Code	Observation technique used.	1X,A1

(continued)

Site/ID		
Field	Description	Format
Station Description	Free-format description of the site, typically the town and/or country	1X,A22
Longitude	Longitude of the site in degrees (−90° to 90°N), decimals	1X,F10.6
Latitude	Latitude of the site in degrees (0° to 360°E), decimals	1X,F10.6
Ellipsoidal Height	Height above ellipsoid of the site in metres	1X,F9.3
Geoidal Height	Height above geoid of the site in metres	1X,F9.3
		92

Site/Receiver Block (Mandatory for GNSS)

List the receiver used at each site during the observation period of interest.

Site/Receiver		
Field	Description	Format
Site Code	Call sign for a site	1X,A9
Point Code	Physical monument used at a site	1X,A2
Solution ID	Solution Number at a Site/Point code for which some parameters are estimated	1X,A4
Observation Code	Observation technique used.	1X,A1
Start Time	Time since the receiver has been operating at the Site/Point defined as year:day_of_the_year:sec_of_the_day.	1X,I4.2,':', I3.3,':',I5.5
	Value 00:000:00000 indicates that the receiver has been operating at least since the "File Epoch Start Time"	
End Time	Time since the receiver has been operating at the Site/Point defined as year:day_of_the_year:sec_of_the_day.	1X,I4.2,':', I3.3,':',I5.5
	Value 00:000:00000 indicates that the receiver has been operating at least since the "File Epoch End Time"	
Receiver Type	Receiver Name & model	1X,A20
Receiver Serial Number	Serial number of the receiver. Takes on value '-----' if unknown	1X,A20
Receiver Firmware	Firmware used by this receiver during the epoch specified above. Takes on value '-----' if unknown	1X,A11
		100

Site/Antenna Block (Mandatory for GNSS)

List of antennas used at each site used in the SINEX_TRO file including the reference to the antenna phase centre model used.

Site/Antenna		
Field	Description	Format
Site Code	Call sign for a site	1X,A9
Point Code	Physical monument used at a site	1X,A2
Solution ID	Solution Number at a Site/Point code for which some parameters are estimated	1X,A4
Observation Code	Observation technique used.	1X,A1
Start Time	Time since the antenna has been installed at the Site/Point defined as year:day_of_the_year:sec_of_the_day.	1X,I4.2,':', I3.3,':',I5.5
	Value 00:000:00000 indicates that the receiver has been operating at least since the "File Epoch Start Time"	
End Time	Time since the antenna has been installed at the Site/Point defined as year:day_of_the_year:sec_of_the_day.	1X,I4.2,':', I3.3,':',I5.5
	Value 00:000:00000 indicates that the receiver has been operating at least since the "File Epoch End Time"	
Antenna Type	Antenna Name & model	1X,A20
Antenna Serial Number	Serial number of the antenna. Takes on value '-----' if unknown	1X,A20
Antenna Calibration Model	Name of the antenna model used in the correction of the observations for phase centre variations	1X,A10
		98

Comments:

- For IGS, the antenna calibration model refers to the ANTEX file provided by the IGS Central Bureau Information System:

  directory: ftp://igscb.jpl.nasa.gov/igscb/station/general
  atx ('wwww' for GPS week of the last update)

- For IGS, standard antenna names please refer to ftp://igscb.jpl.nasa.gov/igscb/station/general/rcvr_ant.tab
- If a receiver antenna is given in this block with a serial number to indicate individual antenna calibration model it has to be assigned in the SITE/ANTENNA Block to a specific station.

Site/Coordinates Block (Mandatory for GNSS)

This block provides the coordinates of the sites. The eccentricities of subsection "SITE/ECCENTRICITIES should be applied to these precise coordinates. The coordinates should be related to SITE point and only if ECCENTRICITIES are zero, then it is the ARP point. For the combination result, it also gives some statistical information.

Site/Coordinates		
Field	Description	Format
Site Code	Call sign for a site	1X,A9
Point Code	Physical monument used at a site	1X,A2
Solution ID	Solution number to which the input in this data line is referred to	1X,A4
Observation Code	Observation technique used	1X,A1
Data Start	Start Time since the site coordinates are valid, defined as year: day_of_the_year:sec_of_the_day.	1X,I4.2,':', I3.3,':',I5.5
	Value 00:000:00000 indicates the validity since the "File Epoch Start Time"	
Data End	End Time since the site coordinates are valid, defined as year: day_of_the_year:sec_of_the_day.	1X,I4.2,':', I3.3,':',I5.5
	Value 00:000:00000 indicates the validity till the "File Epoch End Time"	
Coordinates	x,y,z-coordinate of a site of SINEX_TRO format used.	3(1X,F12.3)
System	Terrestrial Reference System Code	1X,A6
Remark	A remark used to identify the origin of the coordinates (AC acronym or 'Mean')	1X,A5
Standard Deviation	Standard deviation for x,y,z in [mm] (Used only for Mean)	3(1X,I2)
Counter	Number of ACs used for Mean(Used only for Mean)	1X,I2
		110

Site/Eccentricity Block (Mandatory for GNSS)

List of antenna eccentricities from the Marker to the Antenna Reference Point (ARP) or to the intersection of axis.

Site/Eccentricities		
Field	Description	Format
Site Code	Call sign for a site	1X,A9
Point Code	Physical monument used at a site	1X,A2
Solution ID	Solution Number at a Site/Point code for which some parameters are estimated	1X,A4
Observation Code	Observation technique used.	1X,A1
Start Time	Time since the antenna has been installed at the Site/Point defined as year:day_of_the_year:sec_of_the_day.	1X, I4.2,':', I3.3,':', I5.5
	Value 00:000:00000 indicates that the receiver has been operating at least since the "File Epoch Start Time"	
End Time	Time since the antenna has been installed at the Site/Point defined as year:day_of_the_year:sec_of_the_day.	1X, I4.2,':', I3.3,':', I5.5
	Value 00:000:00000 indicates that the receiver has been operating at least since the "File Epoch End Time"	

(continued)

Site/Eccentricities		
Field	Description	Format
Eccentricity Reference System	Reference system used to describe vector distance from monument benchmark to the antenna reference point or intersection of axis:	1X,A3
	'UNE' – Local reference system: Up, North, East	
	'XYZ' – Cartesian Reference System X, Y, Z.	
	All units are in meters	
Up / X Eccentricity	Up / X offset from the marker to the Antenna reference point (ARP)	1X,F8.4
North / Y Eccentricity	North/Y offset from the marker to the Antenna reference point (ARP)	1X,F8.4
East / Z Eccentricity	East / Z offset from the marker to the Antenna reference point (ARP)	1X,F8.4
		77

Trop/Solution Block (Mandatory for values in zenith directions)

This block contains the solution for all epochs.

Trop/Solution		
Field	Description	Format
Marker	Name of the marker	1X,A9
	NOTE: For backward compatibility left – aligned 4- character station codes are also permitted	
Time	Time epoch of the solution: Middle of data Interval, defined as year: day_of_the_year:sec_of_the_day.	1X,I4.2,':', I3.3,':',I5.5
Values	Space separated fields of variable length. Number and order of fields are given in the block TROP/DESCRIPTION.	no format
	Readable by:	
	read(line(20:),*)(val(i),i = 1,n)	
		variable

Slant/Solution Block (Mandatory for values in slant directions)

This block contains the slant solution for all epochs.

Slant/Solution		
Field	Description	Format
Marker	Name of the marker	1X,A9
	NOTE: For backward compatibility left – aligned 4- character station codes are also permitted	
Time	Time epoch of the solution: Middle of data Interval defined as year: day_of_the_year:sec_of_the_day.	1X,I4.2,':', I3.3,':',I5.5
Values	Space separated fields of variable length. Number and order of fields are given in the block TROP/DESCRIPTION.	no format
	Readable by:	
	read(line(20:),*)(val(i),i = 1,n)	
		variable

Examples

Example for Submissions of Trop & Slant Estimates

```
%=TRO 2.00 GOP 2017:157:61799 GOP 2013:168:64500 2013:168:86100 P  MIX
*-------------------------------------------------------------------------------
+FILE/REFERENCE
*INFO_TYPE_________ INFO_____________________________________________________
 DESCRIPTION        GOP - Geodetic Observatory Pecny, RIGTC
 OUTPUT             Solution parameters
 CONTACT            gnss@pecny.cz
 SOFTWARE           G-Nut/Geb
 INPUT              GNSS/NWM/RAO/OTH data
 VERSION NUMBER     001
-FILE/REFERENCE
*-------------------------------------------------------------------------------
+TROP/DESCRIPTION
*_____KEYWORD_____________ _VALUE(S)__________________________________________
 TROPO SAMPLING INTERVAL    300
 SLANT SAMPLING INTERVAL    300
 DATA SAMPLING INTERVAL     300
 GNSS SYSTEMS               G
 TIME SYSTEM                G
 TROPO MODELING METHOD      KALMAN FILTER
 GEOID MODEL                VMF1/EGM96
 OCEAN TIDE LOADING MODEL   FES2004
 ATMOSPH TIDE LOADING MODEL NOT APPLIED
 ELEVATION CUTOFF ANGLE     7
 OBSERVATION WEIGHTING      SINEL
 A PRIORI TROPOSPHERE       EXTERN
 TROPO MAPPING FUNCTION     GMPH/GMPW
 GRADS MAPPING FUNCTION     CHEN_HERRING
 REFRACTIVITY COEFFICIENTS  77.60 70.40 373900.0
 SOURCE OF MET/DATA         NWP
 TROPO PARAMETER NAMES      TROTOT STDDEV TRODRY TROWET TGNTOT STDDEV TGETOT STDDEV   NSAT    GDOP     IWV  PRESS TEMDRY WMTEMP TEMLPS WMTLPS ZWDDEC
 TROPO PARAMETER UNITS       1e+03  1e+03  1e+03  1e+03  1e+03  1e+03  1e+03  1e+03      1       1       1      1      1      1 1e+03  1e+03       1
 TROPO PARAMETER WIDTH          6      6      6      6      6      6      6      6      4       4       6      7      6      6       6       6       6
 SLANT PARAMETER NAMES      SLTTOT STDDEV SLTDRY SLTWET SLTIWV SLTGRD SATRES SATMPT   SAT SATELE SATAZI FACDRY FACWET FACGRD
 SLANT PARAMETER UNITS       1e+03  1e+03  1e+03  1e+03      1  1e+03  1e+03  1e+03     1       1       1      1      1      1
 SLANT PARAMETER WIDTH           8      6      8      6      6      6      6      6     4       7       7      9      9      9
-TROP/DESCRIPTION
*-------------------------------------------------------------------------------
+SITE/ID
*STATION__ PT __DOMES__ T _STATION_DESCRIPTION__ _LONGITUDE _LATITUDE_ _HGT_ELI_ _HGT_MSL_
 GOPE00CZE  A 11502M002 P                        14.785625  49.913706   592.716   630.502
 WTZR00DEU  A 14201M010 P                        12.878912  49.144199   666.119   705.725
 ZIMM00CHE  A 14001M004 P                         7.465279  46.877099   956.324  1000.057
-SITE/ID
*-------------------------------------------------------------------------------
+SITE/COORDINATES
*STATION__ PT SOLN T __DATA_START__ __DATA_END____ __STA_X_____ __STA_Y_____ __STA_Z_____ SYSTEM REMRK
 GOPE00CZE  A    1 P 2013:168:00000 2013:168:86100  3979315.993  1050312.623  4857067.191  IGS08   GOP
 WTZR00DEU  A    1 P 2013:168:00000 2013:168:03300  4075580.457   931853.932  4801568.218  IGS08   GOP
 ZIMM00CHE  A    1 P 2013:168:00300 2013:168:86100  4331296.936   567556.035  4633134.023  IGS08   GOP
-SITE/COORDINATES
*-------------------------------------------------------------------------------
+SITE/ECCENTRICITY
*                                                    UP______ NORTH___ EAST____
*STATION__ PT SOLN T __DATA_START__ __DATA_END____ AXE ARP->BENCHMARK(M)_______
 GOPE00CZE  A    1 P 2013:168:64500 2013:168:86100 UNE   0.1114   0.0000   0.0000
 WTZR00DEU  A    1 P 2013:168:64500 2013:168:86100 UNE   0.0710   0.0000   0.0000
 ZIMM00CHE  A    1 P 2013:168:64500 2013:168:86100 UNE   0.0000   0.0000   0.0000
-SITE/ECCENTRICITY
*-------------------------------------------------------------------------------
+SITE/ANTENNA
*STATION__ PT SOLN T __DATA_START__ __DATA_END____ DESCRIPTION_________ S/N_________________ PCV_MODEL_
 GOPE00CZE  A    1 P 2013:168:64500 2013:168:86100 TPSCR.G3            TPSH ------------------- IGS08_1664
 WTZR00DEU  A    1 P 2013:168:64500 2013:168:86100 LEIAR25.R3          LEIT ------------------- IGS08_1664
 ZIMM00CHE  A    1 P 2013:168:64500 2013:168:86100 TRM29659.00         NONE ------------------- IGS08_1664
-SITE/ANTENNA
*-------------------------------------------------------------------------------
+SITE/RECEIVER
*STATION__ PT SOLN T __DATA_START__ __DATA_END____ DESCRIPTION_________ S/N_________________ FIRMW_____
 GOPE00CZE  A    1 P 2013:168:64500 2013:168:86100 TPS NETG3             ------------------- ----------
 WTZR00DEU  A    1 P 2013:168:64500 2013:168:86100 LEICA GRX1200+GNSS    ------------------- ----------
 ZIMM00CHE  A    1 P 2013:168:64500 2013:168:86100 TRIMBLE NETRS         ------------------- ----------
-SITE/RECEIVER
*-------------------------------------------------------------------------------
+TROP/SOLUTION
*STATION__ ____EPOCH_____ TROTOT STDDEV TRODRY TROWET TGNTOT STDDEV TGETOT STDDEV NSAT GDOP    IWV   PRESS TEMDRY WMTEMP TEMLPS WMTLPS ZWDDEC
 GOPE00CZE 2013:168:64500 2334.3    5.3 2166.8  167.4   0.99   0.85   0.14   0.93    7  2.2  27.26  951.92  299.6  285.7   7.20   7.21   3.32
 GOPE00CZE 2013:168:64800 2334.2    5.2 2166.8  167.4   1.00   0.84   0.17   0.92    6  1.9  27.25  951.90  299.6  285.7   7.20   7.21   3.32
 GOPE00CZE 2013:168:65100 2333.0    5.1 2166.8  166.2   1.00   0.83   0.29   0.91    7  2.2  27.06  951.90  299.6  285.7   7.20   7.21   3.33
...
 ZIMM00CHE 2013:168:85800 2275.0    4.6 2081.5  193.5  -0.18   0.65   0.79   0.86    9  1.1  31.16  913.97  296.3  282.6   7.21   6.74   2.94
 ZIMM00CHE 2013:168:86100 2274.7    4.7 2081.5  193.2  -0.20   0.66   0.84   0.85    8  1.4  31.11  914.01  296.2  282.5   7.20   6.74   2.94
-TROP/SOLUTION
*-------------------------------------------------------------------------------
+SLANT/SOLUTION
*STATION__ ____EPOCH_____ SLTTOT STDDEV   SLTDRY SLTWET SLTIWV SLTGRD SATRES SATMPT  SAT  SATELE  SATAZI    FACDRY    FACWET    FACGRD
 GOPE00CZE 2013:168:64500   8363.0    9.9  7748.2  603.3   98.2   10.4    1.1    0.0  G05  16.000  39.323  3.575822  3.603292 12.159794
 GOPE00CZE 2013:168:64500   5635.5    8.2  5226.3  405.1   66.0   -0.2    4.2    0.0  G06  24.340 276.596  2.411963  2.419605  5.273237
 GOPE00CZE 2013:168:64500   3527.2    6.5  3266.0  252.6   41.1    0.8    7.8    0.0  G16  41.483 305.307  1.507287  1.508554  1.698072
 ...
 ZIMM00CHE 2013:168:86100   6721.5    8.0  6146.0  573.3   92.3   -7.0    9.3    0.0  G28  19.603 279.934  2.952592  2.967259  8.150843
 ZIMM00CHE 2013:168:86100   2366.6    4.7  2156.7  200.2   32.2   -0.2    9.8    0.0  G32  74.810 235.655  1.036111  1.036160  0.281091
-SLANT/SOLUTION
%=ENDTRO
```

Example for Combination Product

```
%=TRO 2.00 ASI 2015:352:42300 EUR 2015:298:01800 2015:304:84600 P MIX
*------------------------------------------------------------------------------
+FILE/REFERENCE
 DESCRIPTION    Weekly combination of trop estimates of EPN Analysis Centers
 OUTPUT         Combined Tropospheric Products of the EPN Network
 CONTACT        rosa.pacione@e-geos.it,ASI/CGS Italy
 Version Number 001
-FILE/REFERENCE
*------------------------------------------------------------------------------
+TROP/DESCRIPTION
*_________KEYWORD_____________ __VALUE(S)_____________________
 TROPO SAMPLING INTERVAL                    3600
 BIAS FROM INTERVAL                      15298 15304
 DELETE FACTOR                             1.0
 GEOID MODEL                            EGM2008
 TIME SYSTEM                                 G
 TROPO PARAMETER NAMES         TROTOT STDDEV #ACTAK #ACDEL
 TROPO PARAMETER UNITS         1.0e+3 1.0e+3      1      1
 TROPO PARAMETER WIDTH              8      8      2      2
-TROP/DESCRIPTION
*------------------------------------------------------------------------------
+CENTERS/INFO_MODEL
*_AC T CUT DATA TROP __TROP_MAPPING_FUNCTION______
 ASI P   3  300 3600    VMF1H/VMF1W
 BEK P   3  180 3600    GMFH/GMFW
 BKG P   3  180 3600    GMFH/GMFW
 COE P   3  180 3600    VMF1H/VMF1W
 ..........................

-CENTERS/INFO_MODEL
*------------------------------------------------------------------------------
+INPUT/FILES
 ASI1_OPE_FIN_2015102500_01D_01H.TRO
 ...........
 ASI1_OPE_FIN_2015103100_01D_01H.TRO
 BEK1_OPE_FIN_2015102500_01D_01H.TRO
 ...........
 BEK1_OPE_FIN_2015103100_01D_01H.TRO
 ...........
 COE1_OPE_FIN_2015103100_01D_01H.TRO
 ...........
-INPUT/FILES
*------------------------------------------------------------------------------
+FILE/COMMENT
 Coordinates taken from EUREF weekly combined solution
-FILE/COMMENT
*------------------------------------------------------------------------------
+SITE/ID
*STATION__ PT __DOMES__ T _STATION_DESCRIPTION__ APPROX_LON_ APPROX_LAT_ _APP_HGT GEOID_HGT
 ACOR00ESP  A 13434M001 P A Coruna, ES           43.364385    -8.398930   66.900   14.821
 ...
-SITE/ID
*------------------------------------------------------------------------------
+SITE/COORDINATES
*STATION__ PT SOLN T DATA_START____ DATA_END_____ ___STA_X____ ___STA_Y____ ___STA_Z____ SYSTEM REMRK SX SY SZ #N
 ACOR00ESP  A    1 P 2015:298:00000 2015:304:86370  4594489.598  -678367.524  4357066.243 ITRF08 Mean   0  0  0
 ...
-SITE/COORDINATES
*------------------------------------------------------------------------------
+SITE/RECEIVER
*STATION__ PT SOLN T DATA_START____ DATA_END_____ DESCRIPTION_________ S/N_________________ FIRMWARE___
 ACOR00ESP  A    1 P 2015:298:00000 2015:304:86370 LEICA GRX1200PRO     -459187              8.20/2.125
 ...
-SITE/RECEIVER
*------------------------------------------------------------------------------
+SITE/ANTENNA
*STATION__ PT SOLN T DATA_START____ DATA_END_____ DESCRIPTION_________ S/N_________________ PCV_MODEL_
 ACOR00ESP  A    1 P 2015:298:00000 2015:304:86370 LEIAT504        LEIS -103033              IGS08_1885
 ...
-SITE/ANTENNA
*------------------------------------------------------------------------------
+SITE/ECCENTRICITY
*                                                UP______ NORTH___ EAST____
*STATION__ PT SOLN T DATA_START____ DATA_END_____ AXE ARP->BENCHMARK(M)_______
 ACOR00ESP  A    1 P 2015:298:00000 2015:304:86370 UNE   3.0460   0.0000   0.0000
 ...
-SITE/ECCENTRICITY
*------------------------------------------------------------------------------
+TROP/SOLUTION
*STATION__ ____EPOCH____ TROTOT _SIG #T #D
 ACOR00ESP 2015:298:01800 2461.6  5.6  4  0
 ACOR00ESP 2015:298:05400 2461.6  4.3  4  0
 ACOR00ESP 2015:298:09000 2457.8  4.6  4  0
 ...
-TROP/SOLUTION
*------------------------------------------------------------------------------
+CENTERS/INFO_SOLUTION
*STATION__ AC_ #D DAY_COD #B _BIAS_ _BIAS_ _BIAS_ _BIAS_ _BIAS_ _BIAS_ _BIAS_
 ACOR00ESP BEK  7 1111111  1    1.4    1.0    0.9    1.3    1.1    1.0    1.2
 ACOR00ESP IGE  7 1111111  1    1.9    1.9    1.9    1.9    1.9    1.9    1.9
 ACOR00ESP IGN  6 1110111  1    1.9    1.5    1.3    1.8    2.0    1.6    1.9
 ACOR00ESP ROB  4 1001101  1   -5.3   -5.0   -5.1   -5.5   -5.3   -4.9   -5.2
 ....
-CENTERS/INFO_SOLUTION
*------------------------------------------------------------------------------
%=ENDTRO
```

Example of Submission for Radiosonde Product

```
%=TRO 2.00 GOP 2017:157:61760 GOP 2013:169:00000 2013:181:21600 S  MIX
*-------------------------------------------------------------------------------
+FILE/REFERENCE
*INFO_TYPE__________ INFO____________________________________________________
 DESCRIPTION         GOP - Geodetic Observatory Pecny, RIGTC
 OUTPUT              Solution parameters
 CONTACT             gnss@pecny.cz
 SOFTWARE            G-Nut/Rao
 INPUT               GNSS/NWM/RAO/OTH data
 VERSION NUMBER      001
-FILE/REFERENCE
*-------------------------------------------------------------------------------
+TROP/DESCRIPTION
*_________KEYWORD_____________ __VALUE(S)_____________________________________
 TROPO SAMPLING INTERVAL       0
 TIME SYSTEM                   UTC
 REFRACTIVITY COEFFICIENTS     77.60 70.40 373900.0
 TROPO PARAMETER NAMES         WVPDEC WMTLPS TEMLPS ZWDDEC WVPRES    IWV  PRESS HUMSPC TEMDRY WMTEMP TRODRY TROTOT TROWET
 TROPO PARAMETER UNITS              1  1e+03  1e+03      1      1      1      1      1      1      1  1e+03  1e+03  1e+03
 TROPO PARAMETER WIDTH              6      6      6      6      6      6      7      6      6      6      6      6      6
-TROP/DESCRIPTION
*-------------------------------------------------------------------------------
+SITE/ID
*STATION__ PT __DOMES__ T _STATION_DESCRIPTION__ _LONGITUDE _LATITUDE_ _HGT_ELI_ _HGT_MSL_
 EZM_11520  A XXXXXXXXX S Czech Republic: PRAHA-  14.446900  50.007800   340.003   378.007
-SITE/ID
*-------------------------------------------------------------------------------
+SITE//COORDINATES
*STATION__ PT SOLN T __DATA_START__ __DATA_END____ __STA_X_____ __STA_Y_____ __STA_Z_____ SYSTEM REMRK
 EZM_11520  A    1 S 2013:169:00000 2013:181:21600  3977538.400  1024729.503  4863607.154  IGS08   GOP
-SITE/COORDINATES
*-------------------------------------------------------------------------------
+TROP/SOLUTION
*STATION__ ____EPOCH_____ WVPDEC WMTLPS TEMLPS ZWDDEC WVPRES    IWV    PRESS HUMSPC TEMDRY WMTEMP TRODRY TROTOT TROWET
 EZM_11520 2013:169:00000   2.99   7.11   7.05   3.73  18.87  32.19  980.00 12.064  294.5  287.8 2230.6 2426.9  196.3
 EZM_11520 2013:169:21600   3.36   6.97   7.13   3.50  21.27  28.78  981.00 13.600  295.3  286.9 2232.9 2409.0  176.0
 EZM_11520 2013:169:43200   3.05   7.22   7.44   3.64  23.94  34.14  980.00 15.337  305.5  288.7 2230.7 2438.2  207.6
 EZM_11520 2013:170:00000   5.19   6.94   7.15   3.27  23.21  29.11  982.00 14.835  294.8  286.6 2235.2 2413.4  178.2
 EZM_11520 2013:170:21600   4.55   6.59   7.02   3.00  22.78  29.56  982.00 14.559  296.8  284.9 2235.2 2417.3  182.1
 EZM_11520 2013:170:43200   3.43   7.05   7.32   4.10  26.41  36.86  981.00 16.918  304.1  288.8 2232.9 2456.9  224.0
 EZM_11520 2013:171:00000   4.02   7.37   7.03   4.73  22.78  29.36  978.00 14.619  297.3  290.5 2226.1 2403.5  177.4
 EZM_11520 2013:171:21600   3.84   7.19   6.86   4.07  22.36  28.93  978.00 14.347  296.9  288.4 2226.1 2402.1  176.0
 EZM_11520 2013:171:43200   3.57   7.31   7.42   4.24  25.46  33.76  977.00 16.370  304.5  290.1 2223.8 2428.1  204.2
 EZM_11520 2013:172:00000   2.10   6.56   6.64   2.87  16.60  32.20  976.00 10.647  293.8  284.4 2221.5 2420.2  198.6
 EZM_11520 2013:172:21600   2.02   5.82   6.15   3.10  16.39  30.38  979.00 10.477  291.9  281.7 2228.3 2417.5  189.2
 EZM_11520 2013:172:43200   2.80   6.24   6.45   3.50  16.39  24.22  980.00 10.466  297.5  282.9 2230.6 2380.8  150.2
 EZM_11520 2013:173:00000   2.30   5.67   6.30   2.45  16.82  26.38  982.00 10.720  292.9  280.3 2235.2 2400.3  165.1
 EZM_11520 2013:173:21600   2.48   5.78   6.06   2.72  16.82  24.83  982.00 10.720  292.1  279.4 2235.2 2391.0  155.9
 EZM_11520 2013:173:43200   2.03   6.02   6.82   3.28  12.94  25.87  981.00  8.244  297.9  280.9 2232.9 2394.4  161.5
 EZM_11520 2013:174:00000   2.43   5.97   6.42   3.48  16.39  29.36  980.00 10.466  291.8  280.6 2230.6 2414.1  183.5
 EZM_11520 2013:174:21600   2.80   5.67   6.19   3.27  16.92  25.55  979.00 10.823  291.5  279.5 2228.3 2388.7  160.4
 EZM_11520 2013:174:43200   2.42   5.60   6.24   2.96  15.56  28.94  979.00  9.944  294.8  278.6 2228.3 2410.5  182.2
 EZM_11520 2013:175:00000   1.88   5.19   6.16   2.04  10.72  22.74  981.00  6.822  290.1  273.9 2232.8 2378.4  145.6
 EZM_11520 2013:175:21600   1.92   5.22   6.12   2.11  12.85  24.83  982.00  8.181  285.5  272.5 2235.1 2394.8  159.7
 EZM_11520 2013:175:43200   2.17   5.16   5.96   2.21  13.46  26.26  983.00  8.564  287.3  273.0 2237.4 2406.1  168.7
 EZM_11520 2013:176:00000   2.00   5.21   6.06   2.21  13.46  26.73  982.00  8.572  285.1  272.7 2235.1 2406.9  171.8
 EZM_11520 2013:176:21600   2.38   4.92   6.16   2.24  13.11  24.14  981.00  8.355  285.1  272.1 2232.8 2388.4  155.5
 EZM_11520 2013:176:43200   2.36   4.73   5.93   2.37  12.77  22.98  983.00  8.118  285.3  271.0 2237.4 2386.0  148.6
 EZM_11520 2013:177:00000   2.26   4.88   5.99   2.48  10.86  20.63  986.00  6.881  283.3  270.3 2244.2 2378.0  133.8
 EZM_11520 2013:177:21600   2.37   4.94   6.07   2.62  11.09  20.91  986.00  7.023  282.9  270.2 2244.2 2379.8  135.6
 EZM_11520 2013:177:43200   2.24   5.18   5.92   2.51  10.08  19.82  988.00  6.368  284.3  270.2 2248.7 2377.3  128.6
 EZM_11520 2013:178:00000   4.09   6.25   6.16   4.34   9.74  13.10  990.00  6.139  282.5  273.2 2253.3 2337.3   84.1
 EZM_11520 2013:178:21600   4.48   5.83   6.60   4.47  10.29  13.26  989.00  6.494  283.9  273.2 2251.0 2336.1   85.1
 EZM_11520 2013:178:43200   2.95   5.82   6.79   4.16   9.34  14.36  988.00  5.901  287.1  273.9 2248.7 2340.7   91.9
 EZM_11520 2013:179:00000   4.18   5.94   6.86   3.94  10.22  13.20  987.00  6.463  281.8  274.3 2246.4 2330.8   84.4
 EZM_11520 2013:179:21600   3.16   5.68   6.58   3.12  10.50  14.60  986.00  6.649  281.5  272.5 2244.2 2338.1   93.9
 EZM_11520 2013:179:43200   2.55   5.81   7.04   3.06   9.60  14.39  985.00  6.086  292.5  273.6 2241.9 2334.1   92.2
 EZM_11520 2013:180:00000   3.15   6.12   6.64   4.04  11.24  16.34  984.00  7.134  284.1  276.1 2239.6 2343.4  103.8
 EZM_11520 2013:180:21600   2.70   5.93   6.39   3.08  11.24  18.31  983.00  7.141  285.5  273.6 2237.4 2354.7  117.3
 EZM_11520 2013:180:43200   2.04   5.67   6.87   2.60  10.72  21.14  981.00  6.822  292.1  273.6 2232.8 2368.3  135.5
 EZM_11520 2013:181:00000   2.79   5.90   6.42   3.42  13.11  22.46  984.00  8.330  285.8  275.5 2239.6 2382.6  143.0
 EZM_11520 2013:181:21600   6.51   5.82   5.77   6.32   9.41   9.06  986.00  5.955  283.8  273.9 2244.2 2302.2   58.0
-TROP/SOLUTION
%=ENDTRO
```

Example of Submission for NWM-derived Parameters

```
%=TRO 2.00 GOP 2017:120:63556 GOP 2013:168:00000 2013:169:00000 N  MIX
*-------------------------------------------------------------------------------
+FILE/REFERENCE
*INFO_TYPE_________ INFO_____________________________________________________
 DESCRIPTION        GOP - Geodetic Observatory Pecny, RIGTC
 OUTPUT             Solution parameters
 CONTACT            gnss@pecny.cz
 SOFTWARE           G-Nut/Shu
 INPUT              GNSS/NWM/RAO/OTH data
-FILE/REFERENCE
*-------------------------------------------------------------------------------
+TROP/DESCRIPTION
*         KEYWORD_____________ _VALUE(S)_____________________________________
 REFRACTIVITY COEFFICIENTS     77.60 70.40 373900.0
 TROPO SAMPLING INTERVAL       3600
 TIME SYSTEM                   UTC
 TROPO PARAMETER NAMES         WVPDEC WMTLPS TEMLPS ZWDDEC WVPRES SCLHGT    IWV   PRESS HUMSPC TEMDRY WMTEMP TRODRY TROTOT TROWET
 TROPO PARAMETER UNITS              1  1e+03  1e+03      1      1  0.001      1       1      1      1  1e+03  1e+03  1e+03
 TROPO PARAMETER WIDTH              6      6      6      6      6      6      6       7      6      6      6      6      6      6
-TROP/DESCRIPTION
*-------------------------------------------------------------------------------
+SITE/ID
*STATION__ PT __DOMES__ T _STATION_DESCRIPTION__ _LONGITUDE _LATITUDE_ _HGT_ELI_ _HGT_MSL_
 GOPE00CZE  A 11502M002 N                        14.785625  49.913706   592.716   630.502
 WTZR00DEU  A 14201M010 N                        12.878912  49.144199   666.119   705.725
 ZIMM00CHE  A 14001M004 N                         7.465279  46.877099   956.324  1000.057
-SITE/ID
*-------------------------------------------------------------------------------
+SITE/COORDINATES
*STATION__ PT SOLN T DATA_START____ DATA_END______ __STA_X_____ __STA_Y_____ __STA_Z_____ SYSTEM REMRK
 GOPE00CZE  A    1 N 2013:168:00000 2013:169:00000  3979316.100  1050312.600  4857067.400  IGS08   GOP
 WTZR00DEU  A    1 N 2013:168:00000 2013:169:00000  4075580.800   931853.900  4801568.800  IGS08   GOP
 ZIMM00CHE  A    1 N 2013:168:00000 2013:169:00000  4331297.300   567556.000  4633134.600  IGS08   GOP
-SITE/COORDINATES
*-------------------------------------------------------------------------------
+TROP/SOLUTION
*STATION__ ____EPOCH___ WVPDEC WMTLPS TEMLPS ZWDDEC WVPRES SCLHGT    IWV   PRESS HUMSPC TEMDRY WMTEMP TRODRY TROTOT TROWET
 GOPE00CZE 2013:168:00000   2.58   6.23   6.51   2.80  12.51  8.081  22.67  953.04  8.202  293.1  280.1 2169.4 2311.4  142.0
 GOPE00CZE 2013:168:03600   2.49   6.21   6.50   2.74  12.21  8.081  22.79  953.13  8.006  292.7  279.9 2169.6 2312.5  142.9
 GOPE00CZE 2013:168:07200   2.41   6.18   6.49   2.68  11.91  8.082  22.92  953.22  7.810  292.4  279.8 2169.8 2313.6  143.7
 GOPE00CZE 2013:168:10800   2.33   6.16   6.48   2.62  11.61  8.082  23.05  953.32  7.614  292.1  279.7 2170.0 2314.6  144.6
 GOPE00CZE 2013:168:14400   2.24   6.13   6.47   2.57  11.31  8.082  23.17  953.41  7.418  291.8  279.5 2170.2 2315.7  145.5
 GOPE00CZE 2013:168:18000   2.16   6.11   6.46   2.51  11.02  8.082  23.30  953.50  7.222  291.4  279.4 2170.5 2316.8  146.3
 GOPE00CZE 2013:168:21600   2.08   6.08   6.45   2.45  10.72  8.082  23.42  953.59  7.026  291.1  279.3 2170.7 2317.8  147.2
 GOPE00CZE 2013:168:25200   2.11   6.17   6.52   2.52  11.23  8.089  23.79  953.60  7.361  291.9  279.8 2170.7 2319.9  149.2
 GOPE00CZE 2013:168:28800   2.18   6.30   6.62   2.64  11.97  8.098  24.24  953.57  7.847  293.0  280.5 2170.6 2322.2  151.6
 GOPE00CZE 2013:168:32400   2.27   6.45   6.74   2.77  12.84  8.109  24.74  953.51  8.418  294.3  281.3 2170.5 2324.7  154.2
 GOPE00CZE 2013:168:36000   2.36   6.60   6.86   2.92  13.74  8.120  25.27  953.42  9.010  295.6  282.2 2170.3 2327.4  157.1
 GOPE00CZE 2013:168:39600   2.44   6.75   6.97   3.06  14.57  8.131  25.81  953.30  9.556  296.9  283.1 2170.0 2330.0  160.0
 GOPE00CZE 2013:168:43200   2.50   6.89   7.06   3.17  15.23  8.141  26.34  953.15  9.992  298.0  283.8 2169.7 2332.5  162.9
 GOPE00CZE 2013:168:46800   2.46   6.97   7.12   3.22  15.38  8.149  26.83  952.95 10.096  298.7  284.3 2169.2 2334.8  165.6
 GOPE00CZE 2013:168:50400   2.40   7.05   7.16   3.25  15.37  8.155  27.31  952.73 10.091  299.2  284.7 2168.7 2337.1  168.4
 GOPE00CZE 2013:168:54000   2.33   7.10   7.19   3.26  15.27  8.161  27.78  952.49 10.031  299.5  285.0 2168.2 2339.3  171.1
 GOPE00CZE 2013:168:57600   2.26   7.15   7.21   3.27  15.16  8.166  28.23  952.26  9.966  299.7  285.3 2167.7 2341.3  173.7
 GOPE00CZE 2013:168:61200   2.21   7.19   7.21   3.29  15.12  8.171  28.65  952.05  9.950  299.7  285.5 2167.2 2343.3  176.1
 GOPE00CZE 2013:168:64800   2.19   7.21   7.20   3.32  15.24  8.174  29.04  951.90 10.033  299.6  285.7 2166.8 2345.2  178.3
 GOPE00CZE 2013:168:68400   2.28   7.22   7.15   3.42  15.94  8.176  29.31  951.90 10.486  299.1  286.0 2166.8 2346.7  179.9
 GOPE00CZE 2013:168:72000   2.37   7.23   7.11   3.51  16.64  8.177  29.59  951.90 10.940  298.7  286.2 2166.8 2348.3  181.4
 GOPE00CZE 2013:168:75600   2.46   7.24   7.07   3.61  17.33  8.179  29.87  951.90 11.394  298.2  286.5 2166.8 2349.8  183.0
 GOPE00CZE 2013:168:79200   2.55   7.25   7.02   3.71  18.03  8.180  30.15  951.90 11.848  297.7  286.7 2166.8 2351.4  184.5
 GOPE00CZE 2013:168:82800   2.64   7.26   6.98   3.80  18.72  8.182  30.43  951.90 12.301  297.3  287.0 2166.8 2352.9  186.1
 GOPE00CZE 2013:169:00000   2.73   7.27   6.94   3.90  19.42  8.184  30.71  951.90 12.755  296.8  287.2 2166.8 2354.5  187.6
 ...
 ZIMM00CHE 2013:168:00000   3.02   7.12   6.87   3.86  18.78  8.106  28.07  912.71 12.261  294.8  284.1 2078.5 2253.5  175.0
 ZIMM00CHE 2013:168:03600   3.01   7.15   6.89   3.83  18.40  8.107  27.54  912.56 12.165  294.7  284.1 2078.2 2249.9  171.8
 ZIMM00CHE 2013:168:07200   3.00   7.18   6.91   3.80  18.02  8.108  27.01  912.41 12.069  294.5  284.1 2077.8 2246.3  168.5
 ZIMM00CHE 2013:168:10800   2.99   7.21   6.93   3.77  17.64  8.108  26.49  912.26 11.973  294.4  284.1 2077.5 2242.7  165.3
 ZIMM00CHE 2013:168:14400   2.98   7.24   6.95   3.74  17.26  8.109  25.96  912.11 11.877  294.3  284.1 2077.1 2239.2  162.0
 ZIMM00CHE 2013:168:18000   2.97   7.27   6.97   3.72  16.88  8.110  25.43  911.96 11.781  294.2  284.1 2076.8 2235.6  158.8
 ZIMM00CHE 2013:168:21600   2.96   7.30   6.98   3.69  16.49  8.111  24.91  911.81 11.685  294.0  284.1 2076.4 2232.0  155.5
 ZIMM00CHE 2013:168:25200   2.93   7.30   7.07   3.65  16.31  8.115  24.84  911.75 11.520  294.8  284.2 2076.3 2231.4  155.1
 ZIMM00CHE 2013:168:28800   2.90   7.28   7.18   3.62  16.20  8.120  24.94  911.71 11.347  295.8  284.3 2076.2 2231.8  155.6
 ZIMM00CHE 2013:168:32400   2.86   7.26   7.29   3.58  16.16  8.126  25.19  911.69 11.190  296.9  284.5 2076.2 2233.2  157.0
 ZIMM00CHE 2013:168:36000   2.82   7.24   7.42   3.53  16.17  8.131  25.57  911.68 11.070  298.1  284.7 2076.2 2235.4  159.3
 ZIMM00CHE 2013:168:39600   2.77   7.21   7.54   3.48  16.24  8.137  26.05  911.66 11.009  299.3  284.9 2076.1 2238.4  162.2
 ZIMM00CHE 2013:168:43200   2.71   7.19   7.65   3.42  16.34  8.143  26.63  911.63 11.031  300.2  285.0 2076.0 2241.9  165.8
 ZIMM00CHE 2013:168:46800   2.63   7.20   7.76   3.34  16.45  8.149  27.27  911.47 11.217  300.9  285.0 2075.7 2245.6  169.9
 ZIMM00CHE 2013:168:50400   2.55   7.21   7.87   3.24  16.60  8.155  28.02  911.29 11.488  301.5  285.1 2075.3 2249.9  174.7
 ZIMM00CHE 2013:168:54000   2.47   7.22   7.96   3.15  16.80  8.160  28.82  911.12 11.807  301.9  285.0 2074.9 2254.7  179.8
 ZIMM00CHE 2013:168:57600   2.39   7.22   8.02   3.06  17.01  8.164  29.64  911.01 12.138  302.1  285.0 2074.6 2259.8  185.1
 ZIMM00CHE 2013:168:61200   2.32   7.21   8.05   2.98  17.25  8.166  30.43  910.99 12.445  302.0  284.9 2074.6 2264.8  190.2
 ZIMM00CHE 2013:168:64800   2.27   7.19   8.04   2.92  17.50  8.165  31.15  911.09 12.692  301.7  284.7 2074.8 2269.7  194.9
 ZIMM00CHE 2013:168:68400   2.28   7.11   7.90   2.92  17.76  8.158  31.57  911.58 12.704  300.8  284.3 2075.9 2273.6  197.7
 ZIMM00CHE 2013:168:72000   2.29   7.04   7.75   2.93  18.01  8.150  32.00  912.08 12.716  299.9  283.9 2077.1 2277.6  200.5
 ZIMM00CHE 2013:168:75600   2.31   6.96   7.61   2.93  18.27  8.143  32.42  912.57 12.728  298.9  283.6 2078.2 2281.6  203.4
 ZIMM00CHE 2013:168:79200   2.32   6.88   7.47   2.93  18.53  8.135  32.85  913.07 12.740  298.0  283.2 2079.3 2285.5  206.2
 ZIMM00CHE 2013:168:82800   2.33   6.81   7.33   2.94  18.78  8.128  33.27  913.56 12.753  297.0  282.8 2080.4 2289.5  209.0
 ZIMM00CHE 2013:169:00000   2.34   6.73   7.19   2.94  19.04  8.120  33.70  914.05 12.765  296.1  282.5 2081.6 2293.4  211.8
-TROP/SOLUTION
%=ENDTRO
```

Acknowledgments This activity is carried out in the framework of WG3 'GNSS for Climate' of the COST Action ES1206 'Advanced Global Navigation Satellite Systems tropospheric products for monitoring severe weather events and climate (GNSS4SWEC)'. e-GEOS work was done under ASI contract 2015-050-R.0. The work at GOP was carried out under the framework of the national project (No. LD14102) by the Ministry of Education, Youth and Sports of the Czech Republic provided in support of the COST Action ES1206. D. Offiler (Met Office UK), H. Brenot (BIRA), M. Bender (DWD), H. Vedel (DMI), O. Lewis (Met Office UK) are acknowledged for useful suggestions.

References

Askne, J., & Nordius, H. (1987). Estimation of tropospheric delay for microwaves from surface weather data. *Radio Science, 22*(3), 379–386.

Bevis, M., Businger, S., Chiswell, S., Herring, T. A., Anthes, R. A., Rocken, C., & Ware, R. H. (1994). GPS Meteorology: mapping zenith wet delays onto precipitable water. *Journal of Applied Meteorology, 33*, 379–386.

'COST-Format' File Specification for Ground-based GNSS Delay and Water Vapour Data, http://egvap.dmi.dk/support/formats/egvap_cost_v22.pdf.

Davis, J. L., Herring, T. A., Shapiro, I. I., Rogers, A. E. E., & Elgered, G. (1985). Geodesy by radio interferometry: Effects of atmospheric modelling errors on estimates of baseline length. *Radio Science, 20*, 1593–1607.

Douša, J., & Eliaš, M. (2014). An improved model for calculating tropospheric wet delay. *Geophysical Research Letters, 41*. https://doi.org/10.1002/2014GL060271.

Gendt, G. (1997). *SINEX TRO—Solution (software/technique) independent exchange format for combination of Tropospheric estimates version 0.01*. March 1, 1997. https://igscb.jpl.nasa.gov/igscb/data/format/sinex_tropo.txt.

IERS convention. 2010. Gérard Petit and Brian Luzum (eds.). (IERS Technical Note; 36) Frankfurt am Main: Verlag des Bundesamts für Kartographie und Geodäsie, 2010. 179 pp., ISBN 3-89888-989-6.

Saastamoinen, J. (1972). Atmospheric correction for the troposphere and stratosphere in radio ranging of satellites. In S. W. Henriksen et al. (Eds.), *The use of artificial satellites for geodesy* (Vol. 15). Washington, DC: Geophysics Monograph Series, A.G.U.

Smith, W. L. (1966). Note on the relationship between total precipitable water and surface dew point. *Journal of Applied Meteorology, 5*, 726–727.

SINEX Format, http://www.iers.org/IERS/EN/Organization/AnalysisCoordinator/SinexFormat/sinex.html.

The U.S. Standard Atmosphere. (1976). Sponsorship of National Oceanic and Atmospheric Administration, National Aeronautics and Space Administration, U.S. Air Force, U.S. Government Printing Office, Washington, DC.

WMO. (2001). *Manual on codes*. WMO-306, Vol. 1.2, Part B, 2001 with Supplement 3, 2007, WMO, Geneva. See online version at http://www.wmo.ch/pages/prog/www/WMOCodes.html.